

THE JOURNAL OF
PHYSICAL
CHEMISTRY

Volume 68

JANUARY—APRIL, 1964

PAGES 1—982

W. ALBERT NOYES, JR., *Editor*

L. O. MORGAN, *Associate Editor*

CHARLES R. BERTSCH, *Senior Production Editor*

RICHARD H. BELKNAP, *Director of Fundamental Journals Division*

EDITORIAL BOARD

A. O. ALLEN
J. BIGEISEN
L. F. DAHL
B. P. DAILEY
F. S. DAINTON
D. D. ELEY
J. R. FRESCO

C. J. HOCHANADEL
C. KEMBALL
W. KLEMPERER
A. D. LIEHR
S. C. LIND
F. A. LONG
J. L. MARGRAVE
J. P. McCULLOUGH

W. J. MOORE
R. G. PARR
G. PORTER
J. E. RICCI
M. B. WALLENSTEIN
W. WEST
B. ZIMM

EASTON, PA.
MACK PRINTING COMPANY
1964

THE JOURNAL OF PHYSICAL CHEMISTRY

W. ALBERT NOYES, Jr., *Editor*

L. O. MORGAN, *Assistant Editor*

RICHARD H. BELKNAP, *Director of Fundamental Journals Division*

CHARLES R. BERTSCH, *Senior Production Editor*

EDITORIAL BOARD: A. O. ALLEN, J. BIGELEISEN, L. F. DAHL,
B. P. DAILEY, F. S. DANTON, D. D. ELEY, J. R. FRESCO,
C. J. HOCHANADEL, C. KEMBALL, W. KLEMPERER, A. D. LIEHR,
S. C. LIND, F. A. LONG, J. L. MARGRAVE, J. P. McCULLOUGH,
W. J. MOORE, R. G. PARR, G. PORTER, J. E. RICCI,
M. B. WALLENSTEIN, W. WEST, B. ZIMM

© Copyright, 1964, by the American Chemical Society.

Published monthly by the American Chemical Society at 20th and Northampton Sts., Easton, Pa. Second-class postage paid at Easton, Pa.

The Journal of Physical Chemistry is devoted to the publication of selected symposia in the broad field of physical chemistry and to other contributed papers.

Manuscripts originating in the British Isles, Europe, and Africa should be sent to F. C. Tompkins, The Faraday Society, 6 Gray's Inn Square, London W. C. 1, England.

Manuscripts originating elsewhere should be sent to W. Albert Noyes, Jr., Department of Chemistry, University of Texas, Austin, Texas 78712.

Correspondence regarding accepted copy, proofs, and reprints should be directed to Fundamental Journals Production Office, American Chemical Society, 20th and Northampton Sts., Easton, Pa. 18043. Senior Production Editor: Charles R. Bertsch. Assistant Editor: Edward A. Borger.

Advertising Office: Reinhold Publishing Corporation, 430 Park Avenue, New York, N. Y. 10022.

Articles must be submitted in duplicate, typed, and double spaced. They should have at the beginning a brief Abstract, in no case exceeding 300 words. Original drawings should accompany the manuscript. Lettering at the sides of graphs (black on white or blue) may be pencilled in and will be typeset. Figures and tables should be held to a minimum consistent with adequate presentation of information. All footnotes and references to the literature should be numbered consecutively and placed in the manuscript at the proper places. Initials of authors referred to in citations should be given. Nomenclature should conform to that used in *Chemical Abstracts*, mathematical characters be marked for italic, Greek letters carefully made or annotated, and subscripts and superscripts clearly shown. Articles should be written as briefly as possible consistent with clarity and should avoid historical background unnecessary for specialists.

Notes are similar to articles in every way except as to length and are subjected to the same editorial appraisal. In their preparation particular attention should be paid to brevity and conciseness. Material included in Notes must be definitive and may not be republished subsequently.

Communications to the Editor are designed to afford prompt preliminary publication of observations or discoveries whose value to science is so great that immediate publication is imperative. The appearance of related work from other laboratories is in itself not considered sufficient justification for the publication of a Communication, which must in addition meet special requirements of timeliness and significance. Their total length

may in no case exceed 1000 words or their equivalent. They differ from Articles and Notes in that their subject matter may be republished.

Symposium papers should be sent in all cases to Secretaries of Divisions sponsoring the symposium, who will be responsible for their transmittal to the Editor. The Secretary of the Division by agreement with the Editor will specify a time after which symposium papers cannot be accepted. The Editor reserves the right to refuse to publish symposium articles, for valid scientific reasons. Each symposium paper may not exceed four printed pages (about sixteen double spaced typewritten pages) in length except by prior arrangement with the Editor.

The American Chemical Society and the Editors of *The Journal of Physical Chemistry* assume no responsibility for the statements and opinions advanced by contributors.

Business and Subscription Information

Remittances and orders for subscriptions and for single copies, notices of changes of address and new professional connections, and claims for missing numbers should be sent to the Subscription Service Department, American Chemical Society, 1155 Sixteenth St., N.W., Washington, D. C. 20036. Changes of address for *The Journal of Physical Chemistry* must be received on or before the 30th of the preceding month. Please include an old address label with the notification.

Claims for missing numbers will not be allowed (1) if received more than sixty days from date of issue, (2) if loss was due to failure of notice of change of address to be received before the date specified in the preceding paragraph, or (3) if the reason for the claim is "missing from files."

Subscription rates (1964): members of American Chemical Society, \$12.00 for 1 year; to nonmembers, \$24.00 for 1 year. Postage to countries in the Pan-American Union, \$0.80; Canada, \$0.40; all other countries, \$1.20. Single copies for current year: \$2.50. Postage, single copies: to Canada and countries in the Pan-American Union, \$0.15; all other countries, \$0.20. Rates for back issues are available from the Special Issues Sales Department, 1155 Sixteenth St., N.W., Washington, D. C. 20036.

Publications of the American Chemical Society include: *Analytical Chemistry*, *Biochemistry*, *Chemical Abstracts*, *CA Section Groupings*, *Chemical and Engineering News*, *Chemical Reviews*, *Chemical Titles*, *Chemistry*, *Industrial and Engineering Chemistry*, *Inorganic Chemistry*, *Journal of Agricultural and Food Chemistry*, *Journal of the American Chemical Society*, *Journal of Chemical Documentation*, *Journal of Chemical and Engineering Data*, *Journal of Medicinal Chemistry*, *The Journal of Organic Chemistry*, and *The Journal of Physical Chemistry*. Rates on request.

No. **29** in the
**ADVANCES IN
 CHEMISTRY
 SERIES**

PHYSICAL PROPERTIES OF CHEMICAL COMPOUNDS—III

This handbook of basic data contains 456 full-page tables on 434 aliphatic compounds and 22 miscellaneous compounds and elements—all carefully worked out by R. R. Dreisbach of The Dow Chemical Co.

It is a sequel to **PHYSICAL PROPERTIES—II** (Advances No. 22), which covers 476 organic straight-chain compounds, and **PHYSICAL PROPERTIES—I** (Advances No. 15), which presents data on 511 organic cyclic compounds.

This series provides you with a breadth of data that you can get in no other way. For each compound 15 physical properties are given: purity—freezing point—vapor pressure—liquid density—vapor density—refractive index—rate of change of boiling point with pressure—latent heat of fusion—latent heat of evaporation—critical values—compressibility—viscosity—heat content—surface tension—solubility. Parameters are also furnished for interpolating and extrapolating determined data for almost all the compounds. To get this information by ordinary means you would have to seek out many sources.

PHYSICAL PROPERTIES—III offers the extra advantage of a cumulative index to **all three volumes** (1443 compounds and elements). Use it and the earlier compilations to save yourself hours of laboratory time, and to answer questions quickly.

489 pages.

Cloth bound.

Price: \$6.50

PHYSICAL PROPERTIES—II — 491 pages • cloth bound • price: \$6.50

PHYSICAL PROPERTIES—I — 536 pages • cloth bound • price: \$5.85

Order from:

Special Issues Sales/American Chemical Society/1155 Sixteenth Street, N.W./Washington 6, D.C.

THE JOURNAL OF PHYSICAL CHEMISTRY

Volume 68, Number 1 January, 1964

Raymond M. Fuoss and Lars Onsager: The Conductance of Symmetrical Electrolytes. IV. Hydrodynamic and Osmotic Terms in the Relaxation Field.	1	Robert S. Neale: A Correlation of Bond Dissociation Energy with Ionization Potential and Electron Affinity.	143
F. S. Pettit: Thermodynamic and Electrical Investigations on Molten Antimony Sulfide.	9	Maxwell Goldblatt: The Density of Liquid T ₂ O.	147
W. L. Masterton and Jacqueline A. Scola: Activity Coefficients of 2:1 Complex Ion Electrolytes: Nitropentamminecobalt(III) Chloride, Chloropentamminecobalt(III) Perchlorate, and Fluoropentamminecobalt(III) Chloride.	14	Morris L. Nielsen and J. V. Pustinger, Jr.: Phosphorus-31 Nuclear Magnetic Resonance Studies of Phosphorus-Nitrogen Compounds.	152
T. S. Nagarjuna and Jack G. Calvert: The Photooxidation of Carbon Monoxide on Zinc Oxide.	17	Ruth R. Benerito, Ralph J. Berni, and John B. McKelvey: Hydrolysis Rates and Distribution Coefficients of <i>d,l</i> -Butadienediepoide between Carbon Tetrachloride and Aqueous Sodium Hydroxide.	158
Peter J. Dunlop: Frictional Coefficients for Binary and Ternary Isothermal Diffusion.	26	James E. Blair and J. W. Williams: The Sedimentation Velocity Experiment and the Determination of Molecular Weight Distributions.	161
Milton Manes: On the Application of Thermodynamics and Kinetics to Some Near-Equilibrium Systems.	31	Everett Douglas: Solubilities of Oxygen, Argon, and Nitrogen in Distilled Water.	169
Harold W. Goldstein: The Reaction of Active Nitrogen with Graphite.	39	H. Diebler and N. Sutin: The Kinetics of Some Oxidation-Reduction Reactions Involving Manganese(III).	174
John C. Trowbridge and Edgar F. Westrum, Jr.: Anhydrous Perchloric Acid: Heat Capacities and Thermodynamic Functions from 5 to 300°K.	42	S. N. Vinogradov and Martin Kilpatrick: Association of N-H Compounds. II. Infrared Spectroscopic Investigation of the Self-Association of 3,5-Dimethylpyrazole in Benzene and in Carbon Tetrachloride.	181
Peter Castle, Richard Stoesser, and Edgar F. Westrum, Jr.: Triethanolamine Borate. The Heat Capacity and Thermodynamic Functions from 5 to 350°K.	49	J. Calvin Giddings: General Combination Law for <i>C_i</i> Terms in Gas Chromatography.	184
Y. Amenomiya, J. H. B. Chenier, and R. J. Cvetanović: Application of Flash-Desorption Method to Catalyst Studies. IV. Adsorption of Ammonia on Alumina and Its Effect on Adsorption of Ethylene.	52	L. C. Fischer and Gilbert J. Mains: The Temperature Dependence of the Flash Photolysis of Diethyl Ketone.	188
S. B. Tricklebank, L. Nanis, and J. O'M. Bockris: Diffusion in the System Molten Sodium Iodide-Potassium Chloride.	58	NOTES	
K. M. Myles and A. T. Aldred: Thermodynamic Properties of Solid Vanadium-Iron Alloys.	64	A. Greenville Whittaker and David C. Barham: Surface Temperature Measurements on Burning Solids.	196
S. Gilman: The Mechanism of Electrochemical Oxidation of Carbon Monoxide and Methanol on Platinum. II. The "Reactant-Pair" Mechanism for Electrochemical Oxidation of Carbon Monoxide and Methanol.	70	A. R. Lawrence and A. J. Matuszko: The Electric Moments of Some Nitrate Esters. II. Hindered Rotation.	199
E. W. Anacker, R. M. Rush, and J. S. Johnson: Equilibrium Ultracentrifugation and Light Scattering of Sodium Lauryl Sulfate and Dodecyltrimethylammonium Bromide Solutions.	81	E. M. Morimoto and Milton Kahn: Isotopic Exchange of Iodine Atoms between Tetrabutylammonium Iodide and <i>p</i> -Nitrobenzyl Iodide in Carbon Tetrachloride-Nitrobenzene Mixtures.	201
L. H. Kaplan: Photoetching of Thin Lead Films with Nitromethane.	94	B. Brocklehurst, G. Porter, and J. M. Yates: γ -Excitation of the Singlet and Triplet States of Naphthalene in Solution.	203
Yung-Fang Yu Yao: Chemisorption of Amines and Its Effect on Subsequent Oxidation of Iron Surfaces.	101	A. MacLachlan: Radiation Synthesis of Iodonium Compounds.	205
Kenneth Schug and Ahmad Dadgar: The Relative Free Energies of Sodium, Potassium, Rubidium, Cesium, and Strontium Ions in Methanol and Methanol-Water Mixtures.	106	D. L. Bidlack and D. K. Anderson: Mutual Diffusion in the Liquid System Hexane-Hexadecane.	206
Ahmad Dadgar and Kenneth Schug: The Relative Free Energies of Sodium and Potassium Ions in Ethanol, Ethylene Glycol, Ethanolamine, and Ethylenediamine.	112	G. P. Mohanty, L. J. Fiegel, and J. H. Healy: On the System Niobium Pentoxide-Tantalum Pentoxide.	208
G. R. McMillan, Jack G. Calvert, and Sandra S. Thomas: Nitrosomethane Formation in Photolysis of <i>t</i> -Butyl Nitrite.	116	Ralph P. Seward and Paul E. Field: The Solubility of Thallous Bromide and Silver Chloride in Molten Nitrate Solvents.	210
Robert R. Dewald and James L. Dye: Absorption Spectra of the Alkali Metals in Ethylenediamine.	121	H. Hiraoka and J. H. Hildebrand: The Solubility and Entropy of Solution of Certain Gases in (C ₄ F ₉) ₃ N, CCl ₂ F-CClF ₂ , and 2,2,4-(CH ₃) ₃ C ₅ H ₉	213
Robert R. Dewald and James L. Dye: Solubilities and Conductances of Alkali Metals in Ethylenediamine.	128	William M. Moore and Marshall D. Ketchum: The Limiting Quantum Yield for the Photoreduction of Benzophenone with Isopropyl Alcohol.	214
James L. Dye and Robert R. Dewald: A Model for Metal-Amine Solutions.	135	K. A. Kini: Surface Area of Active Carbon and Carbon Black by the B.E.T. Method Using Argon, Carbon Dioxide, Methanol, Krypton, and Xenon.	217
		COMMUNICATION TO THE EDITOR	
		C. A. Angell: Success of Free Volume Model for Transport in Fused Salts.	218

AUTHOR INDEX

- Aldred, A. T., 64
 Amenomiya, Y., 52
 Anacker, E. W., 81
 Anderson, D. K., 206
 Angell, C. A., 218

 Barham, D. C., 196
 Benerito, R. R., 158
 Berni, R. J., 158
 Bidlack, D. L., 206
 Blair, J. E., 161
 Bockris, J. O'M., 58
 Brocklehurst, B., 203

 Calvert, J. G., 17, 116
 Castle, P., 49
 Chenier, J. H. B., 52
 Cvetanović, R. J., 52

 Dadgar, A., 106, 112
 Dewald, R. R., 121, 128, 135
 Diebler, H., 174
 Douglas, E., 169
 Dunlop, P. J., 26
 Dye, J. L., 121, 128, 135

 Fiegel, L. J., 208
 Field, P. E., 210
 Fischer, L. C., 188
 Fuoss, R. M., 1

 Giddings, J. C., 184
 Gilman, S., 70
 Goldblatt, M., 147
 Goldstein, H. W., 39

 Healy, J. H., 208
 Hildebrand, J. H., 213
 Hiraoka, H., 213

 Johnson, J. S., 81

 Kahn, M., 201
 Kaplan, L. H., 94
 Ketchum, M. D., 214
 Kilpatrick, M., 181
 Kini, K. A., 217

 Lawrence, A. R., 199

 MacLachlan, A., 205
 Mains, G. J., 188
 Manes, M., 31
 Masterton, W. L., 14
 Matuszko, A. J., 199

 McKelvey, J. B., 158
 McMillan, G. R., 116
 Mohanty, G. P., 208
 Moore, W. M., 214
 Morimoto, E. M., 201
 Myles, K. M., 64

 Nagarjunan, T. S., 17
 Nanis, L., 58
 Neale, R. S., 143
 Nielsen, M. L., 152

 Onsager, L., 1

 Pettit, F. S., 9
 Porter, G., 203
 Pustinger, J. V., Jr., 152

 Rush, R. M., 81

 Schug, K., 106, 112
 Scola, J. A., 14
 Seward, R. P., 210
 Stoesser, R., 49
 Sutin, N., 174

 Thomas, S. S., 116
 Tricklebank, S. B., 58
 Trowbridge, J. C., 42

 Vinogradov, S. N., 181

 Westrum, E. F., Jr., 42, 49
 Whittaker, A. G., 196
 Williams, J. W., 161

 Yao, Y.-F. Y., 101
 Yates, J. M., 203

THE JOURNAL OF PHYSICAL CHEMISTRY

Registered in U. S. Patent Office © Copyright, 1964, by the American Chemical Society

VOLUME 68, NUMBER 1 JANUARY 15, 1964

The Conductance of Symmetrical Electrolytes.^{1a} IV.

Hydrodynamic and Osmotic Terms in the Relaxation Field

by Raymond M. Fuoss and Lars Onsager

Contribution No. 1742 from the Sterling Chemistry Laboratory, Yale University, New Haven, Connecticut
(Received September 18, 1963)

Using (1) the differential equation which defines that part of the total potential which has hydrodynamic origin, (2) the corresponding Poisson equation, and (3) the appropriate boundary conditions, the term ΔX_p in the relaxation field is calculated up to terms of order $c^{3/2}$ in concentration in the conductance function $\Lambda(c)$. The Boltzmann factor e^{ξ} is kept explicit as $\exp(-\beta e^{-\kappa r}/r)$ throughout the computation; the principal approximations made are to drop terms of order $\kappa^3 \sim c^{3/2}$. The leading term contains the negative exponential integrals $E_n(2\kappa a)$ and $E_n(\kappa a)$ and thus contributes $c \log c$ terms to $\Lambda(c)$; these are identical with our previous result.^{1b} The next term, linear in c , has a coefficient $P_2(b)$, $b = \epsilon^2/aDkT$, which contains most of the function $K(b)$ which appeared in the electrostatic part ΔX_e of the relaxation field. The kinetic term in $\Lambda(c)$ is also computed to the same degree of approximation; combined with ΔX_v , it gives the complete function $K(b)$, multiplied by a small coefficient.

In the first paper of this series, the equation of continuity for solutions of symmetrical electrolytes was reduced to the form

$$\nabla \cdot e^{\xi} \nabla \mu_{21} = -V(r) \cos \vartheta \quad (1)$$

where

$$\zeta = \epsilon^2 e^{-\kappa r}/rDkT \equiv \beta e^{-\kappa r}/r \quad (2)$$

is the ratio of the electrostatic potential energy of two ions of opposite charge to the thermal energy kT , and μ_{21} is the potential of the total directed force acting on an ion of species 1 located by spherical coordinates (r, ϑ) with respect to an ion of species 2 at the origin. The direction of the external field X_i is along the x -axis ($x = r \cos \vartheta$). The discussion is limited to symmetrical electrolytes, so that $\epsilon_1 = -\epsilon_2$; by convention, we shall

consider species 1 as cations. Then for 1-1 electrolytes, $\epsilon_1 = +\epsilon$ and $\epsilon_2 = -\epsilon$, where ϵ is the elementary charge, 4.8022×10^{-10} e.s.u.

The function $V(r) \cos \vartheta$ is defined by the equation

- (1) (a) Corrections to previous papers of this series: I, R. M. Fuoss and L. Onsager, *J. Phys. Chem.*, **66**, 1722 (1962): eq. 1.25, divide $(v_1 + v_2)$ by $(\omega_1 + \omega_2)$; eq. 1.27, divide right-hand side by $(\omega_1 + \omega_2)$; eq. 2.2, multiply right-hand side by $\cos \vartheta$; eq. 2.5, right-hand side is $[-V(r) \cos \vartheta]$; eq. 2.7, right-hand side is $[-V(r) \cos \vartheta]$; eq. 2.31, replace φ by ϑ . II, R. M. Fuoss and L. Onsager, *ibid.*, **67**, 621 (1963): eq. 12, replace Δ by ∇ and insert minus sign before $V(r)$; eq. 15, insert minus sign before $V(r)$; eq. 72, divide $\tau^2 N'(b)$ by 3; eq. A4, second term on right-hand side is e^b/b ; p. 625, fifth line under (71), the exponent of (DT) is $3/2$. III, R. M. Fuoss and L. Onsager, *ibid.*, **67**, 628 (1963): eq. 16, replace ξ by ζ ; Table I, column headings are b ; $F(b)$; b ; $F(b)$; b ; $-F(b)$. Symbols used in I, II, and III will be used in general without redefinition here. Equations derived in these papers will be cited as I (1.25), etc. (b) R. M. Fuoss and L. Onsager, *J. Phys. Chem.*, **61**, 668 (1957).

$$-V(r) \cos \vartheta \equiv 2e^{\zeta}(v_x \cos \vartheta + v_r) \times \\ (\mathrm{d}\zeta/\mathrm{d}r)/(\omega_1 + \omega_2) \quad (3)$$

where v_x and v_r are the field and radial components of the velocity of an ion of species 1 in the vicinity of an ion of species 2, and ω_j is the reciprocal of the friction coefficient of an ion of species j , so that

$$\mathbf{v}_j^0 \equiv X_{\epsilon_j \omega_j} \mathbf{i} \quad (4)$$

The potential μ_{21} was separated into two terms, μ_{21}' and μ_{21}'' , where μ_{21}' is the purely electrostatic part of the potential, satisfying by definition the homogeneous equation

$$\nabla \cdot e^{\zeta} \nabla \mu_{21}' = 0 \quad (5)$$

The solution of this equation was given in part II. We now present a treatment of the equation

$$\nabla \cdot e^{\zeta} \nabla \mu_{21}'' = -V(r) \cos \vartheta \quad (6)$$

which gives the part of the relaxation field which derives from the motion produced at the location of a given ion by the motion of its neighbors. This result, plus the osmotic term,² calculated with the Boltzmann factor e^{ζ} explicit, will be combined in the following paper with our previous results to give the following conductance equation

$$\Lambda = \Lambda_0 - S c^{1/2} + 2E' c \ln \tau - [E_1' \Lambda_0 H(b) - \\ E_2' G(b)] c - (2b - 3) \Lambda_0 \tau^3 / b^2 - 6E' c e^{-2\tau} K(b) \quad (7)$$

where³

$$\tau = \beta \kappa / 2 = 4.2016 \times 10^6 c^{1/2} / (DT)^{3/2} \quad (8)$$

$$b = \beta / a = \epsilon^2 / DkTa \quad (9)$$

and the functions H , G , and K are explicit functions of the Bjerrum parameter b . The coefficients

$$S = \alpha + \beta_0 \Lambda_0 \quad (10)$$

and

$$E' = E_1' \Lambda_0 - E_2' \quad (11)$$

are determined by the valence type of the electrolyte, the temperature of the system, and the dielectric constant and viscosity of the solvent. They are the same ones which appeared in our first solution of the problem.⁴ It will be noted that the functional form of $\Lambda(c)$ is the same as before; what will be changed is the dependence on a of the coefficient of the term linear in concentration, which is now separated into four terms. These include our former $J(a)$, plus new terms which appear as a consequence of retaining the Boltzmann factor e^{ζ} explicitly in (1) instead of approx-

imating it by the first few terms of its series.⁵ As pointed out in part II, one of the new terms predicts for lower dielectric constants a decrease in conductance of the form which previously required the hypothesis of a thermodynamic equilibrium between free ions and ion pairs. The terms calculated in this paper slightly decrease this "ion pair" term from ΔX_e .

1. *The Hydrodynamic Term in the Relaxation Field.* We designate by ΔX_e that part of the relaxation field which is produced by the velocity term $(\mathbf{v}_1 + \mathbf{v}_2)/(\omega_1 + \omega_2)$ in the equation of continuity⁶; in principle, it can be derived by the following sequence of operations. First, the corresponding part of the equation of continuity (6) is solved for μ_{21}'' , where

$$\mu_{21}'' \equiv kT \chi_{21}'' + \epsilon^2 \theta'' \quad (1.1)$$

and χ_{21}'' and θ'' , respectively, measure the changes in distribution function f_{j1} and potential ψ_j produced by the velocity field. The result is substituted in the corresponding Poisson equation⁶

$$\Delta \theta'' = -(\kappa^2 kT / 2\epsilon^2) e^{\zeta} \chi_{21}'' \quad (1.2)$$

$$= -(\kappa^2 / 2\epsilon^2) e^{\zeta} \mu_{21}'' + \kappa^2 e^{\zeta} \theta'' / 2 \quad (1.3)$$

Solution of (1.3) then gives θ'' , and the component in the direction of the external electrical field of the force on the central ion due to the hydrodynamic motion of its neighbors is given by

$$\Delta X_e = -\epsilon \nabla_x \theta''(a) \quad (1.4)$$

i.e., by the x -component of the negative gradient of the potential $\epsilon \theta''(r, \vartheta)$ calculated at $r = a$. The fact that only the value of $(\partial \theta'' / \partial x)$ at $r = a$ is desired, rather than θ'' as an explicit function of r and ϑ , permits considerable simplification of the mathematical problem. As we shall show, it is necessary to integrate neither the equation of continuity nor the Poisson equation in order to evaluate (1.4), because an adequate approximation can be expressed as a definite integral in terms of $V(r)$ by using the properties of μ_{21}'' and θ'' as defined by their differential equations, (6) and (1.3), and the boundary conditions which these functions must satisfy.

The quantity $V(r) \cos \vartheta$ is an abbreviation for the scalar product $\mathbf{v} \cdot \nabla e^{\zeta}$ which appeared on expansion of the divergence of the product of distribution function and velocity. We shall use our previous value⁷ of velocity

(2) R. M. Fuoss and L. Onsager, *J. Phys. Chem.*, **62**, 1339 (1958).

(3) R. M. Fuoss and L. Onsager, *Proc. Natl. Acad. Sci. U. S.*, **47**, 818 (1961).

(4) R. M. Fuoss and L. Onsager, *J. Phys. Chem.*, **61**, 668 (1957).

(5) See eq. I (1.25).

(6) See eq. I (1.19).

(7) R. M. Fuoss, *J. Phys. Chem.*, **63**, 633 (1959).

$$\mathbf{v} = \mathbf{i} f_1(r) + \mathbf{r}_1 f_2(r) \cos \vartheta \quad (1.5)$$

where $f_1(r)$ and $f_2(r)$ are given explicitly by eq. 8 of ref. 7, and the constants B and E which appear in them have the values given by (5), (6), and (15) of the same paper. Since ζ is only a function of r (i.e., is spherically symmetric)

$$\nabla e^\zeta = \mathbf{r}_1 e^\zeta (d\zeta/dr) \quad (1.6)$$

and the scalar product reduces to

$$\mathbf{v} \cdot \nabla e^\zeta = e^\zeta [f_1(r) + f_2(r)] (d\zeta/dr) \cos \vartheta \quad (1.7)$$

because $\mathbf{i} \cdot \mathbf{r}_1 = \cos \vartheta$. Substituting explicit values of the constants and functions from ref. 7, the result is

$$\nabla \cdot e^\zeta \nabla \mu_{21}'' = [X \epsilon e^\zeta / \pi \eta \kappa^2 (\omega_1 + \omega_2)] F(r) (d\zeta/dr) \cos \vartheta \quad (1.8)$$

where

$$F(r) = C_1/r^3 - C_2 e^{-\kappa r} (1 + \kappa r)/r^3 \quad (1.9)$$

with

$$C_1 = (1 + \kappa a + \kappa^2 a^2/3)/(1 + \kappa a) \quad (1.10)$$

and

$$C_2 = e^{\kappa a}/(1 + \kappa a) \quad (1.11)$$

Introduction of a new dependent variable $\varphi(r)$ simplifies the form of (1.8) considerably by absorbing into the coefficient the parts which are independent of the coordinates; it is defined by the equation

$$\mu_{21}''(r, \vartheta) \equiv \beta X \epsilon \varphi(r) \cos \vartheta / \pi \eta \kappa^2 (\omega_1 + \omega_2) \quad (1.12)$$

The equation of continuity then reduces to

$$\nabla(\varphi \cos \vartheta) + \nabla \zeta \cdot \nabla(\varphi \cos \vartheta) = -[F(r) \cos \vartheta / \beta] (d\zeta/dr) \quad (1.13)$$

It will be noted that e^ζ divides out at this stage; it will reappear in the Poisson equation. After making the vector operations indicated in (1.13), $\cos \vartheta$ can next be factored out, leaving an ordinary differential equation in one variable. Further simplification is obtained by approximating $d\zeta/dr$ by $(-\beta/r^2)$ in the gradient term. (This neglects long range screening, but gives a close approximation near the ion, $r < 1/\kappa$, where accuracy is needed.) These manipulations reduce the equation of continuity to the form

$$d^2\varphi/dr^2 + (2/r - \beta/r^2)(d\varphi/dr) - 2\varphi(r)/r^2 = F(r)e^{-\kappa r}(1 + \kappa r)/r^2 \quad (1.14)$$

We next consider the Poisson equation (1.3). Substitution of $\varphi(r)$ gives

$$\Delta \theta'' - \kappa^2 e^\zeta \theta''/2 = -[\beta X \epsilon \varphi(r) \cos \vartheta] / 2\pi \eta \epsilon (\omega_1 + \omega_2) \quad (1.15)$$

Now $\theta''(r, \vartheta)$ must be of the form $H''(r) \cos \vartheta$ and by use of the boundary conditions⁸ which the potential must satisfy, we find

$$\Delta X_v = -\epsilon_1 H''(a)/a \quad (1.16)$$

Again to simplify the coefficients, we introduce a new function $Q''(r)$, defined by

$$Q''(r) \cos \vartheta = -\epsilon_1 \theta''(r, \vartheta)/Xa \quad (1.17)$$

so that the desired result can be stated in the compact form

$$\Delta X_v/X = Q''(a) \quad (1.18)$$

that is, if we can evaluate Q'' for $r = a$, the problem is solved. Using the new dependent variable, the Poisson equation becomes

$$d^2Q''/dr^2 + (2/r) dQ''/dr - (2/r^2 + \kappa^2 e^\zeta/2) Q''(r) = b e^\zeta \varphi(r) / 2\pi \eta (\omega_1 + \omega_2) \quad (1.19)$$

The hammer and tongs approach to the problem would now be to solve (1.14) for φ , adjust the solution to the boundary conditions, substitute the result in (1.19), solve this equation in turn and adjust its solution to the boundary conditions, differentiate partially with respect to x , and then set r equal to a .

Preliminary investigation, however, showed that ΔX_v is in general small compared to ΔX_e and therefore can have little numerical influence on the total linear coefficient. An adequate upper estimate for ΔX_v can be found by a much less laborious route than by the formal attack just outlined. If we drop the term $\kappa^2 e^\zeta/2$ compared to $2/r^2$ in (1.19), the differential equation which defines $Q''(r)$, we still have a good approximation to a description of the situation near the ion where $r < 2e^{-b/2}/\kappa$; in effect, long range screening is being neglected again. The net effect will be to suppress a damping function $e^{-\gamma r}(1 + \gamma r)$ in the integrand of the equation which determines ΔX_v ; as we shall show in the Appendix, such approximation introduces no catastrophic errors. The equation for $Q''(r)$ thus becomes

$$d^2Q''/dr^2 + (2/r)(dQ''/dr) - (2/r^2)Q''(r) \approx b e^\zeta \varphi(r) / 2\pi \eta (\omega_1 + \omega_2) \quad (1.20)$$

Now consider the identity

$$\frac{1}{r^2} \frac{d}{dr} \left(e^{\beta/r} r^2 \frac{d\varphi}{dr} \right) = e^{\beta/r} \left[\frac{d^2}{dr^2} + \left(\frac{2}{r} - \frac{\beta}{r^2} \right) \frac{d}{dr} \right] \varphi(r) \quad (1.21)$$

The quantity in brackets is recognized as the operator in

(8) See eq. II (19-26).

the differential equation which defines $\varphi(r)$ (and hence which determines μ_{21}''). By substituting (1.21) in (1.14), rearranging, and integrating, we obtain

$$\int_a^\infty e^{\chi} \varphi(r) dr = \frac{r^2 e^{\chi}}{2} \frac{d\varphi}{dr} \Big|_a^\infty - \frac{1}{2} \int_a^\infty e^{\chi} F(r) e^{-\chi r} (1 + \chi r) dr \quad (1.22)$$

that is, the integral on the left is given in terms of the integral of *known* functions and the values of $d\varphi/dr$ at the boundaries.

The integral on the left of (1.22) is also proportional to the result of multiplying (1.20) by dr and integrating between limits a and ∞ . Noting that

$$d[2Q''/r]/dr = (2/r) dQ''/dr - 2Q''/r^2 \quad (1.23)$$

and that by virtue of the boundary conditions on the potential at $r = a$

$$r(dQ''/dr)_a = Q''(a) \quad (1.24)$$

$$(dQ''/dr)_\infty = 0 \quad (1.25)$$

$$Q''(\infty) = 0 \quad (1.26)$$

the integral of (1.20) becomes

$$3Q''(a)/a = -[b/2\pi\eta(\omega_1 + \omega_2)] \int_a^\infty e^{\chi} \varphi(r) dr \quad (1.27)$$

Now combining (1.27) and (1.22), we obtain

$$Q''(a) = -\frac{\beta r^2 e^{\chi}}{12\pi\eta(\omega_1 + \omega_2)} \frac{1}{a} \frac{d\varphi}{dr} \Big|_a^\infty + \frac{\beta}{12\pi\eta(\omega_1 + \omega_2)} \int_a^\infty e^{\chi} F(r) e^{-\chi r} (1 + \chi r) dr \quad (1.28)$$

We thus have the estimate of $Q''(a)$ expressed in terms of the values of $d\varphi/dr$ at the boundaries $r = a$ and $r = \infty$, and a definite integral over known functions.

The boundary condition for μ_{21}'' at $r = a$ is⁹

$$[2\mathbf{v}/(\omega_1 + \omega_2) + \nabla\mu_{21}''] \cdot \mathbf{r}_1 = 0 \quad (r = a) \quad (1.29)$$

Using our previous⁷ value for \mathbf{v} , we obtain

$$(\mathbf{v} \cdot \mathbf{r}_1)_a = X\epsilon \cos \vartheta / 6\pi\eta a (1 + \chi a) \quad (1.30)$$

From the definition (1.12) of $\varphi(r)$

$$\mathbf{r}_1 \cdot \nabla\mu_{21}'' = [\beta X\epsilon \cos \vartheta / \pi\eta\chi^2 (\omega_1 + \omega_2)] [d\varphi/dr] \quad (1.31)$$

Substitution of these last two results (1.30) and (1.31) in the boundary condition (1.29) gives

$$(d\varphi/dr)_a = -\chi^2 / 3\beta a (1 + \chi a) \quad (1.32)$$

Since we shall eventually drop terms of order $c^{1/2}$, we may neglect χa compared to unity in the denom-

inator here. At the upper limit, $d\varphi/dr$ vanishes, of course. Combining these results, we finally obtain

$$\Delta X_e / X = -\chi^2 a e^b / 36\pi\eta (\omega_1 + \omega_2) + [\beta / 12\pi\eta (\omega_1 + \omega_2)] \int_a^\infty e^{\chi} F(r) e^{-\chi r} (1 + \chi r) dr \quad (1.33)$$

The hydrodynamic part of the relaxation field is seen to be determined by a definite integral over known functions, one of which is the radial part of the inhomogeneous term in the differential equation which defines μ_{21}'' . The presence of the screening function $e^{-\chi r}$ guarantees the convergence of the integral.

We now proceed to the evaluation of this integral; it is clearly a function of concentration through χ . Since our ultimate goal is a conductance function valid up to terms of order $c^{3/2} \sim \chi^3$, we shall develop the integral as a series and drop terms of order χ^3 and higher. To this approximation, the constants C_1 and C_2 defined by (1.10) and (1.11) can be simplified as

$$C_1 = 1 + \chi^2 a^2 / 3 + O(\chi^3 a^3) \quad (1.34)$$

$$C_2 = 1 + \chi^2 a^2 / 2 + O(\chi^3 a^3) \quad (1.35)$$

Define $I(\chi)$ as the integral in (1.33). Then

$$I(\chi) = \int_a^\infty e^{\chi} F(r) e^{-\chi r} (1 + \chi r) dr$$

is the integral which is to be evaluated. Using the approximations for C_1 and C_2 above

$$I(\chi) = I_1(\chi) + (\chi^2 a^2 / 3) \int_a^\infty e^{\chi} e^{-\chi r} (1 + \chi r) dr / r^3 - (\chi^2 a^2 / 2) \int_a^\infty e^{\chi} e^{-2\chi r} (1 + \chi r)^2 dr / r^3 \quad (1.36)$$

where

$$\begin{aligned} I_1(\chi) &= \int_a^\infty e^{\chi} [1 - e^{-\chi r} (1 + \chi r)] e^{-\chi r} (1 + \chi r) dr / r^3 \\ &= \int_a^\infty e^{\chi} e^{-\chi r} (1 + \chi r) dr / r^3 - \int_a^\infty e^{\chi} e^{-2\chi r} (1 + 2\chi r) dr / r^3 - \chi^2 \int_a^\infty e^{\chi} e^{-2\chi r} dr / r \\ &= I_2 - I_3 - \chi^2 I_4 \end{aligned} \quad (1.37)$$

The last two terms of (1.36) above can be considerably simplified, because they have coefficients χ^2 . The integrals are functions of χ , which converge for $\chi = 0$; going to this limit, we see that the last two terms combine to give

$$-(\chi^2 a^2 / 6) \int_a^\infty e^{\beta/r} dr / r^3 = -A\chi^2 a^2 / 6 \quad (1.39)$$

where A is a constant which will be evaluated below. Hence

(9) See eq. I (1.31).

$$I(x) = I_1(x) - Ax^2a^2/6 \quad (1.40)$$

and only $I_1(x)$ remains to be calculated.

In (1.38), I_2 and I_3 are both of the pattern

$$I_2(\lambda x) = \int_a^\infty e^\zeta e^{-\lambda x r} (1 + \lambda x r) dr/r^3 \quad (1.41)$$

with λ equal to one or two. We shall therefore first evaluate this auxiliary integral. As shown in part II,¹⁰ e^ζ may be approximated by $e^{-2\tau}e^{\beta/\tau}$, where $e^{-2\tau}$ is the square of the activity coefficient. Using this

$$e^{2\tau}I_6(\lambda x) = \int_a^\infty e^{\beta/\tau} e^{-\lambda x r} dr/r^3 + \lambda x \int_a^\infty e^{\beta/\tau} e^{-\lambda x r} dr/r^2 \quad (1.42)$$

and expanding through terms of order x^2

$$e^{2\tau}I_6(\lambda x) = A + Bx + Cx^2E_n(\lambda xa) + Dx^2 \quad (1.43)$$

Setting x equal to zero evaluates the first coefficient, which also appeared in (1.39)

$$A = I_6(0) = \int_a^\infty e^{\beta/\tau} dr/r^3 \quad (1.44)$$

Substitution of $\mu = \beta/\tau$ converts this to an elementary form which integrates to

$$A = [e^b(b-1) + 1]/\beta^2 \quad (1.45)$$

Next, partial differentiation of (1.43) with respect to x gives

$$\partial I_6/\partial x = -\lambda^2 x \int_a^\infty e^{\beta/\tau} e^{-\lambda x r} dr/r \quad (1.46)$$

$$= B + 2Cx E_n(\lambda xa) - Cx e^{-\lambda xa} + 2Dx \quad (1.47)$$

The integral on the right of (1.46) contains an exponential integral

$$\int_a^\infty e^{\beta/\tau} e^{-\lambda x r} dr/r \equiv \int_a^\infty (e^{\beta/\tau} - 1)e^{-\lambda x r} dr/r + E_n(\lambda xa) \quad (1.48)$$

which, with

$$C = -\lambda^2/2 \quad (1.49)$$

just cancels the exponential integral on the right of (1.47). This reduces (1.46) and (1.47) to

$$-\lambda^2 x \int_a^\infty (e^{\beta/\tau} - 1)e^{-\lambda x r} dr/r = B + \lambda^2 x e^{-\lambda xa}/2 + 2Dx \quad (1.50)$$

Again setting $x = 0$, we see that B must vanish

$$B = 0 \quad (1.51)$$

Then x may be divided out of (1.50) and for D we finally find

$$D = -\lambda^2 e^{-\lambda xa}/4 - (\lambda^2/2)j_p(b) \quad (1.52)$$

where

$$j_p(b) = E_p(b) - \ln b - \Gamma \quad (1.53)$$

is the function introduced in the discussion of the electrostatic part of the relaxation field.¹¹

If the above results are substituted in (1.37), we find for I_1

$$e^{2\tau}I_1(x) = x^2[E_n(2xa) - E_n(xa)/2 + j_p(b)/2 + 3/4] + O(x^3a) \quad (1.54)$$

This is substituted in (1.36) and the result in (1.33), to give for the hydrodynamic term

$$\Delta X_o/X = [x^2\beta e^{-2\tau}/12\pi\eta(\omega_1 + \omega_2)]P_1(b) \quad (1.55)$$

where

$$P_1(b) = E_n(2xa) - E_n(xa)/2 + j_p(b)/2 + 3/4 - e^b/2b + e^b/6b^2 - 1/6b^2 \quad (1.56)$$

The part of $P_1(b)$ which is sensitive to b is

$$2P_2(b) = E_p(b) - (e^b/b)(1 - 1/3b) \quad (1.57)$$

which is almost the pattern of $K(b)$, where

$$3K(b) = E_p(b) - (e^b/b)(1 + 1/b) \quad (1.58)$$

2. *The Osmotic Term.*¹² In our previous calculation of this term, we used F_{12} , the perturbation to the distribution, which was calculated on the basis of the approximation

$$e^\zeta \approx 1 + \zeta + \zeta^2/2 \quad (2.1)$$

In order to be consistent with the present calculations of relaxation and electrophoresis in which e^ζ is kept explicit, we must recalculate the virtual force ΔP on the ion produced by the local concentration gradients, using $n_1 n_2 e^\zeta$ for f_{12}^0 , the unperturbed distribution function. As before, this force is given by the integral

$$\Delta P = \int \Pi \cos \vartheta dS \quad (2.2)$$

where

$$\Pi = (f_{12} - f_{12}^0)kT/n_1 \quad (2.3)$$

and the integration is over the sphere of radius a which contains the ion. Since

$$dS = 2\pi a^2 \sin \vartheta d\vartheta \quad (2.4)$$

and

$$f_{12} - f_{12}^0 = \chi_{12} f_{12}^0 \quad (2.5)$$

(10) See eq. II (55-57).

(11) See eq. II (A3).

(12) R. M. Fuoss and L. Onsager, *J. Phys. Chem.*, **62**, 1339 (1958). In eq. 14, ΔP should be replaced by $\Delta P/e$.

the integral becomes

$$\Delta P = [2\pi kT a^2 f_{12}^0(a)/n_1] \times \int_0^\pi \chi_{12}(a, \vartheta) \sin \vartheta \cos \vartheta \, d\vartheta \quad (2.6)$$

Using our results (and symbols) from part II

$$\chi_{12} = -(\epsilon_2 X/kT)[R(a) - a] \cos \vartheta - \epsilon^2 \theta/kT \quad (2.7)$$

Since $\theta(a) \sim \psi'(a)$ is of order κa , we neglect it here compared to $[R(a) - a]$. At $r = a$

$$e^{\epsilon} \approx e^{-2\tau} e^b \quad (2.8)$$

as before; for symmetrical electrolytes

$$\kappa^2 = 8\pi\eta\epsilon^2/DkT = 8\pi n\beta \quad (2.9)$$

Substituting in the expression (2.6) for ΔP and inserting the factor of $2/3$ from integration over ϑ , we obtain

$$\Delta P = (\kappa^2 a^2 X \epsilon e^b e^{-2\tau}/6\beta)[R(a) - a] \quad (2.10)$$

At $r = a$, $R(a)$ can be evaluated easily by expanding $e^{-\kappa a}$ as a series and dropping higher terms

$$(1 - T_1)R(a) = -T_1[a - (\beta/\kappa^2 a^2)\{1 - e^{-\kappa a}(1 + \kappa a)\}] + e^{-b}[a - (\beta/\kappa^2 a^2)\{1 - e^{-\kappa a}(1 + \kappa a + \kappa^2 a^2)\}] \quad (2.11)$$

After expansion and rearrangement, this gives

$$R(a) = ae^{-b}b^3/4(1 - T_1) + O(\kappa a\beta) \quad (2.12)$$

where

$$T_1 = e^{-b}(1 + b + b^2/2) \quad (2.13)$$

Substitution in (2.10) then gives

$$\Delta P/X\epsilon = \kappa^2 a^2 b^2/24(1 - T_1) - \kappa^2 a^2 e^b e^{-2\tau}/6b \quad (2.14)$$

The first term will give a small linear term in the conductance equation; its multiplier $e^{-2\tau}$ has been dropped because it would lead only to a term of order $c^{3/2}$. This multiplier will be retained in the second term of (2.14), however, because this one (also small) will be combined with other terms in which the difference between $e^{-2\tau}$ and unity can become significant. We note that the second term contains a factor $ae^b/b = \beta e^b/b^2$, and that ΔX_v contains a function which differs from $K(b)$, the essentially exponential function which appeared in ΔX_e , by the term in e^b/b^2 . Now the x -component of the velocity function used in setting up the differential equation (6) for μ_{21}'' reduces at $r = a$ and $\kappa = 0$ to

$$v_x^0 = (X\epsilon/4\pi\eta)(R^2/6a^3 + 1/2a) \quad (2.15)$$

Here R [not the $R(a)$ of (2.7)!] is the distance at which

the radial component of the velocity vanishes.¹³ If we set $R = a$ in (2.15) and use the definition of ω in

$$v_x^0 = X\epsilon\omega \quad (2.16)$$

it is easily shown that

$$3\pi\eta a(\omega_1 + \omega_2) = 1 \quad (2.17)$$

Writing a^2/b in the equivalent form $\beta a/b^2$ in the second term of (2.14) and using (2.17) to replace a in the result, we finally have for the osmotic term

$$\Delta P/X\epsilon = \kappa^2 a^2 b^2/24(1 - T_1) - [\kappa^2 \beta e^{-2\tau}/12\pi\eta(\omega_1 + \omega_2)](2e^b/3b^2) \quad (2.18)$$

It will be seen that the second term now naturally combines with the $e^b/6b^2$ in the function $P_2(b)$ of (1.57) in ΔX_e . Then this term, together with $e^b/2b$ and the exponential integral from $j_p(b)$, combine to give the same function

$$3K(b) = E_p(b) - (e^b/b)(1 + 1/b) \quad (2.19)$$

which appeared in the electrostatic term ΔX_e of the relaxation field.

3. *Combination of Hydrodynamic and Osmotic Terms.* The contribution to the relaxation field from the velocity field is given by (1.55). To this we add the osmotic term just derived, with the coefficient of the second term converted to hydrodynamic symbols. The result is

$$\Delta X_v/X + \Delta P/X\epsilon = [\kappa^2 \beta/12\pi\eta(\omega_1 + \omega_2)] \times [P_3(b) + 3e^{-2\tau}K(b)/2] + \beta^2 \kappa^2/24(1 - T_1) \quad (3.1)$$

where

$$2P_3(b) = 2E_n(2\kappa a) - E_n(\kappa a) - \ln b - \Gamma + 3/2 - 1/3 b^2 \quad (3.2)$$

In the next paper of this series, this result will be combined with the electrostatic relaxation field from part II and the electrophoresis from part III to give the conductance function (7) announced in the introduction.

Appendix

In discussing the differential equation which defines $Q''(r)$, an approximation was made which will now be investigated. The full differential equation is

$$\Delta(Q'' \cos \vartheta) - \gamma^2 e^{\epsilon} Q''(r) \cos \vartheta = A e^{\epsilon} \varphi(r) \cos \vartheta \quad (A1)$$

where A is the coefficient shown in (1.19). This equation, whose operator is of course precisely the same one which appeared in treating ΔX_e , has the solutions¹⁴ for its homogeneous form

(13) Reference 4, eq. 5.21 and 5.22; ref. 7, eq. 10-16.

(14) See eq. II (39, 40).

$$f_1(r) = e^{-\gamma r}(1 + \gamma r)/\gamma^2 r^2 \quad (A2)$$

$$f_2(r) = e^{\gamma r}(1 - \gamma r)/\gamma^2 r^2 \quad (A3)$$

and use of Green's function as before will lead to the result

$$Q''(a) = B \int_a^\infty e^{-\gamma r}(1 + \gamma r)e^{\xi} \varphi(r) dr \quad (A4)$$

in analogy to II (47). If the term in γ^2 in (A1) is dropped, the result would be

$$Q''(a) \approx B \int_a^\infty e^{\xi} \varphi(r) dr \quad (A5)$$

i.e., the screening function $e^{-\gamma r}(1 + \gamma r)$ disappears. Since

$$e^{-\gamma r}(1 + \gamma r) \leq 1 \quad (A6)$$

for all values of γ and r and is monotone decreasing, the integral (A5) is an upper bound for the desired integral (A4). We shall show, by investigation of two closely related integrals, that (A5) is an adequate approximation to (A6), and therefore our result, which was obtained by dropping the γ^2 term in (A1), is likewise justified.

The point at issue really is whether neglect of the screening function (A6) introduces serious error; convergence of the integral is already guaranteed by the $e^{-\kappa r}$ terms in $\varphi(r)$. The Boltzmann factor e^{ξ} is always greater than unity, but for large distances, $r > 1/\kappa$, rapidly converges to unity

$$\lim e^{\xi} = \lim \exp(\beta e^{-\kappa r}/r) = 1 \quad (A7)$$

Hence we shall consider the two integrals

$$I(\gamma) = \int_a^\infty e^{-\gamma r}(1 + \gamma r)\varphi(r) dr \quad (A8)$$

and

$$I(0) = \int_a^\infty \varphi(r) dr \quad (A9)$$

in order to study the long range effects of the damping function, $e^{-\gamma r}$.

Since we are interested here in long range effects, we shall approximate the differential equation (1.14) for $\varphi(r)$ by

$$d^2\varphi/dr^2 + (2/r) d\varphi/dr - 2\varphi(r)/r^2 = F(r)e^{-\kappa r}(1 + \kappa r)/r^2 \quad (A10)$$

i.e., the short range term $(-\beta/r^2)$ in the operator is dropped. The operator in (A10) can be rearranged to

$$L(\varphi) = \frac{1}{r^3} \frac{d}{dr} \left[r^4 \frac{d}{dr} \left(\frac{\varphi}{r} \right) \right] \quad (A11)$$

which permits us to obtain a particular integral of

(A10) by quadratures. The result is, after approximating C_1 and C_2 in $F(r)$ by unity

$$\varphi_p(r) = (e^{-\kappa r}/4r^3)(1 - \kappa r/3 + \kappa^2 r^2/6 - \kappa^3 r^3/6) + (\kappa^4 r/24)E_n(\kappa r) - e^{-2\kappa r}/4r^3 \quad (A12)$$

To this, we add C_3/r^2 , the solution of the homogeneous equation $L(\varphi) = 0$ which vanishes at $r = \infty$, and use the boundary condition (1.32) to evaluate C_3 . To terms of order κ^2

$$C_3 = -\kappa/6 + O(\kappa^2 a) \quad (A13)$$

Substitution of

$$\varphi(r) = \varphi_p(r) - \kappa/6r^2 \quad (A14)$$

in (A8) and performance of the indicated integrations gives

$$I(\kappa) = \kappa^2 f_1(\kappa, \gamma) E_n(p\kappa a) - (7\kappa^2/16) E_n(s\kappa a) + \kappa^2 f_2(\gamma, a) E_n(\kappa a) - \kappa e^{-\gamma a}/6a + f_3(\gamma, a) e^{-p\kappa a}/8a^2 - f_4(\gamma, a) e^{-s\kappa a}/8a^2 \quad (A15)$$

where

$$\gamma^2 = q^2 \kappa^2 = \kappa^2/2 \quad (A16)$$

$$p = 1 + q \quad (A17)$$

$$s = 2 + q \quad (A18)$$

$$f_1(\kappa, \gamma) = 3/16 - \kappa^2/8\gamma^2 \quad (A19)$$

$$f_2(\gamma, a) = (\kappa^2 e^{-\gamma a}/8\gamma^2)(1 + \gamma a + \gamma^2 a^2/3) \quad (A20)$$

$$f_3(\gamma, a) = 1 + \kappa a(q - 5/3) - (\kappa^2 a^2/24p)(3/q + 2 - q) - \kappa^3 a^3/24 \quad (A21)$$

and

$$f_4(\gamma, a) = 1 - \kappa a(2 - q) \quad (A22)$$

In the limit of γ (or q) going to zero, $I(\gamma)$ reduces to $I(0)$. No singularities appear. On expanding $e^{-\gamma a}$ in $f_2(\gamma, a)$, the terms in γ^{-2} from f_1 and f_2 are seen to cancel and are therefore harmless. The $(3/q)$ in f_3 is matched by a term of opposite sign, which appears when $E_n(p\kappa a)$ is expanded as a Taylor's series in γ

$$E_n(p\kappa a) = E_n(\kappa a) - \gamma e^{-\gamma a}/\kappa + \gamma^2 e^{-\kappa a}(1 + \kappa a)/2\kappa^2 + O(q^3) \quad (A23)$$

The whole integral is of order $\kappa^2 \ln \kappa a$ and higher, because the term $(-\kappa e^{-\gamma a}/6a)$ cancels out when the exponential functions $e^{-p\kappa a}$ and $e^{-s\kappa a}$ are expanded as series and the indicated multiplications are carried out. The final result after series expansions and the above cancellations is

$$I(\gamma) = (\kappa^2/16)[4E_n(\kappa a) - E_n(p\kappa a) - 7E_n(s\kappa a)] - (79 + 22q)\kappa^2 a^2/192 + O(\kappa^3 a^3) \quad (\text{A24})$$

Expanding the exponential integrals, and regrouping terms, (A24) becomes

$$I(\gamma) = \kappa^2[0.25 \ln \kappa a + 0.12104] \quad (\text{A25})$$

while

$$I(0) = \kappa^2[0.25 \ln \kappa a - 0.06875] \quad (\text{A26})$$

Since the equations are not to be used when the distance $1/\kappa$ becomes less than about $5a$ (due to failure of both model and mathematical approximations), $0.25 \ln \kappa a$ in absolute value is at least 0.40 and becomes numerically greater as concentration decreases. At $\kappa a = 0.2$, $I(\gamma) = -0.38\kappa^2$ and $I(0) = -0.47\kappa^2$; the difference is about 25% and, as just mentioned, decreases as concentration decreases. Hence as asserted in section 2, suppression of the screening factor $e^{-\gamma r}(1 + \gamma r)$ in the integral produces no gross error.

We shall next show that the net error in the coefficient of the linear term of $\Lambda(c)$ is still smaller and becomes negligible as the dielectric constant decreases. Terms from ΔX_e always appear in the conductance function with the coefficient E'_2 times a factor of order unity while terms from ΔX_e have coefficient $E'_1\Lambda_0$ times factors of order unity. Consider, for example, the coefficient of the term in $\ln \tau$

$$E' = E'_1\Lambda_0 - E'_2 \quad (\text{A27})$$

The $E'_1\Lambda_0$ part comes from ΔX_e , the E'_2 part from $\Delta \bar{X}_e$. The values

$$E'_1 = \beta^2\kappa^2/24c = \tau^2/6 \quad (\text{A28})$$

and

$$E'_2 = \beta\kappa\beta_0/16c^{1/2} \quad (\text{A29})$$

where the Onsager electrophoresis coefficient β_0 is defined as

$$\beta_0 = \mathfrak{F}\epsilon\kappa/3\pi\eta\sigma c^{1/2} \quad (\text{A30})$$

are substituted in (A27). Here σ (equals 10^{-8} times the velocity of light) is the factor which converts e.s.u. potentials to volts and \mathfrak{F} is the Faraday equivalent. The result is

$$E' = E'_1\Lambda_0[1 - (\mathfrak{F}\epsilon/2\pi\sigma)(1/\Lambda_0\eta\beta)] \quad (\text{A31})$$

Substituting numerical values for the universal constants

$$E' = E'_1[1 - 2.460 \times 10^{-8}/\beta\Lambda_0\eta] \quad (\text{A32})$$

Since

$$\beta = 560.4 \times 10^{-8}/D_{25} \quad (\text{A33})$$

and the Walden product $\Lambda_0\eta$ usually varies between one half and unity, it is seen that the second term in the brackets (the hydrodynamic part) is small, and eventually negligible as D decreases, compared to the leading electrostatic term.

Thermodynamic and Electrical Investigations on Molten Antimony Sulfide

by F. S. Pettit¹

Max-Planck-Institut für physikalische Chemie, Göttingen, Germany (Received September 24, 1968)

The S/Sb ratio, y , in Sb_2S_3 melts at 650° has been determined as a function of the $\text{H}_2\text{S}/\text{H}_2$ ratio in a coexisting gas atmosphere. The homogeneity range of liquid Sb_2S_3 has been found to extend from $y = 1.30$ for coexistence with liquid antimony up to $y = 1.75$ for coexistence with sulfur vapor at 1 atm. Experimental results for y as a function of the $\text{H}_2\text{S}/\text{H}_2$ ratio are in accord with an equation deduced from the ideal law of mass action for the disproportionation reaction, $2\text{Sb}^{3+} = \text{Sb}^+ + \text{Sb}^{5+}$. Conductivity and e.m.f. measurements indicate ionic conduction and n-type semiconduction due to a two-electron exchange between Sb^+ and Sb^{3+} ions.

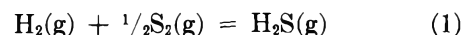
Statement of the Problem

Phenomena typical of solid semiconducting compounds have also been observed in the liquid state. For instance, the electrical conductivity of molten Cu_2S rises considerably when excess sulfur is added.² In the system Fe-S, the conductivity as a function of the S/Fe ratio has a minimum corresponding to a transition from prevailing n-type to prevailing p-type conduction.³ In the case of solid semiconducting compounds, it has been found to be expedient to investigate both deviations from the ideal stoichiometric composition and the electrical conductivity as functions of the activity of the metallic or nonmetallic component in order to test appropriate models for defects which contribute to electrical conduction. In the case of liquid semiconductors, an analogous approach seems to be promising. In what follows, the results of investigations on molten Sb_2S_3 with excess Sb or S are presented.

Thermodynamic Investigations

According to Jaeger and van Klooster,⁴ Sb_2S_3 has a congruent melting point at 546° . The boundaries of the homogeneity range of molten Sb_2S_3 above 546° are determined by the equilibrium with solid or liquid Sb on one side and with sulfur vapor on the other side. To establish thermodynamic relations, it is expedient to consider the activity of sulfur as the decisive variable in addition to temperature and total pressure. The activity of sulfur, a_s , may be predetermined either with the help of $\text{H}_2\text{S}-\text{H}_2$ mixtures, or with the help of sulfur vapor with a known partial pressure of S_2 molecules.

Both data are interrelated by the equilibrium constant of the reaction



In what follows, the activity of sulfur, a_s , is expressed in terms of the partial pressure ratio

$$p_{\text{H}_2\text{S}}/p_{\text{H}_2} \equiv q \quad (2)$$

In case sulfur vapor is actually used, the corresponding value of q may be calculated with the help of the equilibrium constant for reaction 1.⁵

The composition of an antimony sulfide melt may be expressed in terms of the ratio y of the number of S atoms to the number of Sb atoms, or in terms of the sulfur excess

$$\delta = y - \frac{3}{2} \quad (3)$$

which has a negative value in the case of excess antimony, *i.e.*, if $y < \frac{3}{2}$.

To establish the relation between sulfur activity and composition, Sb_2S_3 melts were equilibrated with gas atmospheres with known sulfur activities and the re-

- (1) Pratt and Whitney Aircraft, North Haven, Conn.
- (2) M. Bourgon, G. Derge, and G. M. Pound, *J. Metals*, **9**, 1454 (1957).
- (3) D. Argyriades, G. Derge, and G. M. Pound, *Trans. AIME*, **215**, 909 (1959).
- (4) F. M. Jaeger and H. S. van Klooster, *Z. anorg. allgem. Chem.*, **78**, 246 (1912).
- (5) J. F. Elliott and M. Gleiser, "Thermochemistry for Steel-making," Addison-Wesley Publishing Co., Inc., Reading, Mass., 1960, p. 244.

sulting S/Sb ratio was determined after quenching. For these investigations, Sb_2S_3 was synthesized from antimony and sulfur purified according to von Wartenberg⁶ in sealed Pyrex tubes in a two-stage furnace where Sb was kept at about 580° and sulfur at 300° . Low sulfur activities were obtained by bubbling H_2S - H_2 mixtures through the Sb_2S_3 , using flowmeters similar to those described by Schuhmann and Moles.⁷ Higher sulfur activities in evacuated and sealed off Supremax tubes were provided by using sulfur vapor whose pressure was determined by a reservoir of liquid sulfur kept at temperatures ranging from 280 to 447° . The corresponding S_2 partial pressures at 650° were interpolated from data reported by Braune, Peter, and Neveling.⁸

To obtain the S/Sb ratio, a stream of H_2 was passed over weighed portions of the quenched samples at 600° whereby the sulfur was converted into H_2S . The stream of H_2 and H_2S was passed through a solution of cadmium acetate⁹ whereupon CdS was precipitated whose amount was determined by an iodometric titration at $\text{pH} \sim 5$, using the reaction



Analysis of Sb_2S_3 samples heated in H_2S below the melting point with virtually ideal stoichiometric composition had an error less than 0.6% provided that starch used as an indicator was added before the beginning of the titration in order to keep the sulfur in colloidal solution and to prevent occlusion of CdS not yet completely reacted. Results are shown in Fig. 1.

To obtain a theoretical expression interrelating δ and the activity of sulfur given by the value of $q = p_{\text{H}_2\text{S}}/p_{\text{H}_2}$, it is tentatively assumed that the melt contains monovalent and pentavalent cations Sb^+ and Sb^{5+} as minor-

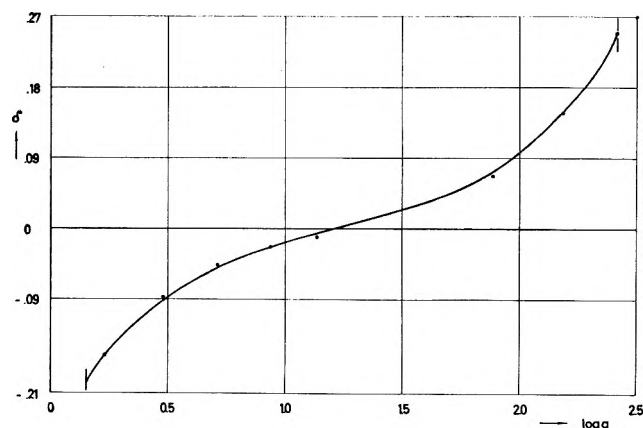
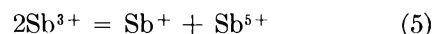
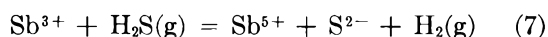
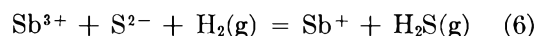


Figure 1. Sulfur excess $\delta = y - \frac{3}{2}$ vs. $\log q = \log (p_{\text{H}_2\text{S}}/p_{\text{H}_2})$ at 650° . The curve is drawn in accord with eq. 13 with $q^* = q(\delta = 0) = 17.1$ and $K_1^{1/2} = 1.6 \times 10^{-2}$. The vertical lines at the ends of the curve indicate the limits of the one-phase region.

ity constituents in addition to Sb^{3+} and S^{2-} ions as majority constituents, whereas ions of other valence states such as Sb^{2+} , Sb^{4+} , or S^- are neglected. The valence state 1 for Sb is assumed in view of results recently obtained for liquid BiCl_3 and BiI_3 with excess Bi.^{10,11} The valence state 5 is assumed in view of the occurrence of stable compounds such as Sb_2O_5 . Thus, properties of liquid Sb_2S_3 are assumed to be determined by the disproportionation reaction



In view of the equations



the sulfur excess δ is

$$\delta = y_v - y_I \quad (8)$$

where y_I and y_v are the ratios of the number of Sb^+ and Sb^{5+} ions, respectively, to the total number of antimony ions. Applying the ideal law of mass action to eq. 5 and using a constant concentration of Sb^{3+} ions for $\delta \leq 0$ as a fair approximation, one has

$$y_I y_v = K_1 \quad (9)$$

Substitution of eq. 9 in eq. 8 yields

$$\begin{aligned} \delta &= K_1^{1/2}(y_v/K_1^{1/2} - K_1^{1/2}/y_v) \\ &= 2K_1^{1/2} \sinh \ln (y_v/K_1^{1/2}) \end{aligned} \quad (10)$$

Applying the ideal law of mass action to eq. 7, one has

$$\frac{y_v}{y_v(\delta = 0)} = \frac{q}{q^*} \quad (11)$$

where $q = p_{\text{H}_2\text{S}}/p_{\text{H}_2}$ according to eq. 2 and q^* is the $p_{\text{H}_2\text{S}}/p_{\text{H}_2}$ ratio over a melt of ideal stoichiometric composition ($\delta = 0$) in which in view of eq. 8 and 9

$$y_I(\delta = 0) = y_v(\delta = 0) = K_1^{1/2} \quad (12)$$

Substitution of eq. 11 and 12 in eq. 10 yields

$$\delta = 2K_1^{1/2} \sinh \ln (q/q^*) \quad (13)$$

Using the experimental value of δ for the smallest and the largest value of q , one obtains from eq. 13 q^*

(6) H. von Wartenberg, *Z. anorg. allgem. Chem.*, **286**, 243 (1956).

(7) R. Schuhmann, Jr., and O. W. Moles, *J. Metals*, **3**, 235 (1951).

(8) H. Braune, S. Peter, and V. Neveling, *Z. Naturforsch.*, **6a**, 32 (1951).

(9) One liter of aqueous solution contained 170 g. of glacial acetic acid, 200 g. of $\text{NaC}_2\text{H}_3\text{O}_2$, 20 g. of $\text{Zn}(\text{C}_2\text{H}_3\text{O}_2)_2$, and 5 g. of $\text{Cd}(\text{C}_2\text{H}_3\text{O}_2)_2$.

(10) R. A. Osteryoung, North American Aviation Science Center, private communication.

(11) D. O. Raleigh, *J. Chem. Phys.*, **38**, 1677 (1963).

$= q (\delta = 0) = 17.1$ and $K_1^{1/2} = 1.6 \times 10^{-2}$. Values of δ as a function of q calculated from eq. 13 with the foregoing values of q^* and $K_1^{1/2}$ are shown in Fig. 1 as the solid curve which fits the experimental points satisfactorily. If a disproportionation equilibrium between Sb^{2+} , Sb^{4+} , and Sb^{3+} ions is assumed, an expression analogous to eq. 13 is obtained but with $(q/q^*)^{1/2}$ instead of (q/q^*) . The present results are not in accord with such an expression. From the data of Britzke and Kapustinski,¹² $q = 1.42$ for the two-phase equilibrium

$\text{Sb}/\text{Sb}_2\text{S}_3$. Consequently, upon extrapolating the curve of Fig. 1 to $q = 1.42$, the homogeneity range of liquid Sb_2S_3 is found to extend from $y = 1.30$ for coexistence with liquid antimony to $y = 1.75$ for coexistence with sulfur vapor at 1 atm.

Data available for the system Bi-S indicate¹³ that the Bi/S ratio in Bi_2S_3 melts as a function of sulfur activity may also be expressed in a form similar to eq. 13.

Conductivity Measurements

Figure 2 shows the conductivity cell which was used for measurements on melts equilibrated with $\text{H}_2\text{S}-\text{H}_2$ mixtures. This cell consisted of two quartz tubes which had capillary constrictions on one end and standard tapered joints on the other. The standard tapered joints were used to connect the cell to the $\text{H}_2\text{S}-\text{H}_2$ train. These quartz tubes along with a quartz thermocouple well and a Pyrex tube for the exit gases were sealed into a brass tube with picein. The brass tube fit into a brass flange with double O-ring seals. The brass flange was machined such that it could be attached to a large quartz tube which contained the antimony sulfide. Each of the quartz tubes with capillaries contained two graphite rods. Solid antimony sulfide was placed in the large outer quartz tube and the cell was heated to 650° . During heating a well defined mixture of $\text{H}_2\text{S}-\text{H}_2$ flowed through the system. When the antimony sulfide was liquid, the brass flange was moved upward along the brass tube and the capillaries were immersed into the melt with the gas mixture bubbling through the melt. The resistance of the melt was determined upon stopping the flow of gas and allowing the antimony sulfide to flow into the capillaries, thus providing a well defined resistance. A d.c. current was passed through the two graphite rods on opposite sides of the cell and the voltage drop across the inner two graphite rods was measured by a standard d.c. potentiometer technique. The capillaries were calibrated at room temperature using mercury as a standard. The resistance of the melt was determined at various times until a constant value was obtained for a given gas mixture.

The cell which was used to determine the resistance of melts in equilibrium with pressures of sulfur greater than those obtained from $\text{H}_2\text{S}-\text{H}_2$ mixtures was basically the same as that of Fig. 1. It was constructed entirely of Supremax glass. The electrodes could not be removed from the melt and a sulfur reservoir was attached directly to the cell. Moreover, since the lowest temperature of the cell had to be that of the sulfur reservoir, the platinum leads were sealed directly

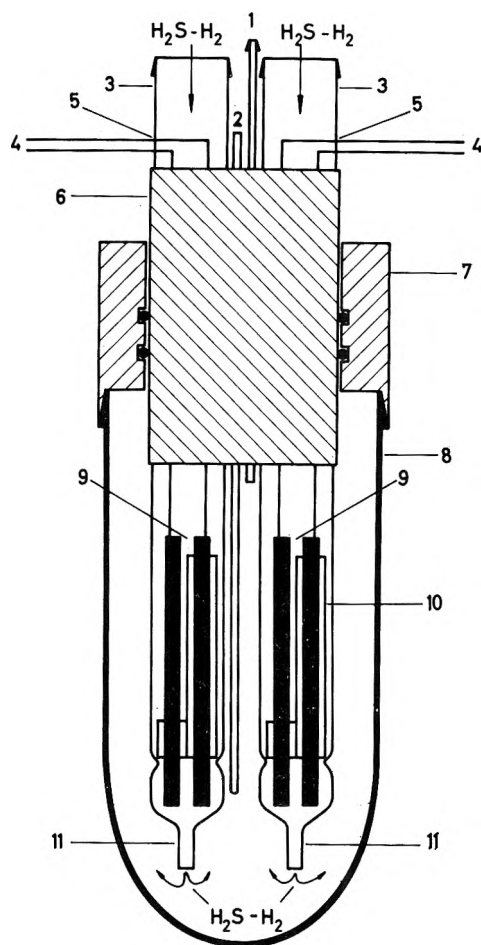


Figure 2. Schematic diagram of the conductivity cell which was used for measurements on melts equilibrated with $\text{H}_2\text{S}-\text{H}_2$ mixtures. The nomenclature of parts numbered on the diagram is as follows: 1, Pyrex tube for exit gases; 2, thermocouple well; 3, quartz tubes containing graphite electrodes; 4, platinum wires extending from graphite electrodes to electrical circuit; 5, platinum wires sealed in quartz tubes with picein; 6, brass tube to contain quartz tubes; the tubes were sealed in the brass tube with picein; 7, brass flange with double O-ring seals; 8, large quartz tube which contained antimony sulfide melt; 9, graphite electrodes (2 mm. in diam., 20 cm. long); 10, small quartz tubes used to insulate and position graphite electrodes; 11, capillary constrictions (0.5–1.0 mm. in diam., 1 cm. long) on the end of quartz tubes which contained graphite electrodes.

(12) E. V. Britzke and A. F. Kapustinski, *Z. anorg. allgem. Chem.*, **194**, 323 (1930).

(13) D. Cubicciotti, *J. Phys. Chem.*, **67**, 118 (1963).

into the Supremax glass. Antimony sulfide was placed in the cell and sulfur was placed in the sulfur reservoir. The cell was evacuated to 10^{-4} mm. and sealed. Upon heating in a two-stage furnace, the antimony sulfide melted and flowed into the capillaries.

Results are shown in Fig. 3. Independence of the conductivity, κ , on q for $q \gg 1$ indicates that ionic conduction prevails if $q \gg 1$. Higher values of κ for

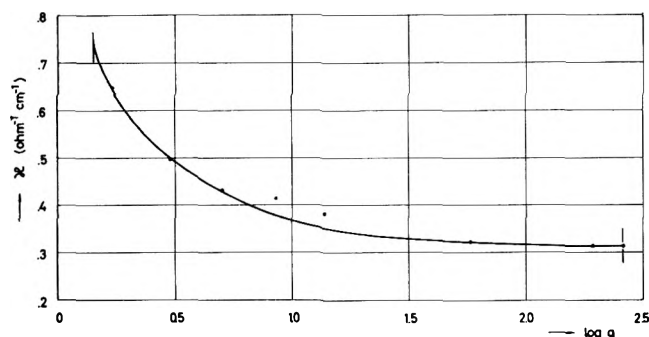


Figure 3. Electrical conductivity, κ , of liquid antimony sulfide at 650° as a function of sulfur activity, $q = p_{\text{H}_2\text{S}}/p_{\text{H}_2}$. The points are experimental values. The curve has been drawn in accord with eq. 14. The vertical lines at the ends of the curve indicate the limits of the one-phase region.

$q \sim 1$ may be ascribed to occurrence of n-type semi-conduction. In particular, a two-electron exchange between Sb^+ and Sb^{3+} ions may be assumed in analogy to a suggestion made by Raleigh¹¹ for BiI_3 melts containing excess Bi. Thus the total conductivity κ may be written as the sum of two terms, κ_{ion} and κ_e , for ionic and electronic conductivity in accord with determinations on the current efficiency for the electrolysis of molten Sb_2S_3 by Yanagase and Derge.¹⁴ The electronic conductivity is set proportional to y_1 , which in turn is inversely proportional to q in view of eq. 7 and 9. Hence

$$\kappa = \kappa_{\text{ion}} + \kappa_e = \kappa_{\text{ion}} + \kappa_e^0/q \quad (14)$$

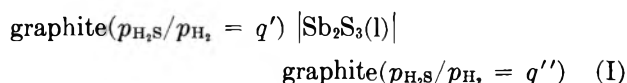
where κ_e^0 is the electronic conductivity extrapolated to $q = 1$. In principle, a third term proportional to q may be added to eq. 14 for electron exchange between Sb^{3+} and Sb^{5+} ions corresponding to p-type conduction. Under the conditions of the present investigation, however, there is no visible increase of the conductivity at higher sulfur activities. Thus the third term in eq. 14 is omitted. The solid curve in Fig. 3 is drawn in accord with eq. 14.

The rise of the conductivity with decreasing sulfur activities is in accord with results obtained by Yanagase and Derge¹⁴ for Sb_2S_3 melts containing excess Sb for temperatures above 700° . The conductivity of

molten Sb_2S_3 has also been determined by Knacke and Strese¹⁵ without fixing the sulfur activity. The value for a Sb_2S_3 melt preheated at 904° is of the same order of magnitude as values shown in Fig. 3. Conductivities reported by Knacke and Strese for Sb_2S_3 melts preheated to temperatures ranging from 660 to 873° are much lower. No explanation for this divergence can be offered.

Electromotive Force Measurements

If the Sb_2S_3 melt exhibited exclusively ionic conduction and deviations from the ideal stoichiometric composition were negligible, the e.m.f., E , of a cell involving molten Sb_2S_3 as electrolyte and graphite electrodes with different sulfur activities given by the $\text{H}_2\text{S}/\text{H}_2$ ratios q' and q''



would be

$$E = \frac{RT}{2F} \ln (q''/q') \quad (15)$$

according to Nernst's formula where F is the Faraday constant. On the other hand, the e.m.f. would be zero in the case of exclusively electronic conduction. Actually, the e.m.f. of cell I lies between the two limiting cases as is shown below.

From an atomistic point of view, migration of Sb^{3+} , S^{2-} ions and electrons is to be considered. In addition, migration of Sb^+ , Sb^{5+} ions and complex ions such as SbS^+ may be considered. If a Hittorf transference experiment is made, however, one obtains only transference numbers for appropriately chosen thermodynamic components whose number is less than the number of ionic species. This information is based on the chemical analysis of the cathodic or anodic compartment of a cell before and after passing current. In a binary melt such as Sb_2S_3 , one may use sulfur as the reference component and may report results of a transference experiment in terms of Sb^{3+} ions, $t_{\text{Sb}^{3+}}$, and electrons, t_e , as arbitrarily chosen components¹⁶ where $t_{\text{Sb}^{3+}}$ is the number of equivalents of Sb, equal to one-third of the number of gram-atoms of Sb, which on passing 1 faraday are transferred toward the cathode with respect to sulfur as the reference component and $t_e = 1 - t_{\text{Sb}^{3+}}$. Then,

(14) T. Yanagase and G. Derge, *J. Electrochem. Soc.*, **103**, 303 (1956).

(15) O. Knacke and G. Strese, *Z. Erzhbergbau Metallhüttenw.*, **10**, 207 (1957).

(16) C. Wagner, "The Electromotive Force of Galvanic Cells Involving Phases of Locally Variable Composition," to be published in *Advan. Electrochem. Electrochem. Eng.*

Equating the electrical work done on cell I upon passing 1 faraday and the free energy change corresponding to the transfer of $t_{\text{Sb}^{3+}}$ equivalents ($= 1/3 t_{\text{Sb}^{3+}}$ mole of Sb) from the left-hand to the right-hand side of cell I with a differential difference of the Sb activity, a_{Sb} , one has

$$dE = -\frac{t_{\text{Sb}^{3+}} RT}{3 F} d \ln a_{\text{Sb}} \quad (16)$$

In view of the Gibbs–Duhem equation, one can write

$$d \ln a_{\text{Sb}} + y d \ln a_{\text{S}} = 0 \quad (17)$$

Thus eq. 16 may be rewritten as

$$dE = \frac{t_{\text{Sb}^{3+}} RT}{3 F} y d \ln a_{\text{S}} \quad (18)$$

Hence, the e.m.f., E , of cell I with finite activity differences is

$$E = \frac{RT}{3F} \int_{q'}^{q''} t_{\text{Sb}^{3+}} y d \ln q \quad (19)$$

The cell used for e.m.f. measurements was essentially the same as the conductivity cell shown in Fig. 1. The quartz capillaries were about 2 cm. long. Each quartz tube contained only one graphite electrode which was separated from the capillary by a quartz frit. Small quartz tubes were used in place of the inner graphite electrodes in order to bubble gas through the melt. A mixture with $q' = 1.5$ was bubbled through the melt at one of the electrodes while mixtures with q'' ranging from about 1.7 to 8.5 were bubbled through the melt at the other electrode. The e.m.f. of the cell was measured at various times until a constant E was obtained for a given value of q'' .

Results are shown in Fig. 4. Upon differentiating eq. 19 with respect to $\ln q''$ for a constant value of q' , one has

$$t_{\text{Sb}^{3+}}(q'') = \frac{3F}{y(q'')RT} \frac{\partial E}{\partial \ln q''} \quad (20)$$

where $y = 3/2 + \delta$ is given by Fig. 1.

With the help of eq. 20 and the data shown in Fig. 4, one obtains $t_{\text{Sb}^{3+}} = 0.38$ for $q'' = 1.7$ and $t_{\text{Sb}^{3+}} = 0.64$

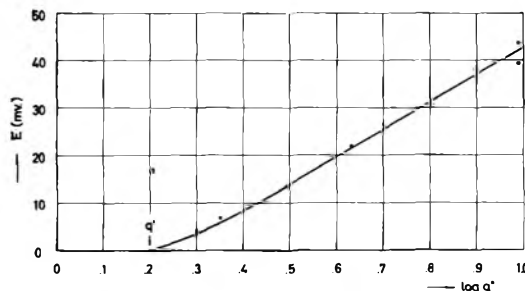
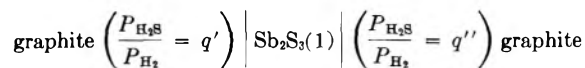


Figure 4. E.m.f. of the cell



vs. $\log q''$ for $q' = 1.5$.

for $q'' = 8.5$. On the other hand, using eq. 14 with $\kappa_{\text{ion}} = 0.31 \text{ ohm}^{-1} \text{ cm.}^{-1}$, one has

$$t_{\text{Sb}^{3+}} = 0.31/\kappa \quad (21)$$

with numerical values $t_{\text{Sb}^{3+}} = 0.48$ and 0.74 for $q = 1.7$ and 8.5 , respectively. These values are consistent with the values deduced from e.m.f. measurements.

Acknowledgments. Sincere thanks are extended to Prof. C. Wagner, who derived the various equations, directed the experimental work, and discussed the results with the writer. The writer also wishes to thank Mr. G. Zintl for helpful discussions, particularly with regard to methods of chemical analysis, and the National Science Foundation for financial support.

Activity Coefficients of 2:1 Complex Ion Electrolytes:

Nitropentaamminecobalt(III) Chloride, Chloropentaamminecobalt(III)

Perchlorate, and Fluoropentaamminecobalt(III) Chloride

by W. L. Masterton and Jacqueline A. Scola¹

The University of Connecticut, Storrs, Connecticut (Received September 3, 1963)

Activity and osmotic coefficients of $[\text{Co}(\text{NH}_3)_5\text{NO}_2]\text{Cl}_2$, $[\text{Co}(\text{NH}_3)_5\text{Cl}](\text{ClO}_4)_2$, and $[\text{Co}(\text{NH}_3)_5\text{F}]\text{Cl}_2$ have been determined at 37° using a vapor pressure osmometer. Measurements have been made from 0.01 *m* to nearly saturated solutions. The calculated activity coefficients are lower than those of simple 2:1 electrolytes and are more nearly comparable to those of 1:2 electrolytes.

Introduction

Comparatively little information is available concerning the activity coefficients, in fairly concentrated solutions, of electrolytes in which the positive ion is a kinetically stable coordination complex. Recently, Brubaker and co-workers²⁻⁵ have investigated 4:1 and 3:1 electrolytes containing the cations $\text{Pt}(\text{en})_3^{+4}$, $\text{Co}(\text{en})_3^{+3}$, and $\text{Co}(\text{pn})_3^{+3}$. Mori and Tsuchiya⁶ have reported activity coefficient data for a single 3:1 electrolyte, $\text{Co}(\text{NH}_3)_6\text{Cl}_3$.

It seemed desirable to extend these studies to complex ion electrolytes of lower charge types. Extensive data on the activity coefficients of simple 2:1 electrolytes (*e.g.*, MgCl_2 , $\text{Zn}(\text{NO}_3)_2$) have been summarized by Stokes.⁷ The interpretation of these data is handicapped by uncertainties concerning the nature of the cationic species present in solution. In particular, it is difficult to assess the effect of hydration of the metal ion. By working with stable 2:1 complex ion electrolytes, this difficulty can be minimized.

The compounds studied in this work were chosen on the basis of relatively high solubility (at least 0.1 *m*) and stability toward aquation. Qualitative observations^{8,9} indicate aquation of $[\text{Co}(\text{NH}_3)_5\text{NO}_2]\text{Cl}_2$ and $[\text{Co}(\text{NH}_3)_5\text{F}]\text{Cl}_2$ to be negligible under the conditions of our measurements. One can calculate from the rate constant and energy of activation reported by Basolo and Pearson⁸ that aquation of $[\text{Co}(\text{NH}_3)_5\text{Cl}](\text{ClO}_4)_2$ at 37° should amount to less than 2% in 1 hr.

Experimental

Compounds. 1. $[\text{Co}(\text{NH}_3)_5\text{NO}_2]\text{Cl}_2$ was prepared as described by Walton.¹⁰ *Anal.* Calcd. for $[\text{Co}(\text{NH}_3)_5\text{NO}_2]\text{Cl}_2$: NH_3 , 32.63; Cl , 27.17. Found: NH_3 , 32.58; Cl , 27.13.

2. $[\text{Co}(\text{NH}_3)_5\text{Cl}](\text{ClO}_4)_2$ was prepared by adding sodium perchlorate to a saturated solution of the chloride salt. The product was recrystallized from water at room temperature by adding perchloric acid. *Anal.* Calcd. for $[\text{Co}(\text{NH}_3)_5\text{Cl}](\text{ClO}_4)_2$: NH_3 , 22.50; ligand Cl , 9.37. Found: NH_3 , 22.52; Cl , 9.24.

3. $[\text{Co}(\text{NH}_3)_5\text{F}]\text{Cl}_2$ was prepared from the nitrate¹¹

- (1) Abstracted in part from a thesis submitted by Jacqueline A. Scola in partial fulfillment of the requirements for the M.S. degree, June, 1963.
- (2) C. H. Brubaker, Jr., *J. Am. Chem. Soc.*, **78**, 5762 (1956).
- (3) C. H. Brubaker, Jr., *ibid.*, **79**, 4274 (1957).
- (4) R. A. Wynveen, J. L. Dye, and C. H. Brubaker, Jr., *ibid.*, **82**, 4441 (1960).
- (5) C. H. Brubaker, Jr., and T. E. Haas, *J. Phys. Chem.*, **65**, 866 (1961).
- (6) M. Mori and R. Tsuchiya, *Nippon Kagaku Zasshi*, **79**, 1164 (1958); *Chem. Abstr.*, **53**, 9793 (1959).
- (7) R. H. Stokes, *Trans. Faraday Soc.*, **44**, 295 (1948).
- (8) F. Basolo and R. S. Pearson, "Mechanisms of Inorganic Reactions," John Wiley and Sons, Inc., New York, N. Y., 1958, p. 122.
- (9) M. Linhard and M. Weigel, *Z. anorg. allgem. Chem.*, **266**, 80 (1951).
- (10) H. F. Walton, "Inorganic Preparations," Prentice-Hall, Inc., New York, N. Y., 1948, pp. 92, 93.
- (11) F. Basolo and R. K. Murmann, "Inorganic Syntheses," Vol. IV, J. C. Bailar, Jr., Ed., McGraw-Hill Book Co., Inc., New York, N. Y., 1953, p. 172.

using an ion-exchange column. A saturated solution of the nitrate (0.025 *m*) was passed slowly through Amberlite IRA-401 resin in the chloride form. The product was brought out of solution by freeze-drying and recrystallized from water by adding alcohol. *Anal.* Calcd. for $[\text{Co}(\text{NH}_3)_5\text{F}]\text{Cl}_2$: NH_3 , 36.39; Cl , 30.31. Found for sample dried over P_2O_5 : NH_3 , 35.96; Cl , 30.17.

After standing for several months, the product was found to contain a small amount of a less soluble impurity which could not be completely removed by recrystallization. Concentrated solutions of $[\text{Co}(\text{NH}_3)_5\text{F}]\text{Cl}_2$ (above 0.2 *m*) were prepared by diluting a filtered, saturated solution whose concentration was determined by chloride analysis.

Apparatus. Osmotic coefficients were measured at 37° with a Mechrolab vapor pressure osmometer. The use of the instrument for this purpose has been described previously.¹² The accuracy of an individual reading is less than that attainable by standard isopiestic techniques. The vapor pressure osmometer, however, can be applied to solutions as dilute as 0.01 *m*; data in this concentration range facilitate the extrapolation to infinite dilution required in the calculation of activity coefficients. Moreover, the time required for a measurement is greatly reduced; readings can be taken on a solution within 1 hr. of the time it is prepared.

The instrument was calibrated with potassium chloride solutions of known molality and osmotic coefficient.¹³ The calibration curve was checked during each run to allow for any drift in resistance of the probe thermistors. Three syringes were filled with solutions of the compound being studied; a fourth syringe contained a potassium chloride solution in the same concentration range.

For each compound, measurements were taken at 0.01 *m* intervals in the range from 0.01 to 0.10 *m*. The data obtained with $[\text{Co}(\text{NH}_3)_5\text{NO}_2]\text{Cl}_2$ are given in Table I. With the more soluble $[\text{Co}(\text{NH}_3)_5\text{F}]\text{Cl}_2$, eight additional readings were taken at approximately equal intervals between 0.10 and 1.0 *m*.

The osmotic coefficient data were smoothed by fitting to a power series of the form shown in eq. 1.

$$1 - \phi = am^{1/2} + bm + cm^{3/2} + \dots \quad (1)$$

For the less soluble salts, all terms beyond the first two were dropped. With $[\text{Co}(\text{NH}_3)_5\text{F}]\text{Cl}_2$, four terms were required to give a satisfactory fit from 0.01 to 1.0 *m*. The average deviation of an experimentally determined osmotic coefficient from the smoothed value was ± 0.005 .

Activity coefficients at 0.01 *m* were calculated from the extended Debye-Hückel equation

$$\log \gamma_{\pm} = \frac{-2A\sqrt{\mu}}{1 + a^0B\sqrt{\mu}} \quad (\mu = 3m) \quad (2)$$

The parameter a^0 was evaluated from the smoothed osmotic coefficient at 0.01 *m*, making use of the derived relation

$$1 - \phi = \frac{4.606A}{\mu(a^0B)^3} \left[x - 2 \ln x - \frac{1}{x} \right] \quad (3)$$

where $x = 1 + a^0B\sqrt{\mu}$. Values of a^0 obtained in this manner were: 4.2 Å. for $[\text{Co}(\text{NH}_3)_5\text{NO}_2]\text{Cl}_2$, 3.9 Å. for $[\text{Co}(\text{NH}_3)_5\text{Cl}](\text{ClO}_4)_2$, and 3.6 Å. for $[\text{Co}(\text{NH}_3)_5\text{F}]\text{Cl}_2$.

Activity coefficients at higher concentrations were obtained by integrating the relation

$$d \ln \gamma_{\pm} = d\phi + (\phi - 1) d \ln m \quad (4)$$

between the limits $m = 0.01$ and *m*. The functional relationship between the osmotic coefficient and molality in this range was obtained from eq. 1.

Discussion

At a given concentration, the activity coefficients of the three compounds listed in Table II are virtually identical. Quite possibly, this agreement reflects the structural similarity of the three cations involved. Work now in progress suggests that the substitution of an ethylenediamine molecule for two ammonia groups noticeably changes the activity coefficient.

The activity coefficients of $[\text{Co}(\text{NH}_3)_5\text{NO}_2]\text{Cl}_2$, $[\text{Co}(\text{NH}_3)_5\text{Cl}](\text{ClO}_4)_2$, and $[\text{Co}(\text{NH}_3)_5\text{F}]\text{Cl}_2$ are markedly lower than those of simple 2:1 salts. The compilation of Stokes⁷ shows that of 33 salts of this valence type in which the cation is an alkaline earth or uncoordinated transition metal ion, 27 have activity coefficients

Table I: Measured Osmotic Coefficients of $[\text{Co}(\text{NH}_3)_5\text{NO}_2]\text{Cl}_2$

<i>m</i>	ϕ	<i>m</i>	ϕ
0.01015	0.904	0.06034	0.797
.01986	.864	.07012	.788
.02991	.840	.08015	.781
.04012	.825	.09094	.776
.05033	.815	.1004	.775

(12) P. O. P. Ts'o, I. S. Melvin, and A. C. Olson, *J. Am. Chem. Soc.*, **85**, 1289 (1963).

(13) Osmotic coefficients of KCl from 0.1 to 1.0 *m* were calculated from data given in H. S. Harned and B. B. Owen, "The Physical Chemistry of Electrolytic Solutions," Reinhold Publ. Corp., New York, N. Y., 1958, p. 415. A small temperature correction was applied to convert from 25 to 37°. Values at lower concentrations were obtained from W. J. Hornibrook, G. J. Janz, and A. R. Gordon, *J. Am. Chem. Soc.*, **64**, 513 (1942).

Table II: Activity Coefficients and Smoothed Osmotic Coefficients at Various Molalities

m	[Co(NH ₃) ₅ NO ₂]Cl ₂		[Co(NH ₃) ₅ Cl](ClO ₄) ₂		[Co(NH ₃) ₅ F]Cl ₂	
	φ	γ _±	φ	γ _±	φ	γ _±
0.01	0.900	0.716	0.898	0.713	0.896	0.709
.02	.866	.638	.864	.634	.862	.631
.03	.843	.588	.841	.584	.840	.581
.05	.812	.521	.810	.518	.809	.514
.07	.791	.478	.790	.475	.788	.472
.10	.771	.434	.772	.431	.766	.426
.20					.723	.342
.30					.698	.297
.50					.663	.243
.70					.634	.210
1.00					.599	.177

greater than 0.50 at 0.1 *m*. In contrast, those of the three complex ion electrolytes studied here average 0.43 at 0.1 *m*. It will also be noted that the activity coefficient of [Co(NH₃)₅F]Cl₂ decreases steadily in the region between 0.1 and 1.0 *m*. Activity coefficients of simple 2:1 salts pass through a minimum in this concentration range.

These same effects are apparent from Brubaker's data for 3:1 complex ion electrolytes. For example, the activity coefficient of Co(en)₃(NO₃)₃ is given as 0.222 at 0.1 *m*; that of aluminum chloride at the same concentration is 0.360. The data for Co(en)₃Cl₃ show no minimum at concentrations up to 1.11 *m*; the activity coefficient of aluminum chloride starts to increase at about 0.2 *m*.

The activity coefficients of the electrolytes we have studied are strikingly similar to those of simple 1:2

electrolytes such as rubidium sulfate. Ten salts⁷ of this type, in which an alkali metal ion is bonded to a divalent anion, have a mean activity coefficient of 0.45 at 0.1 *m*. None of these 1:2 electrolytes shows a minimum in activity coefficient at concentrations up to 1.0 *m*.

The trends pointed out above are explained most readily in terms of hydration of the positive ion. Salts of strongly hydrated cations such as Mg⁺² or Zn⁺² exhibit relatively high activity coefficients, presumably because of the withdrawal of water molecules from their role as solvent. Where cationic hydration is a relatively minor factor, as in the alkali sulfates or 2:1 complex ion electrolytes such as [Co(NH₃)₅F]Cl₂, activity coefficients are comparatively low and decrease steadily with increasing concentration.

It is readily shown that the activity coefficients of [Co(NH₃)₅NO₂]Cl₂, [Co(NH₃)₅Cl](ClO₄)₂, and [Co(NH₃)₅F]Cl₂, at concentrations of 0.1 *m* or greater, fall below the values calculated from eq. 2, where *a*⁰ is assigned a value (4.2, 3.9, and 3.6 Å.) which fits the data at 0.01 *m*. These deviations can be attributed to ion pairing, which should be extensive in compounds of this type where the interionic distance is considerably smaller than Bjerrum's critical value of 7 Å. for a 2:1 electrolyte. Extensive association would also be expected in simple 2:1 salts, but its effect may be obscured by that of hydration, which operates in the opposite direction.

Acknowledgments. This work was supported in part by a grant from the Research Foundation of the University of Connecticut. The authors wish to express their appreciation to Dr. R. Kent Murmann and Ladislav H. Berka for helpful discussions and suggestions.

The Photooxidation of Carbon Monoxide on Zinc Oxide

by T. S. Nagarjunan and Jack G. Calvert

Evans Chemical Laboratory, The Ohio State University, Columbus 10, Ohio (Received September 8, 1963)

The photooxidation of carbon monoxide on zinc oxide solid has been studied in experiments at 0°. Zinc oxide with presorbed oxygen was irradiated with 3660-Å. light in the presence of carbon monoxide gas. Carbon dioxide was formed in the irradiated system, while its rate of formation in the dark was negligible. The reaction was studied under varied conditions: the temperature at which the oxygen was presorbed on the zinc oxide, the pressure of oxygen during the presorption, the pressure of carbon monoxide gas, the time of irradiation, and the intensity and the wave length of the absorbed light. The results confirm that oxygen is adsorbed in at least three different forms on zinc oxide in an amount which depends on the temperature of the treatment. Two of these types of adsorbed species of oxygen react with carbon monoxide to form carbon dioxide on irradiation, while the third type is inactive. The three types may be O_2^- , O^- , and O^{-2} , with the first two the active forms. Carbon monoxide appears to react either from the gas phase or from a weakly adsorbed state. The reaction may occur through two different reaction paths, one much faster than the other. The quantum efficiency of the carbon dioxide formation varies from 0.001 at high intensities to greater than 0.1 at low intensities at 3660 Å. Some aspects of the detailed mechanism are considered. From these and other results some speculation is given concerning the contribution of photooxidations sensitized on suspended solid particulates to the chemistry of the polluted atmosphere. There is a high probability that such reactions are of little importance in the usual polluted atmosphere.

Introduction

The mechanism of formation and the reactions of particulate matter in the polluted atmosphere are rather uncertain at this time. Excellent detailed studies of some aspects of the problem have been made and at least a few points seem clear. For example, under certain conditions organic aerosol formation and light scattering in automobile exhaust-polluted atmospheres can be related to the sulfur dioxide content of the atmosphere.¹ In a very different area of research some evidence of aerosol participation has been found; a marked enhancement of the irritation (as measured by eye irritation, pulmonary flow resistance, etc.) of certain irritants has been observed when an aerosol is present.² The role, if any, which inorganic particulate matter plays in smog formation remains largely unknown. There have been some observations of the acceleration of sulfur dioxide oxidation in the presence of salts of iron and manganese.³ The possible participa-

tion of reactions photosensitized on the surface of inorganic particulates has been considered in a speculative fashion,⁴ but there is no direct evidence which allows a quantitative estimate of the extent of inorganic particulate involvement in the chemistry of the polluted atmosphere. However, particulate matter in automo-

- (1) For a review of the experiments and references to original literature, see P. A. Leighton, "Photochemistry of Air Pollution," Interscience Publishers, Inc., New York, N. Y., 1961, p. 253.
- (2) For a review of the experiments and references to original literature, see "Air Pollution," A. C. Stern, Ed., Vol. 1, Academic Press, New York, N. Y., 1962, p. 319.
- (3) H. F. Johnstone and D. R. Coughanour, *Ind. Eng. Chem.*, **50**, 1169 (1958).
- (4) (a) J. G. Calvert, "Proceedings of the Conference on Chemical Reactions in Urban Atmospheres," Report No. 15, Air Pollution Foundation, Los Angeles, Calif., 1956, p. 91; (b) W. M. Ritchey and J. G. Calvert, *J. Phys. Chem.*, **60**, 1465 (1956); (c) J. G. Calvert, "Proceedings Third Air Pollution Medical Research Conference," Los Angeles, Calif., 1959, p. 55 (State of Calif., Dept. of Health).

bile exhaust-polluted atmospheres has been found to contain significant quantities of at least two metals, lead and iron,⁵ and it has been estimated by Leighton that the rate of sunlight absorption by compounds of these elements can be of the same magnitude as that of other major contaminants present in the polluted atmosphere.⁶ Since photosensitized reactions are known to occur on various oxides, sulfides, etc.,⁴ a possible contribution to the chemistry of the polluted atmosphere may come from these systems. However, the known properties of the automobile exhaust-polluted atmosphere are understood qualitatively in terms of mechanisms which do not involve photoactivated surface reactions, and as a consequence surface reactions usually are neglected in mechanistic considerations. The present work constitutes an effort to improve knowledge of the mechanism and quantum efficiency of reactions photosensitized on solids and is aimed toward the possible evaluation of the importance of these processes in the polluted atmosphere.

Numerous studies of systems containing zinc oxide have been made and much information concerning the interactions of oxygen with irradiated zinc oxide is known.^{7,8} The photooxidation of carbon monoxide, isopropyl alcohol, and other compounds has been shown to occur, although the efficiency is not known for these processes when gaseous reactants are used. Since carbon monoxide is a dominant impurity in polluted atmospheres, it seemed a reasonable choice of simple oxidizable material for this study. In view of the large amount of information available on photosensitized reactions on zinc oxide, we have chosen this solid and the photosensitized oxidation of carbon monoxide for further quantitative studies. Previous work with these systems suggests that the absorption of light of wave lengths less than about 4000 Å. results in the promotion of an electron to the conduction band of the solid, and the subsequent interaction of the promoted electron or the positive "holes" with adsorbed species is presumed to lead to the ultimate chemical changes observed. At least three different forms of adsorbed oxygen are suggested to exist on a zinc oxide surface in contact with oxygen⁸; in addition, photodesorption and photoadsorption of oxygen have been observed for these systems⁹ under certain conditions. In an attempt to simplify the interpretation of the data in our study, we chose to use adsorbed oxygen alone instead of gaseous and adsorbed oxygen; in theory, by proper choice of conditions predominantly any one type of adsorbed oxygen could be made available on the surface, and thus its role in the photooxidation reactions could be studied. The efficiency of the photooxidation of gaseous carbon monoxide on photoexcited zinc oxide containing pre-

sorbed oxygen has been determined in this work under a variety of experimental conditions and is reported here.

Experimental

The apparatus used for this study is shown in Fig. 1. A thin, flat Pyrex cell (C), 10 cm. long, 3.5 cm. wide, and 2-3 mm. thick, was used as the reaction vessel for

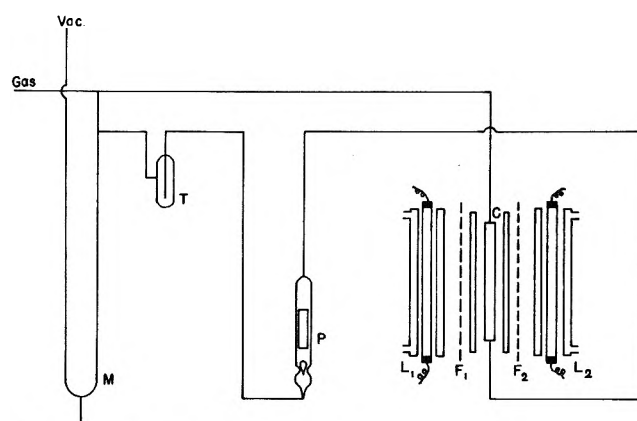


Figure 1. Photochemical apparatus.

the present studies. The circulation of gases through the catalyst and a trap cooled in liquid nitrogen was accomplished through the use of an all-glass circulating pump (P). Two medium pressure mercury arcs, Hanovia Type A, 550 w. (L_1 and L_2), with Pyrex water jackets, were the source of radiation; the arcs were placed on either side of the reaction cell, and about 3 to 5 in. from it in most runs. Glass filters (F_1 and F_2) of appropriate transmissions were placed between the lamps and cell as shown; Corning filters, C.S. 7-37, 4 mm. thick were used in most of the runs. A transparent Pyrex dewar flask served as the bath for the reaction cell and maintained the temperature at 0°; all of the

- (5) "An Aerometric Survey of the Los Angeles Basin," N. A. Renzetti, Ed., Report No. 9, Air Pollution Foundation, Los Angeles, Calif., 1955.
- (6) See ref. 1, p. 98.
- (7) Work related to H_2O_2 formation and photooxidations of organic matter in irradiated zinc oxide-containing systems and references to the earlier literature: (a) T. R. Rubin, J. G. Calvert, G. T. Rankin, and W. MacNevin, *J. Am. Chem. Soc.*, **75**, 2850 (1953); (b) J. G. Calvert, K. Theurer, G. T. Rankin, and W. MacNevin, *ibid.*, **76**, 2575 (1954); (c) I. Komuro, Y. Fujita, and T. Kwan, *J. Res. Inst. Catalysis, Hokkaido Univ.*, **7**, 73 (1959); (d) J. C. Kuriacose and M. C. Markham, *J. Catalysis*, **1**, 498 (1962); (e) F. Romero-Rossi and F. S. Stone, *Actes Congr. Intern. Catalyse, 2e, Paris*, **2**, 1481 (1960).
- (8) (a) T. I. Barry and F. S. Stone, *Proc. Roy. Soc. (London)*, **A255**, 124 (1960); (b) R. Morrison, *Advan. Catalysis*, **7**, 259 (1955).
- (9) (a) Y. Fujita and T. Kwan, *Bull. Chem. Soc. Japan*, **31**, 379 (1958); (b) Y. P. Solonitsin, *Zh. Fiz. Khim.*, **32**, 2142 (1958); (c) Y. Fujita and T. Kwan, *J. Res. Inst. Catalysis, Hokkaido Univ.*, **7**, 24 (1959).

photochemical studies were carried out at this temperature. Under these conditions there was no measurable thermal reaction during the time of the photochemical exposures. The use of the Pyrex walls in the optical path, the filter employed, and the output of the mercury lamp restricted the radiation reaching the cell to the 3660-Å. region in most runs. A set of experiments was conducted to determine the influence of frequency of the radiation on the photooxidation. Three frequency regions were isolated: 3660 Å. (as described previously); 4047 Å. (C.S. 3-74, 1.5 mm., and C.S. 7-51, 2.5 mm.); and 4358 Å. (C.S. 7-59, 3.8 mm., and C.S. 3-73, 3.05 mm.); in this set of experiments the intensities of the three wave length regions were maintained approximately the same through variation of the arc-to-cell distances and the use of calibrated screens.

Reagent grade carbon monoxide (Matheson Co.), pure, dry tank oxygen (with traces of nitrogen), and pure dry tank carbon dioxide (traces of oxygen and nitrogen) were used. Zinc oxide (S.P.) was supplied by the New Jersey Zinc Co. Oxygen for the photooxidation of carbon monoxide was available from the surface of zinc oxide. Before every experiment the dewar around the cell was replaced by a furnace, and the sample was subjected to an outgassing at about 450° for 4–6 hr. Then a presorbed layer of oxygen was prepared on the surface as follows; oxygen (usually at 1 atm.) was kept in contact with the solid for 1 hr., after which the system was evacuated (to 10⁻⁵ to 10⁻⁶ mm.) for 1 hr. This procedure left a presorbed layer of oxygen on the surface. The temperature and pressure at which presorption occurred varied depending on the set of experiments; however, for most experiments, 0° and 1 atm. were used. After the oxygen presorption, carbon monoxide gas was admitted to the cell at the desired pressure, the arcs were warmed up for a 15-min. period, shutters were removed, and the catalyst was irradiated. Immediately after the irradiation, the gas was circulated through the liquid nitrogen trap and circulation continued for at least 30 min.; carbon dioxide collected in the trap was analyzed by mass spectrometry.

In our study of the influence of intensity of irradiation on the photooxidation, copper screens of known transmission were interposed between the arcs and cell. The three screens used in the present study transmitted 57, 33, and 8%, respectively. The intensity of the radiation falling on the two sides of the cell was determined by potassium ferrioxalate actinometry using 0.15 *M* potassium ferrioxalate solution as described by Hatchard and Parker.¹⁰

The catalytic activity of the zinc oxide was qualitatively reproducible in identical check experiments, but there was a considerable scatter of the data, as is the

usual case for heterogeneous photochemical rate data, and there was a gradual loss of activity of the sample after repeated runs. Therefore, the experiments were performed in such a sequence that the lack of reproducibility would not affect the trends observed in that particular set of experiments. After a large number of experiments when the catalyst was observed to lose its activity, the activity was restored by partial reduction of the surface of the zinc oxide with hydrogen at 400° for 1–2 hr.

Studies of adsorption isotherms of CO, CO₂, and O₂ were made in a conventional volumetric adsorption apparatus.

Results

Although the system ZnO–O₂(ads.)–CO was chosen because of its presumed simplicity, the results show some complications which were entirely unexpected. This is apparent in the very nature of the time dependence of the carbon dioxide formation in Fig. 2. The

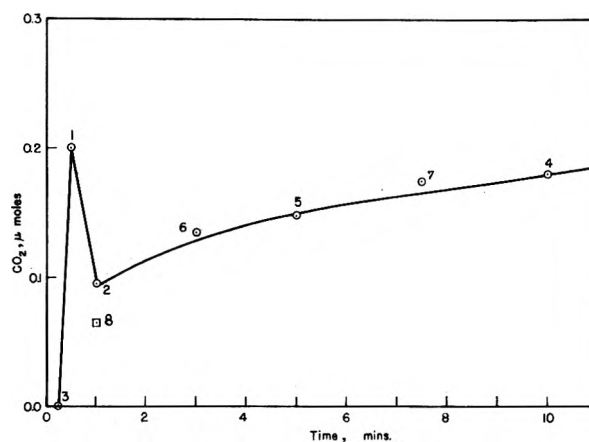


Figure 2. Time dependence of the photooxidation of CO on ZnO: pressure of CO, 250 mm.; temperature, 0°; 3660 Å.

number on each point corresponds to the chronological order of each run. An initial burst of carbon dioxide is evident, followed by a decrease in the amount, and then a steady increase to an apparently limiting value. The effect is reproducible and indeed real, although our theoretical explanation may be open to question. (Note that the same effect in the time dependence is seen in the data of Fig. 3.) The complicated form of the time–carbon dioxide yield data necessitated the careful consideration of irradiation time in determining the effect of the various parameters on the photooxidation.

(10) C. G. Hatchard and C. A. Parker, *Proc. Roy. Soc. (London)*, A235, 518 (1956).

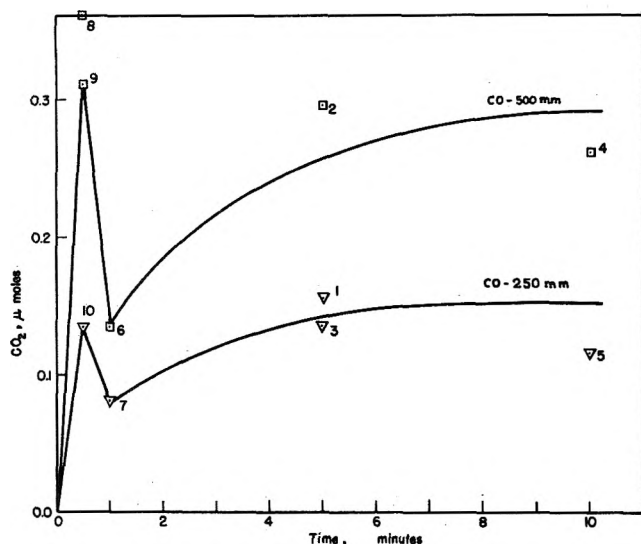


Figure 3. Effect of CO pressure on the photooxidation of CO on ZnO: upper curve, pressure of CO, 500 mm.; lower curve, pressure of CO, 250 mm.; temperature, 0°; 3660 Å.

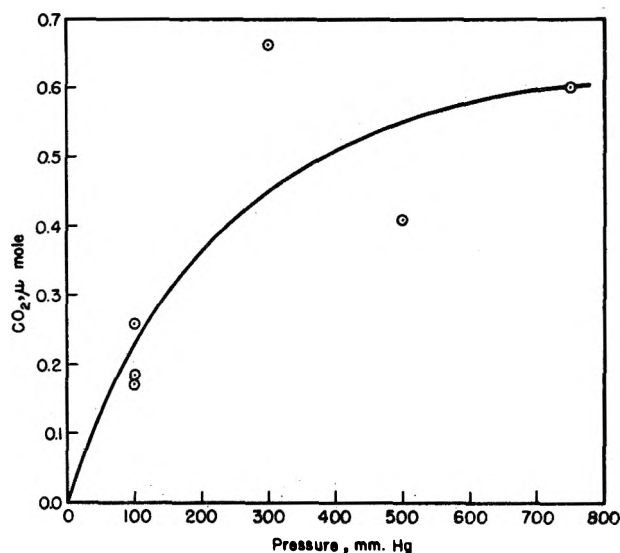


Figure 4. Effect of oxygen-presorption pressure on the photooxidation of CO on ZnO: pressure of CO, 200 mm.; time of exposure, 10 min.; temperature, 0°; 3660 Å.

One would expect the photooxidation of carbon monoxide on zinc oxide to depend on the physical state of the interacting species and the photochemical properties of the catalyst surface. The experiments described here were designed to elucidate these factors. The data of Fig. 3 help in establishing the physical state of the carbon monoxide reactant. The photooxidation was carried out with 250 and 500 mm. of carbon monoxide; the choice of these pressures was made with a knowledge of the adsorption isotherm of carbon monoxide on zinc oxide (Fig. 10). It is seen

that the amount of carbon dioxide formed varies linearly with the pressure of carbon monoxide at all times of exposure used, while the volume of carbon monoxide adsorbed on zinc oxide increases only slightly in this pressure region.

The amount and the type of presorbed oxygen was varied in other sets of experiments. The pressure of oxygen was varied from 100 to 750 mm., keeping the temperature of pretreatment the same (data of Fig. 4), and the temperature of the presorption was varied in the range 0-400° at constant oxygen pressure (data of Fig. 5).

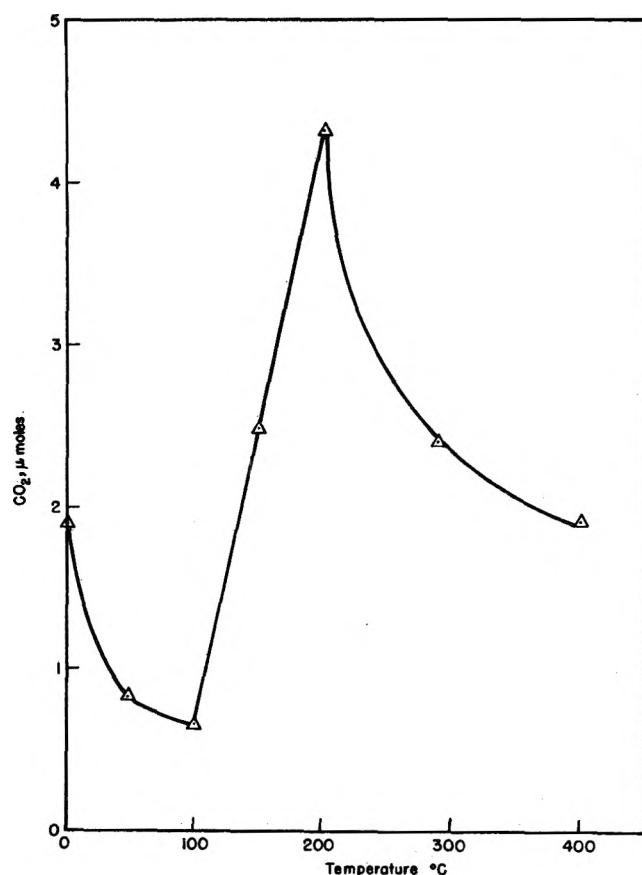


Figure 5. Effect of the temperature of pretreatment of ZnO on the photooxidation of CO: pressure of CO, 275 mm.; time of exposure, 10 min.; temperature, 0°; 3660 Å.

The nature of the interacting species was studied in the series of experiments summarized in Table I. A presorbed layer of carbon monoxide was prepared on the surface of zinc oxide in a manner similar to that used for oxygen presorption (run 2); oxygen was admitted and the experiment conducted under conditions used in the reaction with oxygen presorption. In another experiment, presorbed layers of oxygen and carbon mon-

oxide were prepared in succession (run 4); helium was admitted to facilitate the circulation and condensation of carbon dioxide.

Table I: Photooxidation of Carbon Monoxide on ZnO for Various States of Reactants^a

Expt. no.	Gas presorbed	Gas phase during irradiation	CO ₂ formed, μ moles
1	O ₂	CO (200 mm.)	1.5
2	CO	O ₂ (335 mm.)	0.0
3	O ₂	CO (200 mm.)	0.72
4	O ₂ and CO	He (\sim 200 mm.)	0.0
5	O ₂	CO (200 mm.)	0.39

^a Five-min. exposures, 3660 Å., gases presorbed at 335 mm. and 0°.

In Fig. 6, the effect of the light intensity and time of illumination on the yield of carbon dioxide is shown. From these data and the actinometer experiments the net quantum yields of carbon dioxide formation were calculated; see Fig. 7. Pure crystals of zinc oxide absorb radiations of about 4000 Å. or less. However, in the present study nonstoichiometric zinc oxide was used as a result of outgassing temperatures used and occasional reduction by hydrogen, and absorption could extend to somewhat longer wave lengths. Therefore, it was of interest to study the influence of the longer wave lengths of the mercury arc on the photooxidation. The intensities of the three regions and the yields of carbon dioxide formed in 10-min. exposures are summarized in Table II.

Table II: Effect of Wave Length of the Light on the Photooxidation of Carbon Monoxide on Zinc Oxide at 0°^a

Expt. no.	Wave length, Å.	Incident intensity, quanta/sec. on face of sample ZnO	CO ₂ formed, μ moles
1	3660	3.6×10^{17}	0.18
2	4047	3.2×10^{17}	0.00
3	3660	3.6×10^{17}	0.23
4	4358	4.7×10^{17}	0.00
5	3660	3.6×10^{17}	0.31

^a $P_{CO} = 290$ mm.; oxygen pretreatment at $P_{O_2} = 290$ mm.; 5-min. exposure.

The adsorption properties of the catalyst surface with and without presorbed layers of gases were determined in further experiments. Adsorption isotherms of car-

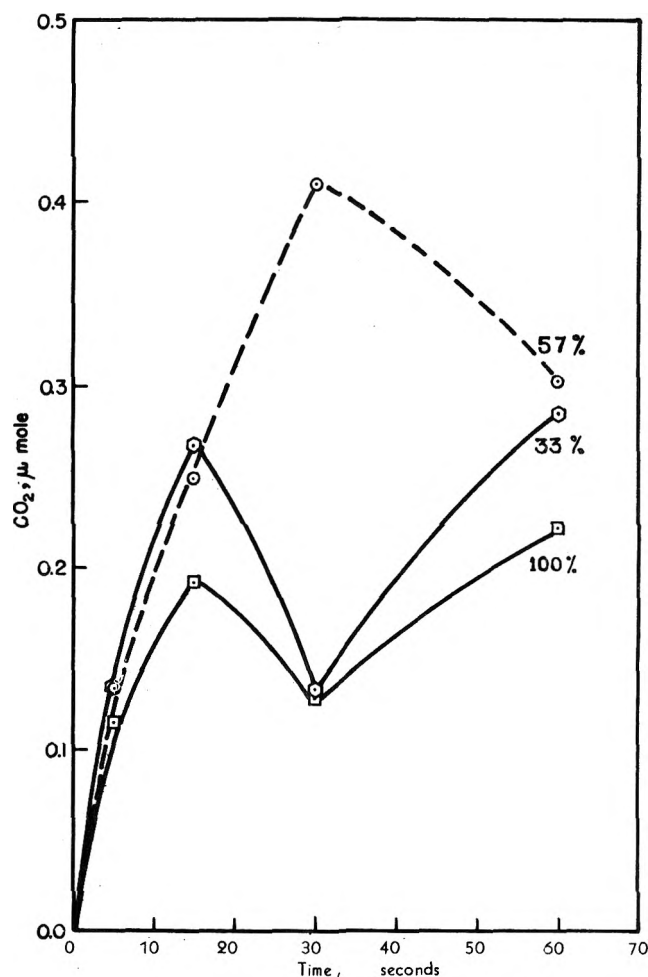


Figure 6. Effect of the light intensity on the photooxidation of CO on ZnO: pressure of CO, 150 mm.; temperature, 0°; 3660 Å.; full intensity, 8.7×10^{17} quanta/sec. over the 70 cm.² of exposed surface.

bon monoxide and oxygen were determined on ZnO, ZnO-O₂ and ZnO-CO surfaces, respectively. The presorbed layers of each gas were prepared as described earlier. The results, Fig. 8, show that the presence of one gas does not influence measurably the adsorption of the other. Adsorption studies of carbon dioxide on zinc oxide, Fig. 9, show that carbon dioxide is adsorbed to a considerable extent even at low equilibrium pressures and that irradiation does not produce a noticeable change at the pressures used in deriving these data. An irreversible photoadsorption of carbon monoxide on zinc oxide is shown in the data of Fig. 10. The photoadsorption isotherm after a dark run shows a much higher adsorption at low equilibrium pressures; however, at higher pressures the adsorption in the dark and in the presence of light is approximately the same. The gas on analysis after the completion of the photo-

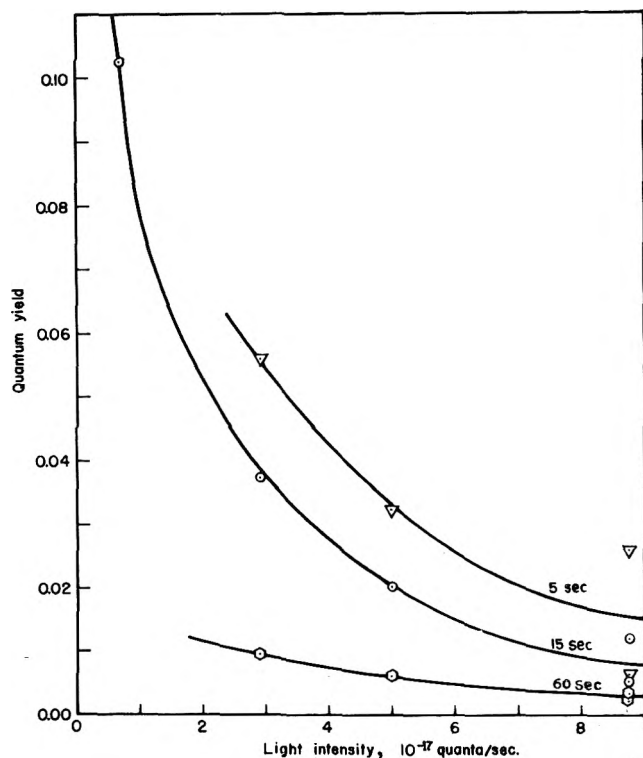


Figure 7. Effect of light intensity on the quantum yield of CO_2 formation in the photooxidation of CO on ZnO: pressure of CO, 150 mm.; temperature, 0° ; 3660 Å.; times of exposure shown.

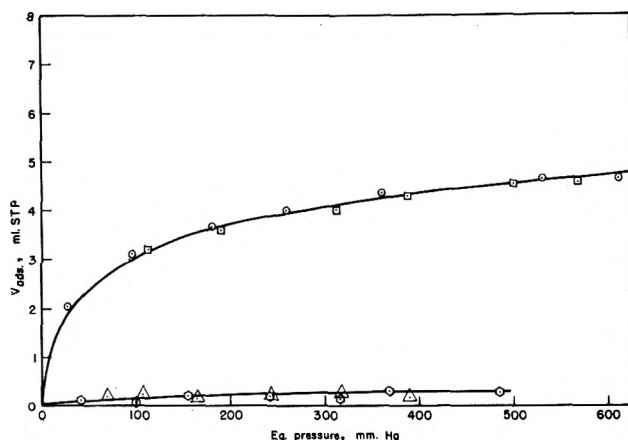


Figure 8. Adsorption studies of CO and O_2 on pretreated and untreated samples of ZnO at 0° : upper curve for CO on untreated ZnO surface (circles) and on O_2 -pretreated ZnO (squares); lower curve for O_2 on untreated ZnO surface (hexagons) and on CO-pretreated ZnO (triangles).

adsorption experiment showed the presence of carbon dioxide. Subsequent adsorption experiments of carbon monoxide in the dark showed a much higher adsorption.

A test was made to detect possible photodesorption of oxygen by following the pressure changes with a thermocouple gage in the reaction cell during irradiation.

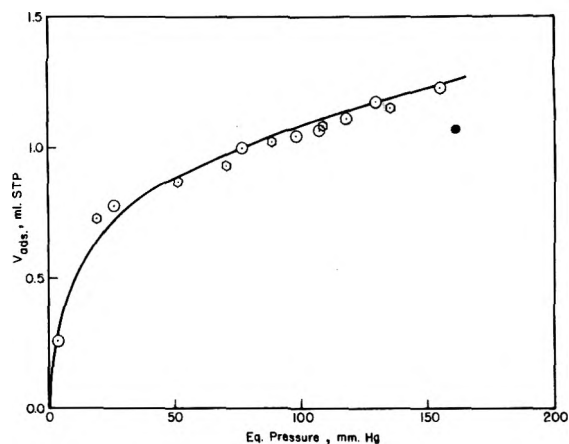


Figure 9. Adsorption studies of CO_2 on ZnO at 0° : dark (hexagons), in 3660-Å. light (circles).

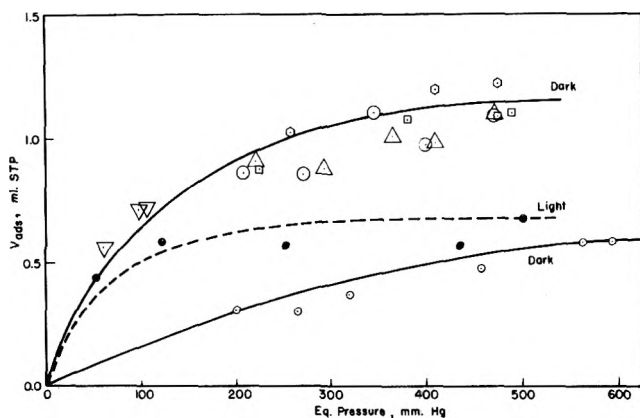


Figure 10. Adsorption studies of CO on ZnO at 0° ; lowest curve is initial run in dark; dashed curve is second run made in 3660-Å. light; upper curve represents data from repeated runs in the dark following the light run.

tion of a presorbed-oxygen-treated zinc oxide surface. There was no measurable photodesorption in our system. In similar experiments using low pressures of pure carbon dioxide, no photoadsorption of carbon dioxide could be detected on irradiation of a zinc oxide surface (with presorbed oxygen) with 3660-Å. light.

Discussion

The Nature of the Reactants in the Photooxidation of Carbon Monoxide on Zinc Oxide. The physical state of the reactants can be inferred from the results obtained here. By the very nature of the experiments performed in this study, the oxygen reactant was available only in the adsorbed state, since gaseous and weakly adsorbed oxygen were removed prior to the run and photodesorption of oxygen was not important for our conditions. However, previous studies suggest that several forms of oxygen exist in the adsorbed state on zinc oxide.^{8,9} Presumably, oxygen adsorbed at low em-

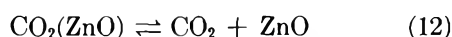
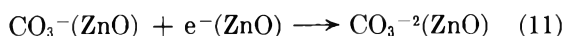
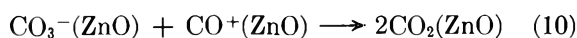
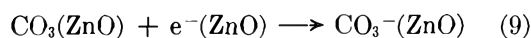
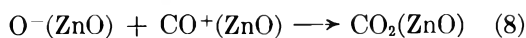
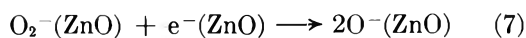
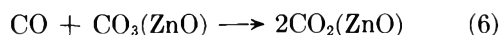
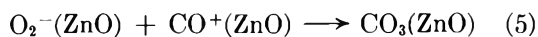
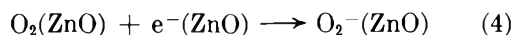
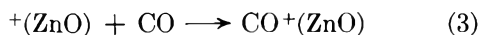
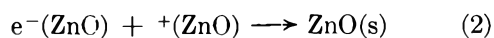
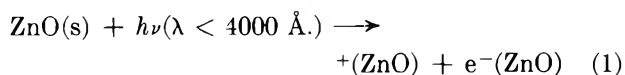
temperatures (below 150°) is largely in the form of the weakly chemisorbed O₂ or as the molecule ion, O₂⁻. This view is in accord with Winter's¹¹ findings that the exchange, O₂¹⁸ + O₂¹⁶ = 2O¹⁶O¹⁸, with adsorbed oxygen on ZnO is only measurable above 120°. Furthermore, it has been shown through conductivity measurements that oxygen adsorbed on zinc oxide is negatively charged.^{8b} Fujita and Kwan^{9c} cite adsorption data which are also consistent with a weak chemical adsorption of oxygen on zinc oxide at low temperatures; they exclude van der Waals adsorption (with an essentially neutral O₂ entity) and favor O₂⁻ as the important surface form of adsorbed oxygen at low temperatures. Presumably such species as O⁻ and O⁻² form at higher temperatures. The results reported here are consistent with these interpretations. The decrease in the amount of carbon dioxide formed in the photooxidation as the temperature of oxygen presorption is raised from 0 to 100° (see Fig. 5) may reflect the gradual decrease in surface concentration of the weakly chemisorbed O₂ and O₂⁻ forms. If one accepts this view, the decrease which occurs corresponds to a heat of adsorption of about 3 kcal./mole. Since the oxygen reactant in our experiments must withstand the 1-hr. degassing procedure at 0°, physically adsorbed oxygen cannot be important in our reaction system; some species involving a partially polarized oxygen and adsorption site must be involved. The absence of photodesorption of oxygen in our samples favors the assumption of the dominance of the O₂ weakly chemisorbed species rather than O₂⁻ here, since photodesorption may be related to the presence of O₂⁻. The increase in carbon dioxide in the temperature range 100–200° suggests a second type of adsorbed oxygen which is reactive; this type must have an appreciable activation energy for adsorption. Conceivably the O⁻ form suggested by others may be the species dominant in this range. At temperatures above 200° the concentration of this species declines due to desorption and/or transformation into a third type of adsorbed oxygen which is unreactive. The latter explanation is favored since previous work has shown that defect zinc oxide (such as that used here) does adsorb oxygen above 200°, and the oxygen is adsorbed in the form of O⁻². In terms of this picture the increase in carbon dioxide formed with increasing pressure of oxygen used in the presorption procedure (see Fig. 4) reflects the increased adsorption and the greater the amount of the weakly chemisorbed O₂ or O₂⁻ reactant which is available on the surface. All of the results are consistent with the dominance of one or both of these species as the initial reactant in the low temperature (0°) presorption which we have employed in most of these experiments.

The form of the reactant carbon monoxide is suggested from the data of Fig. 3 and Table I. The linear dependence of the photooxidation on the carbon monoxide pressure shown in Fig. 3 is consistent with that found for this reaction by Romero-Rossi and Stone^{7e} for somewhat different conditions. The carbon monoxide adsorption data of Fig. 8 show that the carbon monoxide coverage of zinc oxide has increased by only about 15% for the pressure increase from 250 to 500 mm. used in the runs of Fig. 3. From Table I it is seen that strongly chemisorbed carbon monoxide presorbed on the surface does not react with oxygen from the gas phase or from the adsorbed phase. Weakly adsorbed carbon monoxide would be desorbed during the evacuation procedure we employed.¹² The presorption experiments of Fig. 8 show that the presence of one gas as a presorbed layer does not influence the adsorption of the other in the absence of light. However, in Fig. 10 the irreversible photoadsorption of carbon monoxide is evident; a strong interaction exists between the irradiated zinc oxide surface and the carbon monoxide. All of these results point to the conclusion that carbon monoxide reactant at 0° is in the form of a weakly adsorbed species or as a gaseous molecule.

Possible Mechanism of the Photooxidation of Carbon Monoxide on Zinc Oxide Presorbed with Oxygen at 0° and 3660 Å. The wave length dependence of the photooxidation, summarized in Table II, is consistent with the region of strong absorption by zinc oxide crystals, and it is likely that the primary photochemical act is that of energy absorption by the zinc oxide lattice and promotion of an electron to the conduction band of the crystal, e⁻(ZnO), and the formation of a positive hole, +(ZnO), in reaction 1. The extinction coefficient of zinc oxide is such that pair formation will occur within the first few hundred atomic layers from the surface. The selection of an appropriate detailed mechanism which follows this primary process and leads to carbon dioxide formation with the desired kinetics is much more speculative. However, the reactants seem quite well defined in this system, and the present knowledge of this and other related systems excludes participation of many alternatives. It is an unnecessary and unwarranted procedure to review here the evaluation of many possible mechanisms, but it will suffice to consider the present experimental results in terms of the simplest mechanism which we can derive and which is consistent with all the observations.

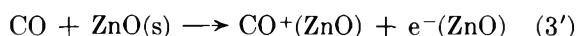
(11) E. R. S. Winter, *J. Chem. Soc.*, 1522 (1954); *Advan. Catalysis*, **10**, 196 (1958).

(12) J. H. Taylor and C. H. Amberg, *Can. J. Chem.*, **39**, 535 (1961).



At the highest light intensity used, the formation of carbon dioxide is very inefficient ($\Phi_{\text{CO}_2} \cong 0.01$, Fig. 7); our mechanism accounts for this inefficiency through the dominance of "hole" and electron combination, reaction 2, under these conditions. At the lower intensities, with the resultant lower electron and "hole" concentrations, (2) would be less probable, interaction with reactant species more important, and the quantum efficiency of carbon dioxide formation would rise as is observed.

If reaction 3, the capture of a carbon monoxide molecule by a "hole," is the rate limiting step in experiments at constant light intensity, then the expected kinetics are consistent with those observed for carbon dioxide formation. This reaction, first suggested by Romero-Rossi and Stone,^{7e} demands a first-order dependence of rate of carbon dioxide on the pressure of carbon monoxide; see Fig. 3. Our results require that the possible thermal reaction



does not occur measurably in the dark at 0° during the time of our experiments. The lack of dark reaction to form carbon dioxide and the adsorption properties of carbon monoxide (Fig. 8) rule it out; if (3') occurred significantly, one would expect an enhancement of adsorption on oxygen-presorbed zinc oxide.¹³ The slowness of (3') is consistent with the findings of Taylor and Amberg,¹² who report the formation of strongly chemisorbed carbon monoxide species on zinc oxide surface only after standing for 24 hr. at room temperature.

Depending on the form of the chemisorbed oxygen, conduction electron capture is presumed to occur with weakly chemisorbed O₂, reaction 4, and/or with O₂⁻ ion, reaction 7. There is a variety of evidence which implicates reaction 4 in many studies of irradiated zinc oxide

in the presence of oxygen.^{7a,b,d} Reaction 7, invoked by Fujita and Kwan in explanation of irreversible photoadsorption of oxygen in zinc oxide, is suggested to be a low temperature photochemical source of O⁻ ion; this is probably the dominant oxygen reactant when oxygen is presorbed at 200°.

According to our mechanism choice, an association of a "hole"-captured carbon monoxide molecule and O₂⁻ and/or O⁻ ions ultimately generates carbon dioxide through the reactions 5, 6, and 8. Presumably, the increased rate of carbon dioxide formation in experiments with oxygen presorption at 200° reflects the importance of the O⁻ reactant and reaction 8 for these conditions.

Apparently unique to this study is the observation of the complicated form of the time dependence of carbon dioxide formation; see Fig. 2 and 3. For our conditions, the amount of carbon dioxide found in the photooxidation using very short exposures is greater than that from extended exposures. Either some intermediate which gives carbon dioxide in short runs reacts in an alternative fashion to lead to other products in long runs, or carbon dioxide formed initially is removed by further reactions. The latter alternative seems unlikely since pure gaseous carbon dioxide when present in the low pressure range involved in the photochemical runs shows no photoadsorption which would be necessary if this effect were the origin of the maximum in the yield curves. Hence the failure to generate some carbon dioxide in long runs must be associated with the reactions involving oxygen and carbon monoxide; reactions 5, 6, 9, 10, and 11 are possible origins of these effects. For our mechanism to fit the observed rate dependence, the thermal reaction (6) must be slow; specifically, it must not occur appreciably during the time of the very short exposures, 5–15 sec., but it must occur largely during the 30-min. dark period of carbon monoxide circulation and carbon dioxide collection which followed each exposure period. According to our mechanism, the development of less carbon dioxide in the runs of longer exposure results because of the depletion of the oxygen reactant; the CO₃ intermediate, which in the shorter runs would develop carbon dioxide in the slow reaction 6 following the run, now competes successfully with oxygen for electrons, and the relatively more stable CO₃⁻ and CO₃²⁻ ions now form. It will be noted that in the extended photolyses the net yield of carbon dioxide seems to approach that of the short runs; see Fig. 2 and 3. This is consistent with the operation of reaction 10 which regenerates carbon dioxide through the continued action of the light,

(13) J. H. deBoer, *Advan. Catalysis*, **8**, 140 (1956).

forming the reactant $\text{CO}^+(\text{ZnO})$, which eventually interacts by (10) to re-form carbon dioxide. Consistent with the formation of the intermediate CO_3 , CO_3^- , and CO_3^{-2} entities in this system is the recovery of small amounts of carbon dioxide during the degassing treatment at 400° following photochemical runs; the gas may arise from the decomposition of the carbonate species which had formed photochemically at the surface. The postulation of the participation of CO_3 in the thermal catalyzed oxidation and the photooxidation of carbon monoxide is not uncommon, but the suggestion of an appreciable lifetime to this species seems new and somewhat unexpected; further experiments with electron spin resonance to test this hypothesis are planned. The fact that the observations here reported have not been found previously may be a consequence of the different catalyst surface preparations used; however, we feel that it is more likely that our reaction conditions are such as to minimize the availability of the good electron acceptor, O_2 , and to allow the reactions other than carbon dioxide formation by the intermediate CO_3 .

The limiting amount of carbon dioxide formed in these experiments corresponds to the ultimate production of one carbon dioxide molecule for every 4 \AA^2 of planar surface irradiated. The total area of the sample to that which is irradiated is at least 3×10^3 . Since the surface coverage by oxygen molecules is low, about one molecule per $100\text{--}500 \text{ \AA}^2$ (see data of Fig. 8), the seemingly high yield of carbon dioxide suggests that the actual surface area which receives radiation is much higher than the planar area of the cell faces (because of the irregular nature of the surface, high incidence angles, etc.) and/or the migration of reactants, adsorbed oxygen, holes, etc., occurs over appreciable distances.

The initial rate data of Fig. 7 show that at low intensities of absorbed light of wave lengths less than 4000 \AA ., there is a quantum efficiency of carbon dioxide formation greater than 0.1 and, within a great uncertainty in the extrapolation to zero time, probably near unity for the initial yield at the lowest intensities employed. Thus the experiments show that a photosensitized reaction of near maximum quantum efficiency (for nonchain processes) can occur on irradiated zinc oxide when there is a significant concentration of carbon monoxide (about 100 mm. pressure) present with presorbed oxygen at intensities below 10^{16} quanta/ $\text{cm}^2 \text{ sec}$. of wave lengths less than 4000 \AA .

Possible Significance of These Results in Evaluation of the Contribution of Oxidations Photosensitized on the Surface of Solids to the Chemistry of the Polluted Atmosphere. The results suggest that oxidation reactions may be sensitized with a quantum efficiency near unity for

solids in contact with relatively large concentrations of oxidizable reactant. To extrapolate these data to conditions prevailing in the polluted atmosphere is largely speculative, since the exact nature (chemical composition and size) of the compounds of iron, lead, etc., exhausted into the atmosphere is not clear at present, and their facility to photosensitize oxidation reactions is not predictable. If the compounds of lead contain the halides and oxides in large part, as seems reasonable from the data available, then photochemical activity of the particulates is likely. In any case it is unlikely that these solids would be more efficient than zinc oxide in these processes for the same wave length region (less than 4000 \AA .); however, they may absorb over a wider region of the solar spectrum and thus might have a higher participation than calculations based on zinc oxide would indicate. With certain assumptions we may derive an estimate of the maximum effects. If we assume that the efficiency of the reactions is comparable to that of zinc oxide, that the linear dependence of the reaction rate on oxidizable reactant observed here holds to the p.p.m. range, that the inorganic solid is present to the extent of 10 \mu g./m^3 , it is of density 10 and average radius 0.25 \mu , and that an absorption only in the $3000\text{--}4000 \text{ \AA}$. region occurs, then following Leighton¹ we would estimate that about 4×10^8 effective quanta/ $\text{cm}^3 \text{ sec}$. will be absorbed by the particles for a zenith angle of 45° . This corresponds to a maximum rate of oxidation of oxidizable matter (such as CO) of 0.003 p.p.h.m./hr. at the 100 p.p.m. level of oxidizable material, 0.0003 p.p.h.m./hr. at 10 p.p.m., and 0.00003 p.p.h.m./hr. at 1 p.p.m. These rates would be increased by factors of two and four if the photosensitive range of the catalyst extended to the 4500 and 5000 \AA . region, respectively. For the conditions stated the rates of such reactions would be negligible compared to others known to occur in these systems. However, if the solid photosensitizer has been loaded with oxidizable material at high pressures (as may occur with lead compounds during the process of combustion), and if this adsorbed layer was maintained for an appreciable period following the exhaust cycle, then the rates of oxidation could approach 6 p.p.h.m./hr. for 3000–4000- \AA . sensitive catalyst, 12 p.p.h.m./hr. for 3000–4500- \AA . sensitive material, and about 24 p.p.h.m./hr. for 3000–5000- \AA . sensitive material present at 10 \mu g./m^3 and subject to the other conditions stated above. These rates are significant, of course, but the chance of having the conditions which are necessary for the higher predictions to hold is extremely low. In view of the present information we conclude that oxidations photosensitized on inorganic particulate matter in the atmosphere are probably of minor importance in the usual

polluted atmosphere. Until more precise information on the nature of the inorganic compounds present in the atmosphere is at hand further speculation is unwarranted.

Acknowledgment. The authors are grateful for the support given this work by grants from the Division of Air Pollution, Bureau of State Services, U. S. Public Health Service, and the National Science Foundation.

Frictional Coefficients for Binary and Ternary Isothermal Diffusion

by Peter J. Dunlop

*Department of Physical and Inorganic Chemistry, University of Adelaide, Adelaide, South Australia
(Received May 2, 1968)*

Starting from a general set of flow equations, relations are deduced which define a set of frictional coefficients for isothermal multicomponent diffusion. These relations are essentially identical with those previously proposed by Lamm, Onsager, Klemm, Laity, and Bearman. Equations are then derived which permit these frictional coefficients to be computed for binary and ternary diffusion from experimental values of diffusion coefficients and corresponding thermodynamic data.

In the past two decades, means of describing multicomponent isothermal diffusion in terms of experimentally measurable diffusion coefficients have been suggested.¹⁻⁴ The diffusion coefficients which appear in one of the above sets of generalized flow equations¹ have been measured for several ternary systems⁵⁻¹² and used, together with the pertinent thermodynamic data, to test the Onsager reciprocal relation (ORR) for ternary isothermal diffusion.⁹⁻¹³ Diffusion in multicomponent systems may also be described in terms of sets of frictional coefficients^{4,14-18} which cannot be measured directly but which, unlike the experimental diffusion coefficients, are independent of the coordinate system of measurement.

It is the purpose of this paper to deduce from a set of generalized flow equations a corresponding set of relations which define frictional coefficients for multicomponent diffusion. These relations are essentially identical with those proposed by Lamm,¹⁴ Onsager,² Klemm,¹⁶ Laity,¹⁷ and Bearman.¹⁸ It is also proposed to derive relationships which enable the frictional coefficients for binary and ternary isothermal diffusion to be computed from experimentally measurable

diffusion coefficients and corresponding thermodynamic data.

- (1) R. L. Baldwin, P. J. Dunlop, and L. J. Gosting, *J. Am. Chem. Soc.*, **77**, 5235 (1955).
- (2) L. Onsager, *Ann. N. Y. Acad. Sci.*, **46**, 241 (1945).
- (3) O. Lamm, *Arkiv Kemi, Mineral., Geol.*, **18B**, No. 2 (1944).
- (4) O. Lamm, *J. Phys. Chem.*, **61**, 948 (1957).
- (5) P. J. Dunlop and L. J. Gosting, *J. Am. Chem. Soc.*, **77**, 5238 (1955).
- (6) I. J. O'Donnell and L. J. Gosting, "The Structure of Electrolytic Solutions," W. J. Hamer, Ed., John Wiley and Sons, Inc., New York, N. Y., Chapman and Hall, London, 1959.
- (7) P. J. Dunlop, *J. Phys. Chem.*, **61**, 994 (1957).
- (8) P. J. Dunlop, *ibid.*, **61**, 1619 (1957).
- (9) P. J. Dunlop, *ibid.*, **63**, 612 (1959).
- (10) L. A. Woolf, D. G. Miller, and L. J. Gosting, *J. Am. Chem. Soc.*, **84**, 317 (1962).
- (11) R. P. Wendt, *J. Phys. Chem.*, **66**, 1279 (1962).
- (12) P. J. Dunlop and L. J. Gosting, *ibid.*, **63**, 86 (1959).
- (13) D. G. Miller, *ibid.*, **63**, 570 (1959).
- (14) O. Lamm, *Acta Chem. Scand.*, **11**, 362 (1957).
- (15) S. Ljunggren, *Trans. Roy. Inst. Tech., Stockholm*, **172**, 1 (1961).
- (16) A. Klemm, *Z. Naturforsch.*, **8a**, 397 (1953).
- (17) R. W. Laity, *J. Phys. Chem.*, **63**, 80 (1959).
- (18) R. J. Bearman, *ibid.*, **65**, 1961 (1961).

Frictional Coefficients for Multicomponent Isothermal Diffusion. Consider a system consisting of $(q + 1)$ nonreacting components numbered $0, 1, \dots, q$ where 0 denotes the solvent. Assume that the flow due to diffusion of each component, $(J_i)_S$, relative to a frame of reference, S, is given by the general relation

$$(J_i)_S = \sum_{k=0}^q (L_{ik})_S X_k \quad (i = 0, 1, \dots, q) \quad (1)$$

where the $(L_{ik})_S$ are phenomenological coefficients for the frame of reference S and the X_k are the forces causing relative motion in isothermal diffusion and are defined by¹⁹

$$X_k = -(\partial\mu_k/\partial x)_{T,P} \quad (2)$$

where

$$\mu_k = \mu_k^\circ + RT \ln C_k y_k \quad (2a)$$

The μ_k are component chemical potentials, the μ_k° are the chemical potentials for the standard states, R is the gas constant, T is the absolute temperature, P is the pressure, the C_k are component concentrations in moles per cc., and the y_k the corresponding activity coefficients. Here we choose to consider flows in moles of a given component crossing one square centimeter in one second in the x direction only. The forces, X_k , are related by the Gibbs-Duhem relation

$$\sum_{k=0}^q C_k X_k = 0 \quad (3)$$

We note that the $(J_i)_S$ are not independent because they are measured with respect to a frame of reference S defined by

$$\sum_{i=0}^q w_i (J_i)_S = 0 \quad (4)$$

where the w_i are weighting coefficients, the values of which fix the frame of reference.²⁰ Because of eq. 3 and 4, all the phenomenological coefficients, $(L_{ik})_S$, the values of which depend on the frame of reference chosen, are not defined.

We now wish to modify eq. 1 so as to introduce a set of phenomenological coefficients which are independent of all the frames of reference defined by eq. 4. This aim may be achieved by taking differences of flows. Equation 1 is written for component j and then multiplied by (C_i/C_j) to give

$$\frac{C_i}{C_j} (J_j)_S = \sum_{k=0}^q \frac{C_i}{C_j} (L_{jk})_S X_k \quad (5)$$

Subtracting eq. 5 from eq. 1 and rearranging yields

$$[C_j(J_i)_S - C_i(J_j)_S] = \sum_{k=0}^q [C_j(L_{ik})_S - C_i(L_{jk})_S] X_k \quad (6)$$

However, each flow may be expressed as the product of a concentration, C_i , and a corresponding diffusion velocity, $(v_i)_S$, measured with respect to the frame of reference S

$$(J_i)_S = C_i(v_i)_S \quad (7)$$

Combining eq. 6 and 7 then yields

$$C_i C_j [(v_i)_S - (v_j)_S] = \sum_{k=0}^q [C_j(L_{ik})_S - C_i(L_{jk})_S] X_k \quad (8)$$

where the coefficients of the dependent forces, X_k , in eq. 8 are now *independent* of the frame of reference S since velocity *differences* appear on the left-hand side of the equation.

Equation 8 contains $(q + 1)^2$ relations, $(q + 1)$ of which are trivial (when $i = j$) and $[q(q + 1)/2]$ of the remaining relations are identical (when i and j are interchanged). Thus $[q(q + 1)/2]$ nontrivial relations ($i \neq j$) are contained in eq. 8. We also note that these $[q(q + 1)/2]$ relations contain $[q(q + 1)/2]$ variables $[(v_i)_S - (v_j)_S]$, but that only $[(q(q + 1)/2) - 1]$ are independent since

$$\sum_{i=0}^q \sum_{j=0}^q [(v_i)_S - (v_j)_S] = 0 \quad (9)$$

Now, remembering the equations which restrict the various variables in eq. 8, we may formally write expressions for the individual dependent forces, X_i , in terms of quantities of the form $C_i C_k [(v_i)_S - (v_k)_S]$, and in order to keep the expressions symmetrical the trivial terms when $i = k$ may be included. The expressions for the forces take the form

$$X_i = \sum_{k=0}^q A_{ik} C_i C_k [(v_i)_S - (v_k)_S] \quad (10)$$

where the coefficients A_{ik} are *not* related to the coefficients of the X_k in eq. 8, since the latter coefficients are not all specified. Equation 8 is simply used as a guide to the form of eq. 10, which may now be rewritten

$$X_i = \sum_{k=0}^q R_{ik} C_k [(v_i)_S - (v_k)_S] \quad (11)$$

$$R_{ik} = C_i A_{ik} \quad (12)$$

(19) Here we choose to neglect the extremely small pressure gradient which must usually exist during isothermal diffusion: see ref. 20.

(20) J. G. Kirkwood, R. L. Baldwin, P. J. Dunlop, L. J. Gosting, and G. Kegeles, *J. Chem. Phys.*, **33**, 1505 (1960).

Because of eq. 3 and 9, we may adopt the convention²¹

$$R_{ik} = R_{ki} \quad (13)$$

which is particularly convenient since it leads to an expression, first derived by Miller,¹³ for testing the ORR for ternary isothermal diffusion.

Equations 11 to 13 define a set of coefficients R_{ik} which are independent of all reference frames defined by eq. 4. Because they are coefficients relating forces, X_i , to velocities, we choose to call the R_{ik} *frictional coefficients*.²² It is clear that only $[q(q+1)/2]$ frictional coefficients are necessary to specify a system of $(q+1)$ dependent forces, X_i . For a two-component system consisting of a solvent 0 and a solute 1, application of eq. 3 to eq. 11 yields $R_{01} = R_{10}$. For systems of more than two components, eq. 13 is equivalent to the assumption of microscopic reversibility^{23,24} since it leads to the ORR (see eq. 34). However, whether or not eq. 13 is valid for a particular system must, in the final analysis, be proved experimentally.

As has been previously suggested,^{2,17} it seems reasonable that any relationships between diffusion processes and macroscopic solution properties, such as viscosity, will most easily be seen if the relative motion of components during isothermal diffusion is described by the set of *frictional coefficients*, R_{ik} , or another similar set, rather than by a set of diffusion coefficients the values of which depend on the frame of reference chosen.²⁰ Whether or not a set of R_{ik} can be determined as accurately as the corresponding set of diffusion coefficients must be tested experimentally.

Frictional Coefficients for Ternary Isothermal Diffusion. The three frictional coefficients which are necessary to describe the diffusion process in a system consisting of three components (a solvent, 0, and two solutes, 1 and 2) may be related to the four measurable diffusion coefficients¹ in the following way. We first write eq. 11 in the form

$$X_1 = R_{10}C_0[(v_1)_S - (v_0)_S] + R_{12}C_2[(v_1)_S - (v_2)_S] \quad (14)$$

$$X_2 = R_{21}C_1[(v_2)_S - (v_1)_S] + R_{20}C_0[(v_2)_S - (v_0)_S]$$

The force X_0 is specified by eq. 3 and the same coefficients R_{ik} that appear in eq. 14. We now choose the frame of reference S to be the volume fixed reference frame.²⁰ This is done by identifying the coefficients w_i in eq. 4 with the partial molar volumes of each component, \bar{V}_i . Equation 4 now becomes

$$\sum_{i=0}^2 \bar{V}_i(J_i)_V = \sum_{i=0}^q \bar{V}_i C_i (v_i)_V = 0 \quad (15)$$

The $(v_i)_V$ are velocities with respect to the volume frame of reference. It is convenient to choose the volume

frame of reference because it becomes identical with the cell or experimental reference frame if the partial molar volumes of all components are independent of concentration.^{20,25} Equation 15 may now be used to eliminate $(v_0)_V$ from eq. 14 after the subscript S has been replaced by V

$$X_1 = [(C_2/C_1)R_{12} + (C_0/C_1)a_{11}R_{10}](J_1)_V + [(C_0C_1)a_{12}R_{10} - R_{12}](J_2)_V \quad (16)$$

$$X_2 = [(C_0/C_2)a_{21}R_{20} - R_{21}](J_1)_V + [(C_1/C_2)R_{21} + (C_0/C_2)a_{22}R_{20}](J_2)_V$$

where

$$a_{ik} = \delta_{ik} + (C_i \bar{V}_k / C_0 \bar{V}_0) \quad (i, k = 1, 2) \quad (17)$$

and δ_{ik} is the Kronecker delta. Equation 7 has been used to introduce the flows in eq. 16.

Now it has already been shown experimentally⁵⁻¹² that flow equations of the form

$$(J_1)_V = -(D_{11})_V (\partial C_1 / \partial x)_{T,P} - (D_{12})_V (\partial C_2 / \partial x)_{T,P} \quad (18)$$

$$(J_2)_V = -(D_{21})_V (\partial C_1 / \partial x)_{T,P} - (D_{22})_V (\partial C_2 / \partial x)_{T,P}$$

may be used to describe the flows $(J_1)_V$ and $(J_2)_V$ of components 1 and 2 in a solvent 0. Here the $(D_{ij})_V$ are diffusion coefficients for the volume frame of reference. But the forces X_i in eq. 16 are related to the concentration gradients in eq. 18 by

$$X_1 = -\mu_{11}(\partial C_1 / \partial x)_{T,P} - \mu_{12}(\partial C_2 / \partial x)_{T,P} \quad (19)$$

$$X_2 = -\mu_{21}(\partial C_1 / \partial x)_{T,P} - \mu_{22}(\partial C_2 / \partial x)_{T,P}$$

where

$$\mu_{ij} = \left(\frac{\partial \mu_i}{\partial C_j} \right)_{T,P, C_k \neq 0, j} \quad (20)$$

It is now convenient to invert eq. 19 to yield expressions which may be used to eliminate the concentration gradients from eq. 18

$$(\partial C_1 / \partial x)_{T,P} = M_{11}X_1 + M_{12}X_2 \quad (21)$$

$$(\partial C_2 / \partial x)_{T,P} = M_{21}X_1 + M_{22}X_2$$

-
- (21) G. J. Hooyman and S. R. de Groot, *Physica*, **21**, 73 (1955).
 (22) Because of the presence of the concentration factors on the right-hand side of eq. 11, it might be more appropriate to name the R_{ik} *frictional resistivities*.
 (23) L. Onsager, *Phys. Rev.*, **37**, 405 (1931).
 (24) L. Onsager, *ibid.*, **38**, 2265 (1931).
 (25) G. J. Hooyman, H. Holtan, Jr., P. Mazur, and S. R. de Groot, *Physica*, **19**, 1095 (1953).

$$M_{11} = -(\mu_{22}/\theta); \quad M_{12} = (\mu_{12}/\theta) \quad (21a)$$

$$M_{21} = (\mu_{21}/\theta); \quad M_{22} = -(\mu_{11}/\theta)$$

where $\theta = |\mu_{ij}| = (\mu_{11}\mu_{22} - \mu_{12}\mu_{21})$. Substitution of eq. 21 into eq. 18 then gives

$$(J_1)_v = -N_{11}X_1 - N_{12}X_2 \quad (22)$$

$$(J_2)_v = -N_{21}X_1 - N_{22}X_2$$

$$\begin{aligned} N_{11} &= [(D_{12})_v\mu_{21} - (D_{11})_v\mu_{22}]/\theta \\ N_{12} &= [(D_{11})_v\mu_{12} - (D_{12})_v\mu_{11}]/\theta \end{aligned} \quad (22a)$$

$$\begin{aligned} N_{21} &= [(D_{22})_v\mu_{21} - (D_{21})_v\mu_{22}]/\theta \\ N_{22} &= [(D_{21})_v\mu_{12} - (D_{22})_v\mu_{11}]/\theta \end{aligned}$$

Equations 22 may now be solved for X_1 and X_2 to yield

$$X_1 = P_{11}(J_1)_v + P_{12}(J_2)_v \quad (23)$$

$$X_2 = P_{21}(J_1)_v + P_{22}(J_2)_v$$

$$\begin{aligned} P_{11} &= -(N_{22}/Q); \quad P_{12} = (N_{12}/Q) \\ P_{21} &= (N_{21}/Q); \quad P_{22} = -(N_{11}/Q) \end{aligned} \quad (23a)$$

$$Q = |N_{ij}| = (N_{11}N_{22} - N_{12}N_{21})$$

In order to obtain expressions relating frictional coefficients to diffusion coefficients, we now equate the coefficients of $(J_1)_v$ and $(J_2)_v$ in eq. 16 and 23, giving

$$\{(C_2/C_1)R_{12} + (C_0/C_1)a_{11}R_{10}\} = P_{11} \quad (24)$$

$$\{(C_0/C_1)a_{12}R_{10} - R_{12}\} = P_{12} \quad (25)$$

$$\{(C_0/C_2)a_{21}R_{20} - R_{21}\} = P_{21} \quad (26)$$

$$\{(C_1/C_2)R_{21} + a_{22}(C_0/C_2)R_{20}\} = P_{22} \quad (27)$$

Equations 24 to 27 may then be solved for the R_{ik} ; thus

$$R_{10} = \frac{C_1(C_1P_{11} + C_2P_{12})}{C_0(C_1a_{11} + C_2a_{12})} \quad (28)$$

$$R_{12} = \frac{C_1(a_{12}P_{11} - a_{11}P_{12})}{(C_1a_{11} + C_2a_{12})} \quad (29)$$

$$R_{21} = \frac{C_2(a_{21}P_{22} - a_{22}P_{21})}{(C_1a_{21} + C_2a_{22})} \quad (30)$$

$$R_{20} = \frac{C_2(C_1P_{21} + C_2P_{22})}{C_0(C_1a_{21} + C_2a_{22})} \quad (31)$$

Equations 28 to 31 permit the frictional coefficients R_{10} , R_{12} , R_{21} , and R_{20} to be computed from measured diffusion and thermodynamic data, but $R_{12} = R_{21}$; hence

$$(a_{12}P_{11} - a_{11}P_{12}) = (a_{21}P_{22} - a_{22}P_{21}) \quad (32)$$

since

$$C_2(C_1a_{11} + C_2a_{12}) = C_1(C_1a_{21} + C_2a_{22}) \quad (33)$$

Now substitution for the P_{ij} in eq. 32 from eq. 22a and 23a yields

$$b_{11}(D_{12})_v + b_{12}(D_{22})_v = b_{22}(D_{21})_v + b_{21}(D_{11})_v \quad (34)$$

$$b_{jl} = \sum_{k=1}^2 a_{kj}\mu_{kj} \quad (34a)$$

Equation 34, which is a consequence of eq. 13, is identical with the expression, first derived by Miller,¹³ for testing the ORR for ternary isothermal diffusion when the diffusion coefficients are measured for the volume-fixed frame of reference.

Frictional Coefficients for Binary Diffusion. Frictional coefficients for binary diffusion are obtained by taking the limits of eq. 28 to 31 as C_1 and C_2 , respectively, tend to zero. The results are obtained quite easily with the aid of the following limits.²⁵

$$(D_{12})_v \rightarrow 0 \text{ as } C_1 \rightarrow 0 \quad (35)$$

$$(D_{21})_v \rightarrow 0 \text{ as } C_2 \rightarrow 0 \quad (36)$$

$$(\theta Q) \rightarrow [(D_{11})_v(D_{22})_v] \text{ as } C_1 \text{ or } C_2 \rightarrow 0 \quad (37)$$

Equation 37 may be obtained by expanding the product (θQ) and utilizing eq. 35 and 36. Thus in the limit $C_2 = 0$

$$(R_{20})_{C_2=0} = \left[\frac{\bar{V}_0}{(D_{11})_v(D_{22})_v} [C_1[(D_{22})_v\mu_{21} - (D_{21})_v\mu_{22}] + C_2(D_{11})_v\mu_{22}] \right]_{C_2=0} \quad (38)$$

$$(R_{12})_{C_2=0} = (R_{21})_{C_2=0} = \left[\frac{1}{(D_{11})_v(D_{22})_v} [C_1\bar{V}_2(D_{22})_v\mu_{11} - [(D_{11})_v\mu_{12} - (D_{12})_v\mu_{11}]] \right]_{C_2=0} \quad (39)$$

$$(R_{10})_{C_2=0} = [C_1\bar{V}_0\mu_{11}/(D_{11})_v]_{C_2=0} \quad (40)$$

The results for $C_1 = 0$ may be obtained by replacing 1 by 2 and 2 by 1 in eq. 38 to 40.

Equation 40 is the expression which relates the frictional coefficient $(R_{10})_{C_2=0}$ to the mutual diffusion coefficient $[(D_{11})_v]_{C_2=0}$ for a binary system consisting of solute 1 diffusing in a solvent 0. In this case eq. 40 may be written

$$R_{10} = [\bar{V}_0RT/D_v][1 + C_1(\partial \ln y_1/\partial C_1)]_{T,P} \quad (41)$$

where $D_v = [(D_{11})_v]_{C_2=0}$ is now the mutual diffusion coefficient for a binary system and y_1 is the solute

(26) Equations 35 and 36 have been tested experimentally; see ref. 6, 7, and 10.

activity coefficient on the concentration scale moles per cc. The above equation may be used to compute values of R_{10} for binary systems from the experimental factors on the right-hand side of the equation.

We note that knowledge of the concentration dependence of the activity coefficients for the solutes 1 and 2 in a ternary system permits $(R_{10})_{C_1=0}$, $(R_{12})_{C_2=0}$, and $(R_{20})_{C_2=0}$ to be determined as follows. If we assume that solutes 1 and 2 are both nonelectrolytes, then the logarithms of the solute activity coefficients, y_i , may be expressed by Taylor series of the form

$$\ln y_i = \sum_{j=1}^2 B_{ij}C_j + \sum_{j=1}^2 \sum_{k=1}^2 B_{ijk}C_jC_k + \dots \quad (i = 1,2) \quad (42)$$

where

$$B_{ij} = \lim_{C_1, C_2 \rightarrow 0} \left(\frac{\partial \ln y_i}{\partial C_j} \right)_{T, P, C_k \neq 0, j} \quad (42a)$$

$$B_{ijj} = \lim_{C_1, C_2 \rightarrow 0} \frac{1}{2} \left(\frac{\partial^2 \ln y_i}{\partial C_j^2} \right)_{T, P, C_k \neq 0, j} \quad (42b)$$

$$B_{ijk} = \lim_{C_1, C_2 \rightarrow 0} \left[\frac{\partial \left(\frac{\partial \ln y_i}{\partial C_j} \right)_{T, P, C_l \neq 0, j}}{\partial C_k} \right]_{T, P, C_l \neq 0, k} = B_{ikj} \quad (42c)$$

and from the B_{ij} and B_{ijk} in eq. 42 the appropriate μ_{ij} may be determined. These values together with the $(D_{ij})_v$ values then permit $(R_{10})_{C_1=0}$, $(R_{12})_{C_1=0}$, $(R_{12})_{C_2=0}$, and $(R_{20})_{C_2=0}$ to be computed by eq. 38 and 39.

Acknowledgments. The author is grateful to Dr. B. J. Steel for many helpful discussions during the course of this work and to Messrs. H. D. Ellerton and D. E. Mulcahy for checking some of the equations. This work was supported in part by a research grant from the National Institutes of Health (AM-06042-02).

On the Application of Thermodynamics and Kinetics to Some Near-Equilibrium Systems

by Milton Manes

Pittsburgh Chemical Company, Research and Development Department, Neville Island, Pittsburgh 25, Pennsylvania
(Received May 3, 1963)

Near-equilibrium systems, including steady-state and nonisothermal systems, appear to be amenable to analysis in terms of classical thermodynamics and kinetics, provided that the actively equilibrating processes in such systems are kinetically independent. In a number of cases the classical analysis (in the linear approximation) has some advantages over the phenomenological approach; it leads to specific suggestions for experiments and to straightforward criteria for judging whether the assumption of equilibrium may be properly applied to a given system. The classical analysis is applied to electrochemical systems with internal leaks, thermocells, thermocouples, electrokinetic systems, and thermal transpiration. It turns out that the nature of the nonequilibrium constraint is less important than its relation to the nature of the leakage processes; nonisothermal systems may be handled with no particular difficulty.

I. Introduction

It has been shown previously¹ that the behavior of near-equilibrium multireaction systems may be understood in terms of classical thermodynamics and kinetics. For each chemical reaction, one uses the fact that for a single reaction, in the linear approximation, the observable rate v is proportional to the thermodynamic force, A , (*e.g.*, free energy, affinity, etc.), *i.e.*

$$v = \tau A \quad (1)$$

The proportionality factor τ can be explicitly related to the equilibration velocity, or "gross" reaction rate, and thereby to the kinetics of the opposing reactions,² and is independent of the manner in which the system is perturbed from equilibrium. In extending eq. 1 to simultaneous chemical reactions, one can write, for example

$$v_1 = r_1 A_1 \quad (2)$$

$$v_2 = r_2 A_2, \text{ etc.}$$

provided that the velocities and affinities refer to the actively equilibrating reactions and that the system conforms to the postulate of Li³ in that the rate of each active reaction is completely determined by its own

affinity in the linear approximation. It has been shown¹ that the identity of the actively equilibrating reactions must in general be determined by what are essentially kinetic investigations.

We shall here be concerned with the extension of eq. 2 to multiprocess two-phase systems in which the transport of heat, matter, and/or electricity takes place between two distinct phases, and we shall place special emphasis on systems that come to a nonequilibrium steady state under some constant external constraint. As long as one can write a thermodynamic force function⁴ for each single process, we can extend eq. 2 to two-phase and multiprocess systems without requiring any new disciplines or any postulates other than the rather modest ones thus far stated.

The approach to be presented amounts to the introduction of kinetics on an equal standing with thermodynamics in the study of the nonequilibrium steady state and a reluctance to apply mysterious terminology before exhausting the possibilities of a straightforward

- (1) M. Manes, *J. Chem. Phys.*, **39**, 456 (1963).
- (2) M. Manes, L. J. E. Hofer, and S. Weller, *ibid.*, **18**, 1355 (1950).
- (3) J. C. M. Li, *ibid.*, **29**, 747 (1958).
- (4) K. G. Denbigh, "The Thermodynamics of the Steady State," John Wiley and Sons, Inc., New York, N. Y., 1951.

analysis. The advantages of this approach, aside from its simplicity, is that it leads to suggestions for further experiments and to straightforward criteria for determining whether or not the Thomson hypothesis⁵ (*i.e.*, the arbitrary separation into "reversible" and "irreversible" processes and the assumption of equilibrium for the "reversible" process) properly applies to a given system. The application of the suggested approach will be illustrated on a highly simplified example, after which its possible applications to other systems will be discussed.

The analysis to be presented resembles that of Thomson,⁵ Eastman,⁶ and Wagner⁷ in the use of classical thermodynamics, but differs in the explicit use of kinetics. It resembles an earlier analysis by Rice⁸ in the use of both thermodynamics and kinetics, but emphasizes processes rather than the "transfer units" of Rice. It uses the idea of "independent" processes as presented by Li,³ with some modifications,¹ differing in the definition of "independence" and in emphasizing the use of near-equilibrium observations and the linear approximation. Finally, although we shall use the matrix language of the phenomenological theory of irreversible thermodynamics,^{4,9} it is emphasized that this language is used for convenience, without any implication that a separate discipline is being used.

The discussion to follow will require several definitions. The term "process" will always be understood as the direct analog of a chemical reaction, in the sense that all of the changes brought about by a single process are understood to be expressible in terms of a single progress variable or a single velocity. Thus, we shall distinguish between pure electrical conductivity, which may exist as a separate process, as against the passage of electrical current when it is one of the effects of an electrochemical reaction. In the latter case the electrochemical reaction is the process, and its electrical effect has the same standing as the appearance or disappearance of each chemical constituent. We shall later see how failure to observe this sort of distinction has led to confusion.

It will be convenient to distinguish between those processes that involve more than one state variable (*e.g.*, chemical reaction, osmosis, Donnan equilibrium) and those processes that involve only a single variable (*e.g.*, pure electrical conduction). We shall refer to the former as "internally coupled" processes and to the latter as "dissipative" or "leakage" processes. For leakage processes, eq. 1 takes a particularly simple form; for example, it becomes Ohm's law for pure electrical conductivity. The utility of the distinction and the justification for expressing a relation as simple

as Ohm's law in the form of eq. 1 will become apparent later.

Finally, we note that the term "independent processes" will refer to sets of processes that are *kinetically* independent, here defined in the sense that one can in principle vary the rate of each process without varying the rates of any of the others.³ One can assume the simultaneous existence of an infinite number of such processes without violating either thermodynamics or microscopic reversibility. Therefore, we shall differ from Li³ in setting no criterion of *linear* dependence on the active processes; their number as well as their identity must in general be determined by direct observation. Although the set of active processes may be linearly independent in many cases, this must be recognized as a fortuitous consequence of the limited number of available reaction paths in a given system rather than the result of a thermodynamic limitation.

II. Kinetic Approach to Simultaneous Near-Equilibrium Processes

Before considering examples, we shall first consider how the active processes may be disclosed, using a modification of a method presented earlier.¹ In the experimental methods suggested by Li³ and by Manes¹ for finding the real processes in a given system, one expresses the observations in terms of the rates of some set of assumed "processes." The experimental information is then used to find the linear transformation that relates the real set to the assumed set. An alternative method, presented here, is to consider the rates of change of each of the extensive variables as the "flows" and the corresponding intensive variables as the "forces," without any prior assumptions as to the nature of the processes. In this language the real processes may be determined by appropriate modification of the equilibration velocities, as described in an earlier article¹; the present approach, however, is somewhat simpler, as shown in the following illustration.

Assume a homogeneous chemical system at constant temperature and pressure containing σ constituents, Q_1, \dots, Q_σ , in which the equations for m actively equilibrating reactions (processes) are

$$\sum_{i=1}^{\sigma} \nu_{ij} Q_i = 0; \quad j = 1, \dots, m \quad (3)$$

(5) W. Thomson, *Math. Phys. Papers*, **I**, 232 (1882).

(6) E. D. Eastman, *J. Am. Chem. Soc.*, **48**, 1482 (1926); **50**, 283 (1928).

(7) C. Wagner, *Ann. Phys.*, **3**, 629 (1929); **6**, 370 (1930).

(8) O. K. Rice, *J. Phys. Chem.*, **61**, 622 (1957).

(9) S. R. DeGroot, "Thermodynamics of Irreversible Processes," Interscience Publishers, Inc., New York, N. Y., 1952.

where ν_{ij} is the stoichiometric coefficient of Q_i in the j th reaction (positive for reactants, negative for products) and where the number m and the identity of the active processes remain to be determined.¹ We can consider ν_{ij} as $-dn_i/d\xi_j$ where n_i is the number of moles of Q_i and ξ_j is the progress variable of the j th reaction. The affinity A_j ($= -\Delta F_j$) of the j th reaction may be written as

$$A_j = \sum_{i=1}^{\sigma} \nu_{ij}\mu_i = \sum_{i=1}^{\sigma} \nu_{ij}\delta\mu_i \quad (4)$$

where $-\Delta F_j$ is the (negative) Gibbs free energy change for the j th reaction, μ_i the chemical potential of Q_i , and $\delta\mu_i$ its deviation from the corresponding value at equilibrium; the second equality follows from the fact that A is zero at equilibrium. If the reactions are kinetically independent, and if v_j is defined as the observable rate of the j th process acting alone, then in the linear approximation

$$v_j = r_j A_j = r_j \sum_{k=1}^{\sigma} \nu_{kj}\delta\mu_k; \quad j = 1, \dots, m \quad (5)$$

where we have used eq. 4 and changed to the index k in summing over all the constituents. Now let \dot{n}_i represent the total rate of change of the number of moles of Q_i and \dot{n}_{ij} the contribution of the j th reaction to \dot{n}_i , so that

$$-\dot{n}_{ij} = \nu_{ij}v_j; \quad -\dot{n}_i = -\sum_{j=1}^m \dot{n}_{ij} \quad (6)$$

By use of eq. 6, 5, and 4, we find

$$-\dot{n}_i = \sum_{k=1}^{\sigma} L_{ik}\delta\mu_k; \quad i = 1, \dots, \sigma \quad (7)$$

where

$$L_{ik} = \sum_{j=1}^m L_{ik}^{(j)}; \quad L_{ik}^{(j)} = r_j \nu_{ij} \nu_{kj} \quad (8)$$

According to eq. 7 and 8, each element L_{ik} in the phenomenological matrix relating the $-\dot{n}_i$ to the $\delta\mu_k$ is the sum of individual contributions $L_{ik}^{(j)}$, from each process, and each such contribution is made up of three factors: (a) r_j , which is related to the equilibration velocity of the j th reaction and therefore to its kinetics; (b) ν_{ij} (arising from eq. 6); and (c) ν_{kj} (arising from eq. 5). If now we can substantially modify r_j of the j th process to $r_j + \Delta r_j$, keeping all other r 's unchanged (using the postulate of kinetic independence), the resulting changes in the matrix elements L_{ik} will be $\Delta r_j \nu_{ij} \nu_{kj}$. This means that the changes in each row and in each column of the \mathbf{L} matrix become proportional to the set of ν_{ij} and therefore suffice to identify the j th process.¹ We have now related the \mathbf{L} matrix directly to

the stoichiometry and thermodynamics of the individual processes (by eq. 5 and 6) and to the kinetics (through the magnitudes of the r_j).²

We note that the extension of the foregoing demonstration to processes involving transport of heat, matter, and electricity is quite straightforward as long as we can write a thermodynamic force function for the individual processes. Thus for a process causing the absorption of q calories of heat at temperature T and its liberation at $T + \delta T$, we would add $(-q/T)\delta T$ to the right side of eq. 4. As Rice³ states, "heat is much like a component." Similarly, we would add a term $z\delta\phi$ for the transport of electrical charge z over the potential difference $\delta\phi$, and a term $V\delta P$ for the volume V over the pressure increment δP . We note, finally, that we have assumed no *a priori* limitation on the number of processes, and that we pay no attention to their linear dependence or independence or to the rank of the \mathbf{L} matrix, since we shall not attempt to invert it. We are now ready to consider how the foregoing ideas apply to some examples.

III. Examples

A. Concentration Cells with Internal Leaks. The preceding analysis leads to some simple but interesting results on application to a two-process system in which one process is internally coupled and the other is a dissipative or "leakage" process. Let us consider as an example a hypothetical concentration cell, which (for simplicity) we assume to be without transference. We shall describe its behavior at stationary and nonstationary states and in the presence and absence of leakage processes, largely for the purpose of later drawing analogies with other systems. The assumed system is shown schematically in Fig. 1; it consists of two electrodes of identical metal M in two half-cells containing solutions of univalent salt MA at respective activities a_I and a_{II} ($= a_I + \delta a$) which are assumed to be nearly equal. The device (B) provides ionic conductance with zero transference; the exact mechanism is not needed for our purpose. We may imagine that the electrodes can be connected to some external constant-voltage source (for example, a large battery) the terminals of which can be maintained at some desired potentials ϕ_I and ϕ_{II} , where the potential difference $\delta\phi$ ($= \phi_{II} - \phi_I$) is small. When connected to the electrodes through switches S_2 and S_3 this source behaves essentially as a potentiometer; when its potential is not in balance with the electromotive force of the cell, a small current i passes from the source to the cell, the positive direction being shown by the corresponding arrow in Fig. 1. The external circuit is assumed (again for simplicity) to have zero resistance. The example therefore rep-

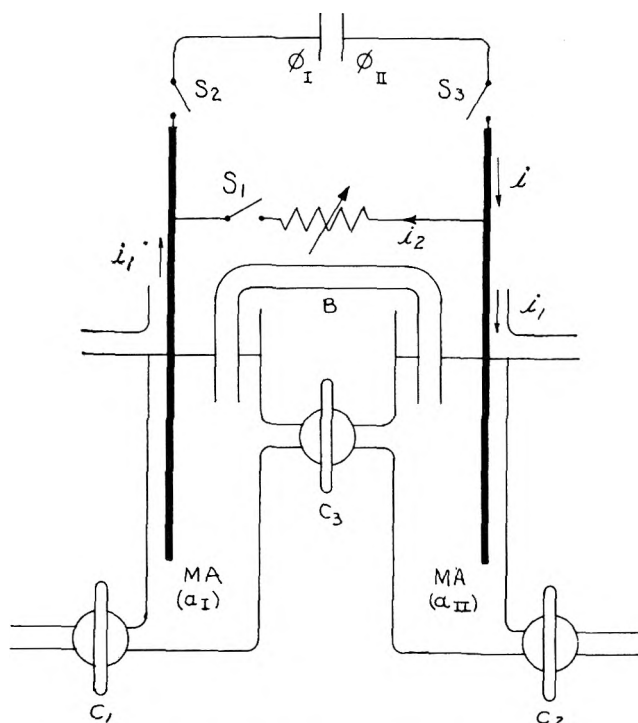


Figure 1. Concentration cell with internal leakage paths.

resents about as simple an electrochemical system as one can postulate.

We shall later wish to consider the effects of leakage processes. We introduce an electrical leak by imagining a variable resistor connected across the electrodes through a switch S_1 ; we shall consider the positive direction of current i_2 in this resistor as shown by the arrow. The current i is the sum of i_2 and the electrochemical current i_1 , that passes through the cell; we shall consider i_1 and i_2 as both being internal currents and i as the current from the source; this choice will make for easier analogies in later discussion. We can now consider the possibility of a diffusion leak, which we could introduce by (fully or partially) opening stopcock C_3 . This would allow the concentrations in the half-cells to equalize without the action of any electrochemical process or electrical leak. Finally, we may imagine that if we should operate the cell sufficiently long to affect the activity difference, we could maintain it at any desired (small) level by flushing through stopcocks C_1 and C_2 from appropriate reservoirs.

We now assume that the over-all electrochemical process consists only of (1) transfer of 1 mole of univalent solute over the (small) activity difference δa and (2) transfer of F coulombs of electricity through the cell over the (small) voltage difference $\delta\phi$. This is our internally coupled process. The electrical leakage across the electrodes through the variable resistor is

ordinary conduction and does not involve any electrochemical effect. We shall first determine the observable effects of our assumed processes and then examine how we would identify the processes from the observations.

We first write a thermodynamic force function, *e.g.*, $-\Delta F$ (joules/mole), for the electrochemical process, for example

$$-\Delta F_1 = F\delta\phi + RT\delta \ln a \quad (9)$$

with R in appropriate units. We can also redefine the units for our convenience, so long as the relative magnitudes of the two terms on the right side of eq. 9 remain invariant. Thus, we can consider that the process consists of the passage of 1 coulomb of electrical current and $1/F$ moles of solute, and we would like to measure the irreversibility of the reaction in volts. We rewrite eq. 9 to get the equally familiar equation

$$E_1 = \delta\phi + (1/F)RT\delta \ln a \quad (10)$$

where $E_1 (= \delta\phi - \delta\phi_{eq})$ is the electrochemical potential.¹⁰

Substitution of E_1 from eq. 10 for A_1 in eq. 2 now gives the rate of the electrochemical process close to equilibrium as

$$v_1 = r_1 E_1 = r_1 \delta\phi + (r_1/F)RT\delta \ln a \quad (11)$$

where r_1 is proportional (in this case, equal) to the conductivity of the cell, the external voltage source being assumed to contribute no resistance. The observable effects are the current and the mass transport effect, which are given by

$$i_1 = r_1 \delta\phi + (r_1/F)RT\delta \ln a \quad (12)$$

$$\dot{n}_1 = (r_1/F)\delta\phi + (r_1/F^2)RT\delta \ln a$$

where $i_1 (= i)$ is the electrical current between the cell and the external capacitor or battery, and where we have assumed that the electrochemical process is the only one operating (S_1 open and C_3 closed in Fig. 1).

We now have a matrix of the observations of the form of eq. 7, where the analog of ν_{11} is 1 coulomb of electricity per coulomb of process advance, ν_{21} is $1/F$ moles per coulomb of process advance, $\delta\mu_1$ is $\delta\phi$ (volts), $\delta\mu_2$ is $RT\delta \ln a$ (joules/mole), and r_1 is the electrical conductivity of the cell in reciprocal ohms. At this point we could easily collapse eq. 12 to eq. 11 because we have a single coupled process. (In DeGroot's terms,¹⁰ "the complication of the electrical potential does not give rise to cross-phenomena in this case.") We now introduce the electrical leakage

(10) See ref. 9, p. 182.

$$v_2 = r_2 \delta \phi \quad (13)$$

the effects of which are

$$i_2 = r_2 \delta \phi \quad (14)$$

$$\dot{n}_2 = 0$$

where we find that $\delta \phi$ is an acceptable thermodynamic force for this process. In order to combine eq. 12 and 14, we must use the same units for the "flows" and "forces," and r_2 turns out to be the conductivity of the leakage path, in reciprocal ohms. Noting now that our current-measuring device is assumed to measure i , the total electric current of *both* processes, we combine eq. 12 and 14 to get a matrix of the over-all "flows" and "forces"

$$i = (r_1 + r_2) \delta \phi + (r_1/F) RT \delta \ln a \quad (15)$$

$$\dot{n} = (r_1/F) \delta \phi + (r_1/F^2) RT \delta \ln a$$

Equation 15 is, like eq. 12, in the form of a phenomenological equation of irreversible thermodynamics. In this case, however, the observations do not lead uniquely to the processes.^{1,3,9}

If we are not aware of the nature of the underlying active processes we may, for example, consider the "cross-terms" to represent "interference" or "drag-coefficients"⁹ between mass transport and electrical flow, when the actual physical picture does not require these concepts. On the other hand, if we start with the idea that the observations result from the combined effects of independent near-equilibrium processes, we can identify them in this case (as outlined in section II), by experimentally varying r_2 ; the fact that only one term in the matrix is thereby affected would be evidence for an uncoupled process. Determination of r_2 and subtraction of $r_2 \delta \phi$ from the matrix eq. 15 would then give eq. 12, which would be recognized as the matrix of a single coupled process by the fact that it is now collapsible to eq. 11. This would complete the identification of the processes. In general, we could not get a unique answer by mathematical analysis alone, even for as simple a case as this one. However, if in our assumed system we are aware of the "leakage" process but not interested in determining its rate, we can still determine the nature of the coupled process by measuring the "flows" at $\delta \phi = 0$ (*i.e.*, with the electrodes short-circuited), under which circumstances the rate of the leakage process is identically zero.

Consider now the stationary state of our assumed two-process system. We now maintain one state variable under a constant constraint and let the other find its stationary value by action of both processes. For

example, we may isolate the half-cells from any external source of fresh solution (C_1 and C_2 closed in Fig. 1), connect the electrodes to the constant voltage source, and allow the concentration difference to find a stationary value. Alternatively, we may remove the voltage source (S_2 and S_3 open in Fig. 1) and maintain the concentration difference in the half-cells at some (small) fixed value, in which case the potential difference across the electrodes would (in this case very rapidly) reach its stationary value. We shall find it useful to distinguish between the constrained variable and the unconstrained variables, and we shall find that the simpler situation to analyze is the one in which the leakage process is associated with the constrained variable. Let us therefore consider first the case where $\delta \phi$ is held constant. If we applied a constant $\delta \phi$ to a system initially at equilibrium, we would expect δa to change as a consequence of the coupled process, and (by Le Chatelier's principle) in the direction of reducing v_1 , until finally

$$v_1 = r_1 \delta \phi + (r_1/F) RT \delta \ln a = 0 \quad (16)$$

i.e., in the electrochemical process the imposed potential difference becomes balanced by the concentration difference. For the second process we apply Ohm's law in the form

$$v_2 = r_2 \delta \phi \quad (17)$$

The perturbation of the two state variables ($\delta \phi$ and $\delta \ln a$) of the internally coupled process so that its rate remains zero is equivalent to its going to a neighboring equilibrium. Therefore, the internally coupled process is at a true state of equilibrium, and

$$RT \frac{\delta \ln a}{\delta \phi} = -F \quad (18)$$

for all values of r_2 . A re-examination of our simple case shows that it can be extended to other two-process systems where the single internally coupled process involves more than two state variables. Moreover, there seems to be no immediate reason why the same analogy should not be applied to a system where the constraint is a temperature difference and the leakage process a heat leak. This would suggest why the assumption of thermodynamic equilibrium in stationary, internally coupled nonisothermal processes (so-called "pseudo-thermostatic" methods⁹) with disregard of the heat leakage process turns out to be exact, and would account for the agreement with experiment of the analyses of, for example, Wagner⁷ and Eastman⁸ (which DeGroot⁹ finds "amazing").

Let us now consider the stationary state of our assumed example when the leakage process involves the

unconstrained variable. Consider our example where we now maintain a constant activity difference, for example by flowing fresh solution through each half-cell with no external source of electricity. (C_1 and C_2 open, S_2 and S_3 closed in Fig. 1.) In this case $i = 0$ at the stationary state (since there is no current flow to or from an outside source) but since neither v_1 nor v_2 is zero, the electrical currents, i_1 and i_2 , of the electrochemical process and of the leakage process are equal and opposite. We can express the v 's at the stationary state in terms of the constraint $RT\delta \ln a$ by solving for $\delta\phi$ in the (upper) eq. 15, *i.e.*

$$\delta\phi = -\frac{r_1}{r_1 + r_2} \frac{1}{F} RT\delta \ln a \quad (19)$$

whence, by substitution in eq. 11 and 13

$$v_1 = \frac{r_1}{F} \left[\frac{-r_1}{r_1 + r_2} + 1 \right] RT\delta \ln a \quad (20)$$

$$v_2 = \frac{r_1}{F} \left[\frac{-r_2}{r_1 + r_2} \right] RT\delta \ln a \quad (21)$$

and $v_1 + v_2 = 0$.

In this case the coupled process is *not* at equilibrium at the stationary state and we could *not* calculate the stationary voltage difference from thermodynamics alone. It would be best to have an independent determination of r_1 and r_2 , since they would relate explicitly to the underlying processes. Lacking this, we could determine the ratio $r_1/[F(r_1 + r_2)]$ from relations derived from eq. 15, *i.e.*

$$\frac{r_1}{[F(r_1 + r_2)]} = -(RT)^{-1}(\delta\phi/\delta \ln a)_{i=0} = (\dot{n}/i)_{\delta \ln a = 0} \quad (22)$$

provided we had sufficient independent justification for the real processes.

We now consider an additional leakage process, *i.e.*, leakage by diffusion through some path between the half-cells, without electron transfer (C_3 open in Fig. 1). The matrix of observations now takes the form

$$i = (r_1 + r_2)\delta\phi + \left(\frac{r_1}{F}\right) RT\delta \ln a \quad (23)$$

$$\dot{n} = \frac{r_1}{F} \delta\phi + \left(\frac{r_1}{F^2} + r_3\right) RT\delta \ln a$$

where r_3 reflects the equilibration velocity of the new leakage process. (We note in passing that we have three independent processes for only two state variables.) If we constrained the voltage to produce a stationary state, we would find $\dot{n} = 0$, where \dot{n} would be the resultant effect of v_1 and v_3 . We note, further, that the

magnitude of the electrical leakage would not affect the value of $RT(\delta \ln a/\delta\phi)$ at the stationary state, this being determined now by the nature and the rates of the two processes involving \dot{n} .

The foregoing example illustrates how the explicit consideration of the individual processes enables us to make specific assumptions about them and to express the consequences of these assumptions in a form amenable to experimental test. It shows, moreover, that we can apply purely thermodynamic criteria only under certain limited circumstances. We shall now draw analogies between this example and other nonequilibrium phenomena.

B. The Thermocell. Having noted that the concentration cell with internal leaks involves no essentially new principles, we now consider thermal effects. We assume that the electrochemical process just described causes q calories of heat to be liberated in half-cell I and an equal amount of heat to be absorbed in half-cell II. We now consider the possibility that the respective half-cells are maintained at absolute temperatures T_I and T_{II} by contact with appropriate heat reservoirs. The thermodynamic force for the (single) electrochemical process now becomes

$$-\Delta F = F\delta\phi + RT\delta \ln a + (q/T)\delta T \quad (24)$$

where $\delta T = T_{II} - T_I$. We first note that if $\delta T = 0$ the contribution of the heat of transport q to the over-all thermodynamic force is identically zero. This is no different from the other terms on the right side of eq. 24; the contributions of mass transport and of charge transport also become zero at $\delta \ln a = 0$ and $\delta\phi = 0$, respectively. The incorporation of the heat of transport into the over-all thermodynamic force therefore involves no nonclassical assumptions. One suspects that sources of difficulty in accepting the heat of transport as a purely thermodynamic quantity on the same standing as what one could call "charge of transport" or "mass of transport" are: (a) constrained temperature differences are less familiar than constrained differences in electrical potential and in activity; (b) constrained temperature differences are always accompanied by heat leaks; (c) heats of transport are hard to measure by direct observation. As we have seen, however, the writing of a thermodynamic force to include thermal effects in half-cells is quite straightforward, and the "cross-effects" that one observes when the process is operating are readily understood.

It should be noted that the heat of transport, q , as used here is a purely thermal quantity; it is the heat that would be observed by direct measurement on the half-cells. Denbigh¹¹ has made this point in discussing

the Soret effect. The attribution of kinetic implications to the heat of transport^{12,13} is correct only when the mechanism is such that the activation energy and the heat of transport are identical. This could be checked experimentally by comparing the heat of transport q with the activation energy of the process as determined by the temperature coefficient of the (isothermal) equilibration velocities.

We can now justify the treatment by Eastman⁶ of the thermocell by setting $\delta \ln a = 0$ in eq. 24 and noting that the electrochemical process (or what we could call the "electrothermochemical" process) is at true equilibrium under a nonisothermal constraint when the leakage process is a heat leak. The analogy with eq. 18 is quite straightforward. Furthermore, one can readily extend the treatment to the case where we have a non-zero $\delta \ln a$ or additional leakage processes. The addition of kinetics therefore not only justifies Eastman's analysis but allows one to consider more complicated cases that would be outside its scope.

C. *The Thermocouple.* Here we recognize that the internally coupled process consists of the transfer of electricity and the concomitant absorption and evolution of heat (Peltier heat) at the junctions. For this process the free energy change may be written

$$-\Delta F = (q/T)\delta T - \delta\phi \quad (25)$$

where q is the Peltier heat absorbed (joules/coulomb) at the higher temperature and $\delta\phi$ is the electrical potential difference in volts. If we apply the temperature constraint, δT , then even in the presence of a heat leak along the thermocouple the internally coupled process is at true equilibrium and we get the well known Thomson relation

$$\frac{\delta\phi}{\delta T} = \frac{q}{T} \quad (26)$$

(For small perturbations we can exclude the Thomson heat, which is a second-order effect.) The accuracy of the Thomson relation and its well known indifference to heat leakage appear as a natural consequence of the nature of the processes, irrespective of the detailed mechanisms.

D. *Electrokinetics.* In electrokinetic systems we find that the effects described by DeGroot¹⁴ could all be rather simply accounted for on the basis of an internally coupled process in which passage of one mole of liquid through a diaphragm carries z coulombs of electric charge, together with a leakage process in which liquid flows through the diaphragm under the pressure difference without carrying any charge. The forces and rates for the two assumed processes may be written

$$v_1 = r_1(-\Delta F_1) = r_1(z\delta\phi + V^*\delta P) \quad (27)$$

$$v_2 = r_2\delta P$$

where V^* is $dV/d\xi_1$ at the high-pressure side (ξ_1 being the corresponding progress variable), and the directions and the units of v_1 , v_2 , $\delta\phi$, and δP ¹⁵ are suitably chosen. The observable effects are an electrical current and a volume flow, which are written as

$$i \equiv I = zv_1 \quad (28)$$

$$\dot{V} \equiv J = V^*v_1 + v_2$$

The matrix of "flows" and "forces" now becomes

$$I = r_1z^2\delta\phi + r_1zV^*\delta P \quad (29)$$

$$J = r_1zV^*\delta\phi + (r_1V^{*2} + r_2)\delta P$$

from which we can immediately get the relations

$$\left(\frac{I}{J}\right)_{\delta\phi=0} = -\left(\frac{\delta P}{\delta\phi}\right)_{J=0} = \frac{z}{V^*} \left[\frac{r_1}{r_1 + r_2/V^{*2}} \right] \quad (30)$$

$$\left(\frac{I}{J}\right)_{\delta P=0} = -\left(\frac{\delta P}{\delta\phi}\right)_{I=0} = \frac{z}{V^*}$$

The analogy to the electrochemical cell with a current leak should be obvious.

The first equalities in eq. 30 represent the symmetry properties of the Onsager¹⁶ relations; they are discussed, for example, by DeGroot¹⁴ and by Prigogine.¹⁷ They have the advantages and the disadvantages of being equally true for real and artificial representations of the underlying processes. The second equalities in eq. 30 represent a particular description of the assumed process that is not derivable from the Onsager relations (since other assumptions would work equally well) and that may be correct or incorrect, but that in any event is subject to experimental verification. The physical description, if true, gives considerable additional information. For example, we would have a relation between $(I/J)_{\delta\phi=0}$ and $(I/J)_{\delta P=0}$, which the cited phenomenological treatments do not consider at all.

(11) K. G. Denbigh, *Trans. Faraday Soc.*, **48**, 1 (1952).

(12) K. S. Pitzer, *J. Phys. Chem.*, **65**, 147 (1961).

(13) R. A. Oriani, *J. Chem. Phys.*, **34**, 1773 (1961).

(14) See ref. 9, p. 185 ff.

(15) It would be easier in the subsequent treatment to write v_2 as $r_2V^*\delta P$, i.e., to measure our leak rate in units of V^* . This might imply, however, that there is some physical significance to using V^* in the leakage process, for which there is no justification.

(16) L. Onsager, *Phys. Rev.*, **37**, 405 (1931); **38**, 2265 (1931).

(17) I. Prigogine, "Thermodynamics of Irreversible Processes," C. C. Thomas, Springfield, Illinois, 1955.

Moreover (as we have seen in our earlier example), if we do have an internally coupled process and a volume leak, the internally coupled (electrokinetic) process is at true equilibrium when a stationary state is maintained by a pressure constraint, in which case we use eq. 26 to determine z/V^* , the charge transfer per unit volume transfer of the electrokinetic process. Finally, the suggested description appears to be more easily visualized than the many alternative representations given, for example, by DeGroot¹⁴ (who considers that four effects exist: two streaming effects and two osmotic effects) or by Prigogine,¹⁷ who states "we have here two irreversible effects, transport of matter under the influence of a difference in pressure and electrical current due to the difference of electrical potential. Moreover, we have a cross-effect related by the coefficients $L_{12} = L_{21}$ which is due to the interference of the two irreversible processes."

E. Thermal Transpiration. Thermal transpiration appears to be an example where there can be leakage in both the constrained and the unconstrained variables. The stationary pressure difference developed when two gas-containing vessels with a sufficiently fine capillary connection are maintained at different temperatures is given by the Knudsen equation

$$P_2/P_1 = (T_2/T_1)^{1/2} \quad (31)$$

which is discussed in some detail by DeGroot¹⁸ and by Prigogine.¹⁹ The prediction of the pressure difference when the capillary connection is enlarged has been a problem of some difficulty; its decrease has been rationalized,¹⁹ although not quantitatively, on the basis that the heat of transport, Q^* , changes with the size of the capillary. An alternative explanation suggested here is that we have in such cases an internally coupled process (diffusion) and a leakage process, the latter being the bulk leakage of gas from high to low pressure under the pressure head. The rates of the two processes may be written

$$v_1 = r_1(\delta \ln P - 1/2\delta \ln T) \quad (32)$$

$$v_2 = r_2\delta P = r_2P\delta \ln P$$

where now the thermodynamic force for the first process comes directly from the Knudsen equation. As we have seen, neither of the two processes is at zero rate at a stationary state under the constraint of a temperature difference because the leak is driven by pressure, and we may ignore the heat leakage. We have, therefore

$$v_1 + v_2 = 0 \quad (33)$$

whence

$$\frac{\delta \ln P}{\delta \ln T} = \frac{1}{2} \frac{r_1}{r_1 + r_2P} \quad (34)$$

which reduces to eq. 31 when $r_1 \gg r_2$. This would occur as the bore of the capillary is reduced, since the diffusion rate decreases as the square of the diameter and the leakage rate as the third to fourth power, depending on pressure.

To subject the preceding picture to an experimental test, one could determine the value of r_1 for a series of capillaries by measuring the rate of pumping when the system is operated as a thermomechanical pump, with no pressure gradient. The value of $(r_1 + r_2)$ could then be determined on the same capillaries by measuring the combined rates of leakage and diffusion under a pressure difference at comparable pressure, in the absence of a thermal gradient. The determination of r_1 and r_2 should now account for $\delta P/\delta T$ over a range of capillary bores in terms of measurable quantities.

IV. Conclusion

Application of classical analysis to near-equilibrium systems requires that thermodynamics and kinetics be assigned approximately equal weight. It is important to recognize that the actively equilibrating processes are the natural units in which to describe the system,³ and to make a clear distinction between the active processes and their stoichiometric equivalents. Once this is recognized, the "cross-effects" of phenomenological theory lose their mystery. It then becomes important to note that the number and identity of the active processes can be determined only by direct observation,¹ and that they can be found through kinetics experiments. Once the idea of a process is properly clarified, we are able to consider leakage processes as distinct entities and, by specific consideration of their rates, to disentangle their effects from those of the internally coupled processes. The recognition of heat leaks as separate processes helps to remove some of the hindrances to considering nonisothermal systems on the same basis as constrained isothermal systems. Finally, although it is not yet certain that the classical approach will be applicable to all systems, some optimism on its further applicability appears to be justified.

(18) See ref. 9, p. 26.

(19) See ref. 17, p. 71.

The Reaction of Active Nitrogen with Graphite

by Harold W. Goldstein¹

Union Carbide Research Institute, Tarrytown, New York (Received May 31, 1963)

The reaction of microwave-activated nitrogen with graphite was studied in the temperature range 1694 to 2365°K. Cyanogen, hydrogen cyanide, and carbon dioxide were the reaction products condensed in traps at liquid nitrogen temperature. Activation energies of 17.6 ± 0.9 kcal. mole⁻¹ and 19.2 ± 2.7 kcal. mole⁻¹ were calculated for the production of cyanogen with TSX graphite and AGOT graphite, respectively. The production of hydrogen cyanide and carbon dioxide is ascribed to the presence of impurities in the nitrogen and graphite.

Introduction

Recently, two studies of the reaction of dissociated gases with graphite have been reported.² Zinman investigated the reaction of carbon with a mixture of active nitrogen and hydrogen at 800° and found that hydrogen cyanide was the principal reaction product. In Giberson's study the graphite was maintained in the discharge region; paracyanogen was produced along with some hydrogen cyanide. In both investigations little care was taken in the outgassing of the graphite.

This study is the first in which the graphite was carefully outgassed and also the first in which the reaction was investigated as a function of the graphite temperature (1694 to 2365°K.). Cyanogen, hydrogen cyanide, and carbon dioxide were the products condensed in traps at liquid nitrogen temperature. The formation of hydrogen cyanide and carbon dioxide is shown to be due to impurities in the nitrogen and graphite.

Experimental

Apparatus and Materials. In the apparatus used, the nitrogen was passed through two liquid nitrogen-cooled traps containing Molecular Sieve 4A,³ a quartz tube containing copper turnings at 600°, and another Molecular Sieve trap at liquid nitrogen temperature. The gas then passed through a Manostat predictability flowmeter, a kerosene-cooled discharge tube, and a converging nozzle about 3 mm. in diameter, and impinged on the hot graphite surface at a distance of approximately 3 cm. from the nozzle (Fig. 1). The graphite was resistance heated by a.c. current passing through the water-cooled copper leads supporting the sample. The reactor was constructed from a 1500-cc.

quartz bulb. Between the discharge tube and the inlet nozzle, provision was made for the introduction of nitric oxide through another Manostat flowmeter. The pumping system included a liquid nitrogen trap, an oil diffusion pump, and a mechanical fore pump. Products collected in four liquid nitrogen traps immediately following the reactor were transferred to a calibrated volume and then to Pyrex break-seals for analysis by a Perkin-Elmer vapor fractometer Model 154D equipped with thermistor and flame-ionization detectors and a silica gel column. In preliminary experiments the same amounts of products were collected with only two traps as with all four.

Pressure in the system was measured with either a Consolidated Electroynamics Corp. Philips gage or a McLeod gage. The temperature of the graphite surface was measured with a Leeds and Northrup optical pyrometer, intercompared with one calibrated by the National Bureau of Standards. Temperature corrections were applied for the sight glass and for the deviation of the pyrometer from the 1948 temperature scale, but not for the emittance of the graphite. A Raytheon Microtherm Model CMD 4 unit (2450 Mc.) run at a setting of 110 watts was used to activate the nitrogen.

Samples of the specially purified nuclear grade graphites designated as TSX and AGOT⁴ were obtained

(1) Martin Company, Research Division, MP-233, Orlando, Florida.

(2) (a) W. Zinman, *Planetary Space Sci.*, 3, 46 (1961); (b) R. C. Giberson, HW-68380 UC-4, Chemistry, Office of Technical Services, Department of Commerce, Washington 25, D. C., 1961.

(3) Linde Company, Division of Union Carbide Corporation.

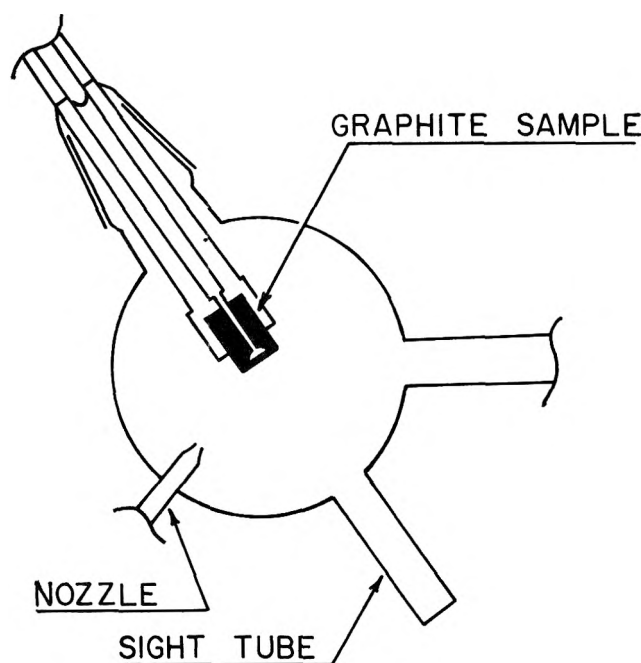


Figure 1. Schematic diagram of reactor.

from the National Carbon Company, Division of Union Carbide Corporation. The specially shaped sample (Fig. 1) had a front surface of about 1.5×1.0 cm. and was mounted in the copper holder so that a beam of active nitrogen impinged on the center of the front surface of the graphite over an apparent area about 5 mm. in diameter. This area showed no temperature differences of more than 5° , while the ends of the front surface and the sides were at least 100° cooler.

The gases used were high-purity dry nitrogen obtained from the Linde Co. and nitric oxide from the Matheson Co. Hydrogen cyanide, prepared by the reaction of sodium cyanide and sulfuric acid, and Matheson cyanogen and "bone dry" carbon dioxide were used to calibrate the vapor fractometer. These three gases were trap-to-trap distilled before use; vapor fractometer analyses revealed no impurities.

Experimental Procedure. The system was evacuated to a pressure less than 10^{-5} torr and the graphite degassed by heating to at least 2050° until the system pressure was again less than 10^{-5} torr. Initial heating of the graphite yielded condensable products in the liquid nitrogen traps, but after using this degassing procedure, no detectable amount of product was collected in 1 hr. After starting the constant nitrogen flow, the temperature of the graphite was adjusted to that desired for the run and the discharge ignited. The collection period for reaction products started when the two traps nearest the reactor were simultaneously immersed in liquid nitrogen (the remaining traps were

immersed immediately following). At the end of the reaction period, the discharge was extinguished, the power to the sample terminated, and the graphite allowed to cool for approximately 10 min. with the nitrogen flowing. The system was isolated from the pumps and the condensable products transferred to the analytical manifold. The graphite was degassed in a similar manner before each run and the same piece of graphite was used repeatedly until visible erosion of the surface occurred.

The concentration of nitrogen atoms for a nitrogen flow of 0.0286 mole min.^{-1} at 1.95 torr was estimated at the jet by titration with nitric oxide.⁵ The titration was performed either before the reaction was initiated or after completion of the reaction. In several hour-long runs the nitrogen atom concentration did not change after the discharge had run approximately 2 min. Therefore, the discharge was initiated at least 5 min. before starting to collect products.

Results and Discussion

Preliminary experiments with molecular and active nitrogen showed a difference in the products collected in traps at liquid nitrogen temperature. Hydrogen cyanide and carbon dioxide were the only products collected from the reaction of molecular nitrogen and graphite, whereas in the case of the reaction of active nitrogen, cyanogen was also formed. The formation of hydrogen cyanide and carbon dioxide was a consequence, it is believed, of the presence of hydrogen, oxygen, and water impurities in the nitrogen. Indeed, direct addition of hydrogen to the nitrogen before activation increased the rate of hydrogen cyanide production by several orders of magnitude. In addition, it was found that the production of hydrogen cyanide and carbon dioxide decreased (but never quite to zero) when the nitrogen was purified before being allowed to react. The presence of small amounts of oxygen and hydrogen impurities in the nitrogen did not affect the rate of production of cyanogen.

In agreement with Stieber,⁶ no significant amount of cyanogen was collected from the reaction with purified molecular nitrogen in the temperature range up to 2365°K . (TSX graphite: Table I). The limit of detection by vapor fractometer analysis was 10^{-8} mole for cyanogen and hydrogen cyanide and 10^{-7} mole for carbon dioxide. In contrast, easily detected amounts of

(4) "The Industrial Graphite Engineering Handbook," National Carbon Company, Division of Union Carbide Corp., New York, N. Y.

(5) P. Harteck, R. R. Reeves, and G. Mannella, *J. Chem. Phys.*, **29**, 608 (1958).

(6) H. C. Stieber, unpublished communication in ref. 2a.

cyanogen were found when active nitrogen was used (TSX: Table III; AGOT: Table IV). In a special check, the rate of formation of cyanogen was constant with time (Table II).

Table I: Products Collected in 30 min. from the Reaction of TSX Graphite and Purified Molecular Nitrogen^a

Temp., °K.	C ₂ N ₂ , mole × 10 ⁶	HCN, mole × 10 ⁶	CO ₂ , mole × 10 ⁶
2212	<0.01	0.05	0.24
2365	Not detected	.02	.32
2365	Not detected	.01	.13

^a N₂ = 0.0286 mole min.⁻¹; P = 1.95 torr.

Table II: Time Dependence of the Products Collected from the Reaction of AGOT Graphite and Active Nitrogen at 2185°K.^a

Time, min.	C ₂ N ₂ , mole × 10 ⁶	HCN, mole × 10 ⁶	CO ₂ , mole × 10 ⁶
5	0.32	Not determined	Not determined
15	0.91	Not determined	Not determined
30	2.06	0.43	0.61

^a N₂ = 0.0286 mole min.⁻¹; N atom = 0.0518 × 10⁻³ mole min.⁻¹; P = 1.95 torr.

The amounts of products collected from the reaction of active nitrogen with TSX and AGOT graphite were determined as a function of the graphite temperature and the nitrogen atom concentration (Tables III and

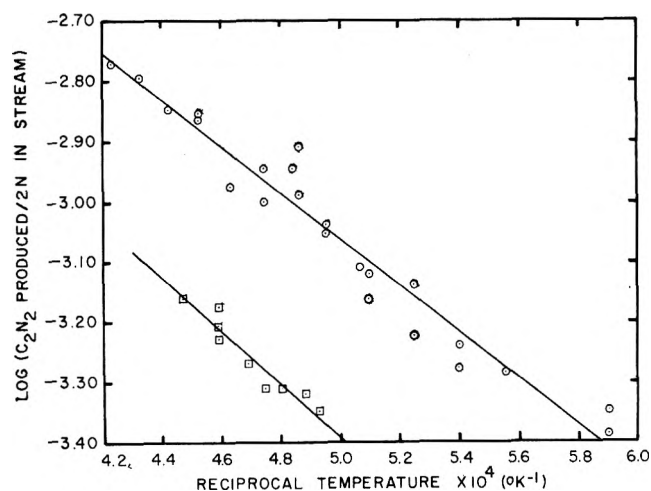


Figure 2. Arrhenius plot for the reaction of graphite and active nitrogen: ○, TSX; □, AGOT.

IV). The corresponding activation energies and entropies for the production of cyanogen, calculated from the least square lines of Fig. 2, are 17.6 ± 0.9 kcal. mole⁻¹ and -2.44 ± 0.45 cal. mole⁻¹ deg.⁻¹ for TSX and 19.4 ± 2.7 kcal. mole⁻¹ and -3.03 ± 1.26 cal. mole⁻¹ deg.⁻¹ for AGOT.

Table III: Products Collected in 30 min. from the Reaction of TSX Graphite and Active Nitrogen^a

Temp., °K.	C ₂ N ₂ , mole × 10 ⁶	HCN, mole × 10 ⁶	CO ₂ , mole × 10 ⁶	N atom, mole min. ⁻¹ × 10 ³	C ₂ N ₂ /2N × 10 ³
1694	1.34	0.12	0.24	0.0539	0.41
1694	1.46	.27	.41	.0539	.45
1800	1.64	.22	.46	.0518	.53
1853	1.85	.12	1.13	.0580	.53
1853	1.88	.12	0.25	.0539	.58
1907	1.85	.07	0.52	.0518	.60
1907	2.25	.03	1.16	.0518	.72
1963	2.13	.40	1.14	.0518	.69
1963	2.36	.10	0.41	.0518	.76
1973	2.53	.03	.29	.0539	.78
2020	2.74	.33	.50	.0518	.88
2020	2.42	.01	1.08	.0394	1.02
2058	2.83	.13	0.31	.0456	1.03
2058	3.97	.03	.33	.0539	1.23
2068	3.69	.15	.34	.0539	1.14
2109	3.22	.29	.28	.0539	1.00
2109	3.54	.13	.14	.0518	1.14
2160	3.28	.20	.21	.0518	1.06
2212	3.74	.26	.47	.0456	1.37
2212	4.8626	.0580	1.40
2263	4.61	.17	.19	.0539	1.43
2314	4.98	.17	.25	.0518	1.60
2365	5.24	.18	.24	.0518	1.69

^a N₂ = 0.0286 mole min.⁻¹; P = 1.95 torr.

Table IV: Products Collected in 30 min. from the Reaction of AGOT Graphite and Active Nitrogen^a

Temp., °K.	C ₂ N ₂ , mole × 10 ⁶	HCN, mole × 10 ⁶	CO ₂ , mole × 10 ⁶	N atom, mole min. ⁻¹ × 10 ³	C ₂ N ₂ /2N × 10 ³
2031	1.40	0.37	0.43	0.0518	0.45
2050	1.72	.52	.71	.0601	.48
2083	1.89	.45	.70	.0643	.49
2108	1.51	.32	.68	.0518	.49
2134	1.75	.41	.61	.0540	.54
2185	2.06	.43	.61	.0518	.66
2237	2.41	.48	.72	.0580	.69

^a N₂ = 0.0286 mole min.⁻¹; P = 1.95 torr.

Acknowledgments. The author wishes to acknowledge the assistance of Dr. E. T. Losin in initially developing this study, Mr. J. Burke in carrying out the experimental measurements, and Dr. W. Weltner, Jr.,

for helpful discussions. This research was sponsored by the Advanced Research Projects Agency Propellant Chemistry Office and was monitored by the Army Missile Command under Contract DA-30-069-ORD-2787.

Anhydrous Perchloric Acid: Heat Capacities and Thermodynamic Functions from 5 to 300°K.

by John C. Trowbridge and Edgar F. Westrum, Jr.¹

Department of Chemistry, University of Michigan, Ann Arbor, Michigan (Received June 3, 1963)

The thermal behavior of anhydrous perchloric acid was studied by adiabatic calorimetry and the data obtained were used as the basis for the evaluation of the thermodynamic functions. The triple point of perchloric acid occurs at 172.0°K. with an associated entropy of melting of 9.67 cal./mole °K.). At 298.15°K. the values of the heat capacity at constant pressure (C_p), the practical entropy (S°), the enthalpy function $[(H^\circ - H_0^\circ)/T]$, and the Gibbs free energy function $[(F^\circ - H_0^\circ)/T]$ are 28.80, 45.02, 23.11, and -21.91 cal./mole °K.). The fusion data conflict with the phase diagram reported by others and provide evidence that HClO_4 does exist as an independent species in the crystalline state. This conclusion is consistent with that obtained from recent infrared and Raman spectra of the solid which reveal bands similar to those of the liquid.

Introduction

Although anhydrous perchloric acid is notorious primarily as a consequence of its marked instability, methods for its preparation were described as early as 1818,² and liquid nitrogen temperatures may be used to retard decomposition.³ Several investigators⁴⁻⁷ have examined its physical properties but few thermal and thermochemical data are available.⁸ Interest in the properties of anhydrous perchloric acid evolved from consideration of the thermodynamics of the hydronium perchlorate (perchloric acid monohydrate) transition. This paper is the first in an endeavor to study the system chlorine heptaoxide-water.

Experimental

Anhydrous Perchloric Acid Sample. The sample for calorimetric investigation was prepared by the method

of Smith,³ with rigorous observation of two precautions: complete exclusion of oxidizable materials including vapor as well as condensed phase contaminants, and adequate temperature control of the distillation reservoir and other portions of the apparatus where perchloric acid vapors are present. Even the pure va-

- (1) To whom correspondence concerning this work should be addressed.
- (2) F. von Stadion, *Ann. chim. phys.*, **8**, 406 (1818).
- (3) G. F. Smith, *J. Am. Chem. Soc.*, **75**, 184 (1953).
- (4) M. Usanovich and T. Sumarokova, *Acta Physicochim. URSS*, **21**, 836 (1946).
- (5) O. Redlich, E. K. Holt, and J. Bigeleisen, *J. Am. Chem. Soc.*, **66**, 13 (1944).
- (6) R. C. Taylor and G. L. Vidale, *ibid.*, **78**, 5999 (1956).
- (7) M. Usanovich, T. Sumarokova, and V. Udovenko, *Acta Physicochim. URSS*, **11**, 505 (1939).
- (8) M. Berthelot, *Ann. chim. phys.*, **27**, 214 (1882).

per is apparently very sensitive to decomposition at slightly elevated temperatures, resulting in pollution of the product.⁹ To meet these criteria the preparation was performed in a Pyrex vacuum line containing no stopcocks or valves. Approximately 1 l. of 20–23% fuming sulfuric acid (reagent grade) was added to a 3-l. distilling flask which contained 0.26 l. of twice-distilled 70% perchloric acid. The vacuum line was then sealed, the flask cooled to 5°, and the system evacuated. At 10° and a pressure of 0.05 mm., perchloric acid was rapidly evolved and was collected as a liquid in a trap cooled with Dry Ice–2-propanol slush. The temperature of the flask was increased gradually to 50° with a heating mantle. It was subsequently sealed from the line under vacuum. An intermediate liquid nitrogen trap prevented the decomposition products formed during seal-off from contaminating the sample. The approximately 100 cc. of product obtained was twice distilled prior to the ultimate distillation into the Pyrex calorimeter liner. Fractional fusion data indicate a maximum of 2.5 mole % impurity (presumably hydronium perchlorate) by the Mastrangelo and Dornte¹⁰ method for impurities which are soluble in both the liquid and solid phases. After completion of the cryogenic investigation the sample was subjected to several chemical tests in an endeavor to determine the acid and perchlorate content. The results of conductometric titrations for both species indicated about 95 wt. % purity and substantiated visual evidence that the sample had further decomposed prior to removal from the calorimeter and that it was still spontaneously decomposing. An increasingly strong yellow sample coloration observed during the unloading deepened to dark orange as the sealed liner stood at 25° for approximately 6 hr. It is presumed that the color is probably occasioned by the presence of ozone as suggested by Smith,¹¹ or of chlorine, which is claimed to be a decomposition product of anhydrous perchloric acid by Zinov'ev and Tsentsiper.¹² Several attempts were made to identify the contaminate by infrared spectroscopy, but the impurity was too dilute to permit detection in a liquid sample and too soluble to isolate as a gas. In all probability the sample was significantly purer for the major portion of the temperature range of heat capacity studies than terminal analyses indicate.

Cryogenic Technique. The Mark III cryostat employed for these low temperature measurements resembles one reported earlier¹³ which has been more fully described by Carlson.¹⁴ Oxidizing power of the sample is such as to preclude even the use of noble metals in contact with the anhydrous perchloric acid. Silver, nickel, copper, and gold specimens subjected to the anhydrous acid at 300°K. were readily oxidized as

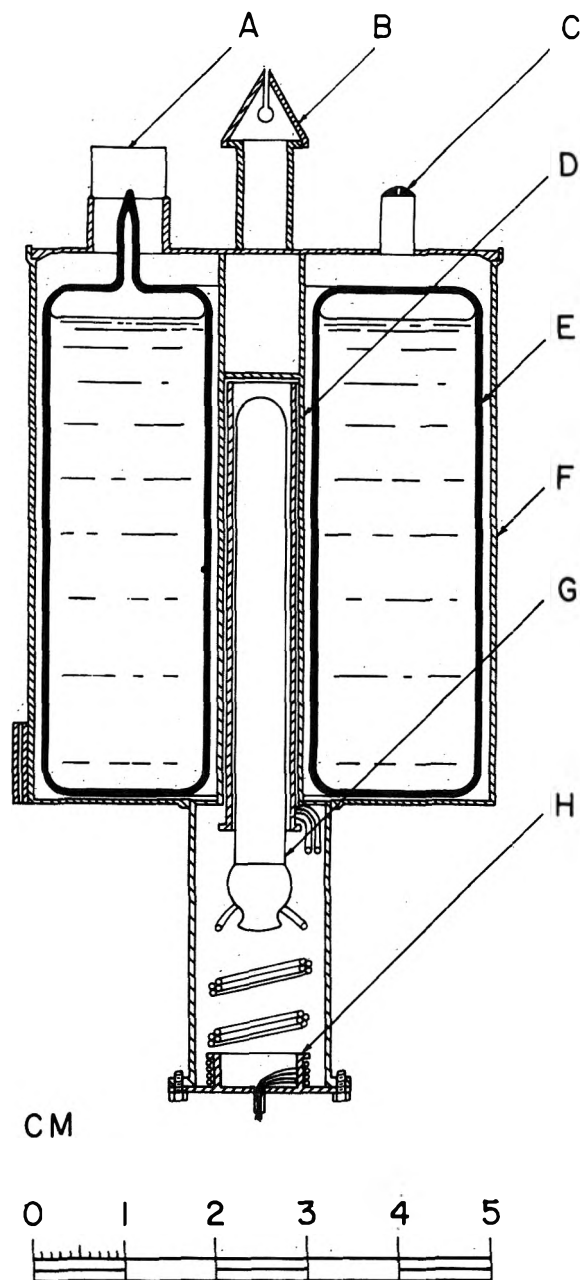


Figure 1. Schematic diagram of calorimeter W-33: A, cap over liner filling tube; B, thermal conductivity cone; C, helium filling tube; D, heater-thermometer well assembly; E, glass liner; F, calorimeter shell; G, thermocouple well; H, spool to equilibrate leads.

- (9) A. A. Zinov'ev, *Zh. Neorgan. Khim.*, **3**, 1205 (1958).
- (10) S. V. R. Mastrangelo and R. W. Dornte, *J. Am. Chem. Soc.*, **77**, 6200 (1955).
- (11) G. F. Smith, personal communication.
- (12) A. A. Zinov'ev and A. B. Tsentsiper, *Zh. Neorgan. Khim.*, **4**, 724 (1959).
- (13) E. F. Westrum, Jr., *J. Chem. Educ.*, **39**, 443 (1962).
- (14) H. G. Carlson, "Thermodynamic Properties of Methyl Alcohol, 2-Methyl- and 2,5-Dimethylthiophene and 2-Methylfuran," Doctoral Dissertation, University of Michigan, 1963; USAEC Report TID-15153 (1962).

shown by a loss in weight. Under the same conditions platinum did not lose weight but its presence resulted in rapid decomposition of the acid. Consequently, a Pyrex liner to contain the sample was used within a modified calorimeter (laboratory designation W-33) of the type shown in Fig. 1 conventionally used in this Laboratory. The copper calorimeter vessel's 0.2 mm. thick cylindrical shell is 5.3 cm. long, 4.4 cm. in diameter, and weighs about 44.3 g. This shell houses an annularly cylindrical Pyrex liner, E, with an internal volume of about 45 cc. and a weight of 36.5 g. Because of the necessity of avoiding even radiation heating of the perchloric acid sample, the liner is first soldered within its gold-plated copper shell and the small diameter Pyrex filling tube is then fused to the vacuum line used for the preparation of the sample. After loading the sample, 72.7128 g. *in vacuo*, and adding 14.4 mm. of purified helium gas to facilitate thermal conduction, the liner filling tube is sealed off and a small Monel cap, A, is soldered in place with low-melting Cerroseal (50% Sn-50% In) solder. This soldering operation is done while the sample is still at liquid nitrogen temperature. The sample in the sealed liner was brought into good thermal equilibrium with the surrounding copper vessel by admitting 17.8 cm. of helium gas pressure to the intervening space at 300°K. and sealing over a small aperture in the Monel tube, C, by fusing Cerroseal solder. The axial entrant well, D, accommodates

the heater-thermometer assembly. The temperature-sensing element is a Leeds and Northrup capsule-type platinum resistance thermometer (laboratory designation A-3) within a cylindrical copper heater sleeve bifilarly wound with Fiberglas-insulated Advance wire having a resistance of 150 ohms. Apiezon-T grease is used to provide thermal contact between thermometer, heater, and calorimeter.

In the Mark III cryostat, the calorimeter is surrounded by a cylindrical adiabatic shield, the three portions of which are individually controlled by separate channels of automatically regulated a.c. power to the heaters. This recording electronic circuitry provided with proportional, rate, and reset control action is used in preference to manual shield control above 50°K. and follows the temperature of the calorimeter to within approximately a millidegree, thereby reducing the energy exchange between the calorimeter and surroundings so that it is negligible compared with other sources of error. Copper-Constantan thermocouples monitor the temperature difference between calorimeter and shield and between shield and the ring used to temper the gradient in the bundle of leads. All measurements of temperature, time, potential, resistance, and mass are referred to calibrations or standards of the National Bureau of Standards.

The heat capacity of the heater-thermometer-liner-calorimeter assembly was determined in a separate set of experiments with the amounts of glass, Apiezon-T grease, and Cerroseal solder carefully adjusted to match those used during the measurements made on the loaded calorimeter or appropriate adjustments applied for the small differences.

Results and Discussion

Heat Capacity. The experimental heat capacity values are listed in chronological sequence in Table I and presented graphically in Fig. 2. These data are presented in terms of the defined thermochemical calorie of 4.184 abs. j., the ice point of 273.15°K., and the 100.465 g. molecular weight of perchloric acid. The approximate temperature increments used can usually be inferred from the differences in the mean temperatures of the adjacent runs in Table I. Adjustment of the observed $\Delta H/\Delta T$ values for curvature was done by the method of Osborne, *et al.*,¹⁵ and had a maximum value of 0.2% below 15°K. and decreased rapidly to less than 0.01% at higher temperatures. No correction for vaporization of the sample was found necessary since the vapor space was minimized and because a

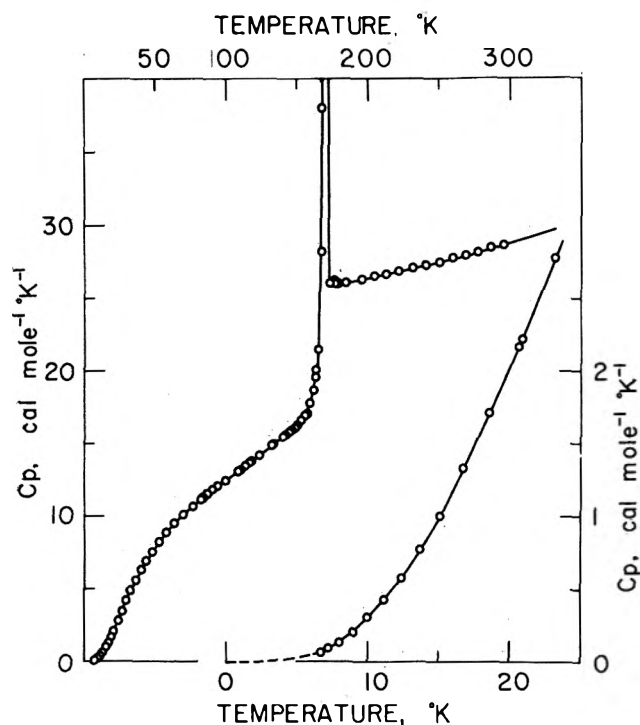


Figure 2. Heat capacity of perchloric acid.

(15) N. S. Osborne, H. F. Stimson, T. S. Sligh, Jr., and C. S. Cragoe, Department of Commerce, Bureau of Standards, Scientific Paper No. 501 (1925), p. 65.

trial calculation showed that the correction would be less than 0.01% at the highest temperature studied. Smoothed heat capacities obtained by a digital computer least-squares fit presented in Table II are essentially identical with those obtained from a large-scale plot.

Melting Behavior. The earliest reported melting temperature of anhydrous perchloric acid, -112° (160°K .), is that of Van Wyk,¹⁶ who used a pentane thermometer calibrated by comparison with a toluene

thermometer from 0 to -70° . Hence he had extrapolated his scale more than 40° and indeed measured the eutectic temperature and assumed the maximum melting point for the pure anhydrous acid was only slightly higher. From the data of this research, the

Table I: Heat Capacity of Anhydrous Perchloric Acid^a

\bar{T}	C_p	\bar{T}	C_p	\bar{T}	C_p
Series I		Series IV		Series IX	
6.64	0.065	144.80	15.83	Fusion run F	
7.18	0.092	150.55	16.39	Series X	
7.97	0.129	156.16	16.96	173.27	26.05
8.92	0.203	161.13	18.57	176.40	26.16
9.98	0.306	164.99	21.43	Series XI	
11.14	0.427	167.63	37.97	Fusion run G	
12.37	0.576	Series V		177.77	26.06
13.65	0.776	Fusion run A		Series XII	
15.06	1.016	Series VI		Series XIII	
16.68	1.329	86.55	11.54	Fusion run H	
18.52	1.712	93.60	12.05	186.82	26.19
20.59	2.170	100.90	12.56	195.30	26.34
Series II		108.51	13.11	204.02	26.52
20.82	2.226	116.24	13.67	212.90	26.68
23.18	2.775	124.39	14.30	221.90	26.84
25.99	3.437	132.61	14.94	231.31	27.08
29.01	4.131	139.72	15.50	240.97	27.28
32.24	4.852	146.54	16.05	250.53	27.49
35.75	5.583	153.23	16.65	259.78	27.78
39.26	6.250	158.78	17.71	268.60	27.95
42.93	6.869	163.55	20.08	277.54	28.19
47.10	7.531	167.03	28.21	286.41	28.47
51.99	8.201	176.10	26.05	295.14	28.86
57.33	8.853	178.64	26.07	Series VIII	
63.01	9.474	181.78	26.10	277.54	28.19
69.14	10.05	Fusion runs B		286.41	28.47
75.93	10.64	186.82	26.19	295.14	28.86
83.38	11.28	195.30	26.34	Fusion run D	
Series III		204.02	26.52	Fusion run E	
82.11	11.18	212.90	26.68	178.83	26.10
90.40	11.83	221.90	26.84	184.49	26.16
99.25	12.44	231.31	27.08	Series VII	
108.11	13.08	240.97	27.28	Fusion run C	
Heated to 181°K .		250.53	27.49	Fusion run C	
		259.78	27.78	Fusion run C	
		268.60	27.95	Fusion run C	
		277.54	28.19	Fusion run C	
		286.41	28.47	Fusion run C	
		295.14	28.86	Fusion run C	

^a Units: cal., mole, $^{\circ}\text{K}$.

Table II: Thermodynamic Functions of Perchloric Acid^a

T	C_p	S°	$H^{\circ} - H_0^{\circ}$	$-(F^{\circ} - H_0^{\circ})/T$
Crystal				
5	0.034	0.011	0.042	0.003
10	0.300	0.088	0.672	0.021
15	1.005	0.330	3.770	0.079
20	2.037	0.755	11.28	0.191
25	3.204	1.334	24.36	0.359
30	4.369	2.021	43.30	0.578
35	5.449	2.777	67.90	0.838
40	6.389	3.568	97.55	1.129
45	7.199	4.369	131.57	1.445
50	7.907	5.164	169.37	1.777
60	9.125	6.717	254.70	2.472
70	10.18	8.205	351.36	3.185
80	11.11	9.627	457.96	3.902
90	11.91	10.983	573.16	4.614
100	12.60	12.273	695.73	5.316
110	13.26	13.505	825.00	6.005
120	13.95	14.688	960.99	6.680
130	14.70	15.834	1104.2	7.340
140	15.50	16.952	1255.2	7.897
150	16.36	18.050	1414.4	8.621
160	(17.33)	19.137	1582.8	9.244
171.13	(18.25)	20.323	1779.0	9.919
Liquid				
171.13	(26.06)	29.999	3436.0	9.919
180	26.14	31.302	3664.7	10.942
190	26.25	32.718	3926.6	12.052
200	26.43	34.069	4190.0	13.119
210	26.62	35.364	4455.3	14.148
220	26.83	36.607	4722.5	15.141
230	27.04	37.804	4991.8	16.100
240	27.26	38.959	5263.3	17.029
250	27.49	40.077	5537.1	17.928
260	27.73	41.160	5813.2	18.801
270	27.98	42.210	6091.7	19.649
280	28.25	43.223	6372.9	20.472
290	28.55	44.229	6656.9	21.274
300	28.75	45.198	6943.8	22.059
273.15	28.07	42.54	6180	19.91
298.15	28.80	45.02	6891	21.91

^a HClO_4 ; 1 mole = 100.465 g.; units: cal., mole, $^{\circ}\text{K}$.

(16) H. J. Van Wyk, *Z. anorg. allgem. Chem.*, **48**, 1 (1906).

triple point of the anhydrous stoichiometric acid is 172.0°K ., suggesting that Van Wyk's calibration was seriously in error. Moreover, he determined his temperature from thermal arrests of less than 1 min. during heating rates of 1.5 to $6^{\circ}/\text{min}$. Zinov'ev and Rosolovskii¹⁷ report from partial thermographic and visual-polythermal data on the system chlorine-heptaoxide-water from 25 to 100 mole % of the former that the eutectic occurs at 53 mole % of Cl_2O_7 and $-100 \pm 2^{\circ}$ ($173 \pm 2^{\circ}\text{K}$.) and in contradiction of their own phase diagram (cf. Fig. 3) describe this as the melting point of

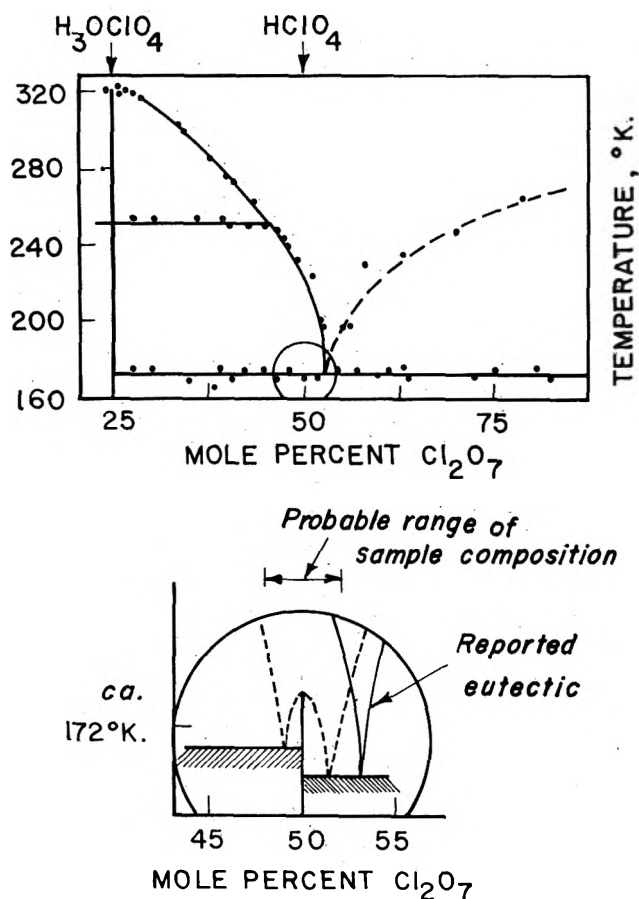
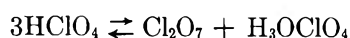


Figure 3. Phase diagram of the system chlorine heptaoxide-water from Zinov'ev and Rosolovskii¹⁷; circular inset: hypothetical congruent melting maximum for molecular perchloric acid species.

perchloric acid. Moreover, they indicated that no "crystallization line" exists for the composition HClO_4 , considered the components of the eutectic to be hydronium perchlorate and either Cl_2O_7 or a metastable compound such as $\text{Cl}_2\text{O}_7 \cdot 2\text{HClO}_4$, and postulated the following equilibrium, to exist at the 1:1 composition



and to shift to the right with decreasing temperature. They report no evidence for either congruent melting or peritectic melting.

If one assumes for discussion the correctness of their melting diagram, the phenomenon observed in these calorimetric studies corresponds to the situation at the eutectic composition (53 mole %) rather than to that indicated at 50 mole % on their diagram. For, were the latter situation correct, a continuing thermal effect should have been obtained over the entire region from the eutectic ($173 \pm 2^{\circ}\text{K}$.) to complete melting of the sample at 222°K . About 90% of the total thermal effect would be expected to appear at the eutectic temperature (from tie line relations) and the remaining 10% over the region 173 to 222°K . with some tendency toward concentration in the upper part of the range if the melting curve slope is reliable. However, since the observed heat capacities at all temperatures above the eutectic appear to be nearly linear and certainly not 4 cal./mole $^{\circ}\text{K}$.) higher than normal over the range 173 to 222°K ., the phase diagram reported may be assumed erroneous in one of two ways. Possibly either (1) the analyses of the samples used in the phase study are faulty, thereby shifting the limit of the saturation curve such that the eutectic is almost exactly at 50 mole % chlorine heptaoxide; or (2) "fine structure" in the vicinity of 50 mole % of the diagram (circled portion in Fig. 2) was not detected; or both.

In the conversion from the weight per cent results of the titrimetric method used by Zinov'ev and Rosolovskii, an error of 0.5% yields a 3% error in the mole per cent in the concentration range near 50 mole % chlorine heptaoxide. Recognition of this fact and realization of the difficulty in analysis of high perchloric acid concentrations make it seem not unlikely that an error in the reported eutectic composition sufficient to place it at 50 mole % could occur.

The presence of a congruent melting point for perchloric acid would suggest its stability and lack of disproportionation in the solid. The circled portion of the phase diagram in Fig. 3 is enlarged at the bottom of the figure showing a hypothetical congruent fusion in the saturation curve and the formation of crystalline perchloric acid. The shaded areas of the figure emphasize that neither eutectic temperature has been sharply defined experimentally except to establish the existence of transitions in this region. The two postulated eutectic temperatures, however, may differ by less than 1° . Moreover, the extent of the postulated solid solution region needs to be delimited. The melting point

(17) A. A. Zinov'ev and V. Ya. Rosolovskii, *Zh. Neorgan. Khim.*, 3 2382 (1958).

is estimated to be about 1° above the eutectic since the temperature of the latter reported by Zinov'ev and Rosolovskii is close to the melting temperature found in the present study.

Recent infrared investigation of crystalline anhydrous perchloric acid by Giguère and Savoie¹⁸ is also consistent with the suggestion of the persistence of the molecular compound into the crystalline region proposed herein and does not support the interpretation of Zinov'ev and Rosolovskii, although the possibility of such an equilibrium does not appear to have been considered in the infrared study. A Raman study at liquid nitrogen temperatures by Dahl, Trowbridge, and Taylor¹⁹ on a portion of the same crystalline HClO_4 used for the calorimetric investigation yielded eight frequencies in good accord with Raman lines observed by Simon and Weist²⁰ on liquid perchloric acid and infrared spectral lines by Giguère and Savoie on the gaseous, liquid, and crystalline states of the acid. Moreover, neither the very intense 921 cm.^{-1} vibration of H_3OClO_4 ,⁶ nor the 501 and 695 cm.^{-1} Raman²¹ and infrared²² bands of Cl_2O_7 were observed. Interference with these bands in the Raman spectra is unlikely and their absence indicates that neither species is present in the crystalline HClO_4 in appreciable amounts. In conclusion, the thermal, infrared, and Raman data all accord with the existence of an HClO_4 species in the crystalline state and provide ample evidence that the phase diagram and its interpretation by Zinov'ev and Rosolovskii are in error. Further investigation of this system in the vicinity of HClO_4 appears desirable for clarification of the nature of the phase relationships.

Considerable apparent premelting is evidenced in the heat capacity data even though heat capacity values as high as $1820\text{ cal./mole }^\circ\text{K.}$ were observed. Table III

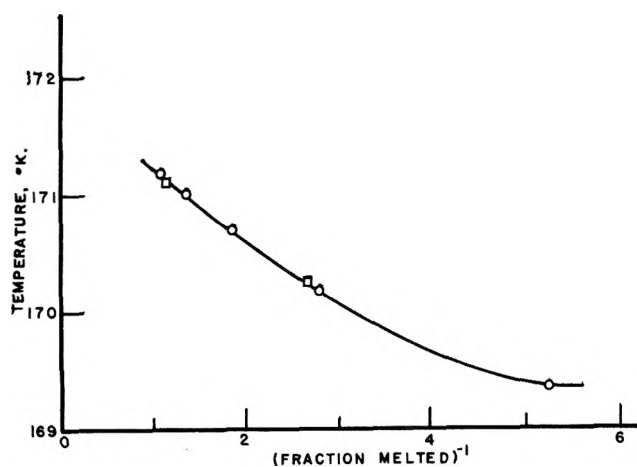


Figure 4. Fractional fusion for perchloric acid: fusion runs B, O; fusion runs G, □.

and Fig. 4 summarize the fractional melting data from two separate series of runs used to calculate purity and melting point. The method of Mastrangelo and Dornte¹⁰ for solid solutions was employed for this cal-

Table III: Fractional Fusion Data for Anhydrous Perchloric Acid^a

\bar{T}_{mean}	ΔT	Apparent C_p	ΔH_{excess}	$1/F^b$	T_{final}
Fusion runs B					
168.830	1.035	284.4	316.50	5.238	169.348
169.765	0.835	352.0	594.92	2.787	170.182
170.444	0.525	593.8	896.95	1.848	170.706
170.857	0.301	1108	1224.78	1.354	171.007
171.092	0.171	1826	1533.09	1.081	171.178
173.073	3.791	57.04	1651.43		174.968
Fusion runs G					
159.672	21.148	46.78	625.38	2.651	170.247
170.684	0.872	980.3	1464.71	1.132	171.119
173.349	4.460	68.47	1655.18		175.579
Melting point: this sample				(1.000)	171.132
Melting point: pure compound				(0.000)	172.008

^a Units: cal., mole, $^\circ\text{K.}$ ^b F is the fraction melted.

ulation and revealed a maximum impurity content of 2.5 mole %. As discussed previously, this is presumed to be largely hydronium perchlorate. On this basis, the melting point of the sample is 171.13°K. and that of pure anhydrous perchloric acid extrapolates to 172.0°K.

The resolution of the normal lattice vibrational (phonon) contributions from excess values was done by extrapolating the heat capacity of crystal and liquid to the transition temperature and resulted in an enthalpy of fusion of 1657 cal./mole and a corresponding entropy increment of $9.67\text{ cal./mole }^\circ\text{K.}$

Thermodynamic Functions. Molal thermodynamic functions obtained by computer integration of the data combined with a Debye T^3 heat capacity extrapolation below 5° are listed at selected temperatures in Table II. The entropy and free energy functions do not include contributions from nuclear spin or isotopic mixing and hence are practical values for chemical thermodynamic purposes.

(18) P. A. Giguère and R. Savoie, *Can. J. Chem.*, **40**, 495 (1962).

(19) A. J. Dahl, J. C. Trowbridge, and R. C. Taylor, *Inorg. Chem.*, **2**, 654 (1963).

(20) A. Simon and M. Weist, *Z. anorg. allgem. Chem.*, **268**, 301 (1952).

(21) R. Fonteyne, *Natuurw. Tijdschr. (Ghent)*, **20**, 275 (1938).

(22) R. Savoie and P. A. Giguère, *Can. J. Chem.*, **40**, 991 (1962).

As a test of the precision of the calorimetry and the heat capacity-type runs in the transition region, several enthalpy increments, each covering the anomalous region, were made and compared with the integral of heat capacity determinations in Table IV. The agreement will be seen to be quite satisfactory.

Table IV: Enthalpy and Entropy Increments of Perchloric Acid^a

Designation	Energy increments	T_{final}	T_{initial}	$H_{150^\circ} - H_{100^\circ}$	$S_{150^\circ} - S_{100^\circ}$
Fusion					
Series VI ^b	12	150.05	150.26	(2244.8)	(13.218)
Series VII	2	151.63	150.00	2250.6	13.252
Series VIII	2	151.61	151.72	2251.4	13.255
Series XI	4	179.96	149.10	2248.5	13.245
Run A ^c	1	153.55	147.21	(2258.8)	(13.300)
Run F	1	175.04	148.57	2250.8	13.252
Run H	1	153.20	149.71	2250.4	13.251
				Average	2250.3
				$H_{150^\circ} - H_{110^\circ}$	
Crystal					
Series VI	5	150.26	112.30	589.69	
Series XII	5	152.24	108.85	588.96	
Run D	1	151.72	110.67	588.16	
				Average	589.27
Numerical quadrature of smoothed curve:				589.42	

^a Units: cal., mole, °K. ^b Rejected from average due to long time (4.5 days) necessary to attain desired drift. ^c Rejected from average by Chauvenet's criterion.

The experimental precision of the thermodynamic functions may be considered to be 0.1% above 100°K. and an estimate of the effect of the apparently impure nature of the sample on the thermodynamic functions can be made on the basis of the following assumptions: that the impurity is entirely perchloric acid monohydrate and that the heat capacities of water and perchloric acid are additive for this substance. Maximum deviations occasioned in the heat capacity, enthalpy, entropy, and free energy functions at 298.15°K. are 0.21 cal./mole °K., 46 cal./mole, 0.20 cal./mole °K., and 0.05 cal./mole °K., respectively.

Comparison with Spectroscopic Entropy. The standard entropy of perchloric acid in the ideal gas state was reported as 70.7 cal./mole °K.¹⁸ and subsequently corrected to 70.5 by Giguère²³ upon incorporating a recalculation of the rotational contribution based on recent electron diffraction data.²⁴ We deduced that a three-fold potential energy barrier of 1.6 kcal. hinders inter-

nal rotation. Utilizing a recent development by Wulff²⁵ which permits evaluation of the barriers to internal rotation from thermal data on condensed phases only, we estimated the torsional frequency of the hydroxyl rotation to be $309 \pm 14 \text{ cm.}^{-1}$ in good accord with the frequency $\nu_{12} = 307 \text{ cm.}^{-1}$ for the gaseous molecule.¹⁸ This datum provides further evidence for the validity of the assumed magnitude of the barrier.

Comparison with the calorimetrically determined entropy (cf. Table V) involves evaluation of the entropy of vaporization, of compression, and of correction from the real to the ideal gaseous state. Unfortunately, definitive data are absent for all three terms. However, application of the Clausius-Clapeyron equation to two single vapor pressure data values (18 mm. at 16°¹⁶ and 56 mm. at 39°²⁶) of questionable reliability from different sources gives an entropy of vaporization of 29.7

Table V: Entropy of Gaseous Perchloric Acid at 298.15°K.^a

0-5°K. Debye extrapolation	0.011
5-171.13°K., solid, numerical integration	20.31
Fusion, 1657.0/171.13	9.67
171.13-298.15°K., liquid, numerical integration	15.02
Vaporization at 28.7 mm., 8850/298.15	29.7
Compression from 28.7 mm. to 760 mm., -R ln (760/28.7)	-6.5
Total, $S^\circ_{298.15}$ (ideal gas, 1 atm.)	68.2
Spectroscopic, ¹⁸ $S^\circ_{298.15}$ (ideal gas, 1 atm.)	70.5

^a Units: cal., mole, °K.

cal./mole °K.) and a vapor pressure of 28.7 mm. at 298.15°K. Compression from 28.7 to 760 mm. at this temperature would give an additional -6.5 cal./mole °K. entropy contribution if the gas is assumed to be ideal. As indicated in Table V, inclusion of these values gives a standard entropy of 68.2 ± 2.0 for gaseous perchloric acid monomer. Consideration of the gas imperfection occasioned by the estimated¹⁸ 3 kcal./mole intermolecular hydrogen bonds (comparable to those in HNO₃ and notably weaker than in H₂O, H₂O₂, and in the alcohols) would tend to increase the entropy somewhat. At present the accord between spectro-

(23) P. A. Giguère, personal communication.

(24) P. A. Akishin, L. V. Vilkov, and V. Ya. Rosolovskii, *Soviet Phys. Cryst.*, **4**, 328 (1960); *Kristallografiya*, **4**, 353 (1959).

(25) C. Wulff, *J. Chem. Phys.*, **39**, 1227 (1963).

(26) D. Vorlander and R. von Schilling, *Ann. Chem.*, **310**, 369 (1900).

scopic and calorimetric entropy can only be said to be within experimental error and does not provide evidence for or against the existence of residual entropy. Further studies on the vaporization and thermodynamics of the gaseous phase are obvious desiderata.

Acknowledgment. The partial financial support of the United States Atomic Energy Commission Division of Research is gratefully recognized. It is a pleasure to acknowledge the counsel and assistance of Professor R. C. Taylor and Dr. Claus A. Wulff.

Triethanolamine Borate. The Heat Capacity and Thermodynamic Functions from 5 to 350°K.

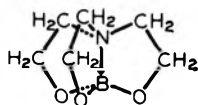
by Peter Castle, Richard Stoesser, and Edgar F. Westrum, Jr.¹

Department of Chemistry, University of Michigan, Ann Arbor, Michigan (Received June 3, 1963)

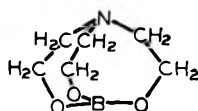
The heat capacity of $B(OCH_2CH_2)_3N$ has been determined by adiabatic calorimetry and its temperature dependence found to be sigmoid with no thermal anomalies over the range 5 to 350°K. Thermodynamic properties were derived by integration of the measured heat capacity data. The heat capacity at constant pressure (C_p), the practical entropy (S°), the enthalpy function ($[H^\circ - H_0^\circ]/T$), and the free energy function $-([G^\circ - H_0^\circ]/T)$ at 298.15°K. in cal./(g.f.w. °K.) are: 44.75, 43.78, 22.48, and 21.30.

Introduction

Thermophysical properties of triethanolamine borate [2,2',2''-nitrilotriethanol borate, $B(OCH_2CH_2)_3N$] are interesting, first because of the possibility of further elucidation of the general thermodynamic characteristics of globular molecules, and second due to the postulated existence of two spatial configurations²⁻⁴ for the molecule. The "triptych" form



involves a postulated bond between boron and nitrogen, while the cage structure



has a nitrogen electron pair on the exterior of the cage.

Kinetic studies of reactions involving attack on the nitrogen electron pair by alkyl iodides,² by mineral acids,² and by hydrolysis,⁵ indicate that reactions at ambient temperatures involving the nitrogen electron pair in triethanolamine borate proceed much more slowly than identical reactions with ordinary tertiary amines. Infrared spectroscopic studies³ indicate the possible formation of a boron-nitrogen bond which requires the triptych structure. In addition, the dipole moments of triethanolamine borate and its derivatives⁵ show the nitrogen electron pair to be almost equally distributed between the boron and nitrogen, which indi-

- (1) To whom correspondence concerning this work should be addressed.
- (2) H. C. Brown and E. A. Fletcher, *J. Am. Chem. Soc.*, **73**, 2808 (1951).
- (3) H. Weidmann and H. K. Zimmerman, Jr., *Ann.*, **620**, 4 (1959).
- (4) H. Steinberg and D. L. Hunter, *Ind. Eng. Chem.*, **49**, 174 (1957); *J. Am. Chem. Soc.*, **82**, 853 (1960).
- (5) H.-C. Fu, T. Psarras, H. Weidmann, and H. K. Zimmerman, Jr., *Ann.*, **641**, 116 (1960).

cates the presence of a boron–nitrogen bond and provides further evidence for the triptych structure. However, the effect of triethanolamine borate on the curing rates of epoxy resins is interpreted as revealing that the nitrogen electrons and the boron orbitals are free to participate in the curing process in the temperature range 150 to 200°. These data then are taken as evidence for the existence of the cage structure,⁶ which purportedly is favored by higher than ambient temperatures. For these reasons investigation of the thermal properties of this substance was initiated; heat capacities at low temperatures presented here do not resolve the structural problem but are of inherent interest.

Experimental

Triethanolamine Borate Sample. The calorimetric sample obtained from the U. S. Borax Corp. was recrystallized from pyridine and sublimed successively *in vacuo* seven times; the final product was handled only in the nitrogen atmosphere of a drybox. Duplicate analyses on separate portions of the sample averaged (by weight): 45.80 ± 0.06% C; 7.75 ± 0.04% H; 8.96 ± 0.03% N; and 6.89% B (theoretical: 45.90% C; 7.71% H; 8.92% N; and 6.89% B). Macroscopic, white, odorless crystals were obtained.

Cryostat and Calorimeter. Measurements were made in the Mark II calorimetric cryostat using a capsule-type platinum resistance thermometer (laboratory designation A-5). The general nature of the cryostat and the use of the adiabatic technique have been described elsewhere.⁷ The Mark II cryostat, however, is a modified version which provides an instrument of greater efficiency, mechanical rigidity, and operating convenience. The metal cryostat is provided with a heat exchanger which utilizes the enthalpy of the effluent helium gas to provide a thermal dam for the conduction of heat by the bundle of electrical leads and thus minimize vaporization of the liquid helium from the lowest temperature reservoir. The calorimeter itself is surrounded by a cylindrical adiabatic shield, the three portions of which are individually controlled by separate channels of automatic regulation of the a.c. power to the heaters. This recording electronic circuitry provided with proportional, rate, and reset control actions is used in preference to manual shield control above 50°K. and controls the temperature to within approximately a millidegree, thereby reducing the energy exchange between the calorimeter and the surroundings so that it is negligible in comparison with other sources of error. Copper–constantan thermocouples monitor the temperature difference between calorimeter and shield and between shield and the ring used to temper the gradient in the bundle of leads.

All measurements of temperature, time, potential, resistance, and mass are referred to calibrations or standards of the National Bureau of Standards.

A gold-plated copper calorimeter (laboratory designation W-28) was loaded in a dry nitrogen atmosphere with a 167.620-g. (*in vacuo*) sample of triethanolamine borate, evacuated, and sealed after adding 88 mm. of He pressure to enhance thermal contact between calorimeter and sample. Amounts of Apiezon-T, Cerroseal solder, and helium gas were adjusted to correspond to the quantities present during the separate heat capacity determinations on the calorimeter–heater–thermometer assembly. The heat capacity of the sample ranged from 88% of the total at 10°K. to a minimum of 62% at 105°K. and gradually increased to 80% above 300°K.

Table I: Heat Capacity of Triethanolamine Borate^a

T^b	C_p^c	T	C_p	T	C_p
Series I		35.01	5.864	156.06	23.518
		37.99	6.527	164.85	24.677
182.53	27.05	Series III		173.68	25.890
Series II				182.51	27.050
				191.44	28.199
		37.30	6.365	200.59	29.497
5.45	0.037	39.60	6.867	208.28	30.407
6.42	0.069	42.69	7.489	217.82	31.938
7.05	0.091	46.52	8.231	227.82	33.420
8.13	0.152	50.85	9.014	237.07	34.852
9.32	0.260	55.00	9.705	246.62	36.279
10.37	0.360	59.28	10.406	255.71	37.678
11.50	0.480	65.37	11.370	265.02	39.173
12.72	0.662	72.78	12.431	274.13	40.667
14.10	0.894	80.25	13.487	283.11	42.180
15.51	1.155	88.12	14.615	292.05	43.718
16.98	1.460	96.57	15.663	301.15	45.271
18.68	1.841	105.15	16.762	310.51	46.941
20.66	2.314	113.42	17.843	319.87	48.633
22.65	2.813	122.07	19.002	328.98	50.328
24.94	3.393	129.99	20.112	337.73	51.992
27.98	4.168	138.58	21.217	346.04	53.599
31.52	5.040	147.29	22.368		

^a Units: cal., g.f.w., °K. ^b T is the mean temperature of the individual heat capacity determinations. ^c C_p is the heat capacity of the crystal at the essentially constant pressure (<1 cm.) of conduction helium plus the saturation sublimation pressure of the sample.

Results of Heat Capacity Measurements. The experimental heat capacity values are presented in chronologi-

- (6) S. H. Langer and I. N. Elbling, *Ind. Eng. Chem.*, **49**, 1113 (1957).
 (7) E. F. Westrum, Jr., J. B. Hatcher, and D. W. Osborne, *J. Chem. Phys.*, **21**, 419 (1953).

Table II: Thermodynamic Properties of Triethanolamine Borate^a

$T, ^\circ\text{K.}$	C_p	S°	$H^\circ - H_0^\circ$	$-(G^\circ - H_0^\circ)/T$
5	0.026	0.009	0.034	0.002
10	0.315	0.091	0.706	0.021
15	1.057	0.345	3.955	0.081
20	2.154	0.793	11.87	0.199
25	3.412	1.407	25.76	0.377
30	4.672	2.141	45.99	0.608
35	5.860	2.952	72.36	0.885
40	6.941	3.806	104.3	1.196
45	7.939	4.682	141.6	1.535
50	8.863	5.567	183.7	1.894
60	10.53	7.334	280.8	2.653
70	12.04	9.072	393.8	3.446
80	13.44	10.77	521.2	4.256
90	14.79	12.43	662.4	5.072
100	16.12	14.06	816.9	5.891
110	17.44	15.66	984.7	6.706
120	18.76	17.23	1165.7	7.518
130	20.08	18.79	1359.9	8.325
140	21.40	20.32	1567.3	9.127
150	22.72	21.84	1787.9	9.924
160	24.04	23.35	2021.7	10.71
170	25.37	24.85	2268.8	11.50
180	26.70	26.34	2529.1	12.29
190	28.06	27.82	2802.9	13.06
200	29.43	29.29	3090.3	13.84
210	30.84	30.76	3391.6	14.61
220	32.27	32.23	3707.2	15.38
230	33.74	33.70	4037.2	16.14
240	35.25	35.16	4382.2	16.90
250	36.80	36.63	4742.4	17.66
260	38.38	38.12	5118.3	18.42
270	40.00	39.59	5510.1	19.18
280	41.65	41.07	5918.3	19.93
290	43.34	42.56	6343.3	20.69
300	45.07	44.06	6785.3	21.44
310	46.85	45.57	7244.9	22.20
320	48.66	47.08	7722.4	22.95
330	50.52	48.61	8218.3	23.70
340	52.42	50.14	8733.0	24.46
350	54.38	51.69	9267.0	25.22
273.15	40.51	40.05	5637	19.42
298.15	44.75	43.78	6702	21.30

^a Units: cal., g.f.w., $^\circ\text{K.}$

cal sequence in Table I. These data are given in terms of the defined thermochemical calorie equal to 4.1840 abs. j., an ice point of 273.15 $^\circ\text{K.}$, and a gram formula weight of 156.990. A small adjustment (<0.1%) has

been made in some regions for the difference between $C_p = (dH/dT)_p$ and the experimental values of $\Delta H/\Delta T$ based on finite temperature increments, which can usually be inferred from the tabulated adjacent mean temperatures. The smoothed heat capacity and thermodynamic functions obtained by integrating these data with a high-speed digital computer are given in Table II. The heat capacity values of Table II were taken from a smooth curve obtained by a least-squares-fit polynomial function through the experimental points and extrapolated below 6 $^\circ\text{K.}$ by means of the Debye limiting law. These values are estimated to have a probable error of 0.08% above 25 $^\circ\text{K.}$, 1% at 12 $^\circ\text{K.}$, which increases to approximately 6% at 5 $^\circ\text{K.}$ The thermodynamic functions are considered to have a precision corresponding to a probable error of less than 0.1% above 100 $^\circ\text{K.}$ Additional digits beyond those significant are given in Table II for internal consistency and to permit interpolation and differentiation. The entropies and Gibbs energies have not been adjusted for nuclear spin and isotope mixing contributions and hence are practical values for use in chemical thermodynamic calculations.

Discussion

Although no thermal anomalies appear in the region from 4 to 350 $^\circ\text{K.}$, the heat capacity appears to increase comparatively rapidly above 250 $^\circ\text{K.}$ as do those of globular molecules with higher temperature transitions. Differential thermal analysis above 350 $^\circ\text{K.}$ reveals the presence of a transition near 473 $^\circ\text{K.}$ and fusion at about 511 $^\circ\text{K.}$ The enthalpy increment associated with fusion appears to be two to three times as large as that of the transition. It has been suggested⁸ that somewhere in the range 430 to 480 $^\circ\text{K.}$ (possibly at the transition temperature) cleavage of the nitrogen-boron bond would result in conversion of triptych to cage structure. Higher temperature calorimetric studies and possibly dielectric constant determinations are desiderata for the elucidation of the mechanism of the transition and the possibility of a higher temperature plastically crystalline phase.

Acknowledgment. The partial financial assistance of the Division of Research of the U. S. Atomic Energy Commission is recognized. P. C. thanks the National Science Foundation for a 1962 Undergraduate Summer Research Participation Award. The cooperation of Evan Suits in the calorimetric measurements is acknowledged with gratitude.

(8) R. Stoesser, personal communication.

Application of Flash-Desorption Method to Catalyst Studies.

IV. Adsorption of Ammonia on Alumina and Its Effect on Adsorption of Ethylene¹

by Y. Amenomiya, J. H. B. Chenier, and R. J. Cvetanović

Division of Applied Chemistry, National Research Council, Ottawa 7, Canada (Received June 26, 1963)

Adsorption of ammonia on an alumina catalyst and its effect on the subsequent adsorption of ethylene have been studied by the flash-desorption method. It has been found that the activation energy of desorption of ammonia increases from 7 to 18 kcal./mole as the surface coverage decreases from 29 to 1.5%. A large excess of ammonia, preadsorbed at 250°, has to be used in order to block the active sites for the strong adsorption of ethylene. When the temperature at which ammonia is preadsorbed is varied between 175 and 900°, the amount of the strongly adsorbed ethylene goes through a minimum (in the neighborhood of 500°). From these results it is concluded that the active sites for ethylene adsorption do not coincide with the highest energy sites for ammonia adsorption, although they are within the distribution range for ammonia.

Introduction

Various methods have been used to determine the surface acidity and the nature of acid sites of catalysts in attempts to explain their activity in acid-catalyzed reactions. Examples of these methods are: titration in aqueous media, titration in nonaqueous media, the chemisorption of basic gases, etc. Of these, the chemisorption of basic gases, such as ammonia or quinoline, seemed to be the most suitable method for determination of the acidity under reaction conditions. The acidity is assumed to be directly related to the chemisorbed amounts of these gases, measured either as the equilibrium amounts at a given temperature and pressure, or as the amount of the gas remaining on the surface after evacuation at a given temperature for a specified time interval. However, it has recently become clear that there is a distribution of surface energies for the adsorption of basic gases on alumina and silica-alumina catalysts.²⁻⁵ In view of this, it would be difficult to specify the proper conditions for the chemisorption or the evacuation of the adsorbed gas which would assure an unambiguous determination of the surface acidity of these catalysts.

Although it has been found that the catalytic

activities for some hydrocarbon reactions are proportional to or at least depend on the measured surface acidities,⁶ it is nevertheless difficult to make direct comparisons between the actual number of active sites on which the reaction takes place and the number of the acidic centers. The authors have found, using a recently developed flash-desorption technique, that at room temperature olefins strongly adsorb on a small part of the surface of an alumina catalyst (about 3% of the total surface) and that this part consists of two different types of active sites.⁷⁻⁹ It was thought, there-

- (1) Contribution No. 7760 from the National Research Council, Ottawa 7, Canada.
- (2) A. C. Zettlemyer and J. J. Chessick, *J. Phys. Chem.*, **64**, 1131 (1960).
- (3) (a) A. Clark, V. C. F. Holm, and D. M. Blackburn, *J. Catalysis*, **1**, 244 (1962); (b) A. Clark and V. C. F. Holm, *ibid.*, **2**, 21 (1963).
- (4) V. Kevorkian and R. O. Steiner, *J. Phys. Chem.*, **67**, 545 (1963).
- (5) Y. Kubokawa, *ibid.*, **67**, 769 (1963).
- (6) For example, A. G. Oblad, T. H. Milliken, Jr., and G. A. Mills, "Advances in Catalysis," Vol. III, Academic Press, New York, N. Y., 1951, p. 199.
- (7) Y. Amenomiya and R. J. Cvetanović, *J. Phys. Chem.*, **67**, 144 (1963).
- (8) Y. Amenomiya and R. J. Cvetanović, *ibid.*, **67**, 2046 (1963).

fore, that it would be useful, prior to a discussion of the correspondence between the catalyst activity and the surface acidity, to investigate the relation between the active sites for ethylene adsorption and the adsorption of ammonia on this catalyst. The results of this study are reported in the present communication.

Experimental

Apparatus. The apparatus, described in detail in part I,⁷ consisted of two parts: (1) a conventional static system for measuring adsorption; and (2) a flashing device by means of which the flash-desorption of the adsorbed gases is effected in a stream of helium by increasing the catalyst temperature uniformly. The concentration of the gas desorbed from the catalyst by flashing was detected by a thermistor-type thermal conductivity cell and recorded. The signal thus recorded is called the flash-desorption chromatogram.

Materials. The alumina was prepared as described in part I, and in all experiments except those with ethylene a sample of 0.152 g. was used. Before use, the catalyst was evacuated for more than 60 hr. at 650° until no more water was condensed in a liquid nitrogen trap connected to the catalyst system. The total surface area of the catalyst after this treatment was 164 m.²/g. as determined by the B.E.T. method with nitrogen. After each run the catalyst was evacuated at 650 to 700° overnight. This treatment was found to be adequate, as evidenced by the reproducibility of the experimental results.

Matheson Co. anhydrous ammonia (99.95%) was passed through a bed of potassium hydroxide pellets and stored in a reservoir containing metallic sodium. Phillips research grade ethylene was condensed in a liquid nitrogen trap, followed by evacuation and fractionation. The middle fraction (one-third) was retained and stored in a reservoir.

Procedure. The isotherm of ammonia on the alumina at room temperature was determined in the usual manner. Desorption measurements were carried out as follows. After the adsorbed amounts were measured under a given set of conditions, the catalyst was heated to the desired temperature in a few minutes and then was evacuated for various time intervals. The desorbed gas was condensed in a liquid nitrogen trap and the amount remaining on the surface after evacuation was calculated from the difference between the amounts adsorbed initially and those collected in the trap during evacuation.

The details of the flash-desorption technique have been given in part I.⁷ The procedure used in other experiments will be indicated in the next section.

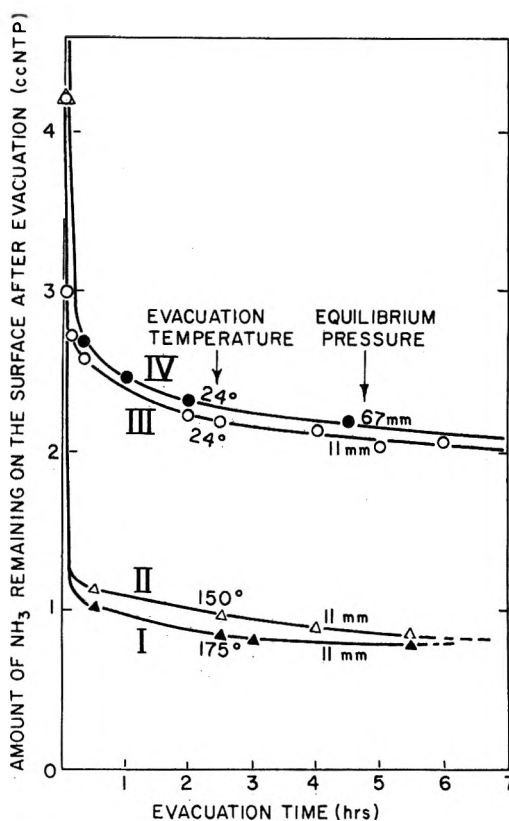


Figure 1. Desorption of ammonia as a function of evacuation time. Weight of alumina 0.152 g.

Results and Discussion

Desorption of Ammonia. The adsorption of ammonia at room temperature reached equilibrium within several minutes. The isotherm was well expressed by the Freundlich equation in the pressure range 0.6 to 130 mm. and the values of the constants were found to be given by the empirical expression

$$a = 19.08p^{1/6.82}$$

where a is the amount adsorbed (cc. NTP/g.) and p is the equilibrium pressure of ammonia (in mm.).

Figure 1 shows the results of the desorption experiments. The amounts of ammonia remaining on the surface after evacuation at different temperatures are plotted against the evacuation time. For curves I, II, and III, the evacuation was carried out after ammonia was adsorbed at 11 mm. at room temperature and for curve IV after adsorption at 67 mm. It is seen from the figure that a large part of the adsorbed ammonia is quickly removed at all temperatures in the first 30 min. and this is then followed by further slow desorption. However, the slow desorption was still

(9) Y. Amenomiya and R. J. Cvetanović, *ibid.*, 67, 2705 (1963).

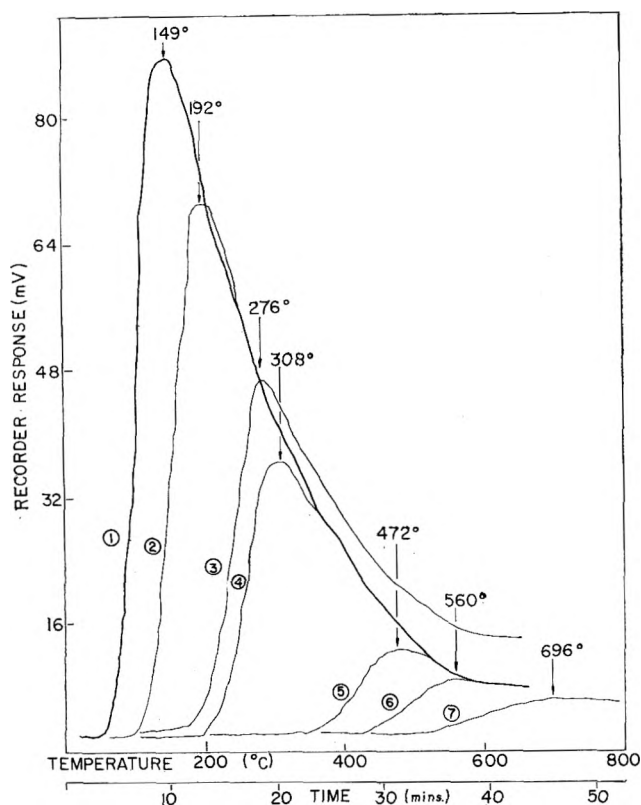


Figure 2. Flash-desorption chromatograms for different amounts of ammonia. The rate of flashing was $15.2^\circ/\text{min.}$; smoothed out chromatograms are reproduced, for simplicity. Evacuations before flashing were made for 2.5 hr. at the following temperatures: 24° (curve 1), 75° (2), 150° (3), 175° (4), 325° (5), 400° (6), and 500° (7).

observed after 6 hr. at 150 and 170° and after 20 hr. at 24° . The difference in amount remaining on the surface for preadsorptions at 11 and 67 mm. (curves III and IV) was found to persist until after 20 hr.

Webb¹⁰ has measured the amounts of ammonia remaining on Alcoa F-10 alumina after evacuation for 2 hr. at 175° and correlated them with the surface acidity determined by titration with KOH. The residual ammonia was very similar to the amount remaining on the catalyst surface in the present work after similar treatment. However, as indicated above, we have found that it was not possible to establish a definite set of conditions of evacuation that would assure that the residual ammonia corresponds only to chemisorption and therefore defines the surface acidity.

Distribution of Surface Energies. When the amount of ammonia remaining on the surface was varied by evacuating at various temperatures for an arbitrarily chosen time interval of 2.5 hr., the subsequent flash-desorption gave the chromatograms shown in Fig. 2. The initial adsorption of ammonia was carried out at a

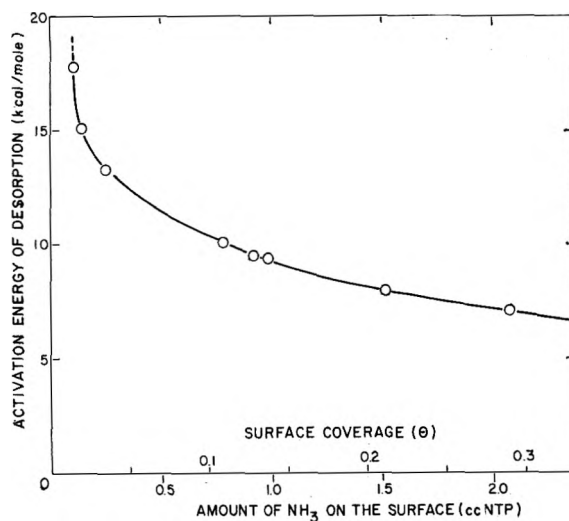


Figure 3. The distribution of the activation energies of desorption of ammonia. The surface coverage (θ) has been calculated assuming 13 \AA^2 for the cross-sectional area of an ammonia molecule.

constant pressure of 11.5 mm. (the adsorbed amount was 4.2 cc. NTP). The amount of ammonia remaining on the surface after the evacuation varied from 2.07 to 0.11 cc. as the evacuation temperature was varied from 24 to 500° . After the evacuation, the catalyst was cooled to room temperature prior to flashing. It is evident from Fig. 2 that the smaller the amount of ammonia remaining on the surface, the higher the temperature at which the peak maximum appears. This indicates a distribution of the activation energies of desorption that depends on surface coverage, as already discussed in connection with the propylene-alumina system in part III.⁹ Had the activation energy of desorption been constant for all sites, the peak maximum would have appeared at the same temperature independently of the amount adsorbed.

In order to obtain the value of the activation energy of desorption for an arbitrarily chosen amount of ammonia on the surface, the temperature of peak maximum, T_M , was followed as a function of the rate of temperature increase used in the flash-desorption (β $^\circ\text{C./min.}$) according to the equation⁷

$$2 \log T_M - \log \beta = E_d/2.303RT_M + \log E_d v_m / R k_0 \quad (1)$$

where E_d and k_0 are the activation energy and the temperature independent factor of the rate constant of desorption, respectively, and v_m is the amount adsorbed in a complete monolayer. The results obtained by

(10) A. N. Webb, *Ind. Eng. Chem.*, **49**, 261 (1957).

keeping the amount of ammonia on the surface constant (0.68 cc. NTP) gave a straight line plot in agreement with the above equation. From the slope and intercept of this plot, E_d and k_0/v_m were found to be 9.8 kcal./mole and $1.47 \times 10^3 \text{ min.}^{-1}$, respectively. It should be pointed out, however, that these experiments were rather difficult because of the shifts in the peak temperatures due to the unavoidable small variations in the adsorbed amounts. The values obtained may therefore be subject to an appreciable experimental error.

By assuming that k_0/v_m is constant for all sites on the surface, the activation energies of desorption corresponding to the peak maxima in Fig. 2 have been calculated from eq. 1, as was done in part III.⁹ These activation energies are plotted against the amount of the gas on the surface in Fig. 3. It is evident that for desorption of ammonia from alumina the activation energies are distributed over a range of values, decreasing as the amount of ammonia on the surface increases. The surface coverages, θ , shown in Fig. 3 were calculated assuming a value of 13 \AA.^2 for the cross-sectional area of ammonia. The values of the activation energies obtained in this manner may be expected to be approximately equal to the heats of adsorption in view of the very fast rates of adsorption even at room temperature.

Although the activation energy of desorption sharply increases at very small surface coverages (close to $\theta = 0.02$) as seen in Fig. 3, there is no indication of a sharp distinction between chemisorption and physical adsorption as indicated by Kubokawa.⁵ Also, there are no maxima nor minima in the energy distribution curve similar to those observed by Kevorkian and Steiner.⁴

Adsorption of Ethylene on Alumina with Preadsorbed Ammonia. It has been reported in part I⁷ that ethylene adsorbed on the alumina used in these studies gives two overlapping peaks in the flash-desorption chromatogram when the catalyst is evacuated for about 10 min. at room temperature before flashing, and that the active sites corresponding to these two peaks occupy about 3% of the total surface. These active sites are called sites I and II, respectively, and have activation energies of desorption of ethylene of 26.8 and 36.4 kcal./mole. Also, particularly sites II seem to be very active for catalytic olefin reactions such as polymerization.¹¹ It is therefore of interest to see how a preadsorption of ammonia on these active sites affects the subsequent chemisorption of ethylene.

After various amounts of ammonia were adsorbed at 250° on the alumina (0.126 g.), the catalyst was cooled to room temperature and ethylene was admitted at an

equilibrium pressure of about 6 mm. The partial pressure of ammonia in the gas phase in these experiments remained always negligibly small. The catalyst was evacuated for 11 min. at room temperature after the adsorption of ethylene, and was then flash-desorbed. The results obtained are shown in Fig. 4, in which the total amount of ethylene initially adsorbed as well as the amount of ethylene flash-desorbed are plotted against the amount of preadsorbed ammonia. It is seen that the flash-desorbed ethylene ("strong"

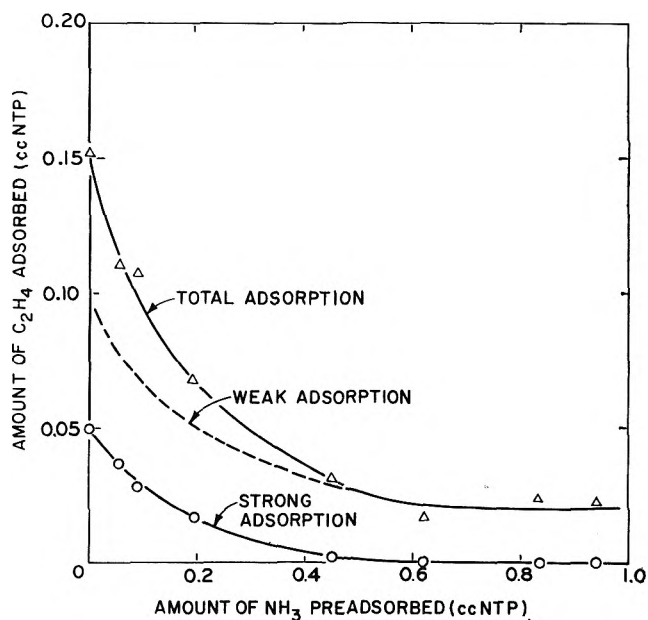


Figure 4. The effect of the amount of the preadsorbed ammonia on the adsorption of ethylene. Weight of alumina, 0.126 g.; adsorption temperature of ammonia, 250° .

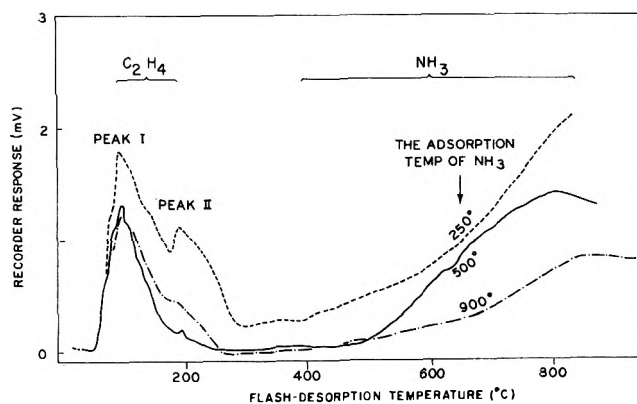


Figure 5. Flash-desorption chromatogram of ethylene on alumina with preadsorbed ammonia. The rate of flashing was about $15^\circ/\text{min.}$

(11) Unpublished results.

Table I: The Effect of Preadsorbed Ammonia on the Adsorption of Ethylene^a

Expt. no.	Preadsorption of NH ₃		Adsorption of C ₂ H ₄		Flash-desorption			Weak adsorption, cc. NTP (a - b)
	Temp., °C.	Amt., cc. NTP	Press., mm.	Amt., cc. NTP (a)	Total C ₂ H ₄ desorbed, cc. NTP (b)	C ₂ H ₄ on sites I, cc. NTP	C ₂ H ₄ on sites II, cc. NTP	
55	5.91	0.145	0.050	0.033	0.017	0.095
46	175	0.064	6.48	0.123	0.040	0.027	0.013	0.083
54	250	0.055	6.08	0.110	0.037	0.025	0.012	0.073
58	350	0.063	6.16	0.111	0.021	0.015	0.006	0.090
57	500	0.063	6.19	0.092	0.017	0.017	Trace	0.075
60	650	0.063	6.19	0.099	0.021	0.019	0.002	0.078
59	700	0.062	6.50	...	0.025	0.019	0.006	...
61	825	0.058	5.88	0.112	0.028	0.022	0.006	0.084
62	900	0.060	6.22	0.116	0.026	0.021	0.005	0.090

^a Catalyst weight 0.126 g.; adsorption temperature of ethylene 24°; evacuation before flashing 11 min. at 24°; rate of flashing about 15°/min.

adsorption) becomes zero at about 0.6 cc. of preadsorbed ammonia. A comparison of this amount with the amount of ethylene strongly adsorbed on the bare surface (0.05 cc.) shows that much more ammonia is needed to "poison" the active sites for ethylene chemisorption than corresponds to the amount of ethylene which just covers these active sites, even after allowing for the fact that the cross-sectional area of ammonia is only one-third to one-half as large as that of ethylene. This suggests that ammonia is not adsorbed selectively on the active sites for ethylene, but is distributed over a wider region on the surface. This matter will be discussed in somewhat greater detail later. It is also of interest that the "weak" adsorption (the "total" minus the "strong" adsorption) is also affected by such relatively small amounts of preadsorbed ammonia, as shown by the broken line in Fig. 4.

The results obtained by maintaining the amount of preadsorbed ammonia constant at about 0.06 cc. and varying its adsorption temperature from 175 to 900° are summarized in Table I. The amount of 0.06 cc. corresponds approximately to the "strong" adsorption of ethylene on the active sites, as described above, and this amount is so small that the pressure of ammonia during preadsorption remained negligible. It should be noted that the ratio of the first peak to the second peak of ethylene varies with the adsorption temperature of ammonia. This is more clearly seen in Fig. 5, where the typical flash-desorption chromatograms are shown. The distribution of the adsorbed ethylene between the two sites was determined approximately by drawing a vertical line on the chromatogram through the minimum between the peaks, as was done in the previous work.⁸ The weak adsorption and the total strong adsorption of ethylene (the sum for the sites I and II), as well as

the adsorption on each of the two sites separately are plotted in Fig. 6 as a function of the adsorption temperature of ammonia. It appears from the plots that the amounts of ethylene adsorbed both on sites I and II show minima at the adsorption temperatures of ammonia of about 350 and 500°, respectively.

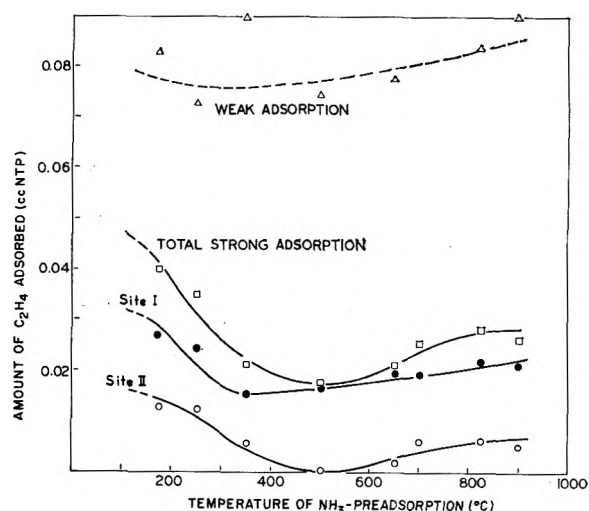


Figure 6. The effect of the adsorption temperature of ammonia on the adsorption of ethylene. Weight of alumina, 0.126 g.; amount of adsorbed ammonia, about 0.06 cc.

These results can be explained by assuming that the active sites for strong ethylene adsorption coincide with the relatively high, but not with the highest energy sites for ammonia adsorption. When a small amount of ammonia is admitted at a low temperature, it is adsorbed rather evenly on the surface because of the fast rate of adsorption, high activation energy of

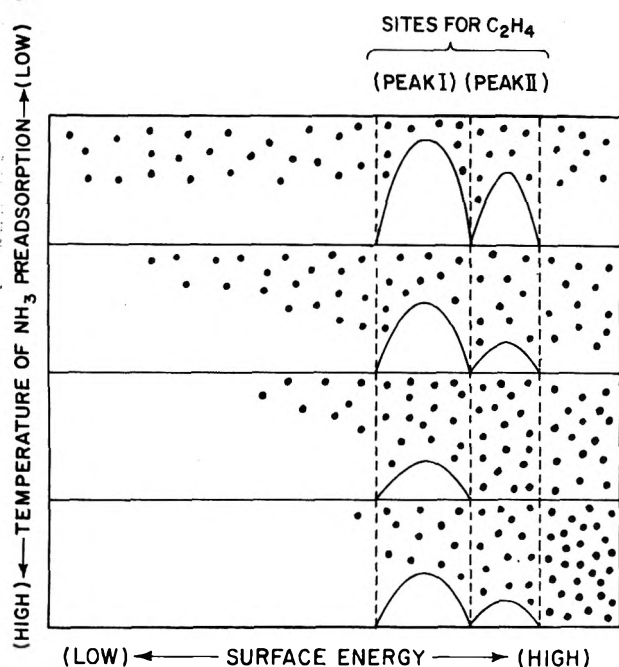


Figure 7. Schematic diagram of the distribution of a small amount of ammonia on the surface sites of alumina at different temperatures of its preadsorption.

desorption, and very low pressure in the gas phase. The high energy sites, which are responsible for the strong adsorption of ethylene, therefore are not occupied by ammonia to an appreciable extent. However, when ammonia is adsorbed at a higher temperature, it cannot go on the low energy sites but is concentrated on the higher energy sites, thus covering the active

sites for ethylene adsorption more efficiently. When the adsorption temperature is very high, ammonia adsorbs preferentially on the sites of still higher energy than those for ethylene chemisorption, and as a consequence the minima shown in Fig. 6 are obtained. These correlations are illustrated schematically in Fig. 7.

The activation energies of desorption of ethylene on the sites I and II are, respectively, 26.8 and 35.4 kcal., as mentioned before, and the difference in these values can explain the fact that the minimum in Fig. 6 for sites I (350°) is lower than for sites II (500°). The "weak" adsorption could perhaps also be explained in a similar manner. Unfortunately, however, the experimental information here is not as quantitative as it is for the "strong" adsorption, because it is easily affected by fluctuations in the equilibrium pressure of ethylene and in the adsorption temperature. The observation that the amount of ammonia needed at 250° to poison the active sites for ethylene chemisorption was far larger than expected, as seen in Fig. 4, is also explainable in terms of the above assumptions.

In conclusion, the results of the present study seem to show that, in general, it is not possible to determine in a simple manner the surface acidity of alumina by measuring the amount of adsorbed ammonia. The difficulty is due to the distribution of surface energies over an appreciable range of values. There is need for further experimental information on these systems, in particular with respect to the relation between the chemisorption of olefins and the acidic centers on the catalyst surface.

Diffusion in the System Molten Sodium Iodide–Potassium Chloride

by S. B. Tricklebank, L. Nanis, and J. O'M. Bockris

The Electrochemistry Laboratory The University of Pennsylvania, Philadelphia 4, Pennsylvania
(Received July 3, 1963)

The diffusion coefficients of Na²² in NaI, 50 mole % NaI–50 mole % KCl, and KCl, and of I¹³¹ into NaI have been measured as a function of temperature. Although special attention to end errors was paid, deviations from the Nernst–Einstein equation are confirmed to be of the same order as those previously measured. The energy of activation for paired diffusion is approximately twice that for the individual ions. The energies of activation for Na⁺ and I[−] in pure NaI are not equal. The energy of activation for Na²² in the system NaI–KCl is greater at the 50–50 composition than for pure NaI or in KCl and $\Delta E_{\text{diffusion}} \approx \Delta E_{\text{conductance}} + RT$. The difference in the energies of activation of Na⁺ and I[−] is interpreted in terms of a significant jump energy arising when the ion concerned is larger than the average hole size. The maximum of the energy of activation of Na²² in the mixture is interpreted in terms of trimer formation.

From self-diffusion results for simple fused salts and the hole theory for liquids, it appears that the energy of activation (ΔE) for diffusion of the ions is equal to the energy to form a hole, which is equal to $3.74RT_m$,¹ where R is the gas constant and T_m the melting point of the salt in degrees absolute. (The singular fact that ΔE depends only on the melting point, *i.e.*, lattice energy of the entire salt, raises the question of how ΔE would behave as a function of interactions in a mixture.) The simplest method of approach is met by the diffusion of M'X into MX (*cf.* Bockris, *et al.*,² where the diffusion of the alkali metal ions into molten sodium chloride has been measured). In the present paper an examination has been made of the effect of diffusion in the reciprocal salt system NaI–KCl, chosen to contain ions of widely differing size.

Of the methods used to determine self-diffusion coefficients in molten salts^{1,3–7} the most convenient method is that of Bockris and Hooper,¹ where the diffusion takes place from a radioactive bulk into an inactive capillary. The advantage of their method is that it avoids the necessity of capillary tube filling in a second vacuum furnace. Therefore, the Bockris and Hooper method was used in the present work.

Experimental

The apparatus and method used were similar to those of Bockris and Hooper. With the measurement

of diffusion of Na²² into the 50 mole % NaI–50 mole % KCl mixture, difficulty in obtaining a constant D was experienced. This was found to be due to the lower melting point salt (NaI) melting first and forming a layer of liquid NaI under solid KCl. The KCl then melted and, being less dense than NaI, formed an upper layer, in spite of the absence of evidence concerning immiscibility from phase diagram studies.⁸ (Similar behavior has been noticed in the preparation of PbCl₂–KCl mixtures.⁹) Hence in the cap of the diffusion cell, an extra hollow slip joint was placed parallel to that carrying the silica capillary holder. A silica capillary was joined to this slip joint through which prepurified

- (1) J. O'M. Bockris and G. W. Hooper, *Discussions Faraday Soc.*, **32**, 218 (1962).
- (2) J. O'M. Bockris, S. Yoshikawa, L. Nanis, and S. R. Richards, to be published.
- (3) E. R. Van Artsdalen, D. Brown, A. S. Dworkin, and F. J. Miller, *J. Am. Chem. Soc.*, **78**, 1772 (1956).
- (4) A. Z. Borucka, J. O'M. Bockris, and J. A. Kitchener, *Proc. Roy. Soc. (London)*, **A241**, 554 (1957).
- (5) C. A. Angell and J. O'M. Bockris, *J. Sci. Instr.*, **35**, 458 (1958).
- (6) S. Djordjevic and G. J. Hills, *Trans. Faraday Soc.*, **56**, 269 (1960).
- (7) See also L. Yang and M. T. Simnad, "Physico-Chemical Measurements at High Temperatures," J. O'M. Bockris, J. L. White, and J. D. Mackenzie, Ed., Butterworths, London, 1959, Chapter 14, p. 295.
- (8) Landolt–Börnstein, **II**, **3**, 158 (1956).
- (9) K. Balasubrahmanyam, private communication.

nitrogen was passed to stir the melt. The melt was mixed both before filling the capillaries and after adding the radioactive pellets. During the work, silica capillaries were replaced by those of platinum. This eliminated any errors associated with corrosion of the capillaries by the melt. Radioactive analyses were made with a Cosmic Radiation Labs., Inc., scintillation counter.

Diffusion coefficients may be calculated for appropriate values of time and tube length by measurement of the total diffusate Q , from the equation¹⁰

$$Q = 2c_0A\sqrt{Dt/\pi} \quad (1)$$

where c_0 is the concentration of the radioactive species in the bulk, A is the cross-sectional area of the capillary, and t is the time.

It was thought by Bockris and Hooper that their method required certain end corrections due to (a) gas-phase transfer of radioactive salt from the bulk to the nonactive salt in the capillaries during equilibration of the tracer with the nonactive material, and (b) adherence of active salt to the mouth of the capillary when the run was terminated. Mechanism (a) was eliminated by holding the mouths of the capillaries 10 cm. above the melt during equilibration, and (b) was corrected for by "zero-time" experiments (runs of 5-sec. duration). Their correction was found to be independent of ion and temperature. Dependence on bath concentration was not examined. D was found to be independent of stirring rate between 4 and 55 r.p.m.

Borucka, Bockris, and Kitchener⁴ suggested that in diffusion measurements by capillary techniques, when the liquid is swept past the mouth of the capillary, some of the liquid in the capillary is "dragged out" and replaced by the surrounding liquid. This gives a positive error to D values in which no account is made for this effect. They established by dye experiments that this " Δl -effect" increased with increasing flow rate across the mouth of the capillary (\bar{v}) and depended upon the capillary diameter (d). By making experiments at different times, Δl was eliminated. The correction factor reduced the D value in NaCl in the temperature range 825–942° by 10–30%.

Berne and Berggren¹¹ confirmed the existence of this Δl -effect. Mills¹² recognized the existence of a possible dependence of an uncorrected D on \bar{v} and stated that it was possible to find an r.p.m. which gave a \bar{v} at which the effect of end errors was zero. Dworkin, *et al.*,¹³ used approximately the same r.p.m. values as Mills and, as their D values did not change with changes in length of capillaries or in length of diffusion time, assumed that their r.p.m. gave a negligible Δl .

Bockris and Hooper confirmed that Δl effects exist

and that for values of \bar{v} of approximately 0–2 mm. sec.⁻¹, an apparent dependence of the measured D value upon \bar{v} existed. However, their D values were apparently independent of \bar{v} over the range 2–30 mm. sec.⁻¹ for NaCl at 928°. They concluded that they had reached the \bar{v} which Mills had found for "zero end error." The observed dependence of D on \bar{v} in the 0–2 mm. sec.⁻¹ region was interpreted in terms of a breakdown of the boundary conditions assumed in (1), due to depletion of the radioactive concentration at the mouth of the capillary.

An alternative explanation, however, is that the change of D with \bar{v} in the region 0–2 mm. sec.⁻¹ is not due to the latter effect, but to the existence of the Δl -effect, changing rapidly with \bar{v} in the lower region and relatively slowly in the upper region (2–30 mm. sec.⁻¹), and that the end-error-free region postulated by Mills is not present. It would then be necessary to subtract from apparent D values an amount corresponding to the counts per minute which accrue from the melt by means of the Δl -effect.

A detailed re-study of a dye system,¹⁴ similar to that performed by Borucka, Bockris, and Kitchener, confirmed the existence of the Δl -effect suggested by these authors, together with a dependence there noted upon \bar{v} and d . An empirical relation has been established between \bar{v} and $\Delta l/d$. Dimensional analysis suggests (see also Thom and Apelt¹⁵) that

$$\Delta l/d = f(\bar{v}d\rho/\eta) = f(\text{Reynolds number}) \quad (2)$$

where ρ is the density and η the viscosity. In the present study, Reynolds numbers have been calculated for the conditions of the experiment, and from the empirical relation established by Richards, Δl was calculated. The corrected value of Q was calculated by subtraction of an amount $c_0A\Delta l$ from the total observed counts in the capillary. This amount, $c_0A\Delta l$, corresponds to the radioactivity swept into the capillary by the Δl -effect. Thus the diffusion coefficients were calculated on the basis of the equation

$$Q_{\text{corrected}} = 2c_0A\sqrt{Dt/\pi} \quad (3)$$

If a constant end correction of 200 counts/min. is taken instead of the Δl correction used in this work, it

- (10) J. Crank, "Mathematics of Diffusion," Oxford University Press, 1957, pp. 18, 31.
- (11) E. Berne and J. Berggren, *Acta Chem. Scand.*, **14**, 428 (1960).
- (12) R. Mills, *J. Am. Chem. Soc.*, **77**, 6116 (1955).
- (13) A. S. Dworkin, R. B. Escue, and E. R. Van Artsdalen, *J. Phys. Chem.*, **64**, 872 (1960).
- (14) S. R. Richards, Ph.D. Thesis, University of Pennsylvania.
- (15) A. Thom and C. J. Apelt, Aeronautical Research Council, R. & M. No. 3090, Her Majesty's Stationery Office, London, 1958.

has been calculated that the energy of activation does not change significantly but D values may be increased by some 10%.

The errors in the measurement have been assessed as: $Q_{\text{corrected}} \pm 3.2\%$, $c_0 \pm 1.6\%$, $A \pm 0.5\%$, and $t \pm 0.2\%$, making the total possible error in D for any one capillary $\pm 10.8\%$, with the average deviation from the mean in this work being $\pm 7\%$.

Results

The results are expressed in terms of

$$D = A \exp[-\Delta E/RT] \quad (4)$$

where D is the diffusion coefficient, ΔE is the energy of activation, R is the gas constant, T is the absolute temperature, and A is a term independent of temperature. Table I gives D values for individual capillaries and Fig. 1-3 show plots of $\log D$ as a function of $1/T$. Table II gives values of A and ΔE calculated by the method of least squares together with the standard deviation of ΔE in each case.

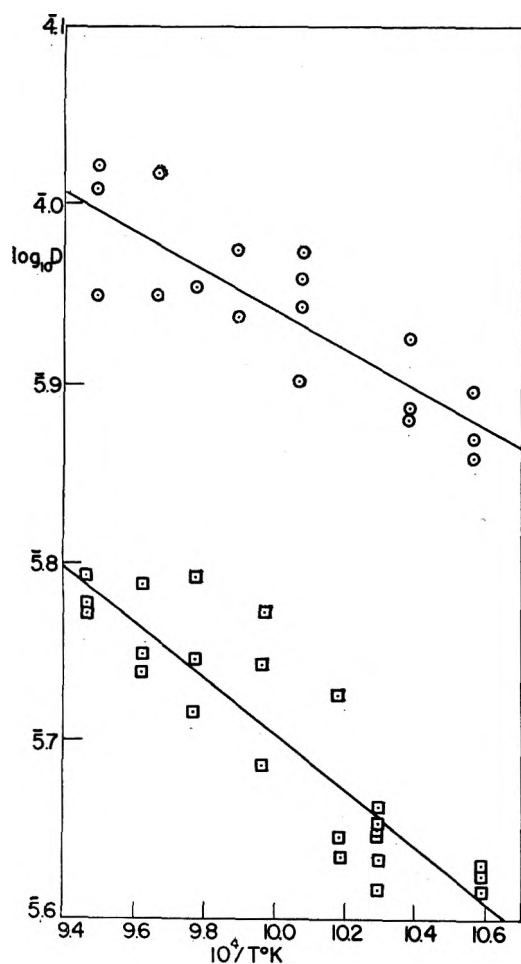


Figure 1. $\log D_{\text{Na}^{22}}$ and $\log D_{\text{I}^{131}}$ in NaI against $1/T$: \circ , Na^{22} ; \square , I^{131} .

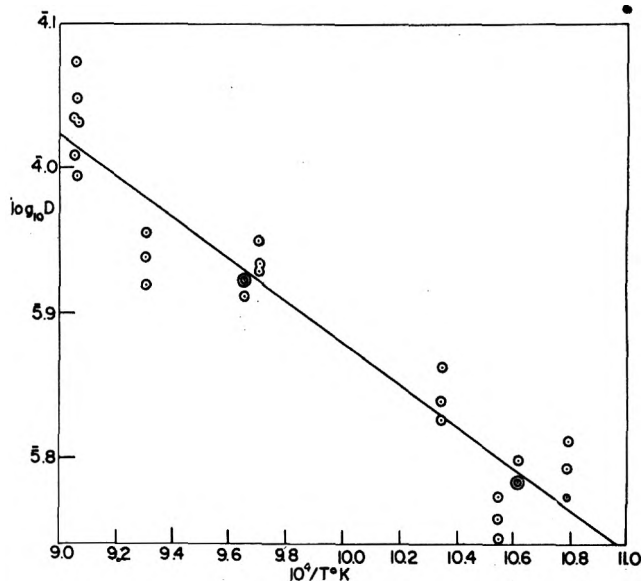


Figure 2. $\log D_{\text{Na}^{22}}$ in 50 mole % NaI-50% KCl against $1/T$.

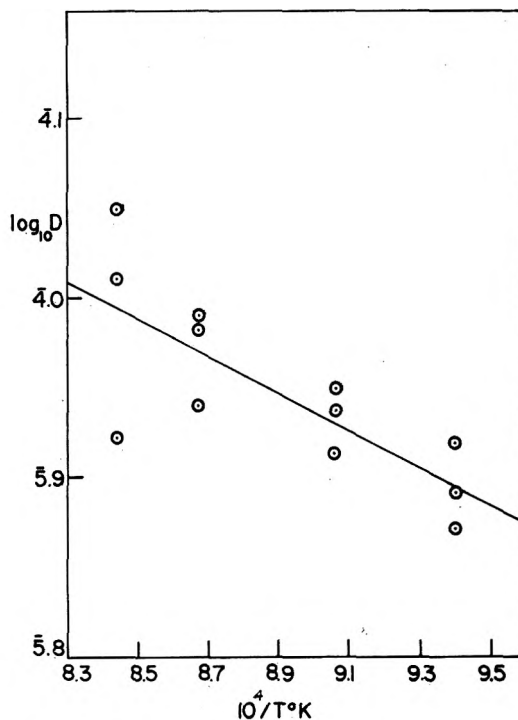


Figure 3. $\log D_{\text{Na}^{22}}$ in KCl against $1/T$.

Discussion

Previous Work. The only previous self-diffusion measurements on NaI have been made by Bockris and Hooper,¹ who found that the energies of activation for diffusion of cation and anion differed by 0.4 kcal. mole⁻¹. Results of the paired vacancy diffusion treatment were inconsistent with those for other alkali

Table I: Average Diffusion Coefficients in the System NaI-KCl

Temp., °C.	$D \times 10^4$, cm. ² sec. ⁻¹	Temp., °C.	$D \times 10^4$, cm. ² sec. ⁻¹
Na ²² in NaI		I ¹³¹ in NaI	
675	0.75	673	0.42
692	.79	700	.44
720	.91	711	.47
722	.81	730	.54
738	.91	751	.57
750	.90	767	.58
763	.95	785	.60
782	.99		
Na ²² in 50% NaI-50% KCl		Na ²² in KCl	
655	0.62	791	0.79
669	.62	831	.86
676	.58	880	.94
694	.70	914	1.00
758	.86		
765	.83		
803	.87		
831	1.06		
833	1.09		

Table II: Constants of the Equation $D = A \exp[-\Delta E/RT]$

System	Tracer	$A \times 10^3$	ΔE , kcal. mole ⁻¹	Temp. range, °C.
NaI	Na ²²	1.09	5.02 ± 0.77	675-782
	I ¹³¹	1.88	$7.21 \pm .76$	673-785
50% NaI-50% KCl	Na ²²	2.08	$6.59 \pm .38$	655-833
KCl	Na ²²	0.73	4.70 ± 1.14	791-914

halides reported in the same paper, where the calculated energy of activation for I⁻ was greater than that for Na⁺. (The energy of activation for NaI pair was not constant, as distinct from the other salts.) The discrepancies in the ΔE values between the present and the former work may be due to some decomposition of NaI which is very sensitive to traces of water and oxygen.

Application of the Nernst-Einstein Equation. Deviations from the Nernst-Einstein equation in molten salt diffusion

$$\Lambda = \frac{F^2}{RT} (D_+ + D_-) \quad (5)$$

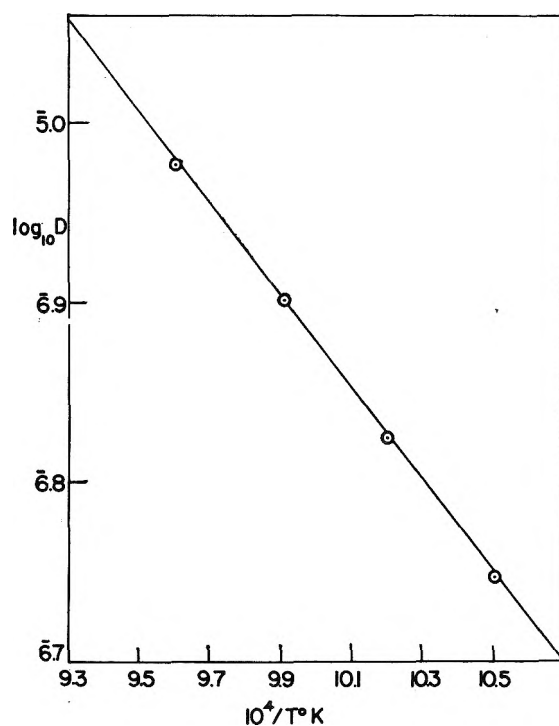
where Λ is equivalent conductance and F is the Faraday constant, have been interpreted by Borucka, Bockris, and Kitchener⁴ and Bockris and Hooper¹ by the existence of some paired diffusion. Tracer diffusion, D^* , is considered to be the sum of two mechanisms of diffusion: (i) the diffusion of a single ion D_+ , D_- into a

vacancy; and (ii) the diffusion of two oppositely charged ions (by rotation), D_p , into a paired vacancy, leading to the equations

$$D_+^* = D_+ + D_p \quad (6)$$

$$D_-^* = D_- + D_p \quad (7)$$

For mechanism (ii) it is not necessary to postulate the existence of "long-lived" paired entities, but it is only necessary that they have a lifetime greater than the time required for a rotational movement of the ion pair into a paired vacancy. Values of the diffusion coefficients, D_{Na^+} , D_{I^-} , and D_{NaI} have been calculated from simultaneous solution of eq. 5, 6, and 7, using conductance data of Yaffe and Van Artsdalen.¹⁶ These are given in Table III together with the activation energy for each diffusion process, as calculated from plots of $\log D_i$ as a function of $1/T$. Figure 4 shows the plot of


 Figure 4. $\log D_{NaI}$ in NaI against $1/T$.

$\log D_{NaI}$ vs. $1/T$. This is linear, which confirms the results obtained by Bockris and Hooper for other alkali halides.

Because end errors in capillary diffusion (by either diffusion of radioactive tracer into or out of the capillary) make the measured diffusion coefficients too large,

(16) I. S. Yaffe and E. R. Van Artsdalen, *J. Phys. Chem.*, **60**, 1125 (1956).

Table III: Derived Diffusion Coefficients for NaI

Temp., °C.	$D \times 10^4, \text{cm.}^2 \text{sec.}^{-1}$		% greater than Nernst-Einstein	$D \times 10^4, \text{cm.}^2 \text{sec.}^{-1}$			$\Delta E, \text{kcal. mole}^{-1}$		
	From conductance ($D_{\text{Na}^+} + D_{\text{I}^-}$)	From tracers ($D_{\text{Na}^+} + D_{\text{I}^-}$)		Calcd. D_{Na^+}	Calcd. D_{I^-}	Calcd. D_{NaI}	$-\text{Rd ln } D_{\text{Na}^+}$ d(1/T)	$-\text{Rd ln } D_{\text{I}^-}$ d(1/T)	$-\text{Rd ln } D_{\text{NaI}}$ d(1/T)
680	1.08	1.19	10.3	0.71	0.37	0.06	4.5	6.4	11.6
708	1.17	1.30	11.4	.76	.40	.07			
737	1.26	1.42	12.7	.82	.44	.08			
769	1.36	1.55	13.9	.87	.49	.09			

and because these end error corrections now have a better experimental basis than those previously used,¹ it is necessary to determine whether the deviations from the Nernst-Einstein equation for NaI are now still maintained. Calculations show that a Δl correction greater by one-third than those used here (*i.e.*, a correction based on independent experimental determinations) would be necessary for no deviation to be observed. This value of Δl lies well outside the limits of uncertainty on the experimental plot of Reynolds number *vs.* $\Delta l/d$ and hence the deviations from the Nernst-Einstein equation are confirmed. A similar conclusion was reached from an evaluation of data in which the end error correction was eliminated by experiments made for two different times.

The calculated energies of activation for diffusion increase in the order of $\text{Na}^+ < \text{I}^- < \text{NaI}$. If

$$\Delta E = \Delta H_{\text{H}} + \Delta H_{\text{J}}^* \quad (8)$$

where ΔH_{H} and ΔH_{J}^* ¹⁷ are the energies to form a hole and jump into a hole, respectively, then it is expected¹ that the work done in forming the average hole for the salt will be the same for cation and anion. The relatively larger energy of activation for I^- could be accounted for by the fact that for I^- , the ion size is larger than the most probable hole size and hence a significant jump energy is required to move the I^- ion into a hole.¹⁸ Although evidence from molecular liquids^{17,19} suggests that $\Delta H_{\text{J}}^* \ll \Delta H_{\text{H}}$, it has been shown in the case of self-diffusion of CCl_4 ²⁰ that a large diffusing species can have a considerable jump energy (in this case $\Delta H_{\text{J}}^* \simeq \Delta E/3$). For the formation of a paired vacancy, a larger energy will be required than that for the formation of single vacancies and, therefore, the energy of activation for NaI diffusion will be larger than that for either Na^+ or I^- . It might be expected that the energy to form a paired vacancy is approximately twice that to form a single vacancy. It might also be expected that the jump energy required for a NaI pair to rotate into a paired vacancy will be small compared with the energy to form that paired vacancy, and hence ΔE_{NaI} would approximate the sum of ΔE_{Na^+} and ΔE_{I^-} . This is

supported by the results reported in this paper (Table III).

Energy of Activation for the Diffusion of Na^{22} in the Mixture. Tests for statistical significance (Fisher "Student" t-test²¹) show that the energy of activation of Na^{22} in the mixture is greater than that of Na^{22} in NaI with a probability of at least 90%. Similarly, there is a 90% probability that the energy of activation of Na^{22} in the mixture is greater than that of Na^{22} in KCl. Predictions based on the hole theory of liquids¹ for the ΔH_{H} component of ΔE are that the energy of activation of Na^{22} in the mixture should be less than that for Na^{22} in either of the pure salts. Therefore, an explanation for this anomalous behavior must be sought.

Bockris, Crook, Bloom, and Richards²² showed that

$$\Delta H_{\text{H}^+} + \Delta H_{\text{J}}^* = \Delta E_{\text{A}} + RT \quad (9)$$

where ΔE_{A} is the energy of activation for conductance. Bockris and Hooper¹ used this equation to compare the energies of activation for single ion diffusion with those for conductance and found good agreement. In this case it is not possible to compare conductance data with single ion diffusion but only with the activation energies for tracer ion diffusion (Table IV). (It is expected that the two comparisons would show the same trends.) The comparison lends support to the indications of higher energy of activation for diffusion of Na^{22} in the mixture as found from the present diffusion data (see Fig. 5).

(17) A. Bondi, *J. Chem. Phys.*, **14**, 591 (1946).

(18) An accurate estimation of the energy of activation for jumping is not possible from existing results for molten salts, but awaits the determination of energies of activation for diffusion at constant volume now being made in this Laboratory.

(19) A. Jobling and A. Lawrence, *Proc. Roy. Soc. (London)*, **A206**, 257 (1951).

(20) H. Watts, B. J. Alder, and J. H. Hildebrand, *J. Chem. Phys.*, **23**, 659 (1955).

(21) A. Hald, "Statistical Theory with Engineering Applications," John Wiley and Sons, Inc., New York, N. Y., 1955, p. 571.

(22) J. O'M. Bockris, E. H. Crook, H. Bloom, and N. E. Richards, *Proc. Roy. Soc. (London)*, **A255**, 558 (1960).

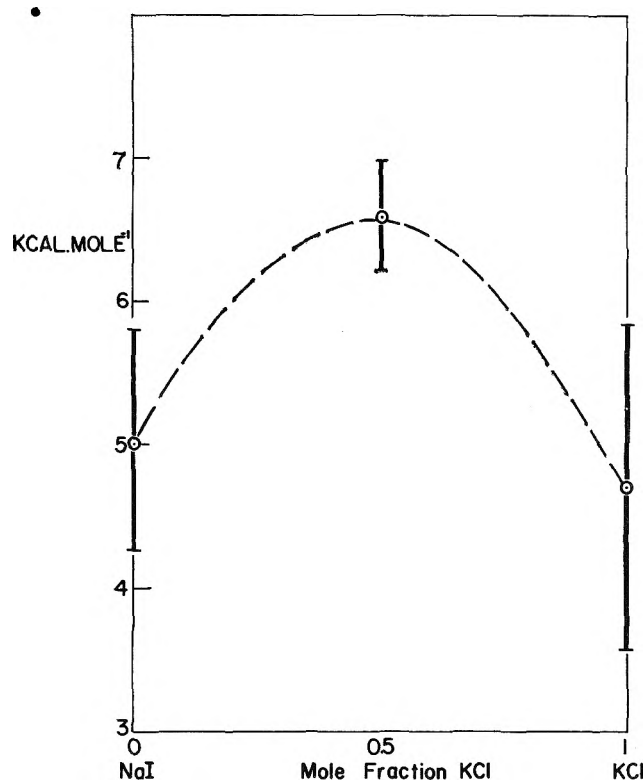


Figure 5. Energy of activation for diffusion of Na^{22} in the system NaI-KCl against composition.

Table IV: Comparison of Energies of Activation for Diffusion of Na^{22} with Those for Conductance

System	ΔE_{diff} , kcal. mole ⁻¹	$\frac{\Delta E_{\Lambda}}{RT}$, ^a kcal. mole ⁻¹	ΔE_{Λ} lit. ref.
NaI	5.0	5.2	Yaffe and Van Artsdalen ¹⁶
50% NaI-50% KCl	6.6	6.0	Bloom, <i>et al.</i> ²³
KCl	4.7	5.3	Van Artsdalen and Yaffe ²⁴

^a $T = 1000^{\circ}\text{K}$.

Bloom, Davis, and James²⁵ have shown that negative values of the surface heat of mixing per unit area, $\Delta H^s/a$, are indicative of the existence of complex ion²⁶ formation. In the system NaI-KCl, negative deviations of $\Delta H^s/a$ reach a maximum value at 50% KCl, which indicates the formation of a species with the composition

$(\text{ClNaI})^-$. This is possible because the polarizing power of Na^+ is greater than that of K^+ , so that Na^+ competes more strongly for the available halide ions. It is doubtful whether this ion is a true covalently bound complex ion, but rather an ionic aggregate or "trimer." The existence of such an ion is supported by evidence from electrical conductivity and molar volume measurements²³ in that deviations from ideality are maximum at the equimolar concentration.

In the present work, the existence of an ion $(\text{ClNaI})^-$ can readily account for the higher $\Delta E_{\text{Na}^{22}}$ in the mixture. There are two possible explanations.

(i) If it is assumed that the trimer is fairly stable, the increase in the energy of activation for Na^{22} in the mixture can be accounted for by a larger energy to form a triple vacancy. However, the probability of forming a triple vacancy is very low, so that, unless the number of trimers present is small, it would be expected that the activation energy would be very much greater than actually found.

(ii) The trimer is not very stable, but sufficiently so as to hinder the diffusion of Na^{22} . With increasing temperature, the trimer will gradually break up and free more Na^{22} , *i.e.*, more Na^{22} will be available for ordinary diffusion as Na^{22} ion. Similar behavior has been reported by Perkins, *et al.*,²⁷ for the diffusion of Pb^{210} in mixtures of PbCl_2 -KCl. At the composition corresponding to $2\text{PbCl}_2 \cdot \text{KCl}$, the diffusion of Pb^{210} is hindered at lower temperatures.

Acknowledgment. The authors wish to thank the Atomic Energy Commission for financial support of the work under Contract No. AT(30-1)-1769 and Mr. S. R. Richards for helpful discussions.

- (23) H. Bloom, I. W. Knaggs, J. J. Molloy, and D. Welch, *Trans. Faraday Soc.*, **49**, 1458 (1953).
- (24) E. R. Van Artsdalen and I. S. Yaffe, *J. Phys. Chem.*, **59**, 118 (1955).
- (25) H. Bloom, F. G. Davis, and D. W. James, *Trans. Faraday Soc.*, **56**, 1179 (1960).
- (26) The significance of this term is discussed in some detail by H. Bloom and J. O'M. Bockris (a chapter in the book "Molten Salts," B. R. Sundheim and D. M. Gruen, Ed., to be published by McGraw-Hill Book Co., Inc., 1963). See also J. O'M. Bockris, D. Inman, A. K. N. Reddy, and S. Srinivasan, *J. Electroanal. Chem.*, in press.
- (27) G. Perkins, Jr., R. B. Escue, J. F. Lamb, T. H. Tidwell, and J. W. Wimberley, *J. Phys. Chem.*, **64**, 1911 (1960).

Thermodynamic Properties of Solid Vanadium-Iron Alloys¹

by K. M. Myles² and A. T. Aldred

*Alloy Properties Group, Metallurgy Division, Argonne National Laboratory, Argonne, Illinois
(Received July 11, 1963)*

The vapor pressure of iron over solid iron and over a series of vanadium-iron alloys has been measured by the torsion-effusion method in the temperature range 1500 to 1700°K. The chemical activities, as well as the free energies, entropies, and enthalpies of formation of the alloys have been computed at 1600°K. from the vapor pressure data. The activities of iron exhibit fairly large negative deviations from Raoult's law throughout the entire compositional range. The activities of vanadium, as determined by the Gibbs-Duhem relation, deviate negatively from ideal behavior in the iron-rich alloys but approach ideal behavior in the vanadium-rich alloys. The positive excess entropies and enthalpies of formation that are found at 1600°K. are considered in relation to the configurational, vibrational, and magnetic changes that occur upon alloying.

Introduction

The thermodynamic properties of transition metal alloys have not been studied to any great extent. This is partly a result of the experimental difficulties encountered, but is due more to the difficulty in interpreting the properties in terms of existing models of metallic solutions. However, the recent emphasis on resolving the factors that govern transition metal behavior requires that the thermodynamics also be considered.

The V-Fe alloy system was selected for the present study because of the extensive mutual solid solubility of the components at elevated temperatures. In addition, other pertinent properties of the system were known.

The torsion-effusion technique was used because of the low vapor pressures involved and because the differences in the volatilities of vanadium and iron enable the design of the experimental apparatus to be simplified. This method also allowed the duration of the experimental runs to be appreciably shortened, and thereby minimized compositional changes in the alloys.

The V-Fe equilibrium diagram is shown in Fig. 1.³ At high temperatures, b.c.c. α -iron and α -vanadium form a continuous series of solid solutions; there is a narrow f.c.c. γ -iron loop. The liquidus and solidus have a minimum at about 33 atom % V and 1740°K. In the equiatomic compositional region, a σ -phase occurs, which dissolves congruently into the α solid solu-

tion at about 1470°K. When an alloy of approximately equiatomic composition is quenched from a temperature where the α -phase is stable and annealed for a short time at 870°K., a metastable CsCl-type ordered structure is formed, which transforms on further annealing to the σ -phase.

The only previous thermodynamic study of the V-Fe alloy system was made by Saxer,⁴ who used the Knudsen effusion method over the temperature range 1550 to 1725°K. The activities and free energies calculated from the vapor pressure data at 1613°K. are in good accord with the present data, although there is disagreement between the two sets of entropy and enthalpy values.

Experimental Techniques

The adaptation of the torsion-effusion method to the study of vapor pressures of metals and alloys has been described by previous authors.^{5,6} In the present arrangement, which has been described in detail else-

- (1) This work was performed under the auspices of the U. S. Atomic Energy Commission.
- (2) This paper is based upon a thesis submitted by K. M. Myles in partial fulfillment of the requirements for the Ph.D. degree at the University of Illinois, Urbana, Ill.
- (3) M. Hansen, "Constitution of Binary Alloys," McGraw-Hill Book Co., Inc., New York, N. Y., 1958.
- (4) R. K. Saxer, "The Chemical Activities of Iron and Vanadium in Binary Iron-Vanadium Alloys and the Vapor Pressures of Pure Cobalt, Iron, and Vanadium," Thesis, The Ohio State University, Columbus, Ohio, 1962.

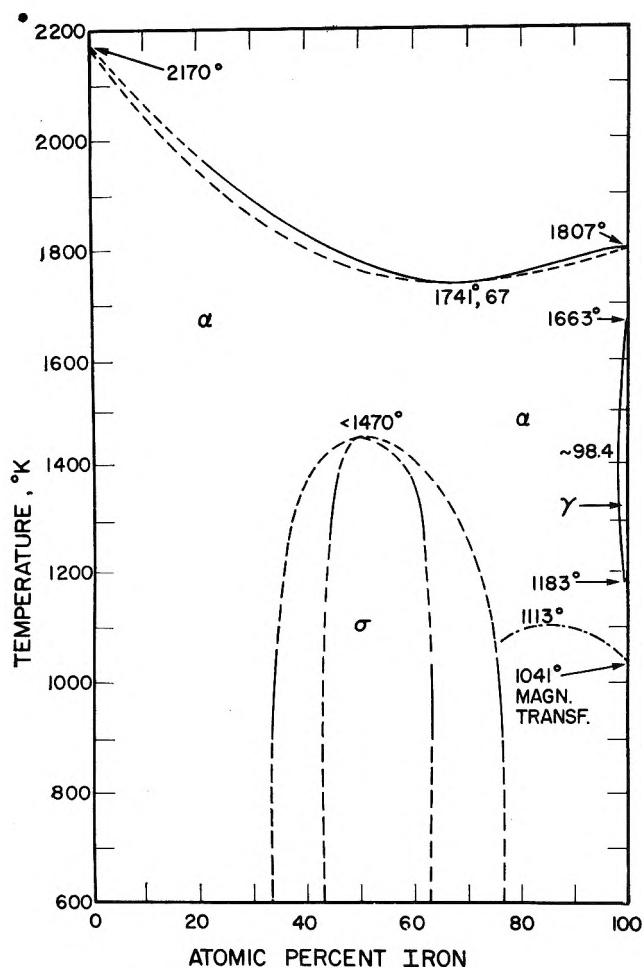


Figure 1. The vanadium-iron equilibrium diagram.

where,⁷ the specimen is enclosed in a tantalum effusion cell that has two eccentrically located orifices. The cell is suspended vertically from a fine tungsten wire in which an elastic torsional strain is induced as the vapor effuses through the orifices. The vapor pressure p is related to the angle θ through which the cell rotates by the expression $p = 2\tau\theta/\Sigma A d f$. Here τ is the torsion constant of the wire, A is the cross-sectional area of the orifice, d is the horizontal distance of the orifice from the suspension axis, and f is the Freeman-Searcy correction factor for an orifice of nonzero length.⁸

The alloys were prepared by arc-melting on a water-cooled copper hearth under a helium-argon atmosphere 99.96% pure iron, obtained from the Metals Manufacturing Control Laboratory, and 99.88% pure vanadium, supplied by the Union Carbide Metal Co. Although weight losses were small, chemical analyses were performed on all the alloys. The arc-melted buttons were machined into the form of coarse turnings, which were loosely packed into the cells to ensure a large surface-to-volume ratio. Each cell was homogenized for 3

hr. and degassed at a temperature at least 50° over the anticipated maximum temperature of the run until a constant deflection was noted. As the weight loss during a run generally did not exceed 0.2%, the compositional changes of a specimen were considered to be insignificant. Chemical analyses indicated that the concentration of vanadium in the effusate was less than 0.1%.

Results

The vapor pressure of iron was measured over pure iron and over nine vanadium-iron alloys. Plots of $\log p$ vs. $1/T$ were linear in form in accord with the Clausius-Clapeyron relation. The constants of the equations representing the plots were evaluated by the method of least squares and are given in Table I with the probable errors for 95% confidence limits.

Table I: Vapor Pressures of Iron over Vanadium-Iron Alloys

$\log p$ (mm.) = $m/T + b$			
N_{Fe}	m	b	Temp. range, °K.
1.000	-20908 ± 109	10.036 ± 0.070	1451-1677
0.913	-20751 ± 117	$9.888 \pm .109$	1467-1672
.807	-20096 ± 110	$9.373 \pm .070$	1472-1666
.704	-19984 ± 115	$9.178 \pm .074$	1468-1629
.596	-19810 ± 119	$8.952 \pm .075$	1454-1668
.501	-20087 ± 127	$8.920 \pm .080$	1469-1669
.399	-20774 ± 125	$9.161 \pm .079$	1468-1704
.304	-21070 ± 100	$9.118 \pm .081$	1474-1756
.206	-21238 ± 66	$8.943 \pm .040$	1527-1767
.0951	-23411 ± 190	$9.331 \pm .110$	1631-1800

The vapor pressure data were used to calculate the thermodynamic properties of the solid alloys at 1600°K. with hypothetical pure α -iron as the reference state. No corrections were made for the difference in free energy between γ - and α -iron^{9,10} since at 1600°K. it falls within the experimental accuracy with which the free energies can be determined. The chemical activities of iron were computed at 1500, 1600, and 1700°K. The activities of vanadium were determined by means

- (5) R. Speiser and J. W. Spretinak, "Determination of the Vapor Pressures of Metals and Alloys," "Vacuum Metallurgy," Electrochemical Society, Inc., 1955.
- (6) J. N. Pratt and A. T. Aldred, *J. Sci. Instr.*, **36**, 365 (1959).
- (7) K. M. Myles, Argonne National Laboratory, Argonne, Ill., ANL-6657 (1963).
- (8) R. D. Freeman and A. W. Searcy, *J. Chem. Phys.*, **22**, 762 (1954).
- (9) J. C. Fisher, *Trans. AIME*, **185**, 688 (1949).
- (10) R. J. Weiss and K. J. Tauer, *Phys. Rev.*, **102**, 1490 (1956).

Table II: Thermodynamic Properties of Vanadium-Iron Alloys at 1600°K.

N_{Fe}	a_{Fe}	a_V	$\Delta\bar{F}_{Fe}$ Cal./g. atom	$\Delta\bar{F}_V$ Cal./g. atom	$\Delta\bar{S}_{Fe}$ Cal./g. atom-deg.	$\Delta\bar{S}_V$ Cal./g. atom-deg.	$\Delta\bar{H}_{Fe}$ Cal./g. atom	$\Delta\bar{H}_V$ Cal./g. atom	ΔF Cal./g. atom	ΔH Cal./g. atom	ΔS Cal./g. atom-deg.
0.9	0.856	0.0138	-494	-13616	1.46	11.26	1842	4400	-1806	2098	2.44
.8	.695	.0466	-1157	-9747	2.54	4.82	2907	-2035	-2875	1925	3.00
.7	.534	.103	-1995	-7226	3.32	2.36	3317	-3450	-3564	1284	3.03
.6	.387	.188	-3018	-5313	3.82	1.46	3094	-2977	-3936	672	2.88
.5	.256	.312	-4332	-3702	4.06	0.985	2164	-2126	-4017	15	2.52
.4	.155	.470	-5927	-2400	4.12	1.09	665	-656	-3811	-131	2.30
.3	.0870	.634	-7763	-1449	4.04	1.13	-1299	359	-3343	-143	2.00
.2	.0460	.787	-9788	-761	4.57	0.935	-2316	735	-2566	122	1.68
.1	.0207	.900	-12327	-335	7.55	0.220	247	17	-1534	-9	0.953

of the Gibbs-Duhem integration. The activities as well as the calculated partial and integral free energies, entropies, and enthalpies of formation are assembled in Table II.

The precision of the activities is estimated to be about $\pm 3\%$ and that of the integral free energies about ± 300 cal./g. atom. Because the calculation of the entropies and enthalpies involves the difference between two large numbers, their precision is considerably lower. A reasonable estimate is about ± 1.50 cal./g. atom-deg. for the entropies and about ± 1500 cal./g. atom for the enthalpies. Possible systematic errors, although believed to be small, preclude an estimation of the accuracy.

Discussion

The vapor pressure of iron, as determined by this study, is plotted in Fig. 2. Values of the latent heat of sublimation at 298.15°K., calculated by means of the third-law test equation, showed no systematic temperature dependence. The average value of ΔH_{298}° , 99,000 \pm 150 cal./g. atom, agrees favorably with the value compiled by Hultgren,¹¹ 99,550 \pm 200 cal./g. atom.

As seen in Fig. 3, the activities of iron exhibit fairly large negative deviations from ideality. The activities of vanadium are also characterized by negative deviations in the iron-rich alloys, but ideal behavior is approached in the vanadium-rich alloys.

The most interesting thermodynamic properties in the present context are the excess quantities, which depict deviations from ideal behavior. The integral excess functions are shown in Fig. 4.

The minimum in the excess free energy occurs at approximately 55 atom % Fe, that is, near the composition of the congruent maximum of the σ -phase. However, in view of the nonconfigurational factors that appear to dominate the excess entropies and enthalpies, it is not believed that the excess free energies can be considered simply in terms of a tendency toward compound formation.

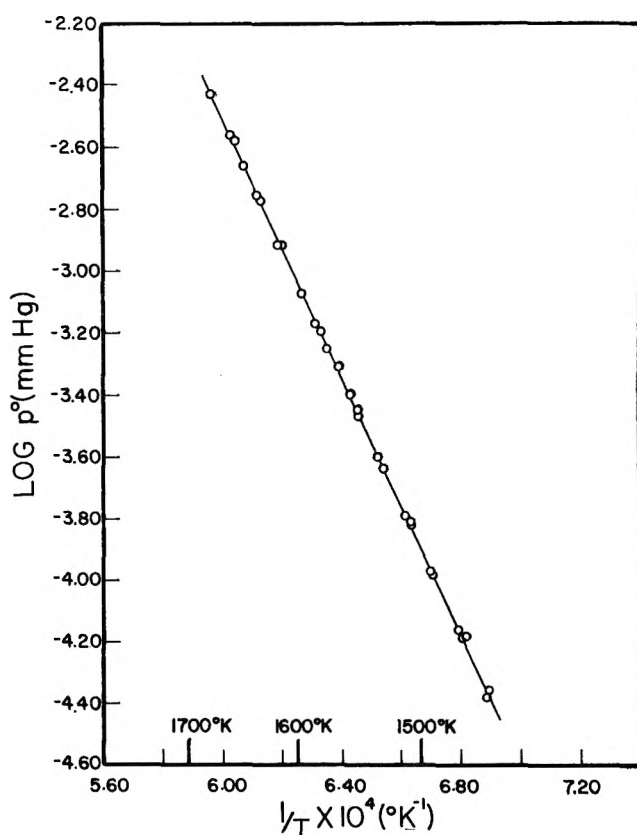


Figure 2. The vapor pressure of iron.

Although the excess free energies are regarded as more reliable, the excess entropies are more amenable to discussion. The excess entropy of formation may be correlated with the nonideal changes that occur in the atomic and electronic structures of the component metals upon alloying, as manifested by the configurational, vibrational, and magnetic characteristics of the alloys.

(11) R. Hultgren, R. L. Orr, P. D. Anderson, and K. K. Kelley, "Selected Values of Thermodynamic Properties of Metals and Alloys," John Wiley and Sons, Inc., New York, N. Y., 1963.

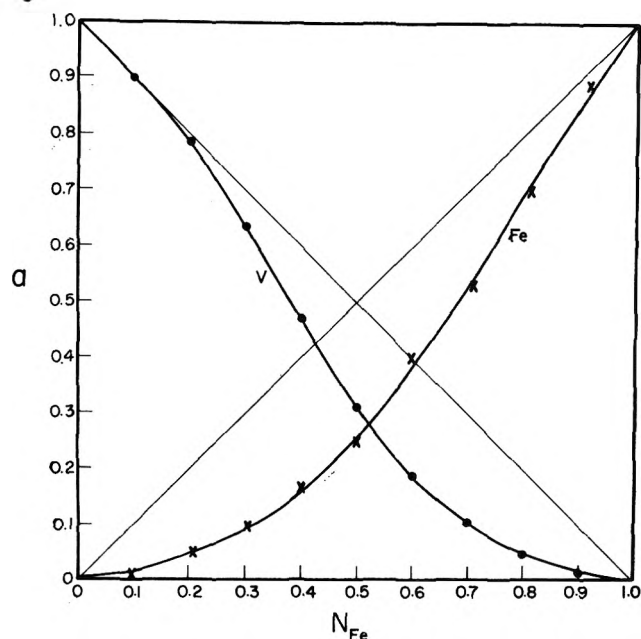


Figure 3. Activities of iron and vanadium at 1600°K.:
 X, experimental values; ●, calculated values.

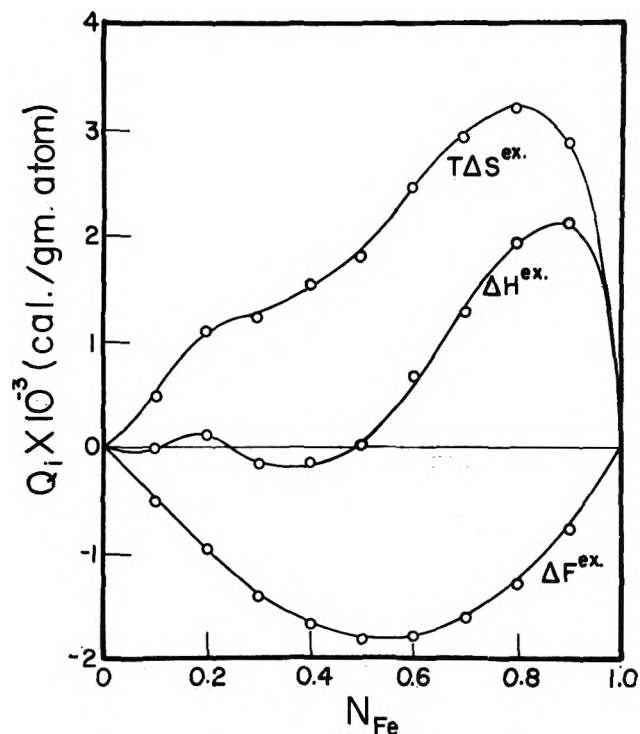


Figure 4. Integral excess free energies, entropies, and enthalpies of formation of vanadium-iron alloys at 1600°K.

The configurational contribution to the excess entropy must of necessity be negative since departures from completely random mixing, whether toward

short-range ordering or clustering, will result in entropies whose values are lower than ideal. In the V-Fe alloy system, the existence of a series of disordered b.c.c. solid solutions at 1600°K. implies that this contribution should be very small, although the occurrence at lower temperatures of CsCl type ordering in the α -phase, and at higher temperatures of a liquidus-solidus minimum suggests that some nonrandomness may exist in the alloys at 1600°K.

The changes in the electronic configurations of the component atoms that occur on alloying¹²⁻¹⁴ could also contribute to the excess entropy, although no theoretical basis for their effect has yet been put forward.

The vibrational entropy, which is associated with the change in the atomic and electronic bonding characteristics upon alloying, is expressed by $\int_0^T \Delta C_p d \ln T$, where ΔC_p represents the deviation of the specific heat from Neumann-Kopp behavior. Although no high-temperature specific heats have been measured in this system, an approximate evaluation of this relation may be made near room temperature by means of the Debye theory of heat capacity and the Debye temperatures and electronic specific heat coefficients determined by Cheng, *et al.*¹² The entropies thus calculated, listed in Table III, are mainly negative. This trend is consistent with the negative deviations of the room temperature lattice parameters from Vegard's law^{15,16} and the decrease in the diffusion rates of a number of solute elements into V-Fe alloys as compared with pure iron.¹⁷ However, it has been suggested¹⁸ that deviations from Neumann-Kopp behavior become more positive as melting temperatures are approached. This is particularly true when a minimum occurs in the liquidus-solidus, as a minimum signifies that the deviations of the activities from ideality in the solid are more positive than in the liquid. The expected misfit energy in the solid leads to an increase in the vibrational frequencies of the atoms in the alloys as compared to those in the pure components, so that the vibrational entropy at high temperatures (1600°K.) may in fact be positive with a maximum value at the composi-

(12) C. H. Cheng, C. T. Wei, and P. A. Beck, *Phys. Rev.*, **120**, 426 (1960).

(13) D. J. Lam, D. O. Van Ostenburg, H. D. Trapp, and D. E. MacLeod, *J. Metals*, **14**, 691 (1962).

(14) D. O. Van Ostenburg, D. J. Lam, H. D. Trapp, and D. E. MacLeod, *Phys. Rev.*, **128**, 1550 (1962).

(15) H. Martens and P. Duwez, *Trans. Am. Soc. Metals*, **44**, 484 (1952).

(16) A. L. Sutton and W. Hume-Rothery, *Phil. Mag.*, **46**, 1295 (1955).

(17) M. A. Krishtal, *Fiz. Metal i Metalloved.*, **9**, 680 (1960).

(18) R. A. Oriani, *Acid Met.*, **3**, 232 (1955).

tion of the liquidus–solidus minimum, in spite of the indications that at lower temperatures it is negative.

The magnetic entropy¹⁹ is dependent upon the degree of randomness in the orientation of the atomic magnetic moments that are associated with the iron atoms in all but the vanadium-rich alloys. Above the Curie temperature, the total entropy of hypothetical paramagnetic iron with no atomic moments is lower than that of paramagnetic iron with randomly oriented moments by an amount $R \ln (\mu_B + 1) = 2.3$ cal./g. atom-deg.¹⁰ Here, μ_B is equal to 2.2, the average atomic magnetic moment per iron atom in Bohr magnetons. Upon alloying either of these two forms of paramagnetic iron with vanadium, which has been assumed to carry no magnetic moment,^{20–22} ideal behavior occurs, insofar as the magnetic entropy is concerned, when the magnetic moment per iron atom remains constant at either 0 or 2.2. This is illustrated by the dashed lines in Fig. 5. Neither of these relations is to be expected in the real

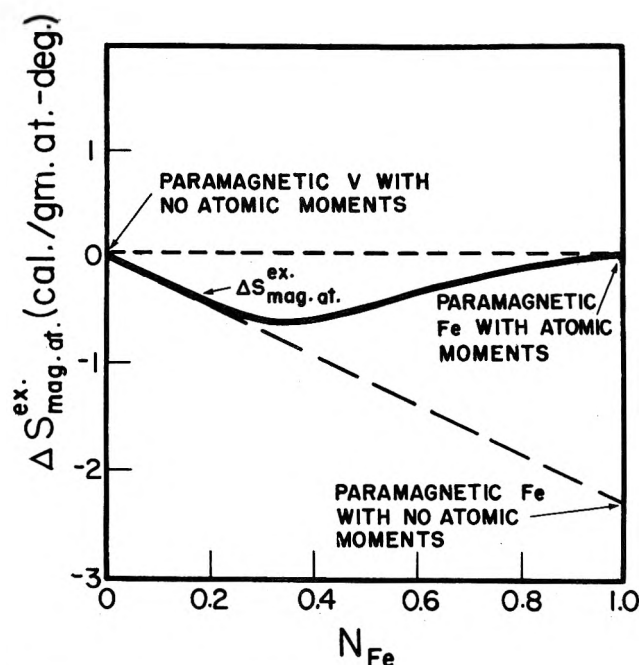


Figure 5. Plot of the magnetic entropy.

alloys as the paramagnetic moment per iron atom gradually decreases with increasing vanadium concentration and disappears at about 22 atom % Fe.²⁰ The resultant magnetic entropy should be approximated by the solid line in Fig. 5.

In summary, the positive excess entropies found experimentally have the wrong sign to be either configurational or magnetic in origin. There is some basis for a belief that a strong vibrational contribution may be made at elevated temperatures.

The enthalpies of formation are also composed of several additive terms related to the changes that occur in the atomic and electronic structures of the component metals upon alloying.

According to the usual nearest neighbor approximations, the configurational contribution to the enthalpy may be expressed in terms of the pairwise bond energies E between nearest neighbors. In a binary alloy that exhibits some degree of clustering, E_{12} is less than $\frac{1}{2}(E_{11} + E_{22})$ and the enthalpy is positive; similarly, if ordering occurs E_{12} is greater than $\frac{1}{2}(E_{11} + E_{22})$, and the enthalpy is negative. Therefore, at 1600°K. the small configurational enthalpy term may be positive at the composition of the liquidus–solidus minimum and negative near the equiatomic composition.

The vibrational enthalpy is related to the thermal excitations of the atoms and electrons through $\int_0^T \Delta C_p dT$. Both the Debye temperatures and the electronic specific heat coefficients indicate that the deviations from Neumann–Kopp behavior at about room temperature are negative; this leads to negative thermal enthalpies (Table III). However, at elevated temperatures, the occurrence of a liquidus–solidus minimum suggests the existence of a misfit energy in the solid alloys. Application of the calculation proposed by Wagner²³ suggests that a positive contribution (about

Table III: Computed Values of the Vibrational Entropy and Enthalpy of Formation at 298°K.^a

N_{Fe}	ΔS_{vib}		ΔH_{vib}	
	at.	el.	at.	el.
	Cal./g. atom-deg.		Cal./g. atom	
1.0	0.00	0.00	0	0
0.67	+0.38	-.19	+45	-42
.45	-1.26	-.12	-130	-17
.34	-0.38	-.04	-31	-6
.20	-2.23	-.30	-242	-44
.15	-2.12	-.22	-224	-33
.08	-1.33	-.13	-131	-19
.0	0.00	.00	0	0

^a Assuming $C_p \approx C_v$.

+370 cal./g. atom) may be made to the vibrational enthalpy of alloys near this composition. Hence, there

(19) R. A. Oriani, *J. Chem. Phys.*, **28**, 679 (1958).

(20) S. Arais, R. V. Colvin, H. Chessin, and J. M. Peck, *J. Appl. Phys.*, **33**, 1353 (1962).

(21) M. V. Nevitt and A. T. Aldred, *ibid.*, **34**, 463 (1963).

(22) D. J. Lam, D. O. Van Ostenburg, M. V. Nevitt, H. D. Trapp, and D. W. Pracht, *Phys. Rev.*, **131**, 1428 (1963).

(23) C. Wagner, *Acta Met.*, **2**, 242 (1954).

is some basis for positive values of the vibrational enthalpy at 1600°K.

The magnetic contribution to the enthalpy could be discussed in a manner similar to the contribution to the entropy, but the theoretical basis is not as well established. However, since the magnetic term affects the heat capacity, the signs of the related entropy and enthalpy contributions must be the same.

Although the activities and free energies of formation obtained at 1600°K. appear to be reliable and self-consistent, the entropies and enthalpies of formation are considerably more difficult to rationalize. The apparent positive excess entropies and enthalpies have

been discussed in terms of the known properties of the alloy system. The present work tends to demonstrate the importance of nonconfigurational contributions to the thermodynamic properties of transition metal alloys. Further elucidation of the thermodynamics of the V-Fe alloy system must await direct measurements of the enthalpies of formation and high temperature heat capacities.

Acknowledgments. The authors are grateful to Professor R. W. Bohl of the University of Illinois and to Dr. M. V. Nevitt of the Argonne National Laboratory for their many helpful discussions during the course of this investigation.

The Mechanism of Electrochemical Oxidation of Carbon Monoxide and Methanol on Platinum.

II. The "Reactant-Pair" Mechanism for

Electrochemical Oxidation of Carbon Monoxide and Methanol¹

by S. Gilman

General Electric Research Laboratory, Schenectady, New York (Received July 15, 1963)

Data were previously reported for surface coverage of platinum with carbon monoxide and "oxygen" after application of a fixed potential to a surface covered with (approximately) a CO monolayer. The data are consistent with a "reactant-pair" mechanism for the electrochemical oxidation of CO. This mechanism assumes that the activated complex in the loss of the first electron from CO involves an adsorbed CO molecule adjacent to an adsorbed water molecule. The reactant-pair mechanism is also consistent with available data for electrochemical oxidation of methanol in acid solution. Some observations suggest that a similar mechanism may be involved in the oxidation of a number of simple organic molecules at the lower range of overvoltages.

Introduction

Considerable information has already been amassed concerning CO and "oxygen" adsorption on platinum under electrochemical conditions.^{2,3} Because of relative structural simplicity and chemical stability, this information was attainable to a higher degree of precision than can likely be obtained for more complicated organic molecules. This makes CO attractive as a model compound in spite of the fact that the electrochemical oxidation occurs at a convenient rate only at potentials at which surface oxidation also occurs. In this study, an attempt is made to deal with this latter complication, and a mechanism is offered in explanation of the resulting data. It is also demonstrated that the mechanism offered for CO is consistent with the data available for methanol. Finally, it is suggested that the oxidation of other simple organic molecules may proceed through an activated complex similar to that proposed for CO.

Experimental

Equipment and reagents used have been described previously.² Where indicated, data taken from pre-

vious²⁻⁴ publications have been utilized. New experimental results were obtained by means of the previously discussed techniques,^{2,3} the potential sequence appearing in Fig. 1, and the procedures listed in Table I.

Results and Discussion

I. *The Electrochemical Oxidation of CO on Platinum in 1 N Perchloric Acid. A. Current-Time Traces at Potential U. Surface Initially Covered with CO.* When the surface is equilibrated with a solution of 1 N perchloric acid saturated with a 1% CO, 99% argon gas mixture or with 100% CO, only about 20% of the sites available for hydrogen deposition remain unobscured by CO² and we may assume the surface almost completely saturated with CO in each case. Under these conditions the current-time trace at constant potential

- (1) This work was made possible by the support of the Advanced Research Projects Agency (Order No. 247-61) through the United States Army Engineer Research and Development Laboratories under Contract Number DA-44-009-ENG-4853.
- (2) S. Gilman, *J. Phys. Chem.*, **66**, 2657 (1962); (b) **67**, 78 (1963).
- (3) S. Gilman, *ibid.*, **67**, 1898 (1963).
- (4) S. Gilman and M. W. Breiter, *J. Electrochem. Soc.*, **109**, 1099 (1962).

Table I

Sequence no.	Figure no.	Step no.	Procedure	Purpose	Final result
I	1a	A	(1) Bubble 99% argon-1% CO mixture with paddle-stirring (200 r.p.m.) for 15 sec.	(1) To keep the solution saturated with gas while removing oxidizable adsorbed impurities from the electrode surface. Also to deposit passive oxygen film	
		B	(2) Bubbling and stirring continued for 20 sec. Stirring without bubbling continued for an additional 10 sec.	(2) To sweep away and dilute molecular oxygen produced during last step. The passive film is retained	
		B	(3) The stirring is discontinued for an additional time τ_B' at step B	(3) To permit the solution to reach a rate of agitation greater than zero but less than that in the actively stirred solution	
		C	(4) Solution is allowed to come to rest for 1.5 min.	(4) The electrode is quickly reduced at $U = 0.4$ v. and CO is brought to the surface by the agitation of the solution (from the previous step). Since the rate of agitation decreases rapidly the surface need not reach equilibrium coverage by the end of the step	(4) The surface is <i>partially</i> covered with CO and the solution is quiet. The concentration of CO adjacent to surface is less than that in the bulk. Additional adsorption of CO during step D is negligible (ref. 2)
		D	(5) The oscilloscope is triggered at the beginning of the potential step	(5) To record the current-time trace corresponding to a surface partially covered with CO	(5) Current-time trace at potential U for partially covered surface
II	1b	A	(1) Solution of 1 M methanol, 1 N perchloric acid; stir for 15 sec. with argon bubbling	(1) To remove oxidizable adsorbed impurities and methanol from the electrode surface	
		B	(2) Continue stirring with argon for 1 min. (3) Allow solution to come to rest for 1.5 min.	(2) To reduce surface and sweep away O_2 and oxidation products and allow adsorption of methanol (3) To allow for mass transport by diffusion only	
	1b	C	(4) Trigger oscilloscope	(4) To record current-time trace	(4) Current-time trace for oxidation of methanol at $U = 0.7$ v.
	1b	D	(5) Continue oscilloscope trace	(5) Record current-time trace	(5) Trace for oxidation of methanol at $U = 0.5$ v. after "activation" at $U = 0.7$ v.

U (1% CO solution) proceeds from a small initial value to a maximum current and then declines to 0.³ At the same time, the surface coverage with CO declines gradually from its initial equilibrium value to 0. The downward trend of current at constant potential is easily explicable on the basis of decreasing surface concentration and hence activity of CO. The rising portion of the trace implies that the over-all rate of the

electrochemical reaction increases as a direct function of (a) increasing time, (b) decreasing surface coverage with CO, or (c) a combination of (a) and (b). A simple situation corresponding to situation (a), for example, is that the reactant or surface undergoes change in reactivity (structure) with time at the applied potential.

To test the relationship between current, time, and θ_{CO} , it is possible to start the experiment with the surface

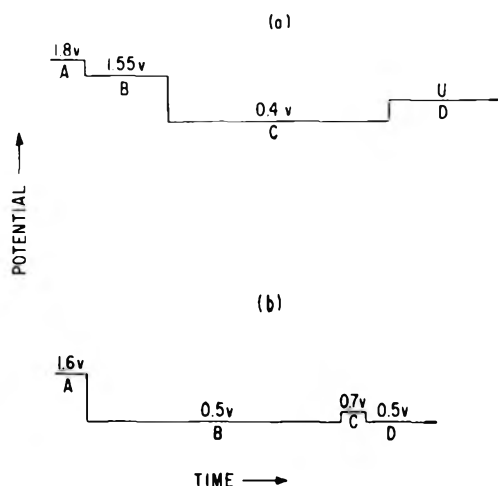


Figure 1. Potential sequences applied to the working electrode.

only partially covered with CO and to observe the current near zero time. This experiment was performed employing sequence I, Table I. $U = 0.80$ v. was chosen since the current at this potential includes no measurable contribution from surface oxidation.^{5,6} Figure 2 presents the results. Trace 1 corresponds to a

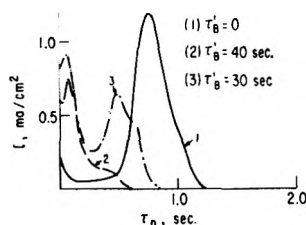


Figure 2. Current-time traces obtained for an electrode partially covered with CO. Trace 1 corresponds to a surface initially equilibrated with CO. Traces 2 and 3 correspond to partially equilibrated surfaces.

surface initially covered to the equilibrium value with CO. After decay of the capacity current, the initial current starts at the familiar low level and rises to a maximum. Traces 2 and 3 correspond to only partial surface coverage with CO. These traces exhibit initial CO-oxidation currents approaching the maximum current of trace 1. This establishes that the increase of current before the maximum of trace 1 depends directly on the surface coverage with CO, and only indirectly on the time, τ_D , elapsed after application of potential U .

If we were to shift traces 1, 2, and 3 of Fig. 2 along the time axis so as to superimpose the points at which the current drops to zero, we would observe that traces

2 and 3 do not simply constitute portions of trace 1. We would not expect such behavior if a single fixed relationship existed between current and θ_{CO} . An explanation for this complication will be offered below on the basis of different initial distributions of ad-molecules on the surface.

B. The Adsorption and Desorption of Carbon Dioxide. It is possible that product CO_2 might act as a "poison" by affecting the surface free energy or desorbing with difficulty, etc. The tendency of CO_2 to adsorb from solution under our conditions was therefore examined to gage the probability of such kinetic considerations. The procedure employed was identical with that previously used to study saturation adsorption of CO .^{2a} The electrolyte was saturated with pure CO_2 and its adsorption was followed with time by application of a linear cathodic pulse and determination of the charge due to hydrogen codeposition. No reduction in the charge due to hydrogen deposition and hence no CO_2 adsorption was observed over 1000 sec. The evidence suggests that CO_2 does not chemisorb under our conditions. This is in accord with the observation that CO_2 does not adsorb from the gas phase at this temperature.⁷ It can thus be safely assumed that dissolved product CO_2 plays no role in the kinetics of CO oxidation. This still allows the possibility that CO_2 formed on the surface desorbs with difficulty. This possibility is in turn rendered unlikely by the observed fact that hydrogen codeposition increases regularly as CO is oxidized.³ This argues against a buildup of adsorbed CO_2 on the surface.

C. The "Reactant-Pair" Mechanism for CO Oxidation. Starting with the observation that the over-all rate of electrochemical reaction increases with decrease in θ_{CO} , we are confronted with a situation which may be described as self-poisoning of the reaction with the reactant. One simple physical situation corresponding to such an observation is that the electrochemical reaction involves adjacent surface sites. For the time being, we will assume that an adsorbed CO molecule and a "free site" (not covered with CO but presumably covered with other solvent species, oxide, etc.) are involved. Corresponding to the situation in which the current is determined by rate of electron transfer from such a "reactant-pair," we may write

$$I_{CO}^B = nK_{CO}^B F S_a \exp(\alpha n' U F / RT) \quad (1)$$

where I_{CO}^B is the partial current for the oxidation of bridged CO; K_{CO}^B is the rate constant for oxidation of

(5) H. A. Laitinen and C. G. Enke, *J. Electrochem. Soc.*, **107**, 773 (1960).

(6) S. Gilman, to be published.

(7) A. C. Collins and B. M. W. Trapnell, *Trans. Faraday Soc.*, **53**, 1476 (1957).

bridged CO; n is the total number of electrons in overall oxidation = 2; F is the Faraday constant; α is the transfer coefficient; n' is the number of electrons in the rate-determining step; and S_a is the density of reactant pairs on the surface. A strictly analogous argument applies to linear CO. It is next necessary to express S_a in terms of the experimentally measurable quantities, Q_{CO}^B , and Q_H . To this end we may regard our reactant pairs as being located between clusters of CO ad-molecules and "free sites." Physical models for this situation will be offered below.

Case 1. Assumptions. Oxidation of CO not adjacent to a "free site" is completely hindered. Increase in the number of reactant pairs may occur only by the outward extension of the line of contact between clusters of adsorbed CO molecules and clusters of "free sites." At high values of θ_{CO} we may regard the clusters of free sites as openings in an otherwise continuously covered surface and

$$S_a' = l' \sum_i C_{F,i} \quad (2)$$

where C_F is the circumference of an individual cluster of "free sites" and l' is a constant. At low values of θ_{CO} , we may regard the CO clusters as openings in an otherwise "free" surface and

$$S_a'' = l'' \sum_i C_{CO}^B, i \quad (3)$$

where C_{CO}^B, i is the circumference of an individual cluster of bridged CO ad-molecules and l'' is a constant. Over the medium range of surface coverage we may therefore write

$$S_a = l \sum_i C_F, i C_{CO}^B, i \quad (4)$$

where circumferences with the same value of i are adjacent.

Initial Conditions at Potential U. The adsorption of a gas on an ideal surface with sites of uniform free energy might be expected initially to result in single isolated ad-molecules (cluster size = 1 molecule/cluster) at low surface coverage. Similarly, at high surface coverages we might expect the size (area) of clusters of "free sites" to be minimal. This would lead to the maximum value for the circumference terms in eq. 4. On the other hand, for a real surface we might expect a distribution of free energies of adsorption on the surface and a corresponding tendency for cluster sizes to be large and for the circumference terms in eq. 4 to approach a minimum for a fixed value of θ_{CO} . Further, we must expect the circumference term in (4) to vary with the path by which the particular surface coverage was established, e.g., adsorption on a completely or

incompletely reduced surface; saturation adsorption followed by some stripping-off by oxidation, etc. It is thus conceivable that the value of S_a and hence the current at constant potential may vary by orders of magnitude at the beginning of an electrochemical oxidation step.

Case 1a. Assumptions. These are the same as for case 1 plus the assumption that (free) site clusters may expand or (CO ad-sites) diminish only isotropically during CO-oxidation.

Let us assume the clusters are initially circular in shape and also let us accept the approximation of equal size for similar clusters. Then

$$C_{CO}^B = 2\pi N_{CO}^B R_{CO}^B \quad (5)$$

where N_{CO}^B is the number of bridged CO clusters and R_{CO}^B is the radius of bridged CO clusters. Also

$$\theta_{CO}^B = Q_{CO}^B / (Q_{CO}^t)_s = m N_{CO}^B \pi (R_{CO}^B)^2 \quad (6)$$

where $(Q_{CO}^t)_s$ is the charge density equivalent to "saturation coverage" with CO, taken as 0.44 mcoulomb/cm.², and m is an appropriate constant. Examination of eq. 5 and 6 reveals that C_{CO}^B is proportional to $(\theta_{CO}^B)^{1/2}$. Similar arguments apply to C_F . Hence over the medium range of surface coverages

$$I_{CO}^B = 2k_{CO}^{B'} F (\theta_{CO}^B)^{1/2} (\theta_F)^{1/2} \exp(\alpha n' F / RT) \quad (7)$$

where $k_{CO}^{B'}$ is a formal rate constant.

Case 1b. Assumptions. These are the same as for case 1, plus the assumption that site clusters may expand only in a decidedly nonisotropic manner. As for case 1a, let us further simplify by assuming all similar clusters equal in size.

Assuming rectangular geometry

$$C_{CO}^B = N_{CO}^B 2(c + d) \quad (8)$$

where c and d are the dimensions of the average site cluster. Also

$$\theta_{CO}^B = m' N_{CO}^B cd \quad (9)$$

where m' is the appropriate constant. Inspection of eq. 8 and 9 reveals direct proportionality between C_{CO}^B and θ_{CO}^B if we assume $c \gg d$. Similar arguments apply to C_F and θ_F . Hence for the medium range of surface coverages we may write

$$I_{CO}^B = 2F k_{CO}^{B''} \theta_{CO}^B \theta_F \exp(\alpha U n' F / RT) \quad (10)$$

where $k_{CO}^{B''}$ is the formal rate constant.

Case 1c. Assumptions—Generalization of Cases 1a and 1b. We may generalize upon eq. 7 and 10 by writing

$$I_{\text{CO}}^{\text{B}} = 2Fk_{\text{CO}}^{\text{B}}(\theta_{\text{CO}}^{\text{B}})^p(\theta_{\text{F}})^q \exp(\alpha Un'F/RT) \quad (11)$$

where p and q are exponents having values between $1/2$ and 1. Equation 11 now carries with it the assumption of cases 1a and 1b that all clusters are equal in area and hence in circumference. It is reasonable, therefore, to term unusually large clusters "inactive" since the circumference per unit area is small. We may make correction for the total inactive surface coverage as

$$I_{\text{CO}}^{\text{B}} = 2Fk_{\text{CO}}^{\text{B}}(\theta_{\text{CO}}^{\text{B}} - a)^p(\theta_{\text{F}} - b)^q \exp(\alpha Un'F/RT) \quad (12)$$

where a and b are fractional "inactive" surface coverages.

Case 2. Assumptions. There is some oxidation of CO ad-molecules not adjacent to a "free" site. This situation would lead to nucleation of new clusters of "free sites." These new clusters would have larger circumference to diameter ratios than the average older clusters and the effect may be to increase the current greatly although θ_{F} increases only slightly. For any nucleation rate, the accelerated dependence of current on θ_{F} may be expected to increase in importance as the number of original clusters of free sites decreases and their average radius increases. The simplest situation would arise when the average nucleated cluster soon attains the same circumference as the average original cluster, when the dependence of the current upon surface coverage could still be represented by eq. 12.

D. Application of the "Reactant-Pair" Mechanism to Constant Potential Data Obtained in a Solution of 1% CO. Interpretation of the data in terms of the individual models discussed does not seem feasible without detailed knowledge of surface morphology and the structure of the ad-layer. It will only be attempted to show that the generalized equation (12) is consistent with the data obtained.

Integration of eq. 12 from zero time to duration of time, τ_{D} , at constant potential U results in a charge corresponding to oxidation of bridged CO. For the surface originally equilibrated with a saturated solution of 1% CO, this charge is in turn equal to the difference between the initial equilibrium value of the charge corresponding to adsorbed CO and its instantaneous value

$$\int_0^{\tau_{\text{D}}} (I_{\text{CO}}^{\text{B}}) d\tau_{\text{D}} = [(Q_{\text{CO}}^{\text{B}})_{\text{e}} - Q_{\text{CO}}^{\text{B}}] = 2Fk_{\text{CO}}^{\text{B}} \int_0^{\tau_{\text{D}}} (\theta_{\text{CO}}^{\text{B}} - a)^p (\theta_{\text{F}} - b)^q d\tau_{\text{D}} \quad (13)$$

In the absence of oxidation of the surface ($U \leq 0.80$ v.), we will assume that hydrogen deposition is a measure of the "free surface"^{2a} and take $\theta_{\text{F}} = Q_{\text{H}}/Q_{\text{H}}^{\text{S}}$. In the presence of surface oxidation ($U > 0.80$ v.) we will

arbitrarily assume PtO stoichiometry^{2a} and take $\theta_{\text{F}} = (Q_{\text{H}} - Q_0/2)/Q_{\text{H}}^{\text{S}}$. Equation 13 is tested for both bridged and linear CO in Fig. 3. In Fig. 3a, values of

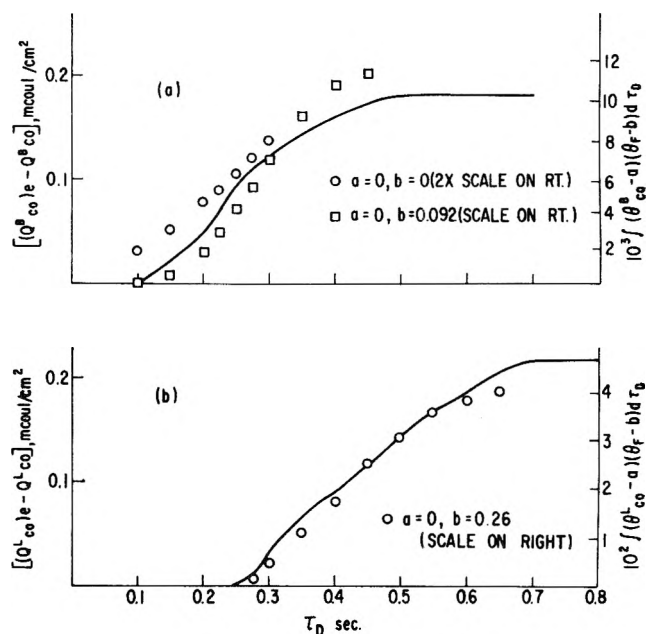


Figure 3. Experimental and theoretical CO-oxidation charge at $U = 0.85$ v.: (a) bridged CO; (b) linear CO.

$[(Q_{\text{CO}}^{\text{B}})_{\text{e}} - Q_{\text{CO}}^{\text{B}}]$ are plotted from previously³ obtained data. The circles on the figure are values of $\int_0^{\tau_{\text{D}}} (\theta_{\text{CO}}^{\text{B}} - a)^p (\theta_{\text{F}} - b)^q d\tau_{\text{D}}$ obtained by graphic integration with $a = b = 0$ and $p = q = 1$. Compared to the smooth curve, these points have values which are too large at small values of τ_{D} . This could correspond to the situation where most of the initially available free sites are "inactive" in the sense discussed above. This may be compensated for by choosing $b = 0.092$, and leaving $a = 0$, $p = q = 1$. The squares of Fig. 3a are the resulting points obtained which (with normalization at $\tau_{\text{D}} = 0.3$ sec.) are a fair fit to the experimental curve. In Fig. 3b a similar analysis was made for linear CO with the circles now corresponding to $b = 0.26$, $a = 0$, $p = q = 1$. An excellent fit of theory to experimental data is obtained. The possible physical significance of different values of b for bridged and linear CO is that the active free sites which are generated by the oxidation of bridged CO ad-molecules initially do not occur in the immediate vicinity of linear CO ad-molecules. Hence the new free sites are "active" for (adjacent to) bridged ad-molecules but "inactive" for (not adjacent to) linear CO ad-molecules. The argument allows us to establish only that a fit of

theory to experimental data may be obtained and does not in itself constitute proof of the theory of any of the detailed situations discussed in cases 1 and 2. No doubt other satisfactory fits may also be obtained with other choices for the constants of eq. 13.

If, for any fixed potential U , the rate of oxidation of CO to CO_2 were determined by an electron transfer, we would expect from eq. 1 that at constant potential U

$$I_{\text{CO}}^{\text{B}}/S_a = nFK_{\text{CO}}^{\text{B}} = \text{constant} \quad (14)$$

The values of K_{CO}^{B} for different values of U might be expected to fall on a Tafel plot. A similar argument applies to the formal rate constant, k_{CO}^{B} , obtained by means of eq. 13. Since the values of the constants of eq. 13 may be different for each potential, and since the choice of constants is in any case fairly arbitrary, it was felt more general and convenient to work with eq. 12 and $a = b = 0$; $p = q = 1$.

The use of eq. 12 requires measurement of a current due to oxidation of a particular CO species, whereas the total current measured includes several other contributions.³ I_{CO}^{B} is thus best obtained by differentiation of the appropriate charge (see eq. 13)

$$I_{\text{CO}}^{\text{B}} = \frac{d}{d\tau_D} [(Q_{\text{CO}}^{\text{B}})_e - Q_{\text{CO}}^{\text{B}}] = \frac{-d}{d\tau_D} Q_{\text{CO}}^{\text{B}} \quad (15)$$

Figure 4b is a plot of $I_{\text{CO}}^{\text{B}}/\theta_{\text{CO}}^{\text{B}}\theta_{\text{F}}$ against U . Figure 4a is a similar analysis for linear CO. The points for any constant value of U correspond to values of $\theta_{\text{CO}}^{\text{B}}$ and $\theta_{\text{CO}}^{\text{L}}$ increasing in intervals of 0.075. Ideally (eq. 14) the points at constant potential would superimpose. The actual tendency of the constant-potential points to cluster may be called "fair" in light of the complicated manner of obtaining the data and the much simplified model employed in its analysis. This difficulty is minimized by the fact that the data may be analyzed further on a logarithmic scale. The best lines through the points from $U = 0.85$ to 1.1 v. result in apparent values of $\alpha n'$ of 0.32 and 0.25 for linear and bridged CO, respectively, and suggest a slow one-electron transfer in each case. Although the values of the ordinate throughout the potential range studied are not greatly different for the two forms of adsorbed CO, the small difference in Tafel slopes results in the values of the intercept at $U = 0$ v. differing considerably. The values are $2Fk_{\text{CO}}^{\text{B}} = 5 \times 10^{-13}$ and $2Fk_{\text{CO}}^{\text{L}} = 5 \times 10^{-9}$ amp./cm.² for the rate at $U = 0$ expressed as current. These may be compared with the values of 10^{-11} amp./cm.² previously reported for methanol oxidation during the ascending sweep of the "polarization curve."⁴ These values all involve extrapolation back to $U = 0$ using uncertain Tafel slopes. A better comparison is probably obtained at $U = 0.8$ v. where the rates for the

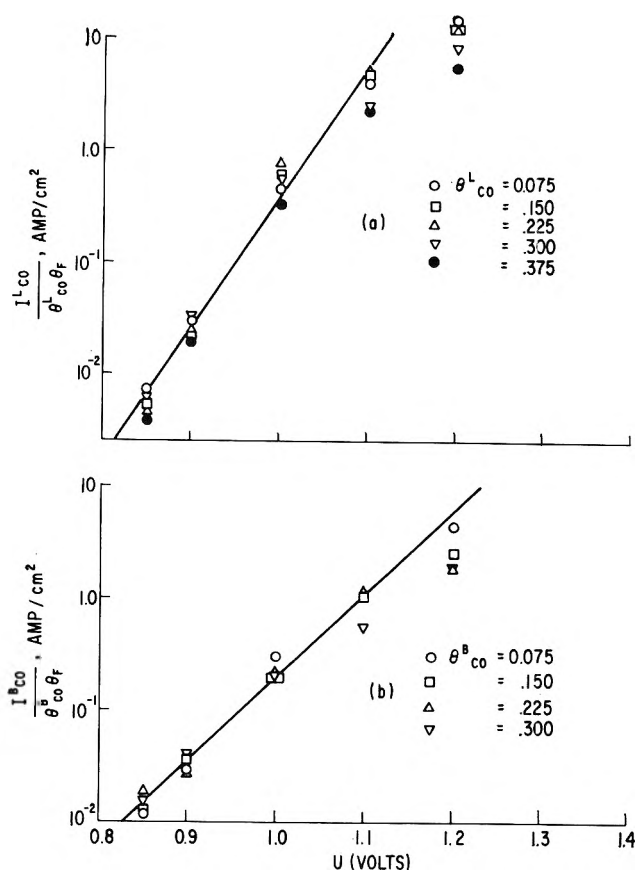


Figure 4. Potential-dependence of the oxidation currents for CO: (a) linear CO; (b) bridged CO.

oxidation of linear and bridged CO are 2×10^{-3} and 6×10^{-3} amp./cm.², respectively. The rate for the oxidation of methanol (assuming a slow electron transfer step first order in methanol and either first or zero order in "free" surface) is 2×10^{-3} amp./cm.² and the rate of the surface oxidation at $\theta_0 = 0.1$ is also 2×10^{-3} amp./cm.².⁶ The similar values of rate constant for CO, methanol, and Pt-surface oxidation already suggest similar rate-controlling steps.

The scatter of the points at constant potential for CO about the mean (Fig. 4) is random with respect to surface coverage with CO, time, and hence also with extent of surface oxidation.³ It does not seem reasonable, therefore, to hold surface oxidation out as the reason for the decided departure of the points for $U = 1.2$ v. from the Tafel lines. One possible explanation for the effect is that the field becomes nonlinear with increasing interfacial potential (and changing structure of the ionic double layer). While the rate shows a tendency to depart from the Tafel line at high potentials, it does not exhibit a maximum in the range examined. Hence the gradual decrease, with increas-

ing potential, of the current measured for the "polarization curve"^{2a} may not be attributed to a decrease in the rate of the electron-transfer step. This matter will be treated further subsequently.

E. Comparison of Constant-Potential Voltammetric Data Obtained with Solutions of 1% and 100% CO. At $U = 1.0$ v. and for a solution of 1% CO the CO-oxidation charge passed before the current decays to virtually (compared with maximum current) zero corresponds almost entirely with CO initially adsorbed on the surface, the additional CO diffusing in from the solution being negligible.³ For the corresponding experiment in a saturated solution of 100% CO, resupply of CO from the solution becomes appreciable. Under these latter conditions, CO supplied from the solution contributes approximately half the total CO oxidation charge passed before the surface concentration drops to zero.³ When, in this latter case, the surface concentration does fall to zero, it is because the diffusion layer thickness has increased to the extent where it may only support the rate of oxidation on the bare surface and no excess of CO flux to the electrode exists which might allow the surface coverage to rise above zero. Hence, at that point the oxidation is diffusion-controlled and occurs with $\theta_{CO} = 0$. Before this situation of diffusion-controlled oxidation current is established, we may expect the CO-oxidation current to be related to θ_{CO} by an expression such as eq. 12, as was found for the experiment which employed a solution of 1% CO. Further, the surface-oxidation current is also limited by CO surface coverage. Hence, if the distribution of CO on the surface were similar for the experiments employing different concentrations of dissolved gas, we might expect the total currents to be similar functions of θ_{CO} . In Fig. 5 total current is plotted as a function of total surface coverage with CO, $\theta_{CO} = Q_{CO}^t / (Q_{CO}^t)_s$. We see that the general appearance of the two curves is quite similar but that the currents of plot b are 0.6 (at the maximum) that of

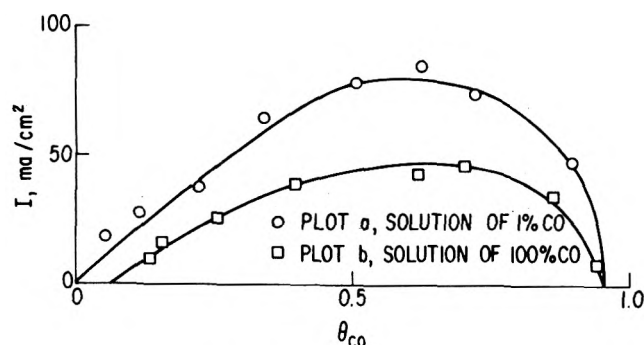


Figure 5. Total anodic current at $U = 1.0$ v.

plot a. The initial values of Q_{CO}^t were 0.41 and 0.43 mCoulomb/cm.², respectively. By the arguments already presented, the number of reactant pairs for plot b must initially be smaller than for plot a, and the number of such pairs will remain smaller if the rate of nucleation of new clusters of free sites is small or zero. This experiment hence lends support to case 1 of the general mechanism offered above.

It was previously suggested that the sudden rise in anodic current with increasing potential of the "polarization curve"^{2a} might be due to higher activity of non-adsorbed (newly diffused to the surface from the solution) CO. Figure 5 establishes that in fact lower currents are supported under the conditions of resupply of CO from the solution. Hence, the sharply rising current in question must be due only to the increase in rate which accompanies decreasing surface coverage (see below).

F. Further Interpretation of the "Polarization Curve." The current-potential traces obtained by application of a slow periodic triangular sweep to a working electrode immersed in 100% CO were previously reported.^{2a} A correlation was demonstrated to exist between θ_F and the measured currents. Further examination of the "polarization curve" in the light of the new material presented here seems warranted.

Figure 6 is a trace taken with a sweep speed of 0.04 v./sec., CO bubbling through the electrolyte, and with

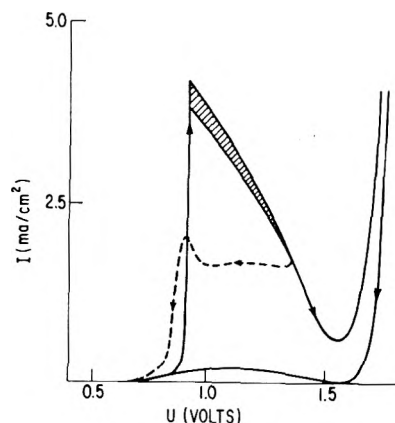


Figure 6. "Polarization curve" for CO in rapidly stirred saturated solution of CO. Triangular sweep applied with potential varying between 0.4 and 1.8 v. (solid trace) or 1.4 v. (dashed trace); $v = 0.04$ v./sec.

paddle-stirring at 200 r.p.m. For the ascending portion of the sweep, virtually no current is observed from 0.4 to 0.91 v. This is in contrast with the appreciable currents which may be obtained for U as low as 0.8 v. in an unstirred solution of 1% CO. The explanation

offered is that the flux of CO to the electrode under these conditions is sufficient to prevent decrease in θ_{CO} , which in turn causes the current to remain low. At $U > 0.91$ v., the rate of oxidation on even the highly covered surface begins to become appreciable with respect to the rate of readsorption of CO from solution at high θ_{CO} (where the rate of adsorption is smaller than the rate of diffusion³). This causes θ_{CO} to drop, which in turn causes the rate of CO oxidation to rise. As θ_{CO} decreases appreciably the rate of readsorption increases and becomes diffusion-controlled. As a result of the demands made on the adjacent solution by the enhanced rates of oxidation and readsorption, the diffusion-layer thickness increases to an equilibrium value. The specific rate with which CO may oxidize on the surface rises to such an extent that all CO on the surface is consumed and any CO which strikes the surface is immediately consumed. We therefore have a type of avalanche effect where the system at $U = 0.91$ v. abruptly moves from a situation at which θ_{CO} is maximum and current is minimum to a situation in which θ_{CO} is zero and current is diffusion-controlled.

In Fig. 6 we see a gradual decline in current from the peak (diffusion-limited) value near 0.91 v. to the minimum value at 1.6 v. It was previously suggested that this decline could be due either to (1) physical masking with surface "oxide" or (2) reduction in the rate constant for electrochemical oxidation of CO. Possibility (1) may still not be ruled out, especially in the light of evidence that the total surface coverage with oxygen at low potentials is more extensive than previously believed (equal to 0.5 monolayer of PtO or 0.25 monolayer of PtO₂ at $U = 1.0$ v. after 1 sec.⁶). Possibility (2) may be eliminated, in view of the finding that the rate of oxidation increases gradually throughout the potential range studied. Actually, if the rate of oxidation were to decrease, readsorption must occur unless this is also hindered. No readsorption of the depolarizer at high potentials (past the current maximum) was found for either CO or methanol.⁸ This leaves the possibility that it is the rate of adsorption that is markedly affected by "adsorbed oxygen" for both of these systems. Since we are speaking of adsorption at a surface coverage of zero, we might alternately think of the process as a "surface activation" and suspect that it is this activation (preceding the electron transfer) which is hindered.

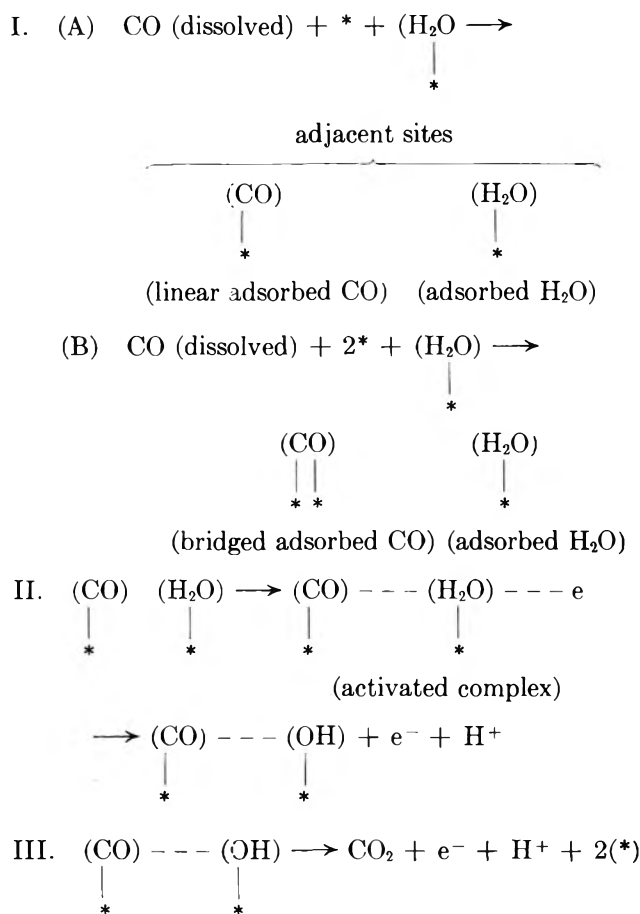
During the descending sweep from 1.4 v. of Fig. 6, we see that the current level reached at the end of the ascending sweep (lower than limiting current) is maintained, establishing that it is the surface oxide directly and not the increase in potential which produced the original current decline. Finally, we observe the

"hysteresis effect" at low potentials. This effect may now be ascribed to the fact that the surface coverage with CO is now smaller than it was during the ascent, hence the number of reactant pairs is larger, and the rate of oxidation is greater.

G. The Structure of the Activated Complex—Summary of the Mechanism We may now consider the possible nature of the "free sites" involved in the postulated reactant-pair. The "free site" adjacent to an adsorbed CO molecule may serve one of two basic functions. (1) It may permit the adsorbed CO to form an additional bond to the surface and be "activated." (2) It may contain an adsorbed species which enters into the activated complex of the rate-determining step. Let us assume that possibility (1) applies. Then, since the current at constant potential tends toward a maximum, we would also expect the number of bonds per adsorbed CO molecule to proceed toward a maximum. Alternatively, we may express the argument in terms of surface concentrations of linear and bridged CO. "Activated" linear CO may be expected to resemble bridged CO physically. Hence, we might expect only bridged (2-site) CO to be active, and the rate of oxidation to be initially proportional to its surface concentration. Linear CO would have to convert to the bridged form to oxidize. Higher currents at constant potential would imply larger surface concentrations of bridged CO. Actually, the linear form tends to decrease at approximately the same rate as the bridged form over the potential range studied, and in any case, no increase in bridged CO over the initial surface concentration is found during oxidation at constant potential.³ It therefore seems reasonable to discard possibility (1) above.

For possibility (2) we might suppose that an adsorbed water molecule (or protonated water molecule) anion, or "oxygen" might be involved. Since perchlorate is involved in this case, the possibility of an adsorbed anion does not seem attractive. The "oxygen" might be present as (stoichiometrically) the hydroxide, oxide, etc. Since CO will oxidize at 0.8 v. where the surface coverage with "oxygen" is immeasurably small, the possibility of "oxygen" as a coreactant seems unattractive. Further, for methanol and formic acid, oxidation may be observed at as low as 0.6 v., making "oxygen" an even less attractive candidate. An adsorbed water species is left as the present most promising choice. The following scheme is therefore offered for the electrochemical oxidation of CO.

(8) M. W. Breiter and S. Gilman, *J. Electrochem. Soc.*, **109**, 622 (1962).



Steps IA and IB are adsorption steps which will be very rapid for any surface coverage slightly less than the equilibrium value and will be rate-controlled by diffusion under any simple experimental situation. Step I determines the initial surface concentration of reactant pairs. The progress of adsorbed linear CO is followed in steps II and III, the argument for the bridged form being identical. Step II is the electron-transfer step, which for any fixed surface concentration of reactant pairs is rate-determining. The loss of the first electron goes through the indicated activated complex. Step III is the final electron transfer which is assumed rapid compared with (II). In a sense, steps II and III resemble reaction of CO with "dissociated water." We may think of CO as lowering the energy of activation for the dissociation of water (surface oxidation). Further, at potentials of $U < 0.80$ v. the product of surface oxidation would tend to be re-reduced, whereas the corresponding back reactions for steps II and III are assumed to have no appreciable rate.

The proposed mechanism for the electrochemical oxidation of CO has some similarity to that proposed for the catalyzed gas-phase oxidation of CO by oxygen.⁹ The latter oxidation is said to involve adjacent adsorbed

molecules of CO and oxygen and the reaction rate therefore also displays a maximum with increase in CO surface coverage as it does in our case.

II. *Application of the "Reactant-Pair" Mechanism to the Electrochemical Oxidation of Methanol in Perchloric Acid Solution.* The electrochemical oxidation of methanol was previously interpreted⁴ on the basis of a rate-controlling one-electron transfer, first order in adsorbed methanol. Two anomalies arose in this interpretation. (1) Values of I/θ_M for $0.3 \geq \theta_M \geq 0.9$ (concentration of methanol = 1 M) do not fall on the Tafel line. (2) A "hysteresis effect" (currents at low potentials are higher during descending than ascending sweeps) more pronounced than that observed for CO occurs. It was previously suggested⁴ that these anomalies might be explained either by a higher rate constant for "unadsorbed CO" or by some mysterious "activation" of the surface. Both of the observed effects, however, suggest similarity with the CO system. Further similarity is suggested by the current-time trace obtained at constant potential. Sequence II of Table I was employed in obtaining Fig. 7. At $U = 0.5$ v., the initial current is virtually zero

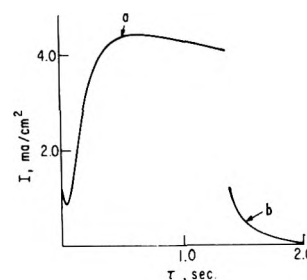


Figure 7. Current-time trace for oxidation of 1 M methanol at constant potential: (a) $U = 0.7$ v.; (b) $U = 0.5$ v.

on the scale employed. Upon raising the potential to $U = 0.7$ v., the current rises from a minimum to a maximum value (trace a) while the surface coverage with methanol decreases somewhat. Upon stepping the potential back to 0.5 v., a considerable transient current is obtained which finally decays to the initial zero value (trace b). Trace a of Fig. 7 is precisely what is to be expected for the reactant-pair mechanism (current reaches a maximum as surface coverage decreases) and differs qualitatively from CO in two main aspects—the minimum current is considerably larger compared with the maximum current and the current does not drop to zero. The relatively large initial

(9) G. C. Bond, "Catalysis by Metals," Academic Press, New York, N. Y., 1962, p. 460.

Current may be ascribed to the presence of considerable free adjacent sites (compared with CO) at the beginning of the experiment. The failure of the current to drop off to zero is simply due to the much higher flux of methanol in this concentrated solution (compared with a saturated solution of CO). This tends to keep the surface coverage with methanol at some "equilibrium value" larger than zero, and it is presumably such values which are sampled at each potential by the "polarization curve" previously reported.⁴ Trace b of the figure would then correspond to the higher currents obtained until the surface coverage again rises toward a monolayer, since the oxidation rate has dropped sufficiently to make this possible.

Because of the structural complexity of methanol (compared with CO) it is also reasonable to attempt an explanation of Fig. 7 on the basis of "intermediates." For trace a of the figure, we might be tempted to argue that the oxidation proceeds only to formaldehyde at the beginning of the trace, but proceeds to CO₂ toward the end of the trace. This allows for a ratio of maximum to minimum currents of only three. This value is clearly exceeded. Two additional explanations for Fig. 7 involve additional current due to nonadsorbed methanol and "surface activation." We have seen that enhanced currents for CO oxidation are certainly not due to nonadsorbed CO and therefore tend to discount this argument by analogy. "Surface activation" due to "oxygen adsorption" is rendered highly unlikely here because of the low potential involved. This leaves us only with a very vague idea of "surface activation" for which the reactant-pair mechanism presently appears the only physical explanation.

In Fig. 8 the data previously reported for 1 M methanol, obtained during a 0.03 v./sec. triangular sweep,⁴ are plotted on semilogarithmic paper employing three different functions for the current ordinate

$$I/\theta_m \quad (a)$$

$$I/\theta_m'\theta_F \quad (b)$$

$$I/(\theta_m'\theta_F)^{1/2} \quad (c)$$

where $\theta_F = Q_H/Q_H^S$ and $Q_m' = 1 - \theta_F$. The first function is the one previously plotted⁴ in support of the simpler electron-transfer mechanism. Functions b and c are for the reactant-pair mechanism, employing generalized eq. 12 with $a = b = 0$ and $p = q = 1$ for function b and $p = q = 1/2$ for function c. For the descending sweep, function b leads to the best linear plot. For the ascending sweep, function a results in the best fit in the medium and high range of potentials, but results in values which are too low in the lower

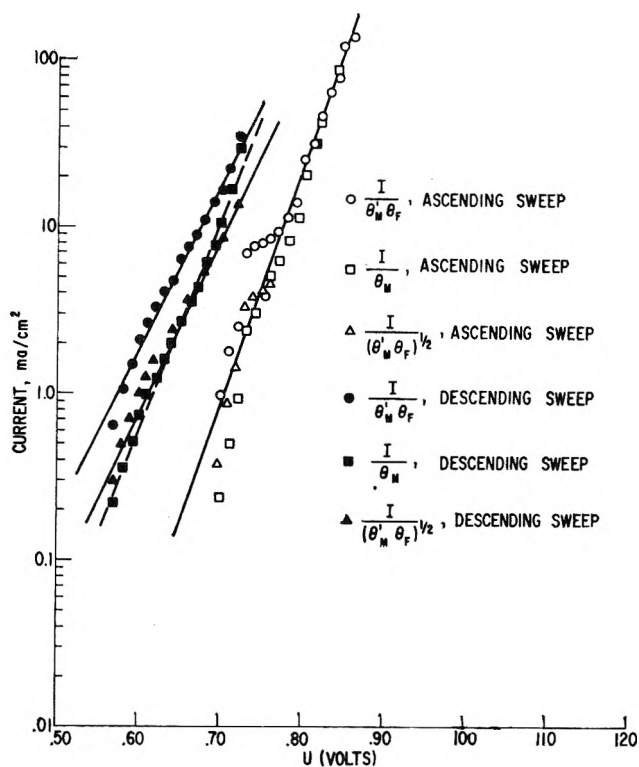


Figure 8. Analysis of methanol "polarization data."

potential range. Function b provides a good linear relationship at the high and low ends of the range, but departs from linearity in the medium range of methanol surface coverages. Function c is satisfactory only in the medium range. It seems reasonable to conclude that the unique validity of either of the proposed mechanisms may not be established by this analysis. Part of the difficulty lies in the nature of the functions themselves. For any fixed value of I and $\theta_m = 0.1$ (high potential range), functions a-c have the values $10I$, $11I$, and $3.3I$. Hence (a) and (b) give similar results. For fixed I and $\theta_m = 0.5$ (medium potential range) functions a-c have the values $2I$, $4I$, and $2I$. Hence (a) and (c) give similar results. Finally for fixed I and $\theta_m = 0.9$ (low potential range), functions a-c have values of $1.1I$, $11I$, and $3.3I$. Hence no similarity of values exist in this one range.

Referring again to Fig. 8 we see that the y -intercepts and hence apparent rate constants for the ascending and descending sweeps differ by over an order of magnitude. Clearly, there is nothing in the model of a simple electron-transfer step first order in adsorbed methanol which will explain this difference. The reactant-pair mechanism explains this effect on the basis of different initial surface concentrations of reactant pairs. During the ascending sweep θ_m is high, θ_F is low, and the

initial density of reactant pairs is small. These may only increase in number as θ_F increases. During the descending sweep, the surface is initially bare and adsorbed methanol molecules tend to deposit in clusters of minimum size; hence, the number of reactant pairs will tend to be a maximum for the particular surface coverage.

One of the most striking differences between the "polarization curves" for methanol⁴ and CO is that the former exhibits the Tafel region, starting at $U > 0.7$ v., whereas the latter has only an abrupt rise at 0.91 v. This difference may be qualitatively explained by the reactant-pair mechanism. For CO, as already proposed in a previous section, the active free surface is initially small at the beginning of the ascending sweep. The current below $U = 0.91$ v. is so small that mass-transport keeps the surface coverage high. When

appreciable decrease in θ_{CO} may be accomplished, the potential is already so large that a sudden rise in current results. For methanol, we propose that the active free surface is initially appreciable. Hence some current flows starting at $U = 0.7$ v. The tendency for the surface coverage to drop abruptly is opposed by the flow of methanol to the electrode which is large (compared to CO) at the concentrations studied. There is finally an abrupt decrease in surface coverage at $U > \sim 0.8$ v. and a corresponding abrupt increase in current.

"Activation" and "hysteresis" effects observed in preliminary experiments with formic acid and formaldehyde suggest that the reactant-pair mechanism might be of general application. The activated complex would involve an adsorbed water molecule (or perhaps OH^- in basic solutions) in all cases.

Equilibrium Ultracentrifugation and Light Scattering of Sodium Lauryl Sulfate and Dodecyltrimethylammonium Bromide Solutions¹

by E. W. Anacker,² R. M. Rush, and J. S. Johnson

Chemistry Division, Oak Ridge National Laboratory, Oak Ridge, Tennessee, and Department of Chemistry, Montana State College, Bozeman, Montana (Received July 26, 1963)

Micellar weights of sodium lauryl sulfate in 0.1 and 0.4 *M* NaCl measured by equilibrium ultracentrifugation and in 0.4 *M* NaCl by light scattering are in good agreement with each other and with values in the literature. The micelles are predominantly monodisperse in 0.4 *M* NaCl, but appear to be polydisperse in 0.5 *M* NaCl. Degrees of aggregation appear to be less in 0.4 *M* LiCl than in 0.4 *M* NaCl. A method of estimation of critical micelle concentration by ultracentrifugation is illustrated. Although the partial specific volume of dodecyltrimethylammonium bromide (DTAB) is too near unity for good estimates of molecular weight by equilibrium ultracentrifugation, the technique does indicate a monodisperse distribution in 0.1 *M* NaBr and polydispersity in 2.0 *M* NaBr. Light scattering values of DTAB degree of aggregation are presented and compared with literature values. Some anomalous observations in the sedimentation of soaps at low centrifugal fields are presented.

A number of different experimental methods have been used in the past to secure information concerning the degree of aggregation of surfactants in solution. In the case of sodium lauryl sulfate, NaLS, for example, these include light scattering,³⁻¹⁰ self-diffusion,¹¹ sedimentation velocity,¹² sedimentation velocity combined with diffusion,¹²⁻¹⁵ centrifugation at solution boundaries¹² (Archibald method), conductivity,^{16,17} osmotic pressure,¹⁸ and X-ray diffraction.¹⁹ Since different procedures have led to substantial variations in estimates of aggregation in some cases, it seemed worthwhile to attempt a study of such systems by equilibrium ultracentrifugation, a method hitherto not applied, to our knowledge.

Although there are disadvantages to equilibrium ultracentrifugation, they are in many instances, at least, different from those of other methods. Dust, for example, is a trivial interference here, in contrast to light scattering; the presence of other impurities would also be expected to be less important. In X-ray scattering,¹⁹ solutions considerably more concentrated than those in question are involved. No assumptions concerning particle shape, which are required in the interpretation of self-diffusion and conductivity, need

be made here. Sedimentation velocity requires auxiliary determination of diffusion coefficients, the measurement of which is complicated by the monomer-micellar equilibria.¹² In the Archibald method, in

- (1) This document is based in part on work performed for the U. S. Atomic Energy Commission at the Oak Ridge National Laboratory, operated by Union Carbide Corporation. Work presented at the 141st National Meeting of the American Chemical Society, Washington, D. C., March 20-29, 1962.
- (2) Department of Chemistry, Montana State College, Bozeman, Montana. ORINS Summer Participant (1957) and ORNL Summer Employee (1959).
- (3) E. Hutchinson and J. C. Melrose, *Z. physik. Chem.* (Frankfurt), **2**, 363 (1954).
- (4) J. N. Phillips and K. J. Mysels, *J. Phys. Chem.*, **59**, 325 (1955).
- (5) L. M. Kushner and W. D. Hubbard, *J. Colloid Sci.*, **10**, 428 (1955).
- (6) H. V. Tartar and A. L. M. LeLong, *J. Phys. Chem.*, **59**, 1185 (1955).
- (7) W. Prins and J. J. Hermans, *Koninkl. Ned. Akad. Wetenschap. Proc.*, **B59**, 298 (1956).
- (8) K. J. Mysels and L. H. Princen, *J. Phys. Chem.*, **63**, 1393 (1959).
- (9) A. Vrij Thesis, Van't Hoff Laboratory, Utrecht, 1959; techniques of interpretation: A. Vrij and J. Th. G. Overbeek, *J. Colloid Sci.*, **17**, 570 (1962).
- (10) H. V. Tartar, *ibid.*, **14**, 115 (1959).
- (11) D. Stigter, R. J. Williams, and K. J. Mysels, *J. Phys. Chem.*, **59**, 330 (1955).

principle similar to equilibrium ultracentrifugation, there is difficulty in the required determination of the concentration gradients at the ends of the liquid columns.²⁰

Equilibrium ultracentrifugation, at least if carried out with columns of solution long in the radial direction, should indicate any substantial polydispersity of the micelles, regardless of whether or not the different species are in rapid chemical equilibrium with one another. Light scattering would not give a simple indication of polydispersity if the distribution were fixed.

Equilibrium ultracentrifugation shares with other sedimentation techniques and with light scattering the disadvantage that, even in the presence of supporting electrolyte, quantities observed depend not only on the molecular weight but on the charge of the solute particles, and an estimate of charge is thus required in interpretation of data. Here this is done by carrying out centrifugations at different soap concentrations, computing the degree of aggregation N for different values of assumed charge, z , and selecting that N and z best satisfying all experiments. A convenient method follows from a definition of components suggested by Scatchard,²¹ in which the polymeric component (component 2) is taken to be $PX_z - (z/2)BX$, P^{+z} being the polymeric ion (the method is symmetrical for negatively charged polymers), X^- , the counter ion, and BX , the supporting electrolyte (component 3). The equation for computation of N for an assumed charge per monomer unit, z' (primes refer to quantities in terms of monomer units), is²²

$$N = \frac{S/A_2'}{1 - (z'/2A_2') \int \ln \left\{ \frac{1 + \eta}{1 - \eta} \right\} / d(x^2)} \quad (1)$$

where $S = d \ln c_2'/d(x^2)$ is the quantity obtained by measuring the concentration distribution of 2 at centrifugation equilibrium; c indicates concentration in moles/l.; $A_2' = M_2'(1 - \bar{v}_2\rho)\omega^2/2RT$; M_2' , the molecular weight of the monomeric unit of component 2, i.e., $M'_{PX_z} - (z'/2)M_{BX}$; \bar{v}_2 is the partial specific volume of 2; ρ , solution density; ω , angular velocity of rotation; R , gas constant; T , absolute temperature; and $\eta = z'c_2'/2c_3$. A number of approximations and assumptions involved in eq. 1 and in the evaluation of S from experimental data are discussed elsewhere²²; the most important probably is the assumption of constancy of activity coefficients. The effect of charge is seen in the second term of the denominator, but it should be noted that charge also affects the value of A_2' and the values of concentration obtained from the

fringe pattern. Application of the method to surfactants is complicated by the presence of appreciable quantities of the monomeric species; the actual amount of nonmicellar species, however, is probably closely approximated by the critical micelle concentration (c.m.c.) for the condition in question. We have included the critical micelle concentration in the supporting electrolyte, component 3, and have defined c_2' as the total surfactant concentration minus this quantity.

All sedimentation techniques suffer from the fact that the partial specific volumes of the surfactants in question here are not greatly different from unity, and the quantity that principally determines the extent of the sedimentation in a given field, $L = M(1 - \bar{v}\rho)$, is thus much less than the molecular weight of the soap. Further, estimates of the molecular weight will be particularly sensitive to the charge, since the concentration independent charge effect (variations in A_2') will be proportional to $L_{PX_z} - (z'/2)L_{BX}$. The light scattering of electrolytic solutions is similarly affected by the charge, but the concentration independent term here is $M_{PX_z} - (z'/2)M_{BX}$, and the estimated values of degree of aggregation therefore are much less affected by uncertainty in z .

A number of authors^{7-9,23-26} have discussed the interpretation of turbidities of ionized solutes from various points of view; the Scatchard definition of components is also useful here.²⁷⁻²⁹ For present

- (12) P. F. Mijnlief, Thesis, Van't Hoff Laboratory, Utrecht, 1958; techniques of interpretation: P. F. Mijnlief and J. Th. G. Overbeek, *Koninkl. Ned. Akad. Wetenschap. Proc.*, **B65**, 221 (1962); P. F. Mijnlief, *ibid.*, **B65**, 334 (1962).
- (13) G. L. Miller and K. J. I. Andersson, *J. Biol. Chem.*, **144**, 475 (1942).
- (14) N. V. Hakala, Thesis, University of Wisconsin, 1943.
- (15) K. Granath, *Acta Chem. Scand.*, **7**, 297 (1953).
- (16) D. Stigter, *Rec. trav. chim.*, **73**, 611 (1954).
- (17) W. Philippoff, *Discussions Faraday Soc.*, **11**, 96 (1951).
- (18) K. Hess and L. A. Suranyi, *Z. physik. Chem.*, **184A**, 321 (1939).
- (19) R. W. Mattoon, R. S. Stearns, and W. D. Harkins, *J. Chem. Phys.*, **16**, 644 (1948).
- (20) E. G. Richards and H. K. Schachman, *J. Phys. Chem.*, **63**, 1578 (1959); see p. 1591.
- (21) G. Scatchard, *J. Am. Chem. Soc.*, **68**, 2315 (1946).
- (22) J. S. Johnson, G. Scatchard, and K. A. Kraus, *J. Phys. Chem.*, **63**, 787 (1959).
- (23) W. Prins and J. J. Hermans, *Koninkl. Ned. Akad. Wetenschap. Proc.*, **B59**, 162 (1956).
- (24) K. J. Mysels, *J. Phys. Chem.*, **58**, 303 (1954); *J. Colloid Sci.*, **10**, 507 (1955).
- (25) D. Stigter, *J. Phys. Chem.*, **64**, 842 (1960).
- (26) E. F. Casassa and H. Eisenberg, *ibid.*, **64**, 753 (1960); H. Eisenberg, *J. Chem. Phys.*, **36**, 1837 (1962).
- (27) P. Doty and J. T. Edsall, "Advances in Protein Chemistry," VI, Academic Press, New York, N. Y., 1951, p. 35.

purposes, we can use the equation given by Scatchard and Bregman,²⁹ which in the present symbolism, with activity coefficients assumed constant, may be written

$$N = \frac{1}{\frac{HV^0m_2'}{\tau - \tau_{c.m.c.}} \left(\frac{dn}{dm_2'}\right)_{m_2}^2 \left[1 + \frac{(dn/dm_3)_{m_2'}}{(dn/dm_2')_{m_2}} z'\eta/2\right]^2 - z'\eta} \quad (2)$$

where $H = 32\pi^3n^2/3N\lambda^4$, $\tau - \tau_{c.m.c.}$ is the turbidity of the solution less the turbidity at the c.m.c.; V^0 is volume of solution containing 1 kg. of solvent; n is refractive index of the solution, λ is the wave length under vacuum; m is concentration in moles/kg. of solvent; and N is Avogadro's number. With eq. 2, one can proceed as with ultracentrifugation, *i.e.*, compute values of N for different assumed values of z' and select the z' for which there is a minimum variation in the computed N values for all concentrations.

In a number of studies, turbidities of surfactant solutions have been interpreted by equations based on the work of Prins and Hermans²³ and Mysels and Princen.⁸ The pertinent expressions for $z = Nz'$ and N are

$$z = \frac{B(c_{c.m.c.}' + fc_{BX}) + [(B/500)(c_{c.m.c.}' + c_{BX})]^{1/2}}{C(1 - 500CE)} \quad (3)$$

$$N = \frac{1}{2}[zE + (1/1000C)] + \frac{1}{2}[zE + (1/1000C)]^2 - (z + z^2)E^2]^{1/2} \quad (4)$$

Here the quantities obtained from the turbidity measurements are the intercept, C , and slope, B , of a plot of $H(dn/dc')^2_{m_{BX}}(c' - c'_{c.m.c.})/(\tau - \tau_{c.m.c.})$ vs. $(c' - c_{c.m.c.}')$. The total molarity of the surfactant on a monomeric basis is c' . The supporting electrolyte is BX ; $f = (\partial n/\partial m_{BX})_{m'}/(\partial n/\partial m')_{m_{BX}}$; m' is the total molality of the surfactant as monomer; $E = (c_{c.m.c.}' + fc_{BX})/(c_{c.m.c.}' + c_{BX})$. An examination of the derivation of eq. 3 and 4 reveals that the refractive index increment for the surfactant (dn/dc') is properly evaluated for constant m_{BX} , rather than for constant c_{BX} ; refractive index measurements were computed on this basis in the work of Princen and Mysels.³⁰ If size distribution is independent of concentration, and z' is the same for all particles, these authors show that one obtains weight average molecular weights.⁸ We shall compare micellar charges and weights computed with eq. 2 with those obtained from eq. 3 and 4.

We report here studies of the micelles of NaLS and of dodecyltrimethylammonium bromide, DTAB, by equilibrium ultracentrifugation and light scattering. NaLS was selected because of the wide attention it has re-

ceived and the variations which exist in published micellar weights. DTAB was selected partly because of its availability and partly because of the contrast which it offered to NaLS. The surface-active ion in DTAB is cationic whereas in NaLS it is anionic. In moderate concentration of supporting electrolyte, NaLS sediments away from the axis of rotation while DTAB sediments toward it. The marked differences existing in published DTAB micellar weights³¹⁻³⁴ served as an additional incentive to examine this substance.

Experimental

Centrifugations were carried out with a Spinco Model E ultracentrifuge equipped with an interference optical system. The majority of the runs were made at 25° in a five-cell rotor; a few were carried out at about 33°. Cells were 12 mm. thick in the light path. Most runs were at about 13,000 r.p.m.

The light scattering studies were conducted with a Brice-Phoenix photometer in the neighborhood of 25°. One determination was made with light of 546 m μ and the rest at 436 m μ . The instrument was calibrated with the aid of the opal glass diffuser provided by the manufacturer. The diffuser constant was checked through a measurement of the excess turbidity of a 0.5% solution of Cornell standard polymer in toluene. The experimental excess turbidities of 3.47×10^{-3} and 3.42×10^{-3} cm.⁻¹ for two runs with blue light are to be compared with 3.50×10^{-3} cm.⁻¹, which is an average of the values obtained by other investigators.^{35,36}

Refractive index increments were determined with a Brice-Phoenix photometer. Three different samples of NaLS were used. NaLS-1 was from the batch employed in the Na⁺ mobility experiments of Mysels and Dulin.³⁷ NaLS-2 and NaLS-3 were prepared from two different lots of lauryl alcohol, each having undergone fractional distillation immediately before use. Esterification of the alcohol and initial purification of the crude NaLS were carried out according to the

- (28) R. S. Tobias and S. Y. Tyree, *J. Am. Chem. Soc.*, **81**, 6385 (1959).
 (29) G. Scatchard and J. Bregman, *ibid.*, **81**, 6095 (1959).
 (30) K. J. Mysels, private communication.
 (31) P. Debye, *Ann. N. Y. Acad. Sci.*, **51**, 575 (1949).
 (32) R. M. Hagen, Thesis, Cornell University, 1949.
 (33) P. A. Smudski, Thesis, Cornell University, 1951.
 (34) H. J. L. Trap and J. J. Hermans, *Koninkl. Ned. Akad. Wetenschap. Proc.*, **B58**, 97 (1955).
 (35) B. A. Brice, M. Halwer, and R. Speiser, *J. Opt. Soc. Am.*, **40**, 768 (1950); authors list values found by others as well as their own.
 (36) S. H. Maron and R. L. H. Lou, *J. Polymer Sci.*, **14**, 29 (1954).
 (37) K. J. Mysels and C. I. Dulin, *J. Colloid Sci.*, **10**, 461 (1955).

procedure of Dreger, *et al.*,³⁸ in each preparation. Extraction with ethyl ether and repeated recrystallization from butanol and from water completed the purification.

The DTAB used in the centrifugations and most of the light scattering work was supplied by H. M. Ghose. Analysis indicated 25.98% Br (theoretical 25.92%). All but one of the centrifugations with this surfactant were carried out with the material as originally received. Because some preliminary light scattering work showed that the turbidity *vs.* concentration plot was considerably rounded in the vicinity of the c.m.c., the DTAB was twice recrystallized from acetone (a small amount of ethanol present) before it was used in our light scattering experiments. A sample of DTAB from H. V. Tartar was used as received for some of the light scattering work. It proved to be indistinguishable from the purified Ghose sample (Fig. 1).

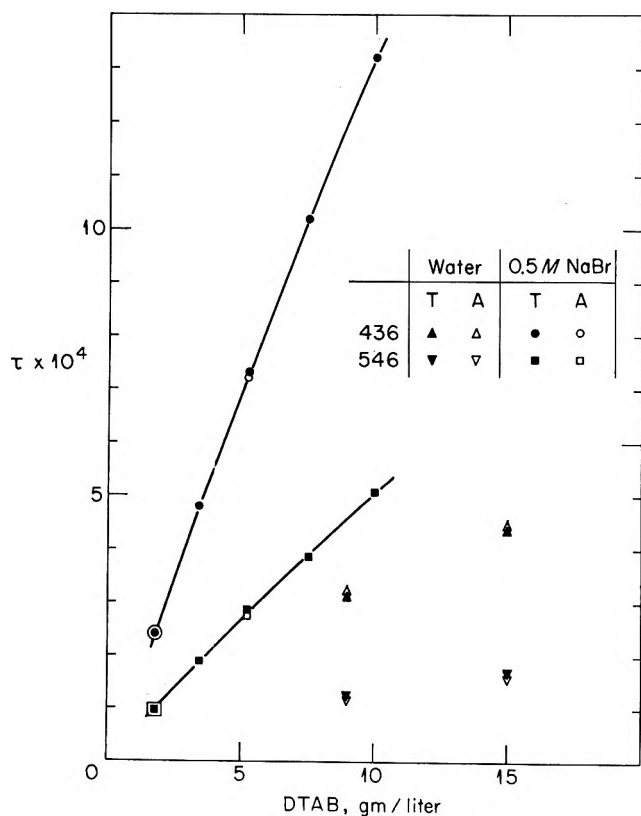


Figure 1. Comparison of turbidities of DTAB solutions prepared from different samples measured under the same conditions: T, Tartar sample; A, material used in this study.

The NaCl and NaBr used as supporting electrolytes were of reagent grade and not further purified. The water used in preparing all solutions was obtained by passing distilled water through a column containing both

cation and anion exchange resins. Except for some of the DTAB solutions used in the light scattering work, solutions were made up by weight. Densities were determined with a *ca.* 24-ml. pycnometer.

Results and Discussion

1. *Volumes and Refractive Index Increments.* The results of apparent specific volume measurements of NaLS and DTAB in the presence of supporting electrolytes are summarized in Table I. Within the accuracy of our measurements and except for the one case mentioned later, no dependence of apparent specific volume, ϕ_v , on concentration was observed in the systems examined. The partial specific volumes of NaLS and DTAB were therefore taken as averages, weighted by a factor proportional to the surfactant concentration, of the appropriate ϕ_v .

The ϕ_v values of DTAB in 2.0 M NaBr were observed to decrease with DTAB concentration. The partial specific volumes required for the ultracentrifugation computations in this situation were estimated by plotting ϕ_v *vs.* log DTAB molality and substituting slopes into the expression³⁹

$$\bar{v} = \phi_v + \frac{d\phi_v}{2.303 d \log m} \quad (5)$$

where m is molality. The values of \bar{v} thus obtained are included in Table I.

The partial specific volumes of NaCl, NaBr, and LiCl were computed from density data in the litera-

Table I: Apparent Specific Volumes of NaLS and DTAB

System	Surfactant molarity at 25°	Apparent specific volume, cc.
NaLS in 0.1 M NaCl	0.010–0.068	0.863
NaLS in 0.4 M NaCl	0.0068–0.068	0.866
NaLS in 0.4 M LiCl	0.017–0.068	0.866
NaLS in 0.5 M NaCl	0.010–0.059	0.866
DTAB in 0.1 M NaBr	0.010–0.100	0.956
DTAB in 0.5 M NaBr	0.025–0.100	0.958
DTAB in 2.0 M NaBr	0.02560	0.977 (0.967) ^a
DTAB in 2.0 M NaBr	0.05097	0.971 (0.963) ^a
DTAB in 2.0 M NaBr	0.1025	0.967 (0.961) ^a
NaLS in 0.4 M NaCl	0.0254 ^b	0.878
NaLS in 0.5 M NaCl	0.025 ^b	0.872

^a Partial specific volume used in calculations. ^b Surfactant molarity at 33°.

(38) E. E. Dreger, G. I. Keim, G. D. Miles, L. Shedlovsky, and J. Ross, *Ind. Eng. Chem.*, **36**, 610 (1944).

(39) G. N. Lewis and M. Randall, "Thermodynamics," McGraw-Hill Book Co., Inc., New York, N. Y., 1923, p. 37.

ture^{40,41} and the values used in the ultracentrifugation calculations are given in Table II.

Table II: Partial Specific Volumes of NaCl, NaBr, and LiCl

Solution	\bar{v} , cc.
0.1 M NaCl	0.2992
0.4 M NaCl	0.3143
0.5 M NaCl	0.3181
0.1 M NaBr	0.2366
2.0 M NaBr	0.2637
0.4 M LiCl	0.4307

It is necessary to know the relation between refractive index and solution concentration to interpret interference patterns obtained in ultracentrifugation. In addition, refractive index increments for the solutes are needed for analysis of light scattering data (eq. 2-4). Increments determined for the soaps in various media are given in Table III. The increments of the nonmicellar soap are possibly different from those of the micelles; instead of listing apparent values ($\Delta n/c'$), as is sometimes done, we report values obtained from the slope of refractive index of solutions *vs.* soap concentration, measured at a constant molarity of supporting electrolytes. Where necessary (for eq. 3 and 4), increments for the soaps at constant supporting electrolyte molality were obtained from these values and the densities of the solutions. The increments used for the supporting electrolytes, mostly taken from the literature,⁴²⁻⁴⁴ are also listed in Table III, and in the computations were assumed to be unaffected by the presence of soap.

2. *Critical Micelle Concentrations (c.m.c.). (a) Values Used in Analysis of Results.* In both the light scattering and ultracentrifugation computations, corrections are necessary for the presence of nonmicellar surfactant (which is assumed to be monomeric in this paper).⁴⁵ In the light scattering work, values of the c.m.c. were selected to give the best linear plots of $H(dn/dc')^2_{\text{MBX}}(c' - c_{\text{cmc}}')/(\tau - \tau_{\text{cmc}})$ *vs.* $(c' - c_{\text{cmc}}')$.

A method of estimation of c.m.c. by ultracentrifugation is illustrated below, but the 25° values used in interpretation of sedimentation results were computed from an empirical equation of c.m.c. in terms of added NaCl, given by Williams, *et al.*⁴⁶ At 35°, the 25° values were also used, but the effect of using a c.m.c. different by an amount suggested by the results of Matijević and Pethica⁴⁷ was tested (section 3). Correction for nonmicellar soap was made by including it in the supporting electrolyte, *i.e.*, the input soap concentration

Table III: Gradients of Refractive Index with Concentration

System	436 m μ , l./mole (dn/dc') ^a	546 m μ , l./mole (dn/dc') ^a
NaLS in 0.1 M NaCl	0.0345	0.0338
NaLS in 0.4 M NaCl	0.0340	0.0335
NaLS in 0.5 M NaCl		0.0331
NaLS in 0.4 M LiCl	0.0342	0.0338
DTAB in H ₂ O	0.0471	
DTAB in 0.1 M NaBr	0.0469	0.0455
DTAB in 0.5 M NaBr	0.0470	0.0458
DTAB in 2.0 M NaBr	0.0472	0.0455
Average used	0.0470	0.0456
LiLS in 0.4 M uni-univalent electrolyte	0.0332 ^b	0.0329 ^b
Supporting electrolytes	(dn/dc)	(dn/dc)
0.4 M LiCl ^c	0.00938	0.00901
0.1 M NaCl ^d	0.01054	0.01015
0.4 M NaCl ^d	0.01022	0.00985
0.5 M NaCl ^d		0.00977
0.1 M NaBr	0.0149	0.0140
0.5 M NaBr	0.0149	0.0140
2.0 M NaBr ^e	0.0142	0.0134

^a Soap values are given for constant moles/l. of supporting electrolyte. ^b Obtained from measurement of NaLS in LiCl solution and converted to LiLS with increments of 0.4 M LiCl and NaCl. Compare with 0.0330 at 436 m μ and 0.0326 at 546 m μ , which were obtained from values in ref. 8 for water by assumption that ratios of increments of LiLS in water and 0.4 M LiCl are the same as those of NaLS in water and 0.4 M NaCl. ^c From ref. 42. ^d From ref. 43. ^e From ref. 44.

was decreased and the supporting electrolyte concentration increased by this amount. The approximation involved in doing this is unimportant, since the soap monomer and supporting electrolyte sediment very little at the speeds of these experiments; further, the molecular weight corrected for buoyancy of NaLS monomer is very close to the value for sodium chloride.

- (40) H. E. Wirth, *J. Am. Chem. Soc.*, **62**, 1128 (1940).
 (41) "International Critical Tables," Vol. 3, McGraw-Hill Book Co., Inc., New York, N. Y., 1928: (a) p. 80; (b) p. 77.
 (42) H. Kohner, *Z. physik. Chem.*, **B1**, 427 (1928); gradients were computed from data in this paper by interpolation.
 (43) A. Kruis, *ibid.*, **B34**, 13 (1936); gradients were computed from data in this paper by interpolation.
 (44) Gradients were computed assuming that percentage decrease from initial value to that at 2.0 M concentration is the same for 436 and 546 m μ as for Na-D light. Percentage decrease in gradient for Na-D computed from data given in "International Critical Tables," Vol. 7, McGraw-Hill Book Co., Inc., New York, N. Y., 1930, p. 72.
 (45) G. D. Parfitt and A. L. Smith, *J. Phys. Chem.*, **66**, 942 (1962).
 (46) R. J. Williams, J. N. Phillips, and K. J. Mysels, *Trans. Faraday Soc.*, **51**, 728 (1955).
 (47) E. Matijević and B. A. Pethica, *ibid.*, **54**, 587 (1958).

In computation of ultracentrifugation results, the input refractive index increments and values of L for the supporting electrolyte were averages for NaCl and soap weighted according to the concentration of NaCl and nonmicellar soap.

Critical micelle concentrations for DTAB were obtained from our light scattering results and could be represented by the equation

$$\log c_{\text{cmc}}' = -0.610 \log (c_{\text{cmc}}' + c_s) - 2.958$$

where c_s is the concentration of NaBr. These values were used in interpretation of both light scattering and ultracentrifugation.

(b) *C.m.c. by Ultracentrifugation.* It was mentioned above that estimates of the c.m.c. can be obtained by ultracentrifugation. In order to do this, a solution whose concentration is not a great deal higher than the c.m.c. is centrifuged to equilibrium; an interference pattern similar to that in Fig. 2a is obtained. One then analyzes the pattern in the usual manner to get a graph of $\ln c_2'$ vs. x^2 (Fig. 2b). At high radius,

where most of the soap is present in the form of aggregates, a straight line will be obtained; at low radius, however, the points will fall above this line, since an appreciable fraction of total soap will be present as slightly sedimenting monomer. By extrapolating the straight line, an estimate of the micellar concentration can be obtained for the points at low radius, and the difference gives an estimate of the c.m.c. A more refined approximation may be obtained by subtracting this value from the soap concentration at each point in the figure (the monomer concentration will be effectively constant at all radii), replotting the logarithm of corrected soap concentration vs. x^2 , and adding the new difference to the first estimate. Rather soon, since convergence is rapid, the graph of $\ln c_2'$ vs. x^2 will be a straight line for the whole range. An equivalent alternate procedure is to select that value of the c.m.c. which gives a straight line when used to correct the input soap concentration.

Since the table of $\ln c_2'$ will be affected somewhat by the assumed value of z' , the value of c.m.c. obtained at low soap concentration should for a completely consistent solution be iterated with experiments at higher concentration to obtain charge. However, in practice, the c.m.c. obtained is only moderately sensitive to the assumed value of z' . In the example in Fig. 2, with our best estimate of $z' = 0.16$, we obtain a c.m.c. for NaLS of 0.0017 M in 0.1 M NaCl, which compares with 0.0015 given by Williams, *et al.*,⁴⁶ and with 0.0016 given by Corrin and Harkins.⁴⁸ If z' is assumed zero, *i.e.*, charge is neglected, the value estimated by ultracentrifugation is not greatly different, 0.0019.

The conditions of this experiment were not optimum; more precision in this determination should be possible with a lower soap concentration, centrifuged in a cell of greater light path length.

3. *Equilibrium Ultracentrifugation of NaLS.* From eq. 1 it can be seen the degree of aggregation cannot be determined independently of charge. Although it is possible in principle to determine both N and z' from a single centrifugation,⁴⁹ it is usually necessary in practice to make several runs under different conditions and to compare the results to obtain an aggregation number and charge simultaneously. For each run N or $1/N$ is computed from eq. 1 and plotted for a plausible range of assumed z' . The intersection of the various curves or the point at which they make closest approach yields N and z' .

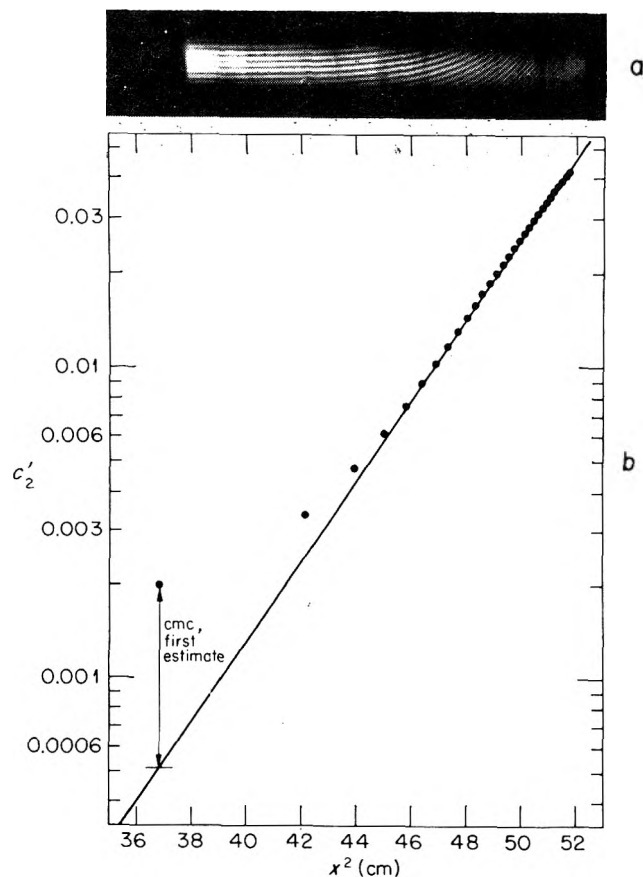


Figure 2. Estimation of c.m.c. by equilibrium ultracentrifugation: 0.010 M NaLS in 0.1 M NaCl, 25°, 24,630 r.p.m., computed for $z' = 0.16$.

(48) M. L. Corrin and W. D. Harkins, *J. Am. Chem. Soc.*, **69**, 683 (1947).

(49) R. W. Holmberg, K. A. Kraus, and J. S. Johnson, *ibid.*, **78**, 5506 (1956).

The procedure implies that at a given sodium chloride concentration, N of the micellar part of the soap is independent of soap concentration. The fact that higher concentrations of soap give lower apparent values of N computed for $z' = 0$ indicates that this assumption is reasonable for supporting electrolyte concentrations of $0.4 M$ and below. In addition, graphs of $\ln n^*$ vs. x^2 for individual centrifugations (n^* being refractive index difference between solution and background), which tend to be concave upward with polydisperse solutes, are to a good approximation linear under these conditions. Solutions $>0.4 M$ NaCl are discussed later.

Although values of N and z' can be selected fairly well by inspection, in the present study, since we wish to compare results with those obtained by light scattering and other methods, we have adopted a systematic procedure which we feel is reasonable, if somewhat arbitrary. Greater angles of intersection are obtained with $1/N$ vs. z' graphs for greater differences in soap concentration, and consequently should give a more sensitive estimate of charge than the intersections for experiments having lesser differences in concentration. In estimating z' , therefore, we have weighted the values of z' obtained at each intersection of curves for different concentrations by the ratio of the higher to the lower concentration. In $0.1 M$ NaCl, since there were only three centrifugations, all intersections were used; for $0.4 M$ NaCl, there were more experiments and all intersections for which the ratio was less than 1.5 were rejected. Once the value of z' was selected, an average of the values of N obtained for each centrifugation at this charge was selected for degree of aggregation. Heavy points on the figures show the results of this procedure.

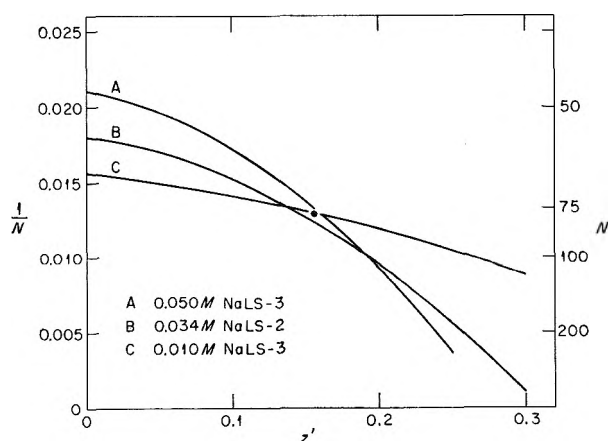


Figure 3. Equilibrium ultracentrifugation of NaLS in $0.1 M$ NaCl at 25° ; degree of aggregation N computed as a function of charge z' .

Figure 3 illustrates the procedure just described for the case of NaLS in $0.1 M$ NaCl at 25° . The best N and z' appear to be 76 and 0.16, respectively, whereas in $0.4 M$ NaCl they are close to 119 and 0.20 (see Fig. 4). In agreement with turbidity results, the values of

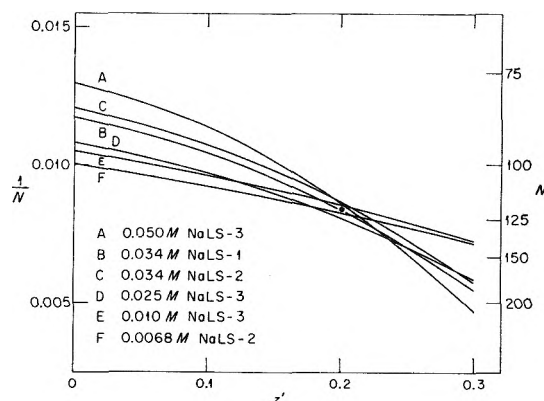


Figure 4. Equilibrium ultracentrifugation of NaLS in $0.4 M$ NaCl at 25° ; degree of aggregation N computed as a function of charge z' .

z' indicate that the micelles bind counterions extensively; the difference between the values for 0.1 and $0.4 M$ NaCl probably is not significant. The crossover point for two solutions (0.01 and $0.025 M$ in NaLS, both $0.4 M$ in NaCl) centrifuged at 33° corresponded to $N = 94$ and $z' = 0.15$. Although the latter values cannot have a high degree of certainty since there are only two runs, they do indicate that micellar weights decrease as the temperature is raised. These results were computed with 25° values of the c.m.c., but variation of this parameter over a reasonable range had only a small effect on N . Similar behavior by DTAB micelles has been observed.³¹

In $0.5 M$ NaCl, the values of N computed for $z' = 0$ are higher for higher initial soap concentration (Fig. 5). Such behavior indicates that the micellar weight increases with increasing c_{NaLS} , since the effect of charge would be in the opposite direction. Graphs of $\ln n^*$ vs. x^2 also indicate polydispersity by concavity upward; this is illustrated by deviations from a straight line, plotted in Fig. 6. For $0.025 M$ NaLS at 25° , insignificant deviations from linearity of $\ln n^*$ vs. x^2 are observed for $0.4 M$ NaCl; at $0.45 M$ NaCl, definite polydispersity is indicated, and at 0.50 , the concavity upward is striking. Similar, though less marked, observations were obtained for 33° and for $0.01 M$ NaLS (not shown) at 25° .

Since estimates of z' are not possible under these circumstances, we do not attempt to evaluate N from

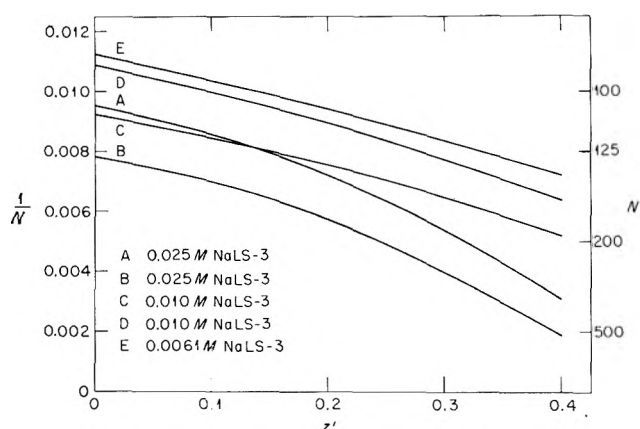


Figure 5. Equilibrium ultracentrifugation of NaLS in 0.5 *M* NaCl at 25°; degree of aggregation *N* computed as a function of charge *z'*; centrifugation of B and C carried out *ca.* 16 months later than others.

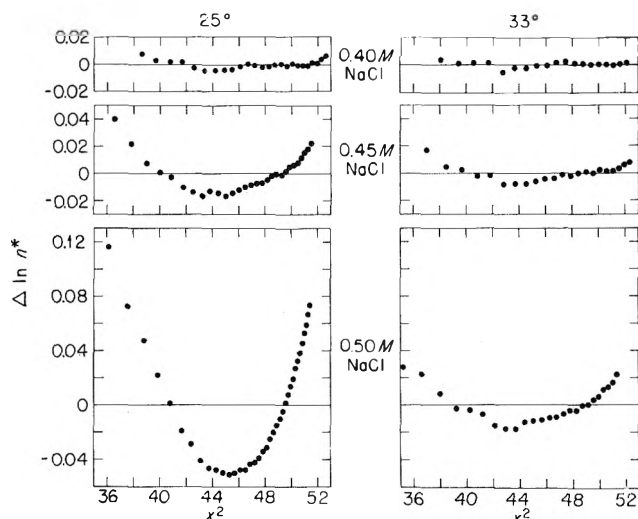


Figure 6. Effect of supporting electrolyte concentration on polydispersity of 0.025 *M* NaLS.

these results. In this connection it is perhaps significant that values of the molecular weight did not seem as reproducible for centrifugations carried out at different times in 0.5 *M* NaCl as they were in 0.4 *M* NaCl. Centrifugations of both 0.01 and 0.025 *M* NaLS (from NaLS-3) solutions in 0.5 *M* NaCl gave molecular weights, computed for $z' = 0$, about 20% higher (Fig. 5) than those obtained in experiments made on solute from the same batch at the same concentrations about a year earlier (when most of the experiments reported were carried out). All gave indications of polydispersity, very clear in the case of 0.025 *M* NaLS. A solution of 0.025 *M* soap concentration in 0.4 *M* NaCl solution, however, centrifuged at the later time, gave a result consistent with the earlier results at the same support-

ing electrolyte concentration; it is included in Fig. 4. A possible explanation is that sedimentation behavior in the polydisperse region is more sensitive to the presence of products produced by possible deterioration of the soap than in the monodisperse region. It should also be noted that in the light scattering measurements of Mysels and Princen,⁸ no indication of polydispersity at 0.5 *M* NaCl was apparent. For these reasons, the ultracentrifugation results in this medium must be viewed with some reservation, particularly quantitatively. However, because the indication of polydispersity was reproducible, and because a similar observation was made with DTAB at high supporting electrolyte concentrations, we report these results.

A single ultracentrifugation of 0.034 *M* NaLS in 0.4 *M* LiCl was also carried out. In analyzing the results, it was found that the aggregation number obtained depended strongly on assumptions made concerning the preferential complexing of Na⁺ and Li⁺. The study was therefore not extended, and the results are not reported in detail. Even if z' was assumed to be as high as 0.25, however, the value of *N* obtained for the assumption giving the highest molecular weight (complete preference for Li⁺) was less than 100, or substantially less than found for solutions 0.4 *M* in NaCl.

4. *Light Scattering by NaLS Solutions.* The light scattering data are recorded in Fig. 7 in the form of turbidity *vs.* concentration plots. Micellar aggregation numbers and charges as computed from eq. 2-4 are listed in Table IV.

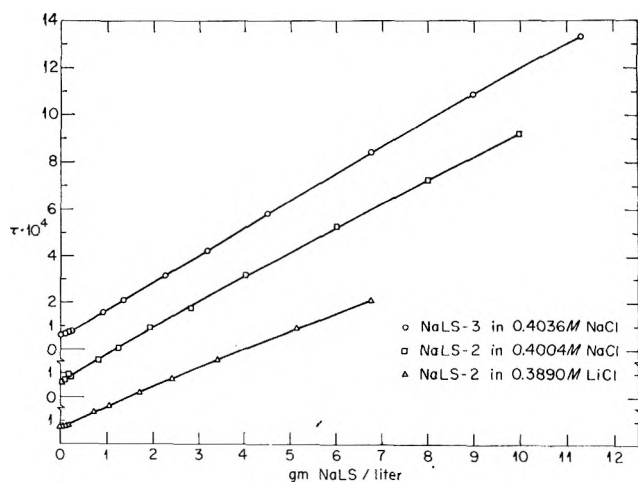


Figure 7. Light scattering of NaLS in 0.4 *M* NaCl and LiCl.

5. *Comparison of NaLS Results.* The increase in *N* for NaLS micelles from 76 to 119 (ultracentrifugation results) as the NaCl supporting electrolyte level is raised from 0.1 to 0.4 *M* is in agreement with the conclu-

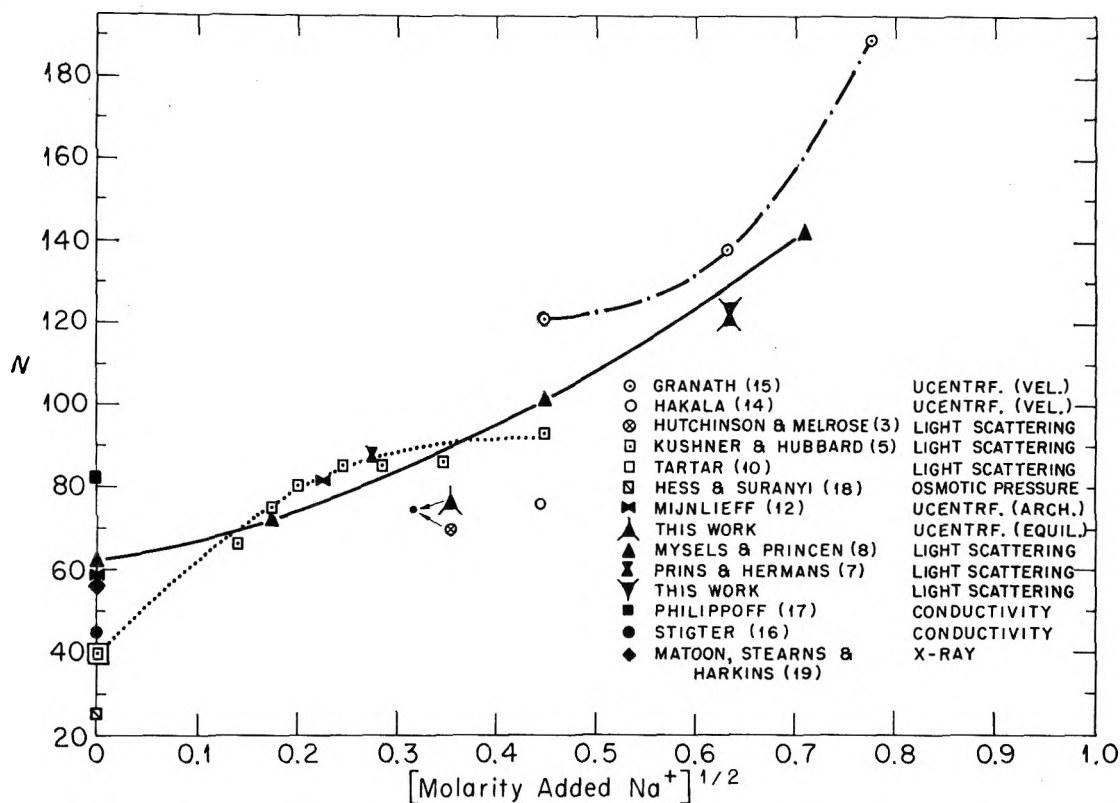


Figure 8. Comparison of reported NaLS aggregation numbers: open points, no charge correction; solid points, charge correction attempted.

Table IV: NaLS Aggregation Numbers

NaLS sample	Supporting electrolyte	Procedure ^a	Temp., °C.	λ , m μ	N	z'
2, 3	0.1 M NaCl	E.U.	25	546	76	0.16
1, 2, 3	0.4 M NaCl	E.U.	25	546	119	0.20
3	0.4 M NaCl	E.U.	33	546	94	0.15
2	0.4 M NaCl	L.S. (2)	25	436	125	0.15
2	0.4 M NaCl	L.S. (3,4)	25	436	123	0.17
3	0.4 M NaCl	L.S. (3,4)	25	436	120	0.10
2	0.4 M LiCl	L.S. (3,4)	25	436		
		I			92	0.22
		II			98	0.21
		III			98	0.21

^a E.U.: Equilibrium ultracentrifugation; L.S.: light scattering. Equations used in interpretation of light scattering given in parentheses. In computing micellar weights in LiCl solutions, refractive index increments of micelles and supporting electrolytes computed on basis that all cations complexed by aggregates are I, Na^+ ; II, Li^+ ; III, in proportion to the stoichiometric concentrations of Li^+ and Na^+ .

sion drawn in earlier work^{4,7,19,31,50} that micelle size is a function of supporting electrolyte concentration. This view has been opposed by Hutchinson.⁵¹

The aggregation numbers of NaLS micelles in 0.4 M

NaCl as found by light scattering for two of the NaLS samples (prepared and examined approximately a year apart) are in good agreement with each other and the ultracentrifugation value. It is also to be noted that eq. 2 gave substantially the same values for N and z' as did eq. 3 and 4 in the common case (NaLS-2 in 0.4 M NaCl) examined. This should not be too surprising since the two procedures originate in expressions for excess turbidity (Stockmayer's equation⁵² on the one hand and Zernike's equation²³ on the other) which can be shown to be equivalent.

For the purposes of comparison, some of the published NaLS micellar weights and those found in the present work are plotted in Fig. 8 against the square root of the molarity of added Na^+ . Micellar weights found in references 4, 6, 9, 11, and 13 have not been included. In two cases the original work was re-examined and only the last results^{8,10} are shown. In two other cases, NaLS of questionable purity was involved. In the remaining case,¹¹ an experimental procedure was later discovered to be of doubtful value.

(50) K. Granath, *Acta Chem. Scand.*, **4**, 103 (1950).

(51) E. Hutchinson, *J. Colloid Sci.*, **9**, 191 (1954).

(52) W. H. Stockmayer, *J. Chem. Phys.*, **18**, 58 (1950).

A solid point designation in Fig. 8 indicates that in the interpretation of the related experimental data some attempt was made to correct results for charge and unaggregated surfactant. An open point designation signifies that either no corrections were made or that such corrections were not discernible from the literature. The single X-ray value was evidently computed by a method not sensitive to charge. A correction for unaggregated surfactant was not deemed necessary because the solution examined was a highly concentrated one and the c.m.c. only a small fraction of the total concentration. Consequently, a solid point designation is used.

The greatest disparity in published micellar weights occurs in the absence of supporting electrolyte. This is not too surprising since micelle interactions are relatively large and difficult to evaluate in solutions of low ionic strength. Observations would also be much more sensitive to electrolyte impurities under these conditions and consideration of ionization in analysis of turbidity measurements is particularly important. The fact that the micellar weights for NaLS in water reported by Tartar and by Kushner and Hubbard are lower than those of Mijnlief and of Mysels and Princen is accounted for in part by neglect of charge on the part of the former. In light scattering (though not in ultracentrifugation of solutes having density so close to that of the solvent), the charge effect is relatively much smaller in solutions high in added salt than at low supporting electrolyte.

If curvature is disregarded, the light scattering results of all investigators are in reasonably good agreement for added Na^+ of 0.02 to 0.20 M . That of Hutchinson and Melrose is a little low, presumably because of neglect of corrections for charge and c.m.c.; both of these would tend to raise the value. It is not, however, outside the range of values given by the various methods.

Our ultracentrifugation results, as well as those of Mijnlief, are in fair agreement with those of light scattering. The results of Hakala and Granath for 0.2 M Na^+ seem considerably out of line.

Values of N computed for solutions of NaLS in LiCl from turbidity measurements are also affected (Table IV) by the relative preference of the micelles assumed for the two ions, though not so much as in ultracentrifugation. Results are listed for different assumptions concerning this preference. It seems clear, in agreement with the indication given by sedimentation, that the micelles are smaller in this medium than at the same concentration of NaCl. It is interesting that no such difference is reported⁸ for LiLS and NaLS in absence of supporting electrolyte.

6. *Equilibrium Ultracentrifugation of DTAB.* Solutions of DTAB at two different levels of supporting electrolyte concentration were centrifuged. The $\ln n^*$ vs. x^2 plot for DTAB in 0.10 M NaBr was essentially linear, an indication that the micelles are predominantly monodisperse. Unfortunately, the $(1 - \bar{v}_2\rho)$ term is small—about 0.040. The $1/N$ vs. z' curves were so nearly parallel that the charge is essentially undetermined; they are also steep, since the value of L of the Scatchard component is very sensitive (on a percentage basis) to the assumed charge. A meaningful estimate of N was thus precluded. If our light scattering value of N , 71, is taken as correct, equilibrium ultracentrifugation of both 0.025 and 0.05 M DTAB in 0.1 M NaBr implies a somewhat higher charge, $z' \sim 0.2$, than that obtained from analysis of the turbidities. Since ultracentrifugation in this case is much more sensitive to charge than light scattering, the value may be better.

In 2 M NaBr, the $(1 - \bar{v}_2\rho)$ term for DTAB is approximately -0.110. Sedimentation takes place in the direction of the meniscus. The $\ln n^*$ vs. x^2 plot is concave upward, *i.e.*, is similar to that obtained with the polydisperse NaLS solutions in 0.5 M NaCl. Also analogous to the anionic soap at high supporting electrolyte concentration, the graphs of $1/N$ vs. z' for different concentrations of DTAB do not intersect. The DTAB micelles thus appear to be polydisperse in 2 M NaBr.

7. *Light Scattering by DTAB Solutions.* Some of the experimental results are presented in Fig. 9 as turbidity

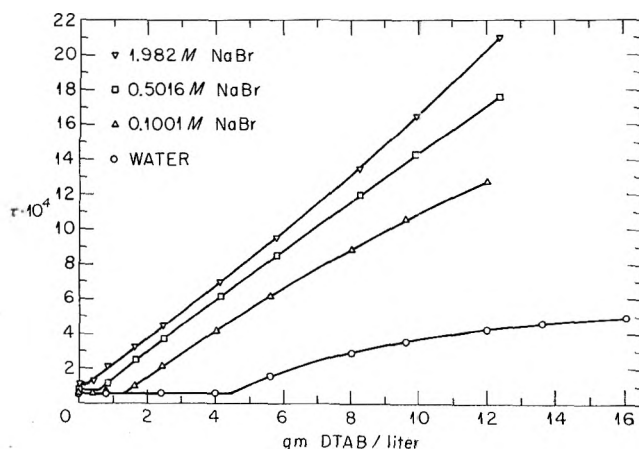


Figure 9. Light scattering of DTAB in NaBr solutions.

vs. concentration plots. Computed values of N and z' are given in Table V. The upward curvature of the DTAB turbidity plot at the 2.0 M NaBr level may reflect the polydispersity indicated in the ultracentrifugation experiments at the same NaBr concentration.

Equations 3 and 4 are useless for interpreting the data for this run since the negative B encountered leads to a complex number for charge.

8. *Comparison of DTAB Results.* All published DTAB micellar weights known to us were determined by light scattering. No correction for charge was made in any of them, the micellar weight being taken in each case as $M'/1000C$ or its equivalent. So as to obtain a meaningful comparison of our results with those in the literature, we have plotted $1/1000C$ (micellar degree of polymerization computed for zero charge) vs. molarity of added Br^- in Fig. 10. Tartar's first published micellar weight for DTAB⁶ is not included, but his latest value is.¹⁰

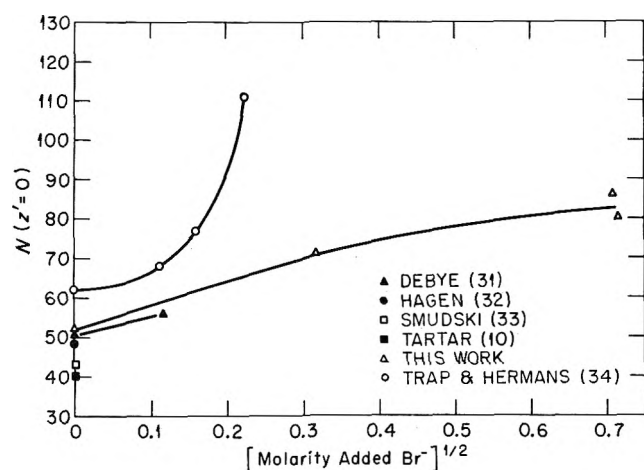


Figure 10. Comparison of reported DTAB aggregation numbers ($z' = 0$) obtained by light scattering.

The micellar weights of Trap and Hermans seem excessively high. If corrected to 25° for a closer comparison with our results, they become still higher by approximately 5%.^{31,33} The refractive index increment used by Trap and Hermans is larger than the one we found for the same wave length. Substitution of our increment for theirs would add an additional 9% of the micellar weight to their values. The reason(s) for the difference in results must lie elsewhere.

Trap and Hermans used KBr as a supporting electrolyte whereas we used NaBr . It is doubtful that the substitution of one cation for another could be the explanation for the observed differences. Because of the high potentials existing at the micelle surface, cations would likely be so strongly repelled as to be ineffective in influencing micelle structure.^{31,53} In any event, replacement of one supporting electrolyte by another could in no way explain the different findings for the system $\text{DTAB-H}_2\text{O}$. If errors in instrument

Table V: Light Scattering of DTAB Solutions at 25°

NaBr concentration, mole/l.	Wave length of light, $m\mu$	Equations used	N	z'	$N(z' = 0)$
0	436	3, 4	61	0.15	52
0.1001	436	3, 4	74	0.12	71
0.5016	436	3, 4	90	0.15	86
0.51	546	3, 4	87	0.23	81
0.51 ^a	546	2	89	0.25	
0.51 ^a	436	3, 4	86	0.22	79
0.51 ^a	436	2	86	0.22	

^a From turbidities in Fig. 1. Somewhat different refractive index increments were found for these solutions (0.0480 for 436 $m\mu$ and 0.0467 for 546 $m\mu$) than those listed in Table III and for consistency were used in computation of N . There were also differences in turbidity; essentially the same aggregation number was obtained. Temperature differences of the measurements may explain part of the differences in turbidity. From other results, we believe the refractive index increments in Table III are more correct. See also E. W. Anacker and H. M. Ghose, *J. Phys. Chem.*, 67, 1713 (1963).

calibration were responsible for differences in the results obtained by two different investigators, one would expect micellar weights to be in constant ratio to one another if paired at identical supporting electrolyte concentrations. This is obviously not the situation.

We suspect that sufficient impurity was present in Trap and Herman's DTAB sample to cause the solutions to exhibit a higher turbidity than would otherwise have been the case. The marked curvature in all of their turbidity plots in the vicinity of the c.m.c (see Fig. 1 of ref. 34) supports this suspicion. As mentioned earlier, our DTAB sample originally showed similar behavior which disappeared after two recrystallizations from acetone.

Whatever lack of agreement exists among the results of the remaining investigations is not easy to explain. We have already stated that when Tartar's DTAB sample was compared with ours in the same scattering instrument, they were indistinguishable.

The work which originated in Debye's laboratory³¹⁻³³ was based upon calibrations involving the use of the absolute camera,⁵⁴ an instrument which has given a turbidity for a standard system (0.5% solution of Cornell polymer in toluene) some 30% less than the accepted value.³⁵ Any errors in calibration introduced by the use of this camera may have been compensated in part by simultaneous neglect of volume and refraction

(53) P. Debye, *J. Phys. Colloid Chem.*, 53, 1 (1949).

(54) P. Debye, *ibid.*, 51, 18 (1947).

corrections.⁵⁵ One cannot be certain of this, however. Unassailable calibration methods as well as certain and rapid procedures for the removal of small but detectable amounts of impurities are still needed in the field of light scattering.

One of the present authors⁵⁶ has been associated with a suggestion that silicotungstic acid-water be used for calibration of aqueous systems. The excess turbidities would be computed from the activity coefficients and refractive index increments of the solute. Reasonably good agreement was obtained between turbidities computed from activity coefficient measurements by ultracentrifugation and experimental values based on the manufacturer's opal glass diffuser calibration. Recent light scattering measurements on this system in another laboratory,⁵⁷ however, have disagreed substantially with our values, and the discrepancy will have to be resolved before the procedure in question can be considered useful for calibration.

9. Anomalous Sedimentation of Soaps. The observations we report in this section are put forward with some hesitancy, not only because we do not understand them, but also because we are not at present able to reproduce them at will. However, the behavior to be described has been seen many times, and whether it is a property of some soap solutions or the result of some unknown facet of our experimental technique, we have no doubt that it exists. We have therefore decided to include an account here, in hope that observations of others may shed some light on these phenomena.

In our first centrifugation of a soap solution, 0.034 M NaLS in 0.4 M NaCl, a sequence in many respects typical of the behavior in question occurred. The experiment was started at low speeds, selected to give a favorable distribution for a solute of the molecular weight indicated by light scattering and of the partial specific volume of this material. Normally, in the initial phases of an experiment, interference fringes would be observed to bend down at the left of the picture, as material sediments away from the meniscus, would be flat in the middle, and bend upward at the right, as solute concentrates at high radius (Fig. 11a). In this case, fringes remained flat over most of the cell, and only slowly did the fringes bend up at high radius, *i.e.*, there was an indication of sedimentation in this region. In Fig. 11b are shown the interference and schlieren patterns after 11 days at 13,410 r.p.m. At this time the speed was increased to 27,690 and sedimentation was promptly observed at the meniscus. After about 12 hr. at this speed, speed was decreased to 19,160 for 7 days, at which time equilibrium appeared to be established. The setting was then changed to its original value, 13,410, and at the end of 4 days equi-

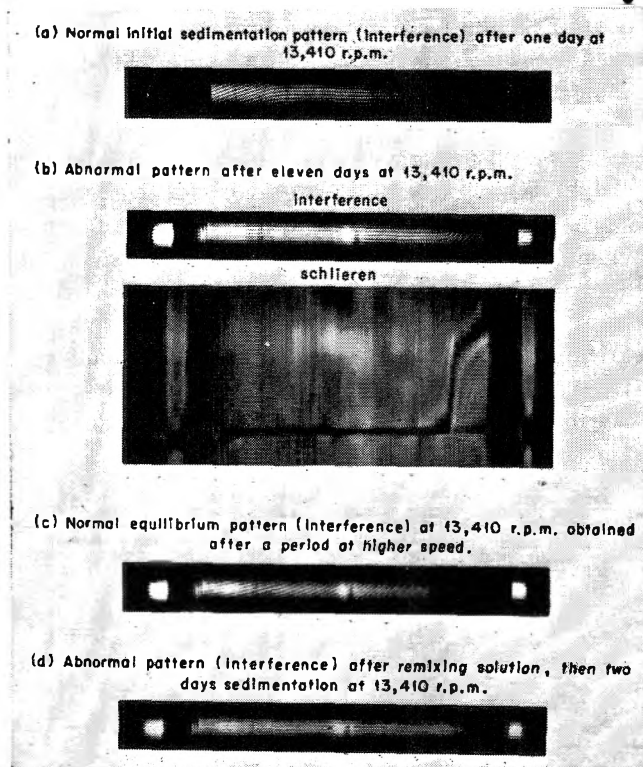


Figure 11. Comparison of normal initial sedimentation pattern (a) with abnormal behavior (b, d); 0.034 M NaLS in 0.4 M NaCl at 25°.

librium seemed essentially attained, with a normal equilibrium pattern (Fig. 11c). The centrifuge was then stopped, the solution remixed by shaking the rotor, and the speed again brought to 13,410. After 2 days, the abnormal pattern (Fig. 11d) was again evident. The difference between Fig. 11b and 11c apparently was not caused by a change in the soap solution. Analysis of the normal equilibrium pattern at 19,160 (schlieren) and at 13,410 (interference) gave the expected molecular weight in this medium; the result at the lower speed is included in Fig. 4.

In another variation of this abnormal behavior, no sedimentation was seen at any radius at speeds of rotation for which very substantial indications would be expected. In many cases, once the speed was raised to a value at which normal sedimentation was observed at all radii, a normal equilibrium pattern would be established if the speed were dropped to a lower value; in some, however, if the speed was dropped enough, the fringes would flatten to a point indicating no significant

(55) C. I. Carr and B. H. Zimm, *J. Chem. Phys.*, **18**, 1616 (1950).

(56) J. S. Johnson, K. A. Kraus, and G. Scatchard, *J. Phys. Chem.*, **64**, 1867 (1960).

(57) M. Kerker, J. P. Kratochvil, R. H. Ottewill, and E. Matijevic, *ibid.*, **67**, 1097 (1963).

concentration variation, even though a substantial gradient would be expected. In other cases a difference between no perceptible and obvious sedimentation was effected by a difference of as little as 50% in the field.

Only with sodium lauryl sulfate were patterns of the type in Fig. 11 seen, though other variations of abnormal behavior were seen with DTAB (0.04 *M* in 0.5 *M* NaBr), cetyl pyridinium bromide (0.03 *M* in 0.4 *M* NaBr), and dodecyl ammonium chloride (0.04 *M* in 0.1 *M* NaCl), though there is a slight question concerning the last. With NaLS the behavior was observed in 0.1 *M* NaCl and in 0.1 and 0.4 *M* LiCl, as well as in 0.4 *M* NaCl, and at 32° as well as at 25°. Although the indications were not conclusive, from experiments carried out at the same time, it appears that the abnormal pattern was more persistent in LiCl than in NaCl and at lower soap and supporting electrolyte concentrations.

As we have implied, the behavior is not altogether reproducible. Solutions which gave abnormal behavior would sometimes exhibit normal initial sedimentations in experiments carried out at a later time under the same conditions; the same was true of similar solutions made up at different times from the same batch of solute (only one somewhat questionable indication of abnormal behavior was given by solutions made of NaLS-3, but clear-cut instances were observed with the other two lots). The reverse was almost never seen; once a solution behaved normally, abnormal behavior under the same experimental conditions was never unambiguously observed. The anomalous observations thus do not seem to arise from some peculiar effect of decomposition of the soap. In this connection, it is of interest that addition of two likely impurities, lauryl alcohol and dilauryl sulfate, to solutions whose sedimentation behavior was normal did not produce abnormal behavior.

It is, of course, possible that these observations are

an experimental artifact. The most plausible explanation to our knowledge would be convection. The fact that in some cases of abnormal behavior a slight bending of the fringes at the meniscus, followed by a straightening, was seen, could be taken to support this. On the other hand, the fact that both normal and abnormal behavior were observed for different solutions in the cells of a five-cell rotor at the same time argues against this possibility.

It is difficult to exclude this explanation completely, but an attempt was made to promote the abnormal pattern with solutions which behaved normally by carrying out experiments under conditions conducive to convection currents, *i.e.*, by misaligning the cell so that the walls did not fall along radii, and by introducing heat to the rotor from the circumference. Only normal patterns were observed.

Convection currents do not seem to us an adequate explanation for the abnormal patterns. The apparent resistance to sedimentation is very difficult to explain in other ways, however. The solutes gave expected values of the molecular weights by light scattering; the short range concentration fluctuations thus seem normal. The explanation may be related to the fact that specific volumes of solvent and solute do not differ greatly, but we have not been able to conceive a model which accounts for all observations.

Acknowledgments. We are indebted to Miss Neva E. Harrison for technical assistance, to Drs. K. J. Mysels, W. Baldwin, H. V. Tartar, and H. M. Ghose for surfactant samples, and to Professor George Scatchard and Dr. K. A. Kraus for a number of profitable conversations. E. W. A. is especially grateful to the Oak Ridge Institute of Nuclear Studies for travel support. This research was supported in part by a grant from the Petroleum Research Fund administered by the American Chemical Society. Grateful acknowledgment is hereby made to the donors of the fund.

Photoetching of Thin Lead Films with Nitromethane

by L. H. Kaplan

*International Business Machines Corporation, Thomas J. Watson Research Center,
Yorktown Heights, New York (Received July 31, 1963)*

Thin evaporated lead films have been photoetched with gaseous nitromethane activated by ultraviolet radiation. The rate of etching (of the order of 10 \AA./min.) varies inversely with the volume of the system, is proportional to the square root of the radiation intensity, and is proportional to the partial pressure of nitromethane and then saturates at a limiting pressure. The presence of nitrogen in the system strongly retards the etching reaction. The rate of reaction has been calculated as a function of the radiation wave length by use of a set of transmission filters. For lead, the wave length band of $2680 \pm 50 \text{ \AA.}$ gives the largest positive contribution to the rate, while a band at $2530 \pm 50 \text{ \AA.}$ inhibits the reaction by about 370% of the observed rate.

Introduction

The formation of thin metallic films, in specific patterns, is a necessity in microminiaturized circuit fabrication technology. A novel method of making such patterns involves the use of a finely focused image of ultraviolet light to initiate photochemical reactions capable of removing metal from the illuminated regions. The image shape being completely arbitrary, any desired configuration could be formed from an initially continuous metallic film.

The investigation described herein is a study of one reaction suitable for such a process. This is the photolytic attack of nitromethane upon metallic lead. This reaction occurs when a film of evaporated metallic lead is exposed to suitable partial pressures of nitromethane and is simultaneously irradiated with ultraviolet light. Exposed portions of the lead film are etched away under these conditions, while the remainder of the film is unaffected. The reaction may be pictured as proceeding by the absorption of a quantum of ultraviolet radiation of the correct frequency by nitromethane, which dissociates *via* a complex reaction series to form free radicals, *e.g.*, CH_3 . The latter, if formed near or on the surface of a Pb film, may then react with the Pb, forming, *e.g.*, volatile tetramethyllead. If we assume a mean free path of the order of 0.1 mm. (the pressures used being of the order of 5 mm.), probably a short-lived free radical created in the gas phase will never reach the lead film to react. As

a result, nearly all photoetching will be confined to those areas which are directly irradiated with ultraviolet light. It is recognized, of course, that the dissociation of nitromethane in the adsorbed state will require radiation of a slightly different frequency than dissociation in the gas phase, since forces holding the molecule to the surface will cause changes in the electronic energy levels and therefore in the quanta required for transitions. A pattern could thus be etched in the Pb film whose dimensional resolution is limited mainly by the optics of the ultraviolet source. The effects of surface diffusion and undercutting by the reactive species are estimated to be small in comparison with optical effects.

In the present study an effort has been made to establish the significant variables which affect the reaction and to optimize the rate of photoetching with respect to each of them. The variables considered most worthy of study were wave length, intensity, and pressure.

Experimental Method

The rates of the reaction under all conditions described were followed by means of the resistance change in a strip of lead 11 mm. long, 0.75 mm. wide, and initially up to 4000 \AA. thick, evaporated on a flat glass substrate. These dimensions remained the same throughout each run. Over a suitably small range of thickness, there should be a linear relationship between resistance and thickness, given by a linear calibration

function. The calibration was established by evaporating Pb strip samples, coating with successive evaporated layers of silicon monoxide (SiO) and silver, and measuring the Pb film thickness by interferometry. The function of the SiO here is to provide a uniform coating over both lead and glass, upon which the silver is deposited to give reflective surfaces. Since the thicknesses of SiO and silver are the same over both lead and glass, the displacement of interference fringes is a function of the Pb film thickness only. Resistance measurements for both calibration and experimental runs were made by measuring and recording the voltage across the film, when a constant current of from 0.05 to 100 μ a. (depending on the resistance range) flowed through it. The calibration curve is shown in Fig. 1.

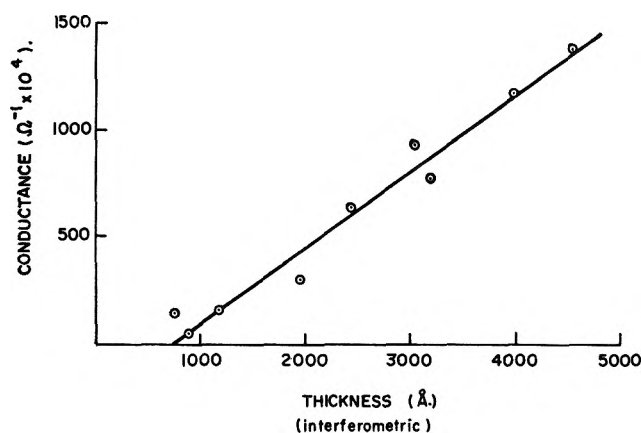


Figure 1. Calibration curve: thickness vs. conductance.

Corrections for thermally caused resistivity changes were judged to be unnecessary here, since even such an unlikely temperature rise as 10° would have caused only a 4% increase in the film resistance. This point was verified by several exposures in which no nitromethane was admitted. Negligible resistance changes were observed in these cases.

The ultraviolet source is a 550-w. quartz mercury arc lamp (Hanovia Model 673 A) mounted in a cylindrical steel housing. The total lamp output is 120 w. between 2000 and 4000 Å. The light emerges from a shuttered port in the shield, passes through a variable aperture, and through any desired filters, and enters the vacuum chamber through a polished quartz window. The glass substrate is held in a stainless steel frame in such a way that painted metallic contacts on each of its ends are isolated from the frame. These contacts are connected through the vacuum wall to a constant current source in parallel with a 10 mv. recording potentiometer. A sliding set of masks is held in

place 0.010 in. from the substrate by two grooves. The substrate holder may be turned 180°, exposing the substrate to either the arc lamp or the metal evaporation source. The latter consists of a tantalum crucible mounted inside a tantalum resistance heater connected to water-cooled electrodes.

In a typical sequence, the lead film was evaporated onto the glass substrate under a pressure of 5×10^{-5} mm. residual gas, using a mask to define the dimensions of the film. Nitromethane was admitted to the desired pressure and the ultraviolet light shutter was opened. The resistance of the film was recorded as a function of irradiation time.

In general, experimental data, expressed as conductance or reciprocal resistance, are plotted against time to obtain a rate curve. Rates are determined as the slope of the best straight line which can be drawn through the points representing the first 20 min. of reaction.

Results

The general form of the curves obtained by plotting film conductance against time of ultraviolet exposure is shown in Fig. 2. It consists of a linear portion from 0 to 70 min., followed by a fairly rapid decrease in slope. The final portions of the curve tend to be non-linear with a slight convexity to the horizontal axis. The slope of the initial linear portion is taken as the rate. The data of this curve may, of course, be converted to thickness measurements by reference to Fig. 1.

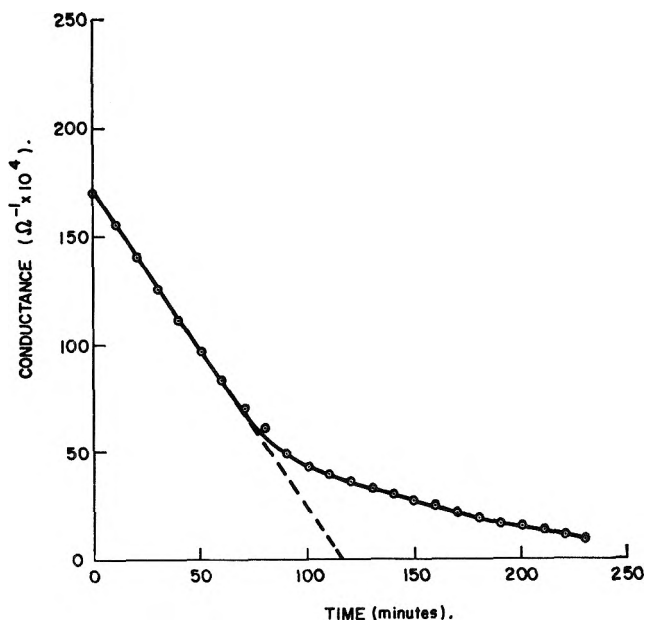


Figure 2. Typical photoetching curve: conductance vs. irradiation time.

Investigation of the effect of nitromethane partial pressure upon the rate of etching produced the curious result shown in Fig. 3. It appears that the rate is a

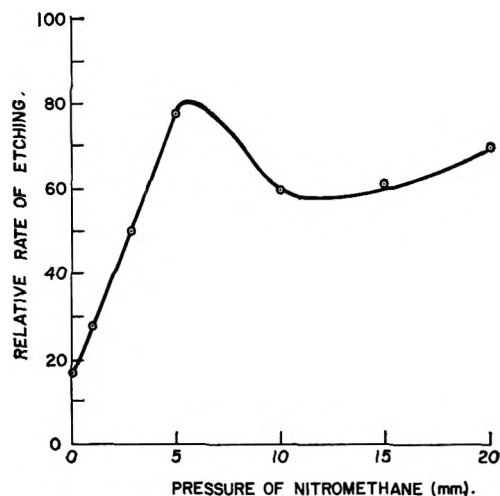


Figure 3. Photoetching rate vs. nitromethane pressure.

reasonably linear function of pressure up to 5 mm. At higher pressures, there is a discontinuity followed by a comparatively small rate increase. One of the most unusual observations made in this investigation involved the effect of the total volume containing the nitromethane on the rate of etching. This effect at the same time suggested the general nature of the reaction mechanism. Figure 4 indicates the effect of system volume upon rate. It should be noted that there was no change in the system geometry in the immediate vicinity of the film. Yet, as the figure indicates, the rate of etching falls off quite rapidly with increasing volume.

The mechanism inferred from this effect is discussed below. One question raised by this mechanism concerns the effect of the addition of an inert gas such as nitrogen upon the rate of the reaction. This aspect was investigated and yielded the results shown in Fig. 5. The rate is drastically reduced by small partial pressures of nitrogen, although subsequent additions have little, if any, effect.

The question of surface reactions, other than those on the lead film itself, seemed of importance. Comparative experiments were therefore run during which the interior surface area of the system was changed. In one experimental series, the walls of that part of the system not in the direct path of the ultraviolet radiation were covered with aluminum foil. The results indicated no change in rate. In another experiment, the well known technique of filling the system with glass

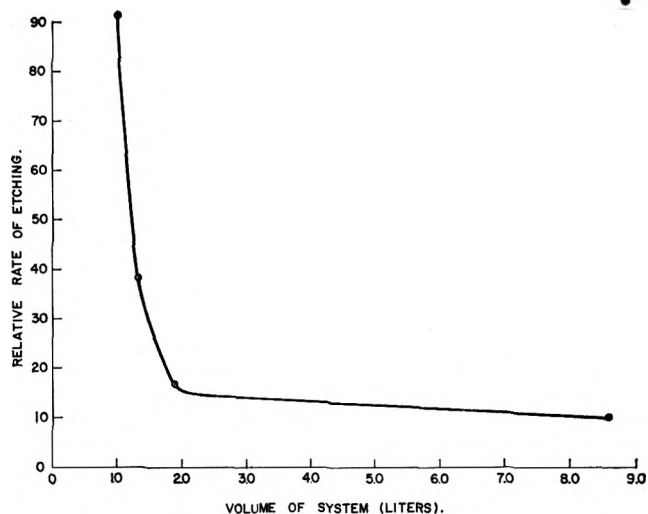


Figure 4. Photoetching rate vs. volume of system.

rods was used to increase the surface area. Once again no significant change in rate was noted. The significance of gas phase reactions was examined by limiting the light beam to a cross section just sufficient to irradiate the area of the lead film. Although the light intensity at the film was unchanged, the volume of irradiated gas was reduced by a factor of five. No significant change in rate was observed, indicating very little contribution of gas phase reactions to the etching process.

The relationship between rate of photoetching and ultraviolet light intensity was studied. Intensity was controlled by insertion of previously calibrated apertures into a specially provided slot in the lamp housing. The amount of radiation reaching the lead film was thus controlled by simple physical blocking with no change in the electrical characteristics of the arc and its spectral distribution. The observed relationship is shown in Fig. 6. It may be noted that a nearly linear plot, with intercepts at the origin, is obtained by plotting the square root of the intensity against the etching rate. The significance of this will be discussed below.

The approach used in determination of the spectral sensitivity of the reaction involved the use of single cut-off filters, mainly Corning flat glass filters. The output of the mercury arc used consists mainly of discrete lines with relatively little background continuum. These lines fall into nine groups in the ultraviolet region, each group having a range of less than 100 Å. During reaction, we may then think of the system as being irradiated with nine wave length bands, each of an intensity determined by the particular filter being used, and each contributing toward the observed reaction rate. For each filter, an equation may be written

$$C_1\sqrt{I_{1a}} + C_2\sqrt{I_{2a}} + \dots + C_n\sqrt{I_{na}} = R_a \quad (1)$$

where I_{na} is the intensity of wave length n when using filter (a), C_n is the rate due to wave length n alone and at unit intensity, and R_a is the total observed rate, using filter (a). Since it has been shown above that the rate of this reaction is proportional to the square root of the intensity, the latter function is used in the equation. For the nine wave length bands described above, there will be nine values of C_n and nine independent equations are necessary to solve for them. This, in turn, necessitates the measurement of rate with nine different filters.

The compositions of the filter elements used are shown in Table I, while the relative intensities of the various bands in the lamp output are listed in Table II.

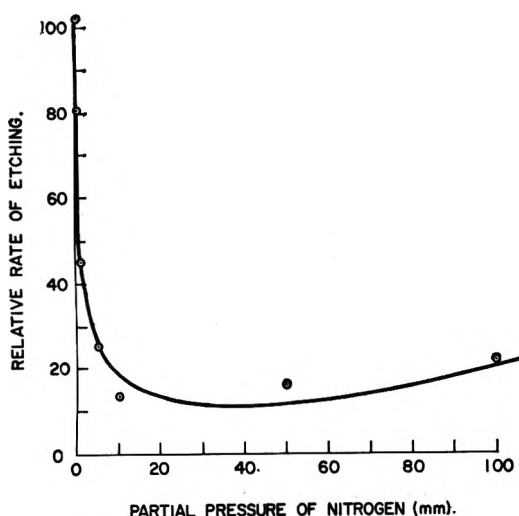


Figure 5. Photoetching rate vs. partial pressure of nitrogen.

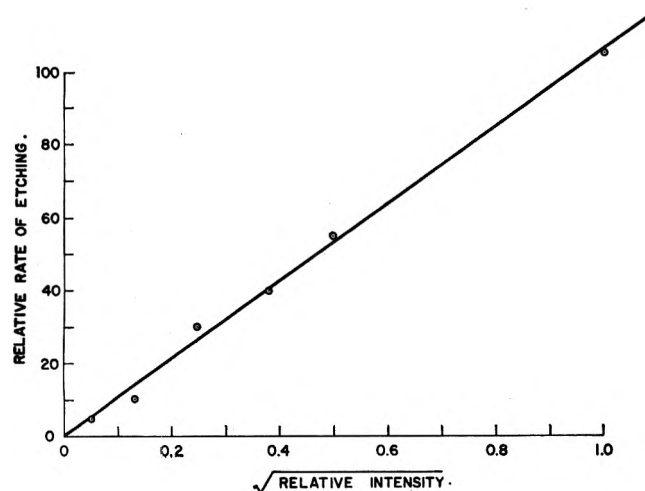


Figure 6. Photoetching rate vs. square root of intensity.

Table I: Ultraviolet Filters

Filter	Composition
1	CuSO ₄ ·5H ₂ O, 100 g./l. H ₂ O; 5-cm. path
2	CoSO ₄ ·7H ₂ O, 45 g./l. H ₂ O; 5-cm. path
3	Corning filter CS 9-54
4	Corning filter CS 0-52
5	Corning filter CS 7-54
6	No filter
7	KHC ₂ H ₄ O ₄ , 5 g./l. H ₂ O; 1-cm. path
8	CCl ₄ , pure liquid, 5-cm. path
9	Corning filter CS 7-51

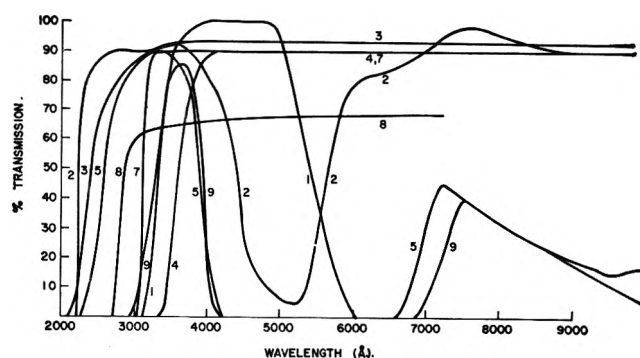


Figure 7. Transmission of filters vs. wave length.

The transmission curves for the various filters used are shown in Fig. 7.

A relation of the type shown in eq. 1 was set up for each filter, using intensities supplied by the manufacturer¹ and experimental rate data. The resultant system of nine linear equations in nine unknowns was solved for the values of the rate coefficients C_1 to C_9 .

The experimentally determined rates obtained using the various filters are shown in Table III. A wide range of activity is evident in the various filters, ranging from little or no etching in some cases to the highest rate, using the unfiltered lamp.

Table IV shows the values calculated for C_1 - C_9 , the unit intensity rates due to each wave length band. It is to be noted that both positive and negative rate coefficients are found, providing definite evidence of strong inhibition by certain wave lengths. The rate coefficients are plotted as a function of wave length in Fig. 8. In order to demonstrate the effect of a rate-intensity relation other than the square root function observed experimentally, this figure also contains a curve calculated using a linear model.

$$C_1I_{1a} + C_2I_{2a} + \dots + C_nI_{na} = R_a \quad (2)$$

(1) Hanovia Lamp Bulletin EH-223.

Table II: Ultraviolet Lamp Output

Band average, wave length, Å.	Band intensity after transmission through each filter, ergs/cm. ² sec.								
	1	2	3	4	5	6	7	8	9
2224	0	20,900	4,640	0	0	32,500	0	0	0
2365	0	57,300	36,400	0	6,190	69,600	0	0	0
2530	0	63,400	50,300	0	0	27,800	72,700	0	0
2676	0	40,200	34,800	0	29,100	44,900	0	0	0
2778	0	24,800	22,400	0	21,600	27,800	0	7,740	0
2931	0	46,400	44,900	0	44,900	52,600	0	30,200	774
3078	2,320	159,000	157,000	0	158,000	179,000	84,400	111,000	27,100
3341	13,200	20,100	20,100	774	19,300	21,600	19,300	13,900	14,700
3660	222,000	212,000	217,000	147,000	191,000	233,000	210,000	152,000	194,000

Table III: Rates of Etching for Various Filters Used

Filter no.	Rate of etching, Å./sec.
1	0.0235
2	.171
3	.190
4	.0329
5	.120
6	.256
7	.0376
8	.0517
9	.0164

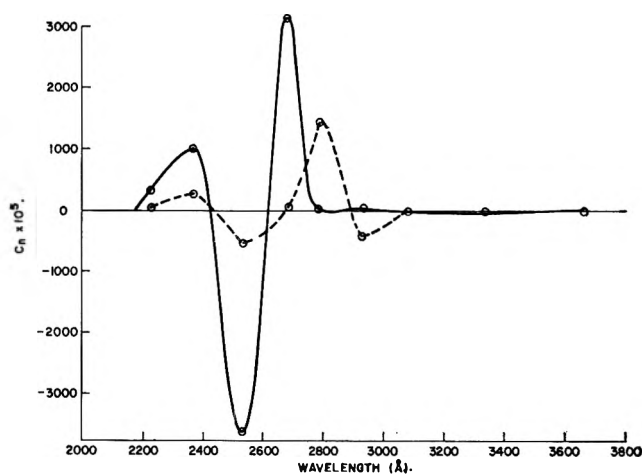
Table IV: Calculated Values of Rate Coefficients (C_n)

Wave length band, Å.	$C_n \times 10^5$, Å.-cm./erg ^{1/2} sec. ^{1/2}	$\sqrt{\text{Intensity}}$ for unfiltered lamp	Unfiltered lamp $C_n \sqrt{I}$, Å./sec.	
C_1	2224	+354	180	+0.63
C_2	2365	+1016	264	+2.65
C_3	2530	-3620	270	-9.80
C_4	2676	+3180	212	+6.72
C_5	2778	+16	167	+0.02
C_6	2931	+27	229	+0.05
C_7	3078	-8	423	-0.03
C_8	3341	-13	147	-0.01
C_9	3660	+11	483	+0.05

Although some shift in wave length and intensity distribution is evident, the basic shape of the curve is certainly preserved, even with this rather drastic change in model.

Discussion

The results obtained give some insight into a possible mechanism for this process. The two most significant observations in this connection are the "break" in the linear etching curve, shown in Fig. 2, and the volume effect, shown in Fig. 4. Any mechanism considered should predict these effects. Two possible explanations

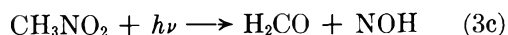
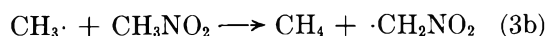
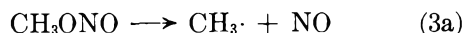
**Figure 8.** Photoetching rate vs. wave length.

for the first effect can be advanced. First, a parallel reaction may be producing a nonvolatile product on the lead film surface, thus making it unavailable for the main reaction. However, it would be difficult to conceive of such a reaction under the experimental conditions indicated. A second, and possibly more realistic explanation, concerns itself with the grain structure of the lead deposit. The latter may, from a simplified point of view, be thought of as a collection of columns, each rising from the underlying substrate, and each the result of an original nucleation site. One might expect each of these columns to grow with a different crystal-line orientation to the plane of the substrate. These diversely oriented grains might well be expected to exhibit different degrees of reactivity when attacked by the etching agent. The rate of etching therefore would not be constant over the entire surface but would vary with the grain orientation. Thus, the conductance of the sample would fall rapidly and linearly at first, while all regions are being etched. When the most active regions are completely gone, a decrease in rate would occur since only sites of lesser activity are left.

This decrease would continue as the individual grains were depleted in the order of their respective activities. Thus, the slowly changing final portions of the curve are to be expected from this picture.

The existence of an effect of total system volume upon a reaction localized on a small surface can only be explained by the inclusion in the reaction mechanism of a step involving an equilibrium gas phase concentration of some activated species. However, the removal of lead exclusively from irradiated areas indicates that a further photochemical reaction occurs on the surface before removal. Since the results quoted above show no effect of surface increase, the volume effect occurs because of a gas phase process rather than because of a wall reaction. Also, since no effect was found by decreasing the irradiated volume of gas, it would appear that the source of this activated species is the irradiated surface of the substrate.

As to the exact nature of the activated species, little more than conjecture is possible with the information available at this point. Current literature seems entirely in agreement that a free methyl radical is produced during the primary photolytic reaction.²⁻⁴ However, the existence of a volume effect implies a rather long lifetime for the activated species, which would be rather unlikely for a methyl radical in this environment.⁵ There is strong evidence^{3,4} to indicate that CH_3ONO is formed in a succeeding reaction step. Further possibilities suggested in the literature are^{2,3,6}



It would seem probable that one of the radicals indicated would be the activated species here.

One interesting result of this work has been the finding that, in addition to the active wave length band at 2680 Å., there exists a band at approximately 2530 Å. which has a definite inhibitive effect upon the etching reaction. The advantage of the method used is that it enables us to view separately the effect of each wave length band and thus obtain a reasonable estimate of the magnitude of the inhibitive effect. In this case, it is seen that in the unfiltered lamp, the effect of the 2530-Å. band is about 114% of that of the 2680-Å. band. Assuming no interaction between the bands, the inhibition reaction would seem to have an effect which is almost four times the actual net rate, calculated by algebraic addition of the $C_1\sqrt{I}$ terms in Table III.

The results obtained may be used to calculate effective quantum yields for the various over-all reactions. It must be first noted, however, that an effective or over-

all quantum yield for a reaction having a nonlinear intensity dependence will always be a function of the intensity.

The quantum yield was calculated for the bands exhibiting the largest negative and the largest positive effects. The irradiated area of the metal film was experimentally measured. The rate of incidence of quanta upon the film was then calculated by

$$\text{quanta/sec.} = \frac{AI_\lambda\lambda}{hc} \quad (4)$$

where I_λ is the intensity of wave length λ in ergs/sec., h is Planck's constant, c is the speed of light, and A is the irradiated area.

The number of metal atoms reacted per second was calculated by

$$\text{atoms/sec.} = \frac{C_\lambda\sqrt{I_\lambda}A\rho \times 6.023 \times 10^{23}}{W} \quad (5)$$

where C_λ and I_λ are, respectively, the rate coefficient and intensity at wave length λ , A is the irradiated area of the metal film, and ρ and W are, respectively, the density and atomic weight of lead.

The quantum yield was then calculated as

$$Q = \frac{\text{quanta/sec.}}{\text{atoms/sec.}} \quad (6)$$

Results for the wave length ranges of 2680 and 2530 Å., respectively, were $76.7/\sqrt{I}$ and $93.7/\sqrt{I}$. For the case of the unfiltered lamp used here, the intensities for the two bands were 4.5×10^4 and 7.3×10^4 ergs/sec. Accordingly, the quantum yields for the two wave lengths at these intensities are 0.362 and 0.347.

Interpretation of these results in terms of the chemical mechanism is fairly obvious. The absorption spectrum of nitromethane exhibits a maximum centering around 2754 Å. Taking into account any shift caused by being in the adsorbed state, we may surmise that the 2680-Å. wave length band corresponds to the initial activation of the nitromethane molecule, and possibly to its dissociation into free methyl radical. Through a series of further steps, a volatile Pb compound must be formed which may then vaporize. Any wave length

- (2) A. J. C. Nicholson, *Nature*, **190**, 143 (1961).
- (3) G. C. Pimentel and G. Rollefson, unpublished work quoted in "Formation and Trapping of Free Radicals," ed. by A. M. Bass and H. P. Broida, Academic Press, New York, N. Y., 1960, Chapter 4, p. 97.
- (4) R. E. Rebert and N. Slagg, *Bull. soc. chim. Belges*, **71**, 709 (1962).
- (5) E. Steacie, "Atomic and Free Radical Reactions," Reinhold Publishing Corp., New York, N. Y., 1946, p. 41.
- (6) H. W. Brown and G. C. Pimentel, *J. Chem. Phys.*, **29**, 883 (1958).

which would tend to decompose this latter organometallic compound would be observed to have a negative effect upon the over-all reaction. The fact that the 2530-Å. band has such an effect is considered strong evidence for the identity of the final product as tetramethyllead, $\text{Pb}(\text{CH}_3)_4$, since the latter, at pressures of about 5 mm., exhibits an absorption continuum below about 2550 Å.⁷

It is of interest here to consider the question of the square root relationship between rate and intensity for this reaction. This has been shown to be the case experimentally for the over-all reaction using an unfiltered lamp. One possible model for a photochemical reaction displaying such kinetics is a chain reaction in which the termination step is second order.⁸ For the etching reaction sequence itself, such a termination may be visualized in terms of some carrier such as free methyl radical (CH_3) or some Pb-containing radical, such as the mono-, di-, or trimethyl derivatives. However, the values calculated above for the quantum yields are sufficiently below unity to make the existence of a chain reaction seem doubtful. Alternatively, the observed square root dependence upon intensity might

be attributed to a nonchain reaction, consisting of a radical forming step followed by a rate determining step requiring simultaneous reaction of two activated species with a lead atom to form a product molecule. In the case of the decomposition of lead tetramethyl, we are again faced with a fractional quantum yield as evidence against a chain reaction. Although such a mechanism has been previously suggested,⁹ the authors propose that only very short chains are involved, as indicated by their value for the quantum yield, which is only slightly above unity. Thus, no radical disagreement exists with the results presented here.

In view of the uncertain nature of the inhibitive reaction, it is perhaps unreasonable to assume a square root rate-intensity relation for this reaction. However, the comparatively small change, resulting in Fig. 2 when a linear relation was assumed over the entire wave length range, makes it doubtful that this point is significant.

-
- (7) P. A. Leighton and R. A. Mortensen, *J. Am. Chem. Soc.*, **58**, 448 (1936).
 - (8) P. J. Flory, "Principles of Polymer Chemistry," Cornell University Press, Ithaca, N. Y., 1953, p. 113.
 - (9) I. Haschlaff and R. G. W. Norrish, *J. Chem. Soc.*, 1580 (1936)

Chemisorption of Amines and Its Effect on Subsequent Oxidation of Iron Surfaces

by Yung-Fang Yu Yao

Scientific Laboratory, Ford Motor Company, Dearborn, Michigan (Received August 6, 1963)

The adsorption of amines and the oxidation of clean and amine prechemisorbed reduced iron surfaces were measured using continuous flowing gas mass spectrometry. The amines used include *n*-butylamine, *n*-hexylamine, *t*-butylamine, cyclohexylamine, pyrrolidine, piperidine, and pyridine. It is shown that although the amines are good inhibitors for corrosion in water solution, they are relatively poor inhibitors for oxidation of iron in a dry atmosphere. The total oxygen uptake by iron surfaces covered with the chemisorbed amines decreases from 95% of that for the amine-free surface to 62% of that for the amine-free surface as the ionization potential of the amines decreases. A tentative explanation of this effect based on the change of contact potential due to chemisorption and the Cabrera and Mott theory of thin oxide film growth is offered. The mass spectra of the gas stream leaving the sample during adsorption and desorption were examined. Deuterium exchange experiments were also conducted. The results show that the chemisorption of amine on the reduced and oxidized iron surface is essentially nondissociative. An amount corresponding to monolayer coverage was chemisorbed on the surfaces for all the amines studied except *t*-butylamine, for which the chemisorption was weaker and the amount adsorbed less. Oxidation of an iron surface covered with chemisorbed amine does not desorb the chemisorbed amines. The amine does not react with the oxygen but is left chemisorbed on the iron oxide surface.

Introduction

The passivity and corrosion resistance of many metals is often attributed to the formation of a thin protective oxide film on the surface. Organic amines function as corrosion inhibitors presumably through chemisorption and the formation of a hydrophobic surface film. However, little is known about the effect of the chemisorbed amines on the oxide film formation. In this investigation such effects are studied by measuring the oxidation of clean and amine prechemisorbed reduced iron surfaces under anhydrous conditions with a view to seeing if any correlation exists between the nature of the amine molecules and their inhibition, if any, of the oxidation of iron.

Adsorption and oxidation from a flowing gas stream followed by continuous mass spectrometry analysis of the gas stream leaving the sample was chosen for this study for the following reasons: (1) Any surface reaction or displacement adsorption which gives off desorb-

able product can be readily detected as it happens. (2) Deuterium exchange experiments can be carried out *in situ*. (3) More than one adsorbate can be studied simultaneously or in sequence on the same sample. (4) The sensitivity is usually higher than that of the conventional volumetric method, particularly in systems with small surface area substrates and low vapor pressure adsorbates.

Experimental

The carbonyl iron powders used have been described previously.¹ The standard reduction condition for all the samples reported here was 500° and 8.5 hr. Hydrogen left on the surface after reduction was removed by sweeping with helium at 500°.

Reagent grade amines were used without further purification. To ensure constant adsorbate concentration in the carrier gas, the liquid amines were held in the

(1) Y. F. Yu Yao, *J. Phys. Chem.*, **67**, 2055 (1963).

pores of a predried SiC catalyst support (Carborundum Co.) in a U-tube. The latter was maintained at a chosen constant temperature at which the vapor pressure of the amine was 0.03 to 0.07 of that at the adsorption temperature, 25° for all the studies reported here. Oxygen was introduced to the system in a premixed O₂-He mixture containing 0.6% of O₂ by volume. Deuterium gas of 99.5% purity was the product of General Dynamics Corp. Helium was used as carrier gas except in the deuterium exchange and hydrogen evolution experiments where argon was used instead.

Teflon-plug stopcocks and Hoke valves were used to avoid any contamination by stopcock grease. The entire system was operated at a pressure slightly above 1 atm. to minimize the leakage of air. A CEC 21-610 type mass spectrometer was used for all the amine and oxygen adsorption measurements. This instrument gives a continuous recording on a strip chart of the peak height of any mass number. Argon adsorption isotherms used to calculate the surface areas were determined using a conventional B.E.T. adsorption apparatus. The flow rate of the gas mixtures was controlled by a needle valve and monitored by a Fisher-Porter variable-area flowmeter. The flow rate was maintained constant to $\pm 2\%$ throughout a run.

The gas mixture was first passed through the system that by-passed the sample bulb until a constant peak height at a characteristic m/e of the amine was attained. This constant peak height was taken as the calibration factor of the particular run. Then the gas mixture was allowed to pass over the hydrogen-free sample and the amount of total adsorption was measured as the time-integrated reduction in peak height as obtained from the recorder chart paper (see Fig. 1). At the end of the run, the peak height of the inlet gas mixture again was measured. The variation in peak height

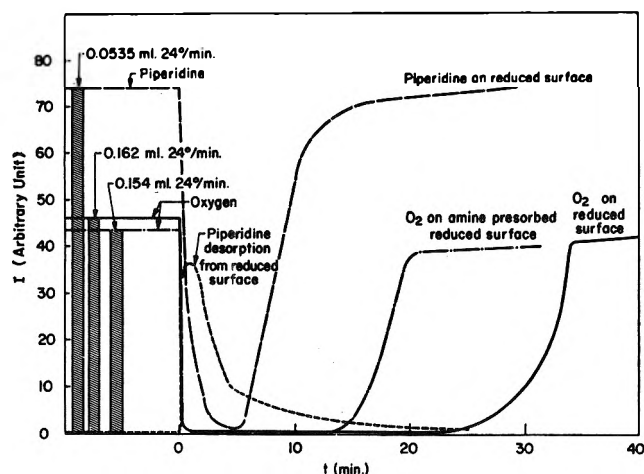


Figure 1.

before and after an adsorption run was seldom over 2%. To measure the desorption at 25°, helium was first passed through the by-pass system to remove the adsorbate left in the mass spectrometer and the connecting tubes. Then the adsorbate inside the sample system was swept out and again measured as the time-integrated peak height obtained from the recorder chart. To correct for the amount of adsorbate taken up or given off by the dead space of the sample bulb, both the adsorption and desorption measurements were also made on a blank sample bulb filled with glass beads under conditions identical with that of an actual sample.

The greatest source of error was probably in the estimation of the vapor pressure of the amines from the bath temperature measured with a thermometer. The vapor pressure data were either taken from the literature or measured by a mercury manometer and a cathetometer at several temperatures. Another factor which could be of importance for some of the amines was the slight uptake and slow desorption of some of the amines by the mass spectrometer and connecting tubes. The overall experimental error for the amine adsorption thus could be as high as 5-10%. In the case of oxidation, there was no adsorption by the system and the same O₂-He mixture was used for all the samples. The experimental error is expected to be insignificant since relative comparisons of the ease of oxidation of different samples rather than their absolute values are of interest in this study.

Results and Discussion

The Chemisorption of Amines by Reduced Iron Surfaces. In the previous study¹ it has been found from the heat of adsorption measurements that *n*-alkylamines are strongly chemisorbed on reduced and oxidized iron surfaces with the chemisorbed bond at the amino group and with the hydrocarbon chain physically adsorbed and randomly oriented. The heat of chemisorption attributable to the amino group is of the same order of magnitude as that of Fe-N covalent bond formation. Emmett and Brunauer² reported that nitrogen is dissociatively chemisorbed on iron catalyst to give a heat of adsorption of about 35 kcal./mole and inhibits the "type A" chemisorption of hydrogen. On the other hand, it is well known that ammonia is dissociatively chemisorbed on iron at near room temperature.³ Kemball and Wolf reported that hydrogen on both carbon and nitrogen of CH₃NH₂ undergo exchange with deuterium over several metal films including iron at

(2) P. H. Emmett and S. Brunauer, *J. Am. Chem. Soc.*, **56**, 35 (1934); **62**, 1732 (1940).

(3) See, for example, P. M. Gundry, J. Haber, and F. C. Tompkins, *J. Catalysis*, **1**, 363 (1962).

room temperature.⁴ Saturated hydrocarbons were found to dissociate on several clean reduced metal surfaces but not on iron.⁵ Therefore, a close examination of the mass spectra of the gas stream leaving the surface during adsorption and desorption of the amines would be desirable in further study of the nature of the chemisorption.

With the mass spectrometer continuously scanning through the mass numbers of 12 to 80 and 1 to 4 in parallel runs, it was found that all the amine peaks in the spectra diminish in the same proportion due to adsorption, and reappear with the same relative heights as that of original free amine upon desorption. No new peak was observed during the adsorption or desorption processes. Only a slight amount of H₂ was found during the amine adsorption at 25°, about 0.004 mole of H₂ per mole of amine adsorbed. After *n*-butylamine adsorption and desorption measurements at 25°, the sample was heated up to 150–170° in a flowing argon stream and some slow hydrogen evolution was observed. The total number of moles of hydrogen evolved in 30 min. at 150° was about 20% of the total number of moles of amine chemisorbed. The peak height at *m/e* of 30 and 41–43 also increased slightly (He used as carrier gas). This suggests that some dissociative desorption takes place upon heating.

To study the chemisorbed state of the amine molecules further, deuterium was admitted and allowed to remain for 12 to 30 min. in contact with a sample that had been prepared by the adsorption of *n*-hexylamine and 1-min. sweeping by helium. The exit gas after this deuterium treatment contained no more HD or that of *m/e* 31 and 32 (deuterated –CH₂NH₂ groups) than that obtained in a blank run. A small amount of exchange was observed when the sample was completely bypassed. This is probably due to exchange taking place at the filament or some parts of the mass spectrometer. Subsequent desorption at 150° did not change the relative peak height at 30, 31, and 32 although a slight increase in absolute heights of these peaks and that of HD was observed. Since exchange of chemisorbed dissociated hydrogen atom is known to be rapid,⁶ the inactivity toward the exchange reaction and the absence of any new peak in the spectra during adsorption or desorption suggest that the chemisorption of amine at 25° is essentially nondissociative.

By setting the mass spectrometer at a characteristic mass number of the adsorbate, the adsorption and desorption can be followed from the change of the peak height at constant flow rate and vapor concentration in the inlet gas. Typical recorded curves are shown in Fig. 1. The areas under the curves can be related to the amount adsorbed on or desorbed from the sample

system. The amount of amine chemisorbed on reduced iron surfaces at 25° was calculated using the following formula and the results are listed in Table I.

$$V_{\text{chemisorbed}} = (V_{\text{total ads}} - V_{\text{blank ads}}) - (V_{\text{total desorb}} - V_{\text{blank desorb}})$$

The surface area of the reduced samples measured by argon adsorption and using the B.E.T. equation was found to be 0.30 m.²/g. Little difference was found among samples prepared under identical conditions. With this information and the amount chemisorbed, the

Table I: Adsorption of Amines on Reduced Iron at 25°

Adsorbate	Relative pressure of adsorption	V _{ads.} ml. STP/g.	V _{des.} ml. STP/g.	V _{chemisorbed.} ml. STP/g.	C.s.a. (exptl.), Å. ²	C.s.a. (calcd. from model), Å. ²
<i>n</i> -Butylamine	0.02	0.058	~0	0.058	20	25 ^a
<i>n</i> -Hexylamine	0.06	0.059	0.009	0.050	23	34 ^a
<i>t</i> -Butylamine	0.05	0.027	0.005	0.022	51	30 ^b
Cyclohexylamine	0.04	0.028	~0	0.028	41	52 ^c
Pyrrolidine	0.07	0.035	0.007	0.028	41	36 ^d
Piperidine	0.15	0.039	0.002	0.037	31	38 ^e
Pyridine	0.05	0.041	0.005	0.036	31	38 ^d

^a Liquid density model, N closest to the surface. ^b Amino group closest to the surface. ^c Chair form, N closest to the surface. ^d Ring parallel to the surface. ^e Boat form, N closest to the surface.

apparent cross-sectional areas of the chemisorbed molecules are calculated and listed in Table I. The slightly higher monolayer capacities (~20%) of the *n*-butyl- and *n*-hexylamine obtained in this study than those obtained previously by volumetric measurements may be attributed to less efficiency in removal of weakly adsorbed amine by helium sweeping than by evacuation (to final pressure of $<1 \times 10^{-5}$ mm. and with liquid nitrogen traps). The same is probably true for all the other amines. Thus the actual amounts of chemisorption could be somewhat less than those listed. From the heat of adsorption, it was shown that the *n*-alkylamines are chemisorbed at the amino group with their

(4) C. Kemball and F. J. Wolf, *Trans. Faraday Soc.*, 51, 1111 (1955).

(5) J. R. Anderson and C. Kemball, *Proc. Roy. Soc. (London)*, A 223, 361 (1954).

(6) G. C. Bond, "Catalysis by Metals," Academic Press, New York, N. Y., 1962, p. 164.

hydrocarbon chains physically adsorbed and randomly oriented on the surface. With this information and the assumptions listed in the footnotes of Table I, Fisher-Hirschfelder models representing the most probable orientation of the chemisorbed molecules were constructed and the projected cross-sectional areas were estimated and are shown in the last column of Table I. Such estimations are undoubtedly crude and can only be considered qualitative. Nevertheless, it shows that the surface is completely covered with chemisorbed amine after adsorption and desorption at 25° with the exception of *t*-butylamine. In this case, the bulky hydrocarbon tails prevent close packing and also weaken the N-Fe bond.

The Oxidation of Freshly Reduced Iron Surfaces. A typical curve recording the change of peak height of *m/e* 32 during oxidation at 25° is included in Fig. 1. Although true quantitative kinetic data cannot be derived from the present results due to the constant flow rate conditions employed, the general feature of a fast oxygen uptake followed by a slow process is the same as that obtained by other methods.⁷ Since the slow oxygen uptake continues indefinitely, an arbitrary cut-off point at a rate of 0.001 ml./min. (~2 layers/day) was chosen as a basis for comparison among all the oxidation experiments reported here. The average amount of oxygen uptake up to this point on 12 freshly reduced surfaces was found to be 0.62 ± 0.03 ml./g. This is about 15% less than that measured volumetrically at low pressure; in that case some localized heating due to poor thermal conduction possibly enhances the oxidation.

The Chemisorption of Amines on Oxidized Iron Surfaces. The iron surfaces, after being used for oxidation studies at 25° as described in the previous section, were used for this study. The amount of amine chemisorbed at 25° on the oxidized surfaces and the apparent cross-sectional areas are calculated in the same manner as that for the reduced surfaces and are listed in Table II. The monolayer capacities are nearly the same as those obtained on the reduced surfaces. Based on the spectra obtained during adsorption and desorption and the deuterium exchange experiments, it again shows that there is no extensive dissociation at 25°. This is consistent with the findings from the heat of adsorption studies that amines are chemisorbed in the same manner on both the reduced and oxidized iron surfaces.

The Oxidation of Reduced Iron Surfaces with Prechemisorbed Amine. As is shown in Fig. 1, the general characteristics of the oxidation of a reduced iron surface covered with chemisorbed amine monolayer are the same as those of a freshly reduced surface but both the fast and slow oxygen uptake are somewhat reduced

Table II: Adsorption of Amines on Oxidized Iron at 25°

Adsorbate	Relative pressure of adsorption	V_{ads} , ml. STP/g.	V_{des} , ml. STP/g.	$V_{chemisorbed}$, ml. STP/g.	C.s.a. (exptl.), Å. ²	C.s.a. (calcd. from model), Å. ²
<i>n</i> -Butylamine	0.02	0.054	~0	0.054	21	25 ^a
<i>n</i> -Hexylamine	0.06	0.046	0.004	0.042	28	34 ^a
<i>t</i> -Butylamine	0.05	0.027	0.006	0.021	54	30 ^b
Cyclohexylamine	0.04	0.025	~0	0.025	45	52 ^c
Pyrrolidine	0.07	0.039	0.004	0.035	33	36 ^d
Piperidine	0.15	0.040	0.005	0.035	32	38 ^e
Pyridine	0.05	0.038	~0	0.038	30	38 ^d

^{a-e} See footnotes in Table I.

Table III: Oxidation of Amine Prechemisorbed Reduced Iron at 25°

Adsorbate	% inhibition ^a	Ionization potential of amine, I_B , e.v.
Piperidine	38	7.85 ^b
Pyrrolidine	36	7.98 ^b
Cyclohexylamine	28	8.32 ^b
<i>n</i> -Hexylamine	23	(9.0) ^c
<i>n</i> -Butylamine	17	9.18 ^b
Pyridine	7	9.76 ^d
<i>t</i> -Butylamine	5	(9.2) ^c

^a % inhibition = $[(V_{O_2}(\text{clean surface}) - V_{O_2}(\text{amine prechemisorbed surface})) / V_{O_2}(\text{clean surface})] \times 100$. ^b See ref. 13. ^c Estimated from I_B s of alkylamine homologs. ^d K. Higasi, I. Omura, and H. Baba, *J. Chem. Phys.*, **24**, 623 (1956).

due to the presence of amine on the surface. The percentages of reduction in total oxygen uptake up to the same cut-off point as defined above are listed in Table III. It is shown that although the amines are good inhibitors for corrosion in water solution, they are relatively poor inhibitors for oxidation of iron in a dry atmosphere.

During the oxidation there was no change of the characteristic amine peak height, nor was any additional amine adsorption observed during or after the oxidation. Since the amine chemisorbed on the reduced surface prior to oxidation corresponds to approximately monolayer coverage and no amine was added or removed from the surface, the same monolayer should also be present on the oxidized surface. Therefore, the possibility of separate sites for oxygen and amine on the surface is ruled out. The oxygen could either diffuse through the

(7) M. W. Roberts, *Trans. Faraday Soc.*, **57**, 99 (1961).

chemisorbed amine layer to react with the underlying metal or it could temporarily displace the amine off the surface. In the latter case, since the amine molecules are also strongly attracted to the oxidized iron surface, they would re-adsorb on the surface immediately without actually being removed. In either case, the final state of the surface is probably one with the oxide film directly on the metal and the amine chemisorbed on the surface of the oxide. As shown in Table III, the percentage of lowering of total oxidation caused by the amine prechemisorbed on the iron surface increases as the ionization potential of the amine decreases. Although this correlation is by no means quantitative and more information along the same line is needed, one can treat this problem qualitatively using the conventional theory of metal oxidation as follows. The theory of very thin oxide film growth proposed by Cabrera and Mott⁸ has been found to be valid for oxidation of Ni, Co, and Cu powders and Cu single crystals at room temperature and below^{9,10} and for evaporated iron films at -195 to 200° .⁷ Therefore, it is not unreasonable to assume that the oxidation of the iron powders also follows the same kinetics. The original theory and its several modifications can best be referred to in the original papers.¹¹ In essence, when the oxidation temperature is low and the oxide film present on the surface is less than $20\text{--}50$ Å. thick, the oxidation rate is controlled by the diffusion of cations into the oxide under the influence of the electrostatic field which results from the contact potential difference existing between the metal-oxide and oxide-oxygen interfaces. Therefore with everything else the same, the greater the contact potential, the faster the oxide film will grow. Chemisorbed amines on the surface could affect the contact potential in two ways. (1) The amine-oxidized metal bond is presumably a coordination covalent bond, that is, electrons are transferred from the amino nitrogen to the cations at the surface. The chemisorbed amines would thus acquire a dipole moment with the positive end away from the iron oxide surface and thus lower the over-all contact potential difference between the metal and the outermost surface (*i.e.*, the positive N atom would repel cations approaching the outer-

most surface). A positive surface dipole has been found in the contact potential measurements by Bewig and Zisman for *n*-alkylamines on oxide-covered platinum.¹² (2) The chemisorbed amine occupies a cation site on the surface that otherwise would be occupied by an oxygen anion. This, too, would result in a decrease in the contact potential difference across the film.

It has been suggested that the ionization potentials of the amines can be used as a measure of their "absolute" Lewis base strength—the tendency of a molecule to donate electrons without the complication of steric effects.¹³ One can then expect that on the same surface those amines with the lower ionization potential would form a stronger coordination bond and have a higher dipole moment than those with higher ionization potential. Therefore, the apparent correlation between ionization potential and the oxidation inhibition as shown in Table III is consistent with the above explanation. The unusually low adsorption and low inhibition efficiency of *t*-butylamine is probably due to a steric effect; the bulky hydrocarbon prevents the N atom from approaching as close to the surface cation as the N atom of the other less hindered amines. The same steric effect was also shown in the heat of adsorption of secondary and tertiary amines reported previously.¹

Acknowledgment. The author is grateful to Dr. J. T. Kummer for suggesting the mass spectrometric method and many valuable discussions throughout the course of this work.

(8) N. Cabrera and N. F. Mott, *Rept. Progr. Phys.*, **12**, 163 (1949).

(9) T. N. Rhodin, Jr., *J. Am. Chem. Soc.*, **72**, 5102 (1950).

(10) J. J. Chessick, Y. F. Yu, and A. C. Zettlemeyer, *Proc. 2nd Intern. Congr. Surface Activity*, **II**, 269 (1957).

(11) See, for example, N. Cabrera, "Semiconductor Surface Physics," R. H. Kingston, Ed., Univ. of Pennsylvania Press, 1957, p. 331; T. B. Grimley, "Chemistry of the Solid State," W. E. Garner, Ed., Academic Press, New York, N. Y., 1955, Chapter 14.

(12) K. W. Bewig and W. A. Zisman, *J. Phys. Chem.*, **67**, 130 (1963).

(13) W. S. Koski and J. J. Kaufman, *J. Am. Chem. Soc.*, **82**, 3263 (1960); J. J. Kaufman, *ibid.*, **84**, 4393 (1962).

The Relative Free Energies of Sodium, Potassium, Rubidium, Cesium, and Strontium Ions in Methanol and Methanol–Water Mixtures¹

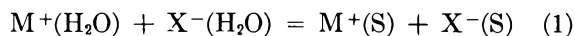
by Kenneth Schug and Ahmad Dadgar²

Department of Chemistry, Illinois Institute of Technology, Chicago 16, Illinois (Received August 7, 1963)

The equilibrium $\text{Na(Hg)} + 1/n\text{M}^{n+}(\text{S}) = \text{Na}^+(\text{S}) + 1/n\text{M(Hg)}$ has been measured for $\text{M} = \text{K, Rb, Cs, and Sr}$, and $\text{S} = 0.30, 0.80, \text{ and } 1.00$ mole fraction methanol (and for Sr also at 0.90 and 0.95 mole fraction methanol) in water–methanol mixtures. These results have been combined with those from similar measurements using water as solvent to yield the standard free energy values for the reaction $\text{Na}^+(\text{H}_2\text{O}) + 1/n\text{M}^{n+}(\text{S}) = \text{Na}^+(\text{S}) + 1/n\text{M}^{n+}(\text{H}_2\text{O})$. The results, when compared with the predictions of the simple Born equation, lead to the conclusion that specific cation solvation effects are of primary importance in determining the relative free energies of the alkali metal ions in these systems. It is also shown that calculations based on a simple ion–dipole model lead to values in reasonable agreement with experiment.

Introduction

The thermodynamic properties of the alkali metal ions in methanol (and aqueous methanol) have been the subject of several investigations.^{3–6} In the cases cited, the free energy change accompanying the transfer of a given pair of ions ($\text{M}^+ + \text{X}^-$) from water to the methanolic solvent S (reaction 1) was obtained from electromotive force or solubility measurements.



Two such transfer processes (with different M^+ but the same X^-) may be combined to give the cation environmental interchange process represented by the following equation (Na^+ has been selected as a convenient reference ion)



Reaction 2 involves the direct comparison of a pair of cations; hence the thermodynamic quantities relevant thereto will reflect the relative solvation properties of these cations in an especially simple way.

This paper reports some standard free energy values for reaction 2 obtained by a direct equilibrium method which appear to be more reliable than free energies calculated from previous e.m.f. data.

The results obtained provide information on the importance of specific ion–solvent interactions for ions

with rare gas electronic configuration and on the dependence of ionic solvation on solvent composition in mixed solvent systems.

Glossary of Symbols

M	= alkali metal atom (or one-half of a strontium atom)
$[\text{M}]_{\text{Hg}}, [\text{M}^{n+}]_{\text{S}}$	= analytical concentration of M in amalgam phase and solvent phase, respectively
$f_{\text{M}}, \gamma_{\text{M}^+}$	= activity coefficient of M in amalgam and M^{n+} in solvent phase, respectively
$R = \frac{[\text{M}]_{\text{Hg}}^{1/n} [\text{Na}^+]_{\text{S}}}{[\text{M}^{n+}]_{\text{S}}^{1/n} [\text{Na}]_{\text{Hg}}}$	= equilibrium quotient for amalgam partition

- (1) This work was supported in part by a Frederick Gardner Cottrell grant from the Research Corporation.
- (2) Based in part on the thesis presented by A. Dadgar to the Graduate School of the Illinois Institute of Technology in partial fulfillment of the requirements for the degree of Master of Science in Chemistry.
- (3) W. W. Latimer and C. Slansky, *J. Am. Chem. Soc.*, **62**, 2019 (1940).
- (4) J. P. Butler and A. R. Gordon, *ibid.*, **70**, 2276 (1948).
- (5) R. W. Gurney, "Ionic Processes in Solution," McGraw-Hill Book Co., Inc., New York, N. Y., 1953, p. 222 ff.
- (6) J. K. Gladden and J. C. Fanning, *J. Phys. Chem.*, **65**, 76 (1961).

$R^\circ = R \left(\frac{f_M^{1/n}}{f_{Na}} \right)$	= R corrected for amalgam activity coefficients
$r_{M^{n+}}$	= crystal radius of M^{n+}
r_{S^+}	= ionic radius of solvated M^+ ion
r_μ^+	= ion-dipole distance in solvated M^+ ion
$K_S^\circ, \Delta G_S^\circ$	= equilibrium constant and standard Gibbs free energy for amalgam partition (reaction 4)
K_i°, G_i°	= the corresponding quantities for cation interchange (reaction 2)
ΔG_{Born}°	= Born free energy for cation interchange using crystal radii
ΔG_S°	= Born free energy for cation interchange using solvated radii
ΔG_μ°	= free energy of formation of gaseous solvated ion
S	= methanol or mixed methanol-water solvent
D_S	= dielectric constant of solvent S
α_S	= polarizability of molecule of solvent S
P_i	= electric dipole induced in solvent molecule by M^+ ion
P_μ	= permanent electric dipole of solvent molecule
$P (= P_\mu + P_i)$	= total electric dipole of solvent molecule in solvated ion

Experimental

Method. The amalgam partition method^{7,8} used in the present work has been described previously. All experiments were carried out at $24.9 \pm 0.1^\circ$ unless otherwise noted.

Materials. Reagent grade halides were used as received or were prepared by the treatment of reagent grade carbonates with an excess of the appropriate acid and evaporation to dryness at 150° .

Alkali metal amalgams were prepared by electrolysis of their aqueous carbonate solutions using a mercury cathode, then washed with water and methanol, dried

by heating under vacuum, and transferred to storage-dispensing vessels under dry nitrogen pressure.

Difficulties were encountered in the preparation of strontium amalgam by the electrolytic method. As an alternative, mixed Sr/Na amalgams of high strontium content were prepared by shaking sodium amalgam with a concentrated aqueous solution of strontium chloride.

All water used had been redistilled in a Barnstead still.

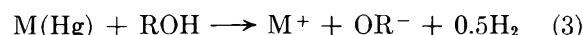
The methanol was reagent grade and was used directly from freshly opened bottles for the $N_{MeOH} = 1.0$ experiments. (A Karl Fischer titration showed a water content of 0.06 mole % H_2O). Solvents with $N_{MeOH} = 0.30$ and 0.80 were prepared by weight from reagent grade methanol and redistilled water.

Analyses. All metal analyses were carried out on the Beckman Model DU flame photometer using aqueous chloride solutions derived from samples removed from the amalgam and solvent phases.⁷

Other auxiliary analyses were performed by standard methods.

Attainment of Equilibrium. In selected experiments it was shown that the value of R° is independent of shaking time after the first 10 min. and independent of the direction of approach to the final equilibrium value. Furthermore, the same R° values are obtained with the anions Cl^- and Br^- .

A possible complication is the decomposition reaction which occurs between the amalgam and the solvent, which can be written in the general form



where $R = H$ or CH_3 . If the rate of decomposition is appreciable relative to the rate of amalgam partition equilibration, the analytical concentrations will not represent the equilibrium values. This potential source of error has been minimized in the present work by using pure mercury for preparation of the amalgams and by carrying out the sampling procedures rapidly.

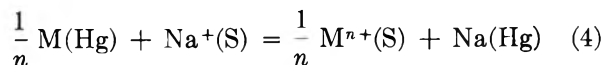
Two further consequences of the decomposition reaction are: (a) it places a practical lower limit on the electrolyte concentration attainable, and (b) it introduces "foreign anions" (HO^- and CH_3O^-) which may interact in a more specific manner with the cations than does the bromide ion. The consistency of the data under rather different experimental conditions suggests that neither of these effects is large enough to introduce appreciable systematic errors.

(7) K. Schug and H. L. Friedman, *J. Am. Chem. Soc.*, **76**, 3609 (1954).

(8) H. L. Friedman and K. Schug, *ibid.*, **78**, 3881 (1956).

Results

For the amalgam partition reaction



we write (see glossary)

$$K_S^\circ = \frac{[\text{Na}]_{\text{Hg}} [\text{M}^{n+}]_{\text{S}}^{1/n} f_{\text{Na}} \gamma_{\text{M}^{n+}}^{1/n}}{[\text{M}]_{\text{Hg}}^{1/n} [\text{Na}^+]_{\text{S}} f_{\text{M}^{n+}}^{1/n} \gamma_{\text{Na}^+}} \quad (5)$$

The concentrations come directly from the analyses and the amalgam activity coefficient ratios from previous work.⁸ This ratio is nearly unity in all of the present experiments.

We may then write

$$K_S^\circ = R^\circ \left(\frac{\gamma_{\text{M}^{n+}}^{1/n}}{\gamma_{\text{Na}^+}} \right) \quad (6)$$

The value of the thermodynamic equilibrium constant K_S° can be calculated from the experimental R° values if either (a) the activity coefficient ratio in eq. 6 is known for any R° , or (b) a suitable extrapolation of R° can be made from the experimental concentration range to infinite dilution. The validity of either of these methods in the present case must be decided on the basis of rather limited information on ionic activity coefficients in nonaqueous solvents. In considering the treatment of the present results, the cell data of Åkerlöf⁹ and of Gladden and Fanning⁶ were examined. Contrary to the statements made by these authors, it was found that the Debye-Hückel limiting law describes the behavior (within 5%) of NaCl and KCl in 90% methanol and of NaCl in 100% methanol up to 0.04 *M* concentration. (There are insufficient data to evaluate the behavior of KCl in 100% methanol.) Since we are dealing with the *ratio* of the activity coefficients of a pair of monovalent ions, it seems reasonable that γ_{Na^+} will also be very nearly equal to γ_{M^+} at somewhat higher concentrations than 0.04 *M*. This conclusion is in accord with the fact that in the present work no concentration dependence of R° is apparent in the range 0.01 to 0.05 *M*. Above 0.05 *M*, a slight but definite increase in R° is observed, suggesting that $\gamma_{\text{Na}^+} > \gamma_{\text{M}^+}$ as is observed at higher concentrations in aqueous solution. It is also reasonable that any effect due to ion-pair formation in the methanolic solvents would also tend to cancel for each pair of alkali halides. The observed agreement between solutions containing Cl⁻ and Br⁻ provides further support for the lack of ion-association effects on R° .

K_S° values were calculated by both of the methods described above, in method a by averaging all R° values below 0.05 *M* total metal ion concentration, and in

method b by carrying out a least squares analysis of R° vs. ($[\text{M}^+] + [\text{Na}^+]$). The choice of the extrapolation function is arbitrary, since there is no readily apparent form for the extrapolation, the variation of R° with concentration arising from *differences* in the ion-atmosphere and ion-pair behavior of Na⁺ and M⁺. The K_S° values obtained by the two methods agreed within the estimated uncertainties (agreement was also obtained for systems containing Sr²⁺, although the above arguments would not be expected to be valid in this case); the values tabulated in Table I were those obtained by method a.

Table I: K_S° Values for the Reaction^a $\text{M(Hg)} + \text{Na}^+(\text{S}) = \text{M}^+(\text{S}) + \text{Na(Hg)}$

M	Mole fraction methanol					
	0 ^b	0.30	0.80	0.90	0.95	1.00
K	2.16	1.96	1.37	1.11
Rb	1.70	1.69	0.99	0.85
Cs	0.68	0.64	.4534
1/2Sr	.20	.30	.38	0.30	0.24	.14

^a Estimated uncertainties: 10% for K, Rb, Cs; 20% for Sr.
^b From ref. 7.

Calculations

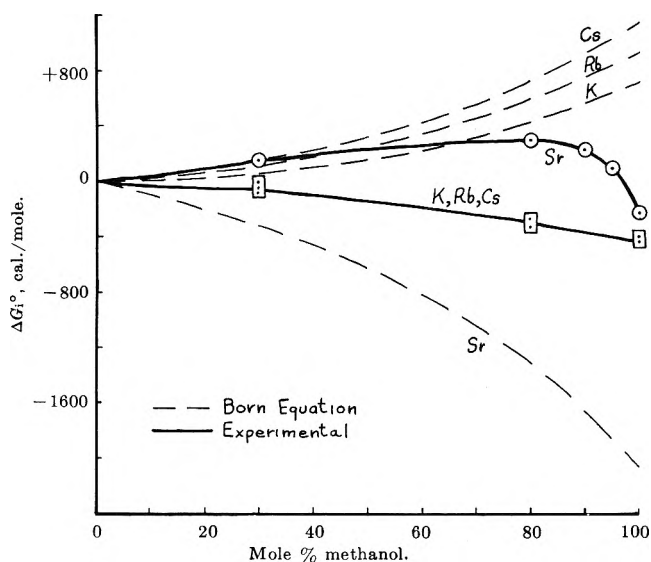
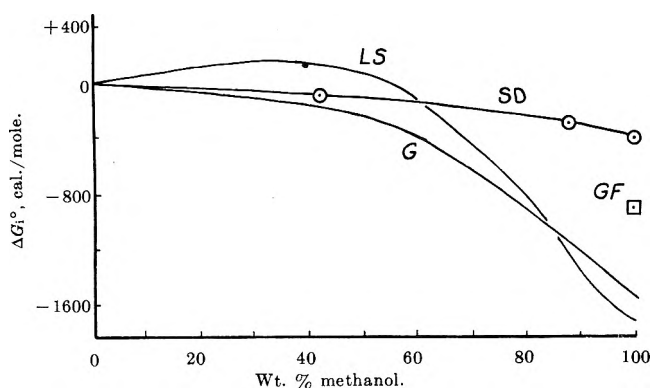
Calculation of K_i° and ΔG_i° . The equilibrium constants for the cation environmental interchange reactions (eq. 2) have been obtained by dividing $K_{\text{H}_2\text{O}}^\circ$ for the amalgam-aqueous partition⁹ reaction by K_S° from the present work. The resulting K_i° values and the corresponding ΔG_i° values are given in Table II, and the free energies are plotted in Fig. 1. Smooth curves have been drawn through the experimental points in each case.

Comparison with Other Data. In Fig. 2, the present values of ΔG_i° for the Na-K system are compared with those calculated from the results of other workers. Latimer and Slansky calculated free energies of solution of MCl (M = Li, Na, K) and KBr from previously reported solubility and activity coefficient data (the latter often obtained from lengthy extrapolations). Combination of their data for KCl and NaCl leads to the curve shown. Gurney as well as Gladden and Fanning studied e.m.f. cells with transference from which the free energies of transfer of MCl (M = Na, K) from water to methanolic solvents were calculated. The difference of these two free energies of transfer gives ΔG_i° .

(9) G. Åkerlöf, *J. Am. Chem. Soc.*, **52**, 2353 (1930).

Table II: Equilibrium Constants and Standard Free Energy Changes for the Reaction $\text{Na}^+(\text{H}_2\text{O}) + \text{M}^+(\text{S}) = \text{Na}^+(\text{S}) + \text{M}^+(\text{H}_2\text{O})$

M	Mole fraction of methanol									
	0.30		0.80		0.90		0.95		1.00	
	K_1°	ΔG_1° , cal.	K_1°	ΔG_1° , cal.	K_1°	ΔG_1° , cal.	K_1°	ΔG_1° , cal.	K_1°	ΔG_1° , cal.
K	1.10	-55	1.57	-270	1.94	-395
Rb	1.00	0	1.71	-320	1.99	-410
Cs	1.06	-35	1.55	-260	2.10	-420
$\frac{1}{2}\text{Sr}$	0.67	+240	0.61	+300	0.67	+240	0.83	+110	1.43	-215

**Figure 1.** Experimental and calculated values of G_1° , the free energy of cation interchange, as a function of solvent composition.**Figure 2.** Comparison of G_1° values for Na-K interchange as obtained in several investigations: LS = Latimer and Slansky GF = Gladden and Fanning, G = Gurney, SD = present results.

There is a striking lack of agreement among the various sets of data. The reasons for this disagreement are not readily apparent, but it is felt that the direct equilibrium method employed in the present work is more likely to give ΔG_1° values free of systematic

error. Thus, the amalgam partition method permits an approach to equilibrium from each side of the reaction and, furthermore, does not involve the erratic behavior frequently reported in potentiometric studies in nonaqueous solvents.

Two features of the present results to be discussed here are: (1) the qualitative lack of agreement between the experimental ΔG_1° values and the predictions of the simple Born equation; it will be shown that an electrostatic model involving the interaction of a point charge with point polarizable dipoles leads to calculated energies in fair agreement with experiment; (2) the dependence of ΔG_1° on solvent composition, particularly for the system involving Sr^{2+} ion.

Comparison with Born Equation. The form of the Born equation applicable to reaction 2 is

$$\Delta G_1^\circ = 165 \left(\frac{1}{r_{\text{Na}^+}} - \frac{1}{r_{\text{M}^+}} \right) \left(\frac{1}{D_{\text{S}}} - \frac{1}{D_{\text{H}_2\text{O}}} \right) \text{ kcal./mole Na}^+ \quad (7)$$

for the alkali metals and

$$\Delta G_1^\circ = 165 \left(\frac{1}{r_{\text{Na}^+}} - \frac{2}{r_{\text{Sr}^{2+}}} \right) \left(\frac{1}{D_{\text{S}}} - \frac{1}{D_{\text{H}_2\text{O}}} \right) \text{ kcal./mole Na}^+ \quad (8)$$

for strontium, when r values are expressed in Ångstrom units.

It has long been recognized that the use of ionic crystal radii in the Born equation involves an oversimplified model of ion-solvent interaction. Some success has been achieved in obtaining a fit with an equation of the Born type by treating the ionic radii as adjustable parameters. In the case of the solvation entropies of gaseous ions in water, an additive term to the cation crystal radii has been shown to be effective in obtaining a fit with an equation of the same form as the Born equation.¹⁰ In the present case, it is clear that such a simple modification will not work because the sign of the observed ΔG_1° is, in most cases, opposite to

(10) W. M. Latimer, *Chem. Rev.*, **18**, 349 (1936).

that predicted by the Born equation. One alternative is to consider the actual free energy change to be the sum of a Born term and a term arising from the specific ion-solvent interaction, *viz.*

$$\Delta G_i^\circ = \Delta G_{\text{Born}}^\circ + \Delta G_{\text{spec}}^\circ \quad (9)$$

Values of $\Delta G_{\text{spec}}^\circ$ calculated for the systems reported here are shown in Table III.

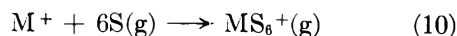
Table III: G_{spec}° from Eq. 9, cal./mole Na^+

	$N = 0.3$	$N = 0.8$	$N = 1.0$
K^+	-260	-910	-1250
Rb^+	-260	-1130	-1490
Cs^+	-360	-1260	-1760
$1/2\text{Sr}^{+2}$	+610	+1780	+1830

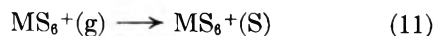
The more negative the value of $\Delta G_{\text{spec}}^\circ$ the greater is the tendency of the indicated ion to go from *methanol* to *water* relative to the reference ion Na^+ . The results indicate that the solvation of an alkali metal ion in methanol relative to its solvation in water decreases with increasing size. For K^+ , Rb^+ , and Cs^+ the change in $\Delta G_{\text{spec}}^\circ$ is just balanced by the opposite change in $\Delta G_{\text{Born}}^\circ$, so that the observed ΔG_i° remains nearly constant. In the strontium case, the positive value of $\Delta G_{\text{spec}}^\circ$ corresponds to a greater preference of the divalent Sr^{2+} ion for the methanolic phase than the univalent Na^+ ion.

The $\Delta G_{\text{spec}}^\circ$ values in Table III apply to a fairly complex process which includes the specific interaction of solvent molecules with ions and local changes in the dielectric constant and structure of the solvent. An attempt to treat the ion-solvent interaction in a more readily visualized way is described in the next section.

Ion-Dipole Model for Solvation. The solvation of a gaseous ion may be represented as the sum of the reactions



and



assuming six-coordination of the solvated ion. Calculations based on this approach have been moderately successful in calculating formation energies of aquo and other complex ions, especially for ions with rare gas structure.¹¹ The energy change accompanying reaction 10 may be calculated on the basis of a model involving the interaction of a point charge (the metal ion) with six octahedrally placed polarizable point dipoles¹²

(the solvent molecules). Three parameters are required—the permanent dipole (P_M) and polarizability (α) of the solvent molecules¹³ and the distance (r_μ) from the charge to the dipole. Suitable r_μ values, although not directly measurable, may be estimated with sufficient accuracy for the present application. For a solvated alkali metal ion, r_μ was obtained from the expression

$$r_\mu = r_{M^+} + r_0 + r_d$$

where r_{M^+} is the crystal radius of M^+ , r_0 the van der Waals radius of oxygen¹⁴ (1.38 Å.), and r_d is the estimated distance from the oxygen nucleus to the center of the electric dipole of the solvent molecule. This latter point was found by assuming charges of $+n$ on each H in H_2O (or on H and the methyl carbon in methanol) and of $-2n$ on oxygen, each charge centered on the nucleus.¹⁵ Required bond angles and bond distances were taken from "Interatomic Distances."¹⁶

The free energy change for reaction 11 was calculated from the Born equation, using solvated radii estimated as described below. It is assumed that the simple Born equation will yield reliable solvation energies for these larger solvated ions.

The model used above to estimate r_μ was extended as follows to estimate r_s , the solvated ionic radius of an alkali metal ion: van der Waals radii¹⁴ were assigned to H (0.30 Å.) and CH_3 (2.00 Å.), the maximum distance from the ion nucleus to the outer edge of H or CH_3 calculated, and the mean of these two distances taken as r_s .

The comparison between the experimental and calculated values has been made by combining ΔG_i° from experiment with ΔG_s° calculated for eq. 11 to get ΔG_μ° (exptl.) for comparison with ΔG_μ° (calcd.). The results (as well as the parameters used) are given in Table IV, for $\text{S} = 100\%$ methanol.

Considering the very large energy values involved in reactions 10 and 11, the results are in good agreement with experiment. Qualitatively, the negative values of ΔG_μ° arise from the greater polarizability of CH_3OH

(11) See F. Basolo and R. G. Pearson, "Mechanisms of Inorganic Reactions," John Wiley and Sons, Inc., New York, N. Y., 1958, pp. 46 ff. and 63 ff., for discussion and references.

(12) The equations needed are given by F. J. Garrick, *Phil Mag.*, 9, 131 (1930); they are also readily derived.

(13) A. A. Maryott and F. Buckley, National Bureau of Standards Circular No. 537, U. S. Govt. Printing Office, Washington, D. C., 1953.

(14) L. Pauling, "The Nature of the Chemical Bond," Cornell University Press, Ithaca, N. Y., 1944.

(15) This treatment corresponds closely to that used by J. D. Bernal and R. H. Fowler, *J. Chem. Phys.*, 1, 515 (1933), and by others.

(16) Special Publication No. 11, The Chemical Society, London, 1958.

Table IV: Comparison of Calculated and Experimental Values of ΔG_{μ}°

Ion	r_{μ}^{+}		r_{B}^{+}		ΔG_{μ}° (calcd.)	ΔG_{μ}° (exptl.)
	H ₂ O	CH ₃ OH	H ₂ O	CH ₃ OH		
Na ⁺	2.65	2.72	4.24	4.81	(0)	(0)
K ⁺	3.01	3.08	4.59	5.15	-0.69	-1.12
Rb ⁺	3.16	3.23	4.74	5.30	-1.10	-1.39
Cs ⁺	3.37	3.44	4.94	5.51	-1.39	-1.65

than H₂O by the smaller Na⁺ ion—the effect being great enough to more than offset a slightly unfavorable solvation term.

Similar calculations with dimethyl ether give somewhat more negative values of ΔG_{μ}° (calcd.). In this case, however, the opposing solvation energy terms are much larger, leading to the conclusion the “extractibility” of an alkali metal from water into ether would increase with increasing size, in qualitative accord with the Born equation.

Solvent Composition. For the alkali metal ions, ΔG_i° varies in a nearly linear monotonic fashion with solvent composition. This simple behavior suggests that these ions do not have a strong preference for either solvent molecule, *i.e.*, that the composition of the primary solvation sheath of an alkali metal ion does not differ appreciably from the stoichiometric composition of the mixed solvent. This conclusion is also consistent with the results of the electrostatic calculations described above.

The variation of ΔG_i° in the Na–Sr system is qualitatively quite different, however, implying a more complex solvation behavior. A tentative explanation for the presence of the maximum can be given if it is assumed that the Sr²⁺ ion prefers H₂O to CH₃OH in its solvation sphere.

At low methanol concentrations ($N_{\text{CH}_3\text{OH}} = 0$ to 0.85) the increase in ΔG_i° (in opposition to the predictions of the Born equation) reflects the effect of the larger size of the highly hydrated strontium ion. As $N_{\text{CH}_3\text{OH}}$ increases further, the decrease in ΔG_i° is due to the “escape” of Sr²⁺ from the methanol-rich solvent due to the preference for H₂O in its solvation sphere. Some

caution is necessary in considering the Sr²⁺ results because of our meager knowledge concerning activity coefficients and ion-pair formation of divalent ions in low dielectric solvents. It is of interest, however, that the variation of ΔG_i° with solvent composition for the Na⁺–Sr²⁺ system is qualitatively the same as ΔG_i° for the Na⁺–H⁺ system as calculated from results reported by Gurney.¹⁷ In the latter case, ΔG_i° shows a much more pronounced maximum near $N_{\text{MeOH}} = 0.80$. Gurney has explained the result on the basis of the greater relative affinity of the proton for H₂O than CH₃–OH, when compared with Na⁺.

Further support may be found for the thesis that Sr²⁺ would discriminate strongly in favor of water from studies on substitution-inert Cr(III) perchlorate solutions in aqueous methanol.¹⁸ For example, at an overall solvent composition of $N_{\text{CH}_3\text{OH}} = 0.72$, the composition of the first coordination shell of Cr(III) is $N'_{\text{CH}_3\text{OH}} = 0.16$.

Enthalpies and Entropies. It would be of great interest to evaluate the separate contributions of ΔH and ΔS to the free energy. Unfortunately, it does not appear possible to do this at present. Published values¹⁹ on the heats of solution of alkali halides can be combined to give ΔH corresponding to reaction 2, but the results are internally inconsistent by amounts up to 800 cal./mole.²⁰

In the hope of obtaining enthalpy (and entropy) data from the temperature coefficient of ΔG_i° , some amalgam partition experiments were carried out at 0°. The results were in qualitative agreement with the calorimetric results, but a realistic estimate of the uncertainty in the derived value of ΔH_i° is about ± 500 cal. It appears that further calorimetric data of proven dependability will be needed to complete the thermodynamic picture.

(17) See ref. 5, p. 225.

(18) E. L. King, J. C. Jayne, and K. Schug, unpublished results. A preliminary report was presented at 71CCC, Stockholm, June, 1962.

(19) C. M. Slansky, *J. Am. Chem. Soc.*, **62**, 2430 (1940).

(20) The errors increase with increasing methanol content. Below 50 mole % methanol, the calorimetric data are fairly consistent.

The Relative Free Energies of Sodium and Potassium Ions in Ethanol, Ethylene Glycol, Ethanolamine, and Ethylenediamine¹

by Ahmad Dadgar and Kenneth Schug²

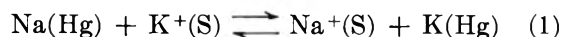
Department of Chemistry, Illinois Institute of Technology, Chicago 16, Illinois (Received August 7, 1963)

The amalgam partition method has been used to measure the relative free energies of Na⁺ and K⁺ in ethanol, ethylene glycol, ethanolamine, and ethylenediamine. The data, together with results taken from the literature for some additional solvents, support the view that specific ion-solvent interactions play a dominant role in the determination of ionic free energies of these ions in nonaqueous solvents.

Introduction

Little is known about the thermodynamic properties of solvated metal ions in solvents of low dielectric constant. Consequently, it is not possible to evaluate the relative importance of various factors which might be expected to affect these properties. An increasing amount of evidence is accumulating, however, to indicate that even for simple ions the predominant effect is due to quite specific ion-solvent interactions. This specificity seems to be less true of ion-ion interactions as expressed, *e.g.*, by ion-pair association constants, which appear to depend primarily on the macroscopic dielectric constant of the solvent. We wish to report some results on the relative free energies of Na⁺ and K⁺ in several solvents obtained by a direct equilibrium method which lend further support to the importance of specific solvation effects.

The experimental method^{3,4} consists of the direct measurement of the equilibrium



between an amalgam phase (Hg) containing the alkali metals and the solution phase containing the ions. The combination of two such equilibria (eliminating the amalgam species) leads to free energies of transfer between the pair of solvents involved.

Experimental

The procedures used conform to those described previously^{3,4} except as noted.

Materials. Ethyl alcohol (Commercial Solvents absolute), ethylene glycol (Fisher Certified), ethylene-

diamine (Fisher Certified) and ethanolamine (Fisher Purified) were used without further purification. Refractive indices at 25°, *n*²⁵_D, agreed closely with reported values⁵ corrected to the same temperature: ethylene glycol, 1.4298 (1.4298); ethanolamine, 1.4525 (1.4519); ethylenediamine, 1.4548 (1.4544).

Dry nitrogen was used to flush the reaction vessels (screw-capped test tubes fitted with Teflon liners) during the addition of the amalgam and solvent.

Analysis. With the ethanolamine and ethylenediamine solutions, the tarry residue left on evaporation of solvent was oxidized with a mixture of nitric and perchloric acids prior to the flame photometer analyses. This procedure was found to give reliable results when applied to solutions of known composition.

Results

The analytical results from each run were combined with activity coefficient data for the amalgam⁴ to evaluate *R*^o defined

$$R^o = \frac{[\text{Na}]_{\text{Hg}}[\text{K}^+]_{\text{S}}f_{\text{Na}}}{[\text{K}]_{\text{Hg}}[\text{Na}^+]_{\text{S}}f_{\text{K}}}$$

where [M]_{Hg} and [M⁺]_S are the total concentration of

- (1) Work supported in part by a grant from the Research Corporation.
- (2) To whom correspondence should be addressed.
- (3) K. Schug and H. L. Friedman, *J. Am. Chem. Soc.*, **76**, 3609 (1954).
- (4) H. L. Friedman and K. Schug, *ibid.*, **78**, 3881 (1956).
- (5) E. M. Arnett, J. G. Miller, and A. R. Day, *ibid.*, **72**, 5635 (1950). Temperature corrections were based on the empirical relation $dn_D/dt = -0.0004 \text{ deg.}^{-1}$.

Table I: Summary of Experimental Results

	Solvent			
	H ₂ NCH ₂ CH ₂ NH ₂	HOCH ₂ CH ₂ NH ₂	CH ₂ CH ₂ OH	HOCH ₂ CH ₂ OH
No. of experiments	13	17	8	15
Equilibration time	15 min.	15 min.	15 min.	15 min.
$\Sigma[M^+]_s$	0.025–0.098 M	0.022–0.056 M	0.020–0.115 M	0.018–0.120 M
$\left(\frac{[Br^-]}{[M^+]}\right)$ range	0.59–0.73	0.40–0.82	0.45–0.81	0.45–0.88
$\left(\frac{[Br^-]}{[M^+]}\right)$ mean	0.64	0.57	0.64	0.72
R° , mean	0.16 ± 0.03	0.33 ± 0.04	2.05 ± 0.07	2.19 ± 0.26

M (M = Na or K) in the amalgam and solution phases, respectively, and f_M is the activity coefficient (hyp. 1 m standard state) of M in the amalgam. Plots of R° vs. total $[M^+]_s$ showed no recognizable concentration dependence over the concentration range studied. The mean values of R° along with other relevant data are given in Table I.

In all experiments a direct reaction occurred between the amalgam and the solvent as evidenced by the fact that the total M^+ in the organic layer after equilibration exceeded that introduced as MBr. This reaction is presumed to be a decomposition of the type



The extent of this reaction was not reproducible and is indicated in Table I as $[Br^-]/[M^+]$, the known bromide concentration divided by the final alkali metal concentration in the organic layer.

The R° values show no dependence on either the relative concentrations of Na⁺ and K⁺ in the organic solution or on the extent of the direct decomposition reaction.

Discussion

Standard Free Energies. The standard free energy change for reaction 1 is given by

$$\Delta G_1^\circ = -RT \ln K_1^\circ \quad (4)$$

For a mixed electrolyte solution containing KBr and NaBr in which ion pairs are the only associated species

$$K_1^\circ = R^\circ \left[\left(\frac{\gamma_K}{\gamma_{Na}} \right) \left(\frac{1 + K_{NaBr}[Br^-]}{1 + K_{KBr}[Br^-]} \right) \right] \quad (5)$$

in which γ_M is the ionic activity coefficient of M^+ in the solution, K_{MBr} the ion-pair association constant for $M^+ \cdot Br^-$, and $[Br^-]$ the free bromide ion concentration.

ΔG_1° values may be calculated from amalgam partition data by extrapolation of R° to infinite dilution or by evaluation of the expression in brackets in eq. 5. In the present work, R° was independent of concentration over an approximate fivefold concentration range.

This behavior could be due to any of the following conditions: (a) $\gamma_K/\gamma_{Na} = \text{constant}$ and $K_{NaBr}[Br^-]$, $K_{KBr}[Br^-] \ll 1$; (b) $\gamma_K/\gamma_{Na} = \text{constant}$ and $K_{NaBr} \cong K_{KBr}$; (c) $\gamma_K/\gamma_{Na} = \text{constant}$ and K_{NaBr} , $K_{KBr} \gg 1$; or (d) a fortuitous cancellation of the contributions from the activity coefficient and ion pair association effects. Cases a and b lead to $K_1^\circ = R^\circ$. The constancy of γ_K/γ_{Na} is reasonable for a pair of similar ions and the available data (discussed below for each solvent) suggest that (b) is the correct description of the present systems.

Ethanolamine ($D = 37.7$ at 25°). Conductance studies of alkali metal salts dissolved in anhydrous ethanolamine⁶ yield rather small values for ion pair association constants (K_A). In particular, K_A values of 5.4 and 5.5 were reported for NaBr and KBr, respectively. These may be considered equal within experimental uncertainty. Furthermore, the value of γ_K/γ_{Na} is undoubtedly near unity, involving as it does a pair of similar ions at a moderate concentration. Further support for rather small association constants is provided by recent conductance studies of solutions of alkali halides in dioxane–water mixtures.⁷ K_A values of 1.5, 0, 0, for KCl, NaBr, and CsI, respectively, at $D = 37$ were estimated from the values reported. (A value of zero means there was no evidence for ion-pair formation.)

Ethylene Glycol ($D = 37.7$ at 25°). There appear to be no direct measurements of ionic activity coefficients or ion-pair formation in ethylene glycol. It is reasonable, however, that ion-association constants will be small for alkali halides and numerically about equal for NaBr and KBr (see discussion above under ethanolamine). Additional support for this statement is provided by the cell measurement data of Gladden and Fanning.⁸ These data have been recalculated using

(6) P. W. Brewster, F. C. Schmidt, and W. B. Schaap, *J. Am. Chem. Soc.*, **81**, 5532 (1959).

(7) J. E. Lind and R. M. Fuoss, *J. Phys. Chem.*, **66**, 1727 (1962); **65**, 1414 (1961); **65**, 999 (1961).

(8) J. K. Gladden and J. C. Fanning, *ibid.*, **65**, 76 (1961).

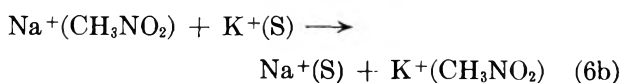
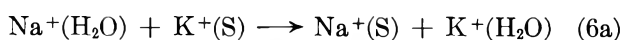
experimental values for aqueous activity coefficients and an extended form of the Debye-Hückel equation to represent activity coefficients in glycol (using $\tilde{a} = 4$). The theoretical slope was obeyed up to about 0.10 M NaCl. These results provide strong support for nearly complete dissociation in the experimental concentration range and for $\gamma_{\text{Na}^+} = \gamma_{\text{K}^+}$.

Ethyl Alcohol ($D = 24.3$ at 25°). Ion-pair association in ethyl alcohol has been reported for several alkali halides.⁹ Expressed as association constants, K_A (NaCl) = 80 and K_A (KCl) = 126 at 25°. These values are somewhat larger than those interpolated for $D = 24.3$ from the work of Lind and Fuoss⁷ in dioxane-water mixtures (40, 29, and 18 for KCl, RbBr, and CsI, respectively). They also show rather greater dependence on the nature of the cation than is usually observed.

In the absence of any direct information on NaBr and KBr in ethanol, it has been assumed that K_A is about 30 and is nearly the same for the two salts. Detailed calculations under these conditions (using the extended Debye-Hückel equation to calculate activity coefficients) give the result that about 20% of the solute is associated as ion pairs in the region 0.01–0.10 M and that the fraction associated is not strongly dependent on K_A for values in the neighborhood of 30.

Ethylenediamine ($D = 12.9$ at 25°). Ion association of alkali halides in anhydrous ethylenediamine has been studied by conductivity¹⁰ and potential¹¹ methods. Although agreement between the two sets of measurements is not very good, ion-pair association constants greater than 10^3 are indicated for the alkali halides. The ratio of ion-association constants for NaX/KX are 0.65, 0.68, and 1.0 for X = Cl, Br, and I, respectively. Despite the much larger ion-pair association constants in this solvent, detailed calculations of the type described above give a degree of association of about 40% and again a relatively slight dependence of this quantity on K_A over the experimental concentration range.

Free Energies of Transfer. In Table II are summarized the values of ΔG_i° for the environmental interchange processes



for a number of solvents as obtained from the present results and from other sources.^{12–17} These values represent the difference in molar free energies of Na⁺ and K⁺ in solvent S relative to this difference in water (6a) or in nitromethane (6b). The choice of nitromethane

as a reference solvent is based on the following considerations: (a) the experimental method employed (for S = H₂O) was capable of higher precision, and (b) specific ion-solvent interactions would be expected to be small for nitromethane so that the ΔG_i° values can be discussed in terms of the effect of the properties of solvent S.

Table II: Free Energy of Interchange of Na⁺ and K⁺ between Solvent S and H₂O or CH₃NO₂ at 25°

S	$-\Delta G_i^\circ$ (H ₂ O)		$-\Delta G_i^\circ$ (CH ₃ NO ₂), kcal.			D^b
	Kcal.	Ref.	Exptl.	Born	Spec.	
CH ₃ NO ₂	+4.30	12	(0)	(0)	(0)	35.9
CH ₃ CN	+1.90	13	-2.40	-0.16	-2.24	37.5
H ₂ O	(0)	..	-4.30	-.85	-3.45	78.5
HOCH ₂ CH ₂ OH	0.01	a	-4.29	-.16	-4.13	37.7
	.08	8				
CH ₃ OH	-.40	14	-4.70	+.05	-4.75	32.6
	-.90	8				
	-1.20	15				
	-1.70	16				
CH ₃ CH ₂ OH	0.01	a	-4.29	+.59	-4.88	24.3
HOCH ₂ CH ₂ NH ₂	-1.09	a	-5.39	-.16	-5.23	37.7
NH ₃ (0°)	-1.55	3	-5.85	+1.15	-7.00	19
H ₂ NCH ₂ CH ₂ NH ₂	-1.66	a	-5.96	+1.85	-7.81	12.9
	-1.4	17				

^a Present work. ^b Dielectric constant at 25°.

Comparison with Other Data. In several cases a comparison is possible between the value of ΔG_i° obtained by amalgam partition and one calculated from other sources. These values have been listed in Table II and will be discussed briefly below. The comparisons can be made on the basis of the ΔG_i° (H₂O) values.

The e.m.f. cell work of Gladden and Fanning⁸ on solutions of KCl and NaCl in ethylene glycol leads to a ΔG_i° value in good agreement with the value obtained from amalgam partition measurements.

The methanol values have been discussed elsewhere,¹⁴

- (9) J. R. Graham, G. S. Kell, and A. R. Gordon, *J. Am. Chem. Soc.*, **79**, 2352 (1957).
 (10) B. B. Hibbard and F. C. Schmidt, *ibid.*, **77**, 225 (1955).
 (11) S. Bruckenstein and L. M. Mukherjee, *J. Phys. Chem.*, **64**, 1601 (1960).
 (12) G. R. Haugen and H. L. Friedman, private communication.
 (13) H. L. Friedman and K. Schug, unpublished observations.
 (14) K. Schug and A. Dadgar, *J. Phys. Chem.*, **68**, 106 (1964).
 (15) R. W. Gurney, "Ionic Processes in Solution," McGraw-Hill Book Co., Inc., New York, N. Y., 1953, p. 222 ff.
 (16) W. M. Latimer and C. Stansky, *J. Am. Chem. Soc.*, **62**, 2019 (1940).
 (17) W. B. Schaap, R. E. Bayer, J. R. Siefker, and F. C. Schmidt, "Advances in the Chemistry of the Coordination Compounds" (6ICCC Proceedings), Macmillan Co., London, 1961, p. 449.

with the conclusion that the direct equilibrium measurements involved in the amalgam partition method probably lead to the most reliable values of ΔG_i° .

Polarographic studies of alkali metal salts in ethylenediamine by Penney and Schlapp¹⁷ lead to a ΔG_i° value 0.26 kcal. more positive than amalgam partition. This probably represents agreement within the combined experimental error.

Examination of the experimental ΔG_i° (CH_3NO_2) values in Table II shows that there is no simple correlation with the macroscopic dielectric constant of the solvent as would be predicted by the Born equation, but instead, a marked tendency for chemically similar solvents to fall together. Since the Born energy must be involved in the process, however, it should be instructive to separate the total free energy change into a Born part and a specific part. This can be done in an approximate way by correcting the experimental value for the Born contribution and examining the resultant values. Column 5 of Table II lists the ΔG_i° values calculated by the Born equation, using ionic radii¹⁸ ($r_{\text{Na}^+} = 0.98$, $r_{\text{K}^+} = 1.33$), and column 6 the ΔG_i° (spec.) values obtained by subtracting ΔG_i° (Born) from ΔG_i° (exptl.). The ΔG_i° (spec.) values show a much better correlation with chemical nature of the solvent than do the original ΔG_i° values. Thus acetonitrile lies about 2 kcal. negative, solvents containing -OH functional groups in the range -4.2 ± 0.8 , solvents with only -NH₂ groups -7.5 ± 0.5 , and ethanolamine (containing both -OH and -NH₂) at -5.23 lies between the -OH and -NH₂ solvents. The ordering suggests that the smaller Na⁺ ion interacts more strongly with solvent molecules than K⁺ in all cases, the difference in-

creasing as we go from CH₃CN, -OH, -OH/-NH₂, -NH₂.

The relatively large difference between acetonitrile and nitromethane deserves some attention in view of the almost identical dielectric constants and expected chemical inertness of this pair of solvents. It is suggested that the main factor here is the ion-dipole interaction between M⁺ and S, the smaller Na⁺ ion interacting relatively more strongly with the slightly more polar CH₃CN molecule. A simple electrostatic calculation (point dipole, point charge, both nonpolarizable) gives $\Delta G_i^\circ = -4.5$ kcal. for the interaction of M⁺ with a single molecule of each solvent, illustrating that the energy difference associated with this model is of the right size.

Some additional evidence for the essential chemical nature of the interactions of Na⁺ and K⁺ with solvents of the type listed comes from studies of ΔG_i° in mixed solvents as a function of solvent composition. For pairs of solvents of the same class ($\text{H}_3\text{O}-\text{CH}_3\text{OH}$,¹⁴ *e.g.*) ΔG_i° has been found to vary smoothly as a function of composition, whereas for mixed-class solvent systems an abrupt and drastic "bending over" occurs as the composition approaches the less strongly solvating component (*e.g.*, $\text{CH}_3\text{NO}_2-\text{H}_2\text{O}$,¹² $\text{CH}_3\text{CN}-\text{H}_2\text{NCH}_2-\text{CH}_2\text{NH}_2$,¹⁹ $\text{H}_2\text{O}-\text{NH}_3^3$). With more highly charged cations, *e.g.*, Sr²⁺ and Cr³⁺ in $\text{H}_2\text{O}-\text{CH}_3\text{OH}$ mixtures,¹⁴ this sharp break has been observed, suggesting that the solvent differences are exaggerated, as would be expected.

(18) L. Pauling, "The Nature of the Chemical Bond," Cornell University Press, Ithaca, N. Y., 1944.

(19) M. Zangen and K. Schug, unpublished observations.

Nitrosomethane Formation in Photolysis of *t*-Butyl Nitrite

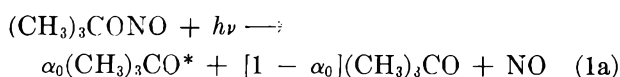
by G. R. McMillan, Jack G. Calvert, and Sandra S. Thomas

Evans Chemical Laboratory, The Ohio State University, Columbus 10, Ohio (Received August 9, 1963)

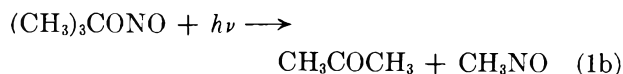
t-Butyl nitrite vapor at low pressure (26 μ) was illuminated with the full light of the quartz medium pressure mercury arc. The reaction was followed *in situ* by scanning the infrared absorption at a 20-m. path length. In contrast to other results at high nitrite pressure, nitrosomethane is a minor product only, amounting to 15% or less of the acetone formed. Acetone appears at the start of the illumination, but nitrosomethane is detectable only after the nitrite has suffered about 20% decomposition. This induction period is increased by addition of small amounts of oxygen and is decreased by addition of nitrogen at a few mm. pressure or nitric oxide at a few microns pressure. Ethane, not found in the high pressure reaction, indicates the presence of methyl radicals in the system. These results suggest that the only important nitrosomethane forming step is combination of methyl with nitric oxide, and the primary process, $(\text{CH}_3)_3\text{CONO} + h\nu \rightarrow \text{CH}_3\text{NO} + \text{CH}_3\text{COCH}_3$, does not occur.

Introduction

Results of photolysis of *t*-butyl nitrite vapor were interpreted in terms of a primary process forming, in part, excited *t*-butoxy radicals.^{1,2}



Decomposition of the excited radicals accounts for the high quantum yields of acetone observed at short wave lengths. Collisional deactivation of the excited radicals was incomplete even at the highest pressures accessible in that work. Even in isoctane solution, where deactivation should be favored, full-arc irradiation of the nitrite produces acetone in 10–15% yield.³ This acetone may or may not be due to decomposition of excited radicals in the liquid phase; formation in the primary process is another possibility.^{4–6}



Further investigation to try to resolve these alternatives seemed warranted. We have now used long-path infrared spectrophotometry to follow vapor phase formation and decay of the elusive product, nitrosomethane.

Experimental

t-Butyl nitrite⁷ was fractionally distilled, treated with

mercury to remove nitrogen dioxide, and stored at -79° . Tank nitric oxide was passed through two gas scrubbers containing sulfuric acid, one containing concentrated potassium hydroxide solution, one containing mercury, and finally through a trap containing silica gel cooled to -79° . Tank nitrogen of high purity was passed over hot, freshly reduced spongy copper, then magnesium perchlorate.

The reaction vessel was a 60-l., cylindrical aluminum tank which fitted closely over the beam supporting the mirrors of the long-path attachment of the Perkin-Elmer Model 21 infrared spectrophotometer. The tank was fixed to the spectrophotometer housing through an O-ring seal. The inner wall of the tank was rendered inactive as previously described.⁸ Six quartz

- (1) G. R. McMillan, *J. Am. Chem. Soc.*, **84**, 4007 (1962).
- (2) G. R. McMillan, *J. Phys. Chem.*, **67**, 931 (1963).
- (3) G. R. McMillan, unpublished results. Dilute solutions of the nitrite were illuminated in quartz with the medium pressure mercury arc at 22° . Less than 5% of the nitrite disappearing formed acetone when the incident radiation was limited to the 3660-Å. region.
- (4) C. S. Coe and T. F. Doumani, *J. Am. Chem. Soc.*, **70**, 1516 (1948).
- (5) P. Tarte, *Bull. soc. roy. Liège*, **22**, 226 (1953).
- (6) B. G. Gowenlock and J. Trotman, *J. Chem. Soc.* 4190 (1955).
- (7) A. I. Vogel, "A Textbook of Practical Organic Chemistry," Longmans, Green and Co., London, 1948, p. 305.
- (8) N. R. Subbaratnam and J. G. Calvert, *J. Am. Chem. Soc.*, **84**, 1113 (1962).

windows were sealed with neoprene gaskets to aluminum window mounts welded along the length of the tank. The windows admitted the light of three Hanovia Type A 550-w. medium-pressure mercury arcs held in a water-cooled quartz condenser. This arrangement permits no confident statement of the wave length distribution of the light absorbed by the nitrite. The full light of the arcs enters the cell, but no wave length is completely absorbed in a single pass through the vapor. The light beam may then undergo several reflections before exiting through the quartz windows. The inner surface of the tank is highly reflective in the visible, but its reflective properties for ultraviolet radiation are unknown. If the extent of light absorption is proportional to the extinction coefficient of the vapor and the fractional output of the lamp at each wave length, then it may be calculated that about 75% of the light absorbed lies at wave lengths shorter than 2550 Å.

The infrared analyzing beam entered the tank through a sodium chloride window, underwent multiple reflections sufficient to give an optical path of 20 m., and left the tank through a second window. A major problem in these systems is leakage of air around the sodium chloride windows into the tank. Here a low rate of leakage was achieved by sealing the windows into place with Glyptal.

Pressure measurements were made with a calibrated stainless steel Wallace and Tiernan FA-160 dial manometer.

An amount of nitrite sufficient to give the desired pressure in the tank was isolated behind a stopcock. Nitrogen was admitted to a pressure of 20 mm., then rapidly pumped away. The nitrite was expanded into the tank, followed by other reactants when desired. In contrast to the usual practice, the vessel was not pressurized to an atmosphere with inert gas.

Formation of nitrosomethane was followed at 6.32 μ using the $\times 5$ scale expansion of the instrument. The wave length was locked and the recorder drum permitted to revolve, so the pen drew the transmittance during the illumination. The true curve of the time dependence of the nitrosomethane absorbance was constructed, taking into account the small but varying contributions of acetone and *t*-butyl nitrite to the absorption at 6.32 μ .

Acetone was measured by the absorption at 5.75 μ , *t*-butyl nitrite by the absorption at 6.05 μ . Beer's law is not obeyed by the last peak under any convenient operating conditions, so accurate measurement of *t*-butyl nitrite could not be made easily. The extinction coefficient of ethane is too low to allow analysis by infrared absorption, so gas chromatography was used. The ethane was collected by admitting nitrogen to the

tank to a pressure of 20 mm., then pumping out through a multiple loop trap over a period of 3 hr. The trap was partially immersed in liquid nitrogen; the upper turns of the loops were maintained at room temperature by a stream of air.

Results

Nitrosomethane is identified by the infrared band at 6.3–6.4 μ . Evidence for assignment of this band has been summarized.⁹ The following points to be discussed in this paper all indicate that the band observed here is due to nitrosomethane: the transiency of the absorption; the behavior of the peak upon addition of nitric oxide before photolysis; and the fair balance, observed under favorable conditions, between methyls introduced and nitrosomethane formed.

Nitrosomethane is a minor product when *t*-butyl nitrite vapor at a pressure of 26 μ is photolyzed at 25°. The typical course of nitrosomethane formation is shown in Fig. 1. The value of the extinction coefficient

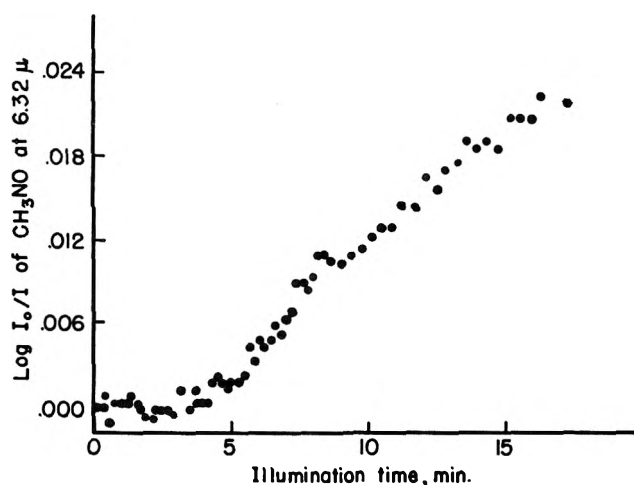


Figure 1. Course of nitrosomethane formation in photolysis of *t*-butyl nitrite: initial nitrite pressure, 0.026 mm.; decomposition is carried to about 55%.

of nitrosomethane is uncertain, so the concentration is expressed in terms of absorbance ($\log I_0/I$) at 6.32 μ . An apparent induction period of about 3 min. is observed, corresponding to about 20% decomposition of nitrite. Examination of curves from many runs indicates that delay in response due to instrument inertia amounts to no more than a few tenths of a minute. This method of determining induction periods fails if the intensity of radiation is high, for under such conditions a displacement of the pen is observed upon sud-

(9) J. G. Calvert, S. S. Thomas, and P. L. Hanst, *J. Am. Chem. Soc.*, **82**, 1 (1960).

denly admitting light to the cell—even with the cell empty.

Figure 2 shows that acetone and ethane are formed without an apparent induction period. To show the material balance, concentrations are presented on a pressure basis in Fig. 2. This requires use of the approximate extinction coefficient of nitrosomethane given from this study.

Addition of small amounts of oxygen prolongs the

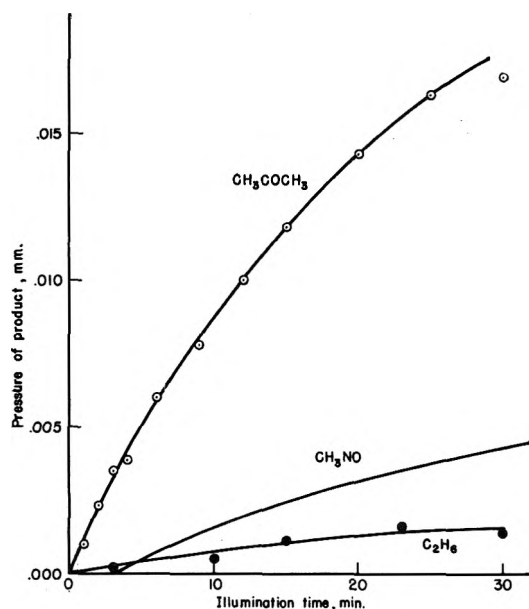


Figure 2. Course of product formation in photolysis of *t*-butyl nitrite at 26°; initial pressure, 0.026 mm.

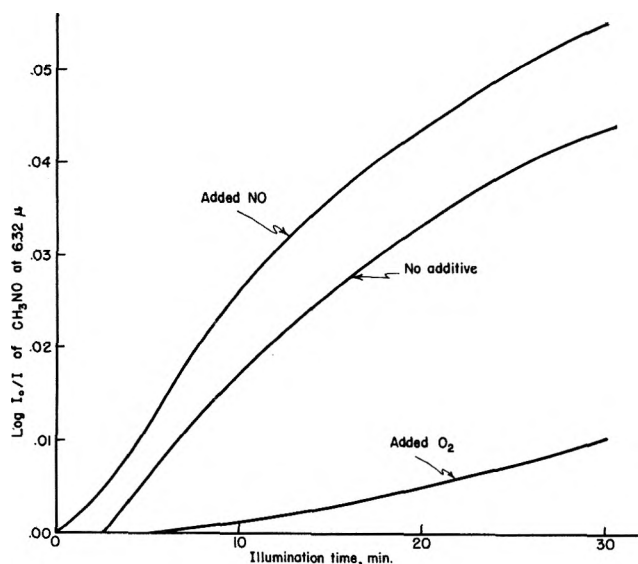


Figure 3. Effect of added nitric oxide (0.0052 mm.) and oxygen (0.13 mm.) on course of formation of nitrosomethane in photolysis of *t*-butyl nitrite (0.026 mm.).

induction period and decreases net nitrosomethane production (Fig. 3). Addition of small amounts of nitric oxide shortens the period (Fig. 3) and increases the maximum rate of nitrosomethane formation (Fig. 4). The induction period was reduced to about 0.5 ± 0.2 min. when the amount of nitric oxide added was just the maximum amount that could be formed by photodecomposition of nitrite by the end of the induction period in the experiment without added nitric oxide. A small but definite decrease in acetone yield is observed as the initial pressure of nitric oxide is increased. A pressure of 0.25 mm. of nitric oxide reduced the acetone yield to 83% of that observed in the absence of added nitric oxide.

Figure 5 shows that addition of nitrogen shortens the induction period. Acetone formation is unaffected. Addition of 20 mm. of nitrogen reduced the ethane yield to 13% of the value expected in the absence of nitrogen.

After the illumination was stopped, disappearance of nitrosomethane absorption was followed. The scatter

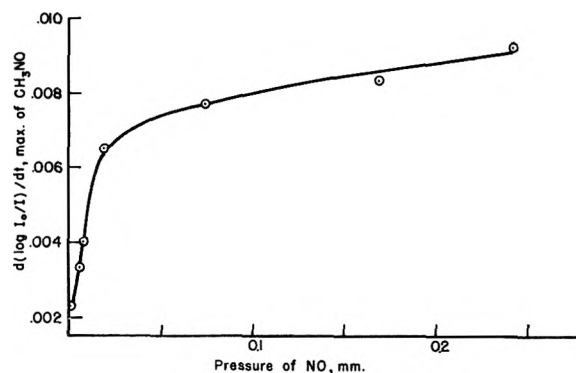


Figure 4. Effect of nitric oxide on maximum rate of nitrosomethane formation; initial nitrite pressure, 0.026 mm.

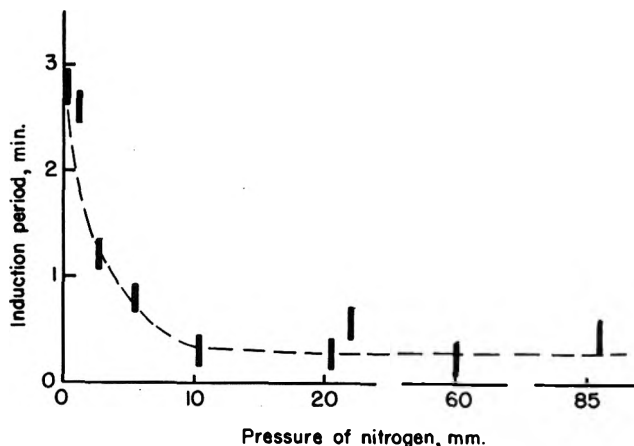


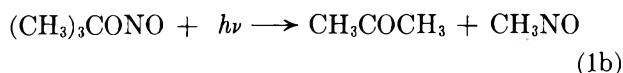
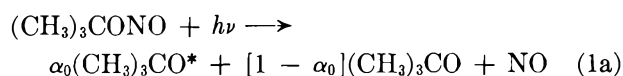
Figure 5. Effect of nitrogen on induction period of nitrosomethane.

of points was too great to establish firmly that the disappearance remains second order in nitrosomethane as has been found for a 20-fold higher concentration.⁹ The average (eight measurements) second-order rate constant was twice the value determined at the higher concentration. We believe this is close enough to indicate that the species examined in the present work really is nitrosomethane. The apparent rate constant of disappearance was not affected by addition of nitric oxide at a pressure of 0.155 mm., 10-fold higher than would be present at the end of an ordinary nitrite experiment.

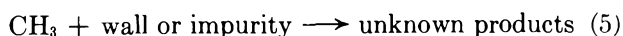
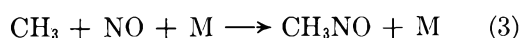
An infrared absorption attributable to formaldoxime was never detected. Neither acetone nor nitrosomethane was decomposed appreciably by light over the course of an illumination.

Discussion

The results give evidence regarding the relative efficiencies of primary processes 1a and 1b.



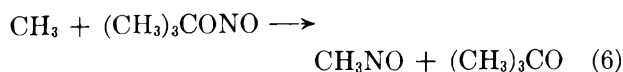
A few of the other probable reactions are



At the lowest pressures used, all radical reactions will be expected to occur at least partly on the vessel wall, so M may be wall as well as a third molecule.

Evidence for writing the primary process as (1a) has been discussed at length.¹

The induction period in nitrosomethane formation, shortened by addition of nitric oxide and lengthened by addition of oxygen, suggests that nitrosomethane is formed principally by combination of methyl with nitric oxide (3). The primary process involving the 1,3 methyl shift (1b)⁴⁻⁶ does not seem to occur. Likewise, the reaction



does not occur at this low temperature and pressure, although it is known under other conditions.¹⁰⁻¹²

In terms of the suggested mechanism, nitrosomethane appears only after sufficient nitric oxide has accumu-

lated to enable (3) to compete favorably with other methyl reactions such as (4) and (5). Addition of nitrogen shortens the induction period by accelerating the third-order methyl-nitric oxide combination and by preventing diffusion of methyl to the wall, where (5) might take place.

As the initial pressure of nitric oxide is increased, the maximum rate of nitrosomethane increases rapidly at first, then more slowly (Fig. 5). This change in slope may be due to inefficient scavenging of a few "hot" methyls formed by decomposition of excited *t*-butoxy formed at the shortest wave lengths. Judging from the amounts of acetone formed, the total number of methyls being produced is decreased by addition of nitric oxide.

Extrapolation of the high pressure deactivation rate¹ indicates that deactivation is negligible at all pressures used in the study; hence, all excited radicals formed in the primary process will decompose. Some unexcited *t*-butoxy may be decomposing too, as shown by the decrease in acetone yield upon addition of small amounts of nitric oxide, which can scavenge the unexcited radicals.

The material balance is generally poor. Acetone accounts for about 90% of the nitrite reacting. One methyl should appear for each acetone, yet even after the large uncertainty in the absolute yield of nitrosomethane is considered, only about half of the methyls are accounted for by the products ethane and nitrosomethane. Reactions such as addition of methyl to nitrosomethane must be occurring to a great extent, but a cursory examination of the infrared spectra has shown no unexplained peaks that might be due to the expected products.^{10,13} When nitric oxide is added, several side reactions are suppressed, early in the reaction most methyls appear as nitrosomethane, and the material balance is improved. Any calculation of the nitrosomethane yield depends upon an uncertain quantity, the extinction coefficient of nitrosomethane in the infrared. It has not been possible to make direct measurements on this very reactive compound. Using an indirect method, Calvert, Thomas, and Hanst⁹ obtained a value of 77 l./mole/cm. at 6.32 μ . If this value is adjusted as best we can to present operating conditions of the instrument, 94 l./mole/cm. is obtained (slit 58 μ). For reference, the measured extinction coefficient of acetone at 5.76 μ was 158 l./mole/cm.

(10) B. Jest and L. Phillips, *Proc. Chem. Soc.*, 73 (1960).

(11) P. Gray and P. Rathbone, *ibid.*, 316 (1960).

(12) B. Bromberger (Jest) and L. Phillips, *J. Chem. Soc.*, 5302 (1961).

(13) L. Phillips, *Proc. Chem. Soc.*, 204 (1961). Other references are given by A. Maschke, B. S. Shapiro, and F. W. Lampe, *J. Am. Chem. Soc.*, 85, 1876 (1963).

(slit 51μ).¹⁴ The maximum rate of nitrosomethane in a typical experiment at high nitric oxide pressure (0.026 mm. nitrite; 0.12 mm. nitric oxide) may be calculated to be 8.2×10^{-4} mm./min., compared with the maximum rate of acetone formation of 8.6×10^{-4} mm./min. Figure 4 shows that all the methyls are probably not scavenged by nitric oxide at this pressure, so the agreement in quoted rates is deceptive.

The reduction in ethane yield upon introducing nitrogen as a diluent perhaps brings the present results into line with the observation, by Coe and Doumani,⁴ that ethane is not a product at higher reactant pressures.¹⁵

Unfortunately, the instrument was not stable enough to permit accurate determination of the rate constant for disappearance of nitrosomethane; however, the absence of any increase in rate constant upon a 10-fold increase in nitric oxide concentration indicates that decay of nitrosomethane by addition of one or two molecules of nitric oxide¹⁶ is not important under our conditions.

Since it appears from this work that (1b) is not an important primary process, the formation of acetone upon photolysis of *t*-butyl nitrite in isoctane solution remains puzzling. Some decomposition of excited *t*-butoxy may be taking place, but photolysis of di-*t*-butyl peroxide, which likewise forms excited *t*-butoxy,¹⁷ gives only *t*-butyl alcohol when the peroxide is in a good

hydrogen-donating solvent.¹⁸ A small contribution of a concerted step like



is another possibility, but this cannot be the only primary process for reasons already given.¹

Acknowledgment. Grateful acknowledgment is made of the generous support of the Division of Air Pollution, Bureau of State Services, Public Health Service, which made possible the pursuance of this work.

-
- (14) The extinction coefficients pertain to a nulled instrument (pen stationary). The values given are roughly independent of nitrogen pressure up to 1 atm.
- (15) The absence of ethane in the products led Coe and Doumani⁴ and others⁶ to favor primary process (1b). They pointed out that formation of nitrosomethane by methyl-nitric oxide combination would imply important formation of ethane by methyl-methyl combination, as the steady-state concentrations of nitric oxide and methyl might not be very different. This is certainly the case provided only these two reactions consume methyl and nitric oxide. At present, several other reactions of these species are known which are likely to occur in the system, so that evidence today perhaps has not its former force. It is possible that the well established reaction 6¹⁰⁻¹² may be the main nitrosomethane forming step during photolysis under the conditions imposed by Coe and Doumani.
- (16) M. I. Christie, *Proc. Roy. Soc. (London)*, **A249**, 248 (1959); L. Batt and B. G. Gowenlock, *Trans. Faraday Soc.*, **56**, 682 (1960).
- (17) G. R. McMillan, *J. Am. Chem. Soc.*, **84**, 2514 (1962).
- (18) H. B. Henbest, J. A. W. Reid, and C. J. M. Stirling, *J. Chem. Soc.*, 5239 (1961).

Absorption Spectra of the Alkali Metals in Ethylenediamine

by Robert R. Dewald¹ and James L. Dye

Kedzie Chemical Laboratory, Michigan State University, East Lansing, Michigan (Received August 12, 1963)

The absorption spectra of the alkali metals in ethylenediamine and the spectra of mixtures of various alkali metal ions with metal solutions are reported. The absorption spectra differ markedly from one metal to another. The species responsible for the various absorption peaks are only slowly interconverted. It is concluded that three types of species are responsible for light absorption, and the presence or absence of any type is a characteristic of the metal.

Introduction

The physical and chemical properties of solutions of alkali metals in liquid ammonia, amines, and ethers have been studied by a large number of investigators. The literature in this field is therefore quite extensive, and the reader is referred to several articles of a review nature for a general survey and additional references.²⁻⁶

The reduction of the solvent with evolution of hydrogen is a major experimental problem, and extreme precautions must be taken to assure the cleanliness and purity of the materials involved. The most stable metal solutions are those in liquid ammonia and these solutions have received the most attention.³ It is now generally agreed that in dilute solutions of the alkali metals in liquid ammonia, the metal is present as ammoniated metal ions and ammoniated electrons. Each electron is believed to exist in a large cavity in the solvent and to be stabilized by orientation and polarization of the ammonia dipoles. The fate of these species as the concentration of metal increases has been interpreted in terms of dynamic equilibria existing among solvated electrons and metal ions and either monomer and dimer units,⁷ or simply electrostatic aggregates of solvated electrons and solvated metal ions.⁸

The properties of amine and ether solutions have generally been explained in terms of the existing theories of metal-ammonia solutions.^{2,9,10} Because of the lower dielectric constant, the species present in metal amine solutions are more highly associated than in liquid ammonia.^{9,10}

There have been many qualitative investigations of the absorption spectra of alkali metals in ammonia and

amines,¹¹ but none has included the absorption spectra of all the alkali metals in a given amine solvent under similar experimental conditions. Windwer and Sundheim⁹ have recently reported the absorption spectra of solutions of sodium, potassium, and rubidium in ethylenediamine. The spectra of sodium and potassium in ethylenediamine had been previously measured by Fowles, McGregor, and Symons.¹¹ The latter authors investigated the absorption spectra of these solutions only up to 1000 m μ , while Windwer and Sundheim examined the range from 300 to 1700 m μ .

Early spectroscopic studies of solutions of the alkali metals in liquid ammonia and in methylamine were carried out by Gibson and Argo.¹² Blades and Hod-

- (1) Work performed in partial fulfillment of the requirements for the Ph.D. degree, Michigan State University, 1963. Paper presented in part before the Division of Physical Chemistry at the 142nd National Meeting of the American Chemical Society, Atlantic City, N. J., September, 1962.
- (2) T. P. Das, "Advances in Chemical Physics," Vol. IV, Interscience Publishers, Inc., New York, N. Y., 1962.
- (3) W. L. Jolly, *Progr. Inorg. Chem.*, **1**, 235 (1959).
- (4) C. A. Kraus, *J. Chem. Educ.*, **30**, 83 (1953).
- (5) M. C. R. Symons, *Quart. Rev. (London)*, **8**, 99 (1959).
- (6) E. C. Evers, *J. Chem. Educ.*, **38**, 590 (1961).
- (7) E. Becker, R. H. Lindquist, and B. J. Alder, *J. Chem. Phys.*, **25**, 971 (1956).
- (8) M. Gold, W. L. Jolly, and K. S. Pitzer, *J. Am. Chem. Soc.*, **84**, 2264 (1962).
- (9) S. Windwer and B. R. Sundheim, *J. Phys. Chem.*, **66**, 1254 (1962).
- (10) D. S. Berns, E. C. Evers, and P. W. Frank, Jr., *J. Am. Chem. Soc.*, **82**, 310 (1960).
- (11) G. W. A. Fowles, W. R. McGregor, and M. C. R. Symons, *J. Chem. Soc.*, 3329 (1957).
- (12) G. E. Gibson and W. L. Argo, *J. Am. Chem. Soc.*, **40**, 1327 (1918).

gins¹³ have reported the spectra of solutions of some of the alkali metals in ammonia, methylamine, and ethylamine. Hohlstein and Wannagat¹⁴ examined the spectra of alkali metals in pure methylamine, pure ethylamine, and mixtures of methylamine and ethylamine with ammonia. Shatz,¹⁵ Eding,¹⁶ and Douthit¹⁷ did further work on the absorption spectra of alkali metals in amine solvents.

It is clear from these studies that solutions of the different alkali metals in amines have quite different optical properties. This paper presents spectral data for solutions of the alkali metals in ethylenediamine and correlates these data with those of other investigators. The interpretation of the results in terms of a new model for metal-amine systems is done in a companion paper.¹⁸

Experimental

Materials. Reagent grade anhydrous ethylenediamine (>99% purity), obtained from Buchs, S. G., Switzerland, was first stored for several days over KOH and then refluxed over a mixture of BaO and KOH in a stream of nitrogen for 2 days. After refluxing, it was distilled in a stream of nitrogen onto sodium wire and lithium pieces. The blue lithium solution formed immediately and was stored for 1 day. The ethylenediamine was then poured into a second distillation flask connected to a 1-m. fractionating column packed with short lengths of 5-mm. glass tubing. The system, including the column, was then evacuated and filled with nitrogen, and the ethylenediamine was refluxed over BaO and KOH in a stream of nitrogen for 2 days and then distilled. The system was designed so that no air came in contact with the ethylenediamine after this stage in the purification. Refluxing and distillation in a nitrogen stream effectively removed traces of ammonia, as indicated by the infrared spectra.

The first fraction of distillate was discarded and the bulk of the ethylenediamine was distilled into a 2-l. flask containing sodium wire and lithium pieces. This flask had been previously evacuated and filled with purified nitrogen. The blue lithium solution was allowed to stand for 1 day, during which time the hydrogen, formed by reaction with dissolved O₂ and H₂O and by decomposition of the solution, was occasionally pumped off. The next flask in the distillation line was connected to the solvent reservoir flask and had a side arm sealed to it which facilitated the distillation of potassium metal. These two flasks were first evacuated and flamed until the pressure stabilized at less than 10⁻⁵ torr. After the potassium metal had been distilled *in vacuo* to form a mirror, the side arm was sealed off and the ethylenediamine was vacuum distilled from the lithium solution onto the potassium.

The receiver flask was cooled with an ice-salt bath. Some potassium dissolved immediately in the ethylenediamine forming a deep blue coloration which lasted for at least several weeks in the presence of excess potassium metal. Portions of ethylenediamine, as needed, were then vacuum distilled into the reservoir flask and covered with purified nitrogen. The purified solvent could be drawn from the reservoir flask into a solution make-up vessel.

Sodium and potassium (E. Merck, A.G., Germany) were obtained in rod form and stored under petroleum hydrocarbons. After washing the metal with dry toluene, the oxides were removed by melting *in vacuo* in a metal degassing and distillation assembly and allowing the melt to pass through constrictions. The metal was then distilled into sample tubes which were sealed off under vacuum. The metal from these tubes was then distilled in an apparatus which facilitated the preparation of fragile glass ampoules as described by Dye, Sankuer, and Smith.¹⁹ Rubidium and cesium (Buchs, S.G., Switzerland) came in sealed ampoules. These metals were also purified by distillation *in vacuo* before transferring them to the fragile glass ampoules. Lithium (E. Merck, A.G., Germany) was stored under mineral oil. Lithium used for solvent purification was only washed with dry toluene. In preparing lithium solutions for measurements, pieces of lithium were cut with a stainless steel knife and forceps from the center of a large piece under toluene. The toluene had previously been dried with sodium wire and lithium pieces and was swept out with argon just prior to cutting the metal. The metal was transferred to the sample make-up vessel while the vessel was being swept out with argon. Reagent grade lithium iodide and lithium chloride (E. Merck, A.G., Germany) were dried at 110° and used without further purification.

Nitrogen used as a covering gas for the solvent was purified by passing it over Cu and CuO at 400°, then through drying towers containing "Ascarite," MgClO₄, and BaO, and finally through a trap containing activated silica gel at liquid air temperatures. The nitrogen was stored on the vacuum line in 2-l. flasks.

Apparatus. Pyrex absorption cells, purchased from

- (13) H. Blades and J. W. Hodgins, *Can. J. Chem.*, **33**, 411 (1955).
- (14) G. Hohlstein and U. Wannagat, *Z. anorg. allgem. Chem.*, **228**, 193 (1956).
- (15) M. H. Shatz, Ph.D. Dissertation, University of Pennsylvania, 1959.
- (16) H. J. Eding, Ph.D. Dissertation, Stanford University, 1952.
- (17) R. C. Douthit, Ph.D. Dissertation, Michigan State University, 1959.
- (18) J. L. Dye and R. R. Dewald, *J. Phys. Chem.*, **68**, 135 (1964).
- (19) J. L. Dye, R. F. Sankuer, and G. E. Smith, *J. Am. Chem. Soc.*, **82**, 4797 (1960).

the American Instrument Co., had nominal path lengths of 0.1 and 1.0 mm. The absorption cell was sealed to a solution make-up vessel. A waste vessel was attached to the apparatus *via* a 19/8 ball joint sealed with Apiezon "W" wax. The entire apparatus was so constructed that solution could be tipped into the absorption cell and then into the waste vessel. This permitted the cell to be rinsed with solution if desired. The solution make-up vessel could be connected to the solvent reservoir flask and the high-vacuum line.

For mixture spectra, the apparatus was modified by attaching a second solution make-up vessel *via* a 19/8 ball joint. In this vessel solutions of metals or lithium salts in ethylenediamine could be prepared. These solutions were then mixed with metal solutions in the delivery tube leading to the absorption cell.

Solution Preparation. The solutions were prepared using two different methods of solvent addition. In the first method, the apparatus, with a metal ampoule and a magnet (sealed in glass) in the solution make-up chamber, was connected directly to the solvent reservoir flask. After evacuation and flaming until the pressure stabilized at less than 10^{-5} torr, the ampoule was broken with the magnet and the solvent was introduced *via* a stopcock. In the second method, more often the case, the apparatus was connected to a distillation flask which was, in turn, connected directly to the solvent reservoir flask. Before attachment, lithium metal was introduced into the distillation flask. The complete assembly was then evacuated and flamed as before, taking care, however, not to heat the lithium. The stopcock between the distillation flask and the absorption cell apparatus was then closed and ethylenediamine was introduced into the distillation flask. The blue lithium solution was allowed to stand for several hours. Finally, after breaking the metal ampoule, the solvent was vacuum distilled into the make-up chamber which was kept at Dry Ice temperature. Upon melting the frozen ethylenediamine, a blue solution readily formed with the metal. It was usually possible to melt a small amount of the solvent not in contact with the metal and transfer this clear solvent to the optical cell. In this way, a small amount of the metal solution could be added to give a solution whose maximum absorbance was less than 2. The absorbance of the saturated solution was too high to permit its measurement directly. Alternatively, a small amount of the solution could be left in the cell and diluted with ethylenediamine by distillation. Finally, in some cases the saturated solution was transferred into the cell and allowed to decompose until the traces were on scale.

Miscellany. For most of the spectral determinations, the glassware was cleaned with hot chromic acid cleaner followed by a hydrofluoric acid cleaner. It was observed that the stability of the solutions increased greatly when the chromic acid cleaning was eliminated. After this observation, all glassware was cleaned first with the hydrofluoric acid cleaner and then with boiling aqua regia.

An oil diffusion pump permitted evacuation to better than 10^{-5} torr as read on a McLeod gage. All stopcocks on the vacuum line were lubricated with Apiezon "N" vacuum grease. Standard taper joints and ball joints were sealed with Apiezon "W" wax. Stopcocks through which liquids were passed were lubricated with Dow Corning high-vacuum silicone grease. Direct contact of mercury vapor with the systems was avoided by using traps.

Determination of Spectra. The spectra were measured with a Beckman DK-2 spectrophotometer at room temperature. Reference cells were filled with pure anhydrous ethylenediamine. The decay of the absorbance as a function of time was followed by allowing the spectrophotometer to cycle as the solutions decomposed. Semilog plots of the absorbance at a given wave length *vs.* time resulted in straight lines or at least smooth curves. This allowed correction of the absorbances at different wave lengths to a common time, thus giving a complete spectrum independent of time. These corrections were normally small and did not alter the shape or peak position significantly. The zero absorbance line, taken to be the trace of the decomposed solution, was also subtracted from the absorbance readings. The absorbance of the decomposed solutions was essentially zero at longer wave lengths, but below about 450 $m\mu$ the absorbance of the decomposed solution became appreciable and continued to rise at shorter wave lengths. Therefore, the relative amount of decomposition product for all of the metals could be estimated from the absorbance of the decomposed solutions.

Results

The wave length range examined and the various absorption maxima are given in Table I. All results reported are qualitative with respect to various peak heights, since analyses were not made. The traces shown in the figures are representative only and many spectra were taken for each metal.

Sodium. Sodium solutions showed only a single peak at 660 $m\mu$ and exhibited only a very small infrared absorption. For example, when the absorbance at 660 $m\mu$ was greater than 2, the absorbance in the infrared was less than 0.03.

Table I: Location of Absorption Maxima in Ethylenediamine^a

Metal	Absorption maximum, $m\mu$
Lithium	660
	1280
Sodium	660
	845
Potassium	660
	845
	1280
Rubidium	660 sh
	890
	1280
Cesium	1030
	1280

^a The range from 400 to 1800 $m\mu$ was scanned for all metals.

Potassium. Potassium solutions in a 0.1-mm. cell showed a broad maximum peaking at 845 $m\mu$ with shoulders in the vicinity of 650 and 1300 $m\mu$. At lower concentrations (using a 1.0-mm. path length), the main absorption was at 660 $m\mu$ with a shoulder at about 840 $m\mu$. Typical traces are given in Fig. 1. Repeated runs at the higher concentrations always gave the 845- $m\mu$ peak. During decomposition in the spectral cell, the 845- $m\mu$ peak in all cases disappeared more rapidly than did the 1280 and 660- $m\mu$ absorption bands. Also, the amount of 660- $m\mu$ absorption varied from one run to another and seemed to increase as the concentration of decomposition products increased. At lower concentrations, for which the maximum occurred

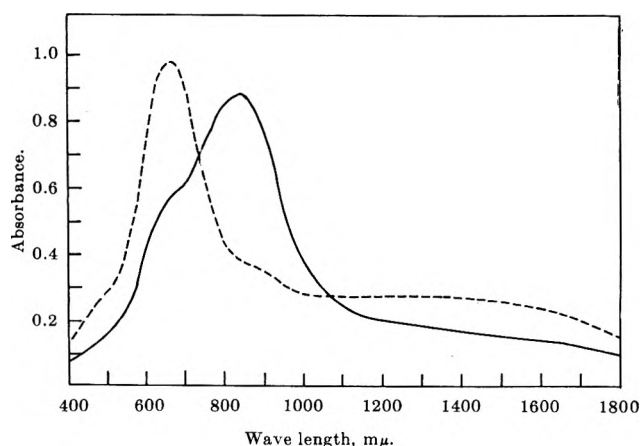


Figure 1. Typical absorption spectra of potassium in ethylenediamine. All spectra were determined at room temperature using a Beckman DK-2 spectrophotometer with automatic slit-width adjustment. Solutions run in the 0.1-mm. cell were generally five to ten times more concentrated than those using the 1.0-mm. cell as indicated by the absorbance: — 0.1-mm. cell (higher concn.), - - - 1.0-mm. cell (lower concn.).

at 660 $m\mu$, the amount of 840- $m\mu$ shoulder also varied from one separate determination to another. In some runs, the 840- $m\mu$ shoulder was rather pronounced, while in others it was small. In all cases, initial 840- $m\mu$ shoulders rapidly disappeared, while the well defined peaks at 660 and 1280 $m\mu$ decayed more slowly. The absorption at 1280 $m\mu$ was always present regardless of the concentration. The intensity of the 1280 peak varied from one run to another, but in most cases the 1280- $m\mu$ absorption band was smaller than either the 845 or the 660- $m\mu$ absorptions.

Rubidium. Rubidium solutions showed a strong absorption peak at 890 $m\mu$ with considerable absorption in the infrared. Under some conditions, a shoulder was also present in the vicinity of 650 to 700 $m\mu$. In these cases, the spectra were similar to the solid curve shown for potassium in Fig. 1 except that the peak occurred at longer wave lengths. Freshly prepared solutions of rubidium had no apparent shoulder in the visible. When new samples were poured into the cell from the vicinity of excess metal, the shoulder tended to appear. In these cases, considerable decomposition product had formed so that an excess of Rb^+ ions were present.

Cesium. Cesium solutions of fairly high concentration, run in the 0.1-mm. cell, showed a maximum at 1030 $m\mu$, as shown in Fig. 2. This absorption band decayed

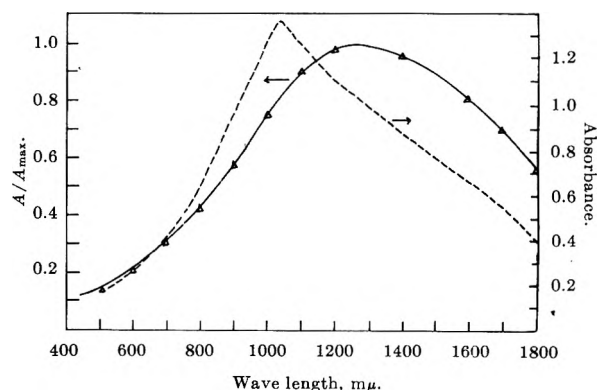


Figure 2. A/A_{max} vs. wave length for the 1280- $m\mu$ peak of cesium in ethylenediamine and spectrum obtained in 0.1-mm. cell showing the 1030 peak: - - - 0.1-mm. cell (fresh soln.), — 1-mm. cell (lower concn.), Δ 0.1-mm. cell (after about 10 min.).

very rapidly (~ 10 min.) leaving an absorption peak at 1280 $m\mu$. When more dilute solutions were studied using a 1-mm. cell, only the 1280 $m\mu$ peak was present as shown in Fig. 2. The absorption band resulting after decomposition of the 1030- $m\mu$ band in the 0.1-mm. cell was identical in shape with the 1280- $m\mu$ band observed in runs using a 1-mm. cell.

Lithium. Lithium solutions generally decomposed more rapidly than solutions of the other alkali metals, probably because lithium could not be purified by distillation. When lithium solutions decomposed, precipitation of the decomposition product usually occurred, which further accelerated the decomposition.

Two absorption maxima (660 and 1280 $m\mu$) were found for lithium in ethylenediamine. In some cases, the 1280- $m\mu$ band was initially much greater than the 660- $m\mu$ band, but in all cases, the infrared band decayed more rapidly leaving a large 660- $m\mu$ absorption. When the cell contained precipitated decomposition product the infrared band disappeared very rapidly. Since in some cases the 1280- $m\mu$ band decayed, leaving only the 660- $m\mu$ peak, it was possible to determine the shape of the 660- $m\mu$ band so that the two absorption bands on other traces could be separated. The traces were first made independent of time by correcting for decomposition as previously described. The contribution of the 660- $m\mu$ absorption band was then subtracted from the total absorbance to give the 1280- $m\mu$ band. The two absorption bands for lithium are shown in Fig. 3 together with other spectra.

In one experiment, blue lithium solution was carefully tipped into the absorption cell from the solution make-up vessel in which a considerable amount of precipitated decomposition product had been present. The spectrum showed only the 660- $m\mu$ peak initially, but as this peak decomposed, the infrared peak built up and finally both peaks decayed as shown in Fig. 4. This shows that the species responsible for the 660- $m\mu$ peak can be converted into the species absorbing at

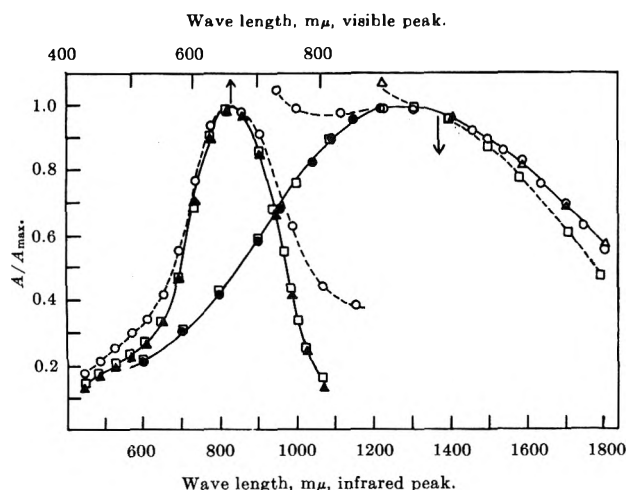


Figure 3. Comparison of the 1280- $m\mu$ absorption band of lithium, potassium, rubidium, and cesium and the 660- $m\mu$ band of sodium, lithium, and potassium, in ethylenediamine: \square , lithium; \blacktriangle , sodium; \circ , potassium; \triangle , rubidium; \bullet , cesium.

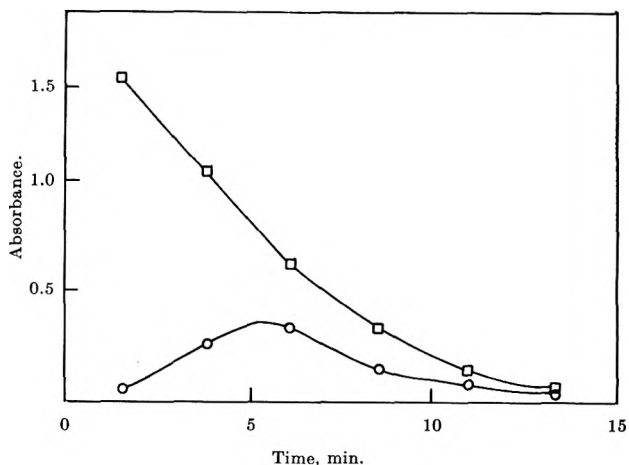


Figure 4. Conversion of 660- $m\mu$ peak into the 1280- $m\mu$ peak for lithium in ethylenediamine (absorbance vs. time): \square , absorbance at 660 $m\mu$; \circ , absorbance at 1280 $m\mu$.

1280 $m\mu$ and that this conversion takes place relatively slowly ($t_{1/2} = 2$ to 4 min.).

Mixture Spectra. The spectral data show that rubidium has only a shoulder at 660 $m\mu$ and that this shoulder becomes more pronounced as the Rb^+ ion concentration increases due to decomposition. On the other hand, cesium has only the 1280- $m\mu$ peak at low concentrations and no peak or shoulder at 660 $m\mu$, even at high concentrations. This suggests that an alkali ion is involved in the 660- $m\mu$ absorbing species and that the low atomic weight metals are preferred. A simple test of this idea involves addition of either lithium or sodium salts to cesium or rubidium solutions to see whether the 660- $m\mu$ peak forms. Generally, the addition of salts like LiCl and LiI markedly increased the rate of decomposition, probably due to impurities in the salts. Another source of lithium or sodium ions is the decomposed solution of the respective metal.

Dilute cesium metal solutions, when mixed with either a lithium chloride solution or a decomposed lithium solution, showed both the 660- $m\mu$ peak and the 1280- $m\mu$ peak. When a solution of rubidium metal was mixed with a decomposed sodium solution, the 660- $m\mu$ absorption band predominated, indicating that the 660- $m\mu$ absorbing species is favored at the expense of the others when sodium ions are present.

Lithium solutions have peaks at 660 and 1280 $m\mu$, while rubidium solutions have the 1280 peak, only a shoulder at 660 $m\mu$, and another peak at 890 $m\mu$. When rubidium and lithium metal solutions were mixed or when rubidium metal solution was added to the decomposition product of lithium, all three peaks were obtained. The spectrum of a solution containing a mixture of lithium metal solution and a decomposed

solution of rubidium again gave the three peaks as well as a solution of lithium iodide mixed with a rubidium solution.

Kinetics of the Decomposition during Absorbance Measurements. The rate of decomposition of the metal-ethylenediamine solutions was studied by following the absorbance as a function of time. It was important that the solutions under study decompose uniformly in the cell proper. This could be determined spectrophotometrically or visually. In some cases it was observed that the decay of the absorbance showed erratic behavior and that there were streaks in the solution between the cell windows, probably because of impurities of the cell walls that catalyzed the decomposition reaction. When this occurred, the cell was rinsed with fresh solution. The rinsing was effective in further cleaning the cell and resulted in uniform decomposition which was then recorded. The decomposition reaction is believed to be surface-catalyzed, since the decomposition rate decreased markedly upon rinsing the cell, and decomposition occurred more rapidly in the absorption cell with its large surface-to-volume ratio than in the waste vessel or the solution make-up vessel.

The decomposition of two independently prepared sodium solutions was strictly first order in the absorbance. In another run, the decay deviated slightly from first-order kinetics, but this may have been due to the presence in this case of a large amount of salt from previous decomposition.

For potassium, the absorbances at different wave lengths did not decay at the same specific rate. Since the absorption bands strongly overlap one another and decay at different specific rates, it is difficult to draw any conclusions about the decomposition kinetics for any single peak. Studies using the 1-mm. cell, which showed only two peaks, fitted a first-order decay law reasonably well.

The optical absorption for rubidium solutions showed essentially first-order behavior. Again, the absorbances at different wave lengths decayed at different specific rates indicating the presence of more than one species.

The decay of the 1280-m μ peak for dilute solutions of cesium fitted first-order kinetics best. The absorbances at different wave lengths decayed at the same specific rate, indicating that the 1280-m μ absorption band is due to a single species. As noted previously, the 1030-m μ absorption band observed in more concentrated solutions disappeared very rapidly.

For lithium solutions, the absorbances at 660 and 1280 m μ decayed at markedly different rates, showing the presence of two species. After the infrared absorbance

had decreased to about 0.05 or lower, the 660-m μ peak decomposed by essentially first-order kinetics.

Discussion

Comparison of Spectra. The 660-m μ peaks for sodium, lithium, and potassium can be compared by plotting A/A_{\max} vs. wave length. Figure 4 shows that the 660-m μ peaks are the same for these metals, both in peak position and in shape. Although the potassium spectrum in Fig. 4 appears to have a different shape, this can be attributed to the contribution of the "tail" of its infrared absorption. The absence of 660-m μ peaks for rubidium and cesium and the results of salt addition to cesium solutions show that the metal is involved in the species responsible for the 660-m μ absorption band. However, from the shape and position of the absorption, we conclude that once a basic metal core is present, the optical transition responsible for the absorption is essentially independent of the metal.

The comparison of the 1280-m μ absorptions is difficult because of the contributions of the other peaks present in the spectra for the different metals. The long-wave length region of the infrared bands can, however, be compared as shown in Fig. 4 by plotting A/A_{\max} vs. wave length, in which A_{\max} is the absorbance at 1280 m μ and A is the absorbance at any given wave length. Within experimental error, cesium, potassium, and rubidium give the same relative absorption spectra from 1300 to 1800 m μ . The tail of the lithium band in this region is slightly below the band for the other metals. This was observed in the spectra of three independently prepared lithium solutions.

The intermediate absorption bands (830-1050 m μ) observed for cesium, rubidium, and potassium solutions resemble one another in shape but are displaced in position. We conclude, therefore, that the species involved in these absorption bands are similar in nature but depend on the metal. That the metal is involved in this species is shown by the fact that when lithium metal solution was added to the decomposition product of rubidium solutions (containing Rb^+ , but no Rb metal), the 660-, 890-, and 1280-m μ peaks were all observed.

Comparison with the Work of Other Investigators. Fowles, McGregor, and Symons¹¹ reported the absorption spectra of sodium and potassium in ethylenediamine up to 1000 m μ . Their results for the spectra in the visible region for dilute solutions of these metals are in general agreement with this work. More recently, Windwer and Sundheim⁹ reported that no absorption could be detected in the infrared region for solutions of lithium, potassium, and rubidium in ethyl-

enediamine. This is in conflict with the spectral results reported in this work.

Because it is difficult to prepare reasonably stable solutions, the differences observed by various workers are not as surprising as might be thought. Traces of impurities can catalyze the decomposition and affect the results obtained. In the case of rather unstable solutions, we conclude that the reported properties might well be the properties of species that decompose rather slowly compared with the species absorbing in the infrared. For example, this work has shown that the conversion of the 660- $m\mu$ species into the infrared absorbing species is a relatively slow process. Another indication of this effect is that Windwer and Sundheim⁹ were unable to obtain cesium solutions stable enough for even simple spectral studies. Since dilute cesium solutions exhibit only the infrared absorption band, this seems to indicate that in their experiments, the decomposition of the infrared-absorbing species was quite rapid. It should also be noted that Dainton, *et al.*,²⁰ report considerable absorption at 1000 $m\mu$ in addition to a 700- $m\mu$ band for solutions of potassium in ethers, whereas Cafasso and Sundheim²¹ reported only the 700- $m\mu$ peak for the same system.

The absorption spectra for solutions of lithium¹⁵ and potassium¹⁶ in methylamine have been reported. Analysis of these data shows that the absorption spectra for lithium and potassium in methylamine are essentially the same as we have found for these metals in ethylenediamine. The stability of metal-methylamine solutions is greater because studies can be made at low

temperatures. Since the results reported in this work are in agreement with the observations reported in methylamine and considering the arguments given above, it seems reasonable to conclude that Windwer and Sundheim⁹ have reported only the optical properties of the most stable species present in these solutions, and that their experimental conditions tended to decompose the species which absorb in the infrared.

The results reported in this paper, particularly the slow conversions, which had also been observed by Eding,¹⁶ forced a re-examination of the general models for metal-amine solutions. We have proposed a model which is in agreement with these observations and those of other investigators. The details of this model are presented in a companion paper.¹⁸

Acknowledgments. The experimental work described in this paper was done at the Max Planck Institut für physikalische Chemie, Göttingen, West Germany. The authors wish to thank Dr. Manfred Eigen for his kind invitation to work in this laboratory as well as the many personnel of the Institut who made their talents available to us. We particularly wish to acknowledge the assistance of Dr. Kahlweit in obtaining spectra. Part of this work was done under a Science Faculty Fellowship from the National Science Foundation (J. L. D.), and it was also supported, in part, by the U. S. Atomic Energy Commission (Contract AT-(11-1)-958).

(20) F. S. Dainton, D. M. Wiles, and A. N. Wright, *J. Chem. Soc.*, 4283 (1960).

(21) F. A. Cafasso and B. R. Sundheim, *J. Chem. Phys.*, **31**, 809 (1959).

Solubilities and Conductances of Alkali Metals in Ethylenediamine

by Robert R. Dewald¹ and James L. Dye

Kedzie Chemical Laboratory, Michigan State University, East Lansing, Michigan (Received August 12, 1968)

The conductances of cesium, rubidium, potassium, and sodium in ethylenediamine have been measured at room temperature as a function of concentration. The equivalent conductance for solutions of cesium, potassium, and rubidium showed the same general concentration dependence while that for sodium solutions exhibited a marked difference in behavior. The *apparent* limiting values of the equivalent conductances of cesium, potassium, and rubidium solutions were evaluated using the Shedlovsky conductance function, and values of 204, 139, and 117 kohlrusch units, respectively, were obtained. The solubilities of the alkali metals in ethylenediamine were also determined.

Introduction

The absorption spectra of solutions of lithium, sodium, potassium, and cesium in liquid ammonia measured up to 0.03 *M* at the absorption maximum and up to 0.2 *M* at other wave lengths have recently been reported by Gold and Jolly.² Their results showed that the alkali metal spectra are practically identical and follow Beer's law from 350 to 1800 $m\mu$ over the concentration range investigated. Conductivities of dilute solutions of sodium and potassium in liquid ammonia are nearly the same,³ and the small differences which do occur may be attributed to the different conductivities of the solvated metal ions.

Metal solutions in amine solvents exhibit absorption spectra which are markedly different from those of metal-ammonia solutions.⁴⁻⁶ Spectroscopic data for solutions of metals in amines and in mixed solvents show the presence of one to three very intense absorption bands depending upon the alkali metal. One of these is in the visible region ($\sim 600-700 m\mu$), one in the near-infrared region ($\sim 800-1000 m\mu$), and the other in the infrared region ($\sim 1200-1500 m\mu$), while metal-ammonia solutions exhibit only an infrared absorption band with a maximum near 1500 $m\mu$.

Conductivities of the different alkali metals in a given amine solvent cannot be readily compared because of the limited conductance data available. Gibson and Phipps⁷ reported the conductance of potassium and cesium in methylamine, but their data have been questioned⁸ because of the probable presence of impurities which tended to decompose their solutions.

Evers, Young, and Panson⁸ made a careful study of the conductance of lithium in methylamine at high concentrations. Later, Berns, Evers, and Frank⁹ successfully reproduced their experimental data in more dilute solutions using a conductance function that had been previously derived by Evers and Frank¹⁰ and used to fit the data of Kraus³ for solutions of sodium in ammonia. This conductance function uses the same mass action equations as Becker, *et al.*,¹¹ and a modified form of the Shedlovsky conductance function.

Since the different metal solutions in a given amine solvent have different spectra, it was thought that they might also show differences in conductance. There-

- (1) Work performed in partial fulfillment of the requirements for the Ph.D. degree, Michigan State University, 1963. Paper presented in part before the Division of Physical Chemistry at the 145th National Meeting of the American Chemical Society, New York, N. Y., September, 1963.
- (2) M. Gold and W. L. Jolly, *Inorg. Chem.*, **1**, 818 (1962).
- (3) C. A. Kraus, *J. Am. Chem. Soc.*, **43**, 749 (1921).
- (4) G. W. Fowles, W. R. McGregor, and M. C. R. Symons, *J. Chem. Soc.*, 3329 (1957).
- (5) T. P. Das, "Advances in Chemical Physics," Vol. IV, Interscience Publishers, Inc., New York, N. Y., 1962.
- (6) R. R. Dewald and J. L. Dye, *J. Phys. Chem.*, **68**, 121 (1964).
- (7) G. E. Gibson and T. E. Phipps, *J. Am. Chem. Soc.*, **48**, 312 (1926).
- (8) E. C. Evers, A. E. Young, and A. J. Panson, *ibid.*, **79**, 5118 (1957).
- (9) D. S. Berns, E. C. Evers, and P. W. Frank, Jr., *ibid.*, **82**, 310 (1960).
- (10) E. C. Evers and P. W. Frank, Jr., *J. Chem. Phys.*, **30**, 61 (1959).
- (11) E. Becker, R. H. Lindquist, and B. J. Alder, *ibid.*, **25**, 971 (1956).

fore, we measured the conductances of alkali metal-ethylenediamine solutions as a function of concentration. Windwer and Sundheim¹² have reported the electrical conductivity of a solution of potassium in ethylenediamine as a function of optical absorbance. With greater accuracy, we have measured the conductances of sodium, potassium, cesium, and rubidium solutions up to saturation. In addition, the solubilities of the alkali metals in ethylenediamine were determined at room temperature.

Experimental

Materials. Purification of materials has been described in the previous paper.⁶

Apparatus. The assembly used in this work was specifically designed for the study of the conductance of these rather unstable systems. It was possible to correct the raw data for decomposition so that the major difficulty encountered in these systems could be overcome. The apparatus is shown in Fig. 1. A solution flask (500-ml.) with a side arm for metal distillation was attached to the solvent reservoir flask of the ethylenediamine purification train, the decomposition vessel of the gas analysis assembly, and the high-vacuum line.

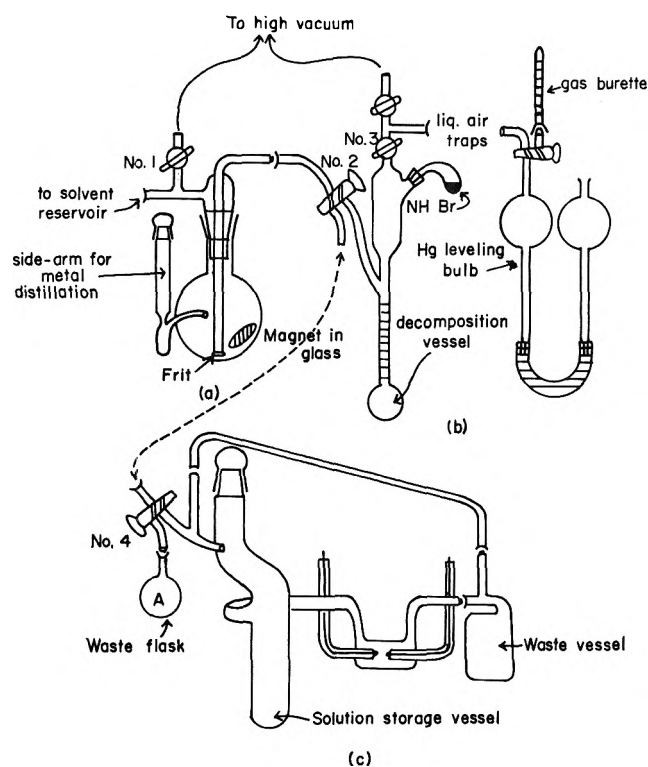


Figure 1. Assembly for conductance and solubility measurements: (a), metal solution make-up flask; (b), gas analysis assembly; (c), conductivity cell apparatus.

A conductance cell with small platinum ball electrodes was constructed of soft glass. The cell was sealed *via* a graded seal to a Pyrex storage vessel and *via* a ball joint to a waste vessel (Fig. 1). The entire apparatus was so constructed that solution could be tipped into the conductivity cell and then into the waste vessel. This allowed rinsing the cell with solution if desired. The cell constant was determined using a series of standard KCl solutions. Conductivity was measured with a Siemens Wheatstone bridge at 100,000 c.p.s. The conductances were determined at room temperature (23–25°) without temperature control since the main source of error was considered to result from decomposition of the solutions.

The gas analysis assembly consisted of a decomposition vessel, two liquid nitrogen traps, a leveling bulb with mercury, and a gas buret.

Operation. A glass tube or capillary of purified metal was broken and introduced into the side arm of the solution make-up vessel. The complete assembly, including the gas analysis apparatus, was then evacuated and flamed until the pressure stabilized at less than 10^{-5} torr. After sealing off the side arm under vacuum, the metal was vacuum distilled into the bottom of the 500-ml. make-up flask. Next, stopcocks 1, 2, and 3 (Fig. 1) were closed and the purified ethylenediamine was introduced into the make-up flask *via* the stopcock on the solvent reservoir flask. The blue solution which formed immediately was then degassed by the high vacuum system through a liquid air trap and stirred constantly with a magnet sealed in glass for about 10 min. after all metal had apparently dissolved.

In preparing saturated solutions of the metals, a large excess of metal was distilled into the make-up flask. The solution was left in contact with the excess metal for 2 hr. with continuous pumping and stirring before transfer. Using this technique, consistent solubilities and conductance values were obtained. Earlier runs had shown that saturation is only slowly attained.

After the blue solution had been degassed, previously purified nitrogen or argon gas, which was stored in 2-l. flasks on the vacuum line, was introduced *via* stopcock 1. The gas pressure forced the blue solution through the frit such that the solution filled the delivery tube up to stopcock 2. The first fraction of the solution was then transferred into the waste flask (A) of the conductivity apparatus *via* stopcocks 2 and 3. Then, the next fraction of the solution was transferred into the decomposition vessel. Finally, the remainder of the

(12) S. Windwer and B. R. Sundheim, *J. Phys. Chem.*, **66**, 1254 (1962).

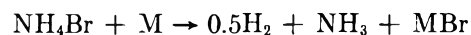
blue solution was transferred into the storage vessel of the conductivity cell apparatus. The time of transfer was recorded. The total time required to make the complete solution transfer was normally less than 15 sec.

Conductivity Readings. Immediately after solution transfer, the conductivity cell was disconnected and the electrodes of the cell were rinsed with blue solution, and then the cell was filled. The resistance was recorded as a function of time for about 1 hr. After this time, the solution was transferred into the waste vessel and a new sample was tipped into the cell for further measurements. The conductivity of the second sample was always lower than the first because of decomposition of the solution in the storage vessel of the conductivity cell apparatus. It has been reported^{4,12} that platinum acts catalytically on the alkali metal-ethylenediamine solutions, accelerating the decomposition. This was also observed in this work, and the rate of decrease of the specific conductance with time was usually two to four times greater in the conductance cell than in the storage vessel. We also observed that during vigorous shaking, the conductance of the solution increased noticeably. This suggests that the solution in the vicinity of the electrodes differs in nature from the solution in the bulk because of decomposition. Before and during each conductivity reading, therefore, the cell was shaken vigorously until the highest steady conductivity reading was obtained.

The log of the specific conductivity is a linear function of time, consistent with the decomposition behavior observed in the spectral cell which also showed essentially first-order decay. The specific conductance as a function of time could be extrapolated back to the time of transfer into the conductance cell. The several values at transfer could then be extrapolated to the time of initial transfer into the storage vessel which was also the time of transfer into the analysis vessel. Usually, this final correction amounted to less than 2% of the initial conductivity reading and normally the conductivity decreased between 5 and 20% during the first hour.

Concentration Determinations. The volume of the solution transferred into the calibrated decomposition vessel was noted. Solid ammonium bromide was then tipped, *via* a side arm, into the blue solution. The evolved H₂ gas was then pumped through two liquid nitrogen traps using a mercury leveling bulb, and collected in a gas buret in which the volume and pressure were measured. During the pumping, the liquid in the decomposition vessel was frozen slowly to ensure removal of all the hydrogen from the decomposed solution. This freezing and pumping process

was repeated until the reading became constant. Usually after the first freezing, no more hydrogen could be pumped off by repeated freezing, melting, and pumping. Finally, the amount of metal could be determined from the stoichiometry of the reaction



To ascertain that this was indeed the correct stoichiometry, a weighed sample of potassium was partially distilled into the analysis vessel and the amount remaining in the side arm was determined by titration. The amount of hydrogen collected agreed with that calculated to within 1%. This method of analysis has the advantage that metal present as decomposition products can be distinguished from the metal present in the zero oxidation state. A number of decompositions were made using water instead of NH₄Br and gave the same results. Mass spectrometric analysis of the gas obtained from the decomposition showed only hydrogen to be present. However, when the solution was allowed to decompose without adding NH₄Br, requiring several days, mass spectrometry showed the presence of significant amounts of low molecular weight decomposition products of ethylenediamine in addition to the hydrogen.

Lithium Conductivity. Since lithium cannot be melted in glass, a bent side arm was attached to the solution make-up flask by a standard taper joint so that it could be rotated into an upright position to tip the metal into the previously evacuated and flamed flask. The lithium metal solution was stirred and pumped on for 20 min. before transfer. Only the conductance of the saturated solution was studied because of the instability of the lithium solutions. Also, these solutions were extremely unstable when in contact with platinum.

Results

Solubility. The solubilities of the alkali metals in ethylenediamine are given in Table I. It was noted that excess sodium, potassium, and rubidium had no noticeable effect on the stability of the solutions, while excess cesium metal appeared to catalyze the decomposition reaction.

Conductance. The values of Λ , κ , and C are given in Table II. The equivalent conductance, Λ , is expressed in kohlrusch units, the specific conductance, κ , in ohms⁻¹ cm.⁻¹, and the concentration, C , in moles per liter. The values of Λ for sodium, potassium, rubidium, and cesium are plotted *vs.* $C^{1/2}$ in Fig. 2. Log-log plots of the specific conductance *vs.* concentration (illustrated by Fig. 3) for these same metals give straight lines, and potassium, rubidium, and cesium have the same

Table I: Solubilities of the Alkali Metals in Ethylenediamine at Room Temperature

Metal	Run no.	Solubility, mole/l.	Average solubility, ^a mole/l.
Lithium	1	0.283	0.287 ± 0.015
	2	0.264	
	3	0.314	
Sodium	1a	2.37 × 10 ⁻³	2.39 ± 0.04 × 10 ⁻³
	1b	2.35 × 10 ⁻³	
	2	2.45 × 10 ⁻³	
Potassium	1a	1.02 × 10 ⁻²	1.04 ± 0.02 × 10 ⁻²
	1b	1.03 × 10 ⁻²	
	2	1.05 × 10 ⁻²	
Rubidium	1	1.07 × 10 ⁻²	1.31 ± 0.02 × 10 ⁻²
	2	1.29 × 10 ⁻²	
	2	1.33 × 10 ⁻²	
Cesium	1	5.43 × 10 ⁻²	5.4 × 10 ⁻²

^a The limits of precision given are average deviations from the mean.

Table II: Conductance-Concentration Data for Solutions of Alkali Metals in Ethylenediamine

Metal and run no.	Concentration, moles/l. × 10 ³	Specific conductance × 10 ⁸	Equivalent conductance
Cs-1	54.3	1420	26.2
Cs-2	48.9	1350	27.7
Cs-5	20.8	742	35.6
Cs-6	7.65	342	44.8
Cs-3	3.55	193	54.4
Cs-7	1.68	113	67.3
Cs-4	0.960	78.6	81.8
Na-2	2.45	62.5	25.5
Na-1b	2.35	60.0	25.5
Na-4	1.04	27.0	25.9
Na-3	0.242	6.36	26.3
K-3	10.7	301	28.1
K-2	10.5	297	28.2
K-1b	10.3	299	29.0
K-10	6.02	201	33.4
K-6	3.68	139	37.8
K-8	3.66	135	36.9
K-4	2.43	103	42.5
K-9	2.37	99.0	42.7
K-5	2.10	92.6	44.1
K-7	2.04	90.8	44.5
K-11	0.416	29.7	71.3
K-12	0.135	12.1	89.7
Rb-1	13.3	321	24.2
Rb-7	6.94	199	28.7
Rb-2	2.85	102	35.8
Rb-6	2.78	98.6	35.5
Rb-3	1.78	70.0	39.5
Rb-5	0.696	35.0	50.3
Rb-4	0.525	30.6	58.3
Li-3	314	15300	48
Li-4	287 ^a	14000	49

^a The average solubility value. Lithium results are only semiquantitative.

The specific conductivity for the concentration range investigated may be expressed by the function

$$\log \kappa = a \log C + b$$

Spectral data showed that solutions tend to decay by a first-order rate law, so that

$$\log C = -kt + d$$

If the decomposition in the conductance cell is also first order, we have

$$\log \kappa = -(k/a)t + (d - b)$$

so that the decay of conductance is consistent with first-order decomposition.

Lithium Conductivity. Semilog plots of the specific conductance vs. time for lithium solutions display

slope but are displaced from one another, while sodium gives a straight line with a different slope. It should be emphasized that each value given in Table II and shown in Fig. 2 represents an independent solution make-up.

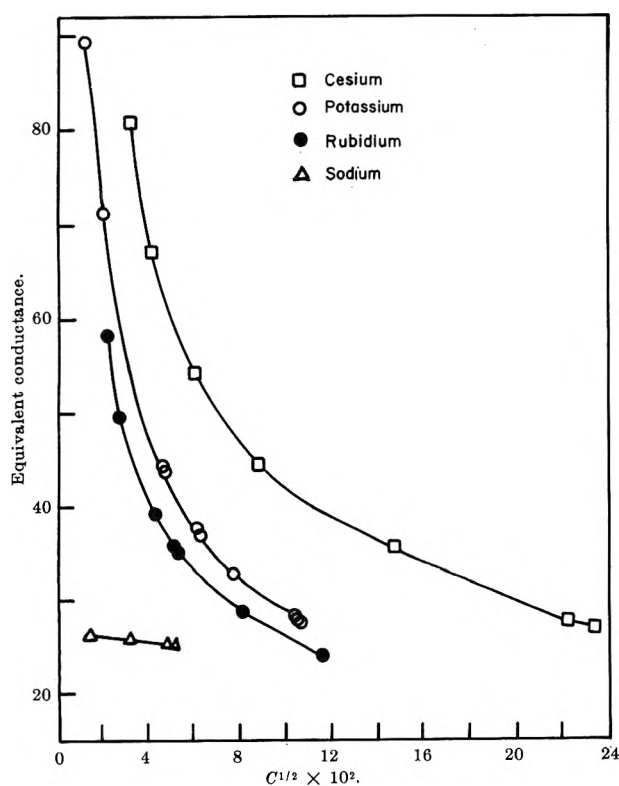


Figure 2. Equivalent conductance vs. $C^{1/2}$ for sodium, potassium, rubidium, and cesium in ethylenediamine.

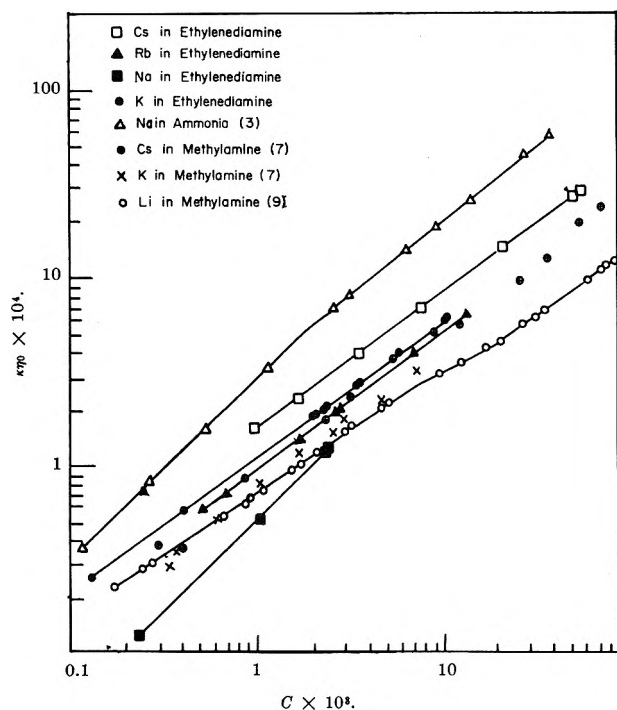


Figure 3. Comparison of the conductance curves for metal-amine systems (log-log plot of $\kappa\eta_0$ vs. C); κ = specific conductance, η_0 = viscosity of the solvent.

three distinct decay rates before the solution is totally bleached. Initially, the decay rate was similar to, but faster than, the rate observed for the other metals and was, of course, accelerated by the catalytic effect of the platinum. After 10–20 min., the specific conductance dropped by about two orders of magnitude within 1 or 2 min. Finally, the lower specific conductance decreased more slowly until it reached the value of the bleached solution. When lithium solutions decompose, precipitation occurs and the lithium spectral data show that precipitate formation results in rapid disappearance of the infrared absorption. The behavior observed during lithium decomposition in the conductance cell is explained as follows. The solutions decompose normally until precipitation occurs. When the precipitate forms near the platinum electrodes, it then speeds the decomposition and results in further precipitation. The infrared species then is rapidly destroyed by the precipitate. This rapid removal of the infrared species causes a sudden drop in the conductivity, followed by a slower decrease as the visible species decomposes. This is in keeping with the idea that the infrared species is the main contributor to the conductivity of the solution.

Conductivity of Decomposed Solutions. The resistances of the solutions approached constant values as the blue color disappeared. The remaining con-

ductivity is considered to be due to metal ions and ethylenediamide ions which result from the decomposition reaction. Conductivity data for the decomposed solutions are given in Table III. These data are of interest because they emphasize the low equivalent conductances of the decomposition products, consistent with the low conductance found for sodium ethanolamide¹³ in ethylenediamine. It is evident from these data that a small accumulation of decomposition product in a metal-ethylenediamine solution would lead to no significant error in the conductance attributed to the metal in the zero oxidation state.

Table III: Conductance-Concentration Data for Decomposed Solutions of Sodium, Potassium, Rubidium, and Cesium in Ethylenediamine

Metal	Concentration, moles/l. $\times 10^3$	Specific conductivity $\times 10^6$	Equivalent conductivity
Cesium	54.3	96.0	1.76
	48.9	87.4	1.78
	20.8	72.5	3.31
	1.68	11.4	6.80
Sodium	2.45	6.40	2.61
	2.35	5.88	2.50
	1.04	3.26	3.13
	0.242	1.06	4.38
Potassium	10.7	31.7	2.96
	10.5	27.3	2.60
	10.3	30.3	2.94
	2.82	12.7	4.67
	2.42	12.3	5.06
	2.10	10.1	4.82
	0.412	3.36	8.16
Rubidium	0.138	2.12	15.4
	13.3	38.7	2.91
	12.9	37.4	2.90
	6.92	22.8	3.29
	2.78	12.7	4.57
0.497	4.89	9.85	

Discussion

Comparison of Conductance Curves. The general form of the conductance curves for potassium, rubidium, and cesium in ethylenediamine is similar to that for alkali metals in methylamine but differs somewhat from that of sodium in liquid ammonia. A method of comparing the different systems, which tends to correct for differences in viscosity, is to plot the log of the product of the specific conductance and viscosity vs. the log of the concentration as shown in Fig. 3. This

(13) W. B. Schaap, R. E. Bayer, J. R. Siefker, J. Y. Kim, P. W. Brewster, and F. C. Schmidt, *Record Chem. Progr.*, **22**, 197 (1961).

figure shows that cesium-amine systems tend to be better conductors than systems of the other alkali metals in amines. It should be noted that the data of Berns⁹ show a deviation from the usual straight-line log-log plot at about 0.02 *M* and then continue at higher concentrations with a straight line having the same slope as before. It is tempting to attribute this anomalous behavior to a systematic error introduced in measurements in the high concentration region. However, the results of a number of runs are consistent.

The conductance behavior of sodium in ethylenediamine (Fig. 2 and 3) differs markedly from that of the other alkali metals in amines. The equivalent conductance of sodium solutions is much lower than for the other alkali metals in ethylenediamine and is almost independent of concentration over the tenfold concentration range investigated. This indicates that the number of current carriers is proportional to the concentration and that the mobility is nearly independent of concentration. Such behavior would not be expected for conventional electrolytes in this medium since extensive ion-pairing would cause the equivalent conductance to be strongly concentration-dependent.

The apparent limiting values of the equivalent conductances, Λ_0 , were evaluated by using the method of Shedlovsky.¹⁴ Also, the apparent pairing constants, K_1 , for solutions of potassium, rubidium, and cesium in ethylenediamine were evaluated. Constants used for the Shedlovsky analysis of the data were $\eta_0 = 1.54 \times 10^{-2}$ poise and $D = 12.9$, where η_0 and D are, respectively, the viscosity and dielectric constant of the solvent. To compute activity coefficients, the extended Debye-Hückel expression

$$\log f_{\pm} = \frac{-7.64\sqrt{C_i}}{1 + 4.86\sqrt{C_i}}$$

was used. This corresponds to a closest approach distance of 6.0 Å. The results for potassium, rubidium, and cesium are plotted in Fig. 4. The intercept and slope, from which apparent values of Λ_0 and K_1 were obtained, were determined by the method of least squares for each set of points in Fig. 4. In order to have enough points in the dilute region for cesium, it was necessary to estimate κ by extrapolation of the log-log plot of specific conductance *vs.* concentration (Fig. 3). This is felt to be valid in view of the data for potassium and rubidium at low concentrations.

Evers and Frank¹⁰ have evaluated the limiting equivalent conductance and the pairing constant for the sodium-ammonia system and Berns⁹ has done so for the lithium-methylamine system. These values, as well as the values obtained in this work, are given in

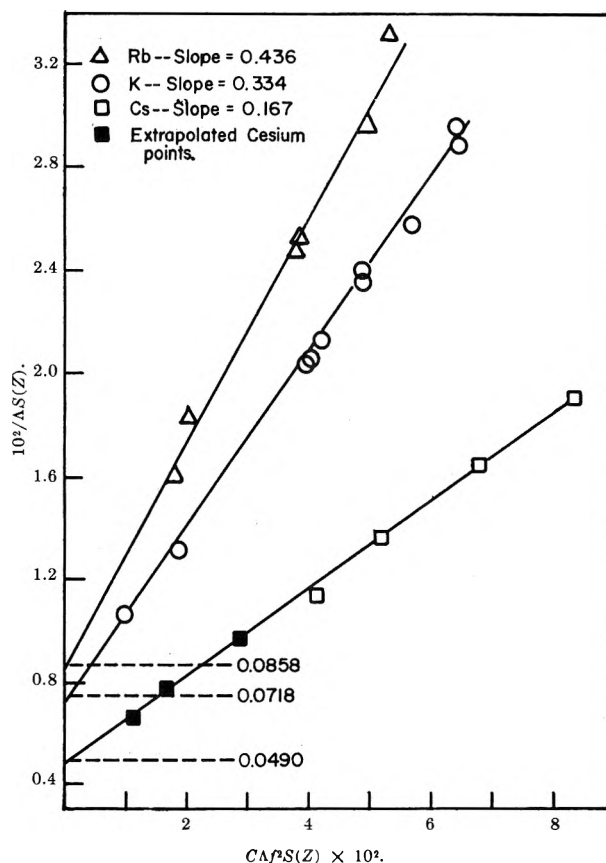


Figure 4. Shedlovsky analysis plots for cesium, potassium, and rubidium in ethylenediamine.

Table IV. The value of Λ_0 for lithium in methylamine reported by Berns may be too high. When the five highest concentration points are eliminated (which also fall in the anomalous region of the plot of $\log \kappa$ *vs.* $\log C$ using the data of Berns), one obtains a value for Λ_0 of about 180 rather than 228.

Table IV shows that the Walden product, $\Lambda_0\eta_0$,

Table IV: Comparison of Limiting Equivalent Conductances

Solvent	Metal	Λ_0	$\Lambda_0\eta_0$	K_1
Ethylenediamine ^a	Cesium	204	3.14	1.44×10^{-4}
	Potassium	139	2.14	1.54×10^{-4}
	Rubidium	117	1.80	1.69×10^{-4}
	Sodium	27 ^b
Methylamine ^c	Lithium	228.3	2.07	5.5×10^{-6}
Ammonia ^d	Sodium	1022	2.61	7.23×10^{-3}

^a Referred to in this work. ^b Estimated from a plot of Λ *vs.* $C^{1/2}$. ^c See ref. 9. ^d See ref. 10.

(14) T. Shedlovsky, *J. Franklin Inst.*, 225, 739 (1938).

for cesium in ethylenediamine is somewhat larger than for the sodium-ammonia system while the Walden products for the other metals in amines are considerably lower than this. Since the spectra of dilute cesium-ethylenediamine solutions exhibit only an infrared absorption band and the conductance behavior appears to be similar to that of the sodium-ammonia system, we conclude that the conductance processes for these two systems are essentially the same. The spectra of dilute solutions of potassium and rubidium in ethylenediamine show absorption bands other than the infrared absorption band. If the contribution to the total conductivity of these species is small and essentially a constant fraction over the concentration range investigated, one concludes that the major contributor to the conductivity of these solutions is the infrared absorbing species. This requires that the general form of the conductance curves be the same for rubidium, potassium, and cesium in ethylenediamine. This is shown to be the case in Fig. 2 and 3. The ion-pair constants given in Table IV are essentially the same for these three metals, and this further indicates the same conduction process. The dissociation con-

stant for sodium in liquid ammonia is somewhat larger than for these metals in ethylenediamine. This would be expected, however, on the basis of the higher dielectric constant of ammonia. The large differences in the apparent limiting equivalent conductance values are difficult to understand and seem to indicate that the other species besides the infrared absorbing species which are present in the metal-ethylenediamine systems either do not dissociate into solvated electrons and solvated metal ions at the dilutions studied, or else that the cation has a strong influence upon the mobility of the solvated electron.

Acknowledgments. The experimental work described in this paper was done at the Max Planck Institut für physikalische Chemie, Göttingen, West Germany. The authors wish to thank Dr. Manfred Eigen for his kind invitation to work in this laboratory as well as the many personnel of the Institut who made their talents available to us. Part of this work was done under a Science Faculty Fellowship from The National Science Foundation (J. L. D.), and it was also supported in part, by the U. S. Atomic Energy Commission (Contract AT(11-1)-958).

A Model for Metal-Amine Solutions

by James L. Dye and Robert R. Dewald

Kedzie Chemical Laboratory, Michigan State University, East Lansing, Michigan (Received August 12, 1963)

A general model is proposed to describe the nature of metal-amine solutions. Three types of species are suggested: (1) solvated electrons similar to those in metal-ammonia solutions are responsible for the infrared absorption band and are the main contributors to the conductivity; (2) covalent dimers, similar to those existing in the gas phase for the alkali metals, form in solutions of K, Rb, and Cs and are responsible for the intermediate absorption; (3) combination of a solvated molecule-ion, M_2^+ , with an electron trapped in the field of this ion gives rise to the absorption at 650–750 $m\mu$ commonly found in metal-amine solutions. Semiquantitative thermodynamic calculations are presented which lend support to the model proposed and help to explain the diversity of behavior observed for the different alkali metals in a variety of solvents.

Introduction

The studies of metal-ethylenediamine solutions reported in the preceding papers^{1,2} prompted us to re-examine the models proposed for metal-amine solutions in general. While no complete theory for these systems has appeared in the literature, some attempts have been made to describe the nature of the various species. In spite of the complexity of the spectra, including the appearance of several bands not found for metal-ammonia solutions, the tendency has been to extend or modify the existing theories of metal-ammonia solutions. Thus, Blades and Hodgins³ proposed the existence of "amine-type" and "aliphatic-type" traps as well as intermediate types to explain their spectral results in methylamine and ethylamine. The "traps" were assumed to be similar to those of the cavity model in ammonia.⁴ Symons has suggested⁵ that the visible absorption (650–750 $m\mu$) is associated with a diamagnetic species such as the dimer of the model of Becker, Lindquist, and Alder.⁶ Cafasso and Sundheim⁷ present results for solutions of the alkali metals in ethers which seem to fit the general description given by Symons. These authors also stress the importance of a well defined negative cavity for the cations as a prerequisite to solubility. Recently, Windwer and Sundheim⁸ have postulated that the visible (650 $m\mu$) absorption is due to a species which shows no e.s.r. absorption, and that the intermediate absorptions (800–900 $m\mu$) for K and Rb solutions might be associated with a dimer.

Dainton, Wiles, and Wright⁹ have presented strong evidence that the visible absorption peak for potassium in dimethoxyethane and tetrahydrofuran arises from the heterogeneous nature of the "solution." They were able to decrease the absorbance repeatedly by centrifugation of the solution. This suggests that the "solutions" are really colloidal in nature. While this may be the case in these solvents, the reproducibility of our solubility and conductance data for ethylenediamine solutions rules out the colloidal hypothesis for these systems. The results of Dainton, *et al.*, are discussed later in this paper in the light of the present model.

Undoubtedly much of the difficulty associated with these systems arises from the conflicting experimental results which have been reported by different investigators and the lack of reproducibility of results by a

- (1) R. R. Dewald and J. L. Dye, *J. Phys. Chem.*, **68**, 121 (1964).
- (2) R. R. Dewald and J. L. Dye, *ibid.*, **68**, 128 (1964).
- (3) H. Blades and J. W. Hodgins, *Can. J. Chem.*, **33**, 411 (1955).
- (4) R. A. Ogg, Jr., *Phys. Rev.*, **69**, 668 (1946).
- (5) M. C. R. Symons, *J. Chem. Phys.*, **13**, 99 (1959); *Quart. Rev. (London)*, **30**, 1628 (1959).
- (6) E. Becker, R. H. Lindquist, and B. J. Alder, *J. Chem. Phys.*, **25**, 971 (1956).
- (7) F. A. Cafasso and B. R. Sundheim, *ibid.*, **31**, 809 (1959).
- (8) S. B. Windwer and B. R. Sundheim, *J. Phys. Chem.*, **66**, 1254 (1962).
- (9) F. S. Dainton, D. M. Wiles, and A. N. Wright, *J. Chem. Soc.*, 4283 (1960).

given investigator.^{1,8,10} These disparities probably arise because of slow conversions of one species into another.

The model presented here is necessarily complex. Even solutions of metals in ammonia, which show only one absorption peak, are thought to contain a minimum of four important species: (1) the cation of the alkali metal, (2) the solvated electron or polaron, (3) the ion-pair or monomer, and (4) the ion quadrupole or dimer.^{11,12} While we believe these species to be present in amine solvents as well, they cannot account for the visible absorption bands, and we postulate in addition the existence of gas-like covalent dimers and electrons trapped by one-electron bonded M_2^+ ions. In spite of the complexity of the model, many diverse experimental results can be explained by it, and the species proposed are at least plausible on thermodynamic grounds.

Experimental Basis for the Model

The spectra of metal-amine solutions clearly require a minimum of three types of absorbing species. For example, potassium and rubidium show three absorption regions having different relative intensities under different conditions. The rate at which the absorbance decays during decomposition varies from one peak to another and from one sample to another so that the spectra cannot arise from fewer than three absorbing species. The shape and position of the absorption peak at $660\text{ m}\mu$ are both independent of the metal, but the intensity of this peak relative to the infrared absorption depends strongly upon the metal, and the peak does not appear at all for solutions of cesium in ethylenediamine. Similarly, the shape and position of the infrared absorption appear to be practically the same for all metals, but sodium shows very little infrared absorption. The position of the intermediate absorption band observed for potassium, rubidium, and cesium solutions depends upon the metal.

The various species are only slowly interconverted. This is most striking in the case of lithium in which the half-time for the conversion is at least several minutes. Other investigators have also commented upon the different decay rates for different spectral bands.^{8,10}

Experiments in which a solution containing one of the alkali metals is mixed with a salt solution of another alkali metal show that the various species are interconvertible and that the $660\text{ m}\mu$ and intermediate species at least depend upon the metal. For example, when a solution of Rb in ethylenediamine (which shows only a shoulder at $660\text{ m}\mu$) is added to a solution containing Na^+ (but not Na), an intense peak appears at $660\text{ m}\mu$. Conversely, when a solution of Li is added to a solution

containing Rb^+ , the peak at $890\text{ m}\mu$, characteristic of Rb solutions, is obtained.

As discussed in the preceding papers,^{1,2} the results obtained by other investigators in a number of solvents can be correlated with our results in ethylenediamine if one bears in mind the slow conversions which are possible among the various species and the possibility that a catalyzed decomposition of one species can occur without immediate disappearance of the others.

We first consider the three types of species separately, discussing the structural features and properties of each one and the experimental evidence for its existence. Then we consider the nature of the conversion reactions and factors which influence the reaction rates. Next, thermodynamic arguments are invoked to explain the diversity of the results observed with different metals and solvents, and, finally, the model is used to explain some experimental observations of other investigators.

Assignment of Absorptions

Infrared Absorption and the Solvated Electron. We postulate that the infrared absorption ($1280\text{ m}\mu$ in ethylenediamine) is due to the solvated electron, existing alone and in ion-pairs, triple-ions, and quadrupoles similar to the principal species in dilute metal-ammonia solutions. The alkali metals and alkaline earth metals in liquid ammonia show only a single absorption (unless a large excess of a common ion is added¹³) in the infrared. This broad absorption band, tailing well into the visible, is attributed to an electron in a cavity surrounded by polarized solvent molecules.¹⁴ The infrared absorption in amines is also very broad and extends into the visible.

A solution of sodium in either methylamine or ethylamine shows only the visible peak, but upon addition of ammonia an infrared absorption maximum appears and the visible absorption decreases,^{3,15} with the infrared peak becoming more pronounced at higher ammonia concentrations. At about 50% ammonia, no visible peak remains. The addition of diethyl ether or tetrahydrofuran to solutions of sodium in ammonia causes a decrease in intensity of the infrared absorption and the appearance of a visible absorption maximum.¹⁵ These results fit in most naturally with the assignment

- (10) H. J. Eding, Ph.D. Thesis, Stanford University, 1952.
- (11) E. C. Evers, *J. Chem. Educ.*, **38**, 590 (1961).
- (12) M. Gold, W. L. Jolly, and K. S. Pitzer, *J. Am. Chem. Soc.*, **84**, 2264 (1962).
- (13) H. C. Clark, A. Horsfield, and M. C. R. Symons, *J. Chem. Soc.*, 2478 (1959).
- (14) J. Jortner, *J. Chem. Phys.*, **30**, 839 (1959).
- (15) G. Hohlstein and U. Wannagat, *Z. anorg. allgem. Chem.*, **288**, 193 (1957).

of the infrared absorption to the "ammonia-like" solvated electron.

The conductances of potassium, rubidium, and cesium in ethylenediamine also support the assignment of the infrared absorbing species to the solvated electron. Dilute cesium solutions show only the infrared absorption. The conductance can be described by the Shedlovsky function including ion association. The value of the limiting equivalent conductance gives nearly the same Walden product as the alkali metals in ammonia. Potassium and rubidium, which show both visible and infrared absorption peaks in dilute solutions, behave in a similar fashion to cesium but with significantly lower values of conductance. Sodium solutions, which show no significant infrared absorption, have a much lower conductance and exhibit a concentration dependence of the equivalent conductance different from the other metals.

Since the dielectric constant of ethylenediamine is significantly lower than that of ammonia, one would expect a greater fraction of the electrons to be present as ion-pairs, triple-ions, and quadrupoles. We would, therefore, expect a lower magnetic susceptibility for the infrared species in ethylenediamine than in ammonia.

To summarize, we attribute the infrared absorption in amine systems to the solvated electron in the species: (e^-) , (M^+e^-) , $(e^-M^+e^-)$, $(M^+e^-M^+)$, and $(M^+e^-)_2$. These species will be collectively referred to as "solvated electrons."

The Intermediate Absorptions.—The absorption maxima at 840, 890, and 1030 $m\mu$ for potassium, rubidium, and cesium, respectively, are attributed to covalent dimers similar to those found in alkali metal vapors. The peak positions for potassium and cesium correlate well with the intense transitions ${}^1\Sigma_u \leftarrow {}^1\Sigma_g$ for the gaseous dimers. The centers of these transitions in the gas phase lie at 860 and 940 $m\mu$, respectively.¹⁶ No data for this transition for the Rb_2 system are given by Herzberg. The absorbance of the dimer is more important relative to the infrared absorbance at high concentrations, consistent with its assignment to a dimeric species.

Interaction of the dimer with the solvent would be essentially through van der Waals forces so that the wave length of the dimer absorption would not be expected to undergo a large shift from the gas phase value. Thermodynamic arguments presented later show that the dimer is reasonable for potassium, rubidium, and cesium, but that its concentration, even in saturated lithium and sodium solutions, should be very small, in agreement with the absence of absorption attributable to the dimer for these metals.

The Species Absorbing at 650–750 $m\mu$. The most novel and puzzling feature of metal-amine solutions is the absorption peak shown by solutions of lithium, sodium, and potassium at 660 $m\mu$ in the ethylenediamine system. This peak appears only when lithium, sodium, or potassium ions are present, although the nature of the absorption is independent of the metal. The studies of spectra show that this species can be converted only slowly into the others, requiring several minutes in the case of lithium solutions. This observation would seem to require the presence of one or more covalent bonds which are broken in the conversion. If the 660- $m\mu$ absorption were due to a "monomer" unit of the Becker-Lindquist-Alder type,⁶ with an electron in an expanded orbital about the solvated ion, the exchange of the electron, according to



would be expected to be rapid.¹⁷ Indeed, we would expect even the exchange of solvent molecules in the primary solvation layer to be very fast.

These observations force us to conclude that at least two alkali metal ions are covalently bonded to one another by at least one electron. This cannot be the normal covalent dimer since the peak position is independent of metal in contrast to the intermediate peaks which we have attributed to the normal dimer. We conclude, therefore, that the one-electron bonded molecule-ion, M_2^+ , is associated with the 660- $m\mu$ species. This conclusion is further strengthened by the fact that for lithium and sodium, at least, the bond strengths of the molecule-ions, Li_2^+ , Na_2^+ , and K_2^+ in the gas phase are apparently *greater* than those of the molecules, Li_2 , Na_2 , and K_2 ,^{18,19} by about 35%. Qualitatively then, it is logical that the ion M_2^+ forms in solution since the bond strength is larger than for M_2 , and the resulting ion and electron can gain solvation energy sufficient to overcome the ionization energy.

It is necessary to describe next the nature of the absorption associated with the molecule-ion. While the M_2^+ "core" is required to explain the slow conversion

(16) G. Herzberg, "Spectra of Diatomic Molecules," D. Van Nostrand Co., Inc., New York, N. Y., 1950.

(17) Prof. J. Jortner, of the Hebrew University, Jerusalem, Israel, indicated in a recent personal communication that this electron transfer could indeed be slow because of the requirements of the Franck-Condon principle. In order for the electron to transfer to a cavity in the solvent, the transition state would have to be made nearly symmetrical by thermal motion and this could be a slow process.

(18) R. F. Barrow, N. Travis, and C. V. Wright, *Nature*, **187**, 141 (1960); E. W. Robertson and R. F. Barrow, *Proc. Chem. Soc.*, 329 (1961).

(19) J. James, *J. Chem. Phys.*, **3**, 9 (1935); J. Faulkner, *ibid.*, **27**, 369 (1957).

of the peak to the infrared absorption, the shape and position of the 660-m μ peak are both independent of the metal. This leads us to propose that the absorbing electron is trapped by the solvated M_2^+ ion in perhaps the same way as the electron is presumed to be trapped in a monomer unit of the Becker-Lindquist-Alder theory. Since the resultant electron density would be largely outside of the primary solvation layer, the nature of the cation in M_2^+ would have little effect upon the electronic energy levels.

The transition occurs at 660 m μ , while the corresponding transition for the solvated electron occurs at 1280 m μ . Therefore, the depth of the potential well for the electron about the cation is probably considerably greater than for the solvated electron. One must explain then why the electrostatic potential around a simple solvated cation does not trap an electron to yield an absorption peak in the visible region. Certainly, if M_2^+ can trap an electron with about 21 kcal. of extra stabilization energy, we would expect the simple ion M^+ to be able to do so as well. A plausible explanation for this difference in behavior of M_2^+ and M^+ may be found by considering the secondary solvation energy. An electron in an orbital about the solvated ion would screen the positive charge so that much of the secondary solvation energy of the ion would be lost. For the simple alkali ions in ammonia, this secondary solvation energy varies from 40.0 to 31.5 kcal. mole⁻¹ for Li^+ and Cs^+ , respectively.²⁰ Unless the excess electronic energy for the electron trapped by the ion is of this magnitude, the "monomer" would not be expected to form. An estimate of the secondary solvation energy of the alkali metal ions and molecule-ions may be made using the Born equation as was done by Coulter for metal-ammonia solutions.²⁰ The solvated ions are not spherically symmetric, but measurements on models yield an average van der Waals radius of about 1.8 Å. for ethylenediamine, which gives secondary solvation energies varying from 29 kcal. mole⁻¹ for Cs^+ to 36 kcal. mole⁻¹ for Li^+ . Similar measurements on a model of Li_2^+ , using an internuclear distance of 2.9 Å.,¹⁹ yield a secondary solvation energy of about 27 kcal. mole⁻¹. We are unable to calculate the increase in binding energy of the electron in going from the solvated state to the positive ion "trap," but the separations of the ground and excited states for the two species differ by about 21 kcal. mole⁻¹. Thus, it seems possible that the electron could be trapped by the large M_2^+ ion but not by a simple M^+ ion because of the lower secondary solvation energy of the former.

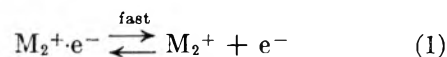
The bonding electron in the molecule-ion and the "trapped" electron would be expected to result in a triplet ground state. However, the visible absorption

in amines has been attributed to a diamagnetic species⁵ based upon the absence of an e.s.r. signal for systems which have only the visible peak. Thus, Fowles, McGregor, and Symons²¹ reported that sodium in ethylenediamine shows no e.s.r. absorption. Windwer and Sundheim⁸ report that it gives a "detectable" signal of 0.75-gauss line width. Recently, Vos,²² using a Varian spectrometer with 100-kc. modulation, observed a relatively strong signal from sodium in ethylenediamine. Estimates of the number of free spins by comparison with DPPH indicated that virtually all of the electrons could have been contributing to the signal. It should be realized, however, that estimating the absolute number of free spins is difficult and can easily be in error by at least an order of magnitude. It is, therefore, not possible to state unequivocally at this time whether the 660-m μ species is paramagnetic or diamagnetic. Quantitative susceptibility studies are urgently needed to answer this question.

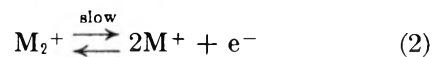
In summary, we propose that the species absorbing at 660 m μ consists of a solvated molecule-ion, M_2^+ , which has trapped an electron outside of its primary solvation sheath. We propose to represent this species by $M_2^+ \cdot e^-$ and to call it the "ionic-covalent dimer."

Equilibria and Conversion Rates

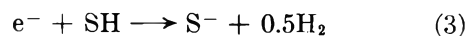
The ionic-covalent dimer is probably in rapid equilibrium with the molecule-ion and the solvated electron according to



This equilibrium is presumed to lie far to the left. The molecule-ion can also undergo the *slow* conversion



If the decomposition reaction involves mainly the solvated electron and the solvent according to



in which SH represents the solvent, then reaction 3 could proceed rapidly enough to reduce the electron concentration to such a low value that only the 660-m μ absorption would be appreciable. Reaction 2 could be slow enough to prevent the rapid disappearance of the 660-m μ absorption. If this is the case, then the discrepancies among the spectral results of different investigators can be accounted for.

(20) L. V. Coulter, *J. Phys. Chem.*, **57**, 553 (1953).

(21) G. W. A. Fowles, W. R. McGregor and M. C. R. Symons, *J. Chem. Soc.*, 3329 (1957).

(22) K. D. Vos, Ph.D. Thesis, Michigan State University, 1962.

The reactions proposed also indicate that a "buffer-effect" should operate when a solution contains solvated electrons and ionic-covalent dimers. As long as an appreciable concentration of solvated electrons exists in the solution, reaction 1 would be suppressed and the 660-m μ absorption should not change much. When the concentration of e⁻ drops to a low value, the 660-m μ absorption is no longer "buffered" and can decrease more rapidly. Such an effect could be responsible for the decay rates observed with a solution of lithium in ethylenediamine, as shown in Fig. 1. After correcting

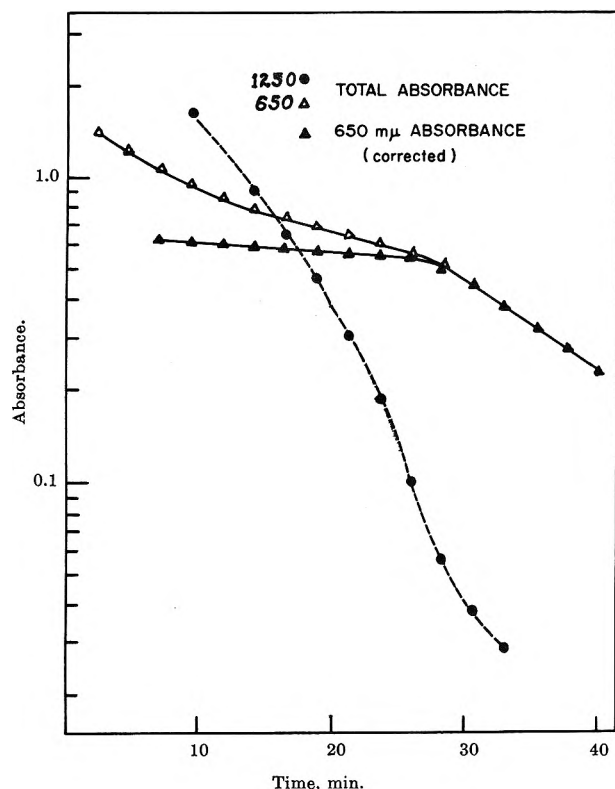


Figure 1. Decomposition of a lithium-ethylenediamine solution (semilog plot of absorbance vs. time). See ref. 1.

for the "tail" of the infrared absorption, it can be seen that the 660-m μ absorbance did not change significantly with time until the solvated electron concentration dropped to a low value.

It is also presumed that the conversion of the covalent dimers in potassium, rubidium, and cesium solutions to the other species is slow as indicated by the decay of the spectra. Of course, the conversions observed were probably heterogeneous in nature so that the true conversion rate is slower than that observed. In addition, the conversions should be more rapid for the heavier alkali metals.

Thermodynamic Considerations

Because of the magnitude of solvation energy effects, it is impossible to make calculations of the concentrations of the various species based upon the properties of the alkali metals alone. It can be demonstrated, however, that the species proposed are plausible on thermodynamic grounds. In addition, calculations can be made which give the trends to be expected as one moves from one metal to another. The general procedure is to assume the presence of the type of species being considered and to estimate its concentration in the saturated solution of one of the alkali metals from experimental data (spectra, solubilities, and conductances). The concentration of the same type of species is then calculated for all of the other alkali metals and compared with experiment.

Solvated Electron Concentration. While the species absorbing at 660 m μ presumably contributes to the conductivity, as evidenced by the conductance of sodium solutions, its contribution is much lower than that due to solvated electrons. Therefore, in calculating the concentration of solvated electrons, the contribution of the 660-m μ species to conductance was ignored.

Cesium shows only the 1280-m μ absorption in dilute solutions, and the equivalent conductance obeys the Shedlovsky equation. The value of the limiting Walden product, $\Lambda_0\eta_0$, obtained by extrapolation, agrees reasonably well with that for metal-ammonia solutions. For these reasons, we used cesium as a "standard" in calculating the conductance and total solvated electron concentration in the saturated solutions of the other metals. A saturated solution of Cs in ethylenediamine at 25° ($C = 0.0543 M$) has an equivalent conductance of 26.2 kohlransch units. Using $D = 12.9$, $\eta_0 = 0.0154$ poise, $\Lambda_c = 204$, and $\delta = 6.0 \text{ \AA.}$, we obtain the equations

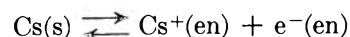
$$\Lambda_i = \frac{204}{1 + 3.87\sqrt{C_i}} \quad (4)$$

$$\log f_{\pm} = \frac{-7.64\sqrt{C_i}}{1 + 4.86\sqrt{C_i}} \quad (5)$$

$$C_i = \frac{\Lambda}{\Lambda_i} C \quad (6)$$

$$K = (C_i f_{\pm})^2 \quad (7)$$

for the equilibrium



For the saturated solution of Cs, this gives: $C_i = 0.0096 M$, $K = 9 \times 10^{-6}$, $\Delta G^\circ = +6.9 \text{ kcal. mole}^{-1}$.

To calculate the concentration of solvated electrons in the saturated solutions of the other alkali metals, the difference between the standard free energies of formation of the particular alkali metal ion and cesium ion in liquid ammonia, obtained from Jolly's tabulation,²³ was assumed to be the same in ethylenediamine. Jolly gives ΔG° values of -54 , -43.6 , -47.0 , -47.5 , and -48 kcal. mole⁻¹ for Li⁺, Na⁺, K⁺, Rb⁺, and Cs⁺, respectively. Using $\Delta G^\circ = +6.9$ kcal. mole⁻¹ for the standard free energy of formation of Cs⁺ and e⁻ in ethylenediamine gives values of $+0.9$, $+11.3$, $+7.9$, and $+7.4$ for the standard free energies of formation of Li⁺, Na⁺, K⁺, and Rb⁺, plus the solvated electron, respectively. From these values and eq. 4, 5, and 7, the specific conductances of the saturated solutions can be calculated and compared with experiment. The apparent dissociation constants of the ion-pairs in K, Rb, and Cs solutions are nearly the same ($\sim 1.5 \times 10^{-4}$), according to the Shedlovsky treatment of conductance data.² We can write, therefore, that

$$K \approx 1.5 \times 10^{-4} = \frac{(C_i f_{\pm})^2}{C' - C_i} \quad (8)$$

in which C' is the total concentration of solvated electrons and C_i is the concentration of dissociated electrons. This equation may be solved for C' using eq. 5 and 7 and the standard free energies given above and compared with the total electron concentration estimated from spectra and solubilities. The results of these calculations are given in Table I. In view of

Table I: Calculated and Observed Specific Conductances and Electron Concentrations in Saturated Solutions of the Alkali Metals in Ethylenediamine

Metal	Specific conductance		Total solvated electron molarity	
	Calcd.	Obsd.	Calcd.	Estimated ^a
Li	Very high ^b	1.5×10^{-2}	$>1^b$	0.1
Na	1.7×10^{-5}	6×10^{-5}	1×10^{-4}	$<3 \times 10^{-5}$
K	4.5×10^{-4}	3.0×10^{-4}	1×10^{-2}	3×10^{-3}
Rb	7.8×10^{-4}	3.2×10^{-4}	3×10^{-2}	5×10^{-3}
Cs	Standard	1.4×10^{-3}	7×10^{-2}	3×10^{-2}

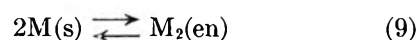
^a Estimated from relative intensities of the infrared absorption band and solubilities. ^b The assumptions break down for Li solutions, and one can predict only that the specific conductance and solvated electron concentration should be high.

the many assumptions made, the agreement is certainly satisfactory. In particular, the differences in standard free energies of formation of the alkali ions in ethylenediamine, estimated from independent data for the ammonia systems, explain why sodium solutions show very

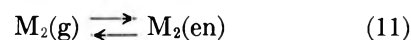
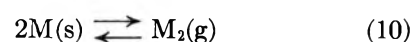
little infrared absorption and low conductivity while lithium solutions and the other alkali metals absorb strongly in the infrared and have relatively high solubilities and conductivities.

Dimer Concentration. It is assumed that the species absorbing at intermediate wave lengths for potassium, rubidium, and cesium solutions are covalent dimers, similar to those which exist in the gas phase. The questions which must be answered are: (1) Is the solvation energy of uncharged dimers sufficient to explain the relatively high concentrations observed for these metals? (2) Why is there no evidence for such dimers in solutions of lithium and sodium?

To answer these questions, it was necessary to estimate ΔG° for the process



This may be viewed as the sum of the free energies for the two steps



Data for ΔH° for reaction 10 are available for all of the alkali metals and ΔG° values are known²⁴ for Li₂(g), Na₂(g), and K₂(g). The molar entropies of Rb₂(g) and Cs₂(g) were calculated from statistical thermodynamics using $\omega_e = 57.28$ cm.⁻¹ and 41.99 cm.⁻¹, respectively, for the ground states of the diatomic molecule.¹⁶ The values $r_e = 4.2$ and 4.5 Å. were used for the equilibrium internuclear distances for Rb₂ and Cs₂, respectively. These values were estimated from an extrapolation of the distances for Li₂, Na₂, and K₂ vs. the single-bond metallic radii.²⁵ The calculations yield 61.8 and 64.9 gibbs, respectively, for the entropy of Rb₂(g) and Cs₂(g) at 25° which result in ΔG° values of 21.1 and 19.5 kcal. mole⁻¹ for reaction 10.

Assuming the molar absorptivity of a dimer to be the same as that of the solvated electron allows us to estimate the concentration of Rb₂ in the saturated solution to be about 10^{-3} M. This gives $\Delta G^\circ = +3.5$ kcal. mole⁻¹ for reaction 9, which yields $\Delta G^\circ = -17.6$ kcal. mole⁻¹ for the standard free energy of solvation of the gas-phase dimer. Using gaseous standard states of 1 mole/l., the solvation free energy is -19.5 kcal. mole⁻¹. This appears to be rather high for the solvation energy of an uncharged species. However, the large alkali metal dimers should be highly polarizable, which would

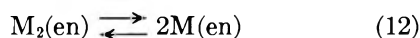
(23) W. L. Jolly, J.C.R.L.-2201, U. S. Atomic Energy Commission, 1953.

(24) National Bureau of Standards (U. S.), Circular 500.

(25) L. Pauling, "The Nature of the Chemical Bond," Third Ed., Cornell University Press, Ithaca, N. Y., 1960.

result in a larger solvation energy than for most uncharged molecules. Even the less polarizable I_2 molecule has a solvation energy of about -6 kcal. mole $^{-1}$ in many solvents.

To estimate the concentration of dimers in saturated solutions of the other alkali metals, we assume that the solvation free energy is the same for all dimers. Actually, the solvation energies for Li_2 , Na_2 , and K_2 would probably be smaller than this, which would lead to high estimates of these concentrations. The concentrations estimated in this way are given in Table II along with the estimated concentration of free atoms. The latter values are obtained by assuming the equilibrium constant for the process



to be the same as for the corresponding gas phase dissociation. Also given in Table II are estimates of the concentrations of dimers using spectral data. It is to be noted especially that this analysis indicates that the dimer concentrations to be expected in saturated solutions of Li and Na are very small, in agreement with the absence of extra absorption peaks for these metals.

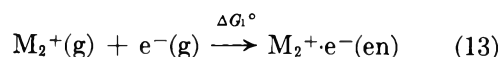
Table II: Calculated Concentrations of Covalent Dimers and Atoms of the Alkali Metals in Ethylenediamine

Metal	Dimer concentration, mole/l.		Atom concentration, mole/l., Calcd.
	Calcd.	Estimated ^a	
Li	10^{-14}	0	...
Na	2×10^{-5}	0	10^{-7}
K	6×10^{-4}	2×10^{-3}	6×10^{-5}
Rb	Standard	3×10^{-3}	5×10^{-4}
Cs	1×10^{-2}	1×10^{-2}	3×10^{-3}

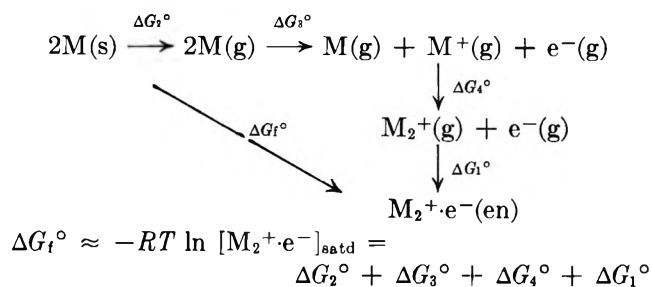
^a Estimated from relative intensities of the intermediate and infrared absorptions and solubilities.

Ionic-Covalent Dimers. Because of unknown differences in solvation energies for the M_2^+ ions, it is difficult to make comparisons of the expected concentrations of this ion for the different alkali metals as could be done for the other species. One can only note the factors involved which affect these concentrations. Both the higher bond strength and the larger solvation energy would favor the Li_2^+ ion compared with the Cs_2^+ ion, for example. On the other hand, the lower ionization potential and lower bond energy in the pure metal would favor the formation of Cs_2^+ .

Although reliable quantitative comparisons cannot be made, it is possible to estimate the free energy change for the process



for the various metals. This represents the sum of three free energy terms; the solvation free energy of the gaseous cation, the solvation free energy of the gaseous electron, and the net free energy for the formation of the ionic-covalent dimer in ethylenediamine from the molecule-ion and the solvated electron. A number of guesses are required for this calculation, which utilizes the cycle



In making these calculations, the following approximations and assumptions were made.

(1) The activity of $M_2^+e^-$ in a saturated solution in ethylenediamine was assumed equal to its concentration which, in turn, was estimated from the solubility and relative intensity of the 660- μ peak. The values used are given in Table III.

Table III: Calculation of the Solvation Free Energy of the Ionic-Covalent Dimer

Metal	Estimated molarity of $M_2^+e^-$ in satd. soln.	ΔG_f° , kcal. mole $^{-1}$	ΔG_1° , kcal. mole $^{-1}$
Li	10^{-1}	+1.4	-144.5
Na	1.1×10^{-3}	+4.1	-124.9
K	1.5×10^{-3}	+3.8	-105.5
Rb	1.5×10^{-3}	+3.8	-100.5
Cs	10^{-4} (?)	+5.5	-89.8

(2) The bond energy of $M_2^+(g)$ was assumed to be 35% larger than that of M_2 as appears to be the case for Li_2 , Na_2 , and K_2 .^{18,19} This value is not very certain and is unknown for the other metals, so that this assumption is probably quite drastic.

(3) The molar entropy of $M_2^+(g)$ was assumed to be the same as that of $M_2(g)$. Gaseous standard states chosen were 1 mole/l. in all cases.

(4) The Sackur-Tetrode equation was used to compute the molar entropy of the gaseous electron.

The results are given in Table III and show the expected trend of decreasing solvation free energy from Li_2^+ to Cs_2^+ . However, the decrease is larger than one would expect based upon the sizes of the ions involved. In addition, while the contribution of the electron to ΔG_1° is unknown, the total solvation free energies seem high. On thermodynamic grounds, therefore, the proposed species seem qualitatively plausible, but the quantitative estimates are not as satisfactory as for the other species.

Comparison with the Results of Other Investigators

Cafasso and Sundheim⁷ have shown that sodium is not soluble in 1,2-dimethoxyethane except in the presence of potassium, and that Na and K dissolve in equimolar amounts. This might be due to the formation of NaK^+e^- which carries sodium into solution.

When diethyl ether is added to solutions of Na in NH_3 , a new peak in the vicinity of 700 $\text{m}\mu$ is formed in addition to the usual infrared peak in ammonia.¹⁵ This would be expected on the basis of the lowering of the dielectric constant of ammonia by ether. As the solvation energy of Na^+ decreases, competition from covalent bond formation in Na_2^+ would occur. There could also be small amounts of this species present even in pure ammonia. Clark, Horsfield, and Symons¹³ have found that the addition of a large excess of NaI to solutions of Na in NH_3 yielded a shoulder at about 800 $\text{m}\mu$ which might be due to the presence of Na_2^+e^- .

Centrifugation of solutions of 1,2-dimethoxyethane by Dainton, Wiles, and Wright⁹ gave an abrupt reduction of the absorbance of the visible peak. These authors noted also the appearance of a precipitate in their systems. We suggest that the precipitate, formed by decomposition, carried along some M_2^+ and/or

M_2^+e^- , resulting in a lower absorbance in the visible region.

Linschitz and Eloranta²⁶ have studied the flash photolysis of solutions of potassium in tetrahydrofuran and in dimethoxyethane. The flash resulted in a large decrease of the 700- $\text{m}\mu$ absorbance and the appearance of a strong absorbance in the near-infrared. This then decayed by a rapid second-order process to give an absorbance maximum at 900 $\text{m}\mu$, followed by a slow first-order return to the initial spectrum. Linschitz has interpreted these data in terms of two types of electron pairs, singlet- and triplet-state pairs. Our interpretation of this result is that the ionic-covalent dimer is dissociated into atoms or into ions and solvated electrons which then combine to form the neutral molecule, K_2 , in a normal singlet state. By a slow first-order process, this would tend to convert to the original mixture containing K_2^+e^- and K_2 .

The spectral data of Shatz²⁷ for lithium in methylamine suggest that the species absorbing in the visible region is dimeric in nature, in accord with the present model. More such studies on the stoichiometry of the various species are needed to complete the identification.

Acknowledgments. This model is derived from experimental results obtained in the Max Planck Institut für physikalische Chemie, Göttingen, West Germany, during 1961-1962. The authors wish to thank Dr. Manfred Eigen for the opportunity which was given to us to study in his laboratory. We also wish to thank the National Science Foundation for a Science Faculty Fellowship (J. L. D.) during this time. This research was also supported in part by the U. S. Atomic Energy Commission (Contract No. AT(11-1)-958).

(26) H. Linschitz and J. Eloranta, *Z. Elektrochem.*, **64**, 169 (1960); *J. Chem. Phys.*, **38**, 2214 (1963).

(27) M. Shatz, Ph.D. Thesis, University of Pennsylvania, 1958.

Correlation of Bond Dissociation Energy with Ionization Potential and Electron Affinity

by Robert S. Neale

Union Carbide Research Institute, Tarrytown, New York (Received August 15, 1963)

Bond dissociation energies $D(X-Y)$ have been linearly related to the ionization potentials (I) of hydrogen and organic radicals and to the differences ($I - E$) of ionization potential and electron affinity of inorganic radicals

A set of empirical constants ϵ has been constructed by Errede¹ to denote the relative contributions of mono- or polyatomic radicals X or Y to any bond dissociation energy $D(X-Y)$ according to

$$D(X-Y) = \lambda \epsilon_X \epsilon_Y \quad (1)$$

The constant λ is characteristic of the type of X-Y species under consideration; thus, λ is 73 for inorganic hydrides, 54 for hydrazines, 84 for disulfides, and 71 when X or Y is a carbon radical. We have now discovered correlations of ϵ with I (the ionization potential) for hydrogen or organic radicals and with $I - E$ (ionization potential minus electron affinity) for inorganic radicals. This is equivalent to correlating $D(X-Y)$ with these same quantities, through eq. 1, without recourse to the ϵ -values. A single correlation is impossible to obtain, however, because λ varies with the type of compound X-Y.

We have considered those organic and inorganic radicals for which an ϵ -value has been calculated¹ and the values of I and, for inorganic radicals, of E are known (Table I). These radicals have been grouped into the following three somewhat arbitrary classes: (A) the unpaired electron is localized on an atom other than carbon which also bears nonbonded s- or p-electrons, *i.e.*, most inorganic radicals; (B) the unpaired electron is formally situated on a carbon atom and is conjugated to a π -electron system, as in (halo)_m-H_{3-m}C·, (C₆H₅)_mH_{3-m}C·, R-C=C-CH₂·, and HC≡C-CH₂·; (C) the remaining radicals (alkyl)_m-H_{3-m}C·, C₆H₅·, CH₂=CH·, CH≡C·, and the hydrogen atom. The CN radical is an exception; as a pseudo-halogen it has been included in class A. The

subscripts A, B, and C used hereafter denote the class of radicals to which the designated symbol is applicable.

The correlations we have observed are summarized by Fig. 1 and eq. 2 and 3 and by Fig. 2 and eq. 4.

$$\epsilon_A = 0.115(I_A - E_A) - 0.07 \quad (2)$$

$$\epsilon_B = 0.115I_B - 0.07 \quad (3)$$

$$\epsilon_C = 0.056I_C + 0.55 \quad (4)$$

It is open to question, with respect to eq. 2 and 3, whether the remarkable coincidence of slope and intercept is significant or fortuitous. The absence of E_B in eq. 3 implies either that E_B has no effect on ϵ_B or that (less probably) E_B is invariably close to zero, contrary to the few published values of 1-2 e.v. (*cf.* Table I). In any case, the correlation of ϵ with I alone for class C radicals according to eq. 4 is greatly different in both slope and intercept; it is probably of useful accuracy, but insufficient examples are available to test it adequately. The maximum deviation of a point from the line of correlation in Fig. 1 is 0.6 e.v. (14 kcal.); however, all but five of the 21 points fall within 0.3 e.v. (7 kcal.) of the line.

In Fig. 2 we have approximated from eq. 1 a new ϵ_C for CH₂=CH· and CH≡C· to accord with the presently accepted² values $D(C_2H_3-H)$ and $D(C_2H-H)$. It was also necessary to redefine ϵ_A for A = F, SH, and I to better accommodate the available D -values involving these radicals. The data for $D(X-CN)$ are few³; ϵ_{CN} was reassigned to accommodate $D(H-CN)$

(1) L. A. Errede, *J. Phys. Chem.*, **64**, 1031 (1960).

(2) B. E. Knox and H. B. Palmer, *Chem. Rev.*, **61**, 247 (1961).

(3) F. H. Field and J. L. Franklin, "Electron Impact Phenomena," Academic Press, Inc., New York, N. Y., 1957, p. 135.

Table I: Physical and Thermochemical Data for Radicals of Classes A, B, and C

Radical	ϵ^a	$D(R-H)^b$	$D(R-CH_3)^b$	I^c	E^c	$I - E$
Class A						
F	(1.42)	135	107	17.42	4.09 ^d	13.33
CN	(1.19)	114	103	14.6	3.2 (2.78) ^e	11.4
OH	1.23	119	90	13.18	2.1 ^{e,e}	11.08
NH ₂	1.05	104	80	11.4	1.2 ^{e,e}	10.2
Cl	1.04	103	80	13.01	3.73 ^d (3.78) ^e	9.28
SH	(0.93)	95 ^f	70	11.1	2.3 ^e (1.65) ^g	8.8
O ₂ H	.93	89.5	...	11.53	3.05	8.48
Br	.86	87	67	11.84	3.55 ^d (3.48) ^e	8.29
I	(.71)	71	53	10.45	3.41 ^d (3.24) ^e	7.04
Li	[.60]	58	...	5.39	0.47 0.35 ^g	4.92 or 5.04
Na	[.49]	47	...	5.14	0.08 0.39 ^g	5.06 or 4.75
K	[.45]	43	...	4.34	0.39 ^g	3.95
Class B						
CF ₃	(1.10)	103	...	10.1
CH ₂ Cl	1.04	9.70
CH ₂ Br	1.00	99	...	9.30
CHCl ₂	0.97	9.30
CCl ₃	.94	90	...	8.78
CH ₂ C≡CH	.94	8.25
CHBr ₂	.92	8.13
CH ₂ C ₆ H ₅	.83	77.5	63	7.76	1.08 ^e	...
CH ₂ CH=CH ₂	.78	77	61.5	8.16
CH ₂ CH=CHCH ₃	.74	7.71
CH(C ₆ H ₅) ₂	.74	7.32 ^h
C(C ₆ H ₅) ₃	.69	6.5 ⁱ
Class C						
H	1.32	103	102	13.595	0.745	...
C≡CH	(1.22)	114 ^j	...	11.3
C ₆ H ₆	1.11	102	89	9.90	2.17 ^e	...
CH=CH ₂	(1.11)	104 ^j	92.5 ^{k?}	9.45 ^l
CH ₃	1.08	102	83	9.85	1.13 ^e	...
C ₂ H ₅	1.05	98	82 ^{k?}	8.78	1.0 ^e	...
<i>i</i> -C ₃ H ₇	1.01	94	...	7.77
<i>t</i> -C ₄ H ₉	0.95	90	...	7.4

^a See ref. 1. Values of ϵ in parentheses were redefined to better accommodate D -values presently described in the literature; values in brackets were calculated directly from $D(M-H)$ and eq. 1. ^b In kcal./mole; values from ref. 5 and from T. L. Cottrell, "The Strengths of Chemical Bonds," 2nd Ed., Butterworths Scientific Publications, London, 1958. ^c In e.v.; 1 e.v. = 23.06 kcal. Data, except as noted, from R. W. Kiser, "Tables of Ionization Potentials," U. S. Atomic Energy Commission, Report TID-6142 (1960). ^d E. Kordes, *Naturwissenschaften*, **21**, 667 (1961). ^e F. M. Page, in ref. 7, p. 68. ^f See ref. 3, p. 143. ^g See ref. 3, Table 45, part 2. ^h A. G. Harrison and F. P. Lossing, *J. Am. Chem. Soc.*, **82**, 1052 (1960). ⁱ See ref. 3, p. 126. ^j See ref. 2; probable best value. ^k C. T. Mortimer, "Reaction Heats and Bond Strengths," Pergamon Press, New York, N. Y., 1962, p. 129. ^l A. G. Harrison and F. P. Lossing, *J. Am. Chem. Soc.*, **82**, 519 (1960).

and $D(Cl-CN)$, although $D(CH_3-CN)$ is better predicted using the original¹ value of ϵ_{CN} .

To determine whether the correlation expressed by eq. 2 was also applicable to the alkali metals, *i.e.*, to

radicals from the left side of the periodic table, approximate ϵ_M values were obtained from $D(M-H)$ by eq. 1 and were plotted *vs.* $(I - E)_M$ for $M = Li, Na,$ and K (Fig. 1, shaded loci). It is evident that the alkali

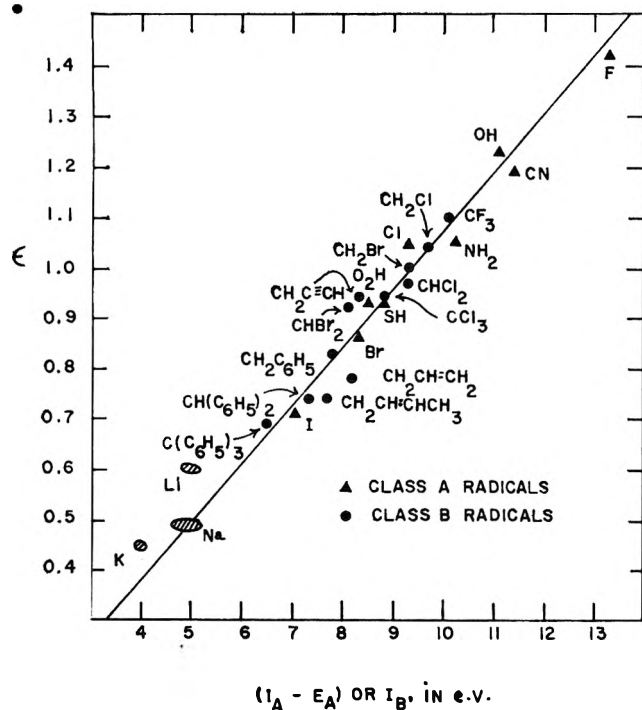


Figure 1. Correlation of ϵ with $(I - E_A)$ for radicals of class A and with I for radicals of class B.

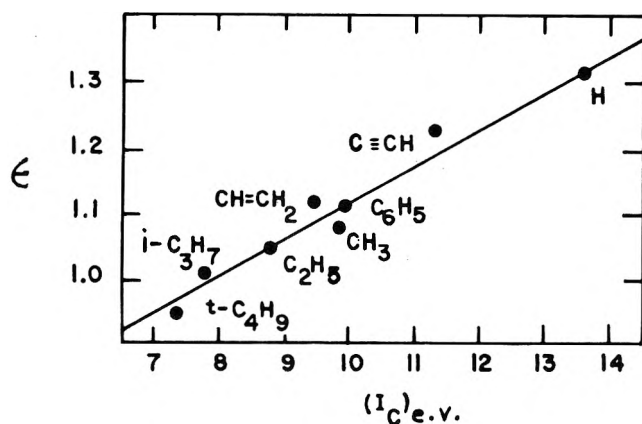


Figure 2. Correlation of ϵ with I for class C radicals.

metals, which by our definition should be class A radicals, fit eq. 2 moderately well. The metal halides are not accommodated by either eq. 2, 3, or 4, but this is not surprising; the metal halides are essentially ionic species, whereas the compounds treated by eq. 2-4 are essentially covalent in the gas phase.

Equations 2-4 are limited only in that a radical X must form a neutral, nonradical, principally covalent species X-H; thus, none of these equations is adaptable to atoms, e.g., O, S, C, B, that are normally found only in polyatomic compounds. Furthermore, the radical X must be neutral. Although one may approximate

a new ϵ_{X^+} from eq. 1, ϵ_H , and a known $D(X^+-H)$, the ϵ_{X^+} are crudely but *inversely* related to $(I - E)_{X^+}$ when the X^+ are positively charged halogen or inert gas atoms.

For each series of compounds with a characteristic λ , one may further write equations in which $D(X-Y)$ is linearly related to the absolute values of I and E , by combining eq. 2, 3, or 4 with eq. 1. For example, $D(X_A-H)$ (i.e., bond dissociation energies of class A hydrides) may be expressed by eq. 5, which results from simple substitution of eq. 2 into eq. 1 (with $\lambda = 73$ and $\epsilon_{Y-H} = 1.32$). Thus

$$D(X_A-H) = 73(1.32)\epsilon_X$$

OR

$$D(X_A-H)_{\text{kcal./mole}} = 11.1(I_X - E_X)_{\text{e.v.}} - 6.8 \quad (5)$$

Equations 6 and 7 for $D(X_B-H)$ and $D(X_C-H)$ are similarly derived ($\lambda = 71$).

$$D(X_B-H)_{\text{kcal./mole}} = 10.8(I_X)_{\text{e.v.}} - 6.8 \quad (6)$$

$$D(X_C-H)_{\text{kcal./mole}} = 5.25(I_X)_{\text{e.v.}} + 51.5 \quad (7)$$

Any other series of compounds may be so treated, for example, $D(X-CH_3)$ by eq. 8-10, and more general equations for $D(X-Y)$ may be derived in the same way, wherein neither X nor Y is fully specified.

$$D(X_A-CH_3)_{\text{kcal./mole}} = 8.8(I_X - E_X)_{\text{e.v.}} - 5.4 \quad (8)$$

$$D(X_B-CH_3)_{\text{kcal./mole}} = 8.8(I_X)_{\text{e.v.}} - 5.4 \quad (9)$$

$$D(X_C-CH_3)_{\text{kcal./mole}} = 4.3(I_X)_{\text{e.v.}} + 42.2 \quad (10)$$

The accuracy of such bond dissociation energy expressions is reasonably good, eq. 5-10, for example, generally reproducing the reported values to within 5 kcal./mole (Fig. 3 and 4).

Equation 5 may be valuable for estimating the electron affinity of an inorganic radical X from known values of $D(X-H)$ and I_X . Use of eq. 5 for this purpose appears feasible because the maximum deviation of $(I - E)_X$ calculated from $D(X-H)$ is only 0.4 e.v. (9 kcal.) over the full range of 71-135 kcal. in $D(X-H)$. The method is particularly attractive because E_X is difficult to measure⁴ and is even less reliably estimated by standard thermochemical cycles, especially for covalently bonded species; $D(X-H)$ and I_X are far more accessible quantities. As examples, we have determined approximate values for E_{PH_2} and E_{NHNH_2} , as described below; however, these are based on unreliable values of I_X and $D(X-H)$ and hence must be considered only as illustrative of the method.

(4) F. H. Field and J. L. Franklin, ref. 3, p. 145.

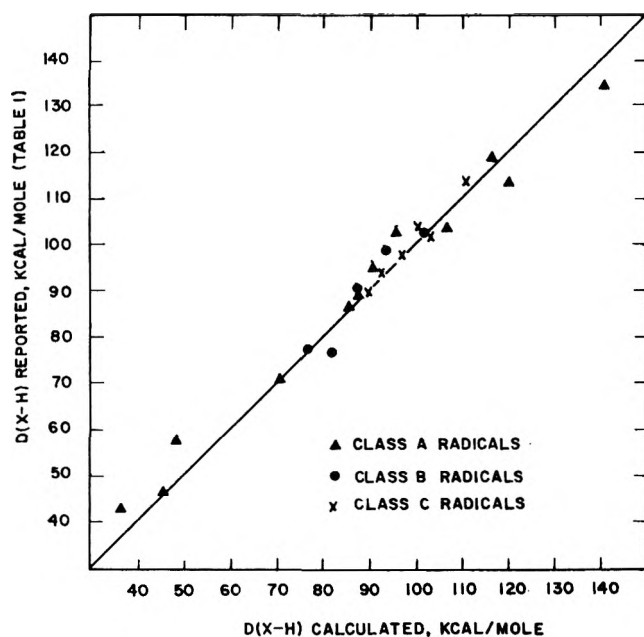


Figure 3. Calculated *vs.* reported bond dissociation energies of inorganic and organic hydrides.

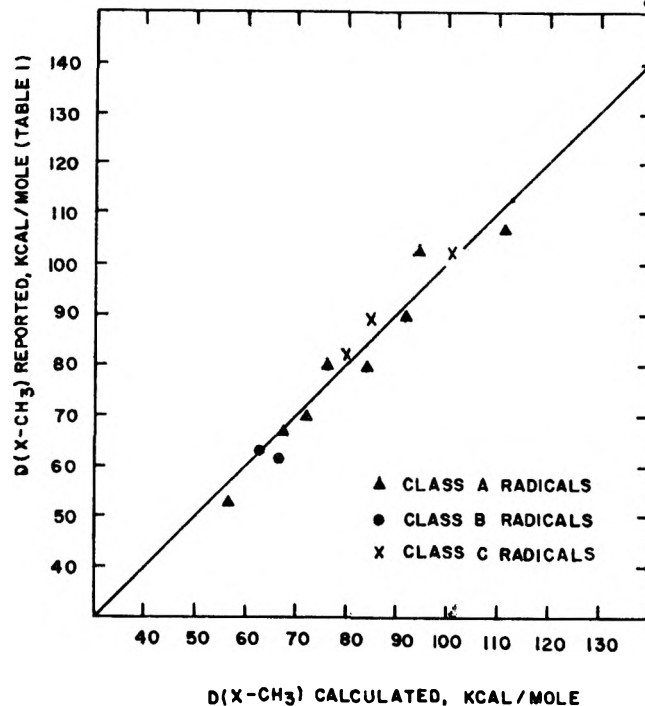


Figure 4. Calculated *vs.* reported bond dissociation energies in the compounds X-CH₃.

The value $D(\text{PH}_2\text{-H})$ is unknown, but has been approximated⁵ from $D_{\text{av}}(\text{PH}_3)$ to be 85 kcal./mole (3.7 e.v.). From the appearance potential of $\text{PH}_2^+ = 13.9$ e.v.,⁶ we obtain an estimated I_{PH_2} of $13.9 - 3.7 = 10.2$ e.v., and from eq. 5 we calculate $E_{\text{PH}_2} \approx 1.8$ e.v. In a similar manner, we have calculated $E_{\text{HNNH}_2} \approx 0.4$ e.v. from $D(\text{H-HNNH}_2) = 76$ kcal./mole and $I_{\text{HNNH}_2} = 7.88$ e.v.⁷

Errede¹ has shown that the ϵ -values for the halogen atoms are given by the quantity $\sqrt{\chi/r}$, where χ is the Pauling electronegativity value⁸ and r the C-X bond length. This relationship, while interesting, suffers from a lack of generality. Pauling⁸ correlated average bond energies with differences in χ , but these are not equal to bond dissociation energies $D(\text{X-Y})$ except in diatomic molecules. Neither Mulliken's values of electronegativity (defined equal to $(I + E)/2$)⁹ nor the χ -values recently defined on the basis of orbital electronegativities¹⁰ appear to be simply related to bond dissociation energies. The present treatment, in contrast, seems to accommodate polyatomic radicals easily and to be quite generally applicable to the prediction of bond dissociation energies.

Better tests of the validity of the relationships depicted herein demand the availability of more precise and mutually consistent experimental data. Theoretical rationalization of these correlations is presently being sought; we conclude only that those factors which determine differences between the values of I or $I - E$ of radicals X and Y may also strongly influence differences between bond dissociation energies in the molecules X-Y.

Acknowledgment. The author is indebted to Dr. Verner Schomaker for several useful discussions.

- (5) C. Walling, "Free Radicals in Solution," John Wiley and Sons, Inc., New York, N. Y., 1957, p. 48.
- (6) F. H. Field and J. L. Franklin, "Electron Impact Phenomena," Academic Press, Inc., New York, N. Y., 1957, p. 299.
- (7) S. N. Foner and R. L. Hudson, "Free Radicals in Inorganic Chemistry," Advances in Chemistry Series, No. 36, American Chemical Society, Washington, D. C., 1962, p. 34.
- (8) L. Pauling, "The Nature of the Chemical Bond," 3rd Ed., Cornell University Press, Ithaca, N. Y., 1960, p. 92.
- (9) R. S. Mulliken, *J. Chem. Phys.*, **2**, 782 (1934).
- (10) J. Hinze, M. A. Whitehead, and H. H. Jaffé, *J. Am. Chem. Soc.*, **85**, 148 (1963).

The Density of Liquid T₂O¹

by Maxwell Goldblatt

*University of California, Los Alamos Scientific Laboratory, Los Alamos, New Mexico
(Received August 15, 1963)*

The density of 99.30 mole % T₂O was determined from 5 to 54° to ±0.015% by a magnetic float method. The density of 100% T₂O depends on temperature according to $D = 1.213124 + 2.9129 \times 10^{-4}t - 1.1954 \times 10^{-6}t^2 + 5.301 \times 10^{-8}t^3$ g./cm.³. The maximum density, 1.21502 g./cm.³, occurred at 13.4 ± 0.1°. Molar volumes are compared with those of H₂O and D₂O. The concentration of T₂O₂ in 98% T₂O was found to be 0.001–0.002 mole/l.

Introduction

Density and thermal expansion measurements on liquid D₂O have been made by several workers.² This paper presents data on the density of liquid T₂O from 5 to 54°. A 1-g. sample of 99.30 mole % T₂O was used.

Due to health hazards a density method had to be used in which the vessel could be filled on a vacuum line and sealed off. Dilatometry was tried but was discarded because gas evolution due to self-radiation caused separation of the liquid in the capillary column. Pressurizing the vessel with T₂ gas kept the liquid thread intact for longer periods but gas bubbles still formed. A magnetic float method similar to that of Richards³ was finally adopted.

Experimental

Density Apparatus. The essential part of the apparatus (Fig. 1) was a small quartz float containing a rod of Mumetal. A coil was set just below the bottom of the density vessel. If the current passing through the coil is gradually decreased, the resulting magnetic field falls below a critical value, allowing the float to rise in the liquid. The effective density of the float was thus changed magnetically. The lower limit of measurable density is the density of the float. This was increased magnetically by as much as 1% in this experiment. The density in this 1% range was read from a graph of density vs. critical current, determined by calibration with liquids of known density.

The coil, a commercial solenoid of 100 ohms, was coated with plastic to prevent shorting in the thermostat. It was fastened to a brass form which also served as a holder for the sample container. Alternating cur-

rent for the coil, taken from a regulated supply (±0.01%), was determined to better than 0.1% with vacuum thermocouples.⁴ Five thermocouples were used to cover a range from 0 to 100 ma.

The float, A, was 3 cm. long and was made from 1.5-mm. o.d. thin-walled quartz tubing. The Mumetal rod, 1-mm. o.d. by 3 mm. long, was waxed in place at the lower end of the float. The mean density of the float was adjusted by adding or removing quartz with a torch until it just floated in nitrobenzene at about 22°. The float density was 1.20076 g./cm.³ at 22.40°, the temperature of flotation in nitrobenzene. The Pyrex density vessel, fitted with break-seals, was sealed off under vacuum just before the density measurements. The side arm (x) was provided for the freezing and condensation of the T₂O. The float section of 8-mm. o.d. tubing fitted the brass holder tightly. The total volume of the vessel was about 30 ml. Calibrating fluids were placed in the density section of the densimeter with a hypodermic syringe. A water thermostat kept the temperature of the density apparatus constant to ±0.005°. The temperature was measured with a Leeds and Northrup platinum resistance thermometer which had been calibrated by the National Bureau of Standards.

Calibration. In this application of the electromagnetic densimeter different densities were obtained by

- (1) This work was done under the auspices of the Atomic Energy Commission.
- (2) I. Kirshenbaum, "Physical Properties of Heavy Water," McGraw-Hill Book Co., Inc., New York, N. Y., 1951, p. 11.
- (3) A. R. Richards, *Ind. Eng. Chem., Anal. Ed.*, 11, 44 (1939).
- (4) F. L. Hermach, *IRE Trans.*, I-8, 235 (1958).

changing the temperature of standard liquids of known density. Account must be taken of the fact that the T_2O and standard are not at the same temperature for the same critical current. Due to the variation of the magnetic susceptibility of Mumetal with temperature and dimensional changes in the apparatus with

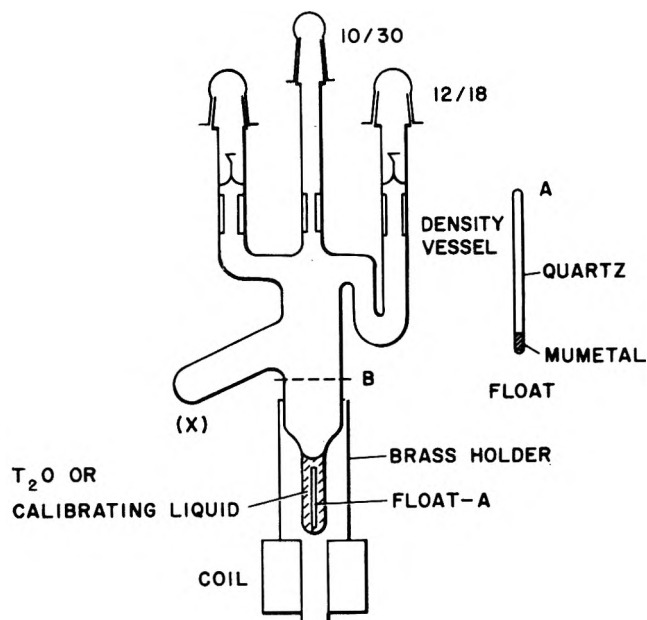


Figure 1. Densimeter apparatus.

temperature, it is necessary to interpolate to the density of a hypothetical standard which does have the same temperature as the T_2O for the measured critical current. For this purpose a calibration curve was obtained with each of four standards over the desired density range, approximately 1.20070 to 1.21400 g./cm.³. For this density range a given standard covered a portion of the temperature range 5 to 54°. A 1.6% (by weight) solution of ethylbenzene in nitrobenzene was used from 4 to 15°; nitrobenzene from 9.5 to 25.5°; β,β' -dichloroethyl ether from 24 to 35°; and a 13.7% solution of bromobenzene in nitrobenzene from 41 to 54°. The densities of the standards were determined by dilatometry to $\pm 0.003\%$. The dilatometers were calibrated with conductivity water.

The way in which the density-current curves were used is illustrated with the help of Fig. 2, which shows two idealized calibration curves. At temperature T_s the measured critical current for T_2O is i . For this current standard 1 has a density D_1 and a temperature T_1 , which is known from its measured density-temperature relationship; similarly for standard 2. For definiteness assume $T_2 > T_s > T_1$. The correct density for T_2O , D_s , is then obtained by a linear interpolation of

density between T_1 and T_2 to T_s . The interpolative corrections amounted to at most 4×10^{-5} g./cm.³, at the highest currents.

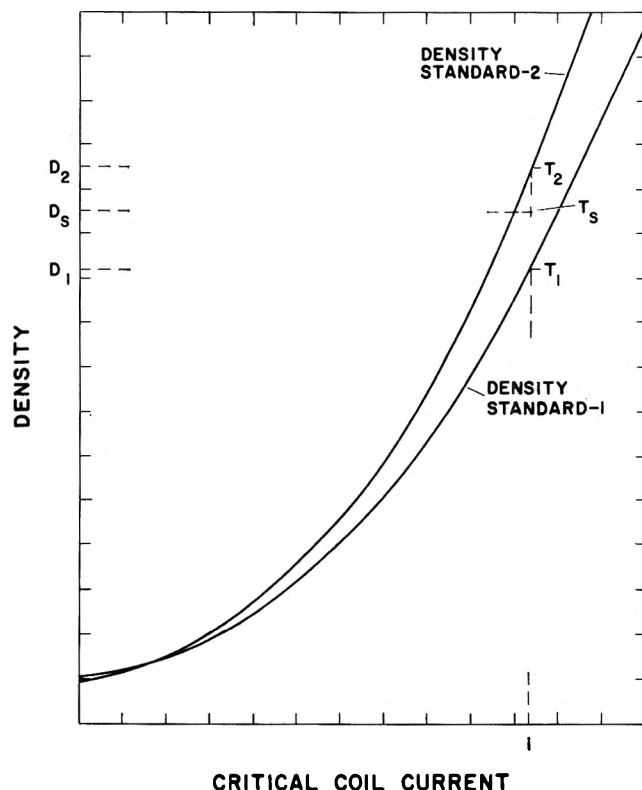


Figure 2. Idealized calibration curves.

A standardized procedure was used. The same applied voltage was used to pull the float into position for each measurement. The current in the coil was reduced slowly and uniformly, the same rate of current change in the coil being used for calibration and for measurement. Four to six measurements of the critical current were made for each density determination. The sensitivity of the densimeter varied from 5×10^{-6} g./cm.³ at low currents, 10–20 ma., to 1×10^{-5} g./cm.³ at the highest currents, 70–80 ma. The long term reproducibility was $\pm 2 \times 10^{-5}$ g./cm.³. Temperature cycling of the apparatus did not shift the calibration curves. The error due to the difference in magnetic susceptibilities of the organic density standard and water causes an error of roughly 1 part in 10^6 .

Preparation of Tritium Oxide. Tritium gas was evolved from UT_3 and a sample was analyzed on a Model 201 Consolidated-Nier mass spectrometer. The gas was converted to T_2O with CuO (350°). The tritium gas passed through a palladium valve and contacted the CuO in a mercury-free system. T_2O vapor was trapped with liquid nitrogen near the exit of the CuO

tube. T₂O was then freed of gases, distilled into a storage vessel equipped with stopcock and ground joint, and kept at liquid nitrogen temperature until needed. Two 1-g. samples of T₂O were prepared. One was used in exploratory work and the other, of better purity, was used in the final density measurements.

Analysis of T₂O. The isotopic composition of the 1-g. sample of T₂O was determined by the iron reduction-mass spectrometer method. The procedure has been described and tested for absolute accuracy with high purity D₂O.⁵ Briefly, 10-ml. STP samples of T₂O vapor, in equilibrium with liquid T₂O at 20.0°, were reduced with powdered iron (500°), and the resulting T₂ was analyzed on the mass spectrometer, previously conditioned with high purity T₂. A correction was made for ΔN_H, the increase in the hydrogen atom fraction of the sample due to pickup of hydrogen in the decomposition system. This was determined⁵ as with D₂O, using 99.0 atom % T₂ gas. ΔN_H was 0.0009 ± 0.0004 for T₂O (0.0006 ± 0.0002 for D₂O). In the D₂O analysis⁵ the deuterium content by the iron reduction method was lower by 0.02% than the n.m.r. and density methods (which gave the same analyses). Although this difference is about the limit of error of the iron reduction method, the tritium atom fraction from the mass spectrometer analysis was increased by 0.0002. A further increase of 0.0009 (ΔN_H) was made to give the tritium atom fraction, N_v, of the vapor in equilibrium with the original liquid. The corrected values of N_v were 0.9922 for each of the two analyses before the density measurements and 0.9924 and 0.9923 for the two analyses after the measurements (see below), giving N_v = 0.9923 (average). The desired tritium atom fraction of the liquid, N_l, was obtained⁶ from

$$(N_l/1 - N_l) = [N_v/(1 - N_v)][P^0_{H_2O}/P^0_{T_2O}]^{1/2} \quad (1)$$

$P^0_{H_2O}/P^0_{T_2O}$ is 1.22 at 20.0°,⁷ giving $N_l = 0.9930$. The estimated uncertainty is ±0.0005.

Temperature Corrections. The T₂O temperature was greater than the bath temperature because of the absorption of self-radiation and heating effects of the coil current. The temperature difference was measured with a differential thermocouple having one junction attached to the float. With 1 g. of 99% T₂O in the densimeter and no current in the coil, the temperature difference was 0.48 ± 0.01° (a calculated estimate was in close agreement). The correction for the temperature increase due to coil current was measured as a function of current for T₂O and the standards at 25.0° and varied from 0.01° at 25 ma. to 0.04° at 70 ma. (a.c.).

Density Measurements. After two analyses the T₂O was transferred to the density vessel. The latter was

attached to a vacuum system, evacuated, conditioned by exposure to T₂O vapor, and again evacuated. The T₂O was distilled into the side arm (x) of the density vessel, which was then sealed off. Upon warming to room temperature the T₂O was poured into the measurement section, and the vessel was set in its brass holder in the thermostat.

Density measurements were first run alternately and repeatedly at 25.20 and 35.06° with a reproducibility of ±0.00002 g./cm.³ at each temperature. Then measurements were made from 5 to 54°. Densities were then remeasured at 25.20 and 35.06° and agreed with the initial measurements. The temperature of flotation of the float in T₂O, without current, was also determined. After completion of this first density series, the liquid T₂O was spilled into the side arm (x), degassed, and analyzed twice. After observation of constant densities for several hours at 25.20 and 35.06°, a second series of measurements was made from 5 to 54°. The 25.20 and 35.06° points were repeated and agreed with the initial values for this series.

On completion of the density measurements the T₂O sample was distilled into a storage container through a break-seal. The portion of the vessel above B, Fig. 1, was carefully replaced with a tapered joint and cap. The vessel and float were washed with water and alcohol and dried *in vacuo*. The complete critical current calibration with nitrobenzene was repeated. The shift from the original calibration was about 2 × 10⁻⁵ g./cm.³ throughout the range. This calibration was averaged with the original for evaluation of the T₂O data. An equal shift was assumed for the other standards.

Results

Density of T₂O. The two series of densities differed by a constant amount, 0.00028 ± 0.00001 g./cm.³, over the temperature range. One-half of this difference, 0.00014 g./cm.³, was added to the density values of the first series, in which the measurements were more numerous, to give the values in Table I. The total absolute error in a density is about ±0.015%.

Density values for 100 mole % T₂O were calculated using Longworth's⁸ equation (2). The density of the T₂O sample is given by

$$D = (N_1M_1 + N_2M_2)/(N_1V_1 + N_2V_2) \quad (2)$$

(5) M. Goldblatt and W. M. Jones, to be published.

(6) G. N. Lewis and R. E. Cornish, *J. Am. Chem. Soc.*, **55**, 2616 (1933).

(7) W. M. Jones, this laboratory, to be published.

(8) L. G. Longworth, *J. Am. Chem. Soc.*, **59**, 1483 (1937).

where M is molecular weight, N is mole fraction, V is molar volume, and subscripts 1 and 2 refer to H_2O and T_2O , respectively. Using $V_1 = M_1/D_1$ and $V_2 =$

The average deviation of the corrected experimental densities from (5) was ± 0.00003 g./cm.³. Densities for pure T_2O from (5) are given in Table II for 2° intervals.

Table I: Densities of 99.30 Mole % T_2O

Temp., °C.	Density, g./cm. ³	Temp., °C.	Density, g./cm. ³
4.98	1.21268	16.72	1.21338
5.51	1.21283	17.91	1.21333
6.49	1.21302	18.64	1.21324
7.62	1.21315	19.06	1.21318
8.00	1.21322	19.54	1.21313
8.60	1.21328	20.53	1.21300
8.98	1.21333	21.73	1.21286
9.63	1.21336	23.09	1.21257
10.10	1.21343	25.20	1.21215
10.59	1.21343	28.17	1.21146
11.66	1.21348	30.10	1.21096
12.17	1.21351	33.09	1.21008
12.68	1.21352	35.06	1.20943
13.09	1.21353	38.07	1.20833
13.53	1.21352	40.04	1.20752
13.99	1.21350	43.17	1.20622
14.70	1.21350	45.13	1.20532
15.07	1.21349	47.88	1.20399
15.71	1.21346	49.98	1.20293
16.06	1.21346	53.04	1.20130
		54.25 ^a	1.20069 ^a

^a Density determined by temperature of flotation.

M_2/D_2 , where D_1 and D_2 are the densities of pure H_2O and T_2O , (2) becomes

$$D_2 = \frac{D}{\frac{M_1(1 - N_2)}{M_2 N_2} \left(\frac{D_1 - D}{D_1} \right) + 1} \quad (3)$$

The physical atomic weights⁹ of hydrogen and tritium were converted to the chemical scale, giving molecular weights (chemical scale) of 18.01573 and 22.03238 for H_2O and T_2O . Then, for $N_2 = 0.9930$, eq. 3 becomes

$$D_2 = \frac{D}{1 - 0.005764(D - D_1)/D_1} \quad (4)$$

The density for H_2O was taken from the International Critical Tables.¹⁰

A least-squares treatment of the 100% T_2O densities derived from the data of Table I gave the following temperature dependence.

$$D_2 = 1.213124 + 2.9129 \times 10^{-4}t - 1.1954 \times 10^{-5}t^2 + 5.301 \times 10^{-8}t^3 \text{ g./cm.}^3 \quad (5)$$

Table II: Density of Pure T_2O

Temp., °C.	Density, g./cm. ³	Temp., °C.	Density, g./cm. ³
6	1.21445	32	1.21194
8	1.21472	34	1.21129
10	1.21489	36	1.21059
12	1.21499	38	1.20984
14	1.21501	40	1.20904
16	1.21494	42	1.20820
18	1.21480	44	1.20731
20	1.21459	46	1.20639
22	1.21431	48	1.20543
24	1.21396	50	1.20443
26	1.21355	52	1.20340
28	1.21307	54	1.20234
30	1.21254		

Maximum Density. Equation 5 gives a maximum density of 1.21502 g./cm.³ at $13.4 \pm 0.1^\circ$. Chang and Chien¹¹ found the maximum density for 100% D_2O to be at $11.21 \pm 0.05^\circ$. The maximum density of ordinary water occurs at 3.98° . The maximum difference in densities of T_2O and H_2O is 0.21692 g./cm.³ and occurs at about 35° .

Relative Molar Volumes. Molar volumes for pure T_2O were calculated at 5° intervals using densities from eq. 5. Molar volumes for pure D_2O were calculated using the densities of Kirshenbaum¹² from 5 to 40° and of Shatenshtein,¹³ raised by five parts in 10⁵ to match those of Kirshenbaum, from 45 to 55°. A molecular weight of 20.02838 was used for D_2O . Molar volumes of D_2O and T_2O relative to those of H_2O are listed in Table III. The number of significant figures is given, at least for T_2O , only for relative accuracy.

Tritium Peroxide Formation. One effect of self-radiation on T_2O is the production of T_2O_2 , which would raise the measured density. Much work has been done

- (9) N. A. Lange, "Handbook of Chemistry," Handbook Publishers, Inc., Sandusky, Ohio, 1956, p. 114.
 (10) "International Critical Tables," Vol. III, 1st Ed., McGraw-Hill Book Co., New York, N. Y., 1928, p. 25.
 (11) T. L. Chang and J. Y. Chien, *J. Am. Chem. Soc.*, **63**, 1709 (1941).
 (12) I. Kirshenbaum, ref. 2, p. 12.
 (13) A. I. Shatenshtein, *et al.*, "Isotopic Water Analysis," AEC-Tr-4136 (1960); 2nd Ed., 1957, p. 69; available from the Office of Technical Services, Department of Commerce, Washington 25, D. C.

on the radiolysis of water¹⁴ but none with the steady-state level of β -radiation present in 1 cm.³ of pure T₂O, 6×10^{17} e.v./cc./sec. A measurement was made of the concentration of T₂O₂ in 1 cm.³ of 98 mole % T₂O using ultraviolet spectrophotometry.

Table III: Relative Molar Volumes of D₂O and T₂O

Temp., °C.	V_{D_2O}/V_{H_2O}	V_{T_2O}/V_{H_2O}
5	1.00555	1.00710
10	1.00485	1.00634
15	1.00430	1.00565
20	1.00393	1.00508
25	1.00359	1.00460
30	1.00329	1.00420
35	1.00303	1.00389
40	1.00280	1.00364
45	1.00265	1.00343
50	1.00247	1.00323
55	1.00235	1.00305

The extinction coefficient curve for T₂O₂ from 2200 to 2750 Å. was estimated from values for H₂O₂¹⁵ and the known shift of the extinction coefficient curve for D₂O₂ relative to H₂O₂. According to Phibbs and Giguère¹⁶ the shift is about 390 cm.⁻¹ toward shorter wave length

and can be attributed to the difference in the zero-point vibrational energies of the peroxides. The shift of T₂O₂ from H₂O₂ was estimated to be 560 cm.⁻¹.

The T₂O was distilled into a 0.5-cm. path length rectangular silica cell fitted with stopcock and ground joint. The transmittance measurements were made against ordinary water in a matched cell on a Beckman DU spectrophotometer. Correction for cell fluorescence was made by subtracting the apparent transmission without the beam from the observed transmission. Measurements were started when the sample was 3.5 hr. old and were continued for 4 days. The concentration of T₂O₂ was constant at 0.002 ± 0.001 mole/l. over this period and from 2200 to 2750 Å. This would cause a 0.002% increase in the density of T₂O. No correction was made.

Acknowledgment. The author gratefully acknowledges helpful discussions with Dr. Wesley M. Jones. He also wishes to thank Mr. R. K. Zeigler for the least-squares treatment of the density data.

- (14) A. O. Allen, "The Radiation Chemistry of Water and Aqueous Solutions," D. Van Nostrand Company, Inc., Princeton, N. J., 1961, pp. 75-96.
- (15) W. C. Schumb, C. N. Satterfield, and R. L. Wentworth, "Hydrogen Peroxide," Reinhold Publishing Corporation, New York, N. Y., 1955, p. 291.
- (16) M. K. Phibbs and P. A. Giguère, *Can. J. Chem.*, **29**, 490 (1951).

Phosphorus-31 Nuclear Magnetic Resonance Studies of Phosphorus-Nitrogen Compounds

by Morris L. Nielsen and J. V. Pustinger, Jr.

Dayton Laboratory, Monsanto Research Corporation, Dayton, Ohio (Received August 16, 1963)

Correlations between P^{31} n.m.r. chemical shifts and structures of 66 phosphorus-nitrogen compounds are made for use in qualitative prediction. Substitution of $-OH$ ($-ONa$) or OPh by $-NH_2$ displaces the chemical shift to lower field, with somewhat greater effect for covalent compounds. Substitution of $-NH-$ for $-O-$ in chain and ring compounds also generally results in negative displacement, with the exception of $R_2P(O)NHP(O)R_2$. The effects of substituting $-NR_2$ for Cl or $-Ar$ groups on phosphorus are shown. Methyl groups on nitrogen attached to phosphorus generally give chemical shifts at lower field than do phenyl groups. In phosphonitrilic compounds, the trimeric derivatives have chemical shifts at lower field than the tetrameric ones. Spin-spin splittings are observed for $P-N-P$ and $P-N-H$ systems, in confirmation of their expected structures.

Phosphorus nuclear magnetic resonance is playing an ever-increasing role in structure characterization and qualitative identification. Chemical shift data for several hundred inorganic- and organophosphorus compounds have been published,¹⁻⁸ and attempts have been made to correlate these data with bond properties and electronic structures of molecules.^{2-4,6,9,10} Comparatively few data have been reported for phosphorus-nitrogen compounds.

To extend the usefulness of the phosphorus magnetic resonance data, we have measured the chemical shifts for some 66 quadruply connected phosphorus-nitrogen compounds. Empirical correlations describing the relative effect of different substituent groups on the phosphorus atom and substitution on the nitrogen atom are presented. Measurements of spin-spin coupling between phosphorus nuclei and protons in the aromatic phosphoramidates establish the presence of considerable covalent bonding in the $P-N-H$ bond networks. The observation of these spin-spin splittings shows minimal electrical quadrupolar interactions arising from the nitrogen nucleus.

Experimental

The n.m.r. spectra were obtained on a Varian Model V-4300-2 high resolution spectrometer with a radio-frequency of 16.2 Mc. and a magnetic field of approximately 9400 gauss, using a Varian magnet, Model V-

4012-A. Chemical shifts, reported in parts per million (p.p.m.) of the applied field, are based upon 85% H_3PO_4 as the standard (zero shift). Upfield shifts are denoted by a plus sign, downfield shifts by a minus sign. The samples were generally contained in a 15-mm. o.d. Pyrex tube, with a narrow (1-2 mm.) tube containing the H_3PO_4 inserted concentrically through the stopper. Accuracy is approximately ± 0.5 p.p.m. For measuring spin-spin coupling constants, samples were contained in 5-mm. o.d. tubes and spun in order to minimize field inhomogeneities.

All data were obtained with samples of pure compounds identified by physical constants or elemental

- (1) H. S. Gutowsky, D. W. McCall, and C. P. Slichter, *J. Chem. Phys.*, **21**, 279 (1953).
- (2) H. S. Gutowsky and D. W. McCall, *ibid.*, **22**, 162 (1954).
- (3) N. Muller, P. C. Lauterbur, and J. Goldenson, *J. Am. Chem. Soc.*, **78**, 3557 (1956).
- (4) J. R. Van Wazer, C. F. Callis, J. N. Shoolery, and R. C. Jones, *ibid.*, **78**, 5715 (1956).
- (5) H. Finogold, *Ann. N. Y. Acad. Sci.*, **70**, 875 (1958).
- (6) C. F. Callis, J. R. Van Wazer, J. N. Shoolery, and W. A. Anderson, *J. Am. Chem. Soc.*, **79**, 2719 (1957).
- (7) K. Moedritzer, L. Maier, and L. C. D. Groenweghe, *J. Chem. Eng. Data*, **7**, 307 (1962).
- (8) R. A. Y. Jones and A. R. Katritzky, *J. Inorg. Nucl. Chem.*, **15**, 193 (1961).
- (9) J. R. Parks, *J. Am. Chem. Soc.*, **79**, 757 (1957).
- (10) L. C. D. Groenweghe, L. Maier, and K. Moedritzer, *J. Phys. Chem.*, **66**, 901 (1962).

analyses. Tabulation of data for these and related compounds will appear elsewhere.¹¹

Results and Discussion

High resolution nuclear magnetic resonance data provide information about the structure of molecules in two ways. The chemical shift data indicate relative degrees of electron screening of the nucleus. Observation of the electron coupled spin-spin interactions provides additional information on the structural relationships of the nonequivalent nuclei in a molecule.

Chemical Shift Data.—Several theoretical treatments¹²⁻¹⁴ of electron shielding have been reported. As yet, a suitable method has not been derived for precise prediction of chemical shifts from n.m.r. theory or empirical relationships. Qualitatively, electron shielding of a nucleus can be considered as being influenced by two opposing effects, namely, electronegativity and the ability to form double bonds.

For quadruply connected phosphorus, the chemical shifts are believed due in significant part to changes in the distribution of π -bonds among the four σ -bonds.¹⁵ In spite of the difficulty in disentangling electronegativity and double bond effects, the data for the phosphorus-nitrogen systems emphasize the influence of the double-bond character of the four σ -bonds.

Substitution of nitrogen for oxygen on quadruply connected phosphorus results in more negative chemical shifts (Table I).

Table I: Displacement of P³¹ N.m.r. Chemical Shift due to Substitution of the -NH₂ Group for -ONa

	Chemical shift, p.p.m.	Displacement of shift per N atom, p.p.m.
(NaO) ₃ PO	-6.0	... ^a
(NaO) ₂ P(O)NH ₂	-8.9	-2.9
NaOPO(NH ₂) ₂	-14.5	-5.6
PO(NH ₂) ₃	-22.0	-7.5
(NaO) ₃ PS	-33.8	... ^b
NaOPS(NH ₂) ₂	-54.2	-9.2
PS(NH ₂) ₃	-61.1	-6.9
(EtO) ₂ P(O)ONa	-3.8	...
(EtO) ₂ P(O)NH ₂	-11.1	-7.3
(PhO) ₂ P(O)ONa	+9.0	...
(PhO) ₂ P(O)NH ₂	-2.8	-11.8
PhOPO(ONa) ₂	0.0	...
PhOPO(NH ₂)ONH ₂	-0.5	-0.5
PhOPO(NH ₂) ₂	-15.2	-7.4
PhPO(ONa) ₂	-13.8	...
PhPO(NH ₂) ₂	-25.4	-5.8
Ph ₂ P(O)ONa	-23.6	...
Ph ₂ P(O)NH ₂	-25.5	-1.9

^a See ref. 8. ^b See ref. 7.

It is probable that the paramagnetic portion of the chemical shift is related to the degree of hybridization of the P-N bond as compared with that of the P-O bond.

For monomeric phosphorus compounds, there appears to be a relation between the type of compound and the extent of the displacement. The displacement is least for compounds having a high degree of ionic character, as, for example, (NaO)₂P(O)NH₂. For the compounds shown, the average displacement is -4 ± 1 p.p.m. per nitrogen atom. Compounds which are characteristically covalent, such as those containing alkyl or aryl groups, show a higher displacement: approximately -8 ± 3 p.p.m. An "oxygen-to-nitrogen shift" of -11 ± 2 p.p.m. was reported by Van Wazer, *et al.*⁴

The nitrogen-for-oxygen displacement is also negative for the linear dimers (pyrophosphates and imido-diphosphates) and trimers (triphosphates and diimidotriphosphates) (Table II). These displacements

Table II: Displacement of P³¹ N.m.r. Chemical Shift due to Substitution of -NH- for -O- in Chain Compounds

	Chemical shift, p.p.m.	Displacement of shift, p.p.m.
(NaO) ₂ P(O)OP(O)(ONa) ₂	+6.0	... ^a
(NaO) ₂ P(O)NHP(O)(ONa) ₂	-2.7	-8.7
(EtO) ₂ P(O)OP(O)(OEt) ₂	+13.4	...
(EtO) ₂ P(O)NHP(O)(OEt) ₂	-2.5	-15.9
(PhO) ₂ P(O)OP(O)(OPh) ₂	+23.9	...
(PhO) ₂ P(O)NHP(O)(OPh) ₂	+10.7	-13.2
(NaO)P α (O)OP β (O)(ONa)OP α (O)(ONa) ₂	+4 (P α) +18 (P β)	... ^a
(NaO) ₂ P(O)NHP(O)(ONa)NHP(O)(ONa) ₂	-1.6	-5.6; -19.6
(PhO) ₂ P α (O)OP β (O)(OPh)OP α (O)(OPh) ₂	+26.6 (P α) +35.2 (P β)	...
(PhO) ₂ P α (O)NHP β (O)(OPh)NHP α (O)(OPh) ₂	+12.5 (P α) +5.9 (P β)	-13.1; -29.3

^a See ref. 4.

are greater for the esters than for the corresponding salts because of the covalent ligands. A comparison of tetraethyl imidodiphosphate with the sodium salt shows that the influence of the imido group is strong enough to offset the displacement caused by substituting EtO- for NaO-. As a consequence, the net difference is zero.

An interesting effect on the chemical shift is produced by the two nitrogens in the pentaphenyl diimidotri-

- (11) M. L. Nielsen, J. V. Pustinger, and J. Strobel, to be published.
- (12) N. F. Ramsey, *Phys. Rev.*, **78**, 699 (1950); **83**, 450 (1951); **85**, 60 (1952); **86**, 243 (1952).
- (13) J. A. Pople, *Proc. Roy. Soc. (London)*, **A239**, 541-550 (1957).
- (14) W. G. Schneider, H. J. Bernstein, and J. A. Pople, *J. Chem. Phys.*, **28**, 601 (1959).
- (15) J. R. Van Wazer, "Phosphorus and Its Compounds, Vol. I. Chemistry," Interscience Publishers, Inc., New York, N. Y.; 1958, p. 50.

phosphate ester, where the triplet due to the middle

$$\begin{array}{c} \text{O} \\ | \\ \text{-NH-P-NH-} \\ | \\ \text{O} \end{array}$$

group (see also Table XI) is at lower field (+5.9 p.p.m.) than the doublet due to the end

$$\begin{array}{c} \text{O} \\ | \\ \text{-PNH-} \\ | \\ \text{O} \end{array}$$

groups (+12.5 p.p.m.). This can be attributed to the strong influence of two -NH- groups on the β -phosphorus. By comparison, the spectrum of pentaphenyl triphosphate ester is similar to that of sodium triphosphate,^{4,6} in which the triplet for the middle group is at higher field than the doublet for the end groups.

In contrast to the esters, if two phenyl groups are attached directly to phosphorus, the displacement in chemical shift resulting from replacement of -O- with -NH- is positive (Table III). This is noted to some degree in the phosphinic compounds in Table I where the difference in the chemical shifts of $\text{Ph}_2\text{P}(\text{O})\text{ONa}$ and $\text{Ph}_2\text{P}(\text{O})\text{NH}_2$ is only -1.9 p.p.m.

Table III: Displacement of P^{31} N.m.r. Chemical Shift due to Substitution of -NH- for -O- in Diphosphinic Compounds

	Chemical shift, p.p.m.	Displacement in shift, p.p.m.
$\text{Me}_2\text{P}(\text{O})\text{OP}(\text{O})\text{Me}_2$	-52.6	... ^a
$\text{Me}_2\text{P}(\text{O})\text{NHP}(\text{O})\text{Me}_2$	-43.4	+9.2
$\text{Ph}_2\text{P}(\text{O})\text{OP}(\text{O})\text{Ph}_2$	-33.1	... ^a
$\text{Ph}_2\text{P}(\text{O})\text{NHP}(\text{O})\text{Ph}_2$	-14.5	+19.1

^a See ref. 7.

In ring compounds (Table IV) the effect due to substituting -NH- for -O- is somewhat greater than in the linear dimers and trimers.

Substitution of $-\text{NH}_2$ for $-\text{OPh}$ on phosphorus causes a negative displacement in the chemical shift (Table V).

Substitution of $-\text{NR}_2$ for $-\text{Cl}$, where R is aliphatic, in the class $(\text{Me}_2\text{N})_n\text{P}(\text{O})\text{Cl}_{3-n}$, generally results in a negative displacement (Table VI). The chemical shift for the trisubstituted phosphoric amide is not as far in the negative direction as expected.

In contrast, substitution of $-\text{N} \begin{array}{l} \text{Ar} \\ \diagup \\ \text{H} \end{array}$ or $-\text{N} \begin{array}{l} \text{Ar} \\ \diagdown \\ \text{Ar} \end{array}$ for -Cl in the classes $(\text{PhNH})_n\text{P}(\text{O})\text{Cl}_{3-n}$ and $(\text{Ph}_2\text{N})_n\text{P}(\text{O})\text{Cl}_{3-n}$ causes little change in the chemical shift (Table VII). Again, the trisubstituted phosphoric amide has a more positive shift than expected.

Comparison of the effect of nitrogen-containing substituents on phosphorus with phenyl substitution

Table IV: Displacement of P^{31} N.m.r. Chemical Shift due to Substitution of -NH- for -O- in Ring Compounds

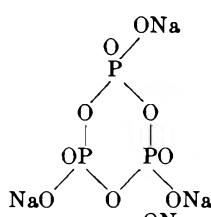
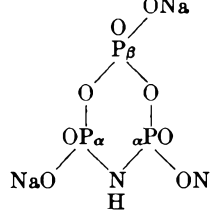
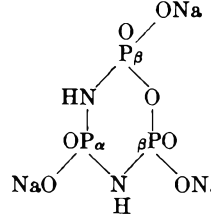
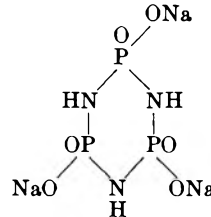
	Chemical shift, p.p.m.	Displacement in shift, p.p.m.
	+21.4
	+10.4 (P_α) +20.2 (P_β)	-11.0
	+4.2 (P_α) +7.9 (P_β)	-6.2 -12.3
	+1.5	-6.4

Table V: Displacement of P^{31} N.m.r. Chemical Shift due to Substitution of $-\text{NH}_2$ for $-\text{OPh}$

	Chemical shift, p.p.m.	Displacement in shift, p.p.m.
$(\text{PhO})_2\text{P}(\text{O})\text{NHP}(\text{O})(\text{OPh})_2$	+10.7	...
$(\text{PhO})_2\text{P}_\alpha(\text{O})\text{NHP}_\beta(\text{O})(\text{OPh})\text{NH}_2$	+8.4 (P_α) -3.8 (P_β)	(-2.3) -14.5
$(\text{PhO})_2\text{P}_\alpha(\text{O})\text{NHP}_\beta(\text{O})(\text{OPh})\text{NHP}_\alpha(\text{O})(\text{OPh})_2$	+12.5 (P_α) +5.9 (P_β)
$(\text{PhO})_2\text{P}_\alpha(\text{O})\text{NHP}_\beta(\text{O})(\text{OPh})\text{NHP}_\gamma(\text{O})(\text{OPh})\text{NH}_2$	+8.4 (P_α) +6.3 (P_β) -0.8 (P_γ)	(-4.1) (+0.4) -13.3

(Table VIII) shows that the chemical shift becomes more positive in the order

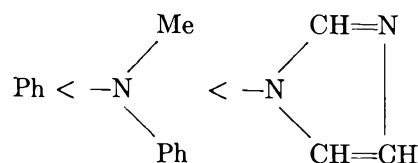


Table VI: Displacement of P³¹ N.m.r. Chemical Shift due to Substitution of -NMe₂ for -Cl

	Chemical shift, p.p.m.	Reference
POCl ₃	-2.2	10
Me ₂ NPOCl ₂	-16.1	7
(Me ₂ N) ₂ POCl	-29.6	
PO(NMe ₂) ₃	-23.4	3
	-27.0	4

Table VII: Displacement of P³¹ N.m.r. Chemical Shift by Substitution of -N< $\frac{\text{Ph}}{\text{H}}$ and -N< $\frac{\text{Ph}}{\text{Ph}}$ for -Cl

	Chemical shift, p.p.m.
POCl ₃	-2.2 ^a
PhNHPOCl ₂	-7.6
(PhNH) ₂ POCl	-4.1
PO(NHPh) ₃	+4.8
Ph ₂ NPOCl ₂	-8.2
(Ph ₂ N) ₂ POCl	-8.1
PO(NPh ₂) ₃	-1.7

^a See ref. 10.**Table VIII:** Displacement of P³¹ N.m.r. Chemical Shift due

	Chemical shift, p.p.m.
Ph ₃ PO	-27.0 ^a
PhPO[N(Me)Ph] ₂	-21.0
PhP(O)(Im)[N(Me)Ph]	-16.6
PO[N(Me)Ph] ₃	-13.0
PhPO(Im) ₂	-6.0
Ph(Me)NPO(Im) ₂	+7.6
PO(Im) ₃	+16.3

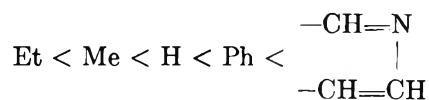
^a See ref. 7.

Substitution of an amido or imido hydrogen by an alkyl or aryl group causes changes in the chemical shift which depend upon the other substituent groups that are present (Fig. 1). In all cases, methyl-substituted compounds have more negative chemical shifts than phenyl-substituted ones. The chemical shifts of the methyl and phenyl derivatives with respect to the hydrogen analogs vary, however, so that both are more negative or are more positive than the hydrogen analogs, or one may be more negative and the other more positive than the hydrogen compound.

For the classes PO(N< $\frac{\text{Y}}{\text{Ph}}$)₃, Me₂NP(O)(N< $\frac{\text{Y}}{\text{Ph}}$)₂, and

PhPO(N< $\frac{\text{Y}}{\text{Ph}}$)₂, the order of the more positive shift is

Me < Ph < H. For the class PhPO(N< $\frac{\text{Y}}{\text{H}}$)₂, the order is



Likewise, for the class PhOPO(N< $\frac{\text{Y}}{\text{H}}$)₂, the order is Me

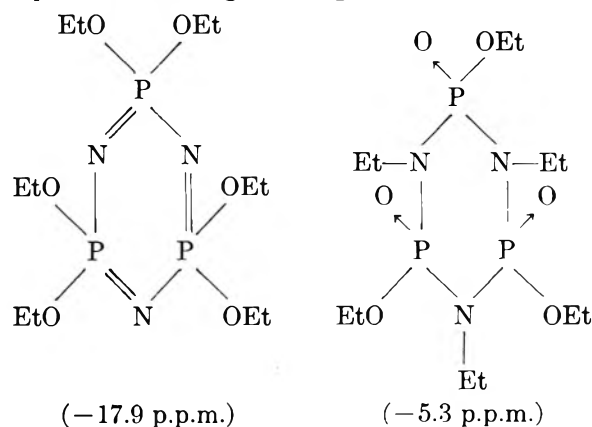
< H < Ph. For the class (PhO)₂P(O)N< $\frac{\text{Y}}{\text{H}}$, as Y is varied, the chemical shift becomes more positive in the order H < Me < Ph. For the class (PhO)₂P(O)N(Y)P(O)(O)(Ph)₂, the order is Me < H < Ph, although the differences are not large.

The chemical shifts of the trimeric and tetrameric phosphonitrilic derivatives (Table IX) differ by 10 to 22

Table IX: N.m.r. Chemical Shift for Phosphonitrilic Derivatives

	Chemical shift, p.p.m.		Difference in shift, p.p.m.
	Trimer	Tetramer	
[PN(OEt) ₂] _n	-17.9	+0.6	18.5
[PN(NCS) ₂] _n	+26.8	+49.1	22.3
[PN(NHC(S)NH ₂) ₂] _n	+10.8	+21.2	10.4
[PN(NHC(S)NHPh) ₂] _n	+2.2	+23.2	21.0

p.p.m., the tetrameric being more positive. This agrees with results reported for the chlorides (PNCl₂)₃ and (PNCl₂)₄ by Lund, *et al.*¹⁶ The cyclic phosphimides, however, show much less difference between the trimer and tetramer: Na₃(PO₂NH)₃, +1.5 p.p.m.; Na₄(PO₂NH)₄, +3.7 p.p.m. Two isomers, C₁₂H₃₀N₃O₆P₃, one of which is a phosphonitrilate and the other a phosphimate, differ in chemical shift, with the phosphonitrilate being more negative



(16) L. G. Lund, N. L. Paddock, J. E. Proctor, and H. T. Searle, *J. Chem. Soc.*, 2542 (1960).

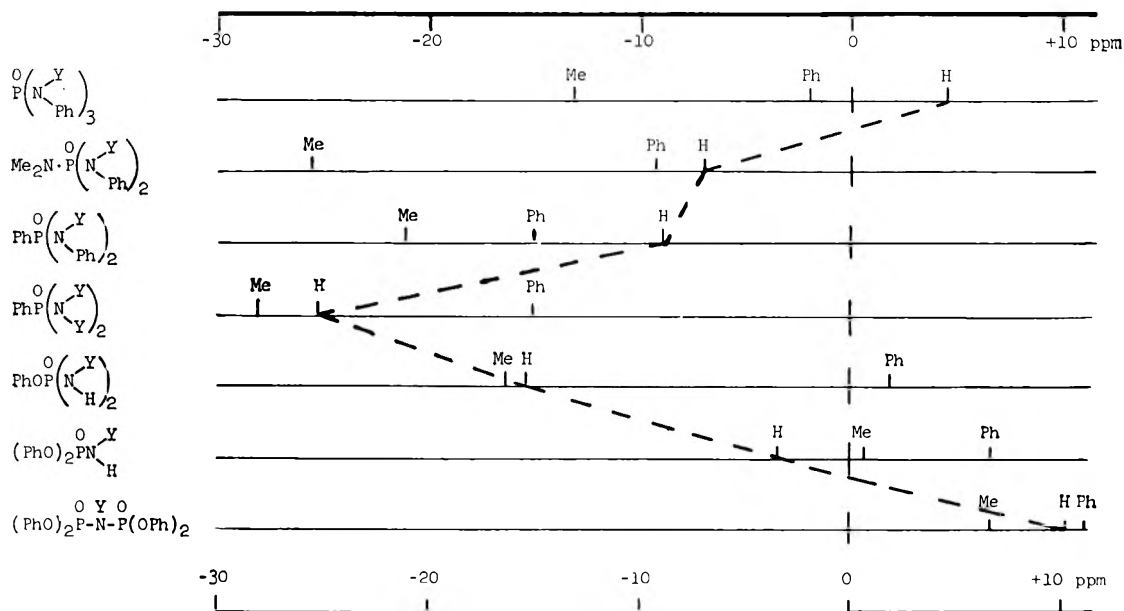
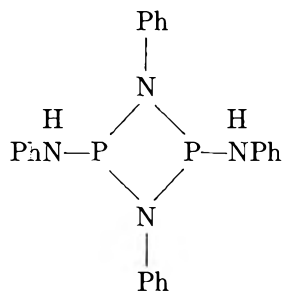
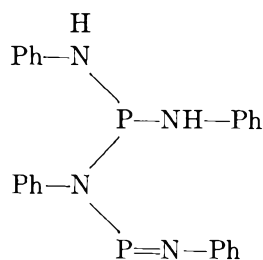


Figure 1. Effect on P^{31} n.m.r. chemical shift by substitution on nitrogen.

Tetraphenyl-2,4-diamino-1,3,2,4-diazadiphosphetidine¹⁷

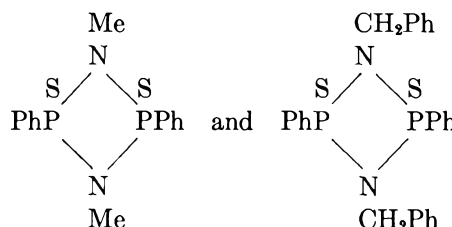


variously identified as "phosphazobenzolanilide"¹⁸ or phenylphosphazoanilide,¹⁷ $PhNHP=NPh$, and phenylimino (phenylamino) phosphine¹⁹



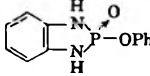
gave a spectrum containing two peaks at -113.6 and -109.2 p.p.m. Since the peak separation is large and dependent upon frequency (71 c.p.s. at 16.2 Mc., 52 c.p.s. at 12.8 Mc.), it is believed that the data represent two separate phosphorus environments. Whether these are due to two isomers of a cyclic structure or to

the linear structure above, suggested by Goldschmidt, *et al.*,¹⁹ has not been resolved and will be the subject of future work. The presence of geometrical isomers in the compounds



was established by Trippett²⁰ from proton magnetic resonance which has not been applicable in this instance.

Table X: P^{31} Spin-Spin Coupling due to Hydrogen on Nitrogen

	Chemical shift, p.p.m.	Number of peaks	J_{P-N} , c.p.s.
$(PhO)_2P(O)NH_2$	-2.8	3	7.5
$(PhO)_2P(O)NHPh$	+6.3	2	10
$PhOP(O)(NHPh)_2$	+2.2	3	10
$PO(NHPh)_3$	+4.8	4	10
	-18.1	3	15

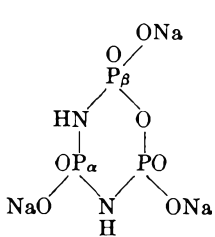
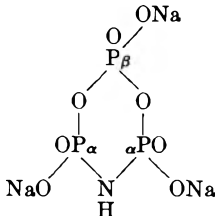
(17) H. W. Grimm, A. Guenther, and J. F. Morgan, *J. Am. Chem. Soc.*, **68**, 539 (1946).

(18) A. Michaelis and G. Schroeter, *Ber.*, **27**, 490 (1894).

(19) S. Goldschmidt and H. L. Krauss, *Ann.*, **595**, 193 (1955).

(20) S. Trippett, *J. Chem. Soc.*, 4731 (1962).

Table XI: P³¹ Spin-Spin Coupling due to Nonequivalent Phosphorus Nuclei

	Chemical shift, p.p.m.	Number of peaks	J _{P-P} , c.p.s.
(PhO) ₂ P _α (O)NHP _β (O)(OH) ₂	+8.1 (P _α)	2	14
	+2.5 (P _β)	2	14
(PhO) ₂ P _α (O)NHP _β (O)(OK)OH	+5.6 (P _α)	2	10
	+4.0 (P _β)	2	10
(PhO) ₂ P _α (O)NHP _β (O)(OK) ₂	+3.3 (P _α)	2	8
	+2.1 (P _β)	2	8
(PhO) ₂ P _α (O)NHP _β (O)(OK) ₂ ·KOH	+5.7 (P _α)	2	31
	-2.2 (P _β)	2	31
(PhO) ₂ P _α (O)NHP _β (O)(OPh)NH ₂	+8.4 (P _α)	2	12
	-3.8 (P _β)	2	12
(PhO) ₂ P _α (O)NHP _β (O)(OPh)NHP _α (O)(OPh) ₂	+12.5 (P _α)	2	13
	+5.9 (P _β)	3	13
(NaO) ₂ P(O)NHP(O)(ONa)NHP(O)(ONa) ₂	-1.6 ^a	Multiple	..
(PhO) ₂ P _α (O)NHP _β (O)(OPh)NHP _γ (O)(OPh)NH ₂	+8.4 (P _α)	4	14
	+6.3 (P _β)	Multiple	8
	-0.8 (P _γ)	4	8
	+4.2 (P _α)	3	8
	+7.9 (P _β)	2	8
	+10.4 (P _α)	2	18
	+20.2 (P _β)	3	18

^a The spectrum consists of a single resonance peak superimposed upon a multiplet. The half-peak width is 2 c.p.s. and the base width is 20 c.p.s. The spectrum approximates the theoretical pattern for an AB₂ system where $J/(\nu_0(\sigma_B - \sigma_A)) = 0.5$.

Spin-Spin Coupling. Interactions between nonequivalent nuclei in a molecule can produce splitting of resonance peaks into multiplets, through a phenomenon called indirect spin-spin coupling.¹ The extent of coupling is reflected in the magnitude of the splitting and is expressed as the coupling constant, J . The magnitude of splitting is dependent, in most part, on the gyromagnetic ratio of the nuclei, the proximity of nonequivalent nuclei, and the degree of covalent bonding in the bond networks.

Spin-spin coupling of the P³¹ resonance with hydrogen on phosphorus, as in (RO)₂P(O)H, or by hydrogen in P-C-H compounds, as in CH₃P(O)(ONH₂)₂, has been reported.^{1,5-7,11} Likewise, that in P-S-C-H, P-O-C-H, and P-N-C-H compounds has been observed.^{3,5,21}

In the present work, splitting by hydrogen in the P-N-H bond networks of phosphorus esters was found (Table X). The number of peaks, as in the cases above, is $n + 1$, where n is the number of hydrogen atoms. The magnitude of the coupling constant, J , probably

indicates to some degree the extent of covalent character in the bond system. No significant perturbation of the phosphorus and proton coupling by the magnetic moment and the electrical quadrupole moment of the interconnecting nitrogen was detected.

Phosphorus-nitrogen compounds in which a phenyl group is connected directly to phosphorus (rather than through oxygen as in the esters) show broad single peaks. For example, Ph₂P(O)NH₂ shows a half-peak width of about 37 c.p.s.; PhPO(NHPh)₂, about 30 c.p.s. Proton resonance data²² indicate spin-spin coupling between the phosphorus nucleus and protons of the phenyl ligand.

Splitting by two or more nonequivalent phosphorus nuclei is observed in most cases (Table XI). However, one compound shows a single peak: (PhO)₂P(O)N=PCl₃, with half-peak width of 3 c.p.s.

(21) R. C. Axtmann; W. E. Shuler, and J. H. Eberly, *J. Chem. Phys.*, **31**, 850 (1959).

(22) J. V. Pustinger and M. L. Nielsen, unpublished data.

Acknowledgment. This work was supported in part by the Air Force Materials Laboratory, Wright-Patterson Air Force Base, Ohio, under Contract AF 33-

(616)-7853. Some of the samples were prepared by T. J. Morrow and L. Parts. The spectra were recorded by J. Strobel and R. Eckstein.

Hydrolysis Rates and Distribution Coefficients of *d,l*-Butadienediepoxyde between Carbon Tetrachloride and Aqueous Sodium Hydroxide

by Ruth R. Benerito, Ralph J. Berni, and John B. McKelvey

Southern Regional Research Laboratory,¹ New Orleans, Louisiana (Received August 19, 1963)

Distribution coefficients at 25° of the *d,l*-isomers of butadienediepoxyde between CCl₄ and aqueous NaOH solutions up to concentrations of 6 *M* and the rates of hydrolysis of the diepoxyde have been measured and compared with values previously reported for the *meso*-isomer in aqueous phases up to 1.5 *M*. In addition, constants for the *meso*-isomer in the more concentrated basic solutions have been determined. The larger solubility of the *d,l*-isomers in the concentrated basic solutions, evidenced by the small distribution coefficients of the *d,l*-isomers as compared to those of the *meso*-isomer, accounts for differences in apparent rates of reaction of the two isomers in relatively strong basic solutions.

Introduction

The distribution coefficients of the *meso*-isomer of butadienediepoxyde (BDE) between a CCl₄ phase and aqueous NaOH phases and the rates of hydrolysis of BDE in the aqueous phases up to 1.5 *M* NaOH have been reported by Klein² and co-workers, who used an adaptation of the method of Larsson.³ Recent work in our laboratories with the *d,l*-isomers of butadienediepoxyde (BDO) necessitated the use of similar two-phase systems. However, it was observed that the *d,l*-isomers could be distributed and caused to react in aqueous phases containing NaOH at much higher concentrations than previously found suitable for treating the *meso*-isomer. Therefore, it was of interest to measure simultaneously the distribution coefficients of BDO between CCl₄ and aqueous NaOH solutions as concentrated as 6 *M* and to measure the rates of hydrolysis of BDO in the aqueous phase. In addition, the constants for the *meso*-isomer in the basic solutions more concentrated than previously used were measured.

Experimental

Materials. The *d,l*-butadienediepoxyde (BDO) was obtained from the Koppers Company.⁴ It was fractionally distilled at 120 mm. pressure. That fraction collected at 85° and used in rate studies had an epoxide equivalent of 2.37 (equiv. per 100 g.) as determined by the method of Durbetaki.⁵

The *meso*-butadienediepoxyde (BDE) was prepared from 1,4-dichloro-2,3-epoxybutane obtained from the Union Carbide Corp.⁴ by the method of Starcher, Mac-

- (1) One of the laboratories of the Southern Utilization Research and Development Division, Agricultural Research Service, U. S. Department of Agriculture.
- (2) E. Klein, J. B. McKelvey, and B. G. Webre, *J. Phys. Chem.*, **62**, 286 (1958).
- (3) L. Larsson, *Acta Chem. Scand.*, **10**, 1071 (1956).
- (4) Mention of trade names and firms does not imply their endorsement by the U. S. Department of Agriculture over similar products or firms not mentioned.
- (5) A. J. Durbetaki, *Anal. Chem.*, **28**, 2000 (1956).

Peek, and Phillips.⁶ The yields of *meso*-isomer obtained were essentially those obtained by the authors, 87%. The BDE used in the rate studies was that fraction collected at 38–39° at 15 mm. This fraction had an epoxide equivalent of 2.34 as determined by the method of Durbetaki.⁵ In addition, both BDE and BDO were characterized by their infrared spectra in CCl₄ solution. Characteristic spectra of both diepoxides have been published previously.⁷

Reagent grade carbon tetrachloride, sodium hydroxide, glacial acetic, and 30% hydrobromic acid in glacial acetic acid were used. All base solutions were carbonate-free and were analyzed against standardized HCl. The HBr titrant was standardized daily against Na₂CO₃ as the primary standard. A stock solution of 0.3710 *M* diepoxide in CCl₄ was standardized daily. All solutions were kept at 25.00°.

Procedure for Rate and Distribution Studies. Water-jacketed solubility burets of approximately 60-ml. capacity and fitted with Teflon plugs were used in all experiments. Before adding a fixed volume (15.00 ml.) of each standardized NaOH solution into the inner chamber of the buret, the outer jacket was filled with water from the constant temperature bath which was maintained at 25.00 ± 0.01°. The time at which the first drop of a fixed volume (15.00 ml. in series A and 25.00 ml. in series B) of the diepoxide stock CCl₄ solution entered the aqueous layer in the inner chamber was taken as the starting time. The buret was shaken immediately and then placed on a tumbling rack in the constant temperature bath. After the approximately predetermined time interval, the water-jacketed weight buret was removed from the bath and the phases were separated. The time of removal of the last of the CCl₄ layer from the weight buret was taken as the final time of the measurement. The concentration of diepoxide in the CCl₄ layer was determined on duplicate 1.00- or 3.00-ml. titers by the method of Durbetaki.⁵ All titrations were made with automatic gravity filling burets of 10-ml. capacity graduated to ±0.05 ml. and filled with standardized (approximately 0.1 *N*) HBr in glacial acetic acid.

In all determinations, a 0.3710 *M* BDO in CCl₄ solution was used. The basic solutions varied from 0.5 to 6 *M* as indicated in the tables of experimental results. For each concentration of base, two series utilizing 15/15 (series A) and 25/15 (series B) volume ratios of organic to aqueous phases were used. At least five points for each volume ratio for each base concentration were determined. The timed intervals varied from 5 min. up to 2 hr.

Results

The following equation gives a relationship between variables based on solute analyses in the organic phase.²

$$\ln [E]_0^0 - \ln [E]_t = \frac{kV_w}{KV_o + V_w} t \quad (1)$$

where $[E]_0^0$ is the concentration of epoxide in the CCl₄ phase after distribution has occurred but before hydrolysis, $[E]_t$ is the epoxide concentration in the CCl₄ phase after any time, t , V_o and V_w are the volumes of organic and aqueous phases, respectively, k is the specific reaction rate constant of the diepoxide in the aqueous phase leading to the first reaction product, and K is the distribution coefficient or molar ratio of epoxide in the organic and aqueous phases, respectively. The slope of a line derived from a plot of $\ln [E]_t$ vs. t gives a value involving both k and K as well as the volumes of both phases. These constants can be evaluated by the solution of simultaneous equations utilizing two slopes obtained by two series at a given base concentration but with two ratios of V_o/V_w . The log of the epoxide concentration (mequiv./ml.) remaining in the CCl₄ layer was plotted against the reaction time for each of the two volume ratios used for each of the base concentrations. All plots were linear, indicating pseudo-first-order reaction mechanism. The slope of each line was determined by the method of least squares, and the standard deviation, σ , associated with each slope was calculated according to the method of Ezekiel.⁸

A summary of the data obtained with BDO is presented in Table I. The activities of the hydroxyl ions given in Table I are on a molality basis and calculated from mean activity coefficients of NaOH as given by Harned and Owen.⁹ (That for the most concentrated base solution is an estimated value.)

Column 7 gives a corrected rate constant, k' , obtained by dividing the apparent rate constant obtained from the experimental data by the mean activity of the hydroxyl ion for each basic concentration. Up to 2 *m* NaOH solutions, the hydrolysis follows the rate equation

$$\frac{-d [E]_w}{dt} = k' a_{\text{OH}^-} [E]_w \quad (2)$$

For these less concentrated basic solutions, the rate constant agrees with that obtained for the *meso*-isomer

(6) P. S. Starcher, D. L. MacPeck, and B. Phillips, U. S. Patent 2,861,084 (Nov. 8, 1958).

(7) P. W. Feit, *Chem. Ber.*, **93**, 116 (1960).

(8) M. Ezekiel, "Methods of Correlation Analysis," 2nd Ed., John Wiley and Sons, Inc., New York, N. Y., 1947, p. 315.

(9) H. S. Harned and B. B. Owen, "The Physical Chemistry of Electrolytic Solutions," 2nd Ed., Reinhold Publ. Corp., New York, N. Y., 1950.

at similar basic concentrations, as Klein² reported an average corrected k of 0.0265 l. mole⁻¹ min.⁻¹ for the *meso*-isomer from 0.5 to 2.0 M NaOH solutions.

Unlike the *meso*-isomer, the *d,l*-isomers were found to be more soluble in the basic solutions, particularly at the higher concentrations. Whereas the *meso*-isomer had a distribution coefficient of 0.509 at 0.5 M NaOH and 1.166 at 2 M NaOH,² the *d,l*-isomer had a distribution coefficient of 0.362 at 0.504 M NaOH and its distribution coefficient was only 1.153 at the 6 M basic concentration. The distribution coefficient of the *d,l*-isomer between CCl₄ and H₂O (pH 7.0) was found to be 0.52.

For comparative purposes, k and K values for the *meso*-isomer were measured for more concentrated basic solutions than reported previously.² Table II is a summary of data obtained in this investigation for the *meso*-isomer. For aqueous phases less concentrated than 3 M NaOH, eq. 1 can be used to calculate both K and k , as the assumptions upon which the equation is

based are followed. In brief, distribution of the solute is established relatively fast compared to the rate of hydrolysis of the solute in the aqueous phase, and the concentration of epoxide in the aqueous phase can be used for its activity (activity coefficients of epoxide were not known). Values of k and K for aqueous phases more concentrated than 3 M are recorded in the tables, but these values are not reliable as the experimental data do not meet the requirements of eq. 1. Values are included to indicate the large differences in distribution constants of the two isomers when the aqueous phase is concentrated base.

Substitution of $[E]_o/K$ for $[E]_w$ in eq. 2 results in the following equation

$$\frac{-d[E]_w}{dt} = k' \frac{[E]_o}{a_{OH^-} K} \quad (3)$$

In the last columns of the tables are recorded values of $k/a_{OH^-}K$.

Table I: Summary of Distribution and Kinetic Data for *d,l*-BDO^a

	NaOH, M	a_{OH^-} , m	Slope $\times 10^3$	Error of slope $\times 10^4$	K^b	k , min. ⁻¹ $\times 10^2$	$k' = k/a_{OH^-}$, l. mole ⁻¹ min. ⁻¹ $\times 10^2$	$k'' = k'K$, l. mole ⁻¹ min. ⁻¹ $\times 10^2$
A ^c	0.5040	0.347	-3.136	0.64	0.362	0.981	2.82	1.02
B ^c	0.5040		-2.664	0.86				
A	1.008	0.679	-5.990	1.78	0.387	1.914	2.81	1.09
B	1.008		-5.050	1.91				
A	1.453	0.984	-8.670	9.76	0.383	2.760	2.80	1.07
B	1.453		-7.230	0.82				
A	2.769	2.100	-13.01	5.06	0.426	4.270	2.03	0.86
B	2.769		-10.85	4.04				
A	4.335	4.116	-14.60	2.40	0.960	6.590	1.60	1.54
B	4.335		-11.01	2.84				
A	6.130	9.113	-9.75	1.16	1.153	4.833	0.53	0.61
B	6.130		-7.18	4.75				

^a Using 0.371 M BDO in CCl₄ vs. NaOH solutions. ^b $K = [\text{epoxide}]$ in CCl₄ layer/[epoxide] in H₂O layer. ^c A, organic phase = 15.00 ml.; aqueous phase = 15.00 ml.; B, organic phase = 25.00 ml.; aqueous phase = 15.00 ml.

Table II: Distribution and Kinetic Data for *meso*-BDE^a vs. Strong NaOH Aqueous Solutions

	NaOH, M	a_{OH^-} , m	Slope $\times 10^3$	Error of slope $\times 10^4$	K^b	k , min. ⁻¹ $\times 10^2$	$k' = k/a_{OH^-}$, l. mole ⁻¹ min. ⁻¹ $\times 10^2$	$k'' = k'K$, l. mole ⁻¹ min. ⁻¹ $\times 10^2$
A ^d	2.868	2.180	-9.53	2.08	0.798	3.947	1.81	1.44
B ^d	2.868		-7.35	1.03				
A	4.599	4.580	-10.99	2.47	5.278	15.88	3.40	17.95
B	4.599		-7.04	3.31				

^a *meso*-BDE (0.371 M) solution in CCl₄. ^b $K = [\text{epoxide}]$ in CCl₄ layer/[epoxide] in H₂O layer. ^c Average k' for dilute base = 2.65×10^{-2} l. mole⁻¹ min.⁻¹ (ref. 2). ^d A, organic phase = 15.00 ml.; aqueous phase = 15.00 ml.; B, organic phase = 25.00 ml.; aqueous phase = 15.00 ml.

For series A, plots of $\log [E]_0$ vs. time resulted in a family of straight lines intersecting at a point corresponding to 33 min. and 0.206 mequiv./ml. for all concentrations up to 3 *M*. For series B, the common point of intersection for lines obtained with aqueous phases less concentrated than 3 *M* NaOH was 34 min. and 0.285 mequiv./ml. In both series, the straight lines for the two most concentrated basic solutions used with BDO did not intersect at the point of intersection of all the other lines. The ratio of the epoxide concentration at the common point of series A to that of series B (0.206/0.285) is 0.723. Molar ratios of BDO in the organic layer

of series A to that in series B at equilibria conditions before finite amounts of epoxide have hydrolyzed can be calculated by use of the distribution coefficient, 0.52, obtained for the distribution of the diepoxide between CCl_4 and water phases. Use of $K = 0.52$ resulted in a molar ratio of 0.73, in agreement with that obtained experimentally, thus indicating that distribution equilibrium is established relatively fast compared to the rate at which the diepoxide hydrolyzes in the aqueous phases for those aqueous phases less concentrated than 3 *M* NaOH.

The Sedimentation Velocity Experiment and the Determination of Molecular Weight Distributions

by James E. Blair and J. W. Williams

Laboratory of Physical Chemistry, University of Wisconsin, Madison, Wisconsin (Received August 21, 1963)

Observations of boundary spreading in sedimentation velocity experiments for the system polystyrene-cyclohexane at the Flory temperature have been utilized largely to demonstrate a procedure whereby solute molecular weight distributions may be obtained. The matter of using the movement of the position of the maximum height of the boundary gradient curve instead of the boundary location as measured from the second moment for the determination of the pressure dependent parameter in sedimentation is considered in some detail. In addition, several other items such as the determination of the zero time correction are discussed.

Introduction

Along with its other attributes, the ultracentrifuge is an instrument by which there may be achieved a physical fractionation of solute molecules of different molecular weights along the radial axis in the rotating cell. Indeed, the possibility so provided of making a molecular weight analysis of a mixture is one of the great advantages of the ultracentrifugal techniques. One may determine the several more common average

molecular weights; in addition and now being considered, procedures are made available by which a complete molecular weight distribution curve may be constructed. In principle, the necessary data may be provided either at sedimentation equilibrium or during sedimentation transport.

The methods which involve the sedimentation equilibrium experiment have been studied by Rinde¹

(1) H. Rinde, Dissertation, Uppsala, 1928.

and by Wales and Williams and their associates.² Using polystyrene as solute it could be shown^{2c} that the molecular weight distribution curve obtained by this route compared well with that constructed from the record of fractional precipitations.

However, there are reasons to believe that the sedimentation transport experiment is the more advantageous from the point of view of resolution and we present here the record of an analysis in which it is used and by which the molecular weight distribution for a typical linear organic high polymer was achieved. It is based upon two ideas, that of a boundary spreading analysis to obtain a distribution of sedimentation coefficient, s , and that of a unique continuous correspondence between sedimentation coefficient and molecular weight for the transformation to a distribution of molecular weight, M . Observations of the behavior and properties of the system polystyrene-cyclohexane at the Flory temperature were used.

As far as we are aware, the original outline for this mode of analysis was described by one of the present authors.³ More recently, it has been the subject of substantial development from several points of view including pressure corrections, the use of systems at the Flory temperature to avoid concentration dependence effects, computational methods, etc.⁴⁻⁸

Theory

The equations descriptive of the transformation of the boundary gradient curve of the sedimentation transport experiment into a distribution of sedimentation coefficients now have appeared in a number of places. Following the presentation of the original and fundamental equation for the distribution by Bridgman⁹ there were developed¹⁰⁻¹² theory and procedures for taking into account the effects of diffusion on the measurement of heterogeneity. However, it soon appeared that, in general, concentration-dependence effects must be also considered in finding the true distribution function by means of an extrapolation for which there is at present no really satisfactory theoretical basis.^{13,14} An excellent survey of the present status of the interpretation of boundary spreading in sedimentation velocity experiments is to be found in the recent Fujita monograph.¹⁵

If for the present the effects of diffusion and concentration dependence are ignored, the distribution of sedimentation coefficient, s , is given by $dc/ds = (dc/dr)(dr/ds)$, except for the radial dilution factor which causes this quantity to diminish with time. To compensate, we write

$$g^*(s) = \frac{1}{c_p} \frac{dc}{dr} \frac{dr}{ds} = \frac{r_b^2 \omega^2 (t - t_0) r}{c_0 r_0^2} \frac{dc}{dr} \quad (1)$$

where c_p represents the decreased concentration of the solution in the "plateau" region, and c_0 is the original concentration of the solution. The asterisk indicates that the distribution has not been corrected for diffusion and concentration dependence; the other symbols have their usual significance.

In working with solutions of organic high polymers at the Flory temperature, it is entirely proper to neglect concentration dependence effects on boundary spreading. Indeed, it is this fact which is probably the greatest single factor in contributing to the success of the analysis for polydispersity. Also, in systems of this kind diffusion effects are relatively unimportant. However, the organic solvents which now must be used are relatively compressible substances as compared to water, and an additional complication is introduced. It is the effect of hydrostatic pressure on the viscosity and the density of this solvent, and on the partial specific volume of the solute as well. The net result is a variation of the sedimentation coefficient with distance in the cell, one which is accounted for by a single pressure dependent parameter.¹⁶

Fujita¹⁵ has developed the equation which relates movement of the boundary position, r , with time, t , for the case of isothermal sedimentation in a system in which the sedimentation coefficient depends on both hydrostatic pressure and concentration. He writes

$$\frac{\ln r/r_0}{\omega^2(t - t_0)} = s_0^{c_0} \left\{ 1 + K \left[\left(\frac{r}{r_0} \right)^2 - 1 \right] \right\} \quad (2)$$

where

$$K = \frac{kc_0 - m(1 + 2kc_0)}{2(1 + kc_0)} \quad (2a)$$

- (2) (a) M. Wales, M. M. Bender, J. W. Williams, and R. H. Ewart, *J. Chem. Phys.*, **14**, 353 (1946); (b) M. Wales, *J. Phys. Colloid Chem.*, **52**, 235 (1948); (c) M. Wales, J. W. Williams, J. O. Thompson, and R. H. Ewart, *ibid.*, **52**, 983 (1948); (d) M. Wales, F. T. Adler, and K. E. Van Holde, *ibid.*, **55**, 145 (1951).
- (3) J. W. Williams *J. Polymer Sci.*, **12**, 351 (1954).
- (4) A. F. V. Eriksson, *Acta Chem. Scand.*, **10**, 360 (1956).
- (5) H. W. McCormick, *J. Polymer Sci.*, **A1**, 103 (1963).
- (6) I. H. Billick, *ibid.*, **62**, 167 (1962).
- (7) M. Wales and S. J. Rehfeld, *ibid.*, **62**, 179 (1962).
- (8) G. Meyerhoff, in "Ultracentrifugal Analysis in Theory and Experiment," Academic Press, New York and London, 1963.
- (9) W. B. Bridgman, *J. Am. Chem. Soc.*, **64**, 2349 (1942).
- (10) R. L. Baldwin and J. W. Williams, *ibid.*, **72**, 4325 (1950).
- (11) J. W. Williams, R. L. Baldwin, W. M. Saunders, and P. G. Squire, *ibid.*, **74**, 1542 (1952).
- (12) L. J. Gosting, *ibid.*, **74**, 1548 (1952).
- (13) J. W. Williams and W. M. Saunders, *J. Phys. Chem.*, **58**, 854 (1954).
- (14) R. L. Baldwin, *J. Am. Chem. Soc.*, **76**, 402 (1954).
- (15) H. Fujita, "Mathematical Theory of Sedimentation Analysis," Academic Press, Inc., New York, N. Y., 1962.
- (16) J. Oth and V. Desreux, *Bull. soc. chim. Belges*, **63**, 133 (1954).

Actually, this equation has been derived to describe the behavior of a monodisperse solute system with the effects of diffusion being neglected. By numerical computations we have justified its later use in connection with polydisperse systems, using the boundary position r_b as the proper value of r . Also, in eq. 2, r_0 is the radial distance from the axis of rotation to the meniscus, t is the time as observed, t_0 is the zero time concentration, ω is the angular velocity, and $s^0_{c_0}$ is the value of the sedimentation coefficient at 1 atm. pressure (superscript zero) and at the initial concentration of the solution. The concentration dependence parameter k is defined by the expression

$$s^0 = \frac{s^0_0}{1 + kc} \quad (3)$$

where s^0_0 is the value of s^0 at infinite dilution. The quantity m , the pressure dependence parameter, takes the form¹⁶

$$m = 1/2\mu\omega^2\rho_0^0r_0^2 \quad (4)$$

where ρ_0^0 is the density of the solvent and μ is a constant characteristic of the solute-solvent system.

For the system polystyrene in cyclohexane at 34.2° (the Flory or θ -temperature) the concentration dependence of s is small compared to that of the pressure dependence and to the limit of precision in determining the constant K

$$K = -m/2 \quad (5)$$

From the usual definition of s (eq. 2 with $K = 0$), one may obtain for use in eq. 1

$$\frac{dr}{ds} = r\omega^2(t - t_0) \quad (6)$$

Now, if the effect of hydrostatic pressure (but not concentration dependence) is included, eq. 6 is modified to read

$$\frac{dr}{ds} = r\omega^2(t - t_0) \frac{d\left[s\left\{1 - \frac{m}{2}\left[\left(\frac{r}{r_0}\right)^2 - 1\right]\right\}\right]}{ds} \quad (6a)$$

Thus

$$\frac{dr}{ds} = r\omega^2(t - t_0) \left[\left\{1 - \frac{m}{2}\left[\left(\frac{r}{r_0}\right)^2 - 1\right]\right\} - \frac{sr m}{r_0^2} \frac{dr}{ds} \right] \quad (7)$$

or

$$\frac{dr}{ds} = \frac{r\omega^2(t - t_0) \left[1 - \frac{m}{2}\left\{\left(\frac{r}{r_0}\right)^2 - 1\right\}\right]}{1 + \frac{mr^2 \ln r/r_0}{r_0^2 \left[1 - \frac{m}{2}\left\{\left(\frac{r}{r_0}\right)^2 - 1\right\}\right]}} \quad (7a)$$

For the usual values of the parameters which occur in sedimentation velocity experiments, eq. 7a can be also written as

$$\frac{dr}{ds} = r\omega^2(t - t_0) \left[\left\{1 - \frac{m}{2}\left[\left(\frac{r}{r_0}\right)^2 - 1\right]\right\} - \frac{mr^2 \ln r/r_0}{r_0^2} \right] \quad (7b)$$

To the degree of approximation that terms in $\left[\left(\frac{r}{r_0}\right)^2 - 1\right]$ and in higher powers of this quantity can be neglected

$$\frac{r^2}{r_0^2} \ln \frac{r}{r_0} \simeq \frac{1}{2} \left[\left(\frac{r}{r_0}\right)^2 - 1 \right] \quad (8)$$

With the introduction of eq. 8 into eq. 7 we find

$$\frac{dr}{ds} = r\omega^2(t - t_0) \left[1 - m \left\{ \left(\frac{r}{r_0}\right)^2 - 1 \right\} \right] \quad (9)$$

Finally, the combination of eq. 9 and 1 gives

$$g^*(s_0^0) \simeq g^*(s^0) = \frac{r\omega^2(t - t_0) \left[1 - m \left\{ \left(\frac{r}{r_0}\right)^2 - 1 \right\} \right] \frac{dc}{dr}}{c_p} \quad (10)$$

This equation is equivalent to forms already arrived at by Billick⁶ and by Wales and Rehfeld,⁷ since in the case of pressure dependent sedimentation the radial dilution law takes the form

$$\frac{c_0}{c_p} = \left(\frac{r_b}{r_0}\right)^2 \left[1 - m \left\{ \left(\frac{r_b}{r_0}\right)^2 - 1 \right\} \right] \quad (11)$$

The analysis we use presupposes in addition a knowledge of the relation between limiting sedimentation coefficient and molecular weight so that there is made available a method of transformation of $g(s^0)$ to $f(M)$, the molecular weight distribution. The relation

$$s = \kappa M^\alpha \quad (12)$$

may be used. Then, if we consider continuous distributions it is possible to write

$$g(s^0)ds = f(M)dM \quad (13)$$

Making the substitution

$$f(M) = g(s^0) \frac{ds}{dM} = g(s^0) \alpha \kappa \left(\frac{s}{\kappa}\right)^{(\alpha-1)/\alpha} \quad (14)$$

For the system polystyrene-cyclohexane at 34.2°, the Flory temperature, the constants α and κ have been

determined by both McCormick¹⁷ and by Cantow.¹⁸ These data are given, in order, by the equations

$$s = (1.69 \times 10^{-2}) M^{0.48} \quad (12a)$$

$$s = (1.35 \times 10^{-2}) M^{0.51} \quad (12b)$$

The equivalent sphere model for the friction coefficient of flexible chain polymers predicts a value of $\alpha = 0.50$ for the poor solvent.

Experimental

Two samples of polystyrene were used in the experiments. One of them, an anionically polymerized material of designation S-103, was furnished to us through the courtesy of Dr. H. W. McCormick of the Dow Chemical Co. The other specimen, 19F, was provided by Prof. J. D. Ferry of this Department. It was originally distributed by Dr. R. F. Boyer, also of Dow Chemical Co., as a preparation having substantially a most probable molecular weight distribution. Both polystyrenes have been the subject of several prior average molecular weight determinations.

Polymer solutions in cyclohexane at 34.2°, the Flory temperature, were studied during sedimentation transport in a Spinco Model E ultracentrifuge. In all experiments double sector cells were used, with solution on one side and solvent on the other, and with both sides being filled to approximately the same level. Four rotational speeds were used: 59,780, 56,100, 47,660, and 39,460 r.p.m. A schlieren optical system was employed to record the redistribution of the components during the sedimentation process.

In the earlier experiments great care was taken to remove water from the cyclohexane. The solvent was distilled from lithium aluminum hydride and the polymer solutions were prepared in a drybox. However, when data taken in this way were compared with those when these precautions were not observed, no consistent or appreciable differences were found. So, these precautions were eventually omitted.

All solutions were prepared by weighing the polymer sample into a 50-ml. long-neck, glass-stoppered flask. The solvent was introduced into the flask and the weight of the solvent was determined by a second weighing. The contents of the flask were then frozen in a Dry Ice bath and the neck of the flask was sealed off. The flask was then placed in an oven at 40° with gentle stirring for at least 1 day to ensure complete solution. After restoration to near θ -temperature, the flask was opened and the solution was removed by hypodermic syringe for insertion into the prewarmed cell. In computing the concentration of a solution, the density of the cyclohexane at 34.2° was taken to be

0.7656 g./ml. and the partial specific volume of the dissolved polystyrene was assumed to be 0.95 cc./g.

The times, t , were measured from the moment the acceleration of the rotor commenced. The acceleration was maintained constant during the speedup period and the times at which the rotor reached two-thirds of its final speed were recorded for comparison with the zero-time correction, t_0 , as ultimately computed. Several methods for the evaluation of this quantity were considered, it having been found that the value of the pressure and concentration dependence parameter K , eq. 2, is rather sensitive to the value of t_0 applied. In this work, the value of t_0 selected was the one which produced the "best fit" of the data to eq. 2; i.e., the t_0 which when inserted produced the minimum standard deviation, σ , defined by

$$\sigma = \left(\frac{1}{n} \sum_{i=1}^n R_i^2 \right)^{1/2} \quad (15)$$

with the residual, R , being defined as

$$R = s_{c_0} \omega^2 (t - t_0) + s_{c_0} K \omega^2 (t - t_0) \left[\left(\frac{r}{r_0} \right)^2 - 1 \right] - \ln \frac{r}{r_0} \quad (15a)$$

The position, $r = r_b$, is the point on the moving boundary gradient curve which has the same velocity as does the corresponding solute molecule ahead of the boundary. The values of r_b were determined by numerical integration of the points along the boundary gradient curve. These, along with the times t which correspond, were fitted to eq. 2 by the method of least squares to determine the quantities s_{c_0} and K . The values of these quantities for a given set of data will be observed to depend upon the value of t_0 which is used.

The results of the calculations made by using various values of t_0 with a given set of r_b and t data are presented in Table I.

It should be also noted that with the schlieren optical system it is not the desired quantity, dc/dr , which is obtained from the photographic plate; it is a number proportional to it. Thus

$$\frac{dc}{dr} = \psi \frac{dh}{dr} \quad (16)$$

Here, ψ is a constant which incorporates dn/dc (the refractive index gradient), the bar angle at which the photograph was taken, and the vertical magnification factor of the optical system. So, the quantity c_p ,

(17) H. W. McCormick, *J. Polymer Sci.*, **36**, 341 (1959).

(18) H. J. Cantow, *Macromol. Chem.*, **30**, 169 (1959).

Table I: Comparison of Data for Quantities $s_{c_0}^0$ and K with Several t_0 Values. Polystyrene S-103 at 59,780 r.p.m. with $c_0 = 0.313$ g./100 ml.

Method	t_0	$s_{c_0}^0$ (in S)	K	$\sigma \times 10^4$
Baldwin ^a	245	4.94	-0.358	2.6
$^{2/3}t_f$	234	4.92	-0.347	2.9
"Best fit"	306	5.08	-0.419	1.8

^a R. L. Baldwin, *Biochem. J.*, **65**, 503 (1957).

the concentration in the so-called plateau region, is given by the statement

$$c_p = \int_{\text{cell}} \left(\frac{dc}{dr} \right) dr = \psi \int \frac{dh}{dr} dr = \psi A \quad (17)$$

where A is the area under the particular boundary gradient curve on the photographic plate. Thus, the essential working equation for the distribution of sedimentation coefficients becomes

$$g^*(s^0) = r\omega^2(t - t_0) \left[1 - m \left\{ \left(\frac{r}{r_0} \right)^2 - 1 \right\} \right] \frac{dh}{dr} / A \quad (10a)$$

The asterisk has been used again because it was found to be necessary to make corrections for the spreading of the boundary due to diffusion. This required an extrapolation of the conventional kind^{10,11} to give the function $g(s^0)$. The details are not provided here.

The information from each experiment was read from the photographic plates by means of a Gaertner tool-maker microscope. From each photograph the location of the inner and outer index marks, the meniscus, and from 19 to 23 values of dh/dr along the boundary gradient curve were determined. The readings always included data for the positions $(dh/dr)_{\text{max}}$ and $(dh/dr) = 0$ at both ends of the curve.

Calculations and Results

1. *Use of r_b and r_H in the Determination of Sedimentation Coefficients.* In the evaluation of the sedimentation coefficient the position at the several times of the maximum of the refractive index gradient, r_H , is often used in place of the boundary position as measured from the second moment, r_b . In order to study this choice further, sedimentation experiments at four different angular velocities with the system polystyrene S-103 in cyclohexane at 34.2° were performed. The data were evaluated to give the quantities $s_{c_0}^0$, t_0 , K , and σ , using the two boundary positions. The time corrections, t_0 , were found by the

method we have evolved. The results are tabulated in Table II.

Table II: Data at Four Rotational Speeds for the System Polystyrene S-103 in Cyclohexane at 34.2°

	r_H	r_b	Difference
Speed = 59,780 r.p.m. $c_0 = 0.313$ g./100 ml.			
$s_{c_0}^0$	5.07	5.08	0.2%
t_0	279	306	27 sec.
K	-0.36	-0.42	15%
$\sigma \times 10^4$	0.93	1.8	..
Speed = 56,100 r.p.m. $c_0 = 0.649$ g./100 ml.			
$s_{c_0}^0$	4.76	4.88	2.45%
t_0	188	246	58 sec.
K	-0.31	-0.44	29.5%
$\sigma \times 10^4$	1.04	1.0	..
Speed = 47,660 r.p.m. $c_0 = 0.7203$ g./100 ml.			
$s_{c_0}^0$	4.67	4.72	1.06%
t_0	338	405	67 sec.
K	-0.19	-0.25	26%
$\sigma \times 10^4$	1.43	1.95	..
Speed = 39,460 r.p.m. $c_0 = 0.7203$ g./100 ml.			
$s_{c_0}^0$	4.77	4.78	0.2%
t_0	581	642	61 sec.
K	-0.17	-0.214	20.5%
$\sigma \times 10^4$	0.599	0.522	..

Although the polymer is one of relatively narrow molecular weight distribution, the asymmetry of the boundary gradient curve introduces a significant error in the value of the parameter K if the displacement with time of the position r_H is used. Furthermore, the error in the determination of K so introduced does not seem to decrease with increased rotational speed. The spreading of the boundary gradient curve due to diffusion is reduced, but with the greater pressure at the cell bottom the actual distortion of the curve is enhanced. The difference in the $s_{c_0}^0$ values is small and random, but the values of t_0 are different in the two cases.

In Fig. 1 and 2 are shown typical boundary gradient curves for the two polystyrenes. They were constructed from photographs taken at late times during the progress of the experiments. The positions r_H and r_b are indicated. In the case of the more nearly homogeneous sample (S-103) $r_H > r_b$, but with the highly polydisperse material (19F) these positions are reversed. The pressure dependence of s tends to skew the curve away from the direction of sedimentation, since the leading molecules tend to be retarded

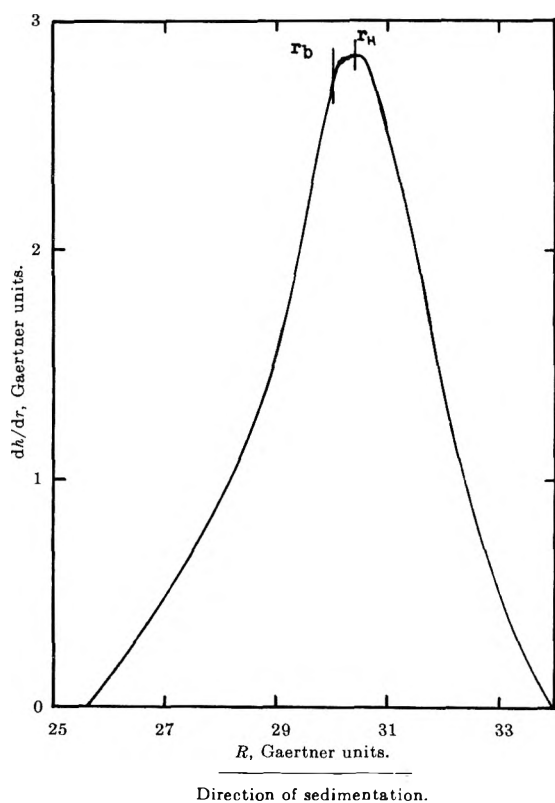


Figure 1. Boundary gradient curve for polystyrene S-103 in cyclohexane at 34.2°; speed, 59,780 r.p.m.

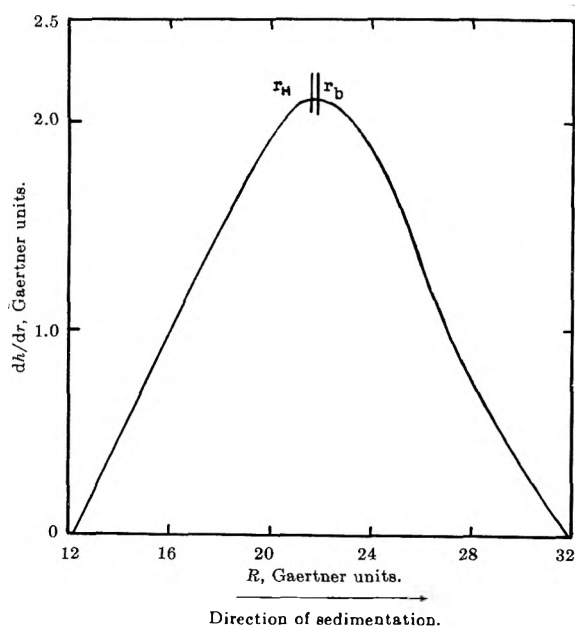


Figure 2. Boundary gradient curve for polystyrene 19F in cyclohexane at 34.2°; speed, 59,780 r.p.m.

in motion when they enter into regions of greater pressure. The "tail" on the weight distribution is in the direction of the heavier molecular weights.

2. *The Effect of Pressure on Sedimentation Velocity Behavior.* During the course of any given sedimentation velocity experiment with a polymer-organic solvent system it appears that the effect of pressure on solute transport predominates over that of concentration dependence. These effects operate in opposite directions, as required by eq. 2a. The plot of $\ln r_b/r_0$ vs. $\omega^2(t - t_0)$ would be linear in the ideal case, but it is concave downward when pressure dependence effects are present exclusively or are more important than those of concentration dependence. By reference to Fig. 3 it will be seen that this situation existed in the experiments we describe.

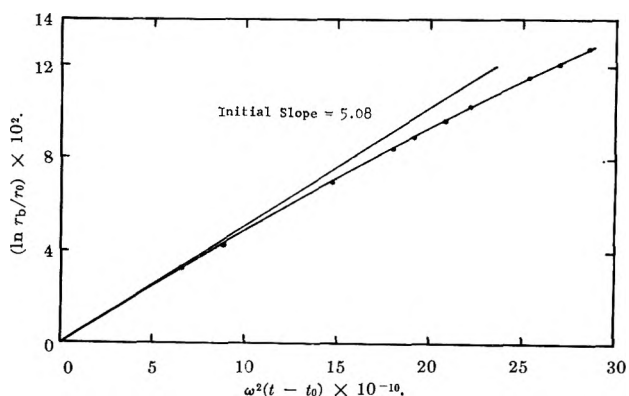


Figure 3. Plot of $\ln r_b/r_0$ vs. $\omega^2(t - t_0)$ for polystyrene S-103 in cyclohexane at 34.2°; speed, 59,780 r.p.m.

From the values of K obtained from the experiments with polystyrene S-103, Table II, the pressure dependence parameter m was computed. From eq. 4 it follows that the quantity m/r_0^2 should be a linear function of ω^2 . The plot, open circles, is shown in Fig. 4.

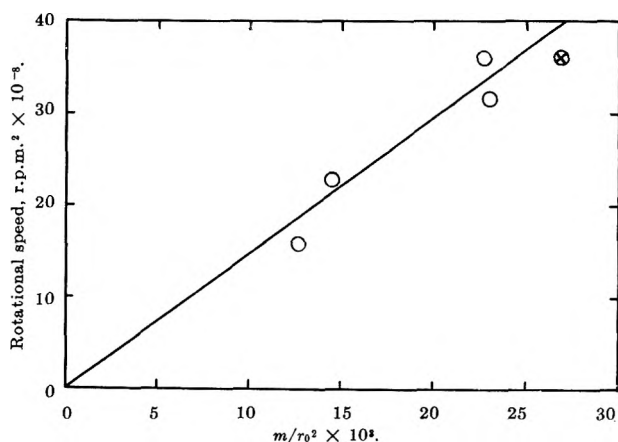


Figure 4. Plot of m/r_0^2 vs. square of rotational speed: O, polystyrene S-103; ⊗, polyisobutylene F-22.

Another point, indicated by a circle with cross, was obtained from the record of an experiment with an isobutylene sample in the same solvent, cyclohexane, and at the same temperature, 34.2°. From the location of this point one is led to suspect that the pressure dependence parameter m is determined primarily by the properties of the solvent.

Another important consequence of the pressure dependence of s during a sedimentation velocity experiment is that the usual square radial dilution law is no longer valid; radial dilution now is described by eq. 11. This is to be seen in a plot of the quantity Ar_b^2 vs. t where A , the area under the boundary gradient curve, is proportional to c_p . The quantity Ar_b^2 would be constant, *i.e.*, independent of time, if there were no pressure dependence.

In Fig. 5 we present plots of Ar_b^2 vs. time, using the data for two experiments at different speeds for the system polystyrene S-103 in cyclohexane. The broken lines represent the expected behavior in the absence of pressure dependence. Allowing for the pressure dependence of s , these plots would be expected to be straight lines of positive slopes, since from eq. 11 it is seen that

$$A_0r_0^2 = Ar_b^2 \left[1 - m \left\{ \left(\frac{r_b}{r_0} \right)^2 - 1 \right\} \right] \quad (18)$$

As a first approximation, for small values of

$$\begin{aligned} s^0 c_0 \omega^2 (t - t_0) \left[1 - \frac{m}{2} \left\{ \left(\frac{r_b}{r_0} \right)^2 - 1 \right\} \right] \\ \left(\frac{r_b}{r_0} \right)^2 = \exp 2s^0 c_0 \omega^2 (t - t_0) \left[1 - \frac{m}{2} \left\{ \left(\frac{r_b}{r_0} \right)^2 - 1 \right\} \right] \simeq \\ 1 + 2s^0 c_0 \omega^2 (t - t_0) \left[1 - \frac{m}{2} \left\{ \left(\frac{r_b}{r_0} \right)^2 - 1 \right\} \right] \quad (19) \end{aligned}$$

hence

$$\left(\frac{r_b}{r_0} \right)^2 - 1 = 2s^0 c_0 \omega^2 (t - t_0) / (1 + ms^0 c_0 \omega^2 (t - t_0)) \quad (20)$$

Now, eq. 18 can be written in the form

$$A_0r_0^2 = Ar_b^2 \left[1 - \frac{2s^0 c_0 \omega^2 m (t - t_0)}{1 + ms^0 c_0 \omega^2 (t - t_0)} \right] \quad (21)$$

or

$$Ar_b^2 = A_0r_0^2 / \left[1 - \frac{2s^0 c_0 \omega^2 m (t - t_0)}{1 + ms^0 c_0 \omega^2 (t - t_0)} \right] \quad (22)$$

For the values of the parameter applicable in these experiments, the quantity $2s^0 c_0 \omega^2 (t - t_0)$ is small, so eq. 22 can be approximated by

$$Ar_b^2 = A_0r_0^2 [1 + 2s^0 c_0 \omega^2 m (t - t_0)] \quad (23)$$

or multiplied out

$$Ar_b^2 = A_0r_0^2 + 2s^0 c_0 \omega^2 m A_0r_0^2 (t - t_0) \quad (24)$$

Hence, a plot of Ar_b^2 vs. time, as in Fig. 5, should be a straight line with slope

$$2s^0 c_0 \omega^2 A_0r_0^2 m$$

3. *Determination of the Molecular Weight Distribution.* Data were taken from a single sedimentation velocity experiment at 59,780 r.p.m. with a solution of polystyrene 19F in cyclohexane, concentration 0.504 g./100 ml., at a temperature of 34.2°. From these data, the distribution of sedimentation coefficients, $g(s^0)$ vs. s , and the molecular weight distribution of the polymer, $f(M)$ vs. M , were determined. In processing the data, the value of the parameter K was taken as -0.45 , as determined from Fig. 4. This number was felt to be more accurate than the value of K which had been computed from any single experiment.

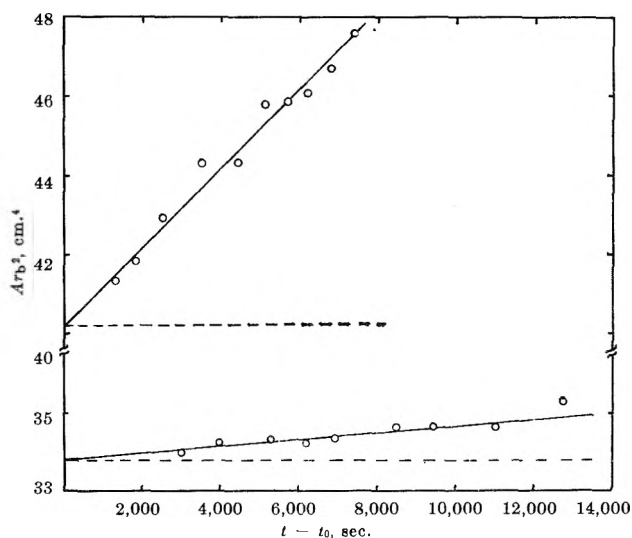


Figure 5. Plot of Ar_b^2 vs. $(t - t_0)$: upper curve, 56,100 r.p.m.; lower curve, 39,460 r.p.m.

The transformation from sedimentation velocity distribution to the weight distribution was then made by means of eq. 14 in which were taken $\alpha = 0.50$ and $\kappa = 1.47 \times 10^{-2}$. The resultant $f(M)$ vs. M curve is shown as the solid line of Fig. 6. The broken line in the figure indicates the weight distribution curve which is obtained when the pressure dependence of s is not taken into account.

Numerical integrations of the corrected distribution curve of Fig. 6 were performed in order to obtain the average molecular weights M_n and M_w . By definition

$$M_n = \frac{\int f(M)dM}{\int \frac{1}{M}f(M)dM} \quad (25)$$

and

$$M_w = \frac{\int Mf(M)dM}{\int f(M)dM} \quad (26)$$

The numerical results are $M_n = 207,000$ and $M_w = 375,000$.

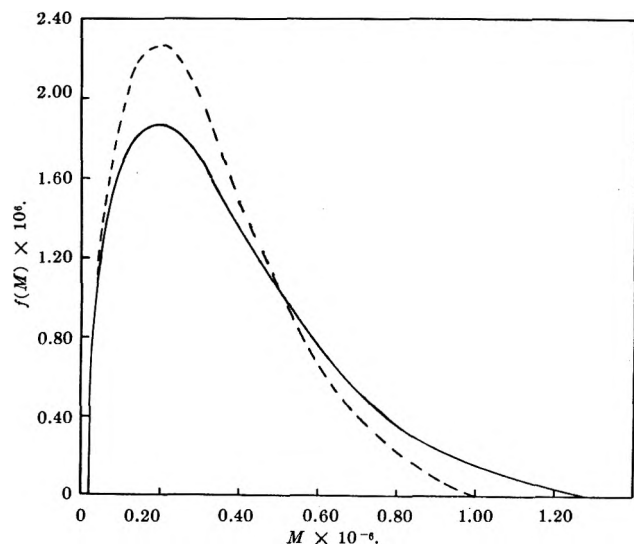


Figure 6. Molecular weight distribution of polystyrene 19F: - - - -, not corrected for pressure dependence; ———, corrected for pressure dependence.

In Table III are summarized the values of M_n and M_w and their ratios for the polystyrene 19F. Similar data for polystyrene S-103 are also included.

It will be noted that the ratio M_w/M_n is essentially unchanged when the pressure correction is neglected in determining the weight distribution of the polystyrene sample 19F, but both M_w and M_n are in error by a considerable amount. This confirms a similar observation which has been made by Billick.⁶ It is seen

from Fig. 6 that failure to correct for the effects of the pressure dependence of s results in a distribution which is richer in low weight polymers and poorer in the heavy species than is the actual case.

Table III: Average Molecular Weight Data for Polystyrenes 19F and S-103

	19F	M_n	M_w	M_w/M_n
Sedimentation velocity with pressure correction (this work)		207,000	375,000	1.81
Sedimentation velocity, no pressure correction (this work)		172,000	313,000	1.82
Light scattering ^a		370,000	1.88
Osmotic pressure ^b		197,000 ± 5%	
S-103				
Sedimentation equilibrium ^c		115,000	117,000	1.02

^a D. J. Streeter and R. F. Boyer, *Ind. Eng. Chem.*, **43**, 1790 (1951). ^b L. D. Grandine, Jr., Dissertation, University of Wisconsin, 1952. ^c A. M. Linklater and J. W. Williams, unpublished.

The important fact to be noted is that the distribution of molecular weights here obtained by velocity sedimentation is for all practical purposes that which corresponds to the distribution required by statistical analysis if the polymerization of the styrene terminates by the disproportionation mechanism. Exactly the same conclusion had been already obtained by using the sedimentation equilibrium experiment with another polystyrene of the same type,^{2a,2c} but now advantage has been taken of the higher sensitivity of the transport process to heterogeneity.

Acknowledgment. This research was made possible by generous grants from the U. S. Army Research Office (DA-ORD-11) and the University of Wisconsin Research Committee, using funds provided by the Wisconsin Alumni Research Foundation. Grateful acknowledgment is hereby made.

Solubilities of Oxygen, Argon, and Nitrogen in Distilled Water

by Everett Douglas

Scripps Institution of Oceanography, La Jolla, California^{1,2} (Received August 26, 1963)

The solubilities of oxygen, argon, and nitrogen in distilled water from 5 to 30° have been determined microgasometrically with an estimated accuracy in α of ± 0.25 to 0.5%, dependent on the solubility of the gas. Comparison of the present results with those from previous workers show the oxygen values to be in good agreement with those of Winkler, whose values have been substantiated by Steen, Elmore and Hayes, and Klots and Benson, while the nitrogen values fall between those of Hamberg, Fox, and Adeney and Becker, but indicate those of Klots and Benson to be somewhat high. The argon values agree with those of Klots and Benson.

Introduction

In reviewing the literature for gas solubilities in distilled water, one is impressed by the nonconformity of values reported by various workers. Until recently, the values of Winkler^{3,4} as used in the "Handbook of Chemistry and Physics"⁵ and the values of Fox^{6,7} were considered the standard values for oxygen. Fox's values are some 1-2% higher than Winkler's. Truesdale, Downing, and Lowden,⁸ in determining the solubility coefficient for oxygen, reported values 4% lower than the accepted values. Since then the solubilities of oxygen have been redetermined and checked by different workers⁹⁻¹³ using gasometric and titrimetric techniques of analysis, all agreeing within $\pm 1\%$ of the values of Winkler. Nitrogen has received less attention since it does not lend itself to titrimetric analysis. Fox's values^{6,7} have been more or less accepted as the standard, with Winkler's values¹⁴ lower and Hamberg's¹⁴ higher. Since then several workers have redetermined the solubility values for nitrogen with resulting inconsistency of values still prevailing.¹⁴⁻¹⁶

Of the major atmospheric gases, argon has received the least attention. The various attempts show little uniformity with one another.^{13,17-22}

The method as described below is similar to that used by Steen with several modifications. In view of these, a detailed description is given, although some parts will necessarily appear repetitive. The present microgasometric method has an estimated accuracy of $\pm 0.25\%$ for O₂ and Ar and $\pm 0.5\%$ for N₂.

Experimental

Principle of Method. The method takes advantage of the fact that the ratio of absorbed gas volume to

- (1) Contribution from the Scripps Institution of Oceanography, University of California, San Diego, Calif.
- (2) This investigation was supported by a research grant (No. GM-05979) from the U. S. Department of Health, Education, and Welfare, Public Health Service.
- (3) L. W. Winkler, *Ber. Deut. Chem. Ges.*, **22**, 1764 (1889).
- (4) L. W. Winkler, *ibid.*, **24**, 89 (1891).
- (5) "Handbook of Chemistry and Physics," 39th Ed., Chem. Rubber Publ. Co., Cleveland, Ohio, 1957.
- (6) C. J. Fox, Intern. Hydrog. Comm. Publication de Circonstance No. 41 (1907).
- (7) C. J. Fox, *Trans. Faraday Soc.*, **V**, 68 (1909).
- (8) G. A. Truesdale, A. L. Downing, and G. F. Lowden, *J. Appl. Chem.*, **5**, 53 (1955).
- (9) A. B. Wheatland and L. J. Smith, *ibid.*, **5**, 144 (1955).
- (10) H. Steen, *Limnol. Oceanog.*, **3**, No. 4, 423 (1958).
- (11) H. L. Elmore and T. W. Hayes, *J. Sanit. Eng. Div. Am. Soc. Civil Engrs.*, **86**, 44 (1960).
- (12) J. C. Morris, W. Stumm, and H. A. Galal, *ibid.*, **87**, 81 (1961).
- (13) C. E. Klots and B. B. Benson, *J. Marine Res.*, **21**, 48 (1963).
- (14) J. H. Coste, *J. Phys. Chem.*, **31**, 81 (1927).
- (15) W. E. Adeney and H. G. Becker, *Sci. Proc. Roy. Dublin Soc.*, **XV**, No. XLIV, 609 (1919).
- (16) T. J. Morrison and F. Billet, *J. Chem. Soc.*, 3821 (1952).
- (17) T. Estreicher, *Z. physik. Chem.*, **31**, 176 (1899).
- (18) L. W. Winkler, *ibid.*, **55**, 345 (1906).
- (19) A. von Antropoff, *Proc. Roy. Soc. (London)*, **A83**, 474 (1910).
- (20) A. Lannung, *J. Am. Chem. Soc.*, **52**, 68 (1930).
- (21) T. J. Morrison and N. B. Johnstone, *J. Chem. Soc.*, 3441 (1954).
- (22) H. Von König, *Z. Naturforsch.*, **18a**, 363 (1963).

liquid volume is constant at a given equilibrium pressure. In contrast to other methods, equilibration is rapid, 30 min., and takes place in a closed system under constant temperature and pressure. Gas-free water is brought into contact with pure gas and after equilibration the amount of gas absorbed by the water is measured volumetrically with a micrometer buret. This ratio gives α when the gas volume is reduced to 0°.

Preparation of Gas-Free Water. Double-distilled water is boiled in a 500-ml. Pyrex suction flask for approximately 1 hr. The mouth of the flask is stoppered, leaving the side arm open for the steam escape, ensuring that no air is in contact with the boiling water. The water, still boiling, is drawn up into a syringe and the needle stoppered. A 10-cc. glass-tip syringe fitted with a blunt-tipped No. 23 needle is inserted through a vaccine stopper in a glass tube leading into the boiling water (Fig. 1a) and flushed several times to rid the dead space of any gas bubbles. The syringe is then filled with the

boiling water. Three syringes are filled from one boiling and stored in a pan of 90° water, thus preventing atmospheric contamination.

Apparatus. The absorption apparatus used (Fig. 1b) is modified from a 0.5-cc. analyzer.²³ It consists of only one side arm, enlarged to deliver approximately 4 cc. of water, to the main absorption chamber of 5-cc. capacity. The rubber stopper is replaced with a small polyethylene plug which is inserted tightly into the capillary of the side arm (Fig. 1c). This completely eliminates elasticity from the system. The water bath is thermoregulated within $\pm 0.01^\circ$ using a Bronwil regulator and all analyses are made in a constant temperature room.

Procedure. Filling the side arm with gas-free water involves having G and D filled with mercury (Fig. 1d), H, the thermobarometer, with water, and the stopcock S-1 closed prior to removing the plug, E. S-2 is in position I. The plug is now removed. No displacement of mercury will occur at this point. The sample syringe is taken from the storage pan and the stopper removed from the needle. The needle is fitted with a short polyethylene tubing adapter and inserted into the side arm (Fig. 1e). S-2 is now turned to position II and S-1 is opened. The side arm is flushed and left filled with gas-free water. S-2 is turned back to position I with S-1 remaining open. The needle is removed and the plug re-inserted. The gas-free sample is now in the side arm. The absorption chamber, G, is filled with mercury to the top of the capillary and the compensating chamber, H, is half-filled with water. A conventional gas-transfer pipet is filled with the pure gas and seated on the capillary. The gas meniscus is pulled down to the mark on the capillary, the micrometer connected to the leveling bulb, position III, and set to zero (V_0) and connected back to position I. To prevent pressure differences in the micrometer, the leveling bulb is always leveled with the mercury in the absorption chamber G. After about 20 micrometer units (mm.) of the gas is drawn into the absorption chamber, the transfer pipet is removed and the water sucked off, leaving an indicator drop in the capillary isolating the gas from the air in H.²⁴ S-1 is positioned and closed.

The volume of the gas is read (V_1) after approximately 2 min. when it remains constant. The gas-free water is then tilted in from the side arm.²⁵ Rapid mechanical shaking is then begun, avoiding bubble

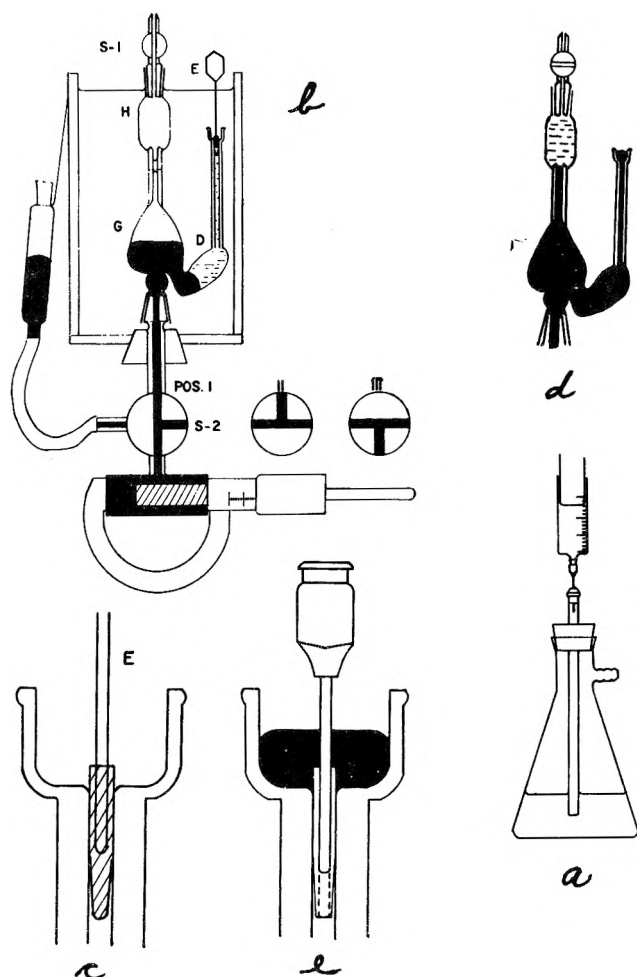


Figure 1.

(23) P. F. Scholander, *J. Biol. Chem.*, **167**, 235 (1947).

(24) For a detailed description, refer to the original paper.²³

(25) This is accomplished by first lowering the water level in the bath and then tilting in the sample water. The water bath level is then appropriately adjusted. The whole operation requires less than 15 sec.

formation, and the indicator drop kept at the mark on the capillary by screwing in the micrometer.

Absorption equilibrium is complete after about 15 min., but shaking is continued for 30 min., after which the volume of gas is read (V_2). Stopcock S-1 is now opened and removed, the indicator drop brought up and carefully drawn off by suction, and the gas expelled by screwing in the micrometer until the lower gas meniscus is at the mark for the reading V_3 .²⁶

The volume of the water, V_4 , is measured by replacing it with mercury from the micrometer. This reading involved five repeated fillings of the micrometer and a common final reading is around 100 mm. Temperature measurements were made using a thermometer calibrated against two certified standards.

Calculation of Data. The equation used for the determination of α is

$$\alpha = \frac{\text{volume of gas absorbed (STPD)}}{\text{volume of water} \times \text{atmospheres of pure gas}}$$

or

$$\alpha_{\text{C.}} = \frac{(V_1 - V_2) \left(\frac{B - b - w}{760} \right) \left(\frac{273}{273 + \text{°C}} \right)}{(V_4) \left(\frac{B - b - w}{760} \right)}$$

where B is the uncorrected barometric reading, b is in brass correction units, and w is the vapor pressure of water. This equation is then reduced to its final form

$$\alpha_{\text{C.}} = \frac{(V_1 - V_2)(273)}{(V_4)(273 + \text{°C.})}$$

It is a significant advantage that with this method, the equilibration pressure remains constant and therefore need not be known.

Results and Discussion

Oxygen. The present results for oxygen are shown in Table I and compared with the values of previous

Table I: Experimental Solubility Coefficients of Oxygen^a

	Temperature, °C.		
	8.00	19.94	29.15
	0.03984	0.03095	0.02651
	.03990	.03098	.02654
	.03986	.03098	.02655
	.03978	.03100	.02653
	.03981	.03092	.02651
Av.	.03984	.03097	.02653

^a α is defined as the volume of gas (STPD) absorbed by a unit volume of water when the pressure of the gas is 760 mm.

workers in Table II. The greatest range of consecutive values at any single temperature was only 0.3% of α , showing the method to have good precision.

Figure 2 (top) shows the per cent difference of previous α values of oxygen from those presently obtained. The present values are in good agreement with those of Winkler and of most other workers, although Fox's values, which are used in "Standard Methods,"²⁷ are definitely higher, and those of Truesdale, *et al.*, are much lower except at the 29° mark. It is important to note the close agreement between the various workers from 5 to 20°, but from there the values begin to diverge. This would tend to indicate that 30° is the limiting temperature for some of these methods. It appears from the present determinations and previous work that Winkler's solubility values for oxygen as given in the handbook should remain the standard values.

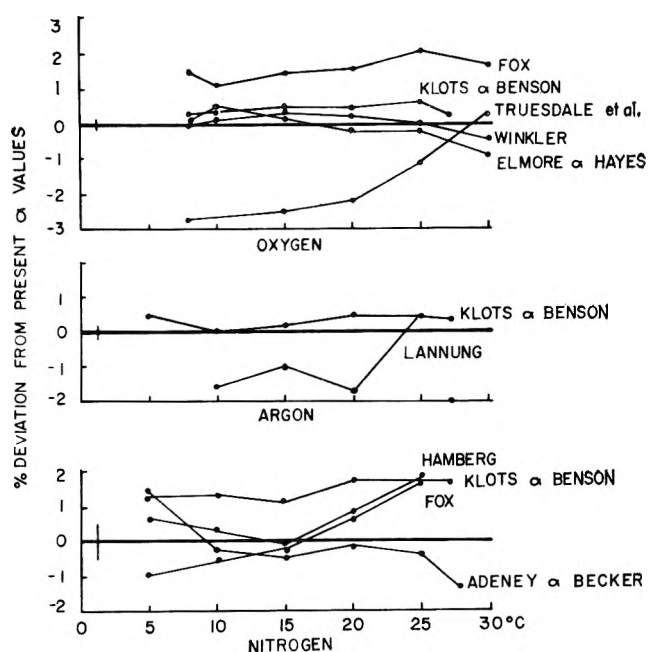


Figure 2.

Argon. Since the solubility coefficient for argon varied greatly between workers, analyses were made at 5° intervals from 5 to 30°. These results are shown in Table III and contrasted with those of the other workers in Table IV. The largest spread in consecutive argon

(26) In most cases V_3 is 0.000 on the micrometer although small amounts of water trapped on the chamber wall at the start would sometimes account for a reading of 0.010 to 0.015 for V_3 . This could be ignored as it entered in the calculation of α in no way.

(27) "Standard Methods," 10th Ed., Waverly Press, Inc., Baltimore, Md., 1955.

Table II: Comparison of Previous α Values of Oxygen with Those Presently Obtained

	Temperature, °C.						
	0	5	10	15	20	25	30
Winkler (1889)	0.04889	0.04287	0.03802	0.03415	0.03102	0.02831	0.02608
Fox (1909)	.04924	.04321	.03837	.03455	.03144	.02890	.02665
Truesdale, <i>et al.</i> (1955)	.04765	.04173	.03698	.03320	.03027	.02800	.02629
Elmore and Hayes (1960)	.04930	.04315	.03816	.03412	.03088	.02824	.02597
Klots and Benson (1963)04303	.03814	.03423	.03111	.02848
Present03797	.03403	.03095	.02830	.02620

Table III: Experimental Solubility Coefficients of Argon

	Temperature, °C.					
	4.62	10.00	15.04	20.00	25.20	29.70
0.04744	0.04178	0.03746	0.03407	0.03111	0.02895	
.04741	.04169	.03749	.03399	.03115	.02907	
.04748	.04182	.03753	.03407	.03112	.02900	
.04749	.04182	.03750	.03405	.03115	.02898	
.04747	.04189	.03751	.03408	.03114	.02905	
Av. .04746	.04180	.03750	.03405	.03113	.02901	

The comparison of the solubility coefficients of nitrogen, Fig. 2 (bottom), shows the present values to be in close agreement with those of Hamberg, Fox, and Adeney and Becker from 5 to 25°, where the values begin to diverge. The values of Klots and Benson remain systematically 1.5% higher.

Table VIII gives the α values of nitrogen from 3 to 30° as taken from a smooth curve.

Sources of Error. 1. Boiling water for 60 min., as

Table IV: Comparison of Previous Argon Values with Present Values

	Temperature, °C.						
	0	5	10	15	20	25	30
Estreicher (1899)	0.05780	0.05080	0.04525	0.04099	0.03790	0.03470	0.03256
Winkler (1906)	.0530042003500300
Antropoff (1910)	.0561043803790348
Lannung (1930)0411	.0371	.0336	.0314	.0289
Morrison and Johnstone (1954)0417	.0367	.0335	.0308	.0282
König (1963)0353	.0328	.0302	.0263
Klots and Benson (1963)04713	.04182	.03759	.03421	.03137
Present04689	.04180	.03753	.03405	.03123	.02888

values was 0.4% experienced at 30 and 10°, while the others remained approximately 0.2%.

The present argon values are compared with previous values in Fig. 2 (middle). It is sufficient to say that the range of values among the various workers is wide. The present values are in good agreement with those of Klots and Benson.

Table VII lists the α values of argon from 5 to 30°. These were taken from a smooth curve fitted through the experimental points.

Nitrogen. Ten consecutive analyses of nitrogen solubilities were made at 7.83, 19.95, and 29.50° with checkpoints at 3.10 and 11.68°. A greater number of nitrogen values were determined at individual temperatures because of its lower solubility. The results for nitrogen are shown in Table V and compared with previous values from other workers in Table VI. The range in values for nitrogen was 1%.

Table V: Experimental Solubility Coefficients of Nitrogen

	Temperature, °C.				
	3.10	7.83	11.68	19.95	29.50
0.02191	0.01953	0.01812	0.01556	0.01349	
.02197	.01966	.01816	.01565	.01348	
.02187	.01961	.01812	.01553	.01349	
	.01957	.01817	.01559	.01363	
	.01959	.01823	.01550	.01352	
	.0195101557	.01351	
	.0195901555	.01356	
	.0195601559	.01356	
	.0196501561	.01359	
	.0193301561	.01359	
Av. .02192	.01959	.01816	.01558	.01354	

described, leaves no detectable amount of gas in solution. To confirm this, 10 cc. of the boiled samples was

Table VI: Comparison of Previous Nitrogen Values with Present Values

	Temperature, °C.						
	0	5	10	15	20	25	30
Hamberg ^a	0.02379	0.02105	0.01881	0.01703	0.01570	0.01468
Fox ^a	.02319	.02068	.01863	.01702	.01572	.01465
Winkler ^a	.02312	.02050	.01829	.01656	.01518	.01410
Adeny and Becker (1919)02122	.01870	.01696	.01555	.01435	0.01327
Morrison and Billet (1952)01743	.01595	.01481	.01377
Klots and Benson (1963)02118	.01899	.01724	.01584	.01466
Present02091	.01875	.01705	.01557	.01441	.01345

^a These values were taken from Coste, ref. 14.

Table VII: Argon Values Interpolated from a Smooth Curve

Temp., °C.	α	Temp., °C.	α
3	17	0.03604
4	18	.03535
5	0.04689	19	.03468
6	.04584	20	.03405
7	.04473	21	.03342
8	.04369	22	.03284
9	.04272	23	.03228
10	.04180	24	.03174
11	.04086	25	.03123
12	.04000	26	.03074
13	.03915	27	.03027
14	.03833	28	.02981
15	.03753	29	.02934
16	.03677	30	.02888

Table VIII: Nitrogen Values Interpolated from a Smooth Curve

Temp., °C.	α	Temp., °C.	α
3	0.02198	17	0.01642
4	.02143	18	.01612
5	.02091	19	.01584
6	.02042	20	.01557
7	.01996	21	.01532
8	.01952	22	.01507
9	.01912	23	.01484
10	.01875	24	.01462
11	.01839	25	.01441
12	.01805	26	.01421
13	.01771	27	.01401
14	.01737	28	.01383
15	.01705	29	.01364
16	.01673	30	.01345

vacuum-extracted over mercury in a 500-cc. chamber, and showed that no gas remained in solution.

2. Diffusion of gas across the indicator drop was investigated. No net movement of the gas occurred

across the drop over a period of 60 min., approximately twice the time limit of equilibration.

3. Complete saturation of the samples was verified by plotting % saturation vs. time, showing that the samples are from 90 to 98% saturated after 7 min. for argon, and 10 min. for nitrogen (Fig. 3). Equilibration time was set at 30 min. to allow for complete saturation.

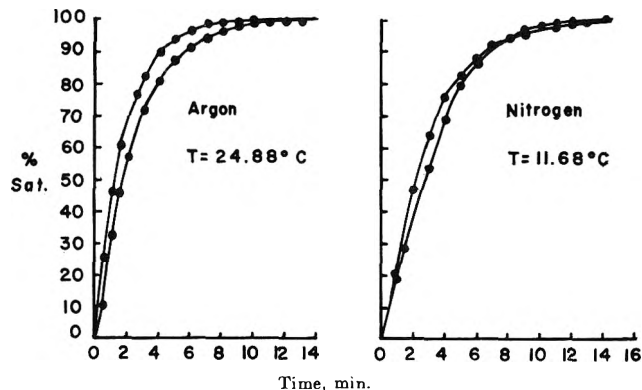


Figure 3.

4. The purity of the nitrogen and argon used was determined on a mass spectrometer, showing the nitrogen to contain 0.04% oxygen and less than 0.03% argon. The argon contained less than 0.1% nitrogen and less than 0.01% CO₂. The purity of oxygen was determined using the Scholander 0.5-cc. analyzer and microgasometric analyzer,²⁸ each showing the oxygen to be at least 99.5% pure.

Estimation of Accuracy. A temperature uncertainty of 0.05° causes an error of less than 0.02% in the values of α . The temperature is known, however, within 0.02°. The micrometer can be estimated to 0.001 mm. using a hand lens. The critical micrometer readings are those of V_0 , V_1 , and V_2 . These three readings could lead to a $\pm 0.15\%$ discrepancy in α . The volume of

(28) P. F. Scholander, L. VanDam, C. L. Claff, and J. W. Kanwisher, *Biol. Bull.*, 109, 328 (1955).

water measured by five stepwise micrometer readings is so large in relation to the others that only a negligible error of 0.04% in α can be introduced here. The temperature differential between the water bath and room temperature could account for a maximum change in α of 0.5%. In practice, however, the maximum error is 0.05% of α , experienced only at the very low temperature determinations. Assuming maximal additive errors, this gives a $\pm 0.26\%$ uncertainty in the determinations.

Acknowledgments. The author wishes to express his thanks to Dr. P. F. Scholander for his interest and encouragement during the course of this work. The author is indebted to Edvard Hemmingsen for the mass spectrometer measurements and to Paul Yeager for the fine glass work on the absorption chamber. Thanks are due to Dr. Scholander, Dr. D. L. Fox, Dr. T. Enns, and George Pickwell for their stimulating discussions and critical reading of the manuscript.

The Kinetics of Some Oxidation-Reduction Reactions

Involving Manganese(III)¹

by H. Diebler² and N. Sutin

Chemistry Department, Brookhaven National Laboratory, Upton, New York (Received August 27, 1963)

The kinetics of several oxidation-reduction reactions involving manganese(III) have been studied spectrophotometrically by the use of a flow technique. The free energies of activation for the oxidation of various substituted tris(1,10-phenanthroline) complexes of iron(II) by manganese(III) in perchloric acid and in pyrophosphoric-sulfuric acid media were found to be linearly related to the standard free energy changes of the reactions. The application of the Marcus theory to the reactions of manganese(III) with iron(II) and with various substituted iron(II)-phenanthroline complexes and to the reaction of cobalt(III) with manganese(II) in perchloric acid leads to an estimate of about $10^{-4} F^{-1}$ sec.⁻¹ for the rate constant of the manganese(II)-manganese(III) electron exchange reaction at 25.0°. Attempts to determine the rate constant for this exchange by a radioactive tracer method were unsuccessful.

Whereas numerous studies of the kinetics of oxidation-reduction reactions have been reported in recent years, very few have dealt with the reactions of manganese(III) in perchloric acid.³ The paucity of data on such reactions is probably due to the belief that free manganic ions cannot exist in significant concentrations in aqueous solution.⁴ Nevertheless, perchloric acid solutions of manganese(III) have been used in a few oxidation-reduction studies. For example, Adamson⁵ has studied the electron exchange reaction between manganese(II) and manganese(III) in perchloric acid

while Ogard and Taube⁶ have used perchloric acid solutions of manganese(III), prepared by the reaction

- (1) Research performed under the auspices of the U. S. Atomic Energy Commission.
- (2) Chemistry Department, Stanford University, Stanford, California.
- (3) For recent reviews of electron transfer reactions, see, for example: (a) H. Taube, *Advan. Inorg. Chem. Radiochem.*, **1**, 1 (1959); (b) J. Halpern, *Quart. Rev. (London)*, **15**, 207 (1961); (c) N. Sutin, *Ann. Rev. Nucl. Sci.*, **12**, 285 (1962).
- (4) W. A. Waters, *Quart. Rev. (London)*, **12**, 296 (1958).
- (5) A. W. Adamson, *J. Phys. Chem.*, **55**, 293 (1951).

of manganese(II) with cerium(IV) or cobalt(III), to study the effect of manganese(III) on the dissociation of CrCl^{2+} . The kinetics of the oxidation of mercury(I) by manganese(III) in perchloric acid has been studied by Rosseinsky.⁷

The stability of manganese(III) can be increased by complexing it with various ligands. Fluoride, sulfate, and pyrophosphate have been used for this purpose. Indeed, solutions of manganic sulfate and manganic pyrophosphate are stable enough to be used as oxidizing agents in volumetric analysis.⁸⁻¹¹ The oxidation of numerous organic compounds by manganic pyrophosphate has been studied by Waters and his collaborators.⁴ Polissar¹² has studied the kinetics of the electron exchange between manganese(II) and the oxalate complexes of manganese(III), while Taube¹³ has studied the kinetics of the oxidation of oxalate ions by manganese(III) in hydrochloric acid.

We have studied the kinetics of the iron(II)-manganese(III) and manganese(II)-cobalt(III) reactions in perchloric acid as well as the oxidation of various substituted phenanthroline complexes of iron(II) by manganese(III) in perchloric acid and by manganese(III) pyrophosphate in a pyrophosphoric acid-sulfuric acid medium. Attempts to study the manganese(II)-manganese(III) electron exchange reaction in perchloric acid were unsuccessful, probably because exchange between the two oxidation states was induced by the separation procedure. The results are discussed in the light of the Marcus theory of electron-transfer reactions.¹⁴ In terms of this theory k_{12} , the rate constant for an electron-transfer reaction, should be related to k_1 and k_2 , the electron exchange rates of the two reactants, and K_{12} , the equilibrium constant for the electron-transfer reaction, by the expression

$$k_{12} = (k_1 k_2 K_{12} f)^{1/2} \quad (1)$$

where

$$\log f = (\log K_{12})^2 / 4 \log (k_1 k_2 / Z^2)$$

and Z is the collision frequency between two uncharged molecules in solution ($\sim 10^{11}$ l. mole⁻¹ sec.⁻¹). Equation 1 is applicable to outer-sphere electron-transfer reactions when the various work terms approximately cancel or are negligible.

Since the completion of this work, a brief report has appeared on the kinetics of the iron(II)-manganese(III) reaction in perchloric acid.¹⁵ The rate constant for this reaction, determined by a polarographic technique, is in good agreement with the value we have determined spectrophotometrically.

Experimental

Chemicals. Manganese(II) and cobalt(II) perchlorates were prepared by dissolving manganese (Fisher Scientific Co.) and cobalt (A. D. Mackay Inc.) in perchloric acid (Baker Analyzed Reagent). Iron(II) perchlorate was obtained from the G. Frederick Smith Chemical Co. Solutions of manganese(III) and cobalt(III) in perchloric acid were prepared by electrooxidation of the lower oxidation states at platinum anodes. The manganese(II) solution was electrolyzed at room temperature at a current density of about 2 ma. cm.⁻² while the cobalt(II) solution was electrolyzed at 0° at a current density of about 50 ma. cm.⁻². Since the tendency of manganese(III) to disproportionate to manganese(II) and manganese(IV) (with the eventual precipitation of MnO_2) is suppressed by high manganese(II) and perchloric acid concentrations, the solutions used in the electrolyses contained up to 0.1 *F* manganese(II) and from 1 to 6 *F* perchloric acid. In most of the studies the manganese(II) concentration was 5×10^{-2} *F*. At lower manganese(II) concentrations, particularly at lower acidities and higher current densities, the solutions turned pink during the early stages of the electrolysis. Spectrophotometric measurements established that this pink color was due to the formation of permanganate; at higher manganese(II) concentrations and acidities the reaction of manganese(II) with permanganate is rapid enough to prevent the formation of an appreciable permanganate concentration during the electrolysis.

The concentrations of manganese(III) and cobalt(III) were determined by adding an excess of standardized iron(II) solution to aliquots of the electrolyzed solutions and titrating the excess iron(II) with cerium(IV). The phenanthroline complex of iron(II) was used as the indicator in the estimation of manganese(III) and cobalt(III) in perchloric acid and its 5,6-dimethyl phenanthroline complex in the estimation of manganese(III) in pyrophosphoric-sulfuric acid.

Manganese(III) pyrophosphate was prepared by electrooxidation of a solution of manganous sulfate

- (6) A. E. Ogard and H. Taube, *J. Phys. Chem.*, **62**, 357 (1958).
- (7) D. R. Rosseinsky, *J. Chem. Soc.*, 1181 (1963).
- (8) A. R. J. P. Ubbelohde, *ibid.*, 1605 (1935).
- (9) J. I. Watters and I. M. Kolthoff, *J. Am. Chem. Soc.*, **70**, 2455 (1948).
- (10) R. Belcher and T. S. West, *Anal. Chim. Acta*, **6**, 322 (1952).
- (11) W. C. Purdy and D. N. Hume, *Anal. Chem.*, **27**, 257 (1955).
- (12) M. J. Polissar, *J. Am. Chem. Soc.*, **58**, 1372 (1936).
- (13) H. Taube, *ibid.*, **70**, 1216 (1948).
- (14) R. A. Marcus, *J. Phys. Chem.*, **67**, 853 (1963).
- (15) M. J. Nicol and D. R. Rosseinsky, *Chem. Ind. (London)*, 1166 (1963).

(Baker Analyzed Reagent) in sulfuric acid (Baker and Adamson) containing a large excess of sodium pyrophosphate (Matheson Coleman and Bell). The iron(II)-phenanthroline complexes were prepared as described previously¹⁶ and standardized spectrophotometrically using published extinction coefficients.^{17,18} Sodium perchlorate was prepared from sodium carbonate (Baker Analyzed Reagent) and perchloric acid. Dibutyl phosphate (Fisher Chemical Co.) was separated from its mixture with the monobutyl compounds by continuous extraction with water.

Procedure. The spectra of the electrolyzed solutions were measured on a Beckman DU spectrophotometer. The formal potentials were measured with a Beckman pH meter by inserting a platinum electrode into the electrolyzed solutions and using a saturated calomel half-cell as reference electrode. It took several hours for the potentials to reach their equilibrium values. The experiments on the manganese(II)-manganese(III) exchange reaction were carried out by adding carrier-free Mn^{54} (as manganese(II)) to a solution containing both oxidation states. The sum of the concentrations of the two oxidation states was varied from 2×10^{-4} to $1 \times 10^{-2} F$ and the perchloric acid concentration of the medium was generally 6 *F*.

The manganese(II) and manganese(III) were separated by both solvent extraction and precipitation methods. Acetylacetone was found to be unsatisfactory as an extracting agent since a two-phase system is not obtained on adding acetylacetone to 6 *F* per-

chloric acid. While a two-phase system could be obtained at lower perchloric acid concentrations, the extraction of manganese(III) was found to be relatively poor and not very reproducible. A very good separation of manganese(II) and manganese(III) could be effected by extraction with a solution of dibutyl phosphate in benzene (volume ratio 1 to 5). It was found that only about 0.5% of the manganese(II) and practically all of the manganese(III) was extracted into the organic phase (as a red dibutyl phosphate complex) after shaking equal volumes of the aqueous and organic solutions for 1 min. Separation by precipitation was accomplished by the addition of either ammonia or a solution of sodium phosphate in ammonia. In the first case MnO_2 , formed by the disproportionation of manganese(III), was precipitated, and in the second case manganese(II) was quantitatively precipitated as $MnNH_4PO_4$ while part of the manganese(III) remained in solution as a phosphate complex.

The oxidation-reduction reactions were studied by the use of the rapid-mixing and flow apparatus which has been described previously.¹⁶ All the reactions were studied at 25.0° by means of the stopped-flow technique.

Results and Discussion

The Nature of Manganese(III) in Perchloric Acid. The spectrum of an electrolyzed solution is shown in Fig. 1, which also contains the spectrum of a manganese(III) pyrophosphate solution. The similarity of the spectra is quite striking. The absorbances of solutions in 6 *F* $HClO_4$ which had been electrolyzed until MnO_2 started precipitating and filtered after they had stood overnight were found to be approximately proportional to the square root of their manganese(II) concentrations. This indicates that the principal absorbing species in these solutions is manganese(III), since the concentration of manganese(IV) should be the same in all the solutions (its saturation value in 6 *F* $HClO_4$). This conclusion is supported by the work of Vetter and Manecke,¹⁹ who found that manganese(III) is the primary product of the electrooxidation of sulfuric acid solutions of manganese(II). On the other hand, the absorbances of the oxidized solutions were independent of their manganese(II) concentrations over wide limits, provided the oxidation was stopped well before the precipitation of MnO_2 commenced. This shows that

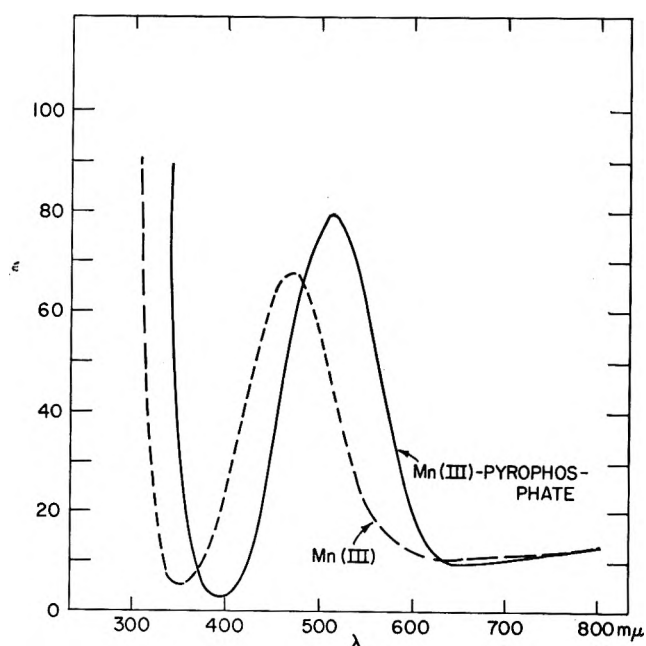


Figure 1. Spectra of manganese(III) in 6 *F* perchloric acid and of manganese(III) pyrophosphate in 0.05 *F* H_2SO_4 .

(16) G. Dulz and N. Sutin, *Inorg. Chem.*, **2**, 917 (1963).

(17) W. W. Brandt and G. F. Smith, *Anal. Chem.*, **21**, 1313 (1949).

(18) W. W. Brandt and D. K. Gullstrom, *J. Am. Chem. Soc.*, **74**, 3532 (1952).

(19) K. J. Vetter and G. Manecke, *Z. physik. Chem.*, **195**, 377 (1950).

even at the lowest manganese(II) concentrations used ($1 \times 10^{-5} F$) the manganese(III) concentrations of the solutions ($1 \times 10^{-4} F$) was at least 10 times larger than their manganese(IV) concentrations. These values lead to an estimate of 1×10^{-2} for the upper limit of the equilibrium constant for the reaction



in $6 F \text{ HClO}_4$ at 23° . This estimate is consistent with the values of 10^{-3} and 10^{-4} in $4 F$ and $7.2 F \text{ H}_2\text{SO}_4$ at 25.0° , respectively, determined spectrophotometrically by Selim and Lingane.²⁰

Values at $470 \text{ m}\mu$ of the apparent extinction coefficient, defined by $\bar{\epsilon} = E/[\text{Mn(III)}]$ where E is the value of the absorbance per cm. of path length, are plotted in Fig. 2 as a function of the manganese(III)

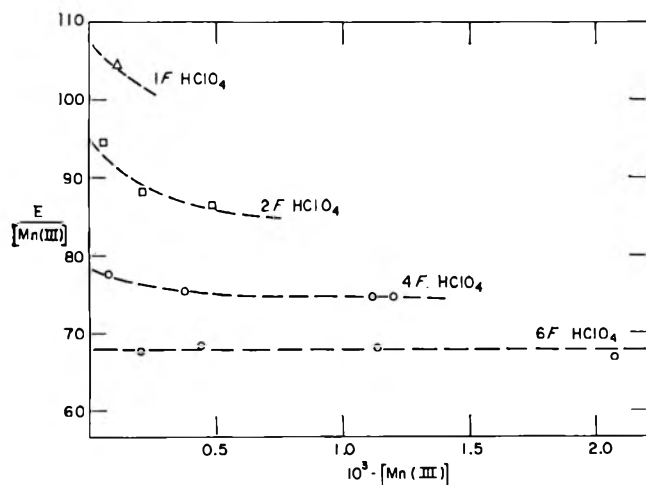
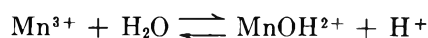


Figure 2. Apparent extinction coefficient of manganese(III) at $470 \text{ m}\mu$ as a function of the manganese(III) and perchloric acid concentrations of the solutions at 23° and an ionic strength of 6.0.

and perchloric acid concentrations of the solutions. The ionic strengths of the solutions were adjusted to 6.0 with NaClO_4 . The large decrease in $\bar{\epsilon}$ with acidity suggests that hydrolyzed forms of manganese(III) are present even at the relatively high acidities used in this work. The slow decrease of $\bar{\epsilon}$ with the manganese(III) concentration of the solutions at perchloric acid concentrations below $6 F$, as well as the gradual decrease of $\bar{\epsilon}$ during the first few days after the preparation of the solutions (the values presented in Fig. 2 were determined 6 days after the solutions were prepared, when no further change with time was observed) suggests that the solutions contain more than one hydrolyzed form of manganese(III). The manganese(III) dependence and the slow changes with time may arise from the slow

formation of dimeric and perhaps higher polymeric forms of hydrolyzed manganese(III).

An attempt was made to obtain a rough estimate of the hydrolysis constant of manganese(III) by extrapolating the $\bar{\epsilon}$ values at constant perchloric acid concentrations to $[\text{Mn(III)}] = 0$ and assuming that MnOH^{2+} was the only hydrolyzed form of manganese(III) present at the very low manganese(III) concentrations. This procedure leads to an estimate of approximately 5 for the value of the equilibrium constant for the reaction



at 23° and an ionic strength of 6.0. While this estimate of K is very crude, it is perhaps worth recalling that other strong oxidizing ions, such as Tl(III) , Ce(IV) , and Co(III) , are also strongly hydrolyzed.²¹ It may be that because of their tendency to attract electrons these powerful oxidizing agents polarize the surrounding water molecules to such a degree that the dissociation of a proton occurs readily.

The Manganese(II)-Manganese(III) Exchange Reaction. The specific activities of the manganese(II) and manganese(III) fractions were found to be the same within about 60 sec. after the addition of the radioactive tracer to the mixture, regardless of the separation procedure employed. This rapid exchange is probably separation-induced, since complete exchange was also found when the tracer was added with the precipitating agents or when it was added after the manganese(II) and manganese(III) had been separated by solvent extraction with dibutyl phosphate and the two phases then remixed by shaking for about 30 sec. These observations suggest that the exchange between manganese(II) and manganese(III)-dibutyl phosphate is rapid, as is the exchange between manganese(II) and the hydrolysis products of manganese(III) [or manganese(IV)] which are formed during the acidity changes required in the precipitation methods. Thus no conclusions about the manganese(II)-manganese(III) exchange rate in perchloric acid can be drawn from these studies. It is likely that the exchange reported by Adamson was also induced by the procedure used to separate the two oxidation states.

The Iron(II)-Manganese(III) Reaction. The oxidation of iron(II) by manganese(III) was studied in 3 and 1 F perchloric acid solutions. The reaction was found to be first order with respect to each of the reactants; the iron(II) and manganese(III) concentrations were

(20) R. G. Selim and J. J. Lingane, *Anal. Chim. Acta*, 21, 536 (1959).

(21) An unusually strong hydrolysis of manganese(III) has also been found by H. Taube (personal communication).

varied from 2.7×10^{-4} to $27 \times 10^{-4} F$ and from 0.5×10^{-4} to $4.9 \times 10^{-4} F$, respectively. The second-order rate constants for the reaction are 1.46×10^4 and $1.67 \times 10^4 F^{-1} \text{ sec.}^{-1}$ in 3.0 and 1.0 F perchloric acid, respectively, at 25.0° and an ionic strength of 3.1 (sodium perchlorate). Individual determinations of the rate constants differed from the mean by less than 7%. The rate constant in 1 F perchloric acid is in good agreement with the value of $6.92 \times 10^3 F^{-1} \text{ sec.}^{-1}$ at 15° in 1.04 F perchloric acid and ionic strength 3.04 determined by Rosseinsky.¹⁵

The equilibrium constant for the iron(II)–manganese(III) may be calculated from the formal potentials of the corresponding couples. The formal potential of the Fe(II)–Fe(III) couple is 0.74 v. in 1 F perchloric acid²² and we have determined the formal potential of the manganese(II)–manganese(III) couple to be 1.56 ± 0.01 and 1.51 ± 0.01 volts in 3 and 1 F perchloric acid, respectively. The rate constant for the iron(II)–iron(III) electron exchange reaction is $4.0 F^{-1} \text{ sec.}^{-1}$ at 25.0° .²³ Substitution of the above values in eq. 1 gives 5×10^{-5} and $3 \times 10^{-4} F^{-1} \text{ sec.}^{-1}$ for the rate constant of the manganese(II)–manganese(III) exchange reaction in 3 and 1 F perchloric acid, respectively, at 25.0° .

The Manganese(II)–Cobalt(III) Reaction. The oxidation of manganese(II) by cobalt(III) was studied in 3.0 F perchloric acid. The manganese(II) concentration was varied from 2×10^{-2} to $5 \times 10^{-2} F$ and the cobalt(III) concentration was $1.3 \times 10^{-4} F$. This reaction was also found to be first order with respect to each of the reactants. The second-order rate constant for this reaction is $1.00 \times 10^2 F^{-1} \text{ sec.}^{-1}$ in 3.0 F perchloric acid at 25.0° . The formal potential of the cobalt(II)–cobalt(III) couple is approximately 1.92 v. in 4 F perchloric acid,²⁴ while the rate constant for the cobalt(II)–cobalt(III) exchange is approximately $7 F^{-1} \text{ sec.}^{-1}$ at 25.0° .²⁵ Substitution of the above values in eq. 1 gives an estimate of $3 \times 10^{-3} F^{-1} \text{ sec.}^{-1}$ for the rate constant of the manganese(II)–manganese(III) exchange reaction in 3 F perchloric acid at 25.0° .

The Iron(II)–Phenanthroline–Manganese(III) Reactions. The second-order rate constants for the oxidation of a number of substituted 1,10-phenanthroline complexes of iron(II) by manganese(III) in 1 and 3 F HClO_4 at 25.0° are presented in Table I, which also contains the formal oxidation potentials of the complexes. Because of the limited solubility of the phenanthroline complexes in perchloric acid, only four compounds could be investigated. The concentrations of the iron(II) complexes and of manganese(III) were varied from 1.5×10^{-6} to $1.2 \times 10^{-5} F$ and from 1.4×10^{-4} to $5.9 \times 10^{-4} F$, respectively. In Fig. 3 values

Table I: Second-Order Rate Constants for the Oxidation of Iron(II)–Phenanthroline Complexes by Manganese(III) in 1 and 3 F Perchloric Acid at 25.0°

Ligand	E^0 , v.		k_{12} , $F^{-1} \text{ sec.}^{-1}$	
	1 F HClO_4 ^{a,b}	3 F HClO_4 ^{a,c}	1 F HClO_4	3 F HClO_4
5-Methyl-1,10-phenanthroline	1.02	0.96	3.2×10^3	2.5×10^4
1,10-Phenanthroline	1.06	1.00	1.85×10^3	1.55×10^4
5-Chloro-1,10-phenanthroline	1.12	1.06 ^d	3.95×10^2	2.9×10^3
5-Nitro-1,10-phenanthroline	1.25	1.20	0.9×10^2	4.2×10^2

^a The formal oxidation potentials of the complexes are in 1.0 and 3.0 F H_2SO_4 , respectively. ^b G. F. Smith and F. P. Richter, *Ind. Eng. Chem., Anal. Ed.*, **16**, 580 (1944). ^c G. F. Smith and W. M. Banick, Jr., *Talanta*, **2**, 348 (1959). ^d This value was estimated from the formal potential in 1.0 F H_2SO_4 .

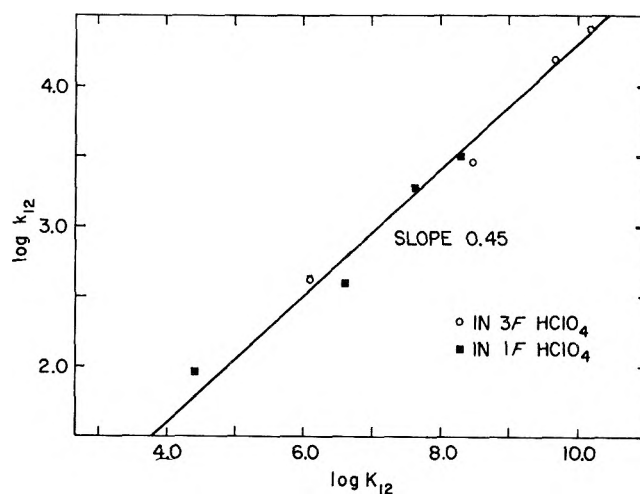


Figure 3. Relationship between the logarithms of the rate constants and the logarithms of the equilibrium constants for the oxidation of various substituted iron(II)–phenanthroline complexes by manganese(III) in 1 and 3 F perchloric acid at 25.0° .

of the logarithms of the rate constants are plotted against the values of the equilibrium constants for the reactions. A reasonably good linear relationship is obtained. Such a linear relationship is predicted by eq. 1 provided $|\log f|$ is small compared to $\log K_{12}$, a condition satisfied in this series. The slope of the straight line in Fig. 3 is 0.45, a value which is in reason-

(22) W. C. Schumb, M. S. Sherrill, and S. B. Sweetser, *J. Am. Chem. Soc.*, **59**, 2360 (1937).

(23) J. Silverman and R. W. Dodson, *J. Phys. Chem.*, **56**, 846 (1952).

(24) B. Warnqvist, personal communication.

(25) N. A. Bonner and J. P. Hunt, *J. Am. Chem. Soc.*, **82**, 3826 (1960).

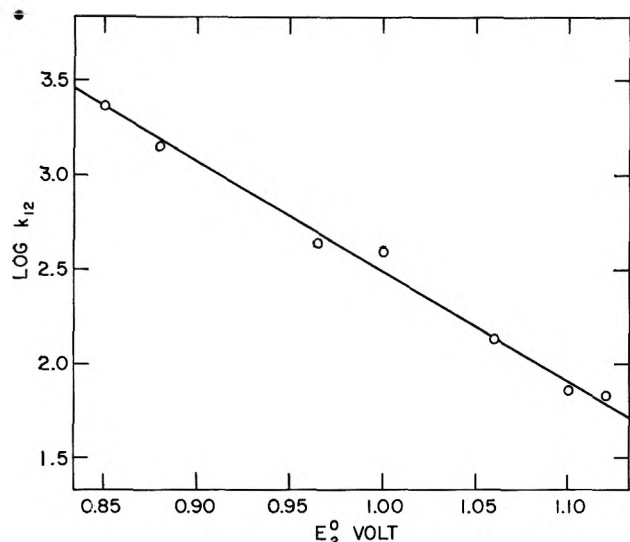
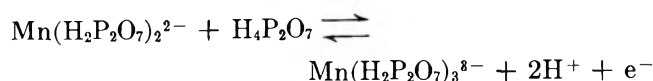


Figure 4. Relationship between the logarithms of the rate constants for the oxidation of various substituted iron(II)-phenanthroline complexes by manganese(III) pyrophosphate (pH 1.0, ionic strength ~ 0.5) at 25.0° and the formal oxidation potentials of the iron(II) complexes.

ably good agreement with the theoretical value of 0.50. Similar linear relationships have also been found for the oxidation of the iron(II)-phenanthroline complexes by cerium(IV)¹⁶ and for the oxidation of iron(II) by the iron(III)-phenanthroline complexes.²⁶

The intercept of Fig. 3 gives -0.22 for the value of $0.50(\log k_1 + \log k_2)$. Substitution of $2 \times 10^3 F^{-1} \text{ sec.}^{-1}$ for the value of k_2 , the effective rate constant for the electron exchange reaction between the phenanthroline complexes of iron(II) and iron(III),¹⁶ gives $2 \times 10^{-4} F^{-1} \text{ sec.}^{-1}$ for the value of k_1 , the rate constant for the manganese(II)-manganese(III) exchange, at 25.0° .

The Iron(II)-Phenanthroline-Manganese(III)-Pyrophosphate Reactions. The medium used in these studies was $0.1 F$ sodium pyrophosphate containing sufficient sulfuric acid to bring the pH to 1.01 ± 0.01 ; the concentrations of the iron(II) complexes were 1×10^{-5} to $2 \times 10^{-5} F$ and the manganese(III) concentration was 1×10^{-3} to $4 \times 10^{-3} F$. The second-order rate constants for the reactions as well as the formal oxidation potentials of the complexes are presented in Table II. According to Watters and Kolthoff,⁹ manganese(II) and manganese(III) are predominantly present in this medium as $\text{Mn}(\text{H}_2\text{P}_2\text{O}_7)_2^{2-}$ and $\text{Mn}(\text{H}_2\text{P}_2\text{O}_7)_3^{3-}$, respectively. The formal potential for the reaction



is about 1.15 v.^9 Because of the change in the number

of pyrophosphate groups coordinated to the manganese in the course of the above reaction, only an over-all equilibrium constant can be calculated for the reactions with the iron(II)-phenanthrolines, but not the equilibrium constant for the actual electron-transfer step. Accordingly the rate constants for the oxidation-reduction reactions have been plotted against the formal oxidation potentials of the complexes in Fig. 4 rather than against the equilibrium constants of the over-all reactions. It will be seen that a reasonably good linear relationship is again obtained. However, the slope of the straight line lies about 30% below the theoretical value. The reason for this discrepancy is not known; it may be that the formal oxidation potentials of the phenanthroline complexes, which were determined in

Table II: Second-Order Rate Constants for the Oxidation of Iron(II)-Phenanthroline Complexes by Manganese(III) Pyrophosphate at 25.0° . Ionic strength ~ 0.5 ; pH 1.0

Ligand	E_0 , v. ^{a,b}	k_{12} , $F^{-1} \text{ sec.}^{-1}$
3,4,7,8-Tetramethyl-1,10-phenanthroline	0.85	2.3×10^3
4,7-Dimethyl-1,10-phenanthroline	0.88	1.4×10^3
3,5,6,8-Tetramethyl-1,10-phenanthroline	0.96 ^c	4.3×10^3
5,6-Dimethyl-1,10-phenanthroline	1.00	3.9×10^2
5-Methyl-1,10-phenanthroline	1.06	1.4×10^3
1,10-Phenanthroline	1.10	7.2×10^1
5-Phenyl-1,10-phenanthroline	1.12	6.8×10^1

^a The formal oxidation potentials of the complexes are in $0.1 F$ H_2SO_4 . ^b See ref. 17 and 18. ^c The E_0 of this complex is reported to be 0.93 v. in ref. 17; we have determined the value reported above. The formal potentials of other phenanthroline complexes we have measured agreed well with the published values.

sulfuric acid, are changed in a systematic manner by the high concentration of pyrophosphate present in these studies. In addition, the rate constants show a large pH-dependence, suggesting that at least two manganese(III) pyrophosphate species are involved in the reactions. The measured rate constants are over-all rate constants and it may well be that the rate constants for the individual steps will give better agreement with eq. 1. Conditions under which the application of eq. 1 to over-all rate constants is appropriate have been described by Marcus.¹⁴

Comparison of Observed and Calculated Rate Constants. The geometric mean of the estimated rate con-

(26) M. H. Ford-Smith and N. Sutin, *J. Am. Chem. Soc.*, 83, 1830 (1961).

stants for the manganese(II)–manganese(III) exchange reaction in 3 *F* perchloric acid at 25.0° is $3 \times 10^{-4} F^{-1} \text{ sec.}^{-1}$. The substitution of this value together with the appropriate exchange rate constants and equilibrium constants into eq. 1 leads to the calculated rate constants presented in Table III. The agreement between the observed and calculated rate constants is encouraging in view of the large differences in the natures of the reactions. It may be noted that, as required for the application of eq. 1, the various work terms either cancel or have been corrected for.^{14,16}

Table III: Comparison of Observed and Calculated Rate Constants in 3 *F* HClO₄ at 25.0°

Reaction	k_{12} (obsd.), $F^{-1} \text{ sec.}^{-1}$	k_{12} (calcd.), ^a $F^{-1} \text{ sec.}^{-1}$
Fe(II) + Mn(III)	1.46×10^4	3×10^4
Mn(II) + Co(III)	1.00×10^2	3×10^1
Fe(phen) ₃ ²⁺ + Mn(III)	1.55×10^3	1×10^4

^a The rate constants were calculated from eq. 1 on the assumption that the manganese(II)–manganese(III) exchange rate is $3 \times 10^{-4} F^{-1} \text{ sec.}^{-1}$ in 3 *F* HClO₄ at 25.0°.

A more extensive comparison of the values of some observed rate constants with those predicted by eq. 1

has been made recently.¹⁶ The agreement was found to be satisfactory. The one notable exception is the iron(II)–cobalt(III) reaction which proceeds by a factor of about 10^5 more slowly than predicted by eq. 1. In view of the various successful predictions of eq. 1 and the satisfactory agreement of the values in Table III, it is possible that the mechanism of the iron(II)–cobalt(III) reaction is more complex than that of the other reactions considered. Clearly, further studies of cross reactions involving the cobalt(II)–cobalt(III) system and using eq. 1 are in order. A direct determination of the rate constant for the manganese(II)–manganese(III) exchange reaction would also be of considerable value.

It is of interest that the rate constant for the manganese(II)–manganese(III) reaction estimated above is much smaller than the observed rate constants for the iron(II)–iron(III) and cobalt(II)–cobalt(III) exchange reactions. The relative values of the rate constants for these reactions are consistent with calculations of the amount of energy required to reorganize the inner coordination shells of the various reactants prior to the electron transfer.^{3c}

Acknowledgment. It is a pleasure to acknowledge helpful discussions with Drs. R. W. Dodson, R. A. Marcus, and J. K. Rowley.

Association of N-H Compounds.^{1,2} II. Infrared Spectroscopic

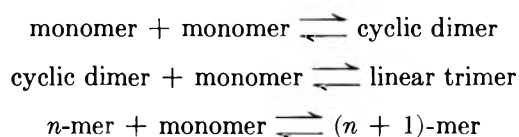
Investigation of the Self-Association of 3,5-Dimethylpyrazole in Benzene and in Carbon Tetrachloride

by S. N. Vinogradov³ and Martin Kilpatrick

Chemistry Department, Illinois Institute of Technology, Chicago 16, Illinois (Received August 29, 1963)

The self-association of 3,5-dimethylpyrazole in C₆H₆ and in CCl₄ was investigated over the temperature range 4 to 60° by means of absorption intensity measurements of the N-H stretching vibration band assigned to monomers. The results were found to be consistent with the formulation that 3,5-dimethylpyrazole self-associates to cyclic dimers and trimers only, in agreement with the recent work of Rossotti and in disagreement with that of Lorenzelli and Mirone. The following heats of association were obtained: in benzene, $\Delta H_{20} = -8.5$ kcal./mole and $\Delta H_{30} = -11.6$ kcal./mole; in CCl₄, $\Delta H_{20} = -9.2$ kcal./mole and $\Delta H_{30} = -13.9$ kcal./mole.

Unlike the O-H···O hydrogen bond, the N-H···N hydrogen bond has been studied very little, even in solution.⁴ There has been a paucity of quantitative data on the thermodynamics of N-H···N hydrogen bond formation. A previous investigation⁵ showed, as the result of the cryoscopic study of the self-association of 3,5-dimethylpyrazole in C₆H₆ over the range 0.02 to 0.12 *m*, that the compound self-associated rather strongly to dimers and trimers with $\beta_{20} = 2.5$ and $\beta_{30} = 2500$ at 5.5°. Since the completion of the present work, reports by two independent investigators on the self-association of 3,5-dimethylpyrazole in CCl₄ studied by infrared absorption spectroscopy have disagreed on the mode of the self-association. Mirone and Lorenzelli⁷ found that a plot of integrated intensity of the fundamental N-H stretching vibration band at 3478 cm.⁻¹ vs. concentration exhibited a plateau between 4 and 15 × 10⁻⁴ *M*. The result was explained by assuming that below 5 × 10⁻⁴ *M*, 3,5-dimethylpyrazole self-associated exclusively to cyclic dimer with $\beta_{20} = 1.7 \times 10^3$ l./mole; for concentrations higher than 2 × 10⁻³ *M*, Mirone and Lorenzelli used the Kempter and Mecke model⁸ to calculate the over-all association equilibrium constant, $K = 770$ l./mole. The authors proposed the following three equilibria to explain their results over the whole concentration range



Rossotti and his collaborators have demonstrated rather convincingly in a careful investigation of the self-association of pyrazole and some of its derivatives including 3,5-dimethylpyrazole, in CCl₄, that these

- (1) Taken in part from the dissertation presented by S. N. Vinogradov to the faculty of the Graduate School of the Illinois Institute of Technology in 1959 in partial fulfillment of the requirements for the degree of Doctor of Philosophy.
- (2) Presented before the Division of Physical and Inorganic Chemistry, 132nd National Meeting of the American Chemical Society, Chicago, Ill., September, 1957.
- (3) Department of Biochemistry, Yale University, New Haven, Conn.
- (4) G. C. Pimentel and A. L. McClellan, "The Hydrogen Bond," W. H. Freeman and Co., San Francisco, Calif., 1960, Chapter VII.
- (5) N. E. White and M. Kilpatrick, *J. Phys. Chem.*, **59**, 1044 (1955).
- (6) The terminology followed is the one of F. J. C. Rossotti and H. Rossotti, "The Determination of Stability Constants," McGraw-Hill Book Co., Inc., New York, N. Y., 1961.
- (7) P. Mirone and V. Lorenzelli, *Ann. chim. (Rome)*, **49**, 59 (1959).
- (8) H. Kempter and R. Mecke, *Z. physik. Chem.*, **B46**, 229 (1940); I. Prigogine and R. Defay, "Thermodynamique Chimique," Desoer, Liege, 1950, p. 449.

compounds self-associate to cyclic dimers and trimers only over the concentration range 10^{-4} to 10^{-2} *M*.⁹ In the case of 3,5-dimethylpyrazole the equilibrium constants were $\beta_{20} = 285 \pm 4$ l./mole and $\beta_{30} = 45,900 \pm 2800$ l.²/mole² at 19°.

Experimental

All measurements were performed on a Perkin-Elmer Model 21 double-beam spectrophotometer equipped with a CaF₂ prism. Demountable nickel cells were fitted inside a copper block placed between the source and monochromator housings. Both sample and reference cells were maintained to better than 0.1° in the range 0–70°. Rolled optical grade AgCl, 1 mm. thick (Harshaw Chemical Co.), was used as window material. The range of cell thicknesses available was 0.05 to 1.2 cm.

3,5-Dimethylpyrazole (Eastman Kodak) was crystallized twice from water and dried under vacuum. It melted at 106.4–107.0° and was used interchangeably with a sample left by White.¹⁰ The literature values range from 106.5 to 107.0°. Eastman Kodak Spectrograde C₆H₆ and CCl₄ were used without further purification. The water content was estimated as 2.5×10^{-5} *M*.

In the case of CCl₄ as solvent, the transmission at 3475 ± 10 cm.⁻¹, the N–H stretching vibration band maximum, was measured over the concentration range 0.0007 to 0.1 *m* at eight temperatures from 277 to 328°K. In the case of C₆H₆, due to its appreciable absorption, the cell thickness range was restricted to 0.05–0.4 cm. and the transmission at 3430 ± 10 cm.⁻¹ was measured over the concentration range 0.002 to 0.14 *m* at five temperatures from 286 to 330°K.

All solutions were made up by weighing. The peak heights of the monomer N–H band were measured at slit widths of 60, 80, and 100 μ in CCl₄ and 100, 120, and 200 μ in C₆H₆. The spectral slit widths were computed from the formulas $S' = 0.18S + 3.0F(s)$ for CCl₄ and $S' = 0.17S + 2.9F(s)$ for C₆H₆¹¹ where *S* is the mechanical slit width in μ .

All our calculations were performed on the IBM 650 computer of the Armour Research Foundation. The data were plotted as $1/\epsilon$ vs. ϵB , where ϵ is the molal absorptivity and *B* is the stoichiometric molality, and fitted by the method of least squares to a polynomial of the type

$$f(X) = \sum_{n=0}^{n=q} a_n X^n$$

with $q = 1, 2, 3,$ and 4 .¹² This treatment of infrared data has been described in detail elsewhere.¹⁸ It is based on the assumption, consistent with the findings of

Rossotti,⁹ that either all polymers are cyclic or that the end N–H groups of linear polymers (if they exist) do not absorb at the same wave length as the N–H groups of monomeric molecules.

Results and Discussion

Figure 1 shows a typical plot of $1/\epsilon$ vs. ϵB . The term involving β_{40} was negative at all temperatures in both solvents, indicating that over the concentration ranges

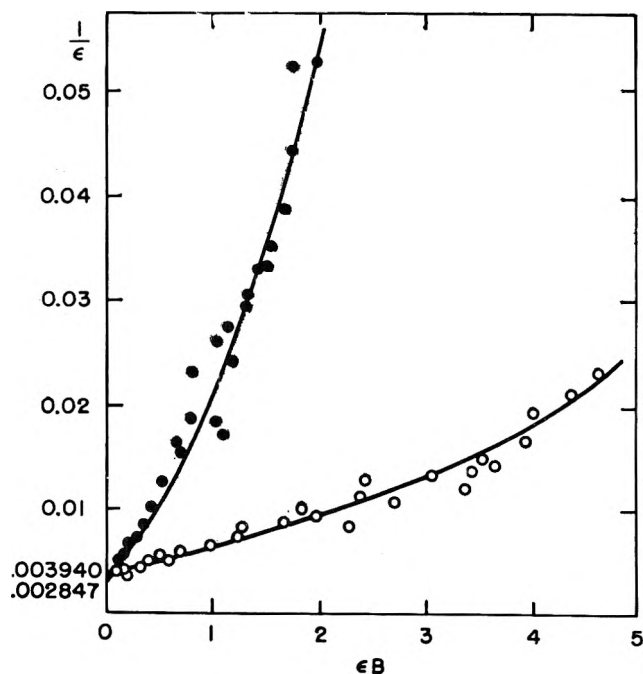


Figure 1. 3,5-Dimethylpyrazole in CCl₄, data at fixed slit width 60 μ ; plot of $1/\epsilon$ vs. ϵB : ●, 227°K.; ○, 326°K.

investigated, 3,5-dimethylpyrazole self-associates to dimers and trimers, in agreement with the conclusion of Rossotti⁹ and contrary to the findings of Mirone and Lorenzelli.⁷ Table I gives the β_{20} and β_{30} obtained from the foregoing treatment of the data taken at the mechanical slit width of 60 μ in CCl₄ and 100 μ in C₆H₆ (spectral slit widths of ~ 12 and 19 cm.⁻¹, respectively, assuming $F(s) = 0.5$). It is evident that 3,5-dimethylpyrazole is much less associated in C₆H₆ than in CCl₄.

(9) D. M. W. Anderson, J. L. Duncan, and F. J. C. Rossotti, *J. Chem. Soc.*, 140, 4201 (1961).

(10) N. E. White, Ph.D. Thesis, University of Pennsylvania, 1954.

(11) R. Barnes, R. S. McDonald, V. Z. Williams, and R. F. Kinnaid, *J. Appl. Phys.*, 16, 77 (1945); V. Z. Williams, *Rev. Sci. Instr.*, 19, 135 (1948).

(12) IBM program 6.0.005.

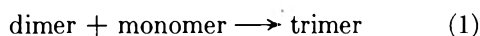
(13) S. N. Vinogradov, *Can. J. Chem.*, 41, 2179 (1963).

Table I: The Monomer-Dimer and Monomer-Trimer Association Equilibrium Constants of 3,5-Dimethylpyrazole

Temp., °K.	CCl ₄		C ₆ H ₆	
	β_{2c} , 10 ³ g. mole ⁻¹	β_{30} , 10 ⁶ g. ² mole ⁻²	β_{20} , 10 ³ g. mole ⁻¹	β_{30} , 10 ⁶ g. ² mole ⁻²
277	790	87 × 10 ³		
281	480	66		
286			34	450
295	200	20	10	280
298	120	16		
310			6.8	
311	110	5.4		
314	94	5.3		
321			6.2	40
326	61	2.2		
328	47	1.9		
331			3.2	34

In benzene the average of data at 100, 120, and 200 μ gave $\Delta H_{20} = -8.5$ and $\Delta H_{30} = -11.6$ kcal./mole. In CCl₄ the average heats of association calculated from the data at 60 and 80 μ were $\Delta H_{20} = -9.2$ and $\Delta H_{30} = -13.9$ kcal./mole.

It is interesting to note that in CCl₄ the strengths of the hydrogen bonds in the dimer, trimer, and the overall change in heat of association for the process



are all equal, $1/2\Delta H_{20} = -4.6$, $1/3\Delta H_{30} = -4.6$, and $\Delta H_{30} - \Delta H_{20} = -4.7$ kcal./mole, while in C₆H₆ the trend, $1/2\Delta H_{20} = -4.3$, $1/3\Delta H_{30} = -3.9$, and $\Delta H_{30} - \Delta H_{20} = -3.0$ kcal./mole, must be due to the solvation by C₆H₆, but it is unclear why the effect would be so pronounced for process 1.

Equally unclear are the reasons for the quantitative discrepancy between the equilibrium constants of this investigation and those of Rossotti⁹ (correcting for the difference in units) and the very considerable difference in the modes of self-association of 3,5-dimethylpyrazole arrived at by the two foregoing investigations and by Mirone and Lorenzelli.⁷ It is possible that the resolutions of the spectrophotometers used could play a role since in all three cases the spectral slit widths were not less than one-fifth the apparent half-band width of the narrow N-H stretching vibration, a condition which was found experimentally and theoretically necessary to eliminate the effect of slit width on absorption band intensity.¹⁴

We consider that although the equilibrium constants obtained from our data cannot be considered as reliable in view of the aforementioned discrepancies and the desirability for further work, the ΔH values obtained should be reliable to $\pm 10\%$. They seem to fall within the range of values of ΔH for N-H...N hydrogen bonding⁵: pyrrole-pyridine, 3.8 kcal./mole (calorimetry),¹⁵ 3.8 kcal./mole (infrared spectroscopy),¹⁶ and 4.3 kcal./mole (n.m.r.)¹⁷; aniline and N-methylaniline with 2-methylpyridine, 8.0 and 4.8 kcal./mole, respectively (calorimetry)¹⁸; indole-pyridine, 3.55 kcal./mole (infrared spectroscopy).¹⁹

(14) G. Pirlot, *Bull. soc. chim. Belges*, **59**, 352 (1950); J. B. Willis, *Australian J. Sci. Res.*, **4**, 172 (1951); R. A. Russell and H. W. Thompson, *Spectrochim. Acta*, **9**, 133 (1957).

(15) S. N. Vinogradov and R. H. Linnell, *J. Chem. Phys.*, **23**, 93 (1955).

(16) H. J. Wimetete and R. H. Linnell, *J. Phys. Chem.*, **66**, 546 (1962).

(17) J. A. Happe, *ibid.*, **65**, 72 (1961).

(18) W. B. Smith, *J. Org. Chem.*, **27**, 4641 (1962).

(19) H. Dunken and H. Fritzsche, *Z. Chem.*, **2**, 379 (1962).

General Combination Law for C_1 Terms in Gas Chromatography

by J. Calvin Giddings

Department of Chemistry, University of Utah, Salt Lake City 12, Utah (Received September 3, 1963)

The dependence of zone dispersion in gas-liquid chromatography on the diffusion of solute in and out of the liquid phase is investigated with the aid of the nonequilibrium theory of chromatography. Although explicit expressions are not obtained for zone dispersion in the (typical) presence of highly complex liquid masses, it is shown that the dispersion can be written as a sum of terms, each referring to a small, relatively simple unit of liquid. The differential equation (of the Poisson type) applicable to each such unit is given and previously obtained solutions are shown. It is demonstrated that the combination law reduces a problem of considerable complexity into its rather simple component parts, and that no practical difficulty stands in the way of solution providing only that the liquid configuration can be determined or estimated.

A basic problem in the study of zone spreading in chromatography, as well as in the broader field of dispersion in any porous material with fluid flow in it, is the manner in which the processes in neighboring regions combine in their over-all contribution to the dispersion of incorporated solute. If rules governing the interaction of such regions can be found, the dispersion problem reduces to the relatively simple one of treating isolated regions. These isolated regions may be complex, but individually they are far less formidable than when considered in total.

The particular system considered here is that generally associated with gas-liquid chromatography in which a finely dispersed partitioning liquid is found on the surface and in the cavities and recesses of a porous material¹ (usually a diatomaceous earth derivative). The over-all liquid configuration is enormously complex. In this paper it will be shown that such a liquid, insofar as its influence on zone spreading is concerned, can be broken into individual liquid units of comparatively simple geometry. The general combination law for the effect of these liquid units will then be elucidated.

The dispersion of a chromatographic zone is usually expressed in terms of the column plate height, H . A definition of this quantity will be presented later. The plate height is composed of a number of additive terms, each representing a particular mechanism leading to zone dispersion. The so-called nonequilibrium processes (next section) lead to a term proportional to

flow velocity, $C\bar{v}$. The C is in turn divided between a C_1 term¹ and a C_g term,² referring to liquid diffusion and gas diffusion processes, respectively. The C_1 term, to be investigated here, is generally the most important source of zone dispersion in gas chromatography. In the following treatment the C_1 term can be obtained as the derived value of H divided by the mean velocity \bar{v} . For convenience, most results will be left in the H form, but it should be remembered that this is only a particular part of the total H , a part most commonly identified by reference to the C_1 term.

Theory

At flow rates which are of practical importance in gas chromatography, zone dispersion is largely a result of various nonequilibrium processes. These arise as the zone's changing concentration profile moves through a given segment and equilibrates at a finite rate with each small region of the column (a qualitative view of nonequilibrium and its effects is given elsewhere³). The nonequilibrium may be controlled by liquid diffusion, gaseous diffusion, or both. The slowness of liquid diffusion makes this term rate-controlling in the largest number of cases. The liquid contribution, only, will be considered here.

(1) J. C. Giddings, *Anal. Chem.*, **34**, 458 (1962).

(2) J. C. Giddings, *ibid.*, **34**, 1186 (1962).

(3) J. C. Giddings, "Chromatography," E. Heftmann, Ed., Reinhold Publishing Corp., New York, N. Y., 1961, Chapter 3.

The quantitative description of nonequilibrium will proceed in terms of the equilibrium departure term, ϵ , defined by the equation⁴

$$m = m^*(1 + \epsilon) \quad (1)$$

where m is the actual value of the local concentration of solute at a given point and m^* is the local concentration assuming that complete equilibrium has been reached within the cross section of column containing that point. The magnitude of ϵ can generally be assumed as small compared to unity. This condition greatly simplifies the mathematical treatment of nonequilibrium⁴ and the consequent zone spreading.

The generalized nonequilibrium theory⁴⁻⁸ indicates that the rate of accumulation of the sample component per unit volume in region i due to nonequilibrium gradients is given by

$$s_i = (v_i - \bar{u})\partial m_i^*/\partial z \quad (2)$$

where v_i is the downstream velocity of phase i at the point under consideration, \bar{u} the mean downstream velocity of the sample zone, and z the distance along the axis of the column. The velocity, v , for the liquid is of course zero and eq. 2 simplifies to

$$s_i = -\bar{u}\partial m_i^*/\partial z \quad (3)$$

where m_i^* is the equilibrium liquid concentration. For diffusion controlled processes, s_i may conveniently be written as $D_1\nabla^2 m_i$, which, with eq. 1 and the condition that m^* is locally constant, becomes $D_1 m_i^* \nabla^2 \epsilon_i$. In this equation, D_1 is the diffusion coefficient of solute in the liquid. The substitution of this into eq. 3 gives one form of the basic differential equation for ϵ_i

$$\nabla^2 \epsilon_i = -\frac{\bar{u}}{D_1} \frac{\partial \ln m_i^*}{\partial z} \quad (4)$$

This equation must be integrated over the entire liquid mass in order to obtain point-by-point ϵ -values.

Once ϵ has been obtained at each point within the liquid, it is not difficult to formulate the effective diffusion coefficient for dispersion or the theoretical plate height which is likewise a measure of dispersion. This is done, as shown elsewhere, by obtaining an expression for the material flux through various cross sections. The effective dispersion coefficient, \mathcal{D} , is shown to be⁷

$$\mathcal{D} = \frac{-\sum \int m_i^* \epsilon_i v_i dA_i}{\partial c^*/\partial z} \quad (5)$$

where A_i is the fraction of total cross-sectional area occupied by the i th phase or region and c^* is the over-all concentration (per unit volume of column rather than per unit volume of a particular phase) at local equilib-

rium. The summation covers all regions of the column, liquid and gas. However, with $v_i = 0$ in the liquid, the summation, effectively, covers only the gas phase. Furthermore, when investigating solely the liquid contribution to zone dispersion, ϵ in the gas phase may be assumed locally constant, ϵ_g . (This assumption and some later ones depends on the additive contribution of gas and liquid terms to \mathcal{D} . The additive condition, discussed elsewhere,⁷ is certainly valid in this case because of the much larger diffusivity of gases compared to liquids, a feature which ensures that each part of a liquid droplet's surface will be bathed at the same concentration). Under these circumstances eq. 5 becomes

$$\mathcal{D} = \frac{-m_g^* \epsilon_g \bar{v} A_g}{\partial c^*/\partial z} \quad (6)$$

where m_g^* is the equilibrium concentration in the gas, \bar{v} the mean downstream fluid (gas in this case) velocity, A_g is the fraction of cross section occupied by gas. Since $m_g^* A_g$ is the gas phase contribution to c^* , the ratio $m_g^* A_g / c^* = R$, a commonly used term denoting the fraction of solute in the mobile phase. Thus the last equation becomes

$$\mathcal{D} = \frac{-R \epsilon_g \bar{v}}{\partial \ln c^*/\partial z} \quad (7)$$

and the plate height, which can be defined as $2\mathcal{D}/R\bar{v}$, is simply

$$H = -2\epsilon_g / \partial \ln c^*/\partial z \quad (8)$$

The ϵ_g and ϵ_i terms are assured by the nature of eq. 4 of being proportional to $\partial \ln c^*/\partial z$ (m_i^* and m_g^* are proportional to c^*); hence the final \mathcal{D} or H expression is not dependent on the concentration gradient. The ϵ_i values from eq. 4 are converted to an ϵ_g value by the local equilibration condition

$$\epsilon_g R = -\bar{\epsilon}_i (1 - R) \quad (9)$$

where $\bar{\epsilon}_i$ is the value of ϵ (or ϵ_i) averaged over the total liquid content.

The Liquid Phase

The bulk of the liquid phase in gas chromatography may be considered to occupy the cavities or pores of the solid support. Between these isolated liquid pools is a thin film of liquid held to the solid by adsorp-

- (4) J. C. Giddings, *J. Chem. Phys.*, **31**, 1462 (1959).
- (5) J. C. Giddings, *J. Chromatog.*, **3**, 443 (1960).
- (6) J. C. Giddings, *Nature*, **188**, 847 (1960).
- (7) J. C. Giddings, *J. Chromatog.*, **5**, 46 (1961).
- (8) J. C. Giddings, *Anal. Chem.*, **35**, 439 (1963).

tion forces.¹ As the chromatographic zone passes through each region the liquid pools first absorb solute, then release it back into the gas stream.³ At any given moment there is a certain flux of solute across the boundaries of a particular pool. Most of this flux typically occurs through the gas-liquid interface. Very little of it occurs through the thin film connecting one pool to another because of the film's dimensions. Virtually none of the flux occurs through the liquid-solid interface because of the solid's impermeability. Thus the diffusion of solute into such pools is governed, in part, by the boundary condition

$$\frac{\partial m_i}{\partial w} = 0 \quad (10)$$

nonflux boundaries

where w is the distance along the outwardly directed normal. This can to good approximation be applied to all such nonflux boundaries, but not to the gas-liquid interface. Somewhat more generally, we shall define a *unit* of liquid as being any liquid mass whose principal gain or loss of solute is through the gas-liquid interface, and whose other boundaries are therefore subject to eq. 10. A nonflux boundary may arise because the liquid is in contact with a solid, or as a result of certain symmetry characteristics. An example of the latter arises in connection with the contact point liquid in glass bead columns. The ring of liquid can be divided by numerous planes of symmetry, and each plane may be regarded as a nonflux boundary. Thus a unit of liquid, as defined above, may be a very small part of the liquid pool. Most pools of the type described above are, however, sufficiently isolated to qualify as a unit. If two nearby cavities are filled in such a way that an exchange of solute takes place between them, the two together must be considered as a unit.

At this point it is necessary to consider the application of eq. 4 to the liquid. If ϕ_i is defined by

$$\phi_i = \epsilon_i \frac{D_1}{R\bar{v} \partial \ln c^*/\partial z} \quad (11)$$

Then, since $\bar{u} = R\bar{v}$ and $\partial \ln c^*/\partial z = \partial \ln m_1^*/\partial z$, eq. 4 becomes

$$\nabla^2 \phi_i = -1 \quad (12)$$

The boundary conditions applying to ϕ_i (where the subscript now refers to unit i) are $\phi_i = \text{constant}$ at the gas-liquid interface (due to the constancy of solute concentration at this interface) and $\partial \phi_i/\partial w = 0$ at all nonflux boundaries. The solution to this equation can be written in the form

$$\phi_i = \theta_i + g_i \quad (13)$$

where g_i is the constant value assumed by ϕ_i at the

gas-liquid interface. The function θ_i is thus obtained as a solution to the equation

$$\nabla^2 \theta_i = -1 \quad (14)$$

subject to the boundary conditions $\theta_i = 0$ at the gas-liquid interface and $\partial \theta_i/\partial w = 0$ at all nonflux boundaries. The solution of this boundary value problem for liquid unit i is a unique function of the geometry of unit i and is thus independent of the configuration of any liquid outside the unit.

The constant g_i , of considerable importance in this treatment, is obtained by combining the definition of this constant (following eq. 13) and eq. 11. Thus $g_i = \epsilon_i(\text{interface})D_1/R\bar{v}(\partial \ln c^*/\partial z)$. The value of $\epsilon_i(\text{interface})$ is, however, simply equal to the constant nonequilibrium term, ϵ_g , of the surrounding gas. Thus

$$g_i = \epsilon_g D_1/R\bar{v}(\partial \ln c^*/\partial z) \quad (15)$$

The expression on the right is constant within a given cross section so that $g_i = \text{the same constant for each of the units of liquid.}$

The average departure from equilibrium in the liquid phase may now be considered with use of the expression

$$\bar{\epsilon}_1 = \Sigma \int \epsilon_i dV_i / \Sigma \int dV_i \quad (16)$$

where the integration extends over the total volume, V_i , of unit i , and the summation extends over all units. By using eq. 13 and 11 this expression for $\bar{\epsilon}_1$ can be formulated in terms of θ_i and g_i

$$\bar{\epsilon}_1 = \frac{R\bar{v}}{D_1} \frac{\partial \ln c^*}{\partial z} \left[\frac{\Sigma \int \theta_i dV_i}{\Sigma dV_i} + g_i \right] \quad (17)$$

The first term in the brackets may be written as $\Sigma(V_i/V_1)\bar{\theta}_i$, where V_1 is the total liquid volume under consideration and $\bar{\theta}_i$ the average value of θ in pore i . This with eq. 15 makes it possible to write

$$\bar{\epsilon}_1 = \epsilon_g + \frac{R\bar{v}}{D_1} \frac{\partial \ln c^*}{\partial z} \Sigma \left(\frac{V_i}{V_1} \right) \bar{\theta}_i \quad (18)$$

The combination of this equation with eq. 9 gives the following expression for ϵ_g

$$\epsilon_g = -(1 - R) \frac{R\bar{v}}{D_1} \frac{\partial \ln c^*}{\partial z} \Sigma \frac{V_i}{V_1} \bar{\theta}_i \quad (19)$$

With this substituted into eq. 7 and 8 we have the dispersivity coefficient

$$\mathfrak{D} = \frac{R^2(1 - R)\bar{v}^2}{D_1} \Sigma \left(\frac{V_i}{V_1} \right) \bar{\theta}_i \quad (20)$$

and the plate height

$$H = \frac{2R(1 - R)\bar{v}}{D_1} \Sigma \left(\frac{V_i}{V_1} \right) \bar{\theta}_i \quad (21)$$

These expressions indicate that the dispersion may be written as a sum of terms, each a function (aside from the total amount of liquid present) solely of the configuration of a given unit of liquid (the dependence of θ_i and $\bar{\theta}_i$ on the configuration of unit i , only, makes this point explicit). This is the desired combination law for the liquid phase contribution to dispersion. Several consequences of this law will be discussed below.

If all units of liquid were identical with unit i the plate height could be written as

$$H_i = 2R(1 - R)\bar{\theta}_i/D_1 \quad (22)$$

The combination law, eq. 21, thus acquires the form

$$H = \Sigma(V_i/V_1)H_i \quad (23)$$

showing explicitly the way in which H is composed of individual plate height contributions.

The nature of the $\bar{\theta}_i$ terms, and the important role they play, can best be shown by writing all distances in dimensionless form. Each unit of liquid will be characterized by a distance d_i (in practice this will generally be the maximum depth of the liquid pool). Dimensionless coordinates will be defined by $x' = x/d_i$, etc. In addition a dimensionless θ_i , θ_i' , will be defined as $\theta_i' = \theta_i/d_i^2$. The equation and boundary conditions for θ_i' will be the same as for θ_i , *i.e.*

$$\nabla'^2\theta_i' = -1 \quad (24)$$

where $\theta_i' = 0$ at the gas-liquid interface, and $\partial\theta_i'/\partial w' = 0$ at all nonflux boundaries. In terms of these dimensionless parameters, the combination law, eq. 21, becomes

$$H = \frac{2R(1 - R)\bar{v}}{D_1} \Sigma \bar{\theta}_i' \left(\frac{V_i}{V_1}\right) d_i^2 \quad (25)$$

Variations in $\bar{\theta}_i'$ will be rather minor compared to variations in d_i^2 . Assuming reasonable values, the latter may vary by a factor of 10^6 from unit to unit, and on account of this variation the contributions of some units of liquid may be immediately discarded.¹ Such is generally the case for the thin film of liquid covering flat or convex solid surfaces.

Equation 25 can be written in a form assumed earlier³ on intuitive grounds

$$H = \Sigma q_i \left(\frac{V_i}{V_1}\right) R(1 - R) \frac{d_i^{2\bar{v}}}{D_1} \quad (26)$$

where q_i , equal to $2\bar{\theta}_i'$, is known as the configuration factor for unit i . From earlier work⁹ it is known that $q_i = 2/3$ for a uniform film, $1/4$ for cylindrical units, $2/15$ for spherical units, and $1/12$ for the ring of liquid surrounding the contact point between two spherical

beads. It is doubtful if the variation in q is ever much larger than that shown here.

Several special cases of the combination law shown by eq. 26 have been derived earlier. In one instance⁷ the units of liquid were limited to the type obtained by the filling of pores of uniform cross section. In another case¹ the cross sectional area of the pores was assumed to increase with some power, n , of the liquid depth. The treatment given here, however, is the first general treatment of this problem, and the only one in which an explicit solution for ϵ_i was not required before proceeding to the formulation of H .

Conclusions

The treatment given above is subject to relatively few restrictive assumptions, and those which are necessary are quite well founded. The assumption that the gas and the liquid diffusion contributions to the plate height are additive is undoubtedly true in view of the large diffusivity of gases. If this is the case, the gas diffusion coefficient may be taken as infinity (due to the nature of the mathematical expression for additivity⁷), and the assumption that all parts of the gas-liquid interface are bathed at equal concentrations is a necessary consequence. The assumption, ϵ_i (interface) = ϵ_g , depends on the requirement that interfacial resistance be small. It has been shown that the accommodation coefficient must be of order 10^{-4} or less for a significant contribution here.¹⁰ Recent evidence^{11,12} shows that such small values are unlikely; for most systems the value is close to unity.

The general plate height expressions derived above obey the mathematical requirement for the additivity of separate liquid units. If a number of rate or diffusion processes are occurring within a column, the plate height is a function of each; *i.e.*, $H \equiv H(D_1, D_2, \dots, k_1, k_2, \dots)$, where the D 's are diffusion coefficients and the k 's are rate constants. Additivity is expressed by⁷

$$H(D_1, D_2, \dots, k_1, k_2, \dots) = H(D_1, \infty) + H(D_2, \infty) + H(k_1, \infty) \dots \text{etc.} \quad (27)$$

In the case under consideration the D values may be assumed to be the diffusivities of the respective units. From eq. 26

$$H(D_i, \infty) = q_i(V_i/V_1)R(1 - R)d_i^{2\bar{v}}/D_1 \quad (28)$$

(9) J. C. Giddings, *Anal. Chem.*, **33**, 962 (1961).

(10) M. A. Khan, Fourth Symposium on Gas Chromatography, Hamburg, 1962.

(11) S. H. Chiang and H. L. Toor, *A.I.Ch.E. J.*, **5**, 165 (1959).

(12) F. Goodridge and D. J. Bricknell, *Trans. Inst. Chem. Engrs.* (London), **40**, 54 (1962)

Application of the additivity expression, eq. 27, yields back eq. 26, a fact which demonstrates the applicability of the additive condition.

As indicated earlier, the combination law derived in this paper reduces the zone dispersion problem to the relatively simple one of treating small isolated units of liquid. The basic equation of the unit, eq. 14, can be solved (numerically if necessary) with little real difficulty, providing an assumption can be made for the configuration of the liquid in the unit. One of the major remaining problems in gas chromatography is that of elucidating the configuration of such units. Some progress has been made in this direction,¹ but the greatest advances have been made with very simple

systems, such as columns packed with glass beads.¹ It has been possible to predict dispersion coefficients in such columns with roughly 20–50% error using independent data.¹³ This is a major advancement over any previous treatment and provides strong evidence for the correctness of the nonequilibrium theory employed here.

Acknowledgment. This work was supported by the Atomic Energy Commission under Contract AT-(11-)-748.

- (13) J. C. Giddings, K. L. Mallik, and M. Eikelburger, *Anal. Chem.*, **34**, 1026 (1962)

The Temperature Dependence of the Flash Photolysis of Diethyl Ketone¹

by L. C. Fischer and Gilbert J. Mains

Department of Chemistry, Carnegie Institute of Technology, Pittsburgh 13, Pennsylvania (Received July 27, 1963)

The flash photolysis of diethyl ketone yielded carbon monoxide, butane, ethylene, ethane, propane, and hydrogen as gaseous products of decreasing importance. Propionaldehyde and methyl ethyl ketone were found among the liquid products. The observation of diethyl ketone-*d*₆ among the flash photolysis products of a mixture of diethyl ketone and diethyl ketone-*d*₁₀ confirmed the importance of the propionyl radical at 24° and its temperature dependence. While most of the products were explainable in terms of the low intensity photolysis mechanism, it was necessary to postulate reactions of vibrationally "hot" species to explain the production of hydrogen, propane, and methyl ethyl ketone and the large yield of ethylene. Tentative values of 0.4 ± 0.1 and 0.15 ± 0.1 were assigned to the disproportion-recombination ratio of ethyl and propionyl radicals into ethylene and propionaldehyde and ethane and methyl ketone, respectively.

Introduction

The vapor phase photolysis of diethyl ketone has been studied extensively at low intensities over a wide range of temperatures; a review of the primary processes in the low intensity photolysis of simple ketones has been published.² However, the photolysis of diethyl ketone at very high light intensities such as that produced by flash photolysis has been the subject of only one experiment,³ and a study of the tempera-

ture dependence of flash photolysis products has not been reported for any compound.

At low intensities, the mechanism for the photo-

- (1) Based upon data submitted by L. C. Fischer in partial fulfillment of the requirements for the degree of Doctor of Philosophy, Carnegie Institute of Technology.
 (2) W. A. Noyes, Jr., G. B. Porter, and J. E. Jolley, *Chem. Rev.*, **56**, 49 (1956).
 (3) D. P. Dingley and J. G. Calvert, *J. Am. Chem. Soc.*, **85**, 856 (1963).

chemical decomposition of this ketone is well understood above 100°. Below this temperature, complicating factors, attributed to the possible stability of C₂H₅CO produced in the primary process, have been recognized both in the liquid^{8,9} and vapor phase studies.^{5-7, 10-13}

In order to gain more information about the primary photochemical steps, the present work was undertaken using a high intensity flash source. At high intensity, second-order radical reactions are expected to predominate over first-order radical reactions and thereby simplify interpretation of the reaction products.

The temperature dependence of the flash photolysis products was investigated over the temperature range 24 to 250°. Also, in an effort to establish the identity of the reacting species, mixtures of diethyl ketone and diethyl ketone-*d*₁₀ were subjected to flash photolysis. In order to gain additional information regarding the reactions of free radicals in this system, some experiments were carried out in the presence of oxygen and nitric oxide as free radical scavengers. Finally, the effect of an inert gas, nitrogen, was also studied.

Experimental

Materials. Matheson diethyl ketone (b.p. 100–102°) was purified by repeated extraction with a saturated sodium bisulfite solution,^{14,15} dried over calcium sulfate, and subjected to fractional distillation. The middle fraction of the distillate exhibited a constant boiling point at 100.2° (uncor.) and was collected for the experiments reported here. The purified diethyl ketone was then thoroughly degassed at -78° using a repeated freeze, pump, and thaw cycle. The air-free sample was then distilled *in vacuo* onto pre-ignited calcium sulfate in a storage ampoule, frozen at -78°, sealed off, and kept in a dark place until used. An aliquot of the diethyl ketone was subjected to gas-liquid chromatography analysis and showed less than 0.05% methyl ketones and ethyl propyl ketone impurities. The mass spectra of this ketone compared very favorably with previously reported patterns¹⁶ except the present sample had lower pattern factors at *m/e* 43 and 72, indicating the absence or very low concentration of the methyl ketones.

Diethyl ketone-*d*₁₀, obtained from Merck, Sharp and Dohme of Canada, was found to be 95.0% diethyl ketone-*d*₁₀ and 5.0% diethyl ketone-*d*₉ by mass spectrometric analysis. No parent peak for diethyl ketone-*d*₈ (*m/e* 91) was found on the mass spectra, indicating that essentially none of this compound was present. Therefore, this sample of diethyl ketone-*d*₁₀ was not further purified.

Matheson Company oxygen, nitric oxide, and nitrogen were used without further purification.

Apparatus. The flash photolysis apparatus consists of a General Electric FT 524 xenon-filled flash lamp which was connected across a capacitance bank of 64.5 μf. The condensers were charged by a high voltage d.c. power supply to the desired voltage and discharged through the lamp by an externally supplied trigger pulse. The discharge voltage was calculated from the current passing through a microammeter in series with a 40-megohm resistance connected across the capacitance bank.

The flash lamp consisted of 8-mm. quartz tubing helically wound into a coil 60 mm. long and 30 mm. in diameter. The radiant energy and irradiance of this lamp have been described previously¹⁷; the lamp was used without a reflector in these studies.

A spectrum of the flash lamp output was obtained by the use of a prism spectrograph. The results showed that the spectral output of the lamp in the ultraviolet region begins at 2100 Å. and extends to at least 4500 Å., the limit of sensitivity for the spectrograph film. The output consists of a continuum upon which are superimposed some of the xenon lines.

Physical actinometry was performed to determine the variation of relative lamp intensity with discharge voltage. The relative intensities were determined from the photographs of the oscilloscope tracings, using a 931 Å. photocell connected through a cathode follower to a Tektronix 515A oscilloscope. The best working range for the lamp was found to be 3800 to 5000 v., most of this work being done at 4000 v., for which this particular lamp has been designed. The lifetime of the discharge was 150 μsec. at this voltage.

- (4) L. M. Dorfman and Z. D. Sheldon, *J. Chem. Phys.*, **17**, 511 (1949).
- (5) M. H. J. Wijnen and E. W. R. Steacie, *Can. J. Chem.*, **29**, 1092 (1951).
- (6) K. O. Kutschke, M. H. J. Wijnen, and E. W. R. Steacie, *J. Am. Chem. Soc.*, **74**, 714 (1952).
- (7) R. K. Brinton and E. W. R. Steacie, *Can. J. Chem.*, **33**, 1840 (1955).
- (8) R. D. Doepker and G. J. Mains, *J. Phys. Chem.*, **66**, 690 (1962).
- (9) P. Ausloos, *Can. J. Chem.*, **36**, 400 (1958).
- (10) A. Shepp and K. O. Kutschke, *J. Chem. Phys.*, **26**, 1020 (1957).
- (11) D. G. L. James and E. W. R. Steacie, *Proc. Roy. Soc. (London)*, **A244**, 289 (1958).
- (12) J. E. Jolley, *J. Am. Chem. Soc.*, **79**, 1537 (1957).
- (13) C. A. Heller and A. S. Gordon, *J. Chem. Phys.*, **36**, 2648 (1962).
- (14) H. W. Huyser and A. Schaafsma, *Chem. Abstr.*, **37**, 139 (1943).
- (15) A. W. Stewart, *J. Chem. Soc.*, **87**, 185 (1905).
- (16) A. G. Sharkey, Jr., J. L. Shultz, and R. A. Friedel, *Anal. Chem.*, **28**, 934 (1956).
- (17) N. A. Kuebler and L. S. Nelson, *J. Opt. Soc. Am.*, **51**, 1411 (1961).

The energy expended per flash at this voltage is 516 j., of which about 5% is obtained as light output in the ultraviolet.

Chemical actinometry was performed to estimate the light intensity per flash. Using uranyl oxalate actinometry¹⁸ and an average quantum yield of 0.57 for decomposition at the wave lengths transmitted by quartz, it was found that the light absorbed by the actinometer at a discharge of 4000 v. through the lamp was about 8.82×10^{18} quanta/flash. Thus, the average absorbed intensity is calculated to be 3.9×10^{21} quanta/cc./sec. (The reaction vessels were filled with 15.0 ml. of uranyl oxalate solution and exposed to 15 flashes; the oxalate decomposition was determined by titration with standard permanganate.)

The reaction vessels used for the high temperature runs were quartz provided with quartz-Pyrex graded seals and Pyrex break-offs as close as possible to the graded seals. The typical reaction vessel was 13 mm. in diameter and 16 cm. long. Provisions were made for loading the reaction vessels through pull-off connections to the vacuum line. The volume of a reaction vessel was about 14 cc.

The reaction vessels used for flash photolyses at room temperature consisted of 13-mm. quartz tubing about 15 cm. long provided with an outer quartz jacket. These reaction vessels were closed by means of vacuum stopcocks. The average volume of a reaction vessel was ca. 40 cc.

Constant temperature was maintained in the high temperature studies by using a heated-air flow tube placed through the coil of the lamp. The flow tube itself was of quartz in the lamp region. The air was filtered and heated prior to entering the lamp area. Heating was achieved by passing a.c. current through coiled (ca. 20 coils/in.) Nichrome V wire wound around the air flow tube for 42.5 in. ahead of the lamp area. Using a small heater similar to this just beyond the flash lamp, it was possible to reduce the temperature gradient across the reaction vessel to within $\pm 0.1^\circ$ at low temperatures and to within $\pm 3.0^\circ$ at the highest temperatures. The temperature of the reaction vessel was measured by a copper-constantan thermocouple placed alongside the reaction vessel between it and the wall of the heated-air flow tube.

Procedure. The usual high vacuum techniques were employed in preparing all samples. Pressures were measured by means of an oil multiplying manometer except in the experiments involving the addition of high pressures of nitrogen when a mechanical pressure gage was used. For all experiments above ambient temperature the reaction vessels were sealed off while the diethyl ketone was frozen at -196° . After

photolysis the gases were separated at -196 and -78° except in the cases where the C_2 hydrocarbon fraction was of particular interest, such as the mixed deuterated experiments or the experiments in the presence of O_2 and NO . In these cases the noncondensables at -160° were separated and their PV product measured. Because residue fractions from the addition of oxygen were not of particular interest, they were not analyzed.

All samples were analyzed using a Consolidated Electro Dynamics Model 21-103C mass spectrometer, except in a few later experiments as noted, where the -78° fraction was analyzed using a flame ionization detector and a 12-ft. gas-liquid chromatography column containing Apiezon L as the liquid phase. The C_2 hydrocarbon fraction from the gas chromatography column was subsequently collected in a trap cooled in liquid N_2 and analyzed using the mass spectrometer.

Results

All the experiments reported here have been carried out using a 4000-v. discharge through the flash lamp. Mass spectrometric and gas-liquid chromatographic analyses showed the photolysis products to be carbon monoxide, butane, ethylene, ethane, propane, propionaldehyde, methyl ethyl ketone, and hydrogen. Trace amounts of propylene and methane were detected but could not be determined quantitatively with any confidence. Over the temperature range studied, the yield of hydrogen was less than 3% of the carbon monoxide yield. Propionaldehyde was detected among the photolysis products at lower temperatures by mass spectrometry; however, the quantitative analysis was complicated by the relatively large amount of butane present. Propionaldehyde was not detected among the photolysis products at higher temperatures, and its quantitative analysis at these higher temperatures was not pursued. Six samples of diethyl ketone were each subjected to twelve flashes at $2 \pm 0.5^\circ$, collected, and the residue analyzed using the gas chromatograph to make a more quantitative determination of the propionaldehyde and methyl ethyl ketone. Effluent gases producing recorder peaks other than those expected were collected in a trap cooled in liquid N_2 and subsequently analyzed by mass spectrometry. These analyses provided definite evidence for the presence of propionaldehyde and methyl ethyl ketone among the photolysis products. The chromatographic analysis also showed a peak with retention time which might be expected for ethyl propyl ketone. The ratio of propionaldehyde to CO was 0.10 and the ratio

(18) W. G. Leighton and G. S. Forbes, *J. Am. Chem. Soc.*, 52, 3139 (1930).

of methyl ethyl ketone to CO was 0.0042. The per cent decomposition of diethyl ketone (as measured by the yield of carbon monoxide) was found to be a linear function of the number of flashes to which the sample was exposed. These data are given in Table I. The pressure of diethyl ketone was 1.9 ± 0.1 cm. unless otherwise stated. It should be noted that the ratios of hydrocarbon products to *n*-butane did not change drastically with the number of flashes. The average ratio of carbon monoxide to butane was 1.06. In Table I are also reported the values for the material balance, defined as $[0.5(C_2H_6 + C_2H_4) + 0.75(C_3H_8 + C_4H_{10})]/CO$.

Table I: Dependence of Hydrocarbon Ratios on the Per Cent Decomposition in the Flash Photolysis of Diethyl Ketone at 24° and 1.9 cm. Pressure

% de-comp. ^a	CO/ C ₄ H ₁₀	C ₂ H ₆ / C ₄ H ₁₀	C ₂ H ₄ / C ₄ H ₁₀	C ₃ H ₈ / C ₄ H ₁₀	C ₂ H ₆ / C ₂ H ₄	Material balance ^b	Method of analysis
1.88	1.17	0.17	0.33	0.11	0.53	1.14	Mass spec.
2.23	n.d. ^c	0.16	0.28	0.13	0.55	n.d. ^c	Gas chrom. and mass spec.
2.52	n.d. ^c	0.15	0.24	0.12	0.61	n.d. ^c	Gas chrom. and mass spec.
3.66	1.07	0.16	0.29	0.09	0.54	1.17	Mass spec.
5.32	1.02	0.15	0.25	0.08	0.60	1.23	Mass spec.
8.69	1.05	0.15	0.28	0.10	0.55	1.22	Mass spec.
11.64	1.06	0.16	0.28	0.10	0.55	1.24	Mass spec.

^a Per cent decomposition calculated on the basis of the carbon monoxide yield. ^b Defined as $[0.5(C_2H_6 + C_2H_4) + 0.75(C_3H_8 + C_4H_{10})]/(CO)$. ^c Value not determined.

The effect of diethyl ketone pressure on the product ratios and material balance was also investigated at 24° over the pressure range 0.59 to 2.70 cm. The product ratios did not vary with initial diethyl ketone pressure. The ethane to butane ratio, expected to increase with pressure if ethyl radical abstraction reactions were important, was found to be 0.14 ± 0.02 over the entire pressure range.

Several experiments were performed to establish the influence of temperature on the product distribution in the flash photolysis of diethyl ketone. Each sample was subjected to twelve flashes; the per cent decomposition at 24° (room temperature) was 5.2% and the per cent decomposition increased linearly with temperature to 11.3% at 252°, the highest temperature studied. Experiments were conducted for the same period of time in the heated-air flow without photolysis to ascertain whether any pyrolysis occurred. No

pyrolysis was observed at 252°. The actual yields of the products for the experiments are given in Table II. Several experiments were conducted at 24° using a spectral filter¹⁹; the filter is a single layer of du Pont cellophane, Type 150PD, wrapped around the reaction vessel. The result of one of these is included in Table II. Actinometry indicated that the intensity

Table II: Temperature Dependence of the Flash Photolysis Products of Diethyl Ketone at 1.9 cm. Pressure Subjected to Twelve Flashes

Temp., °C.	Yields, μmoles						Comments
	CO	C ₄ H ₁₀	C ₃ H ₈	C ₂ H ₆	C ₃ H ₆	H ₂	
24	0.88	0.84	0.17	0.09	0.07	0.03	
24	0.38	0.35	0.09	0.05	0.03	0.01	Cellophane filter
24	n.d. ^a	0.01	0.14	n.d. ^a	42 mm. O ₂ added
24	n.d. ^a	..	0.15	n.d. ^a	40 mm. NO added
37	n.d. ^a	0.01	0.14	0.01	..	n.d. ^a	39 mm. O ₂ added
54	0.91	0.85	0.17	0.09	0.07	0.03	
54	0.93	0.88	0.17	0.10	0.07	0.03	
64	n.d. ^a	..	0.13	n.d. ^a	38 mm. NO added
103	1.08	0.93	0.14	0.10	0.09	0.03	
103	n.d. ^a	0.01	0.38	n.d. ^a	37 mm. NO added
115	n.d. ^a	0.01	0.18	n.d. ^a	40 mm. O ₂ added
154	1.60	1.35	0.21	0.15	0.10	0.04	
164	n.d. ^a	..	0.26	0.01	..	n.d. ^a	38 mm. O ₂ added
165	n.d. ^a	..	0.66	n.d. ^a	37 mm. NO added
196	n.d. ^a	0.02	0.40	0.05	..	n.d. ^a	39 mm. O ₂ added
205	1.67	1.36	0.21	0.13	0.13	0.04	
207	1.32	1.08	0.17	0.10	0.11	0.03	
228	n.d. ^a	0.04	0.47	n.d. ^a	40 mm. O ₂ added
252	1.92	1.60	0.21	0.15	0.12	0.04	

^a Value not determined.

was decreased by at least 25% when the filter was used. Because the filter changed transmission characteristics, it was not used at the higher temperatures.

The data in Table II show some scatter when plotted on a yield vs. temperature graph, which can be reduced to within 2% when corrected for differences in transmission characteristics of the three reaction vessels. These differences were found by chemical actinometry: In order to eliminate this latter effect, the ratios of the yield of hydrocarbon product to the yield of carbon monoxide are shown in Fig. 1. It should be noted that the ratio of ethane to ethylene plotted in Fig. 1 is not 1.0 as anticipated for sole production of these compounds by disproportionation of ethyl radicals; rather it increases in the region from 24 to 120°. The change of material balance with temperature is likewise shown in Fig. 1.

Several experiments were performed with N₂ gas present at 24°. The yields of butane and propane were found to decrease very slightly at higher N₂ pressure, whereas ethane and ethylene yields increased

(19) N. Slagg and R. A. Marcus, *J. Chem. Phys.*, **34**, 1013 (1961).

Table III: Product Yields from the Flash Photolysis of Mixtures of Diethyl Ketone and Diethyl Ketone- d_{10} at Various Temperatures and 1.9 cm. Pressure

Temp., °C.	dEK/dEK- d_{10} initially	% decomp.	CO yield ^a	dEK- d_8 /CO	C ₂ D ₆ /CO	C ₂ D ₈ H/CO	C ₂ H ₆ D/CO	C ₃ H ₈ /CO	C ₂ D ₄ /CO	C ₂ H ₄ /CO	C ₄ D ₁₀ /CO	C ₄ D ₈ H ₂ /CO	C ₄ H ₁₀ /CO
24	0.9	3.3	1.22	n.d.	0.04	0.04	0.07	0.30	0.16	0.14	0.21	0.58	0.44
24 ^b	1.3	1.9	0.73	0.12	0.03	0.07	0.04	0.04	0.19	0.16	0.30	0.48	0.23
26 ^c	0.9	5.7	4.49	0.12	0.04	0.06	0.04	0.02	0.10	0.15	0.26	0.48	0.21
224	0.9	27	8.36	0.02	0.03	0.05	0.04	0.02	0.08	0.11	0.24	0.44	0.18
249	1.0	6.7	1.07	0.02	0.02	0.04	0.02	0.02	0.08	0.06	0.16	0.38	0.20

^a Yield is in μ moles. ^b The reaction vessel was wrapped with one layer of cellophane, Type PD-150. ^c The small high-temperature reaction vessel was used in this experiment.

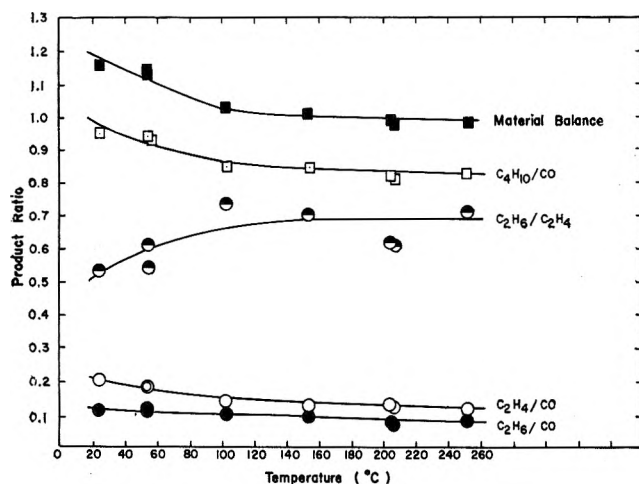


Figure 1. The temperature dependence of the flash photolysis product ratios from diethyl ketone at 1.9 cm. pressure (measured at 24°) subjected to twelve flashes.

very slightly. Although CO was not determined in all experiments, its yield appeared to be relatively constant. Since no drastic shift in product yield was observed, it seems reasonable that local heating effects were not important. Indeed, the maximum calculated temperature rise based on the energy absorbed in the system was 15° in the absence of N₂.

Six experiments were performed at different temperatures with oxygen present. The results of these scavenging studies are included in Table II. The formation of hydrocarbons was suppressed almost completely with the outstanding exception of ethylene. This observation has been confirmed by many previous experimenters in the low intensity photolysis and recently by Dingley and Calvert³ and Cerfontain and Kutschke²⁰ in the flash and high intensity photolysis of azoethane with oxygen. Five experiments with nitric oxide in the system, over a range of temperature similar to the oxygen studies, were also carried out. Results

similar to that observed for the oxygen and diethyl ketone flash photolysis were found. Figure 2 shows the variation of ethylene with temperature formed in the systems when oxygen or nitric oxide was added to the diethyl ketone, and graphical comparison was made with the variation of ethylene yield with temperature when these additives are absent. The yields of the oxygenated and nitric oxide products were not measured.

In Table III are listed the ratios of products to carbon monoxide from the flash photolysis of diethyl ketone-diethyl ketone- d_{10} mixtures. Of primary inter-

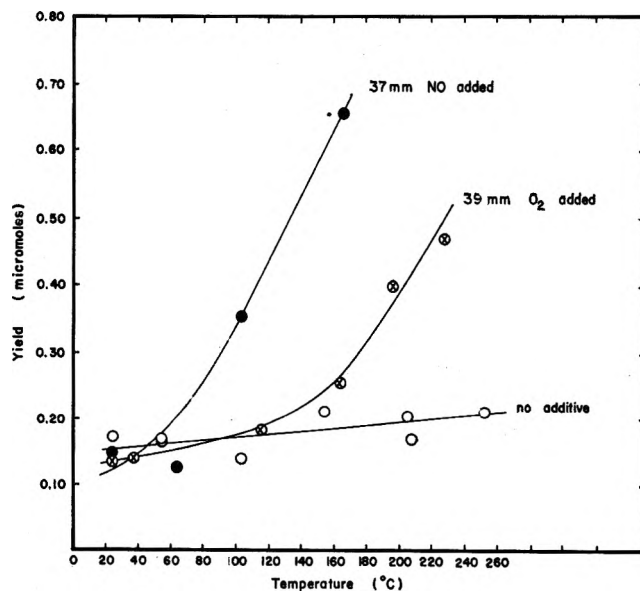


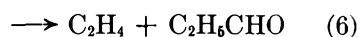
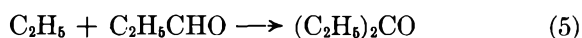
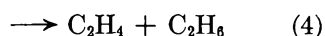
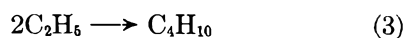
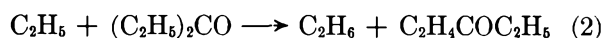
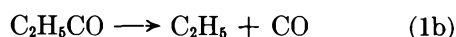
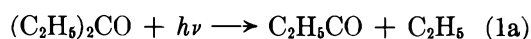
Figure 2. The variation of the ethylene yield with temperature in the presence and absence of oxygen and nitric oxide for diethyl ketone at 1.9 cm. pressure (measured at 24°) subjected to twelve flashes.

(20) H. Cerfontain and K. O. Kutschke, *J. Am. Chem. Soc.*, **84**, 4017 (1962).

est are the ratios of diethyl ketone- d_6 to carbon monoxide. The evidence for the formation of diethyl ketone- d_6 comes from the m/e 91 peak in the mass spectra of the residue fraction after flash photolysis. The parent peak for $C_2H_5COC_2D_5$ does not occur in the spectra of the two pure compounds or in the spectra of their mixture. Also of particular interest is the isotopic composition of the ethanes and ethylenes. The absence of significant yields of CH_3CD_3 and CH_2CD_2 is especially noteworthy.

Discussion

The mechanism usually postulated to account for the major photolysis products at low intensity is



At temperatures over 100° reaction 1b reduces the steady-state concentration of the propionyl radical sufficiently to allow reactions 5, 6, and 7 to be neglected. These latter reactions have been proposed to be important in the low intensity photolysis of diethyl ketone in the liquid^{8,9} and gas⁹ phase.

Although this mechanism does not include reactions of "hot" radicals, their participation in alkyl ketone photolysis reactions seems firmly established, especially at shorter wave length.²¹ A careful investigation of the low intensity photolysis in the presence of oxygen led Jolley¹² to conclude that a fraction of the propionyl radicals, 9%, independent of wave length in the range 2537 to 3130 Å., are "hot" species which inevitably dissociate. The decrease in the yield of butane at high nitrogen pressures (noted earlier) accompanied by an increase in the ethane and ethylene yields are in qualitative accord with this interpretation, provided it is assumed that the nitrogen can remove the excess energy from the "hot" propionyl radicals at high pressures. In a more recent low intensity study of the photolysis of diethyl ketone-biacetyl mixtures, Weir²² concluded that at 3130 Å. the triplet excited state of diethyl ketone was an important electronically excited state. A measure of its importance was found in the reduction of the quantum yields of carbon monoxide, C_2 , and C_4

hydrocarbon formation from the diethyl ketone photolysis to a limiting value which was at least 37% lower in the presence of biacetyl than in its absence. Weir's data at 3130 Å. point to an increased dissociation at higher temperatures, leading to a shorter lifetime. It was concluded that the singlet state of diethyl ketone was a more important electronically excited state and that the dissociation of this state into "hot" propionyl radicals and ethyl radicals increases at higher temperatures.

The observation of relatively large yields of propane and hydrogen among the flash photolysis products in Table II cannot be reconciled with reactions 1 to 7. Furthermore, these reactions predict the ratio of ethylene to ethane to be unity at temperatures above 100° , whereas the data in Table II show ethylene to be the major C_2 flash photolysis product over the entire temperature range 24 to 250° . In order to establish that this unusual product distribution was not arising from an undetected impurity in the diethyl ketone, several low intensity photolyses were conducted at 24° and 2.0 cm. diethyl ketone pressure using a BH6 high pressure mercury lamp. Neither propane nor hydrogen could be detected among the products, and in agreement with previous low intensity studies the ethylene to ethane ratio was 0.9. It seems reasonable to conclude that the formation of propane, hydrogen, and "excess" ethylene, *i.e.*, the ethylene in excess of the ethane produced, is due to reactions arising either as a result of the high light flux or as a consequence of the adsorption of light of short wave length. That these flash photolysis conditions are not leading to pyrolysis reactions is indicated by the failure to eliminate the unusual distribution by either excesses of nitrogen as an inert gas or alteration of the quartz surface by the use of several reaction vessels.

Because of the high light fluxes involved in flash photolysis, the reactions of electronic excited states with each other and with free radicals must be considered, especially if the excited state is long-lived. Rollefson, Roebber, and Pimentel²³ and Marcus and Shilman²⁴ have found it necessary to consider the long-lived triplet state of acetone in their flash photolysis studies. Weir's conclusions make it necessary to consider the triplet state in the flash photolysis of diethyl ketone also. Weir's data at 3130 Å. indicate

(21) P. Ausloos and E. Murad, *J. Am. Chem. Soc.*, **80**, 5929 (1958).

(22) D. S. Weir, *ibid.*, **83**, 2629 (1961).

(23) G. K. Rollefson, J. Roebber, and G. C. Pimentel, *ibid.*, **80**, 255 (1958).

(24) R. A. Marcus and A. Shilman, *Bull. soc. chim. Belges*, **71**, 653 (1962).

an increased dissociation of the triplet state of diethyl ketone at higher temperatures. Therefore, at 250° the triplet excited state, while being formed in these flash photolysis studies, probably decomposes rapidly. As a result of this rapid decomposition, the excess ethylene observed at 250° cannot be attributed to triplet-triplet or triplet-radical reactions.

At lower temperatures, especially 25°, the triplet excited state of diethyl ketone may undergo reactions because of a relatively longer lifetime. However, based upon the temperature dependency of the products and the consistency of the rate constants (to be deduced later) assuming triplet excited state dissociation rather than reaction, it is hereafter considered that the triplet excited state reactions in the flash photolysis of diethyl ketone at 25° are restricted to dissociation into ethyl and propionyl radicals, phosphorescence, and induced dissociation of the propionyl radicals, *viz.*

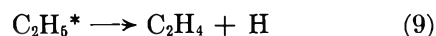


where DEK³ and DEK¹ refer to the triplet and singlet excited states, respectively, of diethyl ketone. This latter reaction is analogous to that proposed in the flash photolysis of acetone by Marcus and Shilman.²⁴

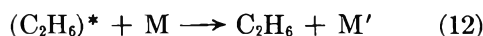
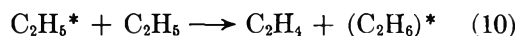
A partial explanation for the "excess" ethylene is the increased relative importance of reaction 6 under flash photolysis conditions. The observation of relatively large yields of diethyl ketone-*d*₆ reported in Table III indicates that reaction 5 is about one-fifth as probable as reaction 1b at 24°. It seems reasonable to conclude that reaction 6 is similarly important, especially in view of the large yield of propionaldehyde observed at 24°. If reaction 6 were the sole source of "excess" ethylene, one would expect the ratio of ethane to ethylene to increase to unity as the temperature was increased. At 250°, the yield of diethyl ketone-*d*₆ indicates that reaction 1b is about 25 times more probable than reaction 5, and by inference, reaction 6. Further support for this interpretation may be found by comparing the relative yield of propionaldehyde with that predicted by assuming two-thirds of the "excess" ethylene to arise *via* reaction 6. The two yields relative to CO are 0.10 ± 0.02 and 0.09 ± 0.02. One further point of interest may be deduced by assuming that the diethyl ketone-*d*₆ yield in Table III is a measure of exactly half of the total ethyl-propionyl recombination in this system. If this reasoning is correct, it is possible to assign a 0.4 ± 0.1 value for the ethyl-propionyl radical disproportionation-combination ratio, *k*₈/*k*₆, at 24°.

It is interesting to consider the source of the remaining one-third of the "excess" ethylene. Calvert and

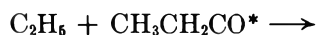
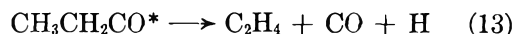
Dingley³ and Futrell and Roquette²⁵ found "excess" ethylene in the flash photolysis of azoethane where the C₂H₅N₂ analog of the propionyl radical is presumably unimportant. They postulate the decomposition of a vibrationally excited ethyl radical, reaction 9.



While reaction 9 may contribute to the remaining "excess" ethylene, it is not possible to exclude the sequence of reactions proposed by Thrush,²⁶ *viz.*

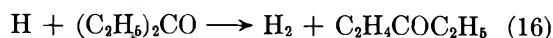


in the flash photolysis of mercury diethyl. Nor can we exclude the analogous reactions of the vibrationally "hot" propionyl radicals.



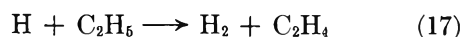
It should be noted that the formation of vibrationally excited ethyl radicals is probably a consequence of the adsorption of light in the 2500–2000 Å. region (which is unaffected by the cellophane filter) and not peculiar to flash photolysis conditions. However, the probability of these excited radicals participating in radical-radical reactions is greatly increased at high light fluxes, *i.e.*, flash photolysis conditions. It is clear that it is possible to account for the remaining "excess" ethylene by some combination of reactions 9 to 14, and in the absence of additional information it is not possible to decide which ones are actually important. Since all of these mechanisms predict the observed formation of only C₂H₄ and C₂D₄ in the isotopic experiments of Table III, no decision can be made on this basis. It seems appropriate to leave this question for future investigations rather than to speculate.

The observation of propane, methyl ethyl ketone, and hydrogen among the flash photolysis products merits consideration. Since these products are completely eliminated in the presence of oxygen and nitric oxide, it is reasonable to assume their precursors are free radicals. Reactions such as

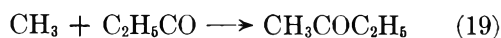
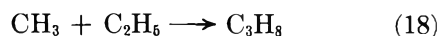


(25) B. C. Roquette and J. H. Futrell, *J. Chem. Phys.*, **37**, 378 (1962).

(26) B. A. Thrush, *Proc. Roy. Soc. (London)*, **A243**, 555 (1958).



and



are consistent with the experimental observations. It should be noted that reaction 11 is not established as the source of methyl radicals since the "atomic" cracking reaction



could also be operative under flash photolysis conditions. It should be possible to distinguish between reactions 11 and 20 as sources of methyl radicals by isotopic analysis of the propanes formed in the flash photolysis of a mixture of diethyl ketone and diethyl ketone- d_{10} . However, the presence of 5% diethyl ketone- d_8 impurity and the lack of mass spectral patterns for the deuterated propanes renders this analysis impossible at present.

It is interesting to note that the ratio of ethane to butane was found to be 0.14 ± 0.02 in all experiments performed at 24° and decreased to 0.09 ± 0.02 at 250° . Since the accepted ratio of rate constants for reaction 4 to reaction 3 is 0.12 ± 0.01 independent of temperature,¹⁹ it is reasonable to assume that reactions 3 and 4 are the principal sources of ethane and butane at 250° . This assumption is partially supported by the isotopic distribution of butanes in Table III. The ratio $(\text{C}_4\text{H}_6\text{D}_6)/(\text{C}_4\text{H}_{10})^{1/2}(\text{C}_4\text{D}_{10})^{1/2}$ is very nearly 2.0 at all temperatures as predicted by simple kinetic theory. If the "excess" ethane, *i.e.*, the ethane above that ascribed to reaction 4, at 24° is ascribed to reaction 7 and, as previously, the extent of reaction 5 is assumed to be exactly twice the yield of diethyl ketone- d_6 at 24° , a value for the ratio of the rate constants for reaction 7 to reaction 5 may be estimated. The value obtained for k_7/k_5 is 0.15 ± 0.1 . Doepker and Mains⁸ report the ratio k_7/k_5 to be 0.50 ± 0.05 in the liquid phase, a value consistent with the ratios of k_6/k_5 and k_7/k_5 deduced in this investigation.

In view of the relative importance of reactions 5, 6, and 7 in flash photolysis at 24° , a reduced quantum yield of CO production is to be expected at high intensity. The quantum yield of carbon monoxide formation estimated on the basis of the actinometry, corrected for the lower adsorption of diethyl ketone vapor, is about 0.5 in the flash photolysis experiments at 24° . At low intensities the reported quantum yield of carbon monoxide formation is 0.60 at 25° . A quantitative comparison would be meaningful only if a monochromatic flash of light were used. Because of the large un-

certainities in the flash photolysis quantum yield, it is not possible to state that the expected decrease is confirmed.

The experiments in the presence of oxygen and nitric oxide require some consideration. It may be observed in Table II that all hydrocarbon yields, except that of ethylene, are rendered negligible in the presence of oxygen and nitric oxide. Because these radical scavengers only slightly depressed the ethylene yield at 24° and because the assignment of the majority of the ethylene production to a molecular process was in conflict with low intensity studies, the effect of temperature on the "unscavenged" ethylene was investigated. The results are shown in Fig. 2. It is clear that oxygen and nitric oxide enter into temperature-dependent reactions which produce ethylene and, as a result, cannot be used to ascertain a "molecular" yield of ethylene. In addition to the observations reported here, the formation of ethylene by ethyl radicals in the presence of oxygen,^{3,27} nitric oxide,²⁷ and iodine²⁸ has been reported previously. Since the scavenger experiments in Table II were conducted only to ascertain the free radical nature of the unexpected hydrogen, propane, and "excess" ethylene products and did not involve a study of the oxidation products, further discussion of the results is unwarranted.

Conclusions

The flash photolysis of diethyl ketone gives rise to new products, hydrogen, propane, and methyl ethyl ketone, and to an unexpectedly large yield of ethylene. The photolysis product distribution has been shown to be temperature dependent, an observation which is attributed to the rapid decomposition of the propionyl radical over the temperature range 24 – 100° . It was found necessary to postulate additional mechanisms for ethylene formation at 250° in flash photolysis. Various ethylene producing mechanisms invoking vibrationally "hot" radicals are considered, but the data do not permit any definite mechanistic assignment. Experiments using diethyl ketone and diethyl ketone- d_{10} mixtures confirm the importance of the propionyl radical at 24° and are consistent with free radical formation of propane and hydrogen.

It is clear that the technique of flash photolysis does not present the gross mechanistic simplifications as hoped for by earlier investigators,^{29,30} but instead

(27) E. L. Metcalf and A. F. Trotman-Dickenson, *J. Chem. Soc.*, 3833 (1962).

(28) M. H. J. Wijnen and J. A. Guercione, *J. Chem. Phys.*, **38**, 1 (1963).

(29) M. A. Khan, R. G. W. Norrish, and G. Porter, *Proc. Roy. Soc. (London)*, **A219**, 312 (1953).

(30) G. J. Mains, G. K. Rollefson, and J. L. Roebber, *J. Phys. Chem.*, **59**, 733 (1955).

introduces many problems not encountered at lower intensities such as the possible reactions of the triplet excited electronic state of diethyl ketone with free radicals and an increased importance of "hot" radical-radical reactions resulting from short wave lengths of the flash lamp output and the high light flux. If the postulation of vibrationally "hot" ethyl radicals in this research and in the flash photolysis experiments of others^{24,26} proves correct, the failure of Thrush²⁶ to determine the ethyl radical absorption spectrum by flash photolysis is readily understood. In spite of its excellent contributions to kinetic spectroscopy, much work remains to be done before the technique of flash

photolysis can be relied upon to deduce the mechanisms of product formation.

Acknowledgment. L. C. Fischer wishes to acknowledge gratefully the financial support provided by a grant from the Air Force Office of Scientific Research. The authors wish to thank Mr. S. Wrbican for determining the mass spectra of the product mixtures and Professor M. H. J. Wijnen of Hunter College for stimulating discussions in the earlier phases of this research. Special thanks are extended to Professor W. A. Noyes, Jr., of the University of Texas for some helpful criticism of an earlier manuscript.

NOTES

Surface Temperature Measurements on Burning Solids^{1a}

by A. Greenville Whittaker^{1b} and David C. Barham

*Sandia Corporation, Albuquerque, New Mexico
(Received June 24, 1963)*

A number of investigators have attempted to measure the surface temperature of burning solid propellants of one sort or another with varying degrees of success.^{2,3} There are a number of reasons why it is difficult to obtain the surface temperature of burning solids. The most important reasons are that solids rarely burn with a smooth surface, the temperature gradients at the surface are very large, and it is difficult to determine when a measuring probe such as a fine thermocouple is really at the surface of the burning material. It is possible to show that there should be a change in slope in the temperature profile at the burning surface due to the latent heat of sublimation of the solid. However, the profiles are always very steep at this point and any change in slope due to this latent heat effect is usually completely lost. Unfortunately, there are no other phenomena that can be used in these systems to determine when the thermocouple has reached the surface of the burning material.

Temperature profile measurements on burning liquids showed that it is easy to find the surface temperature in

a liquid system.⁴ Surface tension causes the liquid to hang onto the thermocouple. This causes a "hold" or "plateau" in the temperature profile which is quite prominent and accurately indicates the surface temperature. This leads one to suspect that it might be possible to measure the surface temperature of pure solids that melt at the burning surface to produce a liquid layer that would be thick enough to act as a burning liquid. The systems chosen for this study were catalyzed ammonium nitrate, catalyzed hydrazine nitrate, and catalyzed ammonium nitrate-hydrazine nitrate eutectic. Preliminary studies of these systems using high speed photography indicated that each one of these systems did indeed form a liquid layer at the burning surface of sufficient depth that the thermocouple would probably be completely covered by liquid before it reached the burning surface.

Experimental

Reagent grade ammonium nitrate was used directly as received. The catalyst used in these studies was

- (1) (a) Work performed under the auspices of the U. S. Atomic Energy Commission; (b) Aerospace Corporation, Laboratories Division, El Segundo, Calif.
- (2) (a) R. Klein, M. Mentser, G. VonElbe, and B. Lewis, *J. Phys. Chem.*, **54**, 877 (1950); (b) A. S. Gordon, M. H. Hunt, and C. A. Heller, "Surface Temperature of Solid Propellants," N.O.T.S., T.M.-971 (1953), China Lake, Calif.
- (3) R. E. Wilfong, S. S. Penner, and F. Daniels, *J. Phys. Chem.*, **54**, 863 (1950).
- (4) D. L. Hildenbrand, A. G. Whittaker, and C. B. Euston, *ibid.*, **58**, 1130 (1954).

chromic oxide and was obtained by thermal decomposition of ammonium dichromate. The chromic oxide thus obtained was screened to various size fractions and then used directly without further treatment. Hydrazine nitrate was prepared by neutralizing a dilute solution of hydrazine with nitric acid to a pH of 3.5 at which the mononitrate exists. The hydrazine nitrate was crystallized from the solution by evaporation at reduced pressure and then dried for 24 hr. in a vacuum system at a pressure of approximately 10^{-5} mm. During these studies the humidity in the laboratory was always 15% or less; hence, no difficulties due to the hygroscopicity of the hydrazine nitrate were encountered. The ammonium nitrate-hydrazine nitrate eutectic was obtained by weighing out appropriate amounts of the components to produce a mixture whose composition was 32 mole % ammonium nitrate and 68 mole % hydrazine nitrate. This mixture has a melting point of 43° .⁵

In every case the strands consisted of cast sticks of material. The substances were heated to just slightly above their melting point and the catalyst was added immediately before casting. This minimized thermal decomposition of the substances and produced sticks containing a minimum number of gas pockets. Only the ammonium nitrate sticks needed to be inhibited. This was done by casting the sticks in glass tubes and leaving the glass in place while the material was burned.

The thermocouples consisted of platinum-platinum + 10% rhodium and they were cast into the sticks in a specially designed mold. The details of the thermocouple preparation and the two-window bomb used in this study have been described previously.⁴ Thermocouples 0.3 mil in diameter were used on the hydrazine nitrate and the hydrazine nitrate-ammonium nitrate systems. Pure ammonium nitrate required the use of 1.0-mil thermocouples. Presumably, stronger couples were required with ammonium nitrate to withstand the dimension changes which accompany the phase changes intrinsic to ammonium nitrate. In all cases the timing was done by high speed photography using a Fastax camera. Ignition of the sticks was accomplished by the "electric match" method. The match material was a stoichiometric mixture of powdered iron and ammonium perchlorate made slightly sticky with a small amount of oil.

Results and Discussion

The anticipated advantages of studying "pure" solids were largely realized. The temperature profiles obtained did indeed show a plateau when the thermocouple was dwelling in the burning surface. In fact, most of the profiles also showed a distinguishable change in slope at the melting point of the material studied.

This made it possible to get an estimate of the accuracy of the temperatures measured and also gave a rough calibration of the couples. Unfortunately, the profiles were not nearly as smooth as those obtained on liquid systems. This was partly due to the fact that the catalyst particle size was large compared to the thermocouple diameter, and that the catalyst did not blow away from the surface immediately as it emerged into the vapor phase. An actual temperature profile is shown in Fig. 1. The temperature rise in the preheat

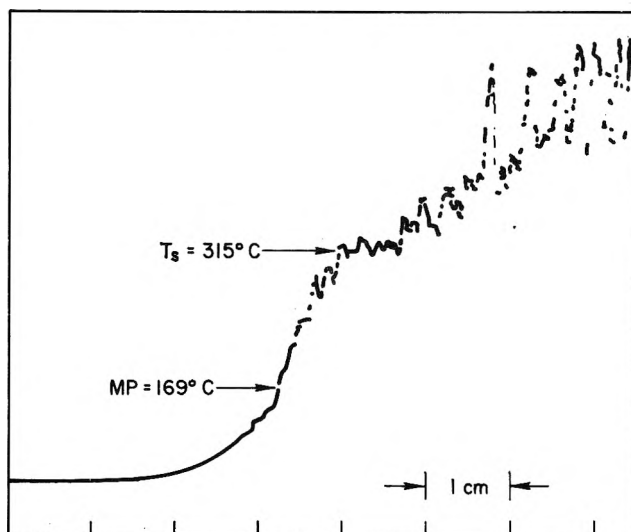


Figure 1. Sanborn recording of a temperature profile for ammonium nitrate containing 1.3% Cr_2O_3 catalyst. Combustion pressure 1000 p.s.i.a.; platinum-platinum 10% rhodium thermocouple 2 mils in diameter; chart speed, 10 cm./sec.

region is smooth and has a shape that indicates preheating by conductive heat flow. When the melting point is reached, the slope of the profile decreases significantly. As the temperature of the liquid layer increases, more thermal noise appears. Presumably, this is due to convection currents that increase in intensity as the viscosity of the melt decreases. Following this, the profile shows a large decrease in slope because the thermocouple is held at the surface of the melt by surface tension. The surface temperature is taken as the temperature corresponding to the beginning of this large change in slope. Finally, the thermocouple breaks out of the surface of the melt and suddenly enters the hot gas phase and collection of hot randomly moving catalyst particles. Presumably, the latter causes the increased thermal noise in this part of the profile. Fortunately, the dwell time in the surface was

(5) Landolt-Bornstein, "Zahlenwerte und Funktionen Aus Physik; Chemie, Astronomie, Geophysik, Technik," 6 Auflage, II Band, 3 Teil, Springer-Verlag, 1956, p. 141.

comparatively long; hence, the thermal noise could be approximately averaged out graphically so that rather accurate surface temperatures could be obtained. The results obtained on the systems studied are given in Tables I, II, and III.

Table I: Surface Temperature *vs.* Burning Rate for Ammonium Nitrate^a

Pressure, p.s.i.a.	Rate, cm./sec.	T_s	M.p.
985	0.17	297	169
1050	.20	269	...
988	.21	302	...
1500	.26	302	159
1500	.29	305	159
1750	.32	326	156
2000	.39	325	...
2000	.40	316	153
2500	.45	287	176
2500	.53	292	162
3000	.50	306	181
3000	.53	317	172
3000	.54	285	...
3500	.65	292	174
3500	.68	298	152
4000	.80	313	191
4000	.89	318	...
4800	.95	317	154
4800	1.11	298	...

^a Obtained with 1-mil diameter Pt-Pt + 10% Rh thermocouple, and containing 2.50% Cr₂O₃ catalyst 70-100 mesh. T_s , surface temperature; m.p., melting point; average T_s = 303 ± 12°; average m.p. = 166 ± 10°.

The average deviation in the surface temperature shown at the bottom of each table is very nearly equal to the temperature drop across the thermocouple due to the thermal gradient in the region of the surface. These gradients were the average measured gradients taken from the temperature profiles. The striking feature about the surface temperature shown in the above tables is that in all cases the surface temperature is constant over a rather wide range of burning rates. This is essentially the same result that was obtained for burning liquids, and may be related to the fact that each of these systems forms a liquid layer at the burning surface. Similar studies on liquids showed that surface temperature was related to pressure by the Clapeyron equation only at very low pressure. As pressure increased, the surface temperature became independent of pressure.⁶ Most liquids would show sustained combustion only in the region where surface temperature was pressure independent. Presumably the liquid

Table II: Surface Temperature *vs.* Burning Rate for Ammonium Nitrate-Hydrazine Nitrate Eutectic^a

Pressure, p.s.i.a.	Rate, cm./sec.	T_s	M.p.	Catalyst ^b
100	0.25	310	50	A
390	.35	284	44	B
385	.35	303	47	B
384	.36	291	..	B
380	.37	303	41	B
388	.38	311	42	B
396	.39	331	50	B
396	.40	299	42	B
565	.43	294	42	B
568	.45	309	..	B
565	.46	309	58	B
580	.46	306	50	B
200	.50	293	..	A
565	.54	298	50	B
310	.66	318	50	A
400	.72	281	44	A
770	.73	323	49	B
400	.73	304	39	A
600	.75	278	46	A
770	.78	320	44	B

^a Obtained with 0.3-mil diameter Pt-Pt + 10% Rh thermocouple. ^b 1.50% Cr₂O₃ catalyst; size A, 70-100 mesh; size B, less than 325 mesh. T_s , surface temperature; m.p., melting point; average T_s = 307 ± 11°; average m.p. = 39 ± 6°.

Table III: Surface Temperature *vs.* Burning Rate for Hydrazine Nitrate^a

Pressure, p.s.i.a.	Rate, cm./sec.	T_s	M.p.	Catalyst ^b
100	0.26	199	..	B
200	.27	208	80	C
200	.27	205	..	C
200	.28	216	76	C
198	.28	206	73	C
200	.32	189	80	C
205	.31	190	79	B
265	.66	194	65	B
300	.70	178	75	C
300	.75	190	..	B
280	.86	192	..	A
280	.87	183	65	A
477	.89	205	80	C
400	1.10	187	65	A
415	1.11	192	68	A
600	1.20	186	77	A

^a Obtained with 0.3-mil diameter Pt-Pt + 10% Rh thermocouple. ^b 1.50% Cr₂O₃ catalyst; size A, 70-100 mesh; size B, 200-325 mesh; size C, less than 325 mesh. T_s , surface temperature; m.p., melting point; average T_s = 195 ± 9°; average m.p. = 74 ± 5°.

(6) D. L. Hildebrand and A. G. Whittaker, *J. Phys. Chem.*, **59**, 1024 (1955).

layer at the surface of these burning solids is operating in this pressure independent regime.

For systems which do not melt at the burning surface (such as ammonium perchlorate) the situation may be different. The second outstanding feature of the results is that the surface temperatures for ammonium nitrate and the ammonium nitrate-hydrazine nitrate eutectic were the same; whereas the surface temperature for hydrazine nitrate was considerably lower than the other two. Presumably, the more easily decomposed hydrazine nitrate escaped from the surface rapidly leaving behind a surface layer consisting almost entirely of ammonium nitrate. Thus, the vaporization (or decomposition) of ammonium nitrate controlled the surface temperature at about the same value as for pure ammonium nitrate.

These results are rather sharply at variance with theoretical models which lead to the result that there is an exponential relation between surface temperature and over-all burning rate.⁷⁻⁹ Andersen, *et al.*, used an Arrhenius-type equation to describe the relationship between burning rate and surface temperature for ammonium nitrate. They made measurements on ammonium nitrate by their "hot plate method" and obtained values for the pre-exponential factor and the activation energy. Their activation energy was reported as 7100 cal./mole and the pre-exponential factor as 1.2×10^2 cm./sec. If the surface temperature for ammonium nitrate is taken as 303° at a burning rate of 0.167 cm./sec. (as shown in the first entry in Table I), one can calculate, using the activation energy and pre-exponential factor given above, the surface temperature which should correspond to the highest burning rate of 1.11 cm./sec. (the last entry in Table I). This calculated surface temperature turns out to be 556°. This is approximately 250° higher than the actual surface temperature measured at this burning rate. It is very doubtful that the errors in our measurements were great enough so that it would be impossible to find a change in surface temperature of this amount. Unfortunately, there are no kinetic data for hydrazine nitrate or for the hydrazine nitrate-ammonium nitrate eutectic. It is evident that an Arrhenius relation between burning rate and surface temperature could not yield the results obtained for these systems.

Clearly, such a model does not fit the experimental results. However, it is difficult to see what sort of mechanism is operating that requires that the surface temperature remain essentially independent of burning rate. Perhaps a possible model for describing this is one in which a near thermodynamic equilibrium exists between liquid and vapor such that the rate of condensation is not quite as large as the rate of evaporation.

This excess of vaporization over condensation would have a cooling effect on the surface and cause the surface temperature to fall below the boiling point of the liquid layer. However, the rate of vaporization (hence the cooling effect) would depend on the temperature gradient at the surface as well as the surface temperature. It is conceivable, therefore, that the burning rate could be almost exclusively controlled by the temperature gradient. In this case, the surface temperature could remain essentially constant over a wide range of burning rates.

Acknowledgment. The author wishes to thank Dr. J. E. Colwell of Aerospace Corporation for his helpful comments.

- (7) O. K. Rice and R. Ginell, *J. Phys. Chem.*, **54**, 885 (1950).
- (8) W. H. Andersen, K. W. Bills, E. Mishuck, G. Moe, and R. D. Schultz, *Combust. Flame*, **3**, 301 (1959).
- (9) B. B. Spalding, *ibid.*, **4**, 59 (1960).

The Electric Moments of Some Nitrate Esters:

II. Hindered Rotation

by A. R. Lawrence and A. J. Matuszko

Research and Development Department, U. S. Naval Propellant Plant, Indian Head, Maryland (Received June 26, 1963)

In a previous paper¹ on the electric moments of nitrate esters, a general increase in the electric dipole moments of the compounds 1,2-dinitroxyethane ($\mu = 3.58$ D.), 1,2-dinitroxypropane ($\mu = 3.95$ D.), and 1,2-dinitroxyptane ($\mu = 4.10$ D.) was observed. It was suggested at the time that the increases in moment were due to the increased size of the attached side chain. This effect has been observed also with dihaloalkanes^{2,3} but the reasons for such behavior have not been discussed.

The increase in electric moment with increasing size of the aliphatic chain can be explained simply for the 1,2-dinitroxyalkanes. First, it is assumed that internal rotation about the bond joining the carbon atoms which bear the nitroxy groups is possible and that no significant rotation occurs about the carbon-oxygen bonds to

- (1) A. R. Lawrence and A. J. Matuszko, *J. Phys. Chem.*, **65**, 1903 (1961).
- (2) M. L. Sherrill, M. E. Smith, and D. D. Thompson, *J. Am. Chem. Soc.*, **56**, 611 (1934).
- (3) A. A. Maryott, M. E. Hobbs, and P. M. Gross, *ibid.*, **63**, 659 (1941).

the nitroxy groups.⁴ This situation is then indicated by Fig. 1.

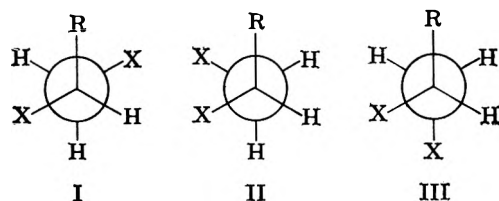


Figure 1. X = ONO₂; R = CH₃, CH₂CH₃, etc.

It is to be noted that (1) when the nitroxy groups are *trans* to each other the dipole moment will be nearly zero, and (2) when the number of molecules with the *trans* conformation decreases, an increase in over-all moment is to be expected. From Fig. 1, then, as the steric size of R increases, rotational isomer III would be expected to predominate at the expense of isomers I and II; the over-all dipole moment would be expected to increase. Thus the electric dipole moments of the series of 1,2-dinitroxyalkanes would be expected to increase as the magnitude of the side chain is increased. This is what is observed.

As a further examination of the way in which side-chain size affects dipole moment, it was decided to determine the moments of *meso*- and *l*-2,3-dinitroxybutane and *dl*-*erythro* and *dl*-*threo*-2,3-dinitroxybutane. If the explanation offered above is valid, the relative magnitudes of the moments of these substances should be explicable in terms of relative side-chain size.

Experimental

Materials. All the nitrate esters were prepared by the nitration of the corresponding diols. The materials were isolated by distillation and were shown to be of at least 95% purity by gas phase chromatography (20% Paraplex on 40-60 mesh Chromosorb-W). The compound *l*-2,3-dihydroxybutane was kindly donated by Dr. R. F. Anderson of USDA. The *dl*-*threo*-2,3-dihydroxypentane was prepared from *cis*-2-pentane via the bromohydrin and epoxide.⁵

Apparatus. The apparatus was the same as was used previously¹ with the exception of the measuring cell. This cell was of new design and consisted of two coaxial brass cylinders, the outer of which was double-walled for the circulation of temperature-regulating fluids. The inner cylinder was suspended from the Teflon stopper which closed the top of the outer cylinder. The bottom of this cylinder was also closed with a Teflon stopper. Both stoppers were held tightly in position by threaded metal "O" rings.

Procedures. All measurements were made in benzene solution at 25° and electric moments were calculated according to the method of Halverstadt and Kumler.⁶ Molar refractivities were calculated from tables⁷ and atom polarizations were ignored. The calculated data are shown as Table I. The probable error is estimated at ±0.03 D.

In order to avoid the tedious computation required, a program for the dipole moment calculation was written by Mr. Frank Ryan of the Computer Branch and the work carried out on an RCA 501 computer. The program was different from that described by Allinger and Allinger⁸ in that it was written directly into RCA 501 machine language. The experimental data were punched on paper tape and fed directly into the computer.

Table I: Empirical Constants and Molar Polarizations of Benzene Solutions at 25°

Compound	E	V_1	a	b	P_2	R_2	μ
<i>meso</i> -2,3-Di-nitroxybutane	2.2734	1.14546	10.71	-0.39	394.9	36.93	4.19
<i>l</i> -2,3-Dinitroxybutane	2.2757	1.14546	8.77	-0.39	337.45	36.93	3.83
<i>dl</i> - <i>erythro</i> -2,3-Di-nitroxybutane	2.2759	1.14407	9.20	-0.33	384.0	41.55	4.09
<i>dl</i> - <i>threo</i> -2,3-Di-nitroxybutane	2.2755	1.14460	8.58	-0.45	354.3	41.55	3.91

Results and Discussion

Since it is possible to rationalize the relative dipole moment magnitudes of 1,2-dinitroxyalkanes on the basis of side-chain size, it is to be expected that the moments of the 2,3-dinitroxyalkanes can be interpreted similarly. It is assumed as before that internal rotation takes place about the central carbon-carbon bond and not about carbon-oxygen bonds or oxygen-nitrogen bonds,⁴ that when the nitroxy groups are *trans* to each other the dipole moment will be nearly zero, and that a decrease in the number of molecules with *trans* conformation results in an increase in over-all moment. Figure 2 represents the resulting situations.

Figure 2a is a stereoprojection of a *meso*- or *erythro*-molecule and Fig. 2b is a stereoprojection representing a

- (4) W. B. Dixon and E. B. Wilson, Jr., *J. Chem. Phys.*, **35**, 191 (1961).
- (5) H. van Risseghem, *Bull. soc. chim. France*, 1661 (1960).
- (6) I. F. Halverstadt and W. D. Kumler, *J. Am. Chem. Soc.*, **64**, 2988 (1942).
- (7) N. A. Lange, "Handbook of Chemistry," 6th Ed., Handbook Publishers, Inc., Sandusky, Ohio, 1946, p. 1025.
- (8) N. L. Allinger and J. Allinger, *J. Org. Chem.*, **24**, 1613 (1959).

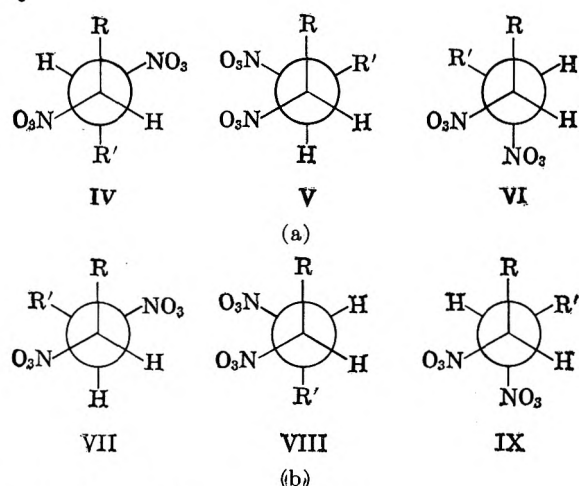


Figure 2. R = CH₃; R' = CH₃, C₂H₅.

threo-molecule (*dl*-mixture). For *meso*- or *erythro*-compounds, it seems clear, upon examination of Fig. 2a, that as the R groups become more bulky, the number of molecules with the *trans* conformation would increase and as a result the dipole moments would decrease in magnitude. Similar consideration of *dl*- or *threo*-compounds indicates that bulky R groups would tend to decrease the number of molecules with *trans* conformation and lead to increasing dipole moments.

Thus the series of *meso*- or *erythro*-compounds would be expected to show decreasing dipole moments while the series of *dl*- or *threo*-compounds would be expected to show increasing dipole moments. It is seen from Table I that the moments of the *meso*- or *erythro*-compounds decrease while those of the *dl*- or *threo*-compounds increase in the predicted fashion.

Additional support for the position taken here may be garnered from the data of Winstein and Wood.⁹ Here again it may be seen that the moments of the *meso*- or *erythro*-compounds decrease while those of the *dl*- or *threo*-compounds increase.

Spin-spin coupling constants between methine protons for the *meso*- and *dl*-forms of 2,3-dibromobutane were recently measured by Anet.¹⁰ The data were interpreted as indicating the presence of larger amounts of rotational isomer with the bromines located *trans* in the *dl*-compound than in the *meso*-compound. This would mean that *meso*-2,3-dibromobutane would have a larger dipole moment than *dl*-2,3-dibromobutane, which is a result in accord with the previous findings of Winstein and Wood.⁹ This explanation of the dipole moment differences between *meso*- and *dl*-isomers based on rotational isomerism gives added plausibility to the interpretation offered here, also based on rotational isomerism, for the dipole moment differences within a homologous series of either *erythro* or *threo* type compounds.

Acknowledgment. It is a pleasure to acknowledge support of this work under the Foundational Research Program of the Bureau of Naval Weapons.

(9) S. Winstein and R. E. Wood, *J. Am. Chem. Soc.*, **62**, 548 (1940).

(10) F. A. L. Anet, *ibid.*, **84**, 747 (1962).

Isotopic Exchange of Iodine Atoms between Tetrabutylammonium Iodide and *p*-Nitrobenzyl Iodide in Carbon Tetrachloride-Nitrobenzene Mixtures¹

by E. M. Morimoto and Milton Kahn

Department of Chemistry, The University of New Mexico, Albuquerque, New Mexico (Received July 8, 1963)

Frequently, in studies of the effect of solvent on the rate of a bimolecular ion-dipole reaction, an attempt is made to correlate the specific reaction rate with the dielectric constant of the solvent medium. The theoretical treatment of Laidler and Eyring² predicts that a plot of the logarithm of the specific reaction rate at zero ionic strength *vs.* the reciprocal of the dielectric constant of the medium should be linear with a positive slope, provided nonelectrostatic effects are negligible. Because of specific solvent effects, this relationship would not necessarily be expected to hold for completely different solvents.³ Even in solvent mixtures the results are not always in accord with this theory.⁴

The work presented here is concerned with the isotopic exchange of iodine atoms between tetrabutylammonium iodide and *p*-nitrobenzyl iodide in carbon tetrachloride-nitrobenzene mixtures at 24.90° over a dielectric constant range from 34.69 to 8.12; the concentrations of both reactants ranged from about 2.00×10^{-6} to 4.00×10^{-6} *F*. The exchange of iodine atoms between an organic iodide and iodide ion is a particularly suitable reaction for the study of solvent effects. Because iodine-131 activity is available in carrier-free form, it is possible, with proper precautions,⁵ to deter-

(1) This communication is based on work done under the auspices of the Atomic Energy Commission (Contract No. AT(11-1)-733).

(2) K. J. Laidler and H. Eyring, *Ann. N. Y. Acad. Sci.*, **39**, 303 (1940).

(3) R. D. Heyding and C. A. Winkler, *Can. J. Chem.*, **29**, 790 (1951).

(4) (a) E. Tommila and P. J. Antikainen, *Acta Chem. Scand.*, **9**, 825 (1955); (b) R. Fuchs and A. Nisbet, *J. Am. Chem. Soc.*, **81**, 2371 (1959).

mine second-order rate constants employing iodide concentrations as low as $10^{-6} M$ and, perhaps less.⁶ At such low iodide concentrations these values of the specific reaction rates should be essentially equal to the hypothetical values at zero ionic strength. Furthermore, at these iodide concentrations the formation of ion pairs should be minimized.

Because hydroxylic solvents are thought to interact with simple anions *via* hydrogen bonding⁷ it is of especial interest to study such reactions in aprotic solvent mixtures.

Experimental

Radioactivity. Iodine-131, obtained from Oak Ridge, was stored as a stock solution, $5 \times 10^{-4} F$ in KI and $5 \times 10^{-4} F$ in NaHSO_3 .

Chemicals. *p*-Nitrobenzyl iodide was prepared as described previously⁸ and purified by seven recrystallizations from absolute ethanol. Eastman Kodak tetrabutylammonium iodide was purified *via* six recrystallizations from absolute ethanol. Both materials were stored in the dark over silica gel. J. T. Baker analytical grade nitrobenzene and Mallinckrodt analytical grade carbon tetrachloride were fractionally distilled through a 20-plate Oldershaw column in the dark, over alumina, under nitrogen, and stored under nitrogen at 10° , in the dark; all solvents were used within 72 hr. of distillation. Erratic results were obtained when no attempt was made to remove oxygen and exclude light from the solvents. Furthermore, such purified solvents yielded similar results 2 weeks subsequent to distillation even though special precautions were taken to exclude light and oxygen during the sampling process.

Ordinary distilled water was redistilled from an alkaline permanganate solution in an all-Pyrex still, boiled, and flushed with nitrogen. Matheson pre-purified grade nitrogen was further dried by passing it slowly through a liquid nitrogen cold-trap. All other chemicals employed were of analytical grade.

Preparation of Reactant Solutions. *p*-Nitrobenzyl iodide solutions were prepared by the dissolution and volumetric dilution of accurately weighed amounts of the solid.

Radioactive tetrabutylammonium iodide solutions were prepared as follows. Approximately 1 ml. of stock iodide tracer solution was treated with 2 ml. of a solution 0.2 *F* in $\text{K}_2\text{Cr}_2\text{O}_7$ and 2 *F* in H_2SO_4 , and extracted with benzene. After several washings with water, the benzene phase was shaken with an aqueous solution of tetrabutylammonium iodide; the resulting active aqueous solution was evaporated to dryness under vacuum over at least 4 hr. and the residue dissolved and

volumetrically diluted with the desired solvent. The concentrations of the resulting tetrabutylammonium iodide solutions were calculated from the concentrations of the original aqueous solutions, the quantitative nature of all the steps in the activation procedure having been experimentally verified.

The reactant solutions were stored in the dark under nitrogen at 10° and found to be stable for at least 48 hr. after preparation. The solvent mixtures were prepared by weight and stored in the dark, under nitrogen, at 10° . All operations in the preparation of solvent mixtures and reactant solutions were conducted in semidarkness with minimum exposure to the atmosphere.

Procedure for Exchange Experiments. The reactant solutions and reaction vessel (10-ml. centrifuge tube with glass stopper) were brought to reaction temperature in a constant-temperature ($\pm 0.01^\circ$) water bath. One-half milliliter of each reactant was then pipetted into the vessel and mixed. After a given interval of time, the reactants were separated and the radioactivity associated with each reactant determined. The procedure was repeated for various time intervals. Preliminary experiments indicated that light had a marked accelerating effect on the rate of the exchange reaction; therefore, all exchange experiments were conducted in the absence of light.

Separation Procedure. The reactants in nitrobenzene-carbon tetrachloride mixtures were separated by shaking with 3 ml. of carbon tetrachloride and 4 ml. of water; benzene was substituted for the carbon tetrachloride when the reaction was conducted in pure nitrobenzene. The resulting two-phase system, with the *p*-nitrobenzyl iodide in the organic phase and the tetrabutylammonium iodide in the aqueous phase, was centrifuged and separated. The organic phase was washed several times with water, the washings being added to the aqueous phase. The efficiency of the extraction of tetrabutylammonium iodide into the aqueous phase was determined through the use of "blank" reaction mixtures in which no *p*-nitrobenzyl iodide was present; corrections were applied whenever necessary. In general, less than 1% of the tetrabutylammonium iodide

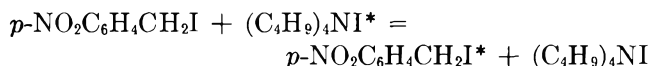
- (5) M. Kahn, "Iodine-131," Chapter 9, "Inorganic Isotopic Syntheses," R. H. Herber, Ed., W. A. Benjamin, Inc., New York, N. Y., 1962.
- (6) E. R. Swart and L. J. le Roux, *J. Chem. Soc.*, 2110 (1956).
- (7) (a) J. A. Learv and M. Kahn, *J. Am. Chem. Soc.*, 81, 4173 (1959); (b) E. A. S. Cavell, *J. Chem. Soc.*, 4217 (1958); (c) E. A. S. Cavell and J. A. Speed, *ibid.*, 1453 (1960); (d) *ibid.*, 226 (1961); (e) J. Miller and A. J. Parker, *J. Am. Chem. Soc.*, 83, 117 (1961); (f) A. J. Parker, *J. Chem. Soc.*, 1328 (1961).
- (8) E. L. Purlee, M. Kahn, and J. L. Riebsomer, *J. Am. Chem. Soc.*, 76, 3796 (1954).

was retained in the organic phase. Also, in each instance, no more than 0.2% of *p*-nitrobenzyl iodide was extracted into the aqueous phase.

Measurements of Radioactivity. The liquid samples were counted with a well-type scintillation detector to expected standard deviations of 1% or less.

Results and Discussion

The reaction investigated was



where the asterisks indicate radioactive atoms. The experimental data were evaluated with the aid of the logarithmic form of the first-order isotopic exchange law.⁹ The reaction was found to be first order with respect to both the *p*-nitrobenzyl iodide and iodide ion. In solvent mixtures of dielectric constant as low as 12.53, the absence of any systematic variation of the observed specific rate constant, *k*, suggests that the salt is completely dissociated; for the solvent mixtures of dielectric constant of 10.00 and 8.12, the values of *k* increase with decrease in tetrabutylammonium iodide concentration, indicating the presence of kinetically inactive ion pairs.¹⁰ Values of the degree of dissociation, α , calculated from the association constants for tetrabutylammonium iodide,¹¹ are in accord with the foregoing observations. In all instances, α was calculated employing the limiting form of the Debye-Hückel activity coefficient expression¹² which should be

valid at the low ionic strengths of the reaction mixtures.

A semilogarithmic plot of \bar{k}/α vs. the reciprocal of the dielectric constant is shown in Fig. 1. Over the range of dielectric constant from 34.69 to 12.53, the plot is linear with a positive slope, in agreement with the theory of Laidler and Eyring.² At lower values of the dielectric constant the specific reaction rate is less than would be predicted from this theory. This departure from theory may be attributed to the accumulation of nitrobenzene around the iodide ion, causing the microscopic dielectric constant to be higher than the bulk value^{11,13} and/or the increase of the "effective size" of the iodide ion with decrease in dielectric constant by virtue of "selective solvation" with nitrobenzene.¹¹

- (9) G. Friedlander and J. W. Kennedy, "Nuclear and Radiochemistry," John Wiley and Sons, Inc., New York, N. Y., 1955, p. 315.
- (10) C. C. Evans and S. Sugden, *J. Chem. Soc.*, 270 (1949).
- (11) E. Hirsch and R. M. Fuoss, *J. Am. Chem. Soc.*, **82**, 1018 (1960).
- (12) C. B. Monk, "Electrolytic Dissociation," Academic Press, Inc., New York, N. Y., 1961, p. 30.
- (13) L. R. Dawson, J. E. Berger, and H. C. Eckstrom, *J. Phys. Chem.*, **65**, 986 (1961).

γ -Excitation of the Singlet and Triplet States of Naphthalene in Solution

by B. Brocklehurst, G. Porter, and J. M. Yates

Department of Chemistry, The University, Sheffield 10, England
(Received August 1, 1963)

The luminescence produced by high energy irradiation of organic solutions has been much studied but the mechanisms of excitation have not yet been fully elucidated. In the case of a dilute solution of a compound with excited states lying lower than those of the solvent, energy transfer processes are commonly involved, *i.e.*, energy absorbed by the solvent is transferred to the solute which emits light. In the field of radiation chemistry, similar effects—sensitized reactions and "protection"—are observed. The transfer of energy is usually discussed in terms of transfer of electronic excitation, but it is also possible that positive charge is transferred, followed by the recombination of the solute ion with an electron or negative ion to produce luminescence or chemical change.

In frozen organic solutions (glasses) which have been bombarded with high energy radiation, the existence of trapped electrons and negative ions has been demon-

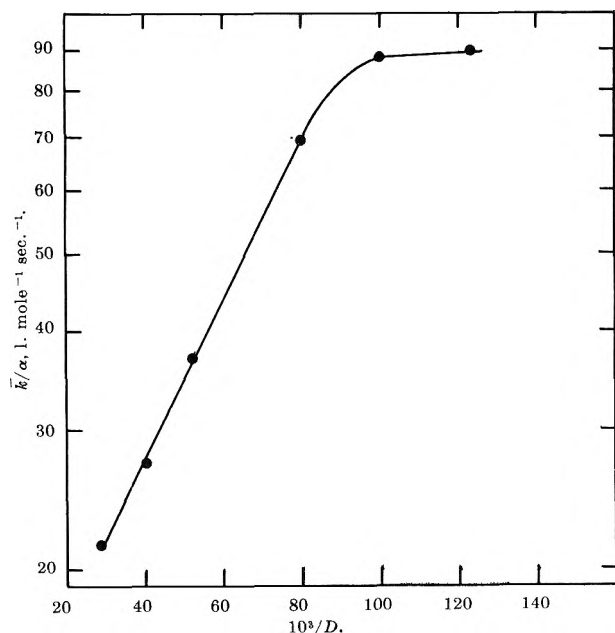


Figure 1. Dependence of specific reaction rate on dielectric constant.

strated,¹ but apparently positive ions have not been observed directly. In glassy solutions of easily ionizable compounds which have been irradiated with ultraviolet light, trapped positive ions and electrons have been observed^{2,3} and it has been shown that luminescence is produced by their recombination; at 77°K. this is a slow process but it can be speeded up by warming (thermoluminescence) or irradiation with infrared light. One criterion of ion recombination should be that triplet and singlet states will be excited in the statistical weight ratio of 3:1, at least approximately, *i.e.*, the phosphorescence/fluorescence ratio should be enhanced, the extent of this depending on the radiationless processes involved. Such an enhancement has been observed in one case² but in another,³ surprisingly, *only* phosphorescence was seen.

Some qualitative observations of thermoluminescence of γ -irradiated glassy solutions have been reported previously,⁴ but no measurements appear to have been published on the ratio, R , of phosphorescence to fluorescence directly excited by high energy radiation or in thermoluminescence following such irradiation. We report here some preliminary results obtained with naphthalene. Observations were made on a deoxygenated 10^{-2} M solution in MP (isopentane-methylcyclohexane) at 77°K. For ultraviolet excitation, the mercury 2537 Å. line was isolated by filters or a monochromator; γ -irradiation was carried out with a 500-c. cobalt source.

After γ -ray doses of 1000–10,000 rads, the sample became green in color. (The naphthalene negative ion is known to be green and the positive ion would be expected to have a similar spectrum.) On removing the sample from the liquid nitrogen it emitted a green glow as the temperature rose. Photographs of the emission spectra in each case showed naphthalene fluorescence and phosphorescence and only traces of emission from impurities in the solvent.

Both fluorescence and phosphorescence were observed during ultraviolet irradiation, γ -irradiation, and thermoluminescence experiments, but it was immediately apparent that, relative to ultraviolet excitation, phosphorescence was enhanced by γ -excitation and the enhancement was still greater in thermoluminescence. Quantitative measurements have been begun using a photomultiplier and filters (Chance glasses OX 9A and OY 18) to isolate the two emissions. The first approximate measurements confirm the enhancement of the phosphorescence. Absolute measurement of the ratio, R , has not yet been attempted, so we put $R = 1$ for ultraviolet excitation; then for γ -excitation we find $R \approx 2$ and for thermoluminescence $R \approx 5$.

The behavior of ultraviolet-excited naphthalene is

not yet fully worked out. Gilmore, *et al.*,⁵ give the absolute value of R as 0.17, the absolute values of the fluorescence and phosphorescence yields being 0.52 and 0.09, respectively. We define here ϕ_s and ϕ_T , the quantum yields of singlet and triplet emission referred to the excitation of singlet and triplet states, respectively. Following Gilmore, *et al.*,⁵ we assume that the excited singlet state can only decay by light emission or conversion to the triplet state; *i.e.*, radiationless decay to the ground state can only occur from the triplet state. Then the normally defined phosphorescence yield (*i.e.*, referred to singlet excitation) is given by $(1 - \phi_s)\phi_T$. Gilmore, *et al.*, calculate $\phi_T = 0.23$ and combine this value with their measured phosphorescence lifetime, τ , to calculate the true radiative lifetime, τ_0 , of the triplet state as 11 sec. This, however, is not consistent with recent measurements^{6,7} of the lifetime (τ) of triplet $C_{10}D_8$ as 16.9, 18.0, or 20.0 sec.; these suggest⁶ that the true radiative lifetime of both $C_{10}D_8$ and $C_{10}H_8$ is at least 20 sec. This figure together with the value of 2.1 sec. for $C_{10}H_8$ measured under the same conditions⁷ gives $\phi_T \leq 0.1$. Because of the difficulty of making accurate absolute measurements of light intensities, we put $\phi_T = 0.1$ and combine this with the ratio, $R = 0.17$, of Gilmore, *et al.*, to calculate $\phi_s = 0.37$.

Then in the case where direct excitation of triplets as well as singlets occurs (in the ratio $x:1$), R is given by

$$\frac{\phi_T}{\phi_s} (1 - \phi_s + x)$$

and we can write

$$\frac{R}{R_0} = 1 + \frac{x}{1 - \phi_s}$$

where R_0 refers to the case $x = 0$ (ultraviolet excitation). Then $x = 3$ gives $R/R_0 = 5.8$; our measured value is about 5 for thermoluminescence, which suggests that it results from recombination of trapped naphthalene ions. Our value of $R/R_0 = 2$ for direct γ -excitation corresponds to $x = 3/6$; if we assume that energy transfer from the solvent only excites singlet

- (1) P. S. Rao, J. R. Nash, J. P. Guarino, M. R. Ronayne, and W. H. Hamill, *J. Am. Chem. Soc.*, **84**, 500, 4230 (1962).
- (2) E. Dolan and A. C. Albrecht, *J. Chem. Phys.*, **37**, 1149 (1962).
- (3) H. Linschitz, M. G. Berry, and D. Schweitzer, *J. Am. Chem. Soc.*, **76**, 5833 (1954).
- (4) H. T. J. Chilton and G. Porter, *J. Phys. Chem.*, **63**, 904 (1959).
- (5) E. H. Gilmore, G. E. Gibson, and D. S. McClure, *J. Chem. Phys.*, **20**, 829 (1952); **23**, 399 (1955).
- (6) C. A. Hutchison and B. W. Mangum, *ibid.*, **32**, 1261 (1960); M. S. de Groot and J. H. van der Waals, *Mol. Phys.*, **4**, 189 (1961).
- (7) B. Smaller, *J. Chem. Phys.*, **37**, 1578 (1962).

states, then this process and charge transfer followed by recombination are occurring in equal proportions.

These calculations are, of course, very approximate and are open to the further objection that we have assumed that the rate of singlet to triplet conversion is independent of the type of excitation; this is usually correct, but exceptions have been found in recent work⁸ on chrysene and hexahelicene where excitation of the higher singlet states leads to a larger phosphorescence/fluorescence ratio. This effect may explain our results with direct γ -excitation; the amount of energy transferred from the solvent is not known, but it is probably much greater than that of the first excited singlet state of naphthalene. Support for this interpretation comes from recent work in this laboratory⁹ on the variation of luminescence with solute concentration in similar systems; the light intensity obeys a simple Stern-Volmer relation which suggests that only one transfer process, rather than two, is involved. It seems improbable that excitation and charge transfer would take place at the same rate.

On the other hand, it seems reasonable to ascribe the thermoluminescence to naphthalene ion recombination since the enhancement of phosphorescence is much larger in this case; if energy is released in the solvent on warming and is transferred to the naphthalene, a different transfer process involving more energy must be invoked. The nature of the negative species is unknown at present; previous work¹⁻³ on electron trapping has always involved much more polar solvents. One would not expect electrons to be trapped in aliphatic hydrocarbons, so we have to assume that they are attached to polar impurities or to other naphthalene molecules, the latter possibility being supported by the green coloration of the irradiated glass.

(8) M. F. O'Dwyer, M. A. El-Bayoumi, and S. J. Strickler, *J. Chem. Phys.*, **36**, 1395 (1962).

(9) G. Porter and J. M. Yates, unpublished work.

Radiation Synthesis of Iodonium Compounds

by A. MacLachlan

Radiation Physics Laboratory, Engineering Department, E. I. du Pont de Nemours and Company, Wilmington, Delaware
(Received August 5, 1963)

Diphenyliodonium triiodide (I) has been detected when iodobenzene is irradiated with γ -rays.^{1,2} Investigations at this Laboratory concerning the radiation chemistry of aromatic compounds found that I is also

formed when iodobenzene is irradiated with 2-6-Mev. electrons. Furthermore, pure iodobenzene is not necessary for excellent yields and, in fact, unsymmetrical iodonium compounds can be obtained when the proper mixture is used. These results prompted the brief mechanism study reported here.

Maximum total yields of iodonium compound could be obtained with only 7% iodobenzene in chlorobenzene or bromobenzene. Diphenyliodonium chloride and bromide are obtained, respectively, complexed with iodine. The iodine complexes were identified by comparison of infrared spectra and melting points with either authentic samples or with the literature values.^{3,4} Precipitation of the iodonium salts occurs spontaneously during irradiation. Dissolution of the iodine iodonium complexes in acetone results in eventual crystallization of the uncomplexed iodonium halides. Comparison of the melting points of the compounds with those given by Beringer, *et al.*,⁵ served as further structure proof.

The effect of iodobenzene concentration was examined by irradiating 93% bromobenzene-7% iodobenzene and 99.2% bromobenzene-0.8% iodobenzene and pure iodobenzene with the same radiation dose. At the higher iodobenzene concentration in bromobenzene, 0.7 g. of product formed, while at the lower only 0.25 g. could be isolated. Irradiation of pure iodobenzene yielded 0.75 g. of diphenyliodonium iodide triiodide.

Free iodine was found to be unnecessary for efficient production of I, and in fact was detrimental. Pure iodobenzene and a slurry, consisting by volume of 95% iodobenzene-5% aqueous sodium thiosulfate (10%), were irradiated with the same total dose. Stirring of the slurry was accomplished with a magnetic stirring bar, such that rapid dissolution of iodine occurred but no emulsion was formed. Irradiation of pure iodobenzene yielded 1.01×10^{-2} mole of diphenyliodonium iodide diiodide along with free iodine. The iodobenzene scrubbed with aqueous thiosulfate during irradiation (thus maintaining the free I_2 concentration at a low level) yielded 1.5×10^{-2} molar equivalent of iodonium compound as the thiosulfate salt. The bisdiphenyliodonium thiosulfate was dissolved in boiling water containing sodium bromide, which on cooling yielded white crystals of diphenyliodonium bromide. Irradiation of

(1) J. D. Parrack, G. A. Swan, and D. Wright, *J. Chem. Soc.*, 911 (1962).

(2) P. F. D. Shaw, *ibid.*, 443 (1951).

(3) M. D. Forster and J. H. Schaeppi, *ibid.*, 101, 382 (1912).

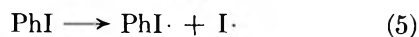
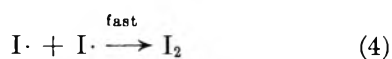
(4) C. Hartmann and V. Meyer, *Ber.*, **27**, 502 (1894).

(5) F. M. Beringer, M. Drexler, E. M. Gindler, and C. C. Lumpkin, *J. Am. Chem. Soc.*, **75**, 2705 (1953).

iodobenzene with I_2 added (0.1 M) resulted in a strong suppression of the iodonium product.

Previous studies of the radiation chemistry of chlorobenzene have shown that the primary chemical reaction upon irradiation is the formation of phenyl radicals and chlorine atoms.⁶ In the presence of iodobenzene the phenyl radical could then add to form the diphenyliodonium radicals. Proof that the phenyl rings do indeed come from both the chloro- and bromobenzene and the iodobenzene was obtained by irradiation of *p*-chlorotoluene and *p*-bromotoluene with 7% iodobenzene. Both these mixtures yielded the mixed iodonium compounds (4-methyl diphenyliodonium chloride and bromide diiodide). Conversion to the known 4-methyl diphenyliodonium bromide (m.p. 174–177⁰⁵) served to prove the structures.

The effect of excess iodine would certainly hinder the phenyl radical attack on iodobenzene. However, the relative ineffectiveness of iodine scavenging indicates that phenyl radical trapping by iodobenzene is a fast reaction. The following scheme is consistent with the results obtained and reported in this study.



(6) A. MacLachlan and R. L. McCarthy, *J. Am. Chem. Soc.*, **84**, 2519 (1962).

Mutual Diffusion in the Liquid System Hexane-Hexadecane

by D. L. Bidlack and D. K. Anderson

Department of Chemical Engineering, Michigan State University,
East Lansing, Michigan (Received August 12, 1963)

Much work has been done recently to study mutual diffusion of binary systems of liquids. Nearly all of the systems studied were either ideal¹ or nonideal with the nonideality attributable to association.² The purpose of this paper is to expand the understanding of liquid diffusion by presenting accurate data for a non-associating, nonideal system. The system chosen was hexane-hexadecane in which the nonideality is caused by the unequal size of the molecules of the two species.

Experimental

Method and Materials. The diffusion data were obtained using a diffusimeter very similar to the one described by Caldwell, Hall, and Babb.³ That paper describes both the apparatus and method in great detail and will not be repeated here. The experimental diffusivities were obtained by measuring the mutual diffusion of two solutions of very nearly equal concentrations. The measured value was taken to be that of a solution with a concentration equal to the average of the two solutions.

To test the accuracy of this diffusimeter, diffusion coefficients for aqueous sucrose solutions with concentrations of 0.3751, 0.5627, and 0.7506 g./ml. were compared with diffusivities reported by Gosting and Morris.⁴ Seven runs were made at these concentrations and the values obtained deviated by less than 1% in all cases from the Gosting and Morris data and had an average deviation of 0.5%.

Viscosities were obtained with an Ostwald-Fenske type viscometer and densities were determined with a 10-ml. glass specific gravity bottle.

The results of this work are recorded in Table I. The mutual diffusion coefficients were measured at a temperature of $25.1 \pm 0.05^\circ$, viscosities at $25.0 \pm 0.05^\circ$, and densities at $25 \pm 1^\circ$.

The chemicals for the investigation were purchased from Matheson Coleman and Bell. The hexane was chromatography or spectroquality grade and the hexadecane was 99+% (olefin-free). In order to test the purity of the chemicals, the refractive index and density were compared with values given by Timmermans⁵ (see Table II).

Activity Data. The choice of the system was based partially on the availability of activity data. McGlashan and Williamson⁶ measured the activities at several different temperatures and showed that at 25°

$$\ln f_A = -0.1105X_B^2 - 0.00736X_B^2(3 - 4X_B) \quad (1)$$

- (1) C. S. Caldwell and A. L. Babb, *J. Phys. Chem.*, **60**, 51 (1956).
- (2) See P. A. Johnson and A. L. Babb, *Chem. Rev.*, **56**, 387 (1956); A. P. Hardt, D. K. Anderson, R. Rathbun, B. W. Mar, and A. L. Babb, *J. Phys. Chem.*, **63**, 2059 (1959); P. C. Carman and L. Miller, *Trans. Faraday Soc.*, **55**, 1838 (1959); D. K. Anderson, J. R. Hall, and A. L. Babb, *J. Phys. Chem.*, **62**, 404 (1958); and footnote references 8–13 for discussion and further references to associated systems.
- (3) C. S. Caldwell, J. R. Hall, and A. L. Babb, *Rev. Sci. Instr.*, **28**, 816 (1957).
- (4) L. J. Gosting and M. S. Morris, *J. Am. Chem. Soc.*, **71**, 1998 (1949).
- (5) J. Timmermans, "Physico-Chemical Constants of Pure Organic Compounds," Elsevier Publishing Co., Inc., New York, N. Y., 1950.
- (6) M. L. McGlashan and A. G. Williamson, *Trans. Faraday Soc.*, **57**, 588 (1961).

Table I: Summary of Experimental Data

	Mutual diffusion coefficients							
	Av. mole fraction hexadecane	0.00417	0.0953	0.1531	0.2504	0.3924	0.6025	0.7422
Difference in mole fraction between upper and lower level in cell	0.00833	0.0082	0.0096	0.0124	0.0108	0.0153	0.0320	0.0293
$D_{AB} \times 10^6$, cm. ² /sec.	2.193	1.933	1.820	1.665	1.492	1.254	1.108	0.8668
	Viscosities							
	Mole fraction, hexadecane	0	0.1995	0.3978	0.5746	0.8011	1.000	
η , centipoises	0.2958	.6062	1.0166	1.4530	2.2091	3.0306		
	Densities							
	Mole fraction, hexadecane	0	.0995	0.1995	0.3978	0.6101	0.7582	1.0000
Density, g./cm. ³	.6550	.6822	.7017	.7277	.7480	.7584	0.7698	

Table II: Comparison of Physical Constants with Previous Data

	Density at 25°		Refractive index at 25° (sodium lamp)	
	This work	Ref. 5	This work	Ref. 5
Hexane	0.6550	0.6549 ^a	1.3720	1.3723 ^a
Hexadecane	0.7698	0.7699	1.4319	1.4325

^a Average of several recorded data.

where f_A is the activity coefficient of hexane and X_B is the mole fraction of hexadecane. From their experimental results and analysis of error, an estimation at $X_B = 0.50$ and 20° shows that $\ln a_A = -0.718 \pm 0.001$, where a_A is the activity of hexane. This is well within the accuracy required for our purposes.

Discussion

Hartley and Crank⁷ have shown that for nonideal systems the behavior of the mutual diffusion coefficient, D_{AB} , is described by

$$D_{AB} = \frac{RT}{N\eta} \left[\frac{X_A}{f_B} + \frac{X_B}{f_A} \right] \frac{d \ln a_A}{d \ln X_A} \quad (2)$$

where X is mole fraction, a is the activity, η is the solution viscosity, f is a friction coefficient dependent on molecular size, and R , T , N have their usual definitions of gas constant, temperature, and Avogadro's number. The subscripts A and B refer to the two species of the system. Although there is some disagreement about Hartley and Crank's arguments,⁸⁻¹⁰ both the absolute rate theory¹¹ and the statistical mechanical approach⁸ agree with the Hartley-Crank theory that the quantity $D\eta/(d \ln a/d \ln X)$ should be a straight line function with mole fraction at constant temperature.

The linearity of $D\eta$ for ideal systems has been verified experimentally by Caldwell and Babb.¹ However,

attempts to test for the linear behavior of $D\eta/(d \ln a/d \ln X)$ for nonideal systems have been unsuccessful.² In all cases the activity correction overcorrects, sometimes by as much as several hundred per cent.¹² In one case, chloroform-ether,¹¹ the activity correction was used with apparent success, but closer examination with more accurate data shows that the correction is also too large for this system.¹³ The tendency to overcorrect is common for both negatively and positively deviating systems from Raoult's law.

The overcorrection has been ascribed to association of the molecules in solution.^{12,13} It is thought that the molecules, instead of acting as monomers during the diffusion process, form dimers and polymers or complexes with the other species in the system and are thus inhibited in their movement.

Miller and Carman¹⁴ recently published a study of another nonideal, nonassociating system, heptane-hexadecane, in which they compared self-diffusion with mutual diffusion.

The activity correction term for this work is derived from eq. 1:

$$\frac{d \ln a_A}{d \ln X_A} = \frac{d \ln a_B}{d \ln X_B} = 1 + \frac{d \ln f_A}{d \ln X_A} = 1 + 0.2210X_A X_B + 0.0442X_A X_B(1 - 2X_B) \quad (3)$$

- (7) G. S. Hartley and J. Crank, *Trans. Faraday Soc.*, **45**, 801 (1949).
- (8) R. J. Bearman, *J. Phys. Chem.*, **65**, 1961 (1961).
- (9) R. Mills, *ibid.*, **67**, 600 (1963).
- (10) J. G. Kirkwood, R. L. Baldwin, P. J. Dunlop, L. J. Gosting, and G. Kegeles, *J. Chem. Phys.*, **33**, 1505 (1960).
- (11) S. Glasstone, K. J. Laidler, and H. Eyring, "The Theory of Rate Processes," McGraw-Hill Book Co., Inc., New York, N. Y., 1941, Chapter IX.
- (12) B. R. Hammond and R. H. Stokes, *Trans. Faraday Soc.*, **52**, 781 (1956).
- (13) D. K. Anderson and A. L. Babb, *J. Phys. Chem.*, **65**, 1281 (1961).
- (14) L. Miller and P. C. Carman, *Trans. Faraday Soc.*, **58**, 1529 (1962).

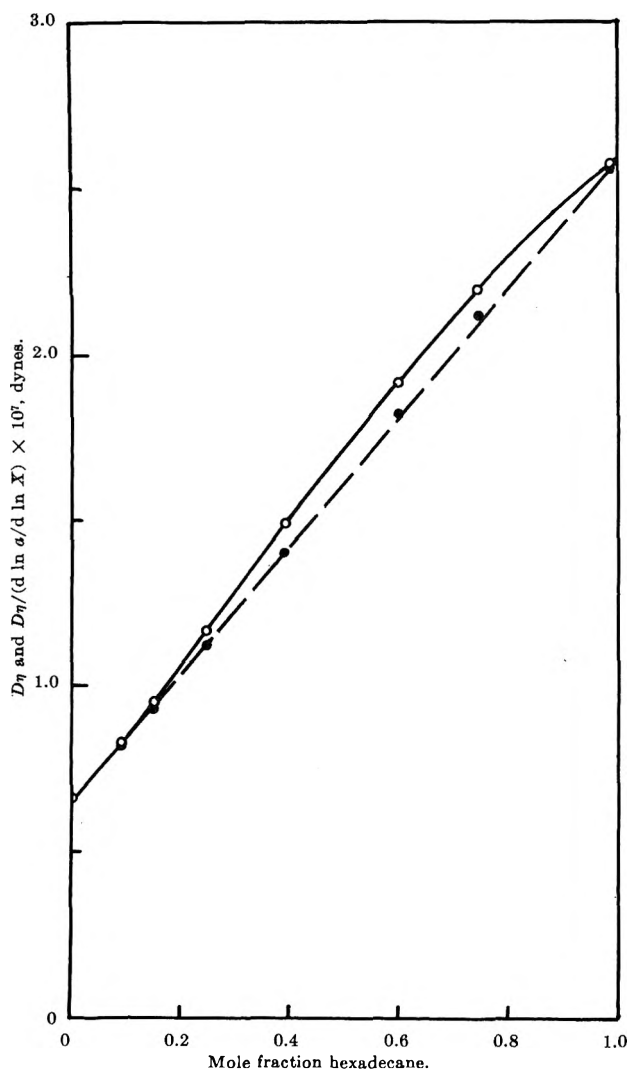


Figure 1.— $D\eta$ and $D\eta/(d \ln a/d \ln X)$ as a function of mole fraction for the system hexane-hexadecane: —○—, $D\eta$; ●, $D\eta/(d \ln a/d \ln X)$; - - - -, linear or ideal behavior.

In Fig. 1, $D\eta$ and $D\eta/(d \ln a/d \ln X)$ are shown as functions of mole fraction along with the predicted linear behavior of $D\eta/(d \ln a/d \ln X)$. The activity corrected product of the diffusivity and viscosity agrees quite closely with theory. At $X_B = 0.5$, $D\eta/(d \ln a/d \ln X) = 1.616 \times 10^{-7}$ dyne, which is 0.2% different from linearity. The maximum deviation of $D\eta/(d \ln a/d \ln X)$ from linearity is 1.7% where the uncorrected $D\eta$ deviates 5.5%. The authors feel that 1.7% is within experimental error since $D\eta/(d \ln a/d \ln X)$ is a result of four different sets of measured data. In any case, the tendency to overcorrect is not found in this system.

Acknowledgment. This work was supported by a grant from the Petroleum Research Fund, administered by the American Chemical Society. Grateful acknowledgment is hereby made to the donors of the fund.

On the System Niobium Pentoxide-Tantalum Pentoxide

by G. P. Mohanty, L. J. Fiegel, and J. H. Healy

A. O. Smith Corporation, Milwaukee 1, Wisconsin
(Received August 16, 1963)

Investigations of phase equilibria in the system Nb_2O_5 - Ta_2O_5 have been reported by Schäfer, Dürkop, and Jori,¹ Goldschmidt,² and Holtzberg and Reisman³ within the past ten years. Because of the variation of the results reported by these workers, it appeared worthwhile to re-examine this system in an attempt to resolve the discrepancies. This paper briefly reports the results of this investigation.

Experimental

Materials. Nb_2O_5 and Ta_2O_5 obtained from A. D. Mackay and Co. were used for preparing all the samples. The purities were given as 99.9% for both the Nb_2O_5 and Ta_2O_5 .

Sample Preparation. Before preparing the binary oxide samples, batches of pure Nb_2O_5 and Ta_2O_5 were pressed and fired in atmospheres of oxygen, argon, and 80% argon-20% oxygen to determine the effects of such treatments on the stoichiometry and structure of the base materials. Changes in the stoichiometry were followed by electrical resistivity measurements. A room temperature value of approximately 10^{10} ohm-cm. was obtained for the Nb_2O_5 sample fired in air at 1400° while approximately 10^{11} ohm-cm. was obtained for Ta_2O_5 fired at 1520° . Attempts were also made at melting the base materials both in an argon arc and in an oxygen acetylene flame. The resistivities of the solid Nb_2O_5 samples prepared in this manner were in the range 10-100 ohm-cm. In comparing these results with those of Greener and Hirthe,⁴ these low values indicated that the materials deviated greatly from stoichiometry, possibly from contaminations during melting. Consequently, the melting procedure was abandoned in favor of the sintering treatment in all subsequent sample preparations.

Determinations of structural changes in Nb_2O_5 confirmed the results reported by Holtzberg, Reisman, Berry, and Berkenblit.⁵ Once Nb_2O_5 undergoes the

- (1) H. Schäfer, A. Dürkop, and M. Jori, *Z. anorg. allgem. Chem.*, **275**, 289 (1954).
- (2) H. J. Goldschmidt, *Metallurgia*, **62**, 211, 241 (1960).
- (3) F. Holtzberg and A. Reisman, *J. Phys. Chem.*, **65**, 1192 (1961).
- (4) E. H. Greener and W. M. Hirthe, *J. Electrochem. Soc.*, **109**, 600 (1962).

structural modification to the monoclinic form (designated as the α -phase), it retains this form no matter what further heat treatments it undergoes. All other forms of Nb_2O_5 are apparently metastable.

Sample Preparation—Quenched Samples. Samples for the annealing treatments were prepared by thoroughly mixing proper amounts of Nb_2O_5 and Ta_2O_5 powders which had been pre-fired at 1000° for 24 hr. After mixing, 3-g. batches of each nominal composition were pressed into the form of flat briquets, placed in covered platinum containers, and fired at appropriate temperatures until complete equilibrium had been achieved in each sample. This required annealing times which ranged from 1 to 8 weeks. Samples were air quenched to room temperature following the annealing treatment.

D.t.a. Measurements. All d.t.a. runs were made in a vertical furnace wound with platinum-40% rhodium wire similar in design to that described by Holtzberg and Reisman.³ The preannealing treatment of the d.t.a. samples was slightly different. The pressed samples were first fired at 1100° , ground, and refired again at 1100° . Following this, the samples were ground again before being pressed into the form suitable for the d.t.a. measurements. This treatment was carried out in an attempt to accelerate attainment of equilibrium conditions in the sample during the d.t.a. runs. Even with this procedure, repeated temperature cycling in the furnace was necessary before reproducible results could be obtained.

X-Ray Diffraction Measurements. In order to deter-

mine the phase distributions after annealing, a diffraction pattern of each fired sample was measured in a G.E. X-RD5 unit equipped with a spectrometer, a proportional counter, a copper anode, stabilized power source, and associated electronic circuitry. Film techniques were used in instances where it was necessary to detect very weak reflections.

A Norelco high-temperature diffractometer attachment using a Pt-40% Rh heating filament as the sample holder was used to determine the at-temperature phase distributions for the Ta_2O_5 -rich samples. Samples for these high temperature diffraction studies were prepared from the same samples used for the room temperature measurements. In order to obtain even temperature distribution over the bulk of the samples, very thin sections cut from repressed powders of the previously fired briquets were used. Temperature was measured by a Pt-Pt/10% Rh thermocouple welded to the bottom of the heating filament and also with an optical pyrometer.

Results and Discussion

The results of this investigation in general support the equilibrium diagram for the Nb_2O_5 - Ta_2O_5 system proposed recently by Holtzberg and Reisman.³ There are certain areas of disagreement, however, and these have been incorporated in the diagram shown in Fig. 1. Because our results generally confirm those reported by Holtzberg and Reisman, only the features which are in variance with their results need to be discussed.

The first of these refers to the region of stability of the compound $2\text{Nb}_2\text{O}_5 \cdot \text{Ta}_2\text{O}_5$. This compound was first reported by Holtzberg and Reisman,³ who indicated it to exist only at the stoichiometric composition; later its existence was confirmed in conjunction with a crystallographic study by Mohanty, Fiegel, and Healy.⁶ The present investigation shows this compound to have limited solubility, especially for Ta_2O_5 . For example, in samples annealed at 1435° , the presence of α - Ta_2O_5 marking the compositional limit of $2\text{Nb}_2\text{O}_5 \cdot \text{Ta}_2\text{O}_5$ was detected only beyond the 36% Ta_2O_5 composition.

Secondly, the temperature where $2\text{Nb}_2\text{O}_5 \cdot \text{Ta}_2\text{O}_5$ undergoes the eutectoid transformation to α - Nb_2O_5 and β - Ta_2O_5 appears to be lower than had been indicated earlier.³ Samples fired directly at 1400° showed the presence of $2\text{Nb}_2\text{O}_5 \cdot \text{Ta}_2\text{O}_5$ from approximately 27 to

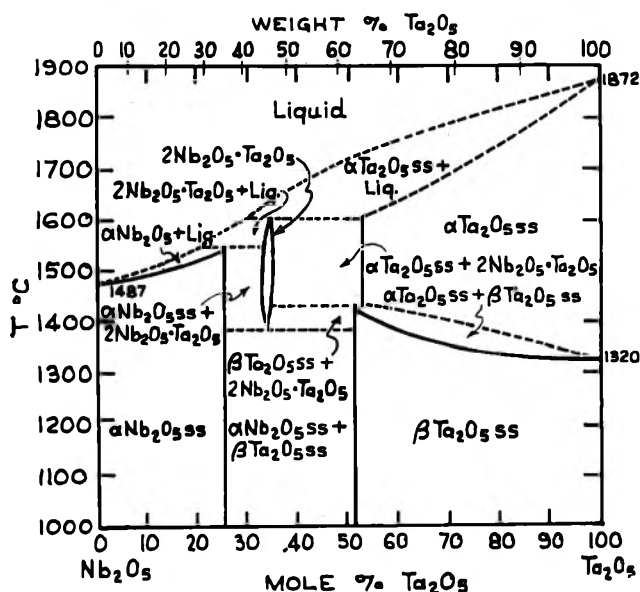


Figure 1. Equilibrium diagram of the Nb_2O_5 - Ta_2O_5 system.

(5) F. Holtzberg, A. Reisman, M. Berry, and M. Berkenblit, *J. Am. Chem. Soc.*, **79**, 2039 (1957).

(6) G. P. Mohanty, L. J. Fiegel, and J. H. Healy, *Acta Cryst.*, **15**, 1190 (1962).

50% Ta_2O_5 along with either $\alpha\text{-Nb}_2\text{O}_5$ or $\beta\text{-Ta}_2\text{O}_5$ (see diagram). At 1350° , on the other hand, only a mixture of the latter two phases was observed in the same composition range. Thus the low temperature limit of $2\text{Nb}_2\text{O}_5 \cdot \text{Ta}_2\text{O}_5$ appears to extend to between 1400 and 1350° and we place the isothermal eutectoid transformation between these two temperatures.

Finally, through a high temperature diffraction study, a more accurate determination of the two-phase region ($\alpha\text{-Ta}_2\text{O}_5 + \beta\text{-Ta}_2\text{O}_5$) extending between the compositions of 50 to 100% Ta_2O_5 was possible. The transformation of pure Ta_2O_5 from α to the β form is readily reversible and indicated the possibility that this tendency might extend into the Ta_2O_5 region. This, indeed, was borne out in the subsequent at-temperature measurements. High temperature diffractometer runs on samples containing 60, 80, 90, and 100% Ta_2O_5 , respectively, showed transition temperatures between the β -phase and the two-phase region which were consistently lower than those which had been obtained from the heat and quench method in this investigation as well as earlier by Holtzberg and Reisman.³ The samples were equilibrated at temperatures for a minimum period of 10 min. before their diffraction patterns were recorded. The temperature at which the first trace of $\alpha\text{-Ta}_2\text{O}_5$ appeared during heating was taken as the transition temperature and these are represented by the solid line in the diagram. Because of possible hysteresis effects, these temperatures are to be taken as the upper estimates. However, it is unlikely that this effect is more than the uncertainty inherent in the temperature measurement of the X-ray samples which is estimated to be within $\pm 10^\circ$. The transformation observed for pure Ta_2O_5 was at $1320 \pm 10^\circ$, which is in agreement with that reported by Lagergren and Magneli.⁷ Attempts to determine the upper transition temperature marking the boundary between the $\alpha\text{-Ta}_2\text{O}_5 + \beta\text{-Ta}_2\text{O}_5$ and $\alpha\text{-Ta}_2\text{O}_5$ regions was less successful. The observed temperatures showed poor reproducibility and these, therefore, have been shown by a dashed line in the diagram, representing the best estimates from the diffraction measurements.

Acknowledgments. The authors thank the United States Atomic Energy Commission for partial financial support in this work, Mr. J. E. Peltier for his assistance in the X-ray investigations, and Messrs. K. W. Easey and G. R. Johnson for assistance in the preparation of samples.

The Solubility of Thallous Bromide and Silver Chloride in Molten Nitrate Solvents

by Ralph P. Seward and Paul E. Field

Department of Chemistry, The Pennsylvania State University, University Park, Pennsylvania¹ (Received August 19, 1963)

The solubilities of salts in fused salt solvents which have no ion in common with the solute have been calculated by a method to be described below from the thermodynamic properties of the pure components. As it was found that solubilities could be calculated which were in reasonable agreement with experimentally determined values in the few cases where the necessary data could be found, it seemed worthwhile to make additional solubility measurements to test further the applicability of the theoretical procedure. Since the calculations require a knowledge of the enthalpies and entropies of solute, solvent, and the reciprocal salt pair at temperatures where the salts are liquid, the number of systems which could be examined is not large. Only systems in which the solute solubility is small have been considered as it was felt that the validity of the theoretical calculations could be more critically tested in these cases. Experimental measurements have been made of the solubility of silver chloride and thallous bromide, at temperatures from 300 to 400° , in various pure and mixed nitrate solvents.

Calculation of Solubilities. The system to be considered is one where n_1 moles of solute AC dissolve in n_2 moles of BD. AC, BD, and the reciprocal salt pair BC and AD are ionic substances having identical ion coordination numbers when in the liquid state. For the purpose of relating the energy of the solution to its composition, it is assumed that the system consists of AC, BD, BC, and AD. The amount of these constituents must be consistent with the total number of moles of A salt being n_1 and the total number of moles of B salt being n_2 . In addition, it is assumed that with random dispersion of anions about cations, and *vice versa*, the ratio of moles of AC to AD, and of moles of BC to moles of BD, is n_1/n_2 . To be consistent with these conditions the composition of the solution is $n_1^2/(n_1 + n_2)$ moles of AC, $n_1n_2/(n_1 + n_2)$ moles of AD, $n_1n_2/(n_1 + n_2)$ moles of BC, and $n_2^2/(n_1 + n_2)$ moles of BD. The free energy of the solution is

(7) S. Lagergren and A. Magneli, *Acta Chem. Scand.*, **6**, 444 (1952).

(1) From the Ph.D. thesis of Paul E. Field, The Pennsylvania State University, August, 1953. Supported by the U. S. Atomic Energy Commission under Contract AT(30-1)-1881.

$$G = \frac{n_1^2}{n_1 + n_2} G_{AC} + \frac{n_1 n_2}{n_1 + n_2} G_{AD} + \frac{n_1 n_2}{n_1 + n_2} G_{BC} + \frac{n_2^2}{n_1 + n_2} G_{BD} \quad (1)$$

As a first approximation, the heat of mixing of the salts in the liquid state may be assumed to be negligible and the entropy increase on mixing to be ideal. With these assumptions, each of the partial molar free energies of eq. 1 may be expressed as

$$G_i = G_i^\circ + RT \ln \frac{n_i}{n_1 + n_2} \quad (2)$$

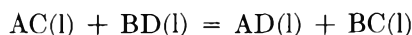
where i refers to any one constituent and G_i° to the free energy of that constituent in the standard state of pure liquid. When appropriate expressions for the individual free energies are substituted in eq. 1 and the resulting equation for G differentiated with respect to n_1 , temperature and n_2 being held constant, the resulting expression for the thermodynamic potential is

$$\left(\frac{\partial G}{\partial n_1}\right)_{T, n_2} = \mu_{AC} = (1 - N_2^2)G_{AC}^\circ + N_2^2 G_{AD}^\circ + N_2^2 G_{BC}^\circ - N_2^2 G_{BD}^\circ + RT \ln N_1^2 \quad (3)$$

Equation 3 may be written

$$\mu_{AC} = G_{AC}^\circ + N_2^2 \Delta G_{AC}^\circ + RT \ln N_1^2 \quad (4)$$

where N_1 and N_2 are mole fractions and ΔG_{AC}° is the standard state free energy change for the reaction



It should be noted that the relationship expressed by eq. 4 was obtained by Flood, Forland, and Grjotheim,² by a lengthier and less direct procedure, however.

For equilibrium with solid AC, the thermodynamic potential of AC in the liquid must equal that of solid AC, which is simply the standard molal free energy $G_{AC(s)}^\circ$. On setting the right side of (4) equal to $G_{AC(s)}^\circ$ and rearranging

$$-RT \ln N_1^2 = \Delta G_{F(AC)}^\circ + N_2^2 \Delta G_{AC}^\circ \quad (5)$$

In (5), $\Delta G_{F(AC)}^\circ$ is the free energy change accompanying fusion of pure AC. This may be evaluated if the heat of fusion of AC and the heat capacities of liquid and solid AC are known. ΔG_{AC}° may be evaluated if the enthalpies of formation and entropies of the four salts as liquids are available. With $\Delta G_{F(AC)}^\circ$ and ΔG_{AC}° known, the value of N_1 may be calculated at any desired temperature.

The neglected heats of mixing, for small values of N_1 at least, would be essentially those for mixing of AD and BC with the large excess of BD. These heats

would contribute an additional term to the free energies of these substances which would appear in eq. 5 as $N_2^2 \Delta H_{mix}$. Whenever such heats are known, this term may be added giving

$$-RT \ln N_1^2 = \Delta G_{F(AC)}^\circ + N_2^2 (\Delta G_{AC}^\circ + \Delta H_{mix}) \quad (6)$$

Experimental

All salts used were purified commercial products except TlBr, which was precipitated by mixing aqueous TlNO₃ with a small excess of aqueous KBr and AgCl which was precipitated by mixing aqueous AgNO₃ and NaCl solutions. All were kept in an oven at 110° before use except LiNO₃ which was kept and handled in a drybox.

About 40 g. of solvent salt was weighed directly into a glass tube. After addition of excess of solute salt, the solvent was melted and the mixture was stirred for 2 hr. or more at the desired temperature. After allowing excess solute to settle, samples of clear solution were removed with a preheated pipet, cooled to room temperature, and weighed. The soluble nitrate was then dissolved, by water in the AgCl studies and by 0.5 M KBr in the TlBr studies. The undissolved AgCl or TlBr was then caught and weighed in a sintered glass crucible.

To provide constant temperatures for the equilibration, the tube containing the solution was set into a larger, vacuum-jacketed tube of 40-mm. inside diameter. Resistance wire wound around a tube of intermediate size just inside the vacuum-jacketed tube provided heat. A relay actuated by a thermistor immersed in the equilibration tube varied the current through the coil to hold the temperature constant to about $\pm 1^\circ$. Temperatures were found from e.m.f. readings of a calibrated chromel-alumel thermocouple whose hot junction was also immersed in the equilibrium solution. E.m.f. measurements were made with a Leeds and Northrup Type K2 potentiometer and Type E galvanometer. Temperature control is probably the limiting factor in determining the accuracy of the solubility measurements. It is thought that errors should not be larger than $\pm 2\%$.

Comparison of Measured and Calculated Solubilities

The ΔG_{AC}° equations of Table I were obtained from the relation $\Delta G_{AC}^\circ = \Delta H_{AC}^\circ - T \Delta S_{AC}^\circ$. Equations for the heats of formation and for the entropies as functions of temperature were set up for each of the four substances involved in the AC + BD reaction. The numerical data needed were the standard heats of for-

(2) H. Flood, T. Forland, and K. Grjotheim, *Z. anorg. allgem. Chem.*, **276**, 289 (1954).

mation and entropies at 298°K. taken from Rossini,³ except the standard entropies of LiNO₃, LiBr, and NaBr, which were values estimated by Latimer.⁴ $H^\circ_T - H^\circ_{298}$ and $S^\circ_T - S^\circ_{298}$ values, heats of fusion, and

Table I: Thermodynamic Data Used in Calculations

Reaction	Standard state free energy changes, cal./mole	
TlBr(l) + LiNO ₃ (l)	$\Delta G^\circ_R = 7460 + 72.86T - 9.97T \ln T$	
TlBr(l) + NaNO ₃ (l)	$\Delta G^\circ_R = 9768 - 2.72T$	
TlBr(l) + KNO ₃ (l)	$\Delta G^\circ_R = 4995 + 52.8T - 7.5T \ln T$	
AgCl(l) + NaNO ₃ (l)	$\Delta G^\circ_R = 19,070 - 46.0T + 6.4T \ln T$	
AgCl fusion	$\Delta G^\circ_F = 2897 + 3.29T + 0.50(10^{-3}) \cdot T^2 - 1.35(10^5)T^{-1} - 1.12T \ln T$	
TlBr fusion	$\Delta G^\circ_F = 1683 + 22.06T + 0.60(10^{-3}) \cdot T^2 - 3.76T \ln T$	
-----Heats of mixing in liquid state, cal./mole-----		
TlNO ₃ in LiNO ₃	-901	NaBr in NaNO ₃ 360
TlNO ₃ in NaNO ₃	142	KBr in KNO ₃ 120
TlNO ₃ in KNO ₃	447	AgNO ₃ in NaNO ₃ 677
LiBr in LiNO ₃	120 (estimate)	NaCl in NaNO ₃ 400

heat capacities were taken from the compilation by Kelley.⁵ Heat capacities of 37.0, 15.5, 16.0, and 16.0 cal. mole⁻¹ degree⁻¹ for liquid TlNO₃, LiBr, NaBr, and KBr were estimated by the authors. Extrapolation to a supercooled state was required in several instances, introducing some uncertainty into the relations. Calculation showed, however, that a change of the heat capacity of liquid TlNO₃ from 37, the estimated value, to 40, for example, altered the ΔG°_R value by no more than about 100 cal. in a total of 7400–7800 cal. in the temperature region of interest. On subtracting the sums of the enthalpy and entropy equations for the reactants from the sums for the products of the exchange reaction, equations for ΔH°_R and ΔS°_R were obtained from which the ΔG°_R equations follow. Heats of mixing are available from the work of Kleppa and co-workers^{6–8} and are included in Table I. These numerical values are the enthalpy increases accompanying the solution of the first named salt in a large amount of the second. It has been assumed that these values are independent of temperature. These heats have been included in eq. 6 for the calculation of solubilities, the appropriate numbers being in each case the sum of the heats of mixing of AD and BC in the large excess of solvent BD.

Solubilities calculated by eq. 6 and the experimentally determined values are presented in Table II. The experimental values were read off at 20° intervals from a plot of the actual determination *vs.* temperature.

Except for TlBr in LiNO₃, the agreement is as good as can be expected. At 600°K., a difference of only 200 cal. in ΔG°_R corresponds to a change of 10% in the calculated solubility. Uncertainties in the thermody-

Table II: Experimental and Calculated Solubilities in Mole %

Solute	Solvent		-T, °K.				
			580	600	620	640	660
TlBr	KNO ₃	Experimental	2.42	3.10	3.87	4.88	6.23
		Calculated	2.18	2.73	3.41	4.28	5.35
		Exptl./calcd.	1.10	1.13	1.13	1.14	1.16
TlBr	NaNO ₃	Experimental	1.88	2.35	2.97	3.79	4.88
		Calculated	1.87	2.34	2.93	3.65	4.52
		Exptl./calcd.	1.00	1.00	1.01	1.04	1.08
TlBr	LiNO ₃	Experimental	1.01	1.33	1.74	2.26	2.98
		Calculated	0.34	0.43	0.54	0.68	0.84
		Exptl./calcd.	2.97	3.10	3.13	3.23	3.55
AgCl	NaNO ₃	Experimental	0.058	0.078	0.106	0.140	0.183
		Calculated	0.047	0.062	0.081	0.104	0.131
		Exptl./calcd.	1.23	1.26	1.31	1.35	1.40

namic data could easily account for this great an uncertainty in ΔG°_R . In view of the small size of lithium ion in comparison with the other ions, it is not surprising that the calculations should be least successful in LiNO₃ solution.

It is perhaps significant that the actual solubilities are greater than the calculated values in all cases. If there is preferential association of the ions of the solute instead of the random dispersion which was assumed, the metathetic reaction would be less complete, the energy increase on dissolving would be smaller, and greater solubility would result. Experimental evidence for this behavior is found in the work of Osteryoung, Kaplan, and Hill.⁹ These investigators found that the solubility of AgCl in KNO₃ in the presence of added KCl could be quantitatively accounted for by assumption of association constants for the formation of AgCl and AgCl₂⁻, the magnitude of these constants corresponding to the existence of a significant fraction of the solute as undissociated AgCl in pure KNO₃ solvent.

- (3) F. D. Rossini, *et al.*, National Bureau of Standards Circular 500, U. S. Govt. Printing Office, Washington, D. C., 1952.
- (4) W. M. Latimer, "Oxidation Potentials," Prentice Hall, New York, N. Y., 1952.
- (5) K. K. Kelley, U. S. Bureau of Mines, Bulletin 584, U. S. Govt. Printing Office, Washington, D. C., 1960.
- (6) O. J. Kleppa and L. S. Hersh, *J. Chem. Phys.*, **36**, 544 (1962).
- (7) O. J. Kleppa, R. B. Clarke, and L. S. Hersh, *ibid.*, **35**, 175 (1961).
- (8) O. J. Kleppa and S. V. Moshchel, *J. Phys. Chem.*, **67**, 668 (1963).
- (9) R. A. Osteryoung, C. Kaplan, and D. L. Hill, *ibid.*, **65**, 1951 (1961).

The Solubility and Entropy of Solution of Certain Gases in $(C_4F_9)_3N$, $CCl_2F \cdot CClF_2$, and 2,2,4- $(CH_3)_3C_6H_9$

by H. Hiraoka and J. H. Hildebrand

Department of Chemistry, University of California, Berkeley, California (Received August 20, 1963)

This investigation is an extension of the systematic study of the solubility and entropy of solution of gases in nonpolar solvents that has been carried out by previous collaborators with the senior author: Taylor,¹ Gjaldbaek,² Reeves,³ Kobatake,⁴ and Archer.⁵ It was undertaken chiefly to add the new solvent, $CCl_2F \cdot CClF_2$, in which Archer had found SF_6 to be much more soluble than the value reported by Kobatake for the same gas in C_7F_{16} .

Experimental

The apparatus and procedures were essentially those employed by Kobatake. The CO_2 was from Western Gas Inc., the N_2 from General Dynamic Corp., the CH_4 from Phillips Petroleum Corp., the Ar, Kr, and SF_6 from the Matheson Co. The $CCl_2F \cdot CClF_2$ was from Union Carbide and the $(C_4F_9)_3N$ from Minnesota Mining and Manufacturing Co.

The gases were passed through cold traps; the liquids were distilled and purity checked by their ultraviolet absorbance.

The vapor pressures of $CCl_2F \cdot CClF_2$ used in calculating the partial pressure of dissolved gases to 1 atm. were those determined by Hiraoka.⁶

Results

The results are given in Table I. The first row of figures for each solution gives temperatures in $^{\circ}C$.; the second row gives the corresponding solubilities as $10^4 x_2$, where x_2 is the mole fraction of gas at the temperature in question and 1 atm. partial pressure. A plot of $\log x_2$ vs. $\log T$ gives straight lines. The values for 25° have been obtained by interpolation on these lines. The figures for the entropy of solution, $\bar{s}_2 - s_2^g$, were obtained by multiplying the slopes of these lines by the gas constant, $R = 1.986$ cal. deg.⁻¹ mole⁻¹.

All of the data of the desired accuracy for the entropy of solution of gases in the solvents 2,2,4- $(CH_3)_3C_6H_9$ ("isooctane"), $CCl_2F \cdot CClF_2$, and three fluorocarbons— C_7F_{16} , $(C_4F_9)_3N$, and $c-C_6F_{11}CF_3$ —are plotted in Fig. 1 against the solubility expressed as $-R \ln x_2$.

Figures for partial molal volumes,⁷ cc. at 25° , were obtained by the method used in earlier investigations as

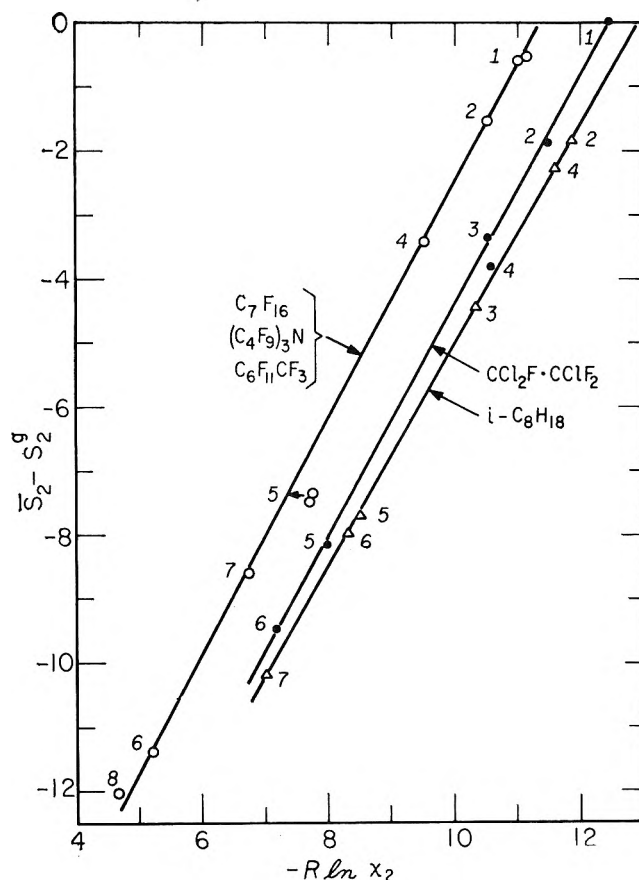


Figure 1. Entropy of solution vs. $R \ln x_2$ at 1 atm. and 25° : 1, N_2 ; 2, Ar; 3, CH_4 ; 4, CF_4 ; 5, CO_2 ; 6, SF_6 ; 7, C_2H_6 ; 8, Cl_2 .

follows: in $CCl_2F \cdot CClF_2$: Ar, 51.8; N, 66.0; CF_4 , 87.7; SF_6 in $(C_4F_9)_3N$, 93.7.

We offer the following comments on these results.

(a) The points for the new data here presented are consistent with those for systems previously studied in falling on a straight line characteristic of the solvent. In this respect the lines for the three fluorocarbon solvents coincide. This linearity is a test for the accuracy of the data.

(b) The slopes of these three lines are 1.82, 1.78, and 1.75, respectively, far in excess of unity, as they

- (1) N. W. Taylor and J. H. Hildebrand, *J. Am. Chem. Soc.*, **45**, 682 (1923).
- (2) J. C. Gjaldbaek and J. H. Hildebrand, *ibid.*, **71**, 3147 (1949); **72**, 609 (1950).
- (3) L. W. Reeves and J. H. Hildebrand, *ibid.*, **79**, 1313 (1957).
- (4) Y. Kobatake and J. H. Hildebrand, *J. Phys. Chem.*, **65**, 331 (1961).
- (5) G. Archer and J. H. Hildebrand, *ibid.*, **67**, 1830 (1963). See also, J. H. Hildebrand and R. L. Scott, "Regular Solutions," Prentice-Hall, Inc., Englewood Cliffs, N. J., 1962.
- (6) H. Hiraoka and J. H. Hildebrand, *J. Phys. Chem.*, **67**, 1919 (1963).
- (7) H. Hiraoka and J. H. Hildebrand, *ibid.*, **67**, 1833 (1963).

Table I: Solubility of Gases in $(C_4F_9)_3N$, $i-C_8H_{18}$, and $CCl_2F \cdot CClF_2$ ^a

						$\bar{s}_2 - s_2^g$, cal. mole ⁻¹ deg. ⁻¹
SF ₆ in $(C_4F_9)_3N$	4.91	14.91	24.96	35.20	25.0	
	1085	888	728	607.9	731	-11.3
CH ₄ in $i-C_8H_{18}$	4.36	14.97	24.77	35.07		
	62.36	(56.88)	53.51	49.89	54.0	-4.2
CO ₂ in $i-C_8H_{18}$	4.48	15.12	24.97	35.05		
	183.8	157.5	138.5	122.8	139	-7.7
CO ₂ in $CCl_2F \cdot CClF_2$	2.90	13.03	24.92	35.35		
	251.4	231.7	182.3	156.0	181	-8.15
CH ₄ in $CCl_2F \cdot CClF_2$	4.00	14.90	25.09	35.00		
	56.51	52.78	49.78	48.72	49.8	-3.35
N ₂ in $CCl_2F \cdot CClF_2$	4.00	15.00	24.98	35.00		
	19.33	19.46	19.31	19.88	19.3	0.00
Ar in $CCl_2F \cdot CClF_2$	0.10	4.21	14.90	20.02	24.91	
	33.4	32.8	31.85	31.40	30.95	30.9
SF ₆ in $CCl_2F \cdot CClF_2$		4.05	14.97	24.98	34.98	
		416.6	341.9	294.1	261.3	294.0

^a Upper row, t , °C., lower row, 10^4x_2 at 1 atm. partial pressure; values at 25° interpolated.

would be if soluble gases involved only the entropy of dilution. This re-emphasizes an important point already made,⁸ that in addition to the entropy of dilution there is a large contribution resulting from increased freedom of motion of solvent molecules adjacent to a solute molecule in progressing to gases with weaker and weaker attractive potentials.

(c) Archer and Hildebrand⁵ had found $10^4x_2 = 279$ for SF₆ in $CCl_2F \cdot CClF_2$, larger than the figure reported by Kobatake and Hildebrand for SF₆ in C_7F_{16} , 224, an incredible discrepancy. Therefore, we redetermined the former, finding the value in Table I, 294, and the same entropy. Our supply of C_7H_{16} is exhausted, so we substituted $(C_4F_9)_3N$, which has nearly the same solvent power, obtaining the value 731, in Table I. Evidently, the value reported by Kobatake contains a gross error that we have been unable to locate.

(d) The order and spacing of the points for the different gases are very different in the several solvents; the positions of the points for CF₄ and SF₆ are especially irregular. These facts express again the conclusion stressed by Archer and Hildebrand,⁵ and again by Hildebrand,⁹ that the energies of interaction between molecules of different types do not all conform to the usually assumed geometric mean "law."

(e) These rather comprehensive systematic values for entropy of solution afford material for carrying out the suggestion made by Hildebrand and Scott⁵ in "Regular Solutions" that we are now in a position to calculate energies of solution and study their relation to

solubility parameters of solvents and "force constants" of gases. This relation is now being examined.

Acknowledgment. We express our gratitude to the Atomic Energy Commission for the support of this work.

(8) J. E. Jolley and J. H. Hildebrand, *J. Am. Chem. Soc.*, **80**, 1050 (1958).

(9) J. H. Hildebrand, *J. chim. phys.*, in press.

The Limiting Quantum Yield for the Photoreduction of Benzophenone with Isopropyl Alcohol

by William M. Moore and Marshall D. Ketchum

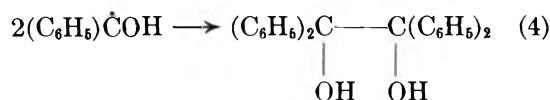
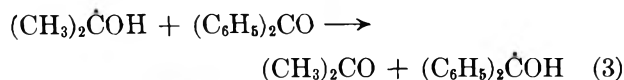
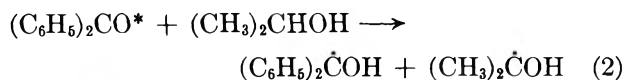
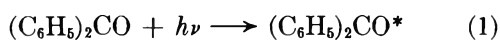
Chemistry Department, Utah State University, Logan, Utah
(Received August 29, 1963)

The photoreduction of benzophenone with isopropyl alcohol is a well known photoreaction that has been used for the synthesis of benzpinacol.¹ As a result of several recent investigations,^{2,3} the general mechanism for the photoreduction of benzophenone is fairly well

(1) W. E. Bachman "Organic Syntheses," Coll. Vol. II, John Wiley and Sons, Inc., New York, N. Y., 1948, p. 71.

understood. Under the influence of absorbed light, photoexcited benzophenone molecules convert to the long-lived triplet state by a highly efficient intersystem crossing. These triplet state molecules abstract hydrogen atoms from suitable hydrogen donors in the rate-determining step forming two free radical species. The properties of the resulting radicals then determine the course of the subsequent reactions.

In at least one case, the benzophenone-isopropyl alcohol system, the subsequent free radical reactions have complicated the basic kinetic measurements. Pitts, *et al.*,⁴ have obtained a quantum yield greater than one for the photoreduction of benzophenone with isopropyl alcohol (the limiting quantum yield of the primary hydrogen abstraction process is one^{2,5}). A mechanism that would account for the products, acetone and benzpinacol, and the high quantum yield, 1.06 ± 0.2 , was given by Pitts, *et al.*⁴ All of the steps except (3) are general reactions that have been postulated for



photoreductions of benzophenone.² Step 3 would have a great effect on the apparent quantum yield for the disappearance of benzophenone, and if it predominated over other processes in the competition for dimethylhydroxymethyl radicals, the limiting quantum yield should be two. Pitts⁴ predicted that this should be the case, since the quantum yield of acetone and benzpinacol was much higher than the corresponding quantum yield for benzophenone. Stoichiometrically, step 3 would predict that: $\Phi_{(\text{acetone})} = \Phi_{(\text{benzpinacol})} = 1/2 \Phi_{(\text{benzophenone})}$ in the limiting case, and a quantum yield of 0.92 was found for acetone and benzpinacol at 3660 Å.⁴

The actinometer system, based on the limiting quantum yield of benzophenone,⁵ was well suited to the benzophenone-isopropyl alcohol system, and since the photolysis of benzophenone has become the condensed phase analog of the gas phase classic, the photolysis of acetone, a reinvestigation of the problem seemed in order.

Experimental

Materials. Benzophenone (reagent grade) was recrystallized twice from ethyl alcohol and water. The

resulting white crystals had a melting range of 47–47.5° (uncor.).

Benzhydrol (reagent grade) was recrystallized once from hot ligroin and then twice from ethyl alcohol and water. The resulting white crystals had a melting range of 66–67° (uncor.).

Isopropyl alcohol (reagent grade) was purified by a method similar to that used by Pitts, *et al.*⁴ It was distilled into anhydrous potassium carbonate and then dried over calcium in a nitrogen atmosphere. It was redistilled and the fraction boiling at 79–79.9° (647.6 mm.) was used for the preparation of solutions.

Triphenylmethane (reagent grade) was recrystallized twice from alcohol and water; the resulting white crystals melted in the range 92–92.5° (uncor.).

2-Propanol-2-*d* was prepared by reducing acetone with lithium aluminum deuteride (Metal Hydrides Corp., 96.6% pure) in anhydrous ether. The infrared spectrum of the compound was identical with that of isopropyl alcohol except for a shift in the C–H stretching frequency from 2855 to 2150 cm.⁻¹. The 2-propanol-2-*d* was purified on an Aerograph vapor phase chromatograph by repeated 0.1-ml. injections. A vapor phase chromatogram taken at high sensitivity showed the alcohol to be uncontaminated by water or other impurities.

Deuterium isopropoxide was prepared by treating sodium metal with excess isopropyl alcohol on an oil bath at 50° overnight. The resulting wet mixture of sodium isopropoxide and sodium hydroxide was dried under vacuum, immediately hydrolyzed with a slight excess of deuterium oxide (99.6% pure), and distilled. The result was a deuterium isopropoxide-isopropyl alcohol azeotrope. The azeotrope was purified on the v.p.c., but complete separation was not possible and further effort was not warranted. The deuterium isopropoxide content of the final mixture was estimated at 83% from infrared analysis.

Procedure. Details of the apparatus, filter system, and general procedure have been given previously.⁵ A collimated light beam from a Westinghouse 800-C SAH mercury arc lamp was filtered to isolate the mercury band centered at 3660 Å. The Beckman DU cell holder was used to locate the photolysis cells in the light beam. Actinometer and sample solutions were photo-

(2) (a) W. M. Moore, G. S. Hammond, and R. P. Foss, *J. Am. Chem. Soc.*, **83**, 2789 (1961); (b) G. S. Hammond, W. P. Baker, and W. M. Moore, *ibid.*, **83**, 2795 (1961).

(3) J. A. Bell and H. Linschitz, *ibid.*, **85**, 528 (1963).

(4) J. N. Pitts, Jr., R. L. Letsinger, R. P. Taylor, J. M. Patterson, G. Recktenwald, and R. B. Martin, *ibid.*, **81**, 1068 (1959).

(5) W. M. Moore and M. Ketchum, *ibid.*, **84**, 1368 (1962).

lyzed simultaneously. All solutions were irradiated *in vacuo*.

Results and Discussion

The method of actinometry developed by Moore and Ketchum⁵ has been applied to the photoreduction of benzophenone with isopropyl alcohol in two ways: (1) the quantum yield for the photoreduction in pure isopropyl alcohol has been determined by the limiting quantum yield of the benzophenone–benzhydrol system in benzene; and (2) the limiting quantum yield of the benzophenone–isopropyl alcohol system in benzene has been determined by comparison with a benzophenone–benzhydrol solution of known quantum yield.

The first method gave erratic results similar to those reported by Pitts, *et al.*,⁴ except that quantum yields as high as 1.8 were obtained. A 0.1 *M* solution of benzophenone in isopropyl alcohol was photolyzed simultaneously with a 0.1 *M* solution of benzophenone and varying concentrations of benzhydrol. The quantum yield was fairly insensitive to moderate changes in the light intensity and the concentration of benzophenone. Increasing the purity of the reagents did not reduce the erratic nature of the results. The average of five intercept determinations (four concentrations of benzhydrol were used for every determination) gave a quantum yield of 1.4 ± 0.4 . Several other determinations were made which would not give any sort of a linear relationship. Several years of operating with the benzophenone–benzhydrol system and the present type light source have shown that both are stable and reproducible. For some unknown reason, the precision that is possible with other benzophenone photoreductions is not achieved in 100% isopropyl alcohol.⁶

By contrast, the second method gave very reproducible and consistent results. The isopropyl alcohol concentration was varied from 1 to 0.025 *M* while a constant benzophenone concentration of 0.10 *M* was maintained. The actinometer standard was 0.10 *M* benzophenone and 0.375 *M* benzhydrol in benzene. The results are shown in Fig. 1 and they obey the standard rate law for photoreduction of benzophenone. The intercept and slope, as determined by the method of least squares, were 0.455 and 0.0421, respectively. The intercept represents the limiting value for the ratio of the quantum yield of the actinometer standard to the quantum yield of the sample. Using a quantum yield of 0.89 for the standard,^{2,5} a limiting quantum yield of 1.96 is obtained for the benzophenone–isopropyl alcohol system.

The experiment was repeated with 2-propanol-2-*d* and the results are also shown on Fig. 1. The intercept and slope, as determined by the method of least squares,

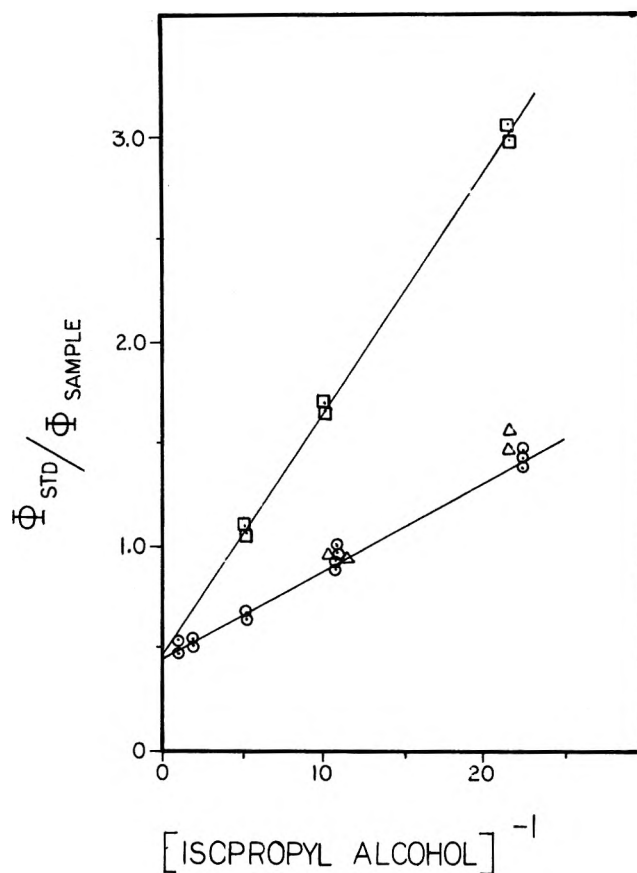


Figure 1. Photoreduction of 0.1 *M* benzophenone with isopropyl alcohol in benzene solution (standard solution contained 0.1 *M* benzophenone with 0.375 *M* benzhydrol in benzene): O, isopropyl alcohol, intercept 0.455, slope 0.0421; Δ , deuterium isopropoxide; \square , 2-propanol-2-*d*, intercept 0.475, slope 0.1166.

were 0.475 and 0.116, respectively. A kinetic isotope effect of 2.78 was calculated from the slopes, which is in good agreement with an isotope effect of 2.7 found for the same photoreduction with benzhydrol.² The intercept represents a limiting quantum yield of 1.88 for the benzophenone–2-propanol-2-*d* system, which is in good agreement with the undeuterated system.

Several runs were made with deuterium isopropoxide and the results are again shown in Fig. 1. No pronounced deviation from the undeuterated system was observed, as might be expected.

One other somewhat disconcerting but useful observation of this system has been made. Triphenylmethane is not a hydrogen donor for photoexcited benzophenone. It is not a quencher since its presence does not seem to affect the photoreduction of benzophenone

(6) Some small impurity in the isopropyl alcohol which is not removed by purification and not detected by the v.p.c. would be the most likely candidate. Also, the yellow intermediate, which has only been observed in the photolysis of benzophenone in isopropyl alcohol,⁴ could possibly quench the photoreaction.

with benzhydrol. However, the quantum yield for the photoreduction of benzophenone with isopropyl alcohol is reduced in a benzene solution saturated with triphenylmethane. Although the products have not been determined and more work needs to be done, a limiting quantum yield of 1.07 was obtained for this system.

These results, in conjunction with the study of Pitts, *et al.*,⁴ confirm the validity of the Pitts mechanism. It has also been demonstrated that the photoreduction of benzophenone with isopropyl alcohol is a special case of the more general mechanism for photochemical hydrogen abstraction reactions.

Step 3, the hydrogen exchange reaction between benzophenone and dimethylhydroxymethyl radical, predominates over other possible secondary reactions involving this radical even when the hydroxyl hydrogen is replaced by deuterium. Pitts observed that oxygen scavenges the dimethylhydroxymethyl radical and lowers the ratio of benzpinacol to acetone.⁴ We have also observed this in the reduced limiting quantum yield for benzophenone. Triphenylmethane can also disrupt step 3, presumably by acting as a hydrogen donor for dimethylhydroxymethyl radical.

The ratio of the slope to the intercept in Fig. 1 will give the ratio k_d/k_r , where k_d is the rate constant for the deactivation of photoexcited benzophenone in solution, and K_r is the rate constant for the hydrogen abstraction reaction. This ratio is 0.0926, which compares with a value of 0.045 for benzhydrol.⁵ In both cases the solvent is principally benzene, so if k_d is assumed to be constant, then K_r (benzhydrol) = $2K_r$ (isopropyl alcohol).

Acknowledgments. This work was supported by Grant U-167 from the Utah State University Research Council.

Surface Area of Active Carbon and Carbon Black by the B.E.T. Method Using Argon, Carbon Dioxide, Methanol, Krypton, and Xenon

by K. A. Kini¹

Division of Coal Research, Commonwealth Scientific and Industrial Research Organization, Sydney, Australia (Received September 9, 1963)

Attention recently has been drawn² to the widely varying values of the B.E.T. surface area obtained by Freeman and Kolb³ for a solid with an area of the order

of several hundred square meters per gram, from adsorption measurements with a homologous series of gases. Freeman and Kolb consider the variation to be a consequence of the assumption of a substantially uniform heat of adsorption in the B.E.T. theory. They have suggested instead a two-energy surface theory, which they consider allows calculation of unambiguous values for surface area.

In this connection it may be of interest to record the results of measurements of the B.E.T. surface areas of two carbonaceous solids, using argon at -195.8° , carbon dioxide at -78° , krypton at -78° , xenon at 0° , and methanol at 30° . These results lend support to the B.E.T. theory in its original form.

Experimental

The samples investigated were "Neospectra" carbon black and an active charcoal (B.D.H.) as supplied for gas adsorption. Adsorption of krypton and of xenon was studied under pressure in a metal adsorption apparatus.^{4,5} Adsorption of argon and of carbon dioxide was measured in a conventional volumetric apparatus, and that of methanol with a McBain sorption balance. The samples were degassed *in vacuo* (10^{-6} cm.) at 150° overnight before the adsorption measurements were made. Adsorption of the rare gases occurred rapidly, equilibrium being reached within a few minutes except in the case of argon on "Neospectra" carbon black at -195.8° , where a small creep was noticed. Methanol, however, was slow to equilibrate. The readings were continued until no further uptake of gas or vapor occurred overnight at each relative vapor pressure studied.

Results and Discussion

As shown in Table I, approximately equal surface area values were obtained for "Neospectra" carbon black with argon, carbon dioxide, and krypton, but the value with xenon was distinctly smaller. Again, for active charcoal, the surface areas obtained with argon and carbon dioxide were almost the same, but xenon and krypton gave a (constant) lower value. It is reasonable to attribute the differences in the areas observed with the various materials to a size effect (*i.e.*, molecular sieve action) of the adsorbed molecule rather than to failure of the B.E.T. theory. The existence of pores of cross-sectional area smaller than 24.9 and 21.0

(1) Department of Fuel Technology, Pennsylvania State University, University Park, Pa.

(2) *Chem. Eng. News*, **40**, No. 38, 66 (1962).

(3) M. P. Freeman and K. Kolb, *J. Phys. Chem.*, **67**, 217 (1963).

(4) K. A. Kini, paper to Sixth Biennial Conference on Carbon; University of Pittsburgh, Pittsburgh, Pa., June, 1963.

(5) K. A. Kini, *Fuel*, **42**, 103 (1963).

Table I: B.E.T. Surface Areas ($\text{m}^2/\text{g}.$) Obtained with Argon, Krypton, Carbon Dioxide, Xenon, and Methanol

	Carbon			Xenon	Methanol
	Argon	dioxide	Krypton		
	at -195.8° (13.8 $\text{\AA}.$) ^a	at -78° (17.0 $\text{\AA}.$) ^a	at -78° (21.0 $\text{\AA}.$) ^a	at 0° (24.9 $\text{\AA}.$) ^a	at 30° (18.1 $\text{\AA}.$) ^a
"Neospectra" carbon black	650	660	670	500	540
Active charcoal	870	860	770	770	860

^a Molecular cross sections calculated from the liquid densities at the stated temperatures by the procedure of P. H. Emmett and S. Brunauer, *J. Am. Chem. Soc.*, **59**, 1553 (1937).

\AA^2 in the carbon black and active charcoal, respectively, seems not unlikely.

Because of the more complicated molecular struc-

ture of methanol, no safe conclusion can be drawn from the results with this adsorbate. However, it may be noted that the methanol area of the active charcoal is the same as that obtained with argon and carbon dioxide. With the carbon black, the value for methanol lies between those for krypton and xenon, a fact which may perhaps be due to incomplete wetting of the surface by the adsorbate.

The results thus suggest that for surface area calculations based on the adsorption of simple adsorbates on carbons of the types examined, it is not necessary to abandon the original form of the B.E.T. theory, at least until more is known concerning the pore structures of such materials.

Acknowledgment. The author is grateful to Dr. M. F. R. Mulcahy for valuable discussions in the course of this investigation and for help in preparing the manuscript.

COMMUNICATION TO THE EDITOR

Success of Free Volume Model for Transport in Fused Salts

Sir: We wish to report a remarkable composition independence in electrical conductance behavior of $\text{Ca}(\text{NO}_3)_2 + \text{KNO}_3$ melts (some compositions in which are glass-forming¹) which has been revealed during a test of Cohen and Turnbull's free volume model² for transport in fused salts.

An adequate test of the free volume model expression for the diffusion coefficient of a species

$$D = AT^{1/2} \exp(-k/(T - T_0)) \quad (1)$$

where T_0 is the temperature below which the liquid contains no "free" volume² and A and k are constants, requires accurate measurement of temperature coefficients. To obtain the necessary precision, conductance measurements were made and the temperature coefficients corrected to correspond to those for a diffusion process. Although questionable in view of possible differences in the temperature coefficients of individual ionic conductances, this procedure seems justified by the results.

Experimentally, the specific conductance, κ , is found to decrease steadily with increasing per cent of Ca-

$(\text{NO}_3)_2$, and, notably, there is no indication of unusual properties in the liquid to correlate with the glass-forming capability of the 30-50 mole % $\text{Ca}(\text{NO}_3)_2$ composition range. The conventional activation energies for specific conductance, E_κ , determined at 4-10° intervals, increase exponentially with decreasing temperature (Fig. 1), the increase being followed to very high values of E_κ (~30 kcal.) in the cases where the measurements were not interrupted by crystallization.

To determine whether this behavior is accounted for by the free volume model, we observe, by differentiation of eq. 1 with respect to $1/T$, that the expression corresponding to the conventional activation energy for diffusion is given by

$$-E_{\text{diff}}/R = \frac{d \ln D}{d 1/T} = -\frac{1}{2}T - k \left(\frac{T}{T - T_0} \right)^2 \quad (2)$$

Hence $E_{\text{diff}} - 1/2RT$ (or in the present case the corrected $E_\kappa - 1/2RT$, hereafter called E_{cor}) should be a

- (1) A. Dietzel and H. J. Poegel, *Proc. 3rd Intern. Glass Congress, Venice, 1953*, p. 213.
- (2) M. H. Cohen and D. Turnbull, *J. Chem. Phys.*, **31**, 1164 (1959).

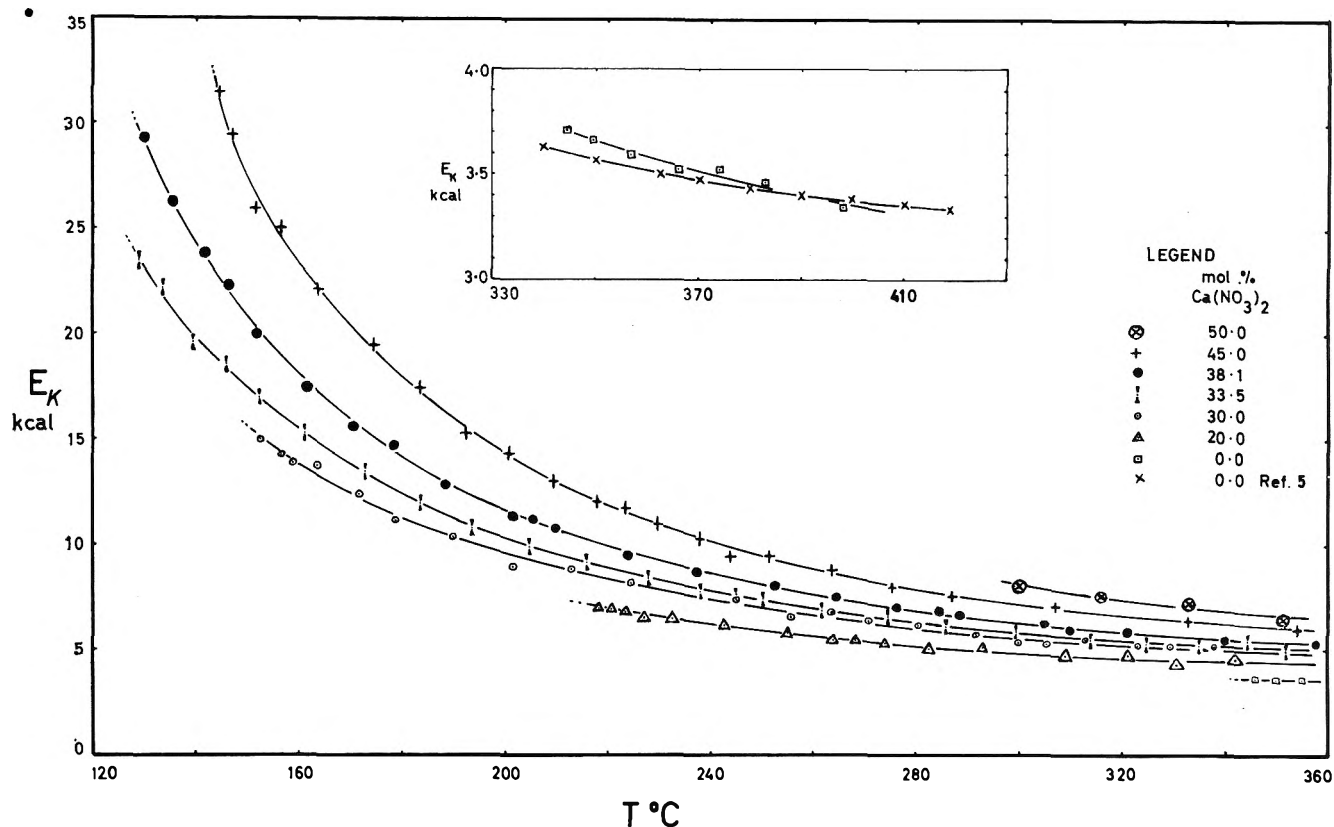


Figure 1. Dependence on temperature of activation energy for specific conductance in $\text{Ca}(\text{NO}_3)_2 + \text{KNO}_3$ melts.

linear function of $[T/(T - T_0)]^2$ which passes through the origin.

For 33.5, 38.1, and 45% $\text{Ca}(\text{NO}_3)_2$ the best choice of T_0 (to $\pm 2^\circ$) leads to a plot (Fig. 2) which is linear within experimental error for all values of T less than $1.7T_0$ ($[T/(T - T_0)]^2 > 6$), a small divergence appearing for higher temperature points. The T_0 -values thus obtained increase linearly with increasing % $\text{Ca}(\text{NO}_3)_2$ (Fig. 2, inset). Most striking, however, is the fact that for these T_0 -values the E_{cor} vs. $[T/(T - T_0)]^2$ plots are indistinguishable, over the whole range of $[T/(T - T_0)]^2$ values. Owing to the divergence from linearity for $T > 1.7T_0$, T_0 could not be determined satisfactorily for melt compositions outside the glass-forming range. However, when T_0 for the appropriate composition is taken from the linear T_0 vs. composition plot (Fig. 2, inset), the E_{cor} vs. $[T/(T - T_0)]^2$ plots in these cases also become virtually indistinguishable from the others. These results are summarized in Fig. 2.

The T_0 -value of 316°K . for 38.1% (50 wt. %) $\text{Ca}(\text{NO}_3)_2$ is in reasonable accord with the "glass transition" temperature, T_g ($\log(\text{viscosity}) = 13$), of 329°K . measured by Dietzel and Poegel.¹ The difference is in the expected direction since the reduction in free volume will become sluggish and effectively cease before the

theoretical zero point, T_0 , is reached, due to the increasingly long relaxation times involved.

The apparent significance of these findings may be summarized as follows.

(i) The free volume model correctly describes transport in molten nitrates without restriction to glass-forming mixtures.

(ii) The temperature-independent term in the exponential of eq. 2 is not dependent on composition in this system. Cohen and Turnbull² give this term as

$$k = \frac{\gamma v^*}{\alpha \bar{v}_m}$$

where α is the mean coefficient of expansion from T_0 to T , v^* is the minimum void volume necessary for diffusive displacement to occur, \bar{v}_m is the mean molecular (or ionic)³ volume, and γ is an overlap factor of value $1/2 < \gamma < 1$. Since α varies by less than 2% over the composition range, we conclude that the void volume to ion volume ratio involved in transport is about the same for all the ions regardless of size or charge. From the present results, this ratio lies in the range

(3) Ion volume here refers to the quantity derived from molar volume rather than from ionic radius.

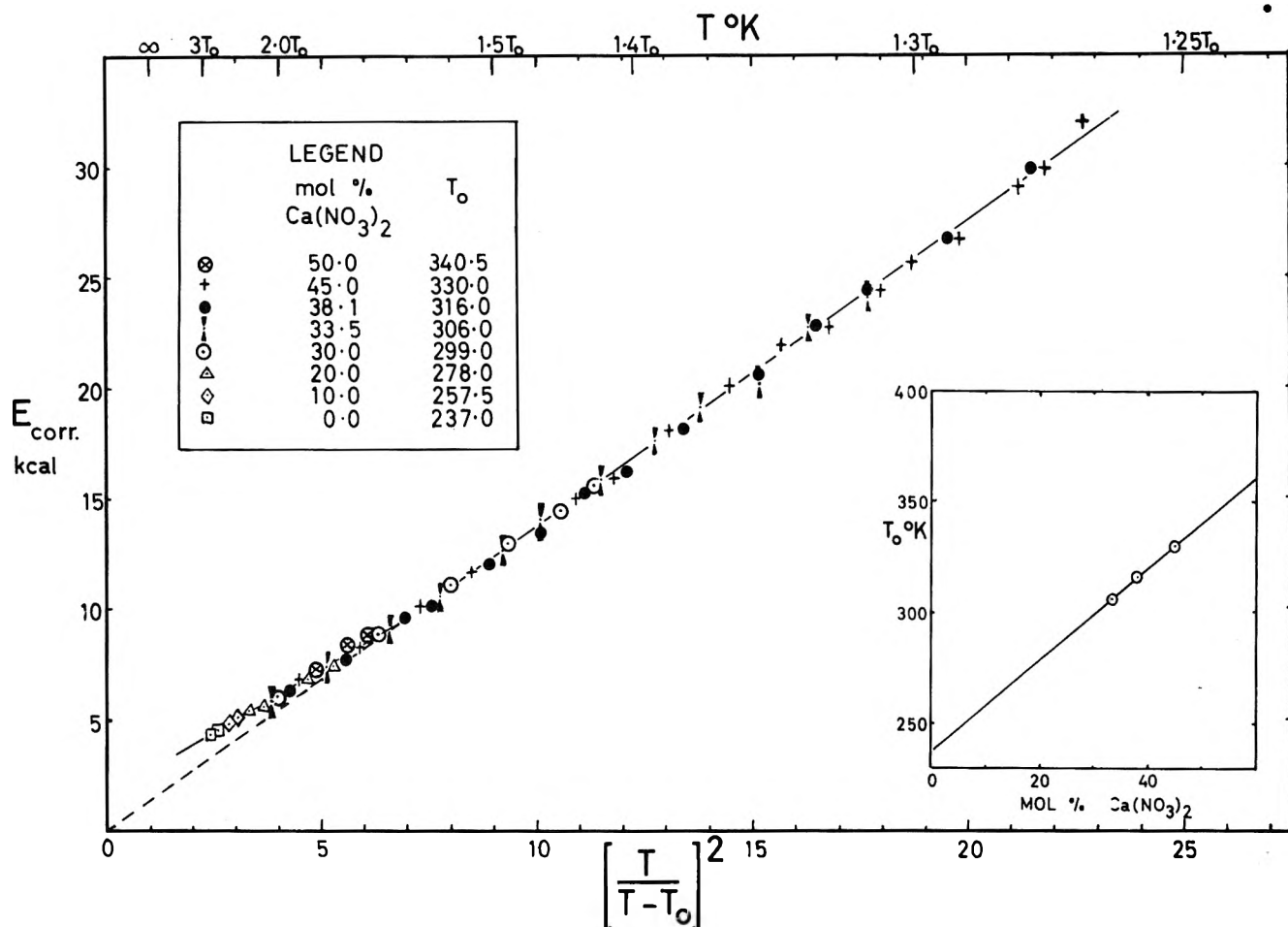


Figure 2. Plot of E_{corr} vs. $[T/(T - T_0)]^2$ for $\text{Ca}(\text{NO}_3)_2 + \text{KNO}_3$ melts. Inset: dependence of T_0 on composition.

0.53–0.26, depending on the value of γ employed. This is about half the values derived by Cohen and Turnbull² for several molecular liquids and seems somewhat low; this factor may need further interpretation for the case of ionic liquids.

(iii) Since the “mean cationic potential” ($\sum N_i z_i / r_i$, where N_i = mole fraction, z_i = ionic charge, and r_i = ionic radius of species i) of the melt increases linearly with % $\text{Ca}(\text{NO}_3)_2$ it follows that the zero point for free volume in these melts, T_0 , is directly proportional to the mean ionic field strength of the melt. Apparently as T_0 is passed, the effect of increasing temperature changes from increase of ionic vibration amplitudes to a production of distributable “extra” volume, this characterizing the liquid state of the glassy material. The associated additional degrees of freedom account for the increase in specific heat known to occur in the transformation range for glassy materials. It may be possible to correlate vibration amplitudes at T_0 with ionic types and predict T_0 for other ionic systems. Figure 2 sug-

gests that T_0 may serve as a basis for obtaining useful reduced temperatures applicable to transport problems.

Finally, we note that activation energy vs. temperature plots of similar character to those described here have been observed in $\text{LiNO}_3\text{--AgNO}_3$ and $\text{KNO}_3\text{--AgNO}_3$ melts⁴ and alkali halides⁵ where there is no suggestion of glass-forming capability.

This work, and further insight provided by diffusion measurements, will be described in greater detail in forthcoming publications.

(4) H. C. Cowen and H. J. Axon, *Trans. Faraday Soc.*, **52**, 242 (1956).

(5) E. R. Van Artsdalen and I. S. Jaffe, *J. Phys. Chem.*, **59**, 118 (1955).

DEPARTMENT OF METALLURGY
UNIVERSITY OF MELBOURNE
PARKVILLE N.2.
VICTORIA, AUSTRALIA

C. A. ANGELL

RECEIVED OCTOBER 21, 1963